MONASH University

Applications of group 15 and group 13 organometallic complexes as therapeutics

Rebekah Nicole Duffin

Bachelor of Science, Bachelor of Science (Honours).

A thesis submitted for the degree of *Doctor of Philosophy* at
Monash University in 2019
(*School of Chemistry*)

Contents

Copyright notice

Declaration

The work described in this thesis if of my original research and contains no material which has been previously accepted for the award of any other degree, or diploma presented at any university or equivalent institution. This thesis, to the best of my knowledge and belief, contains no previously published material written by another person, besides where due reference is made in the text of the thesis.

Rebekah N Duffin

01/08/2019

Dedicated to my friends and family,
whom without, this wouldn't be possible

Publications

Duffin, R. N., Blair, V. L., Kedzierski, L., & Andrews, P. C. (2018). *Comparative stability, toxicity and anti*-Leishmanial *activity of triphenyl antimony (v) and* bismuth *(v) α-hydroxy carboxylato complexes*. Dalton. Trans, **47(3)**, 971-980.

Duffin, R. N., Blair, V. L., Kedzierski, L., & Andrews, P. C. (2018). *Comparative stability, cytotoxicity and anti*-Leishmanial *activity of analogous organometallic Sb (V) and Bi (V) acetato complexes: Sb confirms potential while Bi fails the test*. J. Inorg. Biochem, **189**, 151-162.

Duffin, R. N., Blair, V. L., Kedzierski, L., & Andrews, P. C. (2019). *Alkyl gallium (III) quinolinolates: A new class of highly selective anti-leishmanial agents.* Euro. J. Med. Chem, 111895.

Duffin, R. N., Blair, V. L., Kedzierski, L., & Andrews, P. C. (2019). *Anti-leishmanial activity and cytotoxicity of a series of tris-aryl Sb (V) mandelate cyclometallate complexes.* J. Inorg. Biochem., 110932.

Abbreviations

VL: visceral Leishmaniasis

CL: cutaneous Leishmaniasis

MC: mucocutaneous Leishmaniasis

Ar: general aromatic subsitutent

R, R', R'': general organic substituent

Me: methyl substituent

Ph: phenyl substituent

LH: Free ligand

L: bound ligand

DMSO: *bis-methyl* sulfoxide

Tol: tolyl

THF: tetrahydrofuran

Et_2O: diethyl ether

X: general halide

NMR: nuclear magnetic resonance

IR: infrared spectroscopy

ESI: electron spray ionisation

MS: mass spectrometry

mp: melting point

δ: chemical shift

s: singlet

d: doublet

t: triplet

m: multiplet

o: ortho

m: meta

p: para

br: broad

ppm: parts per million

m: medium

w: weak

sh: sharp

v: wavenumber

AmpB: amphotericin B

ROS: reactive oxygen species

DMEM: Dulbecco's modified eagles' media

M199: medium m199

IC_{50}: Inhibitory concentration 50%

NTI: narrow therapeutic index

SI: selectivity index

Acknowledgements

It is difficult to fathom where to begin. I'd like to thank my parents, Chris Duffin and Lisa Hetherington, for raising me to always chase my dreams and to never say never. For nurturing my love of science from a young age as I continually changed the type of scientist I wanted to be: from an entomologist at age 3, to an ornithologist at age 10, to an MD at age 15 and finally a chemist at age 21. All your support over these 26 years has been phenomenal and I can never repay you for the love and support you have provided for me.

To my loving partner Craig, whom has always supported me from the minute we met. Thank you for your love, for the laughs and all our good times. You mean the world to me, and without you, things would be bleak. Thank you for supporting me emotionally and financially through these past seven years of university. I know it has been tough at times and I appreciate you greatly for this. I look forward to our future together.

To my siblings, Craig (Ceejay), Nathan and Rachelle. We've had our ups and downs but you'll always be in my heart. Especially Rachelle, who shared her journey into science with me for almost four years, I know you're going to be a wonderful researcher one day, keep following your dreams.

Thank you to my supervisor Professor Phil Andrews, for giving me this opportunity to excel in the world of chemistry. Your continuous support has helped me through some of the

toughest of times in this research project. When I wanted to give up, you were always there to give me advice and to push me back into the right direction.

Thank you, Dr. Victoria Blair and Dr. Melissa Werrett. You have both been an inspiration for me, thank you for showing me how a woman can achieve in the world of science. You have both provided excellent roles models for myself and for all young women in science. Vicki, you have always been there to lend me a kind ear when I feel at my lowest, you have helped me grow and mature into the woman in science I am today and I am ever grateful for your support and friendship. Mel, seeing your career take off has been a pleasure, you have given me the insight I need to achieve in this world, and provided me with the best fume-hood buddy any researcher could ask for.

Thank you, Dr. Lukasz Kedzierski, for all your biological assistance, and quick response time to my frantic emails about biology, you've been extremely helpful through the duration of my PhD.

To Sarmi Munuganti, where do I even begin. Girl, without you I don't know how I would have survived this past year. Your undying support, your kind words of encouragement and your friendship have been a shining light for me. You know me best out of anyone in the group, and you know when I am feeling down and are always there to make it better. Thank you for being you, for being a big-hearted, selfless, wonderful human being.

To my other group members past and present, thank you all for a wonderful experience in a research group. Jamie Greer, we started at the same time, both as honours students,

it’s been great getting to know you and seeing us both grow and mature from timid undergraduates, to the postgraduate researchers we are today. You’re always open to discuss research, trivia and pop-culture, and provide helpful tips along the way. Dr. Matt Flynn, though it took me three to four months to be comfortable enough to speak to you, seeing as your desk was behind mine, I’m glad I did. You’ve been very helpful when I am stuck with research, and it’s been great sharing many many Simpsons memes and quotes with someone who understands the reference. I’m glad to call you both my friends, and look forward to more board game nights and dumpling trips with Sarmi, Dimuthu and Peter. Speaking of Dr. Dimuthu Senevirantha, my friend, thank you for your helpful advice through the years, you have been a pleasure to work with and a pleasure to know outside of work. You’re always looking on the bright side of life. Kirralee Burke, we’ll always share that love of Avenged Sevenfold, and the gym, thank you for being a good friend to me. I wish you the best for your future endeavours. Megan Herdman thank you for all the pleasant times in the lab and for your love of parrots, I hope both our birds live long and happy lives just like us. To the rest of my comrades, it difficult to put into a limited amount of words, but you have all been a pleasure to know both in, and out of work, and I wish nothing but the best for you all.

To end off, I’d like to thank the Australian Government Research Training Program (RTP) for providing me with an income to help support my studies.

Abstract

This study aimed to explore the synthesis, characterisation and biological activity of group 13 and group 15 metal complexes. A series of Bi(V) and Sb(V) triphenyl acetic acetates of the general formula [$MPh_3(CO_2R)_2$] and one oxido bridged complex [$(SbPh_3((O_2C\text{-}O\text{-}CO)Me))_2O$], were firstly analysed. Seventeen complexes were characterised, of which fourteen were novel. All Sb(V) complexes were found to be stable to solution state degradation whilst the Bi(V) equivalents decayed over a short period of time. The Bi(V) example complex was found to rapidly react with glutathione, a biological thiol enzyme, degrading in under five minutes. The antimony equivalent reacted much slower, and was able to be successfully tracked by ^1H NMR . Due to the instability and high reactivity of the Bi(V) complexes, non-selective biological activity was observed. The Sb(V) complexes however were selectively toxic to *L. major* promastigotes and amastigotes.

A series of triphenyl Sb(V) *mono*-hydroxido quinolinolate were then probed, forming six-coordinate Sb(V) centres as opposed to the usual five-coordinate. Six novel complexes of the general formula [$SbPh_3(C_9H_4NORR')(OH)$] were synthesised and fully characterised. Similar to the acetic acetates, all quinolinolates were stable to solvent degradation. The complexes exhibited a good degree of biological activity and selectivity, making them an ideal class of candidates for future assays.

Four *bis-methyl* gallium *mono-quinolinolate*s [$Ga(Me)_2(C_9H_4NORR')$], four indium *bis-methyl mono-quinolinolate*s, [$In(Me)_2(C_9H_4NORR')$] and four *mono*-methyl gallium *bis-quinoli*nolates, [$GaMe(C_9H_4NORR')_2$] were then isolated. All complexes were novel. The alkyl indium quinolinolates were unstable in the solution state leading to rapid re-distribution. Several of these changes were successfully tracked by X-ray crystallography, however further analysis is required.

Five of the eight gallium complexes were tested for their biological activity with mixed results. Though exhibiting no cancer or bacterial activity, all five complexes were highly selective and potent anti-Leishmanial complexes.

The last study utilised the previously explored mandelic acid with a change in the aryl group of the triaryl antimony precursor. Ten novel cyclometallates of the formula $[Sb(Ar)_3Man]$ were synthesised, along with two novel perioxo bridged complexes $[(Sb(Ar)_3ManH)_2O_2]$. Though more cytotoxic than the remaining group 13 and group 15 complexes, they showed extremely potent anti-Leishmanial activity leading to a good degree of selectivity. There was no difference of the biological activity between the different enantiomers of the mandelate complexes, concluding that chirality played no role.

1. Introduction

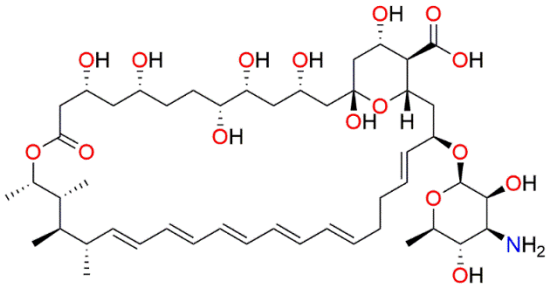

Amphotericin B

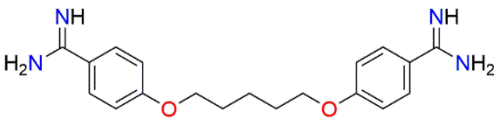

Pentamidine

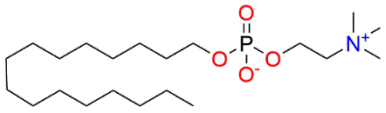

Miltefosine

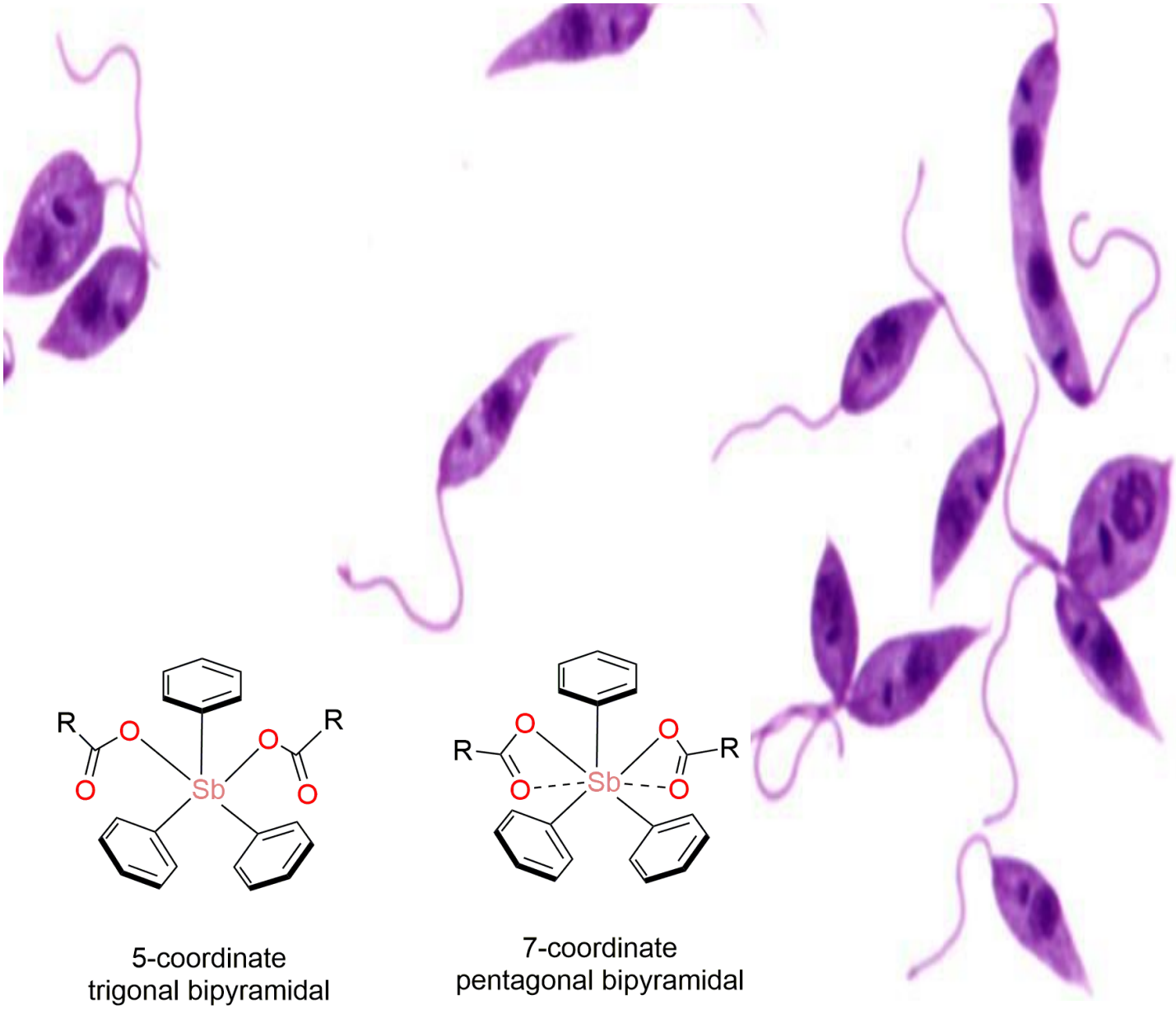

5-coordinate
trigonal bipyramidal

7-coordinate
pentagonal bipyramidal

1.1 *Leishmania*

Leishmania is classified by the World Health Organisation (WHO) as a neglected tropical disease (NTD). Despite its prevalence in over 90 tropical and sub-tropical low socioeconomic countries, interest in medical research for this disease is low on both the political and economic agenda of most first world countries.[1, 2] Approximately 1.5 million new cases of Leishmaniasis were recorded globally by the World Health Organisation (WHO), in 2018.[1] Around 20,000 – 40,000 of these cases resulted in death.[3, 4] Populations in poorer regions are at greater risk of infection, due in part to poor sanitation and lack of proper medical care.[5] The devastating and sometimes fatal visceral Leishmaniasis (VL) is on the rise, with WHO estimating 0.2 – 0.4 million new cases of VL each year.[6] The parasite itself is digenetic, growing and replicating in two distinctive phases. The parasite starts life as the extracellular promastigote in the digestive tract in one of over 30 sand-flies species (*Phelbotomus* and *Lutzomyia).*[7] A large proportion of these *Leishmania spp* are suprapylarian parasites, developing exclusively in the midgut of the sand-fly, whilst several new world species are peripylarian, entering the hindgut prior to migration to the midgut.[6, 8] The parasites undergoes several morphological changes during this stage of development. The whole process takes approximately 6 – 9 days from the initial procyclic promastigote form to the mature infective metacyclic form.[9] When a sand-fly bites a mammalian host, parasites are transferred from the midgut to the proboscis. The metacyclic promastigotes flood the blood stream initiating an immunological response. Macrophages arrive to the site of the infection where the promastigotes attach to the macrophages via a receptor mediated mechanism.[10] Parasites are then taken up into a phagolysosome, an acidic compartment that contains high concentrations of microbicidal peptides and hydrolytic enzymes.[11] The parasites stay hidden within the phagolysosomes by biochemically altering several pathways of the host cell and themselves, enabling survival in the low pH environment.[12] The parasite then undergoes differentiation into the amastigote form. The amastigotes are able to block the harmful production of superoxide and hydrogen peroxide, preventing innate immune response.[13, 14] The amastigotes undergo rapid and

exponential binary fission, bursting the macrophages and flooding the host blood stream. A sand-fly bites the infected host, taking up amastigotes which migrate to the midgut, and the cycle starts again (figure 1.1.1)[15]

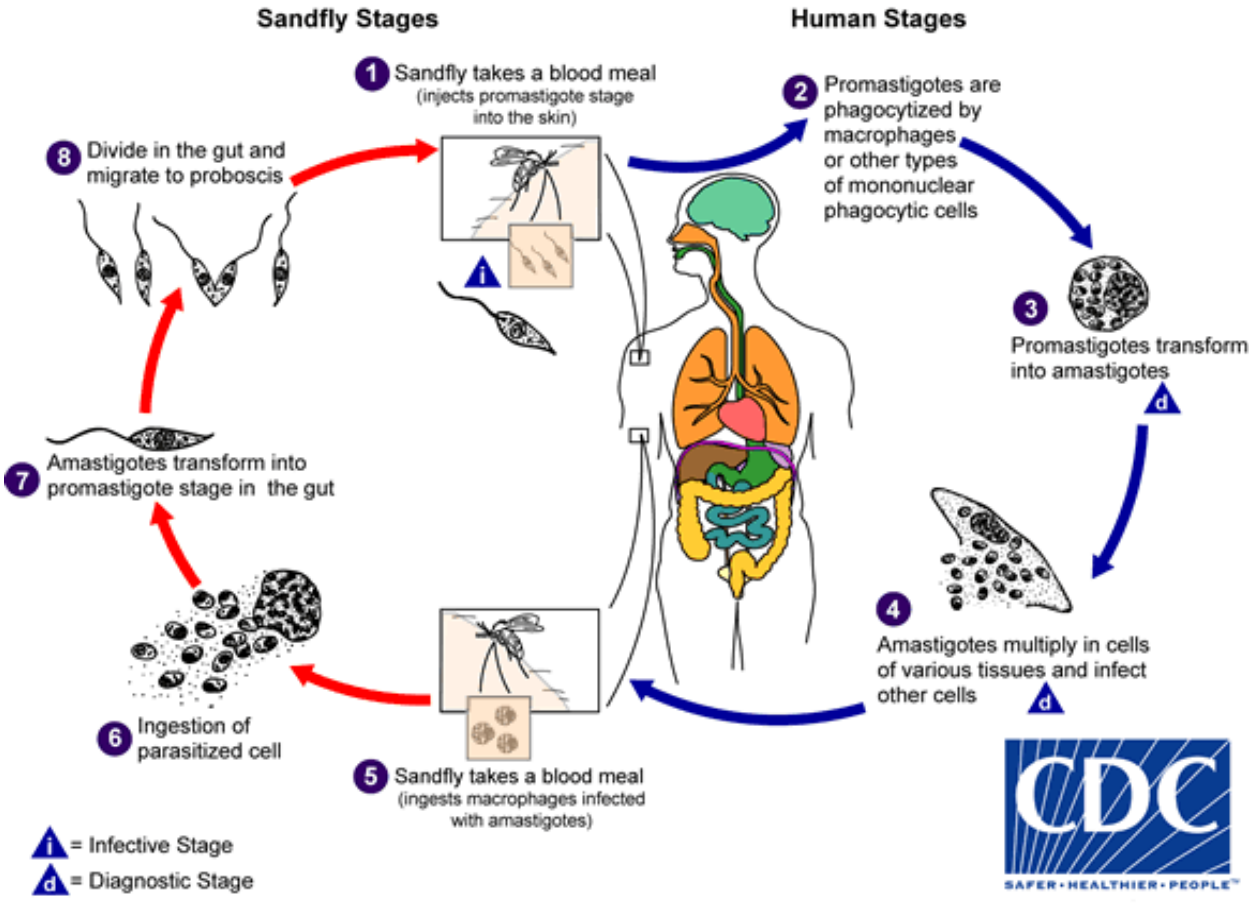

Figure 1.1.1 Life cycle of the Leishmania parasite (https://phil.cdc.gov/Details.aspx?pid=3400, CDC/Alexander J. da Silva, PhD, accessed: 04/07/2019)

1.1.1 Visceral, cutaneous and mucocutaneous Leishmaniasis

Leishmaniasis presents in three distinctive forms: Cutaneous (CT), characterised by lesions of the skin, mucocutaneous (MC), forms as a result of CT and results in infection of the mucosa, and visceral Leishmaniasis (VL), characterised by enlargement of the liver and spleen.[16, 17] VL is often

fatal if left untreated, and can be asymptomatic, making it difficult to diagnose and treat.[18] Cutaneous on the other hand is often self-healing, especially in the case of *L. major* and *L. tropica* infection, with the potential serious outcome of infection scarring of the previously infected area.[19] Similar to VL, MC can present as life threatening if not immediately treated. MC infections are often a result of a prior cutaneous infection and present with symptoms such as persistent nasal congestions, erythema erosions and ulcers of the nasal and mouth area (figure 1.1.2).[19-22]

Figure 1.1.2 Cutaneous and Mucocutaneous Leishmaniasis *infection. Images displayed are from the CDC Public Health Image Library (https://phil.cdc.gov/QuickSearch.aspx?key=true accessed: 04/07/2019)*

1.2 Frontline treatment of *Leishmania* infection

The most cost effective and readily available treatments for Leishmaniasis have relied heavily on the use of pentavalent antimonial complexes. Historically, antimony was first used in the +III oxidation state, in the form of potassium antimony tartrate, or tartar emetic (figure 1.2.1).

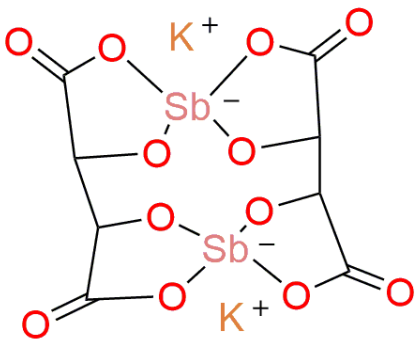

Potassium antimiony tartrate

Figure 1.2.1 Structure of potassium antimony tartrate (tartar emetic)

This complex was intravenously injected into patients suffering from a variety of trypanosome parasites, including *Leishmania.* This was first recorded in 1913, where Machado and Vianna were able to cure infection by injection of the tartar emetic into a Brazilian patient. Attempts to take the drug orally resulted in severe gastrointestinal sickness and vomiting due to its emetic effects.[23, 24] Though an effective anti-Leishmanial, tartar emetic was non-selectively toxic and would induce side-effects, ranging from headaches and muscle pain, to severe or even fatal anaphylaxis.[25] Therefore, it was soon replaced by a new set of antimony complexes, the pentavalent antimonials. These complexes were introduced before the second world war and remain a top choice for the treatment of all forms of the diease.[26] Despite their current use today, these complexes also harbour their own side-effects. Both sodium stibogluconate and meglumine antimonate (figure 1.2.2) are high hydrophilic, and so are unable to be administered by any means other than intravenous or intramuscular injection. Both complexes also have a high renal clearance and so must be injected daily for upwards of a month for an effective treatment.[27, 28]

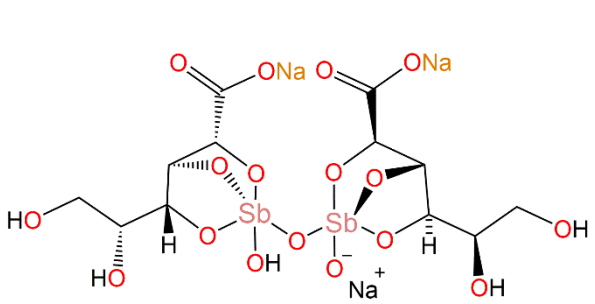

Sodium stibogluconate
(Pentostam ™)

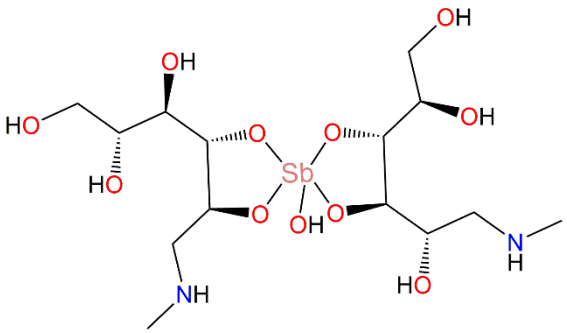

Meglumine antimonate
(Glucantime ™)

Figure 1.2.2. Proposed structures of Pentostam ™ and Glucantime ™

Even at therapeutic doses of 20 mg Sb/kg/day, the complexes harbour problems with toxic side-effects. These are often mild, such as headaches or nausea, but can manifest into more serious cases of elevation of hepatocellular enzymes, cardiotoxicity and pancreatitis.[29, 30] Resistance to these complexes has also become a major issue in recent years, with resistant strains evolving due in part to the administration method yielding non-compliance within infected communities (strict daily injections upwards of a month) and due to biochemical alterations of the parasite. One such biochemical alteration comes as a result of the high levels of arsenic in the drinking water of infected communities in India. The parasite has adapted to this high concentration of As(V) by developing reductase enzymes, these enzymes are able to act upon the Sb(V) drugs prior to their anti-Leishmanial effect, rendering them useless, and allowing the parasite to continue to grow and develop greater resistance.[31-33]

Alternatives to the pentavalent antimonial complexes are organic moieties such as: pentamidine, which was originally designed as an anti-trypanosomal,[34] milteofosine, which found original use as an anti-cancer agent,[35] and amphotericin B (AmpB), of which was developed as an anti-fungal drug (figure 1.2.3).[36]

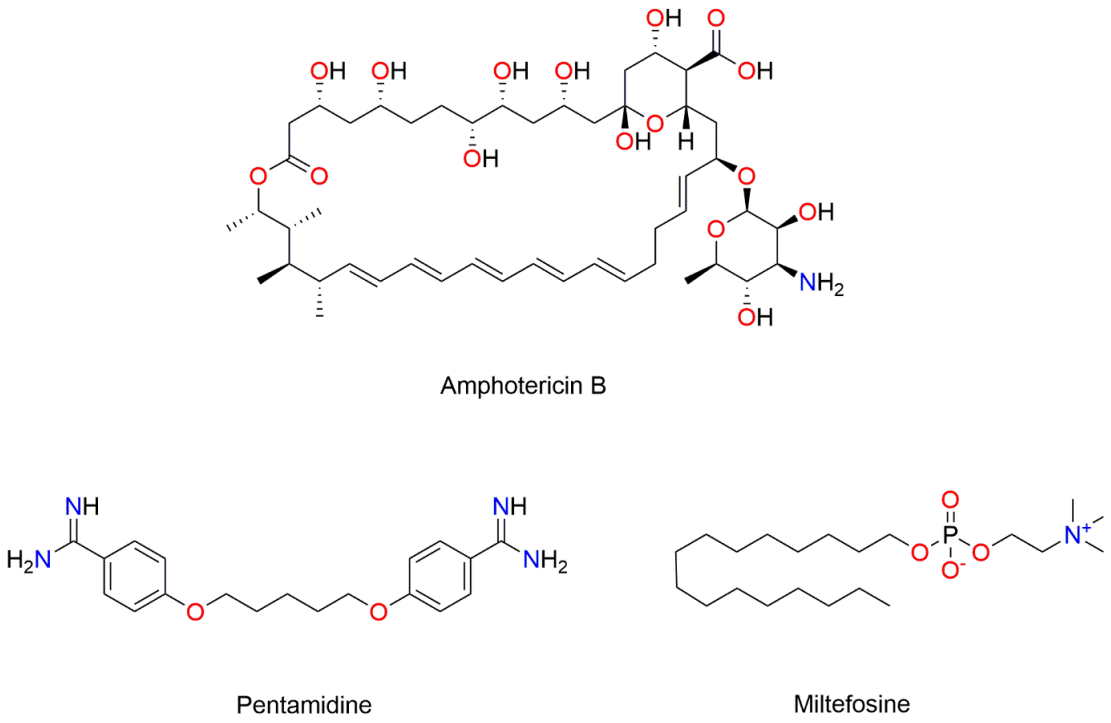

Figure 1.2.3. Structure of the organic drugs, pentamidine, miltefosine and amphotericin B.

Similar to both Pentostam ™ and Glucantime ™, all of these organic compounds harbour unavoidable side-effects, which can often be debilitating. Pentamidine salts were found to induce serious cardiac and gastro toxicity and miltefosine is a known teratogen with a narrow therapeutic window. Even amphotericin B, which is often the last resort drug, is expensive and can cause numerous side effects including renal failure.[37] Not only do these organic alternatives harbour problems associated with toxicity, resistance is also becoming an issue. The orally available liposomal form of amphotericin B (AmBisome ™) was observed to have limited effect on several clinical isolates of the VL causing *L. donavani*, both *in vitro* and *in vivo.*[38] This resistance has been theorised to be associated with an increase in a specific Leishmanial sterol, which alters the fluidity of the membrane, inhibiting the movement of AmBisome ™ into the parasite.[39] A recent study by Veronica *et al* observed resistance to the other orally available drug, miltefosine, to be due in part to increased production of the Leishmanial iron superoxide dismutase (FeSOD).[40]

1.3 Mechanism of action of the front-line treatments

The mechanism of action of the Sb(V) drugs is still being disputed. Current consensus focuses on a reductive pathway as the major constituent of its therapeutic action. The Sb(V) is reduced *in vivo* to the more active +III form, which would make the Sb(V) complexes pro-drugs. This indirect pathway first involves traversing the macrophage membrane, the phagolysosome and finally the parasite membrane. Entry into the parasite is hypothesised to involve recognition of Sb(V) pro-drugs by an interaction with a protein on the cellular surface which recognises gluconate-like sugar moieties.[41] A lipophosphoglycan (LPG) moiety on the cell surface of the parasite interacts in a similar fashion to the macrophages, through identification of mannose-fucose receptors on the macrophage cell surface.[42] This differs from the mechanism of entry for Sb(III) moieties, which traverse the parasite membrane through aquaglyceroporins (AQPs), which are specialised channels that allow the transport of water. This uptake has been observed to be quite rapid in most species of *Leishmania*.[43] Once inside, Sb(V) is reduced by the thiol rich parasite protein trypanothione, to the bio-active Sb(III). Trypanothione is comprised of two units of the mammalian equivalent, glutathione, connected by a single spermidine molecule. Reduction is a pH dependant process, favouring the low pH of the phagolysosome compartment of the macrophage.[44] Reduction interferes with the primary function of the trypanothione, which is to mediate the production of redox active species. This combined with the inhibition of other homeostatic pathways, such as the glycolytic pathway, results in a cascade of reactive oxygen species, leading to enzyme depletion and cell apoptosis.[45] A similar theory involves competitive binding of the Sb(III) with a zinc finger peptide associated with growth and development, disrupting normal cellular function and leading to cell death.[46] The other, less accepted theory, involves the direct action of the Sb(V) complexes prior to reduction. Studies suggest that Pentostam ^{TM} acts as a potent inhibitor of protein phosphatases in *L. donavani,* leading to an increased cytokine response and eventual cell death.[47]

The orally available miltefosine and AmpB act on the parasite in different ways. Miltefosine has been theorised to induce a number of toxic effects. It has been described to increase production of reactive oxygen species (ROS) which exert an apoptosis-like effect,[48, 49] inhibit the production of cytochrome-*c* enzymes within the parasite and affect the metabolism of lipids in the promastigote form.[50, 51] Amphotericin B on the other hand effects the permeability of the protozoal membrane and the respiration of the cell.[52] The mechanism of action however is not that simple and is thought to be multifactorial. One other theorised mechanism involves auto-oxidation and subsequent formation of free radical species.[53] Generation of ROS species seems to be a common factor in anti-Leishmanial complexes, and may be exploited when designing new therapeutics.

1.4 Group 15 complexes in medicine

Complexes of the group 15 metals antimony and bismuth have been used medically for many years now. As previously mentioned in section 1.2, antimony was found to be a potent inhibitor of *Leishmania*, preferentially in the less toxic +V oxidation state. Bismuth too, has been used historically for the treatment of microbes, most notably the Gram-negative bacteria, *Helicobacter pylori* (*H. pylori)*. Commercially available bismuth complexes, bismuth subsalicylate (BBS, tradename: Pepto-*bis*mol ™),[54] colloidal bismuth sub-citrate (CBS, tradename: De-Nol ™)[55] and the most recent addition, ranitidine bismuth citrate, (RBC, tradename: Pylorid ™)[56] have been the front-line treatments for gastric ulcers caused by *H. pylori* (figure 1.4.1). Activity of these drugs is due to the formation of a protective coating of glycoprotein-bismuth complexes, which allow the lesions in the ulcer crater to heal.[57] Bi(III) complexes have also proved to be effective against other infectious diseases such as syphilis and colitis.[58] Studies into the effects of BSS against other bacteria were promising. BSS demonstrated *in vitro* activity against enterotoxigenic *Escherichia coli*, a Gram-negative bacterium notorious for causing diarrhoea in the developing world. The

mechanism of action has been hypothesised to involve the reduction of toxic secretory activity of *E. Coli*, preventing diarrhoeal disorders.[59]

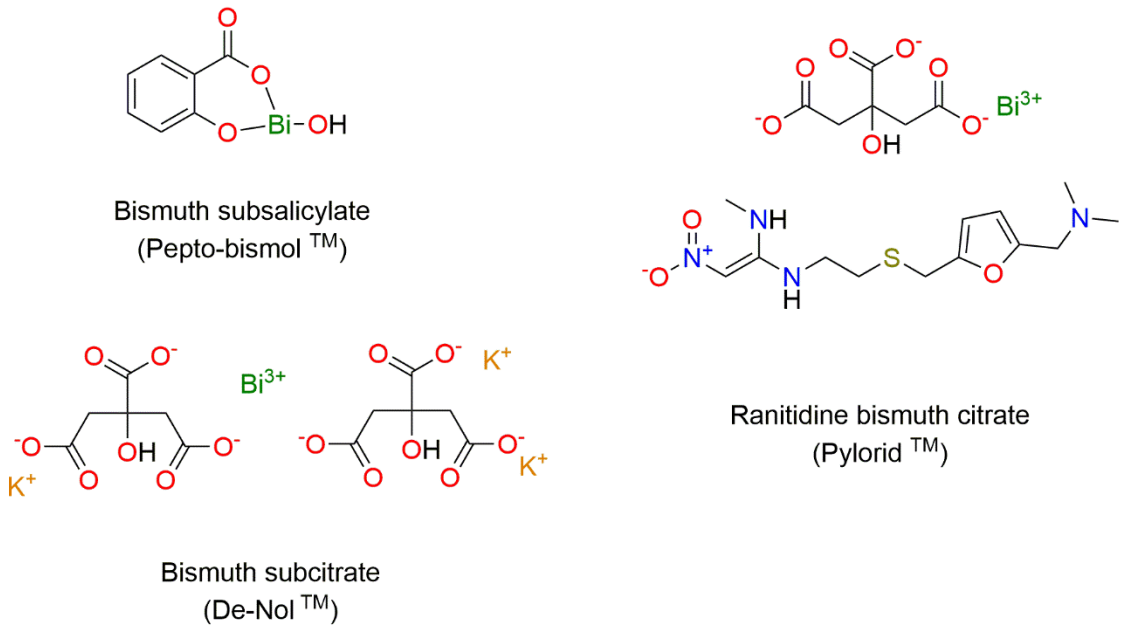

Figure 1.4.1. Empirical structures of gastric treatments of bismuth*, Pepto Bismol TM, De-Nol TM and Pylorid TM.*

Although antimony is still currently used to treat *Leishmania*, it also found use in the treatment of other protozoan disorders such as Schistosomiasis and Trypanosomiasis. Tartar emetic was historically the first efficient treatment for Schistosomiasis.[60] Schistosomiasis is a tropical disease caused by parasitic flatworms of the genus *Schistosoma*. Similar to *Leishmania*, *Schistosoma* requires an intermediate host, of which is snails, prior to human infection.[61] Similar to the treatment for Leishmaniasis, the toxicity of tartar emetic soon caused it to be taken out of circulation as an anti-*Schistosoma*. Several other antimony complexes were employed to combat the parasitic flatworm, including analogues of tartar emetic and several other antimony salts such as: sodium antimony disulfate (Stibophen TM),[62] sodium antimony thiomalate (Anthiomaline TM),[63] sodium antimony gluconate (Tiostan TM)[64] and sodium antimony dimercaptan (Astiban TM). The structure of these are given below in figure 1.4.2.[65] All were intramuscularly injected and

unavoidably toxic, leading to discontinuation of the Sb(III) drugs. All compounds posed a great degree of cardio-toxicity with deaths due to muscle fibre fragmentation observed in Schistosomiasis patients. Nowadays, Schistosomiasis is treated with organic compounds.[66]

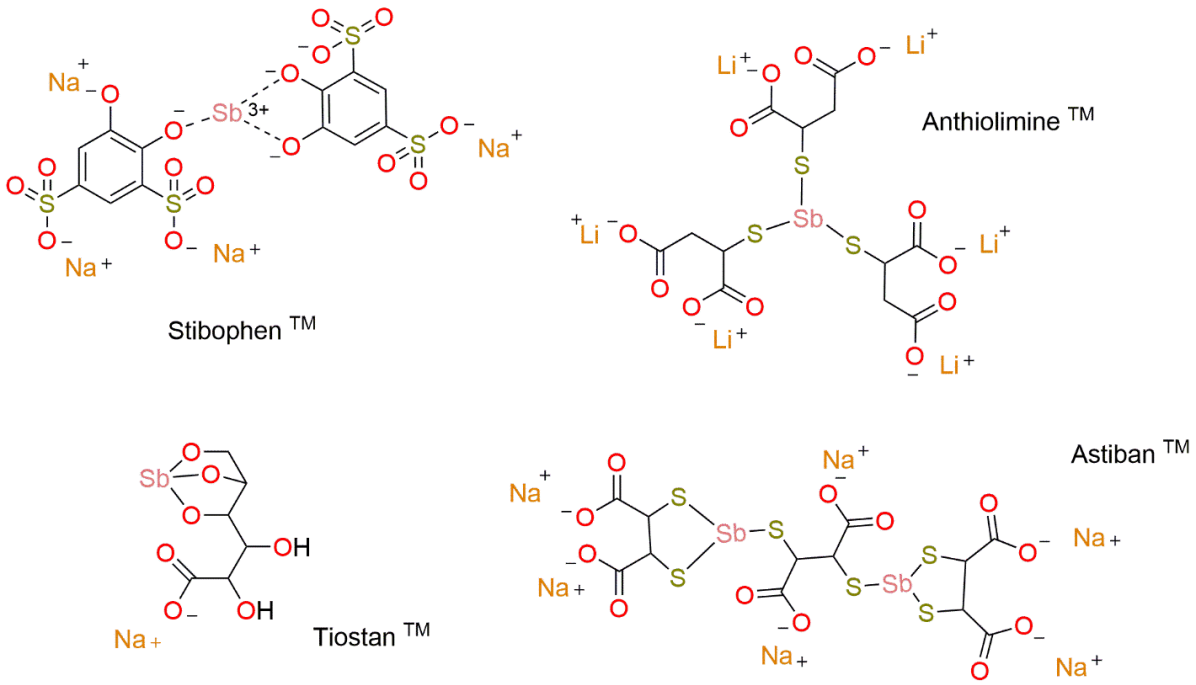

Figure 1.4.2. Structures of traditional anti-parasitic antimony drugs

Similar to *Leishmania*, *Trypanosome* parasites are from the family *kinetoplastidae*, and so share some biological traits. Despite this, antimony complexes were never really a front-line treatment for Trypanosomiasis, with limited research on the trivalent tartar emetic.[67] The elementally related group 15 metalloid arsenic, found its use in the treatment of this parasite instead, in the forms of sodium arsenite and atoxyl TM (figure 1.4.3).[68] Similar to antimony, arsenic poses problems with toxicity and so was eventually removed from circulation. The biological similarities of *Leishmania* to *Trypanosoma* make them ideal common targets in drug development. The use of antimony complexes against *Trypanosoma* therefore could constitute a whole new area of potential therapeutic research.[69]

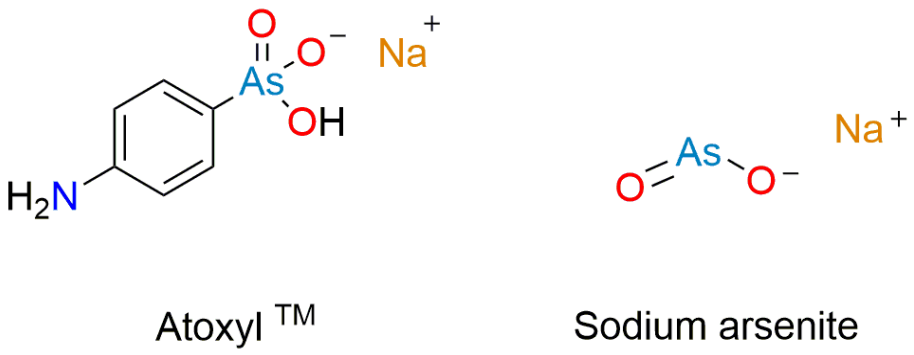

Figure 1.4.3. Structures of Atoxyl and sodium arsenite, used to treat Trypanosomiasis

1.5 Gallium and indium

Gallium and indium are metallic elements of group 13, the triels, along with aluminium and thallium.[70] Both gallium and indium preferentially exist in the +III oxidation state, forming stable complexes with a variety of ligands. Gallium and indium share some chemical similarities, such as a similar Pauling electronegativity of 1.81 and 1.78 respectively.[70] The covalent radius of Ga(III) is understandable smaller than the larger, heavier In(III), with radii of 1.25 Å and 1.50 Å respectively (figure 1.5.1).[71]

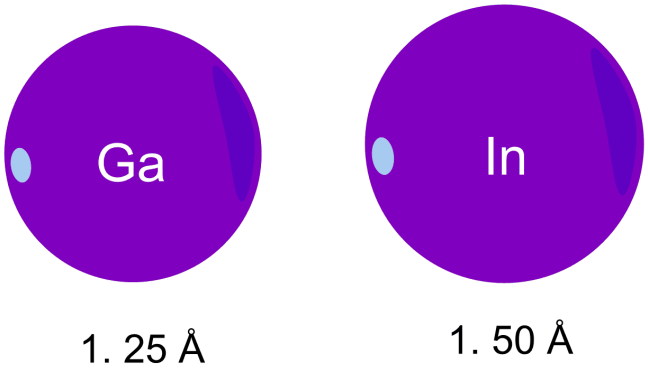

Figure 1.5.1. The ionic radii of Ga(III) and In(III)

Both Ga(III) and In(III) have a propensity to behave as Lewis acids in complex formation.[71] Gallium has already shown medical potential, notably in the treatment of hypercalcemia associated with cancer therapy.[72] Gallium's historic use in medicine will be discussed in greater detail in chapter 2.3.1. Indiums has found use mainly as a semi-conductor, however there are a few medically relevant complexes within the literature, of which will be explored in section 2.3.2.

1.5.1. Gallium and iron

Gallium's medical use has been theorised to be linked to its similarities to iron in the +III oxidation state. Ga(III) and Fe(III) share similar electronegativity, electron affinity, ionic radius and coordination geometry (table 1.5.1).[73]

Table 1.5.1 Similarities of Ga(III) and Fe(III).

	Electronegativity	**Electron affinity**	**Ionic radius**	**Coordination number**
Fe^{3+}	1.96	15.7 kj/mol	0.63 Å	6
Ga^{3+}	1.70	28.9 kj/mol	0.76 Å	6

Both gallium and iron also share similar nuclear radii and ionisation potential.[74] However gallium does not shared the same level of redox activity of iron. Unlike Fe(III), Ga(III) is virtually irreducible under physiological conditions, conversely, Fe(III) to Fe(II) reduction and vice versa, plays an important role in biological pathways. Therefore, gallium may block important redox active pathways by substituting for iron in metallo-proteins and metallo-enzymes. Gallium binds to iron transport proteins such as transferrin and lactoferrin enabling delivery of gallium into cells.[76, 77] The binding affinity of gallium to these proteins has been observed to be more favourable than iron.[78, 79] Not only can gallium bind to these proteins, it also has a more favourable solubility in biological fluids than Fe(III). FeO(OH) in aqueous solutions at physiological, exist as a solid

precipitate, whereas gallate, $Ga(OH)_4^-$, exists in plasma at significant concentrations. This indicates that gallium may also participate in transport and biochemical reactions not possible for plasma Fe(III).[80, 81] Gallium has also been observed to bind to ferritin, the large 440,000 MW protein responsible for iron storage within cells, in particular, macrophages. The transfer of Ga(III) from transferrin and lactoferrin to ferritin appears to be mediated by phosphate containing compounds such as adenosine triphosphate (ATP) and pyrophosphate. Because of its lack of redox activity, Ga(III) is unable to interfere with Fe(II) predominant pathways, which is advantageous. The inability of Ga(III) to enter Fe(II) bearing proteins such as cytochromes and haemoglobin, infers it will not interfere with oxygen transport and therefore has no cytotoxic effect on red blood cells.[82, 83]

1.6 *Leishmania* and iron acquisition

Iron is an essential biological metal, facilitating a variety of homeostatic pathways in all manner of life.[84] *Leishmania*, like all eukaryotes, require iron for growth and maintenance.[85] *Leishmania* encounters a diverse range of environments through its complete life cycle, therefore the parasite has had to evolve sophisticated ways in which to obtain iron from a variety of sources. *Leishmania spp* are able to facilitate iron acquisition from multiple sources such as transferrin, lactoferrin and haemin.[86] The promastigote preferentially acquires iron in the reduced +II ferrous form as opposed to the +III ferric form.[87] However in order to do so, the parasite will often utilise the Fe(III) from transferrin or lactoferrin and reduce it intracellularly to Fe(II) using iron reductase enzymes.[87] The source of this iron has also been shown to be species dependant and will be discussed further in chapter 2.3.3. As the amastigote is found within the phagolysosome of the macrophage, they often face a harsher and less forgiving environment. As such, the acquisition of iron by the amastigote tends to be highly efficient in the iron poor environment of the macrophage. Divalent metals are often removed from the phagolysosome by the natural resistance-associated macrophage protein (Nramp1) transporter, limiting the available iron for the parasite to attain.[88]

A study into specific Leishmanial ferrous transporters observed these proteins are highly up regulated in the amastigotes of the *L. amazonensis* species in particular. The transporter protein was only detectable in the amastigotes that were replicating intracellularly, and was a dependant factor on continuing growth and maintenance.[89]

1.7 Previous work on metal anti-Leishmanials

Over the years more and more research into metal complexes as anti-Leishmanials has emerged, with a large emphasis on transition metal complexes. Between 1990 – present, there have been multiple reports of transition metal anti-Leishmanials, with varying degrees of success. With complexes of platinum,[90-92] iridium,[90] rhodium,[90, 93] gold,[94, 95] silver,[96] and manganese.[97-100] Both bismuth and antimony have also been heavily studied as anti-Leishmanials, with a larger emphasis on the potentially less toxic bismuth. Work by Andrews *et al* into bismuth anti-Leishmanials has focused on both the +III oxidation state and +V oxidation state, with the +V oxidation state found to exhibit non-selective toxicity towards both controls and the parasite.[101-103] The +III state also varied in both cytotoxicity and solubility, making it difficult to rationalise a potential mechanism of action.[104-107] Both Andrews *et al* and Rauf *et al* have provided multiple reports into the activity of triaryl Sb(V) carboxylate complexes, presenting as a more promising class of compounds, with increased stability along with a high degree of selectivity.[101, 108-113]

1.8 This study

As antimony has been observed to be an effective anti-Leishmanial, research into mitigating its toxic side-effects is essential. By exploring a variety of ligand classes, this may help to reduce the observed toxicity, since it has been shown previously that there is often a synergistic effect with ligand and metal.[114] Therefore by adjusting the functionality of the ligands bound to the antimony, it may be possible to alter the biochemical aspects of the complex as a whole.[114, 115] Though found

to be unstable, a final series of tests needs to be completed before ruling Bi(V) out as a potential anti-Leishmanial metal. As previous work with antimony carboxylates has shown success, section 2.1 of this study focuses on assessing a class of two carbon chain acetates. Both antimony and bismuth will be assessed to determine whether further research into both metals should be pursued. Triphenyl antimony and triphenyl bismuth will be utilised as the metal aryl precursor. Previously it has been theorised that by incorporating aryl groups onto the metal centre, it may increase lipophilicity and therefore mitigate the administration methods of the current treatments described in 1.3.

Carboxylates have been the dominant choice of ligand class for anti-Leishmanial aryl antimony complexes, due to their ease of reactivity, good chelation ability and strong antimony – oxygen bond energy of 434 $\pm$ 42 kj mol^{-1}.[58] These complexes form stable five-coordinate antimony complexes, which have the potential to form seven-coordinate structures, via a dative interaction with the carbonyl oxygen (figure 1.8.1). Very little has been done on alternative ligand classes such as thiols or alcohols. This study aimed to investigate the difference in reactivity and stability of a more labile alcoholic Sb – O bond as opposed to the conventional carboxylate. Section 2.2 therefore, focuses on the synthesis and characterisation of aryl antimony complexes with a medically active class of alcohol substituted *N,O* chelating organic heterocycles, the halido-quinolinols.

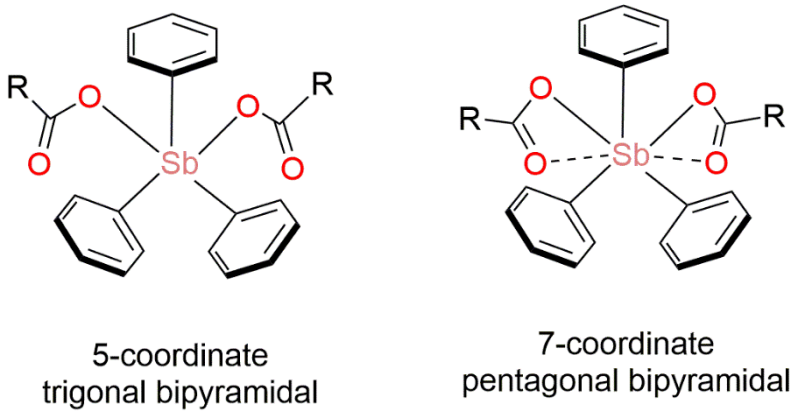

Figure 1.8.1. Binding mode of carboxylate moiety to Sb(V) in relation to geometry.

The use of metals as anti-Leishmanials has been dominated by the group 15 metals bismuth and antimony as well as the transition metals. Very little has been accomplished in the use of other main group metals. The use of the group 13 metal gallium in medicine has been thoroughly explored, but little has been researched in its use as an anti-parasitic. Alkyl gallium complexes have been found to have a high degree of thermodynamic and hydrolytic stability, making them ideal candidates for biological assessment.[116, 117] Section 2.3 focuses on the synthesis and characterisation of two classes of alkyl gallium complexes, with four of the same medically active halido-quinolinols from section 2.1. Similar to the aryl groups on the Sb(V) and Bi(V) complexes, incorporation of the alkyl groups on the gallium was intended to allow for a greater degree of lipophilicity whilst retaining a high degree of stability. The analogous indium complexes will also be explored and their medical potential assessed.

The chelation mode of an acid can vary depending on the other functional groups within the complete molecule. When a hydroxyl is present on the α-position of a carboxylate, there is the possibility of a double deprotonation and formation of dianionic ligand. Previous work with the simple α-hydroxy acid, mandelic acid, observed that with antimony in non-polar solvents, the *bis*-substituted mandelate would form through binding of the carboxylate group. However, when the complex was placed into polar protic solvents, cyclometallation would occur, where the acid becomes deprotonated at the α-hydroxyl, displacing one mandelate to form the dianionic bound *mono*-substituted complex (figure 1.8.2).[101]

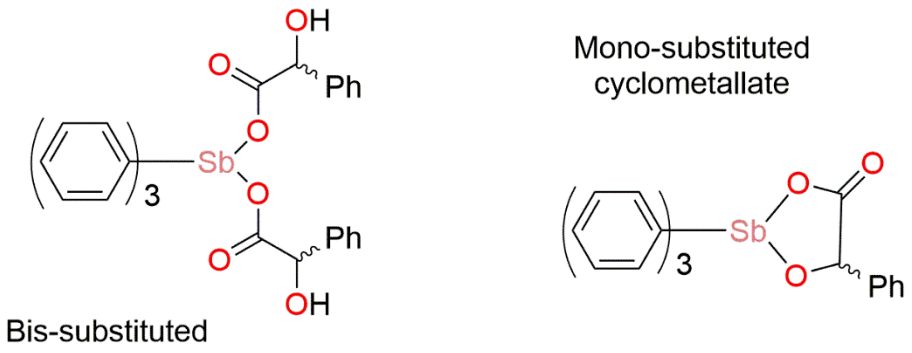

Figure 1.8.2. Bis-substitution and mono-substitution of mandelic acid observed in the synthesis of triphenyl Sb(V) complexes.

The α-carbon of mandelic acid has a chiral centre, therefore the acid is found in both the *R* and *S* enantiomers. It is not an unknown phenomenon in medicinal chemistry that chirality can play a vital role in biological activity.[118-120] Therefore section 2.4 aims to investigate two differing factors in antimony cyclometallate chemistry, a change in aryl group and a change in chirality of the acid, to determine whether any significant differences in the stability and biological activity may arise.

1.9 References

1. W. H. Organization, *Report on the interregional meeting on* Leishmaniasis *among neighbouring endemic countries in the Eastern Mediterranean, African and European regions, Amman, Jordan 23–25 September 2018*, World Health Organization, Regional Office for the Eastern Mediterranean, 2019.
2. W. H. Organization, *Investing to Overcome the Global Impact of Neglected Tropical Diseases: Third WHO Report on Neglected Tropical Diseases 2015*, World Health Organization, 2015.
3. H. A. Fletcher, M. Chatterjee, A. Cooper, T. Hussell, P. M. Kaye, J. Prior, R. Reljic, S. Vermaak, M. Vordermeier and A. Williams, 2018, **7**, 485.
4. J. Alvar, I. D. Vélez, C. Bern, M. Herrero, P. Desjeux, J. Cano, J. Jannin, M. den Boer and W. L. C. Team, *PLoS One*, 2012, **7**, e35671.
5. W. H. Organization, *World Health Organ. Tech. Rep. Ser.*, 2010, xii.
6. S. M. Gossage, M. E. Rogers and P. A. Bates, *Int. J. Parasitol.*, 2003, **33**, 1027-1034.
7. P. Desjeux, *Comp. Immunol., Microbiol. Infect. Dis.*, 2004, **27**, 305-318.
8. P. Bates and M. E. Rogers, *Curr. Mol. Med.*, 2004, **4**, 601-609.
9. S. Kamhawi, *Trends Parasitol.*, 2006, **22**, 439-445.
10. C. Bogdan and M. Röllinghoff, *Parasitol. Today*, 1999, **15**, 22-28.
11. J.-C. Antoine, E. Prina, T. Lang and N. Courret, *Trends Microbiol.*, 1998, **6**, 392-401.
12. J. Alexander, A. R. Satoskar and D. G. Russell, *J. Cell Sci.*, 1999, **112**, 2993-3002.
13. D. G. Russell, *Curr. Opin. Immunol.*, 1995, **7**, 479-484.
14. N. G. Tessarollo, J. M. Andrade, D. d. S. Moreira and S. M. F. Murta, *Parasitol. Int.*, 2015, **64**, 125-129.
15. E. Handman, in *Adv. Parasitol.*, eds. J. R. Baker, R. Muller and D. Rollinson, Academic Press, 1999, 44, 1-39.
16. P. Desjeux, *Clin. Dermatol.*, 1996, **14**, 417-423.
17. C. V. David and N. Craft, *Dermatologic therapy*, 2009, **22**, 491-502.
18. A. Stauch, H.-P. Duerr, J.-C. Dujardin, M. Vanaerschot, S. Sundar and M. Eichner, *PLoS Negl. Trop. Dis.*, 2012, **6**, e1973.
19. M. Maurer, B. Dondji and E. von Stebut, *Med. Microbiol. Immunol.*, 2009, **198**, 137-146.
20. K. Weigle and N. G. Saravia, *Clin. Dermatol.*, 1996, **14**, 433-450.
21. G. L. Machado-Coelho, W. T. Caiaffa, O. Genaro, P. A. Magalhaes and W. Mayrink, *Trans. R. Soc. Trop. Med. Hyg.*, 2005, **99**, 55-61.
22. S. Ahluwalia, S. D. Lawn, J. Kanagalingam, H. Grant and D. N. Lockwood, *BMJ*, 2004, **329**, 842-844.
23. G. C. Low, *Trans. R. Soc. Trop. Med. Hyg.*, 1916, **10**, 37-42.
24. S. Weiss and R. A. Hatcher, *J. Exp. Med.*, 1923, **37**, 97-111.
25. M. Honey, *Br. Heart J.*, 1960, **22**, 601.
26. P. Rees, P. Kager, M. Keating and W. Hockmeyer, *The Lancet*, 1980, **316**, 226-229.
27. P. Manson-Bahr, *Trans. R. Soc. Trop. Med. Hyg.*, 1959, **53**, 123-136.
28. J. Chulay, L. Fleckenstein and D. Smith, *Trans. R. Soc. Trop. Med. Hyg.*, 1988, **82**, 69-72.
29. B. L. Herwaldt and J. D. Berman, *Am. J. Trop. Med Hyg.,* 1992, **46**, 296-306.
30. J. D. Berman, *Clin. Infect. Dis.*, 1988, **10**, 560-586.
31. R. Mukhopadhyay, S. Dey, N. Xu, D. Gage, J. Lightbody, M. Ouellette and B. P. Rosen, *Proc. Natl. Acad. Sci. U.S.A.* 1996, **93**, 10383-10387.
32. D. Légaré and M. Ouellette, *Handbook of* Anti-microbial *Resistance*, 2017, 313-341.
33. G. Mandal, V. Govindarajan, M. Sharma, H. Bhattacharjee and R. Mukhopadhyay, *Antimicrob. Drug. Resist.*, Springer, 2017, 649-665.
34. N. Baker, H. P. de Koning, P. Mäser and D. Horn, *Trends Parasitol.*, 2013, **29**, 110-118.
35. S. L. Croft and J. Engel, *Trans. R. Soc. Trop. Med. Hyg.*, 2006, **100**, S4-S8.

36. G. Cuddihy, E. K. Wasan, Y. Di and K. M. Wasan, *Pharmaceutics*, 2019, **11**, 99.
37. N. Tiwari, M. R. Gedda, V. K. Tiwari, S. P. Singh and R. K. Singh, *Mini Rev. Med. Chem.*, 2018, **18**, 26-41.
38. B. Purkait, A. Kumar, N. Nandi, A. H. Sardar, S. Das, S. Kumar, K. Pandey, V. Ravidas, M. Kumar and T. De, *Antimicrob. Agents Chemother.*, 2011, **56(2)**, 1031-1041.
39. R. A. Demel and B. De Kruyff, *Biochim. Biophys. Acta, Rev. Biomembr.* , 1976, **457**, 109-132.
40. J. Veronica, S. Chandrasekaran, A. Dayakar, M. Devender, V. K. Prajapati, S. Sundar and R. Maurya, *FEB. J.*, 2019.
41. J. Walker, J.-J. Vasquez, M. A. Gomez, J. Drummelsmith, R. Burchmore, I. Girard and M. Ouellette, *Mol. Biochem. Parasitol.*, 2006, **147**, 64-73.
42. J. M. Blackwell, R. Ezekowitz, M. B. Roberts, J. Y. Channon, R. B. Sim and S. Gordon, *J. Expt. Med.*, 1985, **162**, 324-331.
43. E. A. Rauws, W. Langenberg, H. J. Houthoff, H. Zanen and G. N. Tytgat, *Gastroenterology*, 1988, **94**, 33-40.
44. T.-C. Wang, K.-Y. Jan, A. S. Wang and J.-R. Gurr, *Mutat. Res. Fun. Mol. M.*, 2007, **615**, 75-86.
45. A. K. Haldar, P. Sen and S. Roy, *Mol. Med. Int.*, 2011, **2011**.
46. F. Frézard, C. Demicheli and R. R. Ribeiro, *Molecules*, 2009, **14**, 2317-2336.
47. M. K. Pathak and T. Yi, *J. Immun.* 2001, **167**, 3391-3397.
48. N. K. Verma and C. S. Dey, *Antimicrob. Agents Chemother.*, 2004, **48**, 3010-3015.
49. C. Paris, P. M. Loiseau, C. Bories and J. Bréard, *Antimicrob. Agents Chemother.*, 2004, **48**, 852-859.
50. J. R. Luque-Ortega and L. Rivas, *Antimicrob. Agents Chemother.*, 2007, **51**, 1327-1332.
51. M. Rakotomanga, S. Blanc, K. Gaudin, P. Chaminade and P. Loiseau, *Antimicrob. Agents Chemother.*, 2007, **51**, 1425-1430.
52. A. Kumar Saha, T. Mukherjee and A. Bhaduri, *Mol. Biochem. Parasitol.*, 1986, **19**, 195-200.
53. B. Purkait, A. Kumar, N. Nandi, A. H. Sardar, S. Das, S. Kumar, K. Pandey, V. Ravidas, M. Kumar, T. De, D. Singh and P. Das, *Antimicrob. Agents Chemother.*, 2012, **56**, 1031-1041.
54. D. W. Bierer, *Rev. Infect. Dis.*, 1990, **12**, S3-S8.
55. J. Bader, *Digestion*, 1987, **37**, 53-59.
56. A. Scheen, *Rev. Med. Liege*, 1998, **53**, 41-44.
57. J. A. Salvador, S. A. Figueiredo, R. M. Pinto and S. M. Silvestre, *Future. Med. Chem.*, 2012, **4**, 1495-1523.
58. H. Sun, *Biological chemistry of arsenic, antimony and* bismuth, Wiley Online Library, 2011.
59. N. A. Cornick, M. Silva and S. L. Gorbach, *Rev. Infect. Dis.*, 1990, **12**, S9-S10.
60. A. Harder, *Parasitol. Res.*, 2002, **88**, 395-397.
61. B. Gryseels, K. Polman, J. Clerinx and L. Kestens, *The Lancet*, 2006, **368**, 1106-1118.
62. M. J. Miller and H. P. Lyon, *Am. J. Trop. Med Hyg.*, 1955, **4**, 1049-1056.
63. M. Ashkar, *J. Egypt. Med. Assoc.*, 1938, **21**.
64. M. Erfan and S. Talaat, *Trans. R. Soc. Trop. Med. Hyg.*, 1950, **44**, 123-126.
65. Z. Farid, S. Bassily, A. Schulert and E. McConnell, *Ann. Trop. Med. Parasitol.*, 1966, **60**, 165-168.
66. J. R. Coura and M. J. Conceição, *Mem. Inst. Oswaldo Cruz*, 2010, **105**, 598-603.
67. S. Yan, L. Jin and H. Sun, *Metallotherapeutic Drugs and Metal-Based Diagnostic Agents: The Use of Metals in Medicine*, 2005, 441-461.
68. D. Steverding, *Parasit. Vectors*, 2008, **1**, 3.
69. P. Olliaro, J. Lazdins and F. Guhl, *Expert Opin. Emerg. Drugs*, 2002, **7**, 61-67.
70. A. J. Downs, *Chemistry of aluminium, gallium, indium and thallium*, Springer Science & Business Media, 1993.

71. S. Aldridge and A. J. Downs, *The Group 13 Metals Aluminium, Gallium, Indium and Thallium: Chemical Patterns and Peculiarities*, John Wiley & Sons, 2011.
72. R. Warrell, R. Bockman, C. Coonley, M. Isaacs and H. Staszewski, *J. Clin. Invest.*, 1984, **73**, 1487-1490.
73. L. R. Bernstein, *Pharmacol. Rev.*, 1998, **50**, 665-682.
74. F. Minandri, C. Bonchi, E. Frangipani, F. Imperi and P. Visca, *Future Microbiol.*, 2014, **9**, 379-397.
75. K. Logan, P. Ng, C. Turner, R. Schmidt, U. Terner, J. Scott, B. Lentle and A. Noujaim, *Int. J. Nucl. Med. Biol.*, 1981, **8**, 271-276.
76. S. R. Vallabhajosula, J. F. Harwig, J. K. Siemsen and W. Wolf, *J. Nucl. Med.*, 1980, **21**, 650-656.
77. P. B. Hoffer, J. Huberty and H. Khayam-Bashi, *J. Nucl. Med.*, 1977, **18**, 713-717.
78. W. R. Harris, *Biochemistry (Mosc.)*, 1986, **25**, 803-808.
79. W. R. Harris and V. L. Pecoraro, *Biochemistry (Mosc.)*, 1983, **22**, 292-299.
80. R. Weiner, *Nucl. Med. Biol.*, 1996, **23**, 745-751.
81. R. E. Weiner, I. Avis, R. D. Neumann and J. L. Mulshine, *J. Cell. Biochem.*, 1996, **63**, 276-287.
82. R. E. Weiner, G. J. Schreiber, P. B. Hoffer and J. T. Bushberg, *J. Nucl. Med.*, 1985, **26**, 908-916.
83. R. E. Weiner, *J. Nucl. Med.*, 1989, **30**, 70-79.
84. P. Aisen, C. Enns and M. Wessling-Resnick, *Int. J. Biochem. Cell Biol.*, 2001, **33**, 940-959.
85. M. Wilson and B. E. Britigan, *Parasitol. Today*, 1998, **14**, 348-353.
86. M. E. Wilson, R. W. Vorhies, K. A. Andersen and B. E. Britigan, *Infect. Immun.*, 1994, **62**, 3262-3269.
87. M. E. Wilson, T. S. Lewis, M. A. Miller, M. L. McCormick and B. E. Britigan, *Exp. Parasitol.*, 2002, **100**, 196-207.
88. J. R. Forbes and P. Gros, *Trends Microbiol.*, 2001, **9**, 397-403.
89. C. Huynh, D. L. Sacks and N. W. Andrews, *J. Exp. Med.*, 2006, **203**, 2363-2375.
90. S. Croft, R. Neal, D. Craciunescu and G. Certad-Fombona, *Trop. Med. Parasitol.*, 1992, **43**, 24-28.
91. G. Lowe, A. S. Droz, T. Vilaivan, G. W. Weaver, L. Tweedale, J. M. Pratt, P. Rock, V. Yardley and S. L. Croft, *J. Med. Chem.*, 1999, **42**, 999-1006.
92. G. Visbal, E. Marchán, A. Maldonado, Z. Simoni and M. Navarro, *J. Inorg. Biochem.*, 2008, **102**, 547-554.
93. M. Rodriguez-Cabezas, C. Mesa-Valle, S. Azzouz, V. Moraleda-Lindez, D. Craciunescu, M. Gutierrez-Rios, M. De Frutos and A. Osuna, *Pharmacology*, 2001, **63**, 112-119.
94. J. D. S. Chaves, L. G. Tunes, C. H. d. J. Franco, T. M. Francisco, C. C. Correa, S. M. Murta, R. L. Monte-Neto, H. Silva, A. P. S. Fontes and M. V. de Almeida, *Eur. J. Med. Chem.*, 2017, **127**, 727-739.
95. C. Zhang, S. B. Delmas, A. F. Alvarez, A. Valentin, C. Hemmert and H. Gornitzka, *Eur. J. Med. Chem.*, 2018, **143**, 1635-1643.
96. M. Navarro, E. J. Cisneros-Fajardo and E. Marchan, *Drug. Res.*, 2006, **56**, 600-604.
97. J. Benítez, L. Guggeri, I. Tomaz, G. Arrambide, M. Navarro, J. C. Pessoa, B. Garat and D. Gambino, *J. Inorg. Biochem.*, 2009, **103**, 609-616.
98. I. de Aguiar, E. R. dos Santos, A. C. Mafud, V. Annies, M. A. Navarro-Silva, V. R. dos Santos Malta, M. T. do Prado Gambardella, F. de Assis Marques and R. M. Carlos, *Inorg. Chem. Commun.*, 2017, **84**, 49-55.
99. M. Navarro, C. Gabbiani, L. Messori and D. Gambino, *Drug Discov. Today*, 2010, **15**, 1070-1078.
100. M. Navarro, C. Hernández, I. Colmenares, P. Hernández, M. Fernández, A. Sierraalta and E. Marchán, *J. Inorg. Biochem.*, 2007, **101**, 111-116.

101. R. N. Duffin, V. L. Blair, L. Kedzierski and P. C. Andrews, *Dalton Trans.*, 2018, **47**, 971-980.
102. Y. C. Ong, V. L. Blair, L. Kedzierski and P. C. Andrews, *Dalton Trans.*, 2014, **43**, 12904-12916.
103. Y. C. Ong, V. L. Blair, L. Kedzierski, K. L. Tuck and P. C. Andrews, *Dalton Trans.*, 2015, **44**, 18215-18226.
104. P. C. Andrews, V. L. Blair, R. L. Ferrero, P. C. Junk, L. Kedzierski and R. M. Peiris, *Dalton Trans.*, 2014, **43**, 1279-1291.
105. P. C. Andrews, R. Frank, P. C. Junk, L. Kedzierski, I. Kumar and J. G. MacLellan, *J. Inorg. Biochem.*, 2011, **105**, 454-461.
106. A. Loh, Y. C. Ong, V. L. Blair, L. Kedzierski and P. C. Andrews, *J. Biol. Inorg. Chem.*, 2015, **20**, 1193-1203.
107. A. Pathak, V. L. Blair, R. L. Ferrero, L. Kedzierski and P. C. Andrews, *J. Inorg. Biochem.*, 2017.
108. M. I. Ali, M. K. Rauf, A. Badshah, I. Kumar, C. M. Forsyth, P. C. Junk, L. Kedzierski and P. C. Andrews, *Dalton Trans.*, 2013, **42**, 16733-16741.
109. R. N. Duffin, V. L. Blair, L. Kedzierski and P. C. Andrews, *J. Inorg. Biochem.*, 2018, **189**, 151-162.
110. T. Iftikhar, M. K. Rauf, S. Sarwar, A. Badshah, D. Waseem, M. N. Tahir, A. Khan, K. M. Khan and G. M. Khan, *J. Organomet. Chem.*, 2017, **851**, 89-96.
111. R. Mushtaq, M. K. Rauf, M. Bolte, A. Nadhman, A. Badshah, M. N. Tahir, M. Yasinzai and K. M. Khan, *Appl. Organomet. Chem.*, 2017, **31**, e3606.
112. L. Saleem, A. A. Altaf, A. Badshah, M. K. Rauf, A. Waseem, M. Danish, S. S. Azam, M. N. Arshad, A. M. Asiri and S. Ahmad, *Inorg. Chim. Acta*, 2018, **474**, 148-155.
113. S. Sarwar, T. Iftikhar, M. K. Rauf, A. Badshah, D. Waseem, M. N. Tahir, K. M. Khan and G. M. Khan, *Inorg. Chim. Acta*, 2018, **476**, 12-19.
114. K. H. Thompson and C. Orvig, *Dalton Trans.*, 2006, **6**, 761-764.
115. J. Anastassopoulou and T. Theophanides, *Bioinorgnic Chemistry.*, Springer, 1995, 209-218.
116. Y. Shen, Y. Pan, X. Jin, X. Xu, X. Sun and X. Huang, *Polyhedron*, 1999, **18**, 2423-2426.
117. Y.-Z. Shen, Y. Pan, L.-Y. Wang, G. Dong, X.-P. Jin, X.-Y. Huang and H. Hu, *J. Organomet. Chem.*, 1999, **590**, 242-247.
118. A. M. Rouhi, *Chem. Eng. News*, 2003, **81**, 56-56.
119. D. W. Green, J. M. Lee, E. J. Kim, D. J. Lee and H. S. Jung, *Adv. Mater. Interfaces.*, 2016, **3**, 1500411.
120. G. Jaouen, *Bioorganometallics: biomolecules, labeling, medicine*, John Wiley & Sons, 2006.

2. Results and discussion

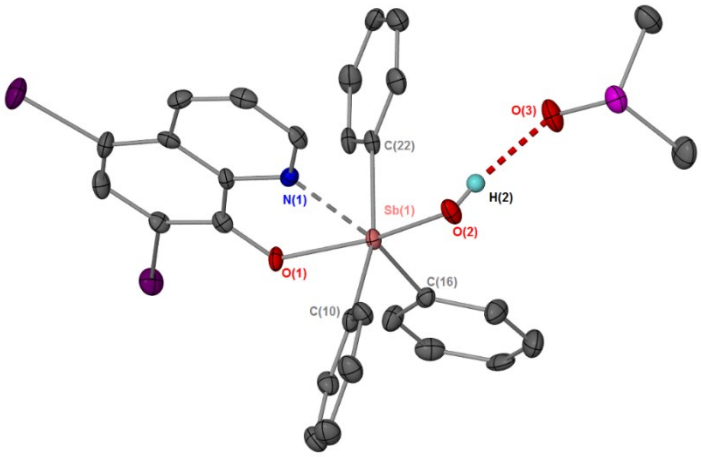

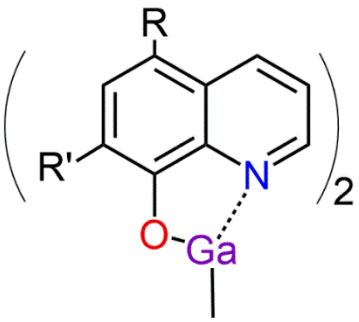

$[GaCH_3(L)_2]$, **(G')**

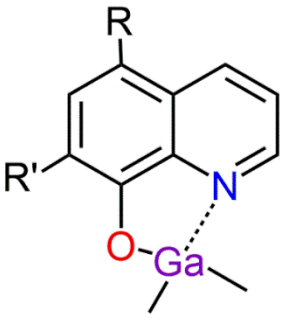

$[Ga(CH_3)_2L]$, **(G)**

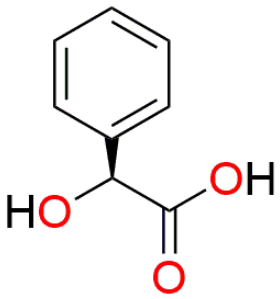

S-Mandelic acid

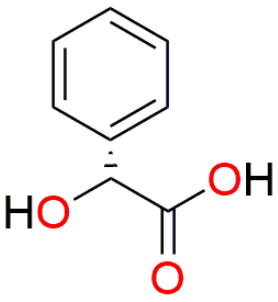

R-Mandelic acid

2.1 Synthesis, characterisation and biological activity of triphenyl Bi(V) and Sb(V) acetic acetates

2.1.1 Sb(V) and Bi(V) aryl carboxylates

The chemistry of carboxylato Bi(V) and Sb(V) aryl complexes, of the general formula $[MPh_3(O_2CR)_2]$, is well established. Reports of the synthesis and characterisation of the bismuth complexes, in particular, dates back to the 1950s, with a brief exploration of the synthetic pathway by Gilman *et al*.[1] Further studies by Goel *et al* in 1970 established changes in the electrical conductance and carboxylate IR stretching frequencies of the final products, along with the molecular nature of the aryl bismuth dihalide precursors.[2] This insight into the synthesis and characterisation of these Bi(V) aryl carboxylates also led to the confirmation of the stable Bi(III) Bi-O-Bi bond, identified in bismuth oxide (Bi_2O_3).[3] Expansion into the comparative chemistry of the analogous Sb(V) complexes was established in 1975 by Ouchi *et al* who highlighted a structural study on triphenyl Bi(V) and Sb(V) alkyl and arylthioacetates.[4] Due to the inherent instability and often air/moisture sensitivity of these Bi(V) aryl arylthioacetates, only their synthetic route was explored. Stabilisation of these complexes was then achieved by the placement of electronegative groups on the substituents.[5] Triaryl Bi(V) tropolonato complexes were then synthesised. As discussed in section 1.4, bismuth complexes have a long historic use against *Helicobacter pylori.* Therefore, the activity of these tropolonato complexes against *H. pylori* was assessed (figure 2.1.1). This opened up a whole new area of research of aryl Bi(V) complexes as potential medicinals.[6]

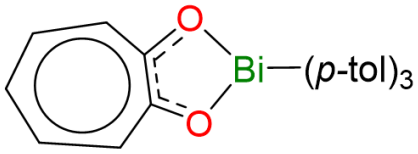

Strain	NCTC 11637	04713 8891	*H.p* 0008	*H.p* 0012	*H.p* 0016	*H.p* 0032	*H.p* 0072	*H.p* 0083
MIC (µg/ mL)	10	10	10	10	10	10	10	10

*Figure 2.1.1. MIC values of tris-p-tolyl*bismuth *tropolonate against eight strains of H. pylori.*[6]

More studies on Bi(V) aryl medicinals followed, highlighting applications as anti-proliferatives and anti-fungals, resulting in interesting and promising preliminary results. Sb(V) analogues were occasionally synthesised and studied for a comparative study in which good selectivity and anti-microbial activity was observed.[7-9] Only a handful of studies have been reported on the anti-microbial activity of both Bi(V) and Sb(V) carboxylate complexes with previous research opting to focus on the +III oxidation state of both bismuth and antimony, with a combination of *O*-donor, *N*-donor, and *S*-donor ligands.[10-13] The +III oxidation state is the more electronically stable for both bismuth and antimony and therefore makes a more favourable candidate in terms of biological activity.[14] In terms of the *Leishmania* parasite, the front-line treatments as discussed in section 1.2, are pentavalent antimonials with *O*-donor ligands, therefore the logical step in the progression of anti-parasitics was to take into account the oxidation state of these front-line treatments. This area of group 15 aryl carboxylates has expanded in the last decade, with reports of both Bi(V) and Sb(V) aryl carboxylates as potent inhibitors of parasitic growth.[15-18]

2.1.2 Acetates

Complexes of Bi(V) have been found to be quite effective anti-microbials, but tend to lack the hydrolytic stability of their antimony counterparts. A study by Andrews *et al* found that the Bi(V)

carboxylates underwent decomposition in DMEM culture media by a reaction with glucose and other substituents which have yet to be identified. This decomposition was very rapid, resulting in half-lives between 1 – 3 hours via exponential decay.[19, 20] When a class of α-hydroxy acid compounds were chelated to triphenyl bismuth an unusual stability arose. Linear decompositions were obtained with half-lives of up to 52 hours. The antimony counterparts were observed to be more stable, forming a cyclometallate complex. This difference in stability may be due to the thermodynamic and entropic stability of a five-membered versus a four-membered chelate (Figure 2.1.2).[17, 21] Therefore more than just chelation was key to the overall stability.

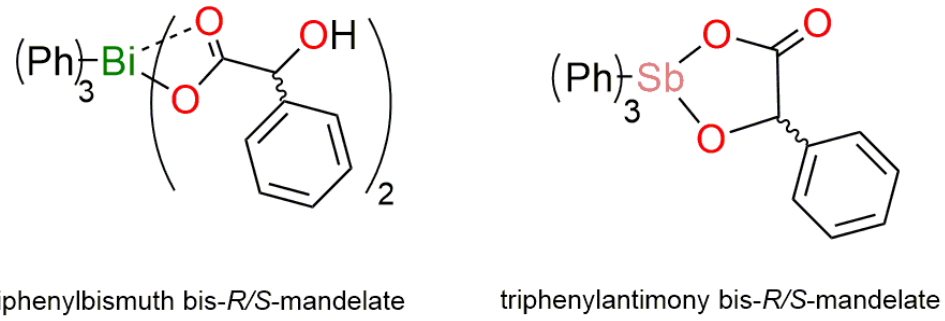

triphenylbismuth bis-*R/S*-mandelate triphenylantimony bis-*R/S*-mandelate

Figure 2.1.2. Chelation mode of mandelic acid with triphenyl Bi(V) versus triphenyl Sb(V).[17]

To assess the structural potential of this increased stability, a class of substituted acetates with the two carbon-chain backbone were selected (Figure 2.1.3). The simplest aryl acetate, phenyl acetic acid ($PhCH_2CO_2H$), has previously shown to exhibit anti-microbial activity,[22] therefore the majority of the selected acetates incorporated a substituted ring. This allowed for an exploration into the chemical effects of ring substitution and how this may impact the overall biology of the complexes. Out of the seventeen complexes synthesised, thirteen were novel.

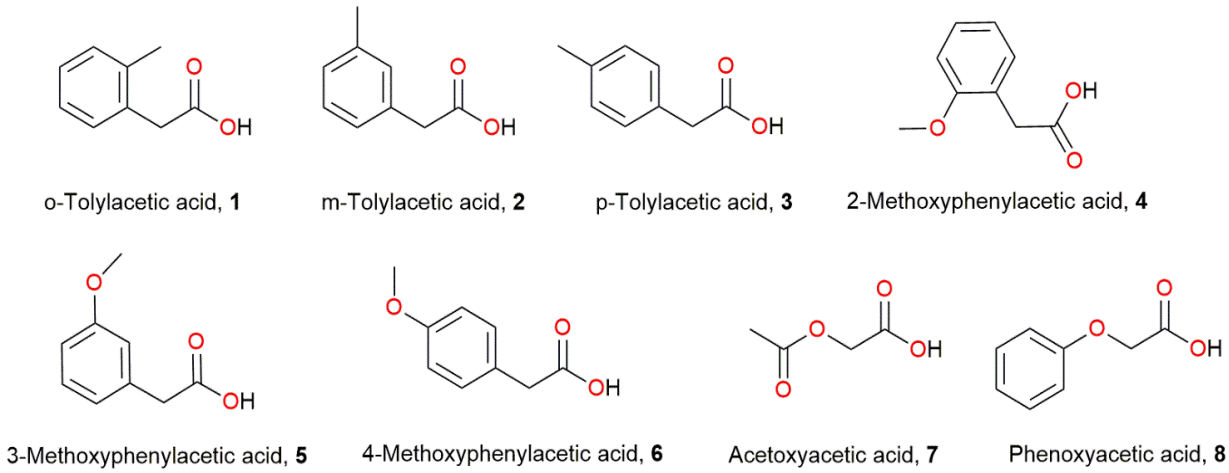

Figure 2.1.3. Substituted acetates explored in this study

2.1.3 Synthesis and characterisation

2.1.3.1 Synthesis

The synthesis pathways for these types of complexes have been previously established, with various routes available, for example: a salt metathesis reaction with the +V oxidation state aryl halide and an alkali or silver salt of the ligand.[18, 23] However, these reactions often require an inert atmosphere and reflux temperatures to obtain the desired aryl group 15 carboxylate. Andrews *et al* developed a one-pot oxidative addition reaction involving hydrogen peroxide which was able to generate the desired products in high yields, eliminating the need for reflux and dry solvents.[19, 20] This technique for the oxidation of the +III metal to the +V state is also very clean, producing only water as a by-product from the formation of the dihydroxido intermediate $[MAr_3(OH)_2]$ and subsequent condensation reaction with the desired acid.[24] Hydrogen peroxide however has its drawbacks due to a short shelf life, light sensitivity and high reactivity, which often lead to the formation of oils in the case of the acetic acetates. To mitigate this, the tertiary-butyl form of the peroxide (t-BuOOH, Luperox ™) was used (scheme 2.1.1). Similar to hydrogen peroxide the overall by-products are water and tertiary-butanol which are easily removed from the reaction.[17] The

reaction pathway utilised similar solvent systems and reaction conditions from a modified synthesis reported by Moiseev *et al*.[25]

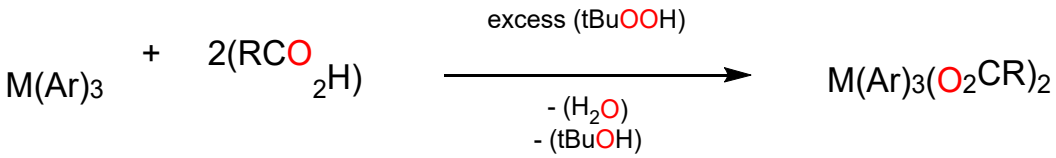

Scheme 2.1.1. Oxidative addition pathway for $M(Ar)_3$ to $M(Ar)_3(O_2CR)_2$

The use of tertiary-butyl hydroperoxide either generates a *mono*-hydroxy-*mono-tert*butoxido intermediate when one equivalent is used in non-polar aprotic solvents, or the dihydroxido intermediate with two equivalents in polar protic solvents (scheme 2.1.2).[26, 27]

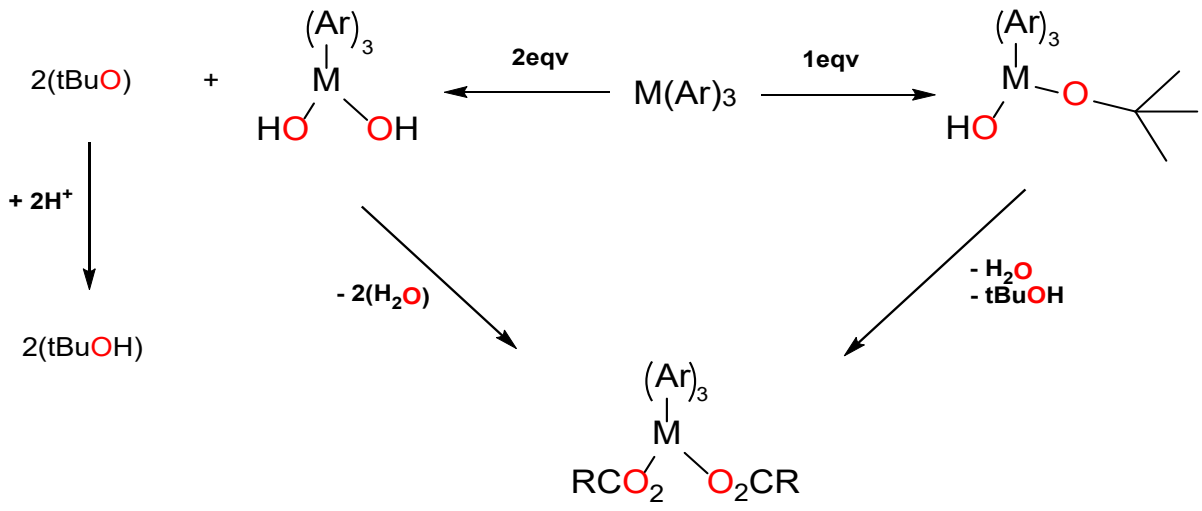

Scheme 2.1.2. Potential routes dependent on the equivalency of peroxide.

The solvent and by-products are then easily removed under vacuum, yielding white to off-white solids which can be purified by hot crystallisation in either toluene or THF. Good to excellent yields for the complexes were obtained, ranging from 64 – 91 % (Figure 2.1.4).[28] Complexes **1B – 8B**, **1S**,

3S, **5S** and **7S/S'** were novel, with complexes **2S**, **4S**, **6S** and **8S** having been previously synthesised and charactised.[18, 23]

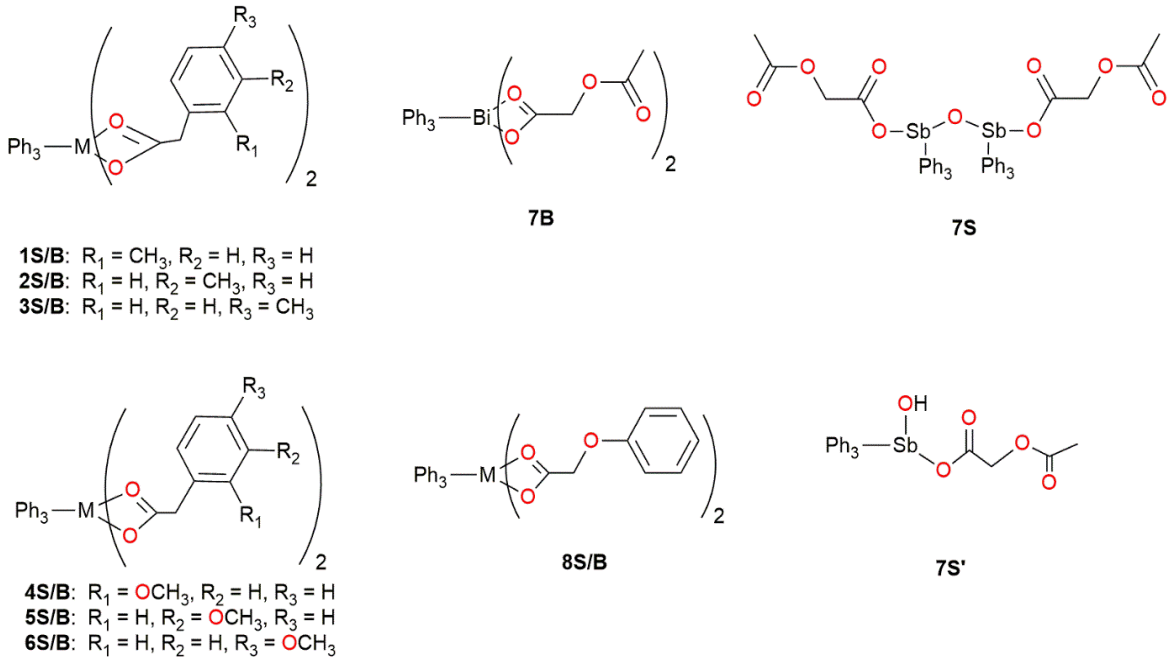

*Figure 2.1.4. Composition of the M(V) aryl complexes [Bi(V) **1B – 8B**, Sb(V) **1S – 8S**].[28]*

2.1.3.2 Characterisation

Complexes underwent characterisation by ^{1}H and ^{13}C NMR, FT-IR, MS, mp and X-ray crystallography. Fifteen of the sixteen complexes were found to adopt the usual confirmation observed for triaryl group 15 carboxylates, incorporating two carboxylate moieties with the general formula $[MPh_3(O_2CR)_2]$, where M = Sb or Bi. The only exception was **7S**, $[(SbPh_3((O_2CCH_2OCO)Me))_2O]$, which was found by X-ray diffraction and elemental analysis, to be an oxido bridged antimony complex. This species was only able to be generated in non-polar aprotic solvents. If the synthesis was attempted and/or the solid product dissolved in a polar protic solvent, **7S** underwent a hydrolysis reaction to form the *mono*-hydroxido **7S'**, $[SbPh_3(O_2CCH_2CO_2CH_3)OH]$ (scheme2.1.3). This hydrolysis pathway was identified after repeated

attempts to obtain the ^{1}H NMR spectrum in $CDCl_3$ yielding two distinct products. A clean ^{1}H NMR spectrum of the oxido bridged complex was unable to be obtained due its insolubility in the usual dry NMR solvent such as C_6D_6 and rapid hydrolysis in $CDCl_3$ and d_6-DMSO. However, each species could be identified based on the proton integration ratio for the oxido bridged complex. For the hydrolysis product, overlap with the $CDCl_3$ solvent signal prevented a definitive integration of the aryl group (Figure 2.1.5).

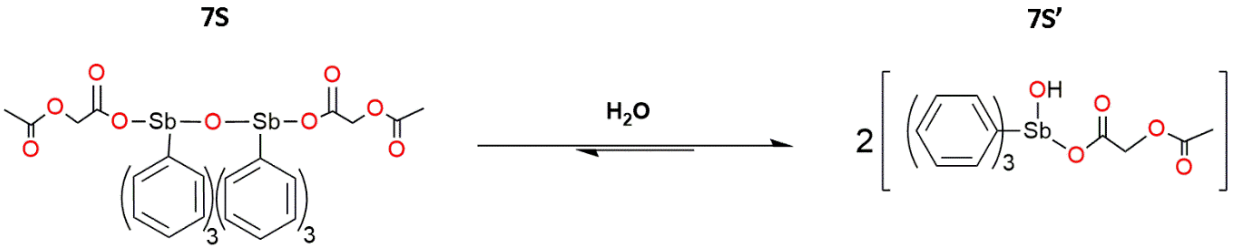

*Scheme 2.1.3. Hydrolysis pathway of **7S,** [(SbPh$_3$((O$_2$CCH$_2$OCO)Me))$_2$O] to **7S',** [SbPh$_3$(O$_2$CCH$_2$CO$_2$CH$_3$)OH].*

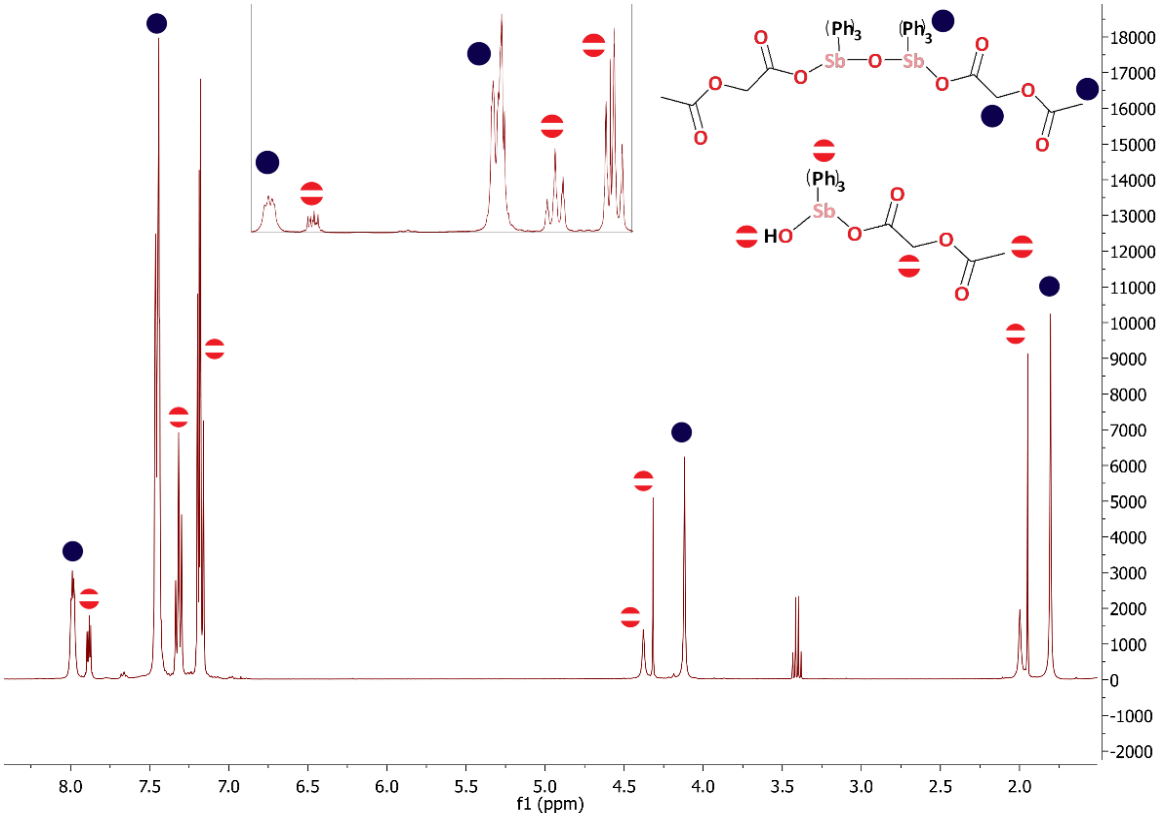

*Figure 2.1.5. ^{1}H NMR of oxido bridged complex, **7S**, [$(SbPh_3((O_2CCH_2OCO)Me))_2O$], (dark-blue, circle) and hydrolysis product, **7S'**, [$SbPh_3(O_2CCH_2CO_2CH_3)OH$] (red, broken circle) Insert of the aromatic region provided, residual solvent signal ($CDCl_3$) and diethyl ether (quartet 3.4 ppm) are not labelled.*

Isolation and solution state chemistry of the hydrolysis product was achieved when crystals of **7S** were dissolved in DMSO and water was added to precipitate **7S',** [$SbPh_3(O_2CCH_2CO_2CH_3)OH$], as a white powder (figure 2.1.6).

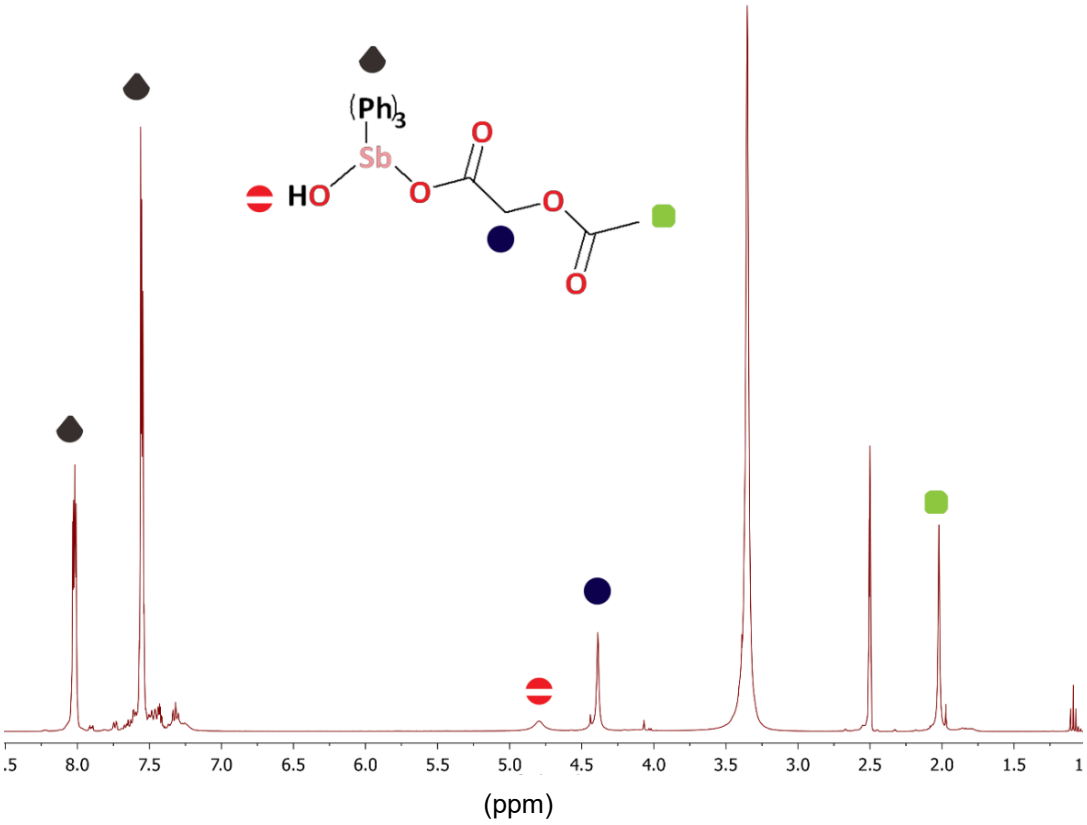

*Figure 2.1.6. ^{1}H NMR spectrum of hydrolysis product, **7S'**, [$SbPh_3(O_2CCH_2CO_2CH_3)OH$], in d_6-DMSO. Residual DMSO signal and H_2O signals can be found at 2.5ppm and 3.3ppm respectively.*

The ^{1}H NMR and ^{13}C NMR for the remaining complexes were as expected. In all complexes synthesised, a high frequency shift of the *o-*, *m-* and *p*-H signals from the parent MPh_3 was observed. These shifts are consistent with previous reports on the formation of triaryl carboxylate complexes of both Sb(V) and Bi(V).[18-20, 29-31] An example of this is given with complexes **1S** and **1B.** A shift is observed for example complexes **1S,** [$SbPh_3(O_2CCH_2C_6H_4CH_3)_2$] and **1B,** [$BiPh_3(O_2CCH_2C_6H_4CH_3)_2$], from the parent acid, **1**, *o*-tolylacetic acid (figure 2.1.3) as well as the triphenyl metal. Upon complexation, the overlap of the aryl protons of the parent acid becomes more resolved and the *o*-Ph, *m*-Ph and *p*-Ph are able to be individually identified. Signals for the methyl group of the tolyl substituent and the CH_2 of the carbon backbone are at similar chemical shifts in both the antimony and bismuth analogue (figure 2.1.7). For full analytical assignment see the experimental section 4.1.

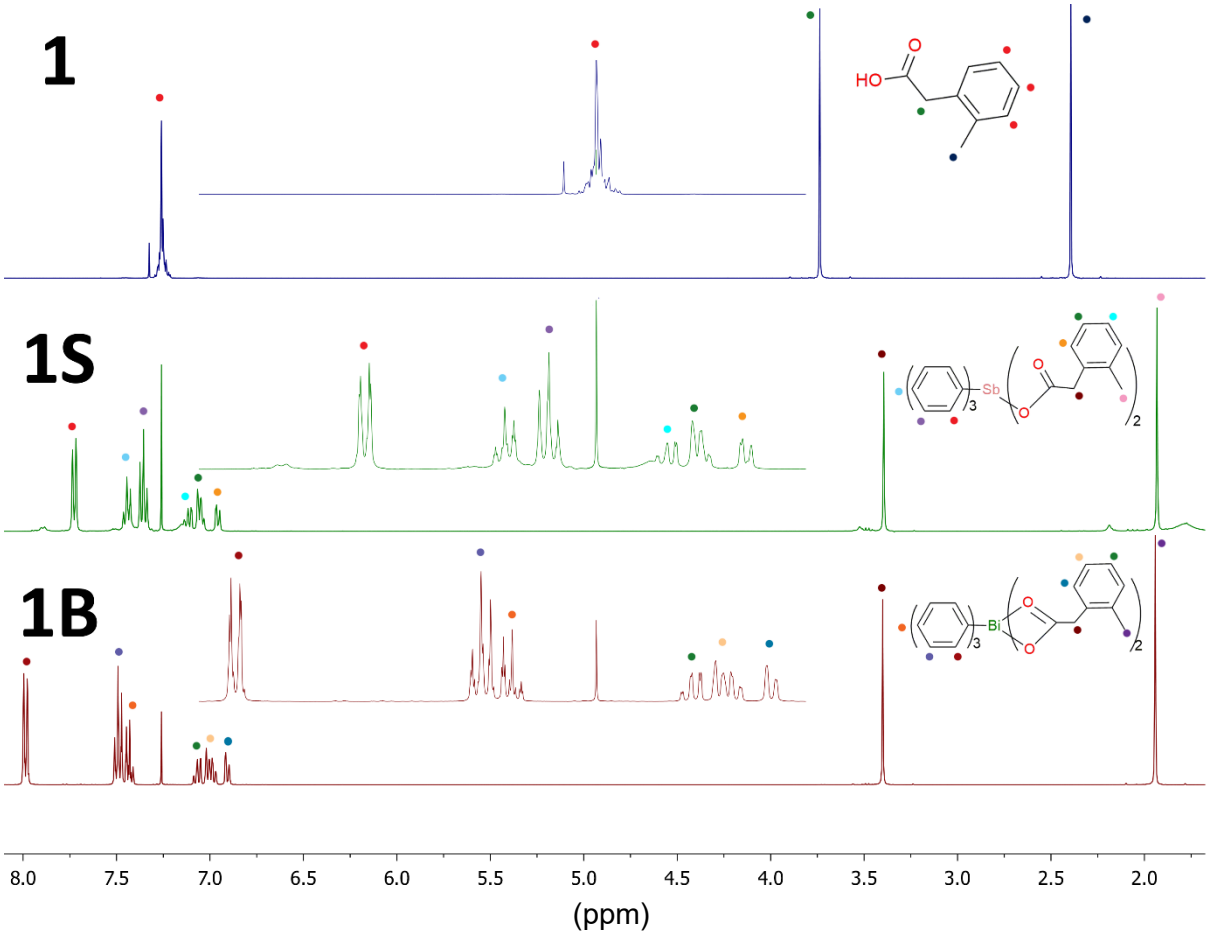

*Figure 2.1.7. ^{1}H NMR of complexes **1S,** $[SbPh_3(O_2CCH_2C_6H_4CH_3)_2]$ and **1B,** $[BiPh_3(O_2CCH_2C_6H_4CH_3)_2]$, against the parent acid, **1**, in $CDCl_3$ (7.26 ppm), aromatic region has been expanded for clarity.*

The ^{13}C NMR spectra are more difficult to assign, however there are several more signals in the complexes versus the free acid due to the presence of the phenyl rings of the complexed MPh_3. For the example complexes **1S** and **1B**, signals corresponding to the tolyl CH_3 and the CH_2 of the carbon backbone are also weaker in both complexes due to a 3:2 ratio of phenyl carbon signals to acetate signals (figure 2.1.8). For full analytical assignment see the experimental section 4.1.

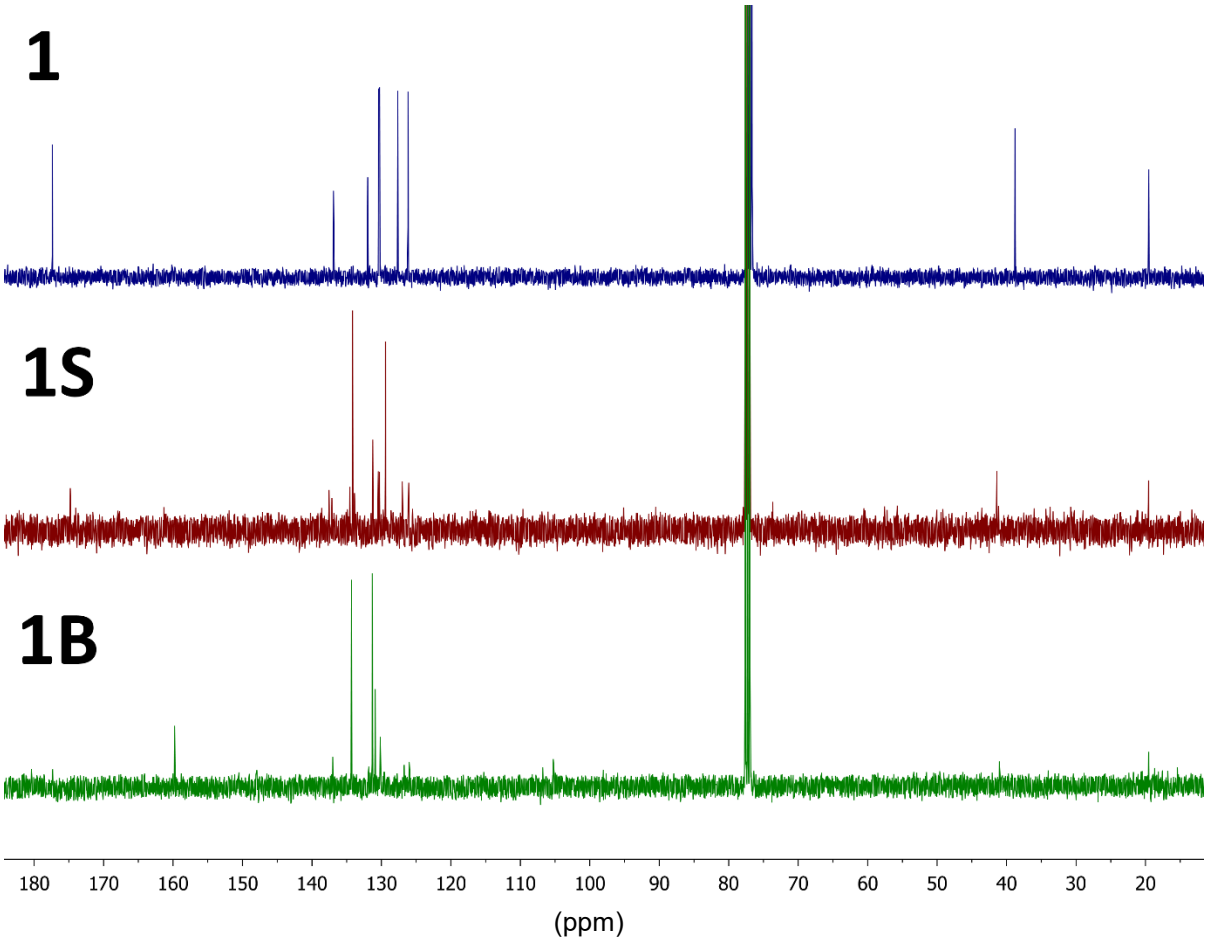

Figure 2.1.8. ^{13}C NMR of complexes ***1S,*** $[SbPh_3(O_2CCH_2C_6H_4CH_3)_2]$ *and* ***1B,*** $[BiPh_3(O_2CCH_2C_6H_4CH_3)_2]$***,*** *against the free acid,* ***1****, in* $CDCl_3$ *(77.3 ppm)*

Further confirmation of the formation of the metal carboxylate complexes was established using FT-IR. This was ultimately determined through interactions with the carboxylate moiety of the individual parent acid against the complex formed. In metal complexes there are several ways in which the carboxylate can interact. The interaction can be *mono*dentate, form a chelate through a *bi*dentate binding mode, or act as a bridging *bi*dentate ligand in a syn-syn, syn-anti or anti-anti configuration. The configuration and denticity of this binding, has an acute effect on the IR stretching frequencies. If the complexes are *mono*dentate, this removes the equivalence of the two oxygen atoms generated through resonance, as such the separation (wavenumber) between the averages of the asymmetric and symmetric frequencies should increase. Conversely, if there

is a covalent interaction from one oxygen and a dative coordination for the other, there should be a relative decrease in the averages of the separation of the asymmetric and symmetric stretching frequencies.[32] To summarise, Deacon *et al* were able to determine a trend that corresponds to the chelation mode of the carboxylate and the average of both the asymmetric and symmetric stretch. For a *bi*dentate binding of the carboxylate through both the carbonyl oxygen via a dative interaction and the covalent bonding of the hydroxyl oxygen, the Δν of the complex will in most cases be < 200 cm^{-1}. Conversely, for a complex that has the carboxylate binding *mono*dentate through a covalent interaction with the hydroxyl oxygen only, the Δν is usually > 200 cm^{-1}.[33] Similar to previous studies by Andrews *et al*, it was found that all the bismuth complexes incorporated a *bi*dentate binding mode of the carboxylate, whereas the antimony complexes were *mono*dentate in nature.[17-20, 28] As bismuth has a larger ionic radius than antimony in the +V oxidation state (0.74 Å versus 0.62 Å respectively) this coordination mode is not unexpected.[34] Further confirmation of the binding mode of each complex was obtained by solid-state analysis by X-ray crystallography, which will be discussed in more detail. The average Δν for the bismuth complexes **1B – 8B** was found to be 186 cm^{-1}, with two distinctive signals observed for both the asymmetric and symmetric stretch. For the antimony complexes **1S – 8S** a single distinctive signal was observed for the asymmetric and symmetric stretch, with an average Δν of 214 cm^{-1}. The hydroxyl signal at ~ 3200 cm^{-1} in the parent acid is also absent upon complexation. An example is given with complexes **1S,** $[SbPh_3(O_2CCH_2C_6H_4CH_3)_2]$ and **1B,** $[BiPh_3(O_2CCH_2C_6H_4CH_3)_2]$ (figure 2.1.9). Table 2.1.1 highlights each individual complex compared against the parent acid.

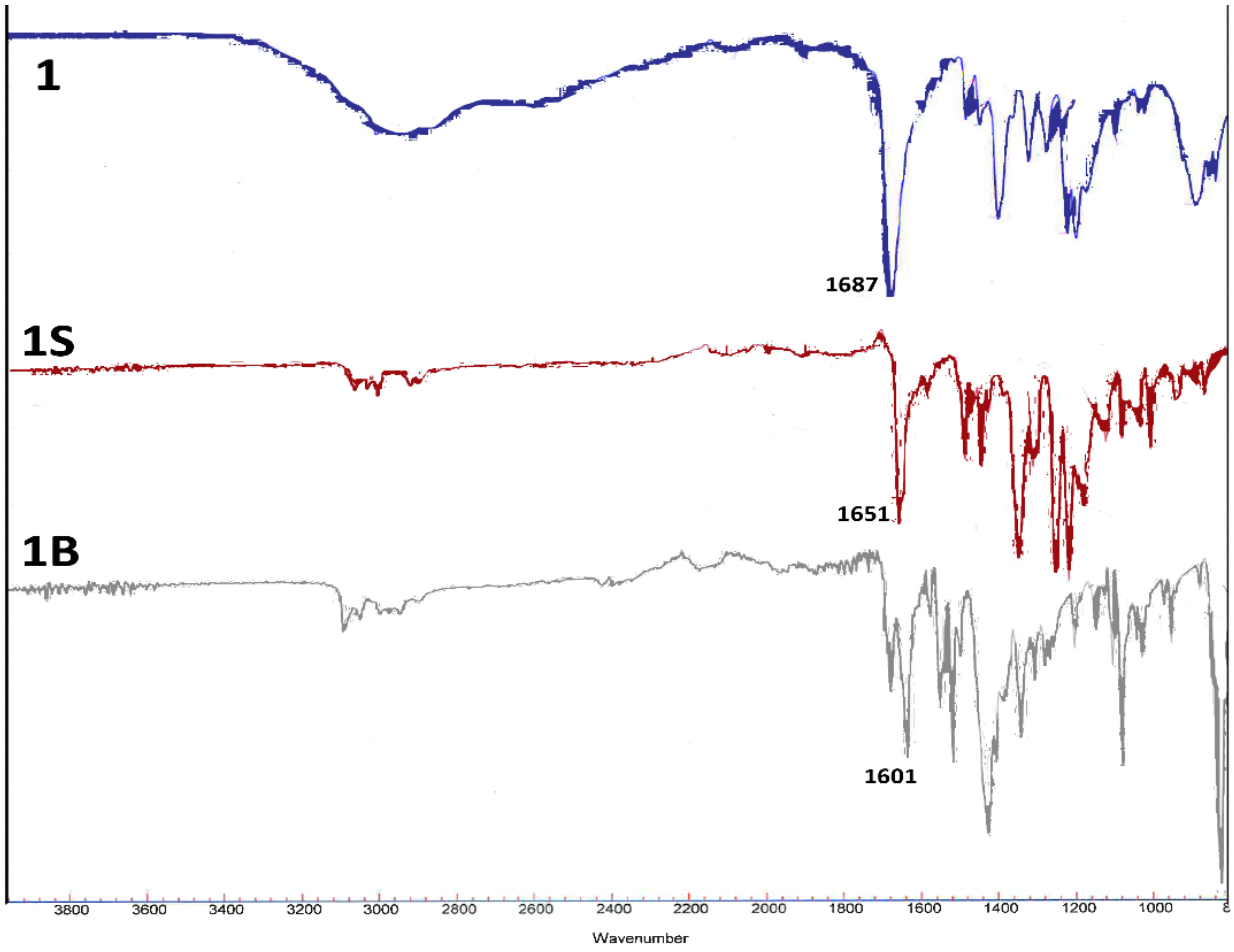

*Figure 2.1.9. IR spectrum of **1S** and **1B** versus the free acid **1**, carboxylate signal has been labelled.*

*Table 2.1.1. Summary of carboxylate stretching frequencies of complexes **1S/1B – 8S/8B***

Compound	ν(-CO_2H) (cm^{-1})	ν(-$CO_{2(aymm)}$) (cm^{-1})	ν(-$CO_{2(symm)}$) (cm^{-1})	Δν (cm^{-1})
1	1687	-	-	-
1B	-	1601 + 1560	1493 + 1470	198
1S	-	1651	1437	214
2	1689	-	-	-
2B	-	1602 + 1559	1490 + 1469	202
2S	-	1653	1435	218
3	1690	-	-	-
3B	-	1600 + 1560	1513 + 1468	179
3S	-	1644	1433	211
4	1705	-	-	-
4B	-	1599 + 1490	1467 + 1425	197
4S	-	1652	1431	221
5	1689	-	-	-
5B	-	1605 + 1489	1466 + 1434	194
5S	-	1619	1413	202
6	1692	-	-	-
6B	-	1596 + 1550	1510 + 1466	176
6S	-	1631	1434	197
7	1722	-	-	-
7B	-	1626 + 1570	1557 + 1470	169
7S	-	1653	1434	219
8	1731	-	-	-
8B	-	1624 + 1598	1557 + 1495	170
8S	-	1669	1437	232

2.1.3.3 X-ray crystallography

All complexes synthesised formed single crystals from either toluene or diethyl ether solutions allowing solid-state analysis by X-ray crystallography, apart from the already reported complex **2S,** $[SbPh_3(O_2CCH_2C_6H_4CH_3)_2]$.[18] For the previously reported complexes **4S**, $[SbPh_3(O_2CCH_2C_6H_4OCH_3)_2]$ **6S,** $[SbPh_3(O_2CCH_2C_6H_4OCH_3)_2]$ and **8S**, $[SbPh_3(O_2CCH_2OC_6H_5)_2]$, no solid-state information had been reported, therefore crystals suitable for X-ray analysis were produced and their structures elucidated. Each complex, excluding the oxido bridged **7S**, $[(SbPh_3((O_2CCH_2OCO)Me))_2O]$, adopts a trigonal bipyramidal geometry, which is the most common conformation seen for bismuth and antimony compounds of the general formula $[M(Ar)_3(O_2CR)_2]$. The aryl groups occupy the

equatorial plane in an orientation reminiscent of a propeller, while the carboxylate moieties sit in the axial plane of the crystal system.[17, 19, 20, 23, 28-30] The major difference between the bismuth and antimony analogues is the coordination number. In the +V state the ionic radii of bismuth is larger than antimony (0.74 Å Bi(V), 0.62 Å Sb(V)),[34] which led to each bismuth complex incorporating both covalent and coordinate bonds from the carboxylate moieties, pushing the coordination number to seven. In contrast, the smaller Sb(V) complexes were found to adopt a five-coordinate geometry, with only the carboxylate hydroxyl interaction present. Antimony structures **3S,** $[SbPh_3(O_2CCH_2C_6H_4CH_3)_2]$, **4S,** $[SbPh_3(O_2CCH_2C_6H_4OCH_3)_2]$, **6S,** $[SbPh_3(O_2CCH_2C_6H_4OCH_3)_2]$ and **7S,** $[(SbPh_3((O_2CCH_2OCO)Me))_2O]$ all have the same monoclinic *C2/c* space group, with the remaining complexes characterised as either monoclinic $P2_1/c$ (**1S,** $[SbPh_3(O_2CCH_2C_6H_4CH_3)_2]$), orthorhombic *Pbcn* (**5S,** $[SbPh_3(O_2CCH_2C_6H_4OCH_3)_2]$) or triclinic *P* (**8S,** $[SbPh_3(O_2CCH_2OC_6H_5)_2]$). Similar to the antimony complexes, the bismuth complexes were dominated by the centrosymmetric monoclinic *C2/c* (**5B,** $[BiPh_3(O_2CCH_2C_6H_4OCH_3)_2]$ **6B,** $[BiPh_3(O_2CCH_2C_6H_4OCH_3)_2]$ **7B,** $[SbPh_3(O_2CCH_2OCO_2CH_3)_2]$, **8B,** $[BiPh_3(O_2CCH_2OC_6H_5)_2]$) with the remaining complexes observed in the space groups triclinic *P* (**1B,** $[BiPh_3(O_2CCH_2C_6H_4CH_3)_2]$ and **3B,** $[SbPh_3(O_2CCH_2C_6H_4CH_3)_2]$), monoclinic $P2_1/c$ (**2B,** $[BiPh_3(O_2CCH_2C_6H_4CH_3)_2]$), and monoclinic $P2_1/m$ (**4B,** $[BiPh_3(O_2CCH_2C_6H_4OCH_3)_2]$). Each complex, disregarding **1S, 1B** and **7S,** are listed below with a brief summary of selected bond lengths and angles. (figures 2.1.10 – 2.1.21). **1S, 1B** and **7S** will be discussed in more detail further in the section.

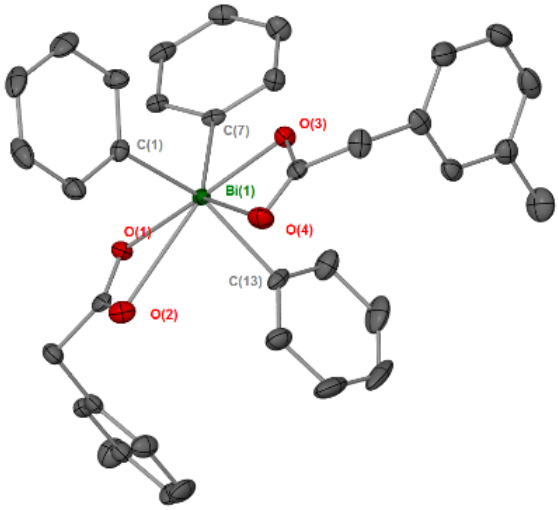

*Figure 2.1.10. Solid-state structure of [$BiPh_3(O_2CCH_2C_6H_4CH_3)_2$], **2B**. Thermal ellipsoids at 50% probability. Hydrogen atoms have been omitted for clarity. Selected bonds lengths (Å) and angles (°). Bi(1) – O(1), 2.326(2), Bi(1) – O(2), 2.726(2), Bi(1) – O(3), 2.258(2), Bi(1) – O(4), 2.703(2), Bi(1) – C(1), 2.195(3), Bi(1) – C(7), 2.204(3), Bi(1) – C(13), 2.194(3); C(7) – Bi(1) – C(13), 108.58(12), C(1) – Bi(1) – C(7), 101.42(12), C(7) – Bi(1) – O(1), 84.79(9), C(7) – Bi(1) – O(3), 86.90(9), O(1) – Bi(1) – O(3), 171.05(8).*

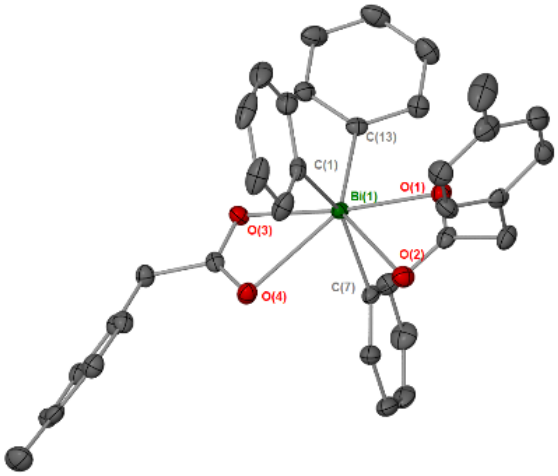

*Figure 2.1.11. Solid-state structure of [$BiPh_3(O_2CCH_2C_6H_4CH_3)_2$], **3B**. Thermal ellipsoids at 50% probability. Hydrogen atoms have been omitted for clarity. Selected bonds lengths (Å) and angles (°). Bi(1) – O(1), 2.277(14), Bi(1) – O(3), 2.308(14), Bi(1) – O(4), 2.703(14), Bi(1) – C(1), 2.205(19), Bi(1) – C(7), 2.185(19), Bi(1) – C(13), 2.195(19); C(7) – Bi(1) – C(13), 143.58(7), C(1) – Bi(1) – C(7), 104.38(7), C(7) – Bi(1) – O(1), 95.17(6), C(7) – Bi(1) – O(3), 91.02(6), O(1) – Bi(1) – O(3), 170.28(5).*

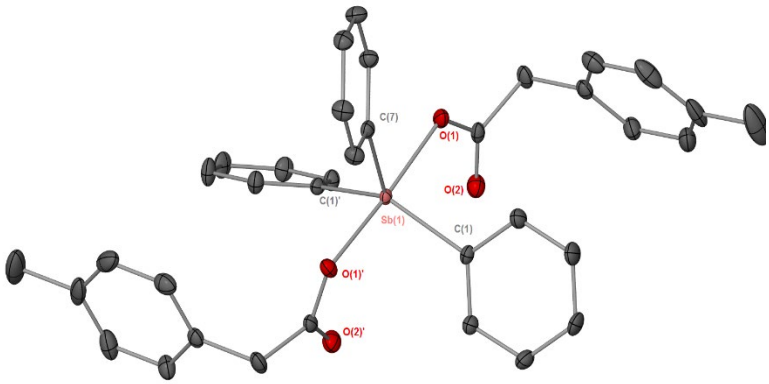

*Figure 2.1.12. Solid state structure of [$SbPh_3(O_2CCH_2C_6H_4CH_3)_2$], **3S**. Thermal ellipsoids at 50% probability. Hydrogen atoms have been omitted for clarity. Selected bonds lengths (Å) and angles (°). Sb(1) – O(1), 2.101(13), Sb(1) – O(1'), 2.101(13), Sb(1) – C(1), 2.100(12), Sb(1) – C(7), 2.092(12); C(7) – Sb(1) – C(1), 110.69(4), C(1) – Sb(1) – C(1'), 138.62(8), C(1) – Sb(1) – O(1), 87.09(3), O(1) – Sb(1) – O(1'), 174.19(6). Symmetry operator: 1 – x, y, 1/2- z*

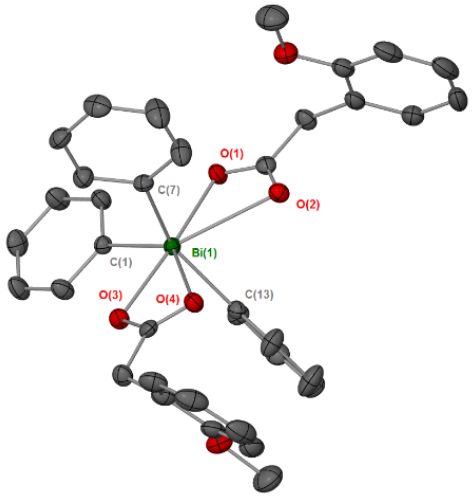

*Figure 2.1.13. solid-state structure of [$BiPh_3(O_2CCH_2C_6H_4OCH_3)_2$], **4B**. Thermal ellipsoids at 50% probability. Hydrogen atoms have been omitted for clarity. Selected bonds lengths (Å) and angles (°). Bi(1) – O(1), 2.289(3), Bi(1) – O(2), 2.759(2), Bi(1) – O(3), 2.298(3), Bi(1) – C(1), 2.205(2), Bi(1) – C(7), 2.181(3), Bi(1) – C(13), 2.186(4); C(7) – Bi(1) – C(13), 149.94(12), C(1) – Bi(1) – C(7), 105.01(10), C(7) – Bi(1) – O(1), 91.48(12), C(7) – Bi(1) – O(3), 90.27(11), O(1) – Bi(1) – O(3), 174.13(7).*

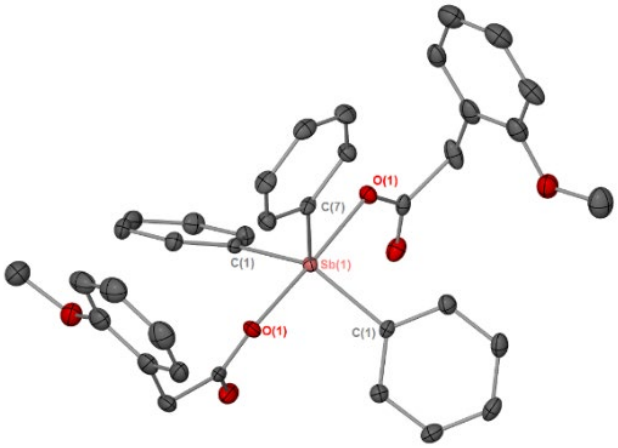

*Figure 2.1.14. Solid state structure of [$SbPh_3(O_2CCH_2C_6H_4OCH_3)_2$], **4S**. Thermal ellipsoids at 50% probability. Hydrogen atoms have been omitted for clarity. Selected bonds lengths (Å) and angles (°). Sb(1) – O(1), 2.107(13), Sb(1) – O(1'), 2.107(13), Sb(1) – C(1), 2.112(2), Sb(1) – C(7), 2.119(3); C(7) – Sb(1) – C(1), 110.69(4), C(5) – Sb(1) – C(5'), 138.62(8), C(1) – Sb(1) – O(1), 87.09(3), O(1) – Sb(1) – O(1'), 174.19(6). Symmetry operator: 1 - x, y, 3/2 - z*

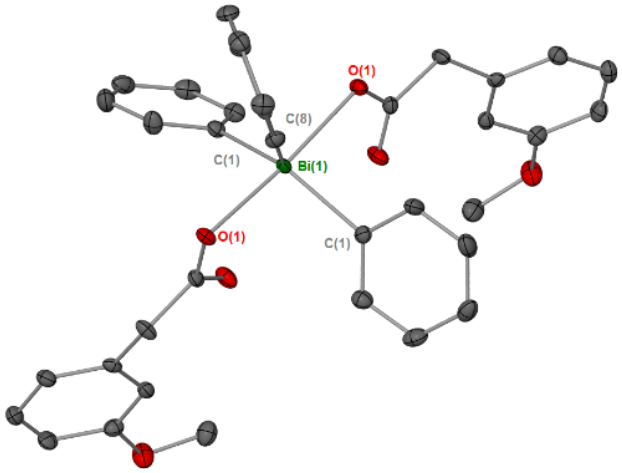

*Figure 2.1.15. Solid-state structure of [$BiPh_3(O_2CCH_2C_6H_4OCH_3)_2$], **5B**. Thermal ellipsoids at 50% probability. Hydrogen atoms have been omitted for clarity. Selected bonds lengths (Å) and angles (°). Bi(1) – O(1), 2.283(12), Bi(1) – O(2), 2.885(12), Bi(1) – C(1), 2.204(18), Bi(1) – C(7), 2.202 (18); C(7) – Bi(1) – C(1), 106.79(5), C(1) – Bi(1) – C(1'), 146.59(11), C(7) – Bi(1) – O(1), 85.82(3), C(1) – Bi(1) – O(1), 90.02(6), O(1) – Bi(1) – O(1'), 171.63(7). Symmetry operator: 1- x, y, 3/2 – z*

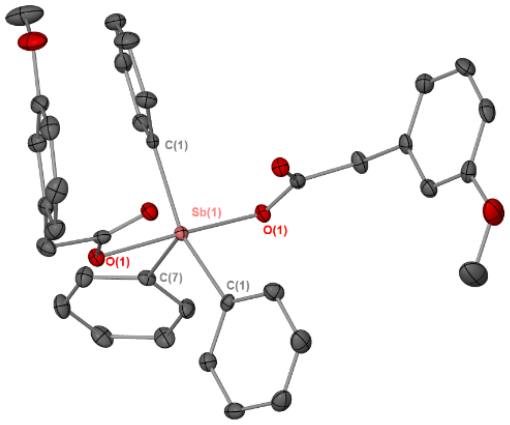

*Figure 2.1.16. Solid state structure of [$SbPh_3(O_2CCH_2C_6H_4OCH_3)_2$], **5S**. Thermal ellipsoids at 50% probability. Hydrogen atoms have been omitted for clarity. Selected bonds lengths (Å) and angles (°). Sb(1) – O(1), 2.139(15), Sb(1) – O(1'), 2.139(15), Sb(1) – C(1), 2.110(2), Sb(1) – C(7), 2.101(3); C(7) – Sb(1) – C(1), 104.97(7), C(1) – Sb(1) – C(1'), 150.06(13), C(1) – Sb(1) – O(1), 89.74(7), O(1) – Sb(1) – O(1'), 174.97(9). Symmetry operator: 1 - x, y, 3/2 - z*

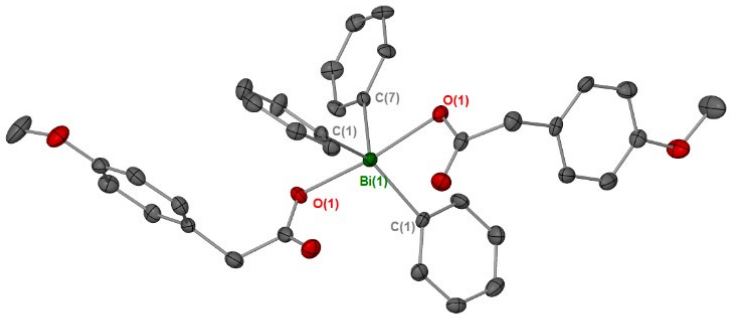

*Figure 2.1.17. Solid-state structure of [$BiPh_3(O_2CCH_2C_6H_4OCH_3)_2$], **6B**. Thermal ellipsoids at 50% probability. Hydrogen atoms have been omitted for clarity. Selected bonds lengths (Å) and angles (°). Bi(1) – O(1), 2.275(4), Bi(1) – O(2), 2.848(4), Bi(1) – O(1'), 2.275(4), Bi(1) – C(1), 2.210(5), Bi(1) – C(7), 2.202(5); C(7) – Bi(1) – C(1), 106.81(15), C(1) – Bi(1) – C(1'), 146.4(3), C(7) – Bi(1) – O(1), 85.32(9), C(1) – Bi(1) – O(1), 93.30(17), O(1) – Bi(1) – O(1'), 170.69(19). Symmetry operator: -x, y, 3/2 - z*

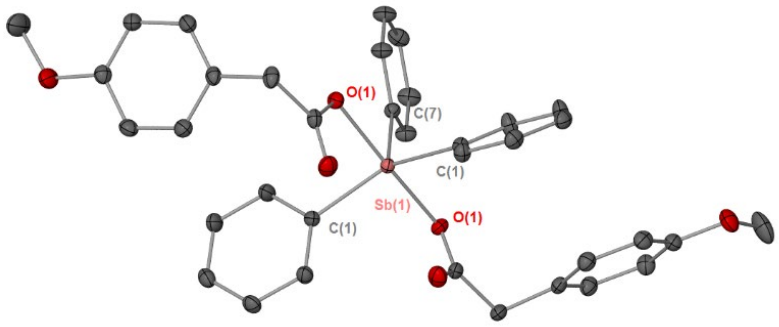

*Figure 2.1.18 Solid state structure of [$SbPh_3(O_2CCH_2C_6H_4OCH_3)_2$], **6S**. Thermal ellipsoids at 50% probability. Hydrogen atoms have been omitted for clarity. Selected bonds lengths (Å) and angles (°). Sb(1) – O(1), 2.109(10), Sb(1) – O(1'), 2.109(10), Sb(1) – C(1), 2.110(12), Sb(1) – C(7), 2.105(17); C(7) – Sb(1) – C(1), 107.41(3), C(1) – Sb(1) – C(1'), 145.17(7), C(1) – Sb(1) – O(1), 89.47(4), O(1) – Sb(1) – O(1'), 175.64(5). Symmetry operator: 1- x, y, 3/2 - z*

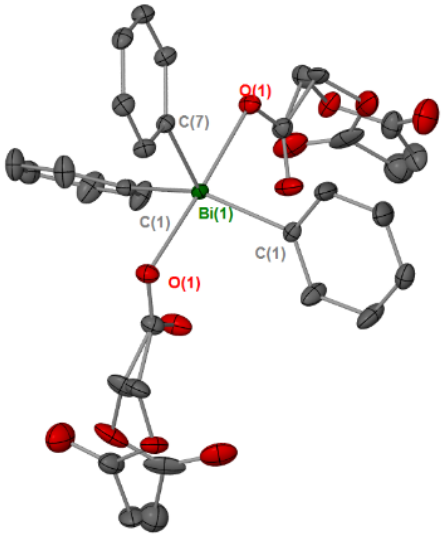

*Figure 2.1.19. Solid-state structure of [$BiPh_3(O_2CCH_2O_2CCH_3)_2$], **7B**. Thermal ellipsoids at 50% probability. Hydrogen atoms have been omitted for clarity. Selected bonds lengths (Å) and angles (°). Bi(1) – O(1), 2.289(19), Bi(1) – O(2), 2.855(19), Bi(1) – C(1), 2.188(3), Bi(1) – C(7), 2.202(4); C(1) – Bi(1) – C(1'), 148.82(12), C(1) – Bi(1) – C(7), 105.59(7), C(1) – Bi(1) – O(1), 87.59(19), C(7) – Bi(1) – O(1), 87.92(5), O(1) – Bi(1) – O(1'), 175.84(10). Symmetry operator: 1 – x, y, 3/2 z. Disorder of the terminal end of the acetoxyacetic acetate has been modelled over two positions*

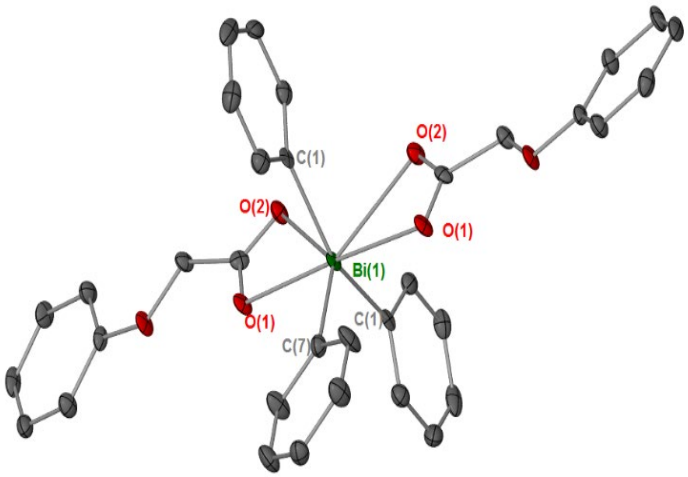

*Figure 2.1.20. solid-state structure of [$BiPh_3(O_2CCH_2OC_6H_5)_2$], **8B**. Thermal ellipsoids at 50% probability. Hydrogen atoms have been omitted for clarity. Selected bonds lengths (Å) and angles (°). Bi(1) – O(1), 2.334(3), Bi(1) – O(2), 2.694(2), Bi(1) – C(1), 2.197(5), Bi(1) – C(7), 2.214(7), Bi(1) – C(11), 2.853(5); C(11) – Bi(1) – C(11'), 133.00(2), C(11) – Bi(1) – C(7), 113.49(10), C(7) – Bi(1) – O(1), 87.53(8), C(7) – Bi(1) – O(2), 139.22(7), O(1) – Bi(1) – O(3), 175.05(16). Symmetry operator: 1 - x, y, 3/2 - z*

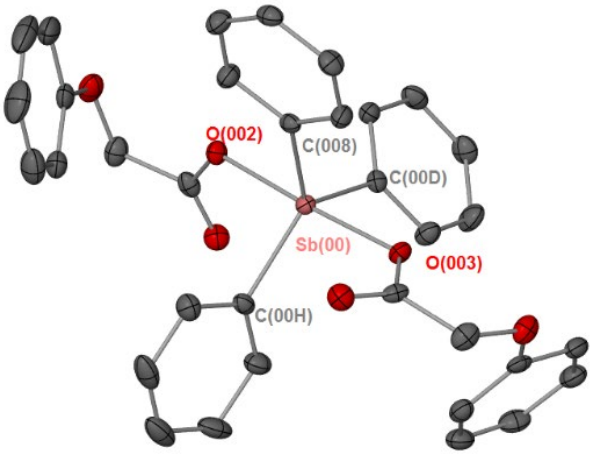

*Figure 2.1.21. Solid state structure of [$SbPh_3(O_2CCH_2OC_6H_5)_2$], **8S**. Thermal ellipsoids at 50% probability. Hydrogen atoms have been omitted for clarity. Selected bonds lengths (Å) and angles (°). Sb(1) – O(1), 2.109(2), Sb(1) – O(3), 2.115(2), Sb(1) – C(1), 2.111(3), Sb(1) – C(7), 2.099(3), Sb(1) – C(13), 2.100(3); C(7) – Sb(1) – C(1), 117.44(11), C(1) – Sb(1) – C(13), 119.25(11), C(1) – Sb(1) – O(1), 94.45(10), O(1) – Sb(1) – O(3), 175.49(8)*

Example complexes **1B** is pentagonal bipyramid with a coordination number of seven, whereas **1S** with a coordination number of five, is trigonal bipyramidal. It was strongly anticipated, from the IR data ($\Delta\nu$ = 2.14 cm^{-1}, table 2.1.1) that the coordination number of **1S** would be five, indicative of a *mono*dentate binding mode of the carboxylate moiety. This was further confirmed in the solid-state by the averaged bonding and non-bonding lengths for the Sb – O interactions (2.120 and 2.970 respectively). For complex **1B** a widening of the trigonal angle of the equatorial plane was observed from the ideal 120 ° to 143.6(7) °, 104.4(7) °, and 112.0(7) ° for the C(7) – Bi(1) – C(13), C(1) – Bi(1) – C(7) and C(1) – Bi(1) – C(13) bond angles respectively. It is possible this deviation is a result of the *cis* configuration of the *o*-tolylacetate ligands in the axial plane which could allow for a greater interaction between the bismuth centre and the carbonyl oxygens. To a lesser extent **1S** also experiences deviation in trigonal angle with angles of 113.6(7), 139.1(7) and 107.3(7) found for C(13) – Sb(1) – C(1), C(1) – Sb(1) – C(7) and C(7) – Sb(1) – C(13) respectively. An in-depth summary of the crystallographic data for these complexes is given in table 2.1.2 and table 2.1.3.

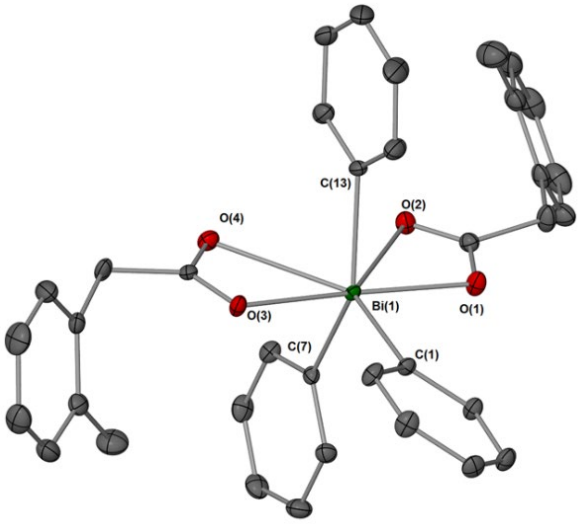

Figure 2.1.22. Solid-state structure of $[BiPh_3((O_2CCH_2C_6H_4CH_3)_2]$, **1B**. Thermal ellipsoids at 50% probability. Hydrogen atoms have been omitted for clarity. Selected bonds lengths (Å) and angles (°). Bi(1) – O(1), 2.278(14), Bi(1) – O(2), 2.703(14), Bi(1) – O(3), 2.308(14), Bi(1) – O(4), 2.703(15), 2.815(14), Bi(1) – C(1), 2.205(19), Bi(1) – C(7), 2.186(2), Bi(1) – C(13), 2.195(2); C(7) – Bi(1) – C(13), 143.6(8), C1 – Bi(1) – C(7), 104.5(7), C7 – Bi(1) – O(1), 95.15(6), C(7) – Bi(1) – O(4), 75.93(6), O(1) – Bi(1) – O(3), 170.3(5).

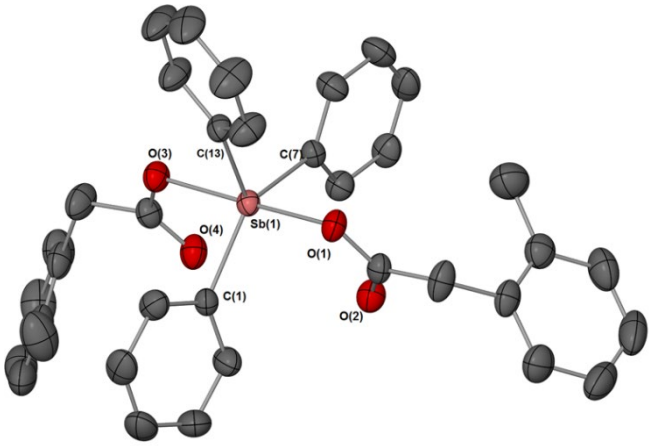

Figure 2.1.23. Solid state structure of $[SbPh_3((O_2CCH_2C_6H_4CH_3)_2]$, **1S**. Thermal ellipsoids at 50% probability. Hydrogen atoms have been omitted for clarity. Selected bonds lengths (Å) and angles (°). Sb(1) – O(1), 2.110(14), Sb(1) – O(3), 2.131(14), Sb(1) – C(1), 2.108(19), Sb(1) – C(7), 2.104(19), Sb(1) – C(13), 2.116(18); C(7) – Sb(1) – C(1), 139.1(7), C1 – Sb(1) – C(13), 113.5(7), C1 – Sb(1) – O(1), 90.71(6), O(1) – Sb(1) – O(3), 174.0(5).

The covalent M – C bond lengths for the antimony complex **1S** (range: 2.108(19) – Å, 2.116(18) Å) and are comparable to analogous structures in the literature.[8, 17, 18, 27-29, 35] Similar to the antimony, the bismuth complex **1B** also shares bonds lengths comparable to previously synthesised complexes, with bond lengths ranging from 2.185(19) Å – 2.205(16) Å.[4, 5, 16, 19, 20, 24, 36] Complex **1B** adopts *bi*dentate binding through both the hydroxyl oxygen and the carbonyl oxygen as suggested by the average bond lengths of 2.759 Å (Bi(1) – O(1), O(3)) and 2.930 Å (Bi(1) – O(2), O(4)) respectively. This is further supported by the IR carboxylate stretching frequencies (table 2.1.1).

Complex **7S** (figure 2.1.24) was the only outlier in this class of acetates, with the formation of a Sb – O – Sb bond.

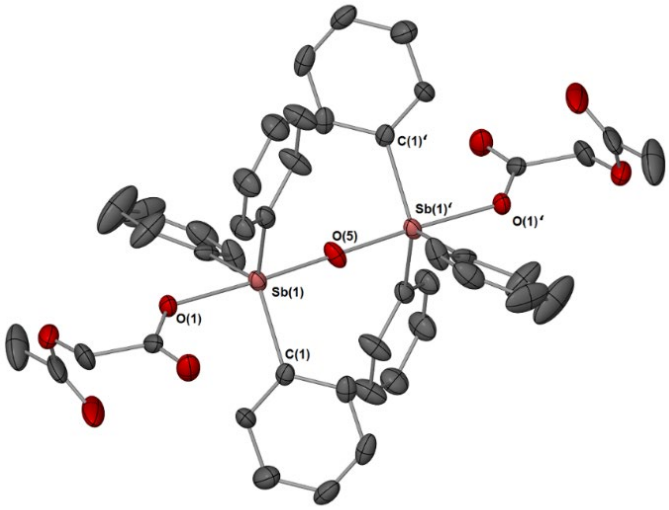

Figure 2.1.24. Solid state structure of [$(SbPh_3(O_2CCR))_2O$], **7S**. Thermal ellipsoids at 50% probability. Hydrogen atoms have been omitted for clarity. Selected bonds lengths (Å) and angles (°). Sb(1) – O(1), 2.147(3), Sb(1) – O(5), 1.951(5), Sb(1) – C(1), 2.110(4), Sb(1) – C(7), 2.108(5), Sb(1) – C(13), 2.106(4); C(7) – Sb(1) – C(1), 126.5(17), C(1) – Sb(1) – C(13), 115.9(17), C1 – Sb(1) – O(1), 90.46(16), O(1) – Sb(1) – O(5), 175.2(8), Sb(1) – O(5) – Sb(1)', 179.9(18). Symmetry operator ' = 1-x, 1-y, 1-z.

The formation of the complex can be rationalised by the likely reaction pathway. The intermediate step of the oxidation of Sb(III) to the Sb(V) forms $SbPh_3(OH)_2$, however the formation of a *bis*-substituted complex does not. Rather, two intermediates of a *mono*-acetate, $SbPh_3(O_2CR)(OH)$, come together, which after the loss of water forms the new Sb – O – Sb bond. This often results due an incorrect stoichiometry of the peroxide oxidant, as shown by Sharutin *et al* in the formation of aryl antimony dioximates.[27] Several repeated syntheses of consistent reaction conditions resulted in the same crystalline sample of **7S**. Therefore, it would seem to be the preferential product for this particular ligand. Crystallographically, **7S** can still be said to adopt the usual trigonal bipyramidal geometry at each of the Sb(V) centres, with a coordination number of five. Bond lengths of 2.110(4) Å (Sb(1) – C(1)), 2.108(5) Å (Sb(1) – C(7)), and 2.106(4) Å (Sb(1) – C(13)) were observed for the M - C and found to be similar to the more typical Sb(V) triaryl dicarboxylates with each of the phenyl groups occupying the usual propeller like orientation.[15, 17,

[18, 23, 28, 29] The carboxylates of the oxido-bridge antimony sit almost linear in the axial plane, with a slight deviation from the ideal 180 ° to 175.2(8) °. The covalent bond interaction with the carboxylate oxygen O(1) of 2.147(3) was found to be longer than the covalent bond with the bridging oxygen O(5) of 1.950(4). This isn't an unusual observation, with Quan *et al*, Abakumov *et* al and Preut *et al*, all reporting shorter Sb – O oxido bridging bond lengths of 1.950(4) Å, 1.968(6) Å and 1.936(1) Å respectively.[37-39] The angle of the Sb – O – Sb bridge is almost linear, with an angle of 179.9(18). Similar linearity was observed in the complex $[(SbPh_3(C_2H_2ClO_2)_2)O]$ characterised by Quan *et al* with a formal angle of 180 ° for the Sb – O – Sb bond.[38] Linearity is not always observed in these bridging antimony complexes however, another complexed characterised by Quan *et al*, $[(SbPh_3(C_6H_3ClNO_2)_2)O]$, exhibits distortion from the ideal 180 ° to a bent angle of 165.1(4) ° for the Sb – O – Sb bond.[37]

*Table 2.1.2. Summary of the crystallographic data of triphenyl Sb(V) acetates, **1S – 8S**.*

	1S	**3S**	**4S**	**5S**	**6S**	**7S**	**8S**
Chemical formula	$C_{36}H_{33}O_4Sb$	$C_{36}H_{33}O_4Sb$	$C_{36}H_{33}O_6Sb$	$C_{36}H_{33}O_6Sb$	$C_{36}H_{33}O_6Sb$	$C_{44}H_{40}O_9Sb_2$	$C_{34}H_{29}O_6Sb$
M_r	651.37	651.37	683.37	683.37	683.37	956.26	655.32
Crystal system, space group	Monoclinic, $P2_1/c$	Monoclinic, $C2/c$	Monoclinic, $C2/c$	Orthorhombic, $Pbcn$	Monoclinic, $C2/c$	Monoclinic, $P2_1/c$	Triclinic, P $P\text{-}1$
Temperature (K)	296	296	123	296	296	296	296
a, b, c (Å)	12.157 (3), 10.382 (3), 24.819 (7)	23.2869 (12), 9.3365 (5), 13.2480 (6)	24.7407 (15), 9.4054 (6), 16.7457 (19)	19.1951 (11), 9.6030 (8), 16.7738 (10)	16.9984 (11), 9.7839 (7), 18.1779 (14)	10.826 (2), 9.7607 (18), 18.663 (3)	9.3167 (5), 9.5733 (5), 18.3654 (9)
V (Å^3)	3086.9 (14)	2871.1 (3)	2995.6 (4)	3091.9 (4)	2993.5 (4)	1958.3 (6)	1399.35 (13)
Z	4	4	4	4	4	2	2
T_{min}, T_{max}	0.675, 0.746	0.691, 0.746	0.616, 0.746	0.672, 0.746	0.664, 0.749	0.646, 0.746	0.667, 0.746
R_{int}	0.043	0.031	0.059	0.056	0.052	0.091	0.059
$(\sin\theta/\lambda)_{max}$ (Å^{-1})	0.716	0.670	0.719	0.646	1.042	0.671	0.667
$R[F^2 > 2\sigma(F^2)]$, $wR(F^2)$, S	0.031, 0.063, 1.06	0.018, 0.043, 1.06	0.032, 0.076, 1.06	0.026, 0.067, 1.00	0.048, 0.121, 0.99	0.049, 0.112, 1.00	0.039, 0.116, 0.76
No. of reflections	9448	3611	4625	3474	13885	4928	6945
No. of parameters	372	188	197	197	197	251	370

*Table 2.1.3 Summary of the crystallographic data of triphenyl Bi(V) acetates, **1B – 8B**.*

	1B	**2B**	**3B**	**4B**	**5B**	**6B**	**7B**	**8B**
Chemical formula	$C_{36}H_{33}BiO_4$	$C_{36}H_{33}BiO_4$	$C_{36}H_{33}BiO_4$	$C_{36}H_{33}BiO_6$	$C_{36}H_{33}BiO_6$	$C_{36}H_{33}BiO_6$	$C_{26}H_{25}BiO_8$	$C_{34}H_{29}BiO_6$
M_r	738.60	738.60	738.60	770.60	770.60	770.60	674.44	742.55
Crystal system, space group	Triclinic, P	Monoclinic, $P2_1/c$	Triclinic, P	Monoclinic, $P2_1/m$	Monoclinic, $C2/c$	Monoclinic, $C2/c$	Monoclinic, $C2/c$	Monoclinic, $C2/c$
Temperature (K)	123	296	173	123	296	296	123	296
a, b, c (Å)	10.2028 (7), 12.0610 (8), 12.5411 (8)	19.9440 (7), 8.5465 (3), 18.0951 (6)	8.8812 (3), 13.2024 (5), 14.8618 (5)	9.5157 (4), 17.9285 (8), 10.3376 (5)	24.6911 (8), 9.6741 (3), 17.3819 (7)	17.0886 (18), 9.7652 (8), 18.467 (2)	20.0227 (10), 9.7510 (5), 15.8259 (7)	13.1884 (6), 20.6913 (9), 12.0533 (8)
V (Å^3)	1467.37 (17)	2948.25 (18)	1487.57 (9)	1565.65 (12)	2948.78 (18)	3047.8 (5)	2485.4 (2)	2768.5 (3)
Z	2	4	2	2	4	4	4	4
T_{min}, T_{max}	0.482, 0.746	0.449, 0.746	0.513, 0.746	0.032, 0.069	0.544, 0.746	0.563, 0.746	0.635, 0.746	0.408, 0.746
R_{int}	0.047	0.051	0.038	0.028	0.062	0.062	0.032	0.089
$(\sin\theta/\lambda)_{max}$ (Å^{-1})	0.721	0.720	0.717	0.716	0.719	0.674	0.720	0.646
$R[F^2 > 2\sigma(F^2)]$, $wR(F^2)$, S	0.019, 0.042, 1.02	0.031, 0.062, 1.02	0.024, 0.060, 1.08	0.018, 0.039, 1.01	0.020, 0.035, 0.72	0.045, 0.089, 1.00	0.023, 0.048, 1.12	0.036, 0.079, 1.02
No. of reflections	9150	9171	9145	4947	4376	3743	3863	3082
No. of parameters	372	372	372	381	197	197	208	187

2.1.4 Stability and Selectivity

2.4.1.1 General stability

An ideal attribute of any potential medicine is its ability to remain stable in aqueous media such as those in biological systems. To exhibit anti-microbial activity a high degree of stability is preferential. As such, a series of analyses in both the solid and solution state of the complexes **1B – 8B** and **1S – 8S** were conducted. Stability in the solid state was confirmed by conducting melting point analyses over several months after exposure of the solids to atmospheric conditions. Initial studies on the solution state were conducted through the use of ^{1}H NMR spectral data in either $CDCl_3$ or d_6-DMSO over a period of one week. Complex spectra were recorded at approximately t = 0, t = 48 hours and finally t = seven days. No significant changes in the chemical shifts and/or integrations of any of the complexes were observed, excluding **7S** which was previously discussed to undergo hydrolysis at the oxido-bridge to form two equivalents of the *mono*-hydroxido **7S'**. **7S** then was concluded to be unstable in polar protic solvents with the hydrolysis product **7S'** being the thermodynamically favoured and more stable of the two forms.

Though these complexes often exhibit stability in both NMR solvents ($CDCl_3$ and d_6-DMSO), those of the general formula $[BiAr_3(O_2CR)_2]$ readily undergo decomposition in culture media. This decomposition is limited to bismuth complexes, with studies by Andrews *et al* on both phenyl and tolyl bismuth carboxylates undergoing exponential decomposition in DMEM culture media, with half-lives of approximately 2 hours.[19, 20] However when a class of chelating α-hydroxy acids were employed, the stability of the bismuth complexes increased from exponential to linear, with half-lives found to exceed fifty hours.[17] To establish whether the two carbon chain backbone has any significant effect on the stability of the bismuth complexes, a class of acetate ligands were selected **1** - **8** (figure 2.1.3). Unfortunately, it was observed the decomposition process was found to take approximately five to six hours. Despite this, the decomposition was still linear rather than

exponential. Even with this decomposition, significant biological activity was still observed on both mammalian and parasitic cells.

All bismuth complexes **1B** – **8B** were tested for their initial solubility in DMEM and M199 culture media. It was found that all complexes except for **7B,** $[BiPh_3(O_2CCH_2O_2CCH_3)_2]$ and **8B,** $[BiPh_3(O_2CCH_2OC_6H_5)_2]$ showed an ideal degree of solubility. To get an idea on the exact time-frame of the decomposition of the bismuth acetates, a representative complex, **3B**, $[BiPh_3(O_2CCH_2C_6H_4CH_3)_2]$, was selected. A known amount of **3B** was dissolved into d_6-DMSO to a concentration of 10 mM, 50 µL of this was then transferred to 1 mL of DMEM which had been previously freeze dried and resuspended in D_2O to minimise the NMR signal from H_2O. **3B** was monitored over a period of t = 0 hours to t = 24 hours. At the 24 hour mark the complex had almost completely dissociated into the parent acid (*p*-tolylacetic acid) and triphenyl bismuth, with minimal signals from **3B** remaining. The decomposition was monitored by the appearance of the aromatic signals for triphenyl bismuth at 7.2, 6.6 and 6.5 ppm after several hours. Overlap of the parent acid, **3**, with a signal from the culture media and triphenyl bismuth occurs at 7.2 ppm. However, the appearance of a multiplet beside the large singlet at 7.2 ppm occurs as **3B** undergoes decomposition into **3** and triphenyl bismuth (figure 2.1.25). To elucidate the half-life of the complex a 12 x 1 hour ^1H NMR study was then conducted, along with the analogous antimony complex **3S,** $[SbPh_3(O_2CCH_2C_6H_4CH_3)_2]$**.** The signal corresponding to the *p*-CH of the phenyl group was compared over time to a constant signal from the culture media at 5 ppm. A rapid decay was observed, however unlike previously rapid decaying bismuth carboxylate complexes, the decay was found to be linear in nature, comparable to the α-hydroxy complexes, though not as stable. The decomposition was exhibited to be zero-order, and a rate constant of approximately 48 µM /hr was calculated, decaying from the original 500 µM concentration after 5.2 hours (figure 2.1.26).

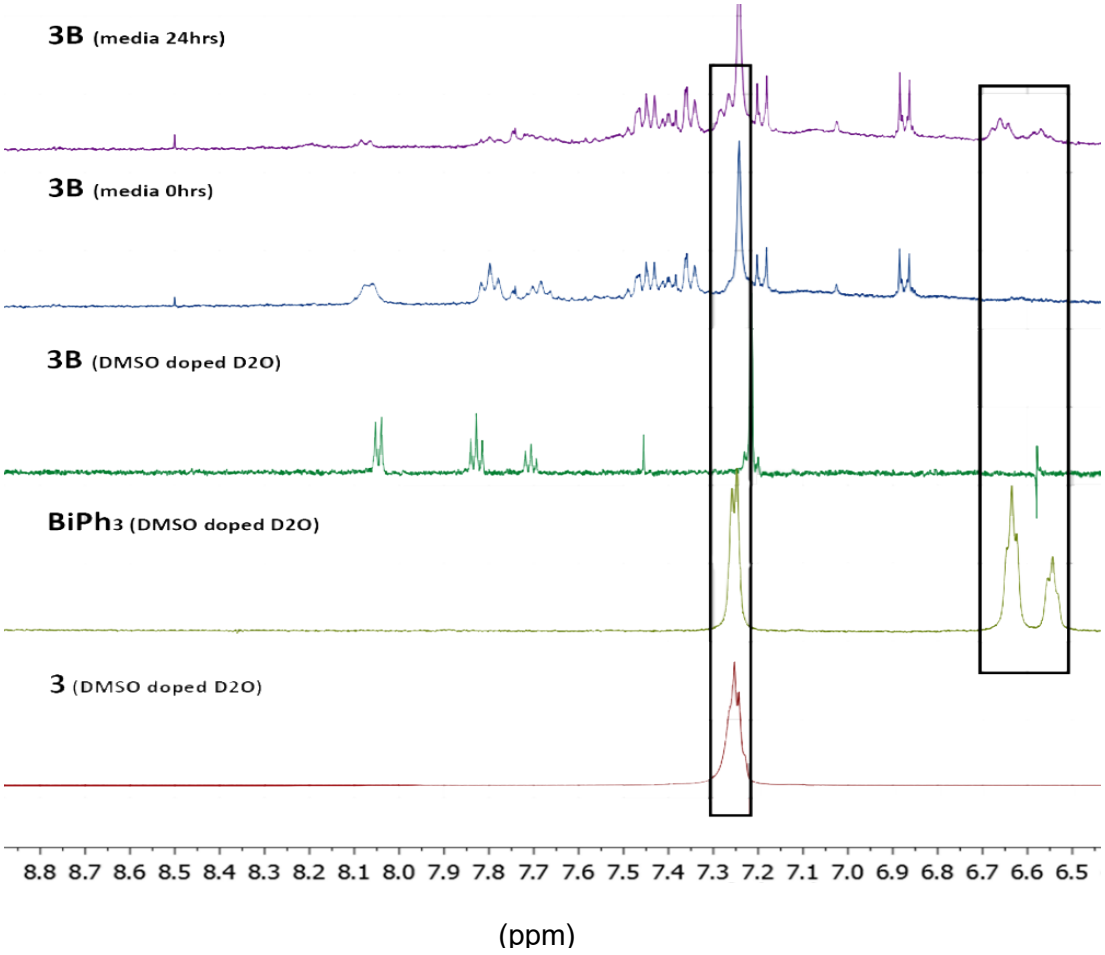

*Figure 2.1.25. ^{1}H NMR analysis of the decomposition of complex **3B,** [$BiPh_3(O_2CCH_2C_6H_4CH_3)_2$], in d_6-DMSO doped freeze dried D_2O DMEM culture medium, at 25 ^{o}C at 0 hrs and 24 hrs, references of the complex, **3B**, $BiPh_3$ and free ligand **3,** p-tolylacetic acid in d_6-DMSO:D_2O given.*

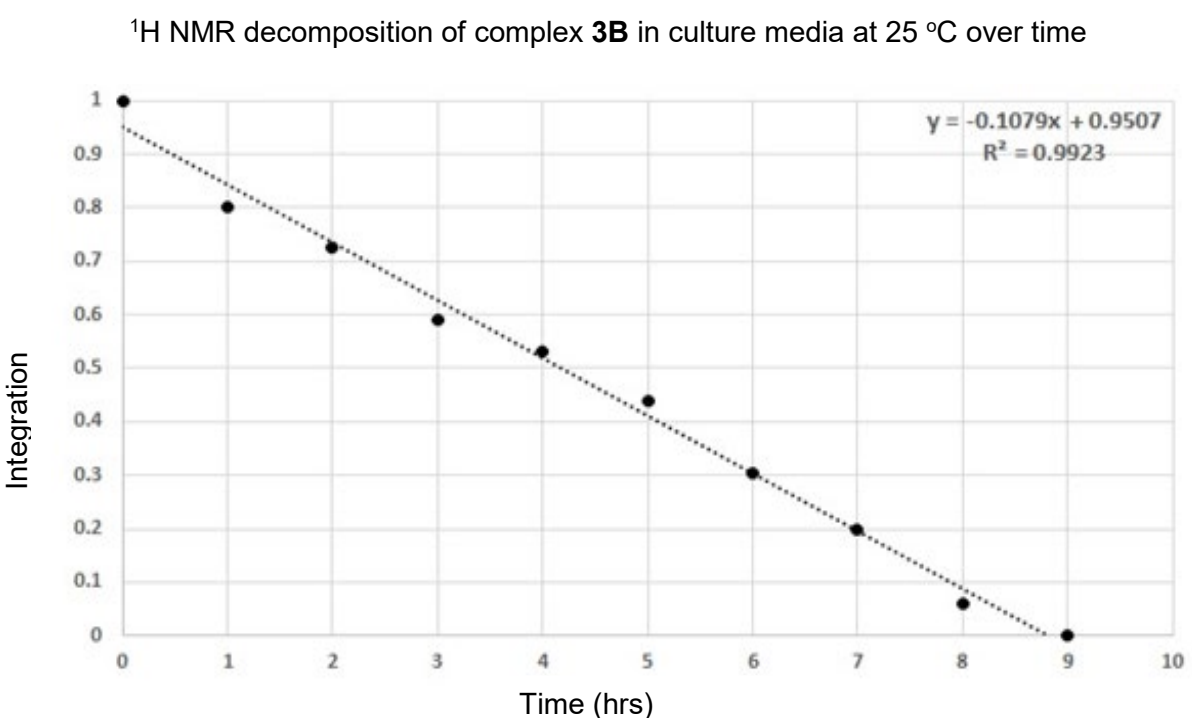

*Figure 2.1.26. ^{1}H NMR analysis of the decomposition curve of [$BiPh_3(O_2CCH_2C_6H_4CH_3)_2$], **3B** at 10 mM, in DMEM culture medium at 25 °C vs time. Half-life = 5.2 h, rate constant = 48 µM/h, R^2 = 0.992.*

Unsurprisingly, the antimony analogue exhibited no decomposition in the culture media with no significant changes in the *o*-CH protons of the phenyl rings relative to the same media signal at 5 ppm observed over a period of 12 hours (figure 2.1.27).

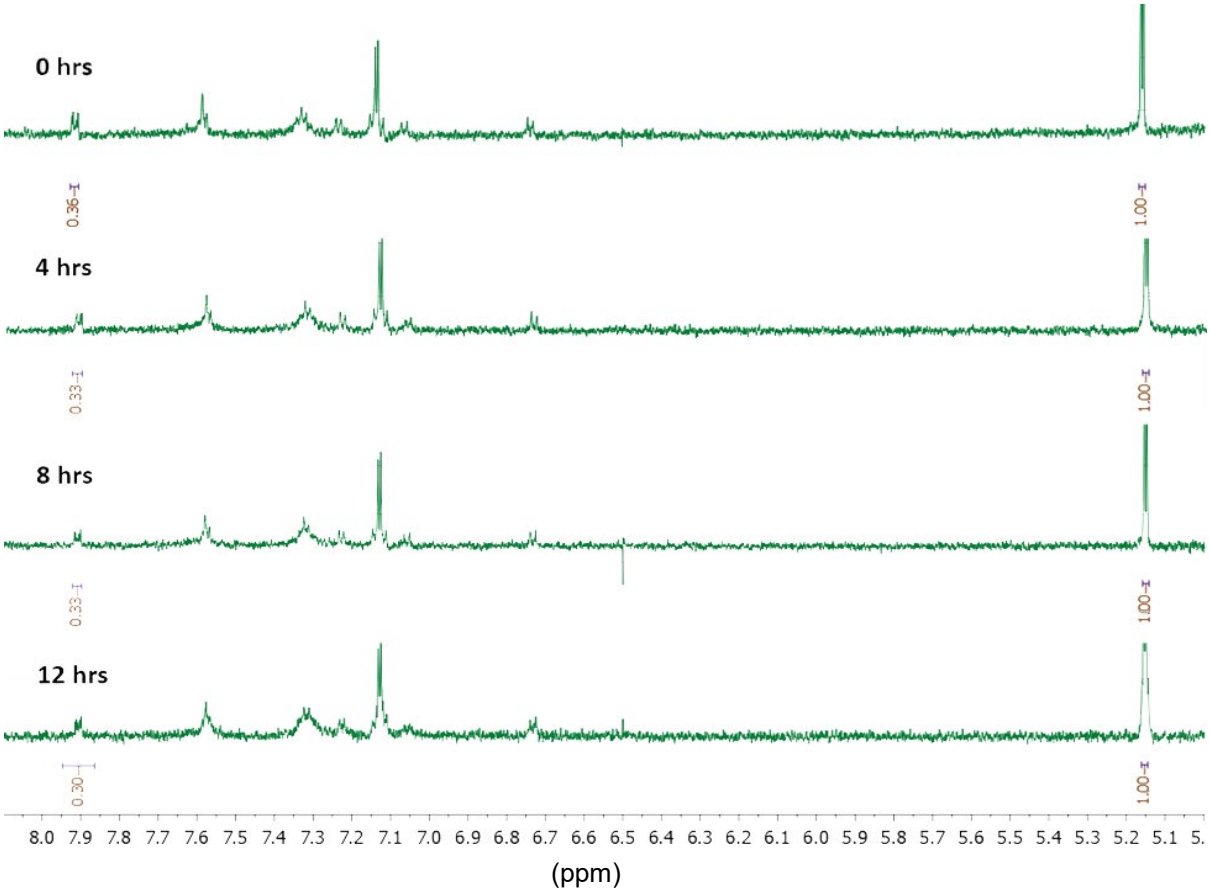

Figure 2.1.27. ^{1}H NMR study of complex $[SbPh_3(O_2CCH_2C_6H_4CH_3)_2]$, ***3S,*** *$[SbPh_3((O_2CCH_2C_6H_4CH_3)_2]$ at 10mM, in DMEM culture medium, at 25 ^{o}C at 0, 4, 8 and 12 hours.*

2.1.4.2. Glutathione studies

To further clarify the reactivity and selectivity of both antimony and bismuth, a study on the reaction with the mammalian sulfur rich tripeptide glutathione was conducted. Glutathione (GSH) is found in large concentrations in mammalian cells. It acts directly and indirectly in cellular functions including synthesis of proteins, DNA transport, enzyme activity, metabolism and the protection of cells (antioxidant activity).[40] It exists in both a reduced and oxidised form, dependent on biological redox activity the oxidised form is a combination of two single units bound by a disulfide bridge (GSSG). The reduction of pentavalent antimony complexes (meglumine antimonate) by glutathione has been studied by Frezard *et al*, concluding that the reduction is seemingly pH and temperature dependant, with a pH and temperature similar to the lysosomes

of the macrophage promoting reduction at a faster rate than standard laboratory conditions.[41, 42] They were also able to hypothesise a stoichiometric ratio for glutathione to meglumine antimoniate of 5:1. However no studies into the activity of glutathione with either bismuth or antimony organometallics has been conducted. It was predicted from the results of the biological assays (2.1.5) that bismuth would most likely show enhanced reactivity with glutathione, due in part to its very high reductive potential in comparison to antimony (for M(V)/M(III), 2.00V versus 0.605V).[43] To establish the reactivity, a ^{1}H NMR study was conducted. A known concentration of complex **3S,** $[SbPh_3(O_2CCH_2C_6H_4CH_3)_2]$ or **3B,** $[BiPh_3(O_2CCH_2C_6H_4CH_3)_2]$ in d_6-DMSO, was added to an NMR tube and frozen at -80 ^{o}C. An excess of glutathione in D_2O:DMSO was then added to the still frozen tube to halt any reaction. A ^{1}H NMR was taken every hour for antimony, and for bismuth a reading was repeatedly after the last up to a period of one hour. As hypothesised, the bismuth complex readily reduced to the parent acid and $BiPh_3$ after as little as five minutes (figure 2.1.28 and figure 2.1.29). Even at time point "0" i.e. the time it took for the machine to load the frozen tube and begin the NMR analysis, the bismuth complex had already begun to react with the glutathione. Therefore, it can be assumed the reaction is favourable and most likely due to the high reductive potential of Bi(V)/Bi(III).[43]

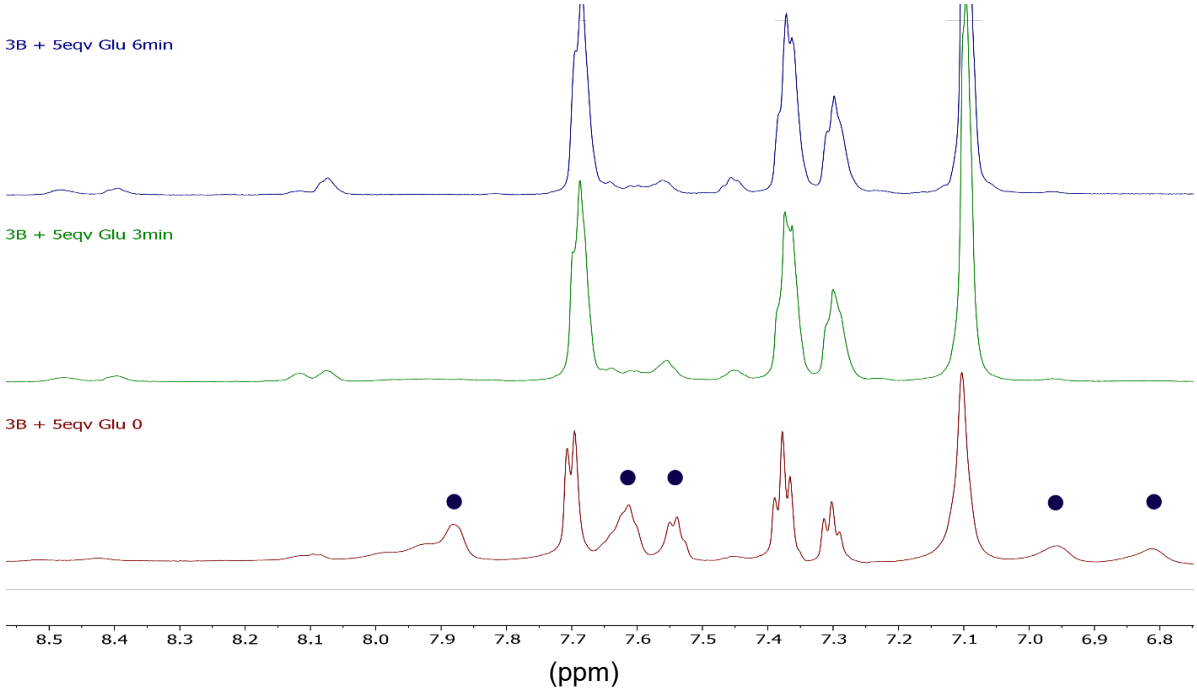

*Figure 2.1.29. ^{1}H NMR of complex **3B,** [$BiPh_3(O_2CCH_2C_6H_4CH_3)_2$], with an excess of GSH in d_6-DMSO:D_2O mix at time intervals t = "0" minutes, t = 3 minutes and t = 6 minutes. The complex **3B** has been labelled with dark-blue circles.*

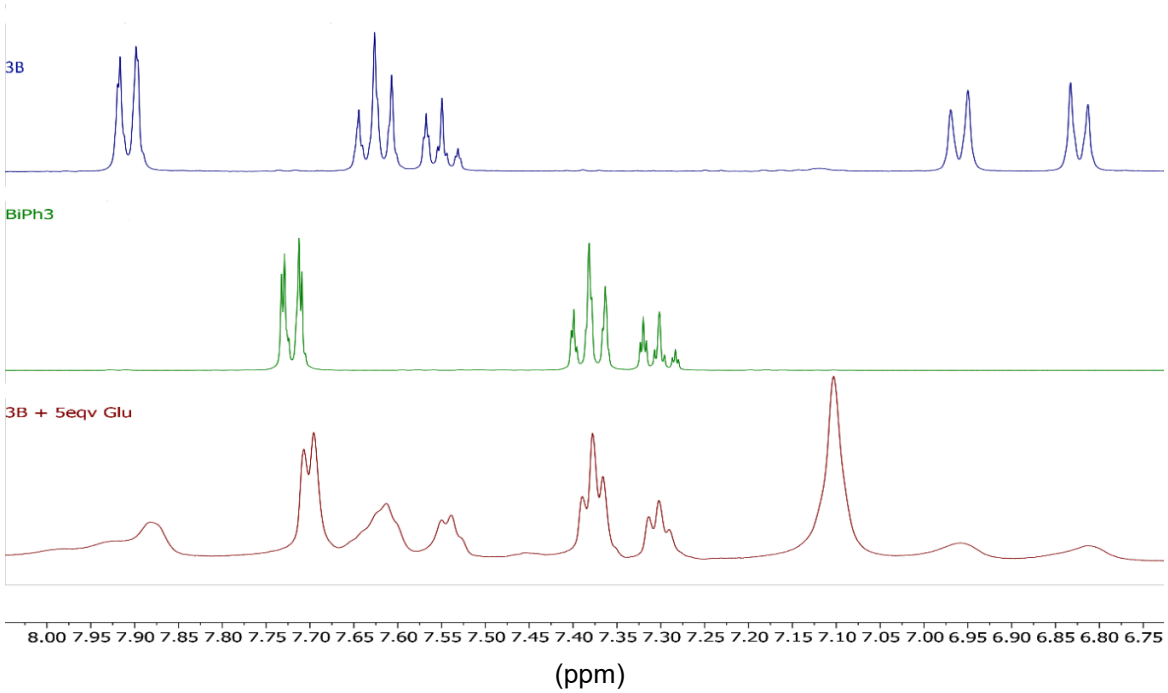

*Figure 2.1.30. ^{1}H NMR overlay of complex **3B**, [$BiPh_3(O_2CCH_2C_6H_4CH_3)_2$], $BiPh_3$ and **3B** + GSH (t = "0") highlighting the presence of both **3B** and $BiPh_3$ in the reaction mixture.*

The antimony complex took longer to react, though substantially faster than meglumine antimonate. Complex **3S** exhibited a half-life of approximately 54 minutes with a logarithmic decay observed (figure 2.1.31).

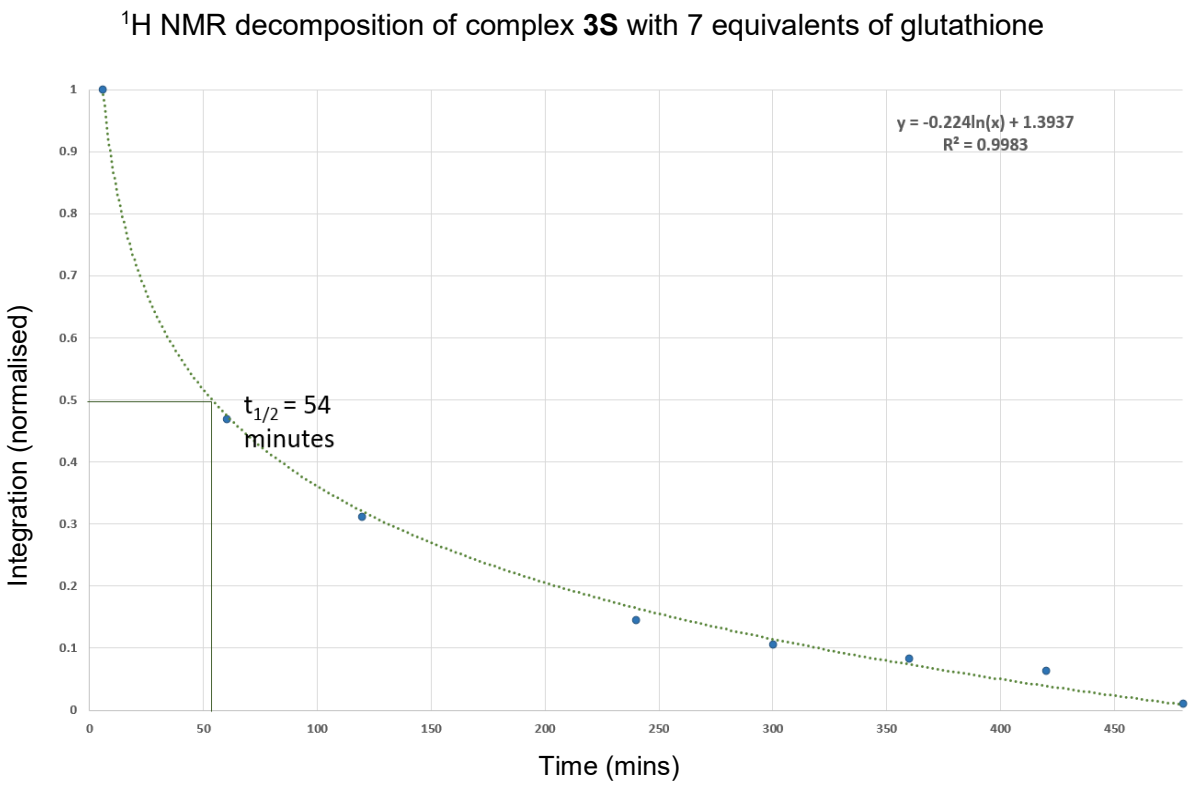

*Figure 2.1.31. ^{1}H NMR decomposition graph of **3S**, [$SbPh_3(O_2CCH_2C_6H_4CH_3)_2$], with an excess of GSH in d_6-DMSO:D_2O. Readings were taken hourly on a 600MHz Bruker NMR spectrometer at 25 ^oC. A decreasing signal of the original complex was compared to an increasing signal of $SbPh_3$ and a proton ratio obtained.*

As complex **3S** differs significantly from meglumine antimonite both structurally and chemically, it can be assumed that the reaction stoichiometry theorised by Frezard *et al* differs for that of our organometallic triaryl antimony and bismuth compounds. Utilising ^{1}H NMR a speculated reaction stoichiometry was predicted based on the hypothesis of Frezard *et al* in which Sb(V) will form $Sb(GS)_3$ upon reduction.[41] From the ^{1}H NMR experiment, it was clear that the parent acid, *p*-tolylacetic acid (**3**), and triphenyl antimony were present at the conclusion of the reaction in addition to the new signals for GSSG (figure 2.1.32). It has been suggested that glutathione undergoes oxidation by DMSO at concentrations equivalent to the cryoprotectant concentration

of 1.1 – 1.7 M, however as this oxidation was observed to be quite slow.[44] The rapid formation of GSSG in the NMR of both **S1** and **B1** suggests the complexes are causing the bulk of the oxidation, resulting in their own reduction. Both **S1** and **B1** are stable in wet DMSO exposed to the atmosphere for days, indicating that the addition of GSH does play a key role in their reduction.

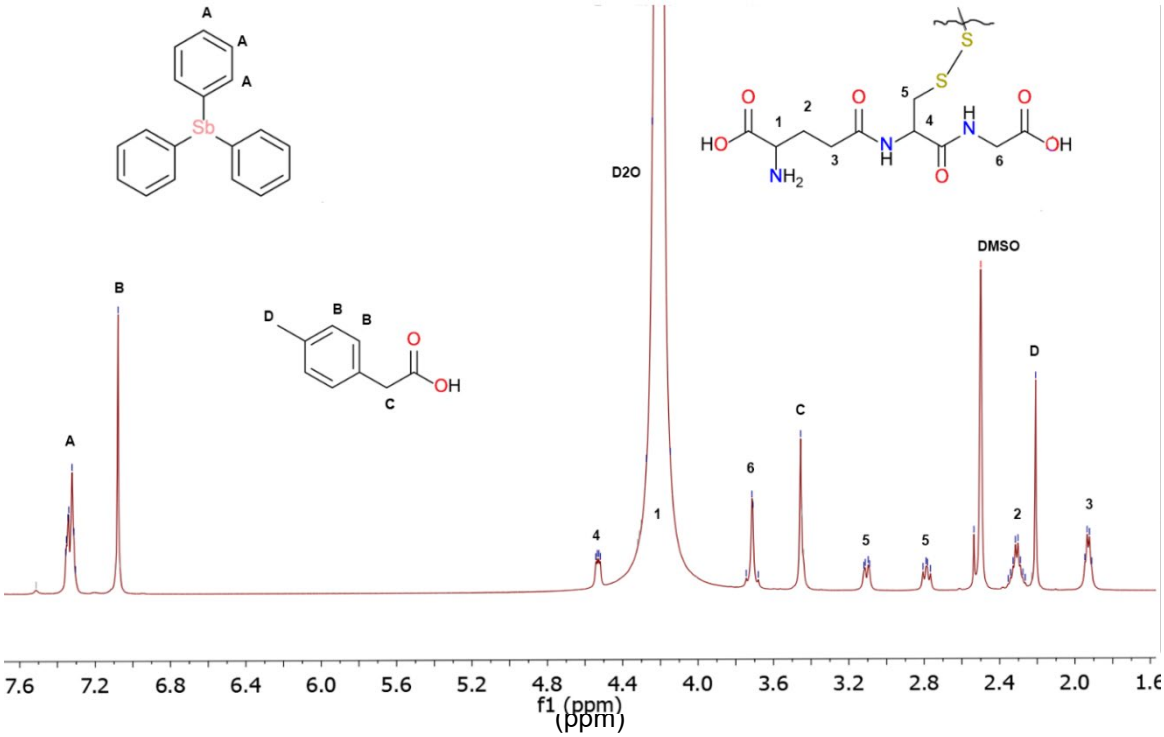

*Figure 2.1.32. ^1H NMR of complex **3S,** $[SbPh_3(O_2CCH_2C_6H_4CH_3)_2]$, with excess GSH after 24 hours. Assignments are given on the spectrum. d_6-DMSO and water are not labelled but appear at 2.50ppm and 4.22ppm respectively.*

From this a predicted stoichiometric equation was determined in which two equivalents of the organometallic complex would react with seven equivalents of GSH to form an equivalent of $SbPh_3$, four equivalents of *p*-tolylacetic acid (**3**), three equivalents of benzene and possibly the two equivalents of oxidised disulfide bridged GSSG (though difficult to determine an excess of GSH was used) and potentially $Sb(GS)_3$ (scheme 2.1.4).

Scheme 2.1.4. Speculated stoichiometry of antimony complexes with glutathione. Reaction conditions and all by-products have not been listed.

Despite this reaction of **3S**, and speculatively, all the antimony complexes with glutathione, complexes **1S**, **3S** – **7S'** were all found to exhibit little to no mammalian toxicity (2.1.5).

2.1.5. Biological activity

2.1.5.1 Leishmania promastigote and fibroblast assays

Despite bismuth complexes **1B** – **8B** exhibiting predicted instability in the culture media, all complexes were still included in the initial assays against both human fibroblasts and *L. major* promastigotes. This allowed for an assessment of their biological activity and mammalian toxicity to be compared to the analogous antimony complexes. Unsurprisingly the antimony complexes yielded a higher degree of solubility in the culture media, and based on the assessment of **3S**, $[SbPh_3(O_2CCH_2C_6H_4CH_3)_2]$, a higher degree of stability. Complexes **7B,** $[BiPh_3(O_2CCH_2O_2CCH_3)_2]$ and **8B,** $[BiPh_3(O_2CCH_2OC_6H_5)_2]$ showed some precipitation in the culture media, hindering an accurate concentration gradient to be established. This makes accurate IC_{50} values, and therefore an accurate assessment of toxicity difficult to obtain. As complexes **2S,** $[SbPh_3(O_2CCH_2C_6H_4CH_3)_2]$ and **8S,** $[SbPh_3(O_2CCH_2OC_6H_5)_2]$ have been tested previously on *L. major* and human fibroblasts, no further assays were conducted.[18] Though complexes **4S,** $[SbPh_3(O_2CCH_2C_6H_4OCH_3)_2]$ and **6S,** $[SbPh_3(O_2CCH_2C_6H_4OCH_3)_2]$ have been previously tested against *L. tropica* (with IC_{50} values of 18.3 µM and 20.9 µM respectively),[23] due to the physiological difference to *L. major* it was concluded to be appropriate to include them in the assay. Resistance to commercially available drugs has develops rapidly in the *L. major* species, making them a more pressing target.[45] To eliminate the possibility of the ligands themselves acting as anti-microbials, a separate study of the parent acetic

acids **1** – **8** was assessed, with their potential toxicity towards both mammalian cells and *L. major* promastigotes yielding little to no activity. IC_{50} values of $\geq$ 100 µm was obtained for all but **3** (*p*-tolylacetic acid) which yielded an IC_{50} value of 79.2 µM. Acids **6,** *p*-methoxyphenylacetic acid, **7,** acetoxyacetic acid and **8,** phenoxyacetic acid, exhibited a small degree of activity, with a slight drop in the % viability curve at concentrations > 12.5 µM, however they all still retained a viability of $\geq$ 100 µM. This change was insignificant in comparison to the complexed bismuth and antimony analogues **1B/S** – **8B/S** (figure 2.1.33).

All bismuth complexes were found to be non-selectively toxic, acting upon both human fibroblasts and *L. major* promastigotes. Conversely all antimony complexes, with the exception of **7S**, were found to be selective in their activity (figure 2.1.34). This was most likely attributed to their increased stability and solubility as opposed to the bismuth complexes.

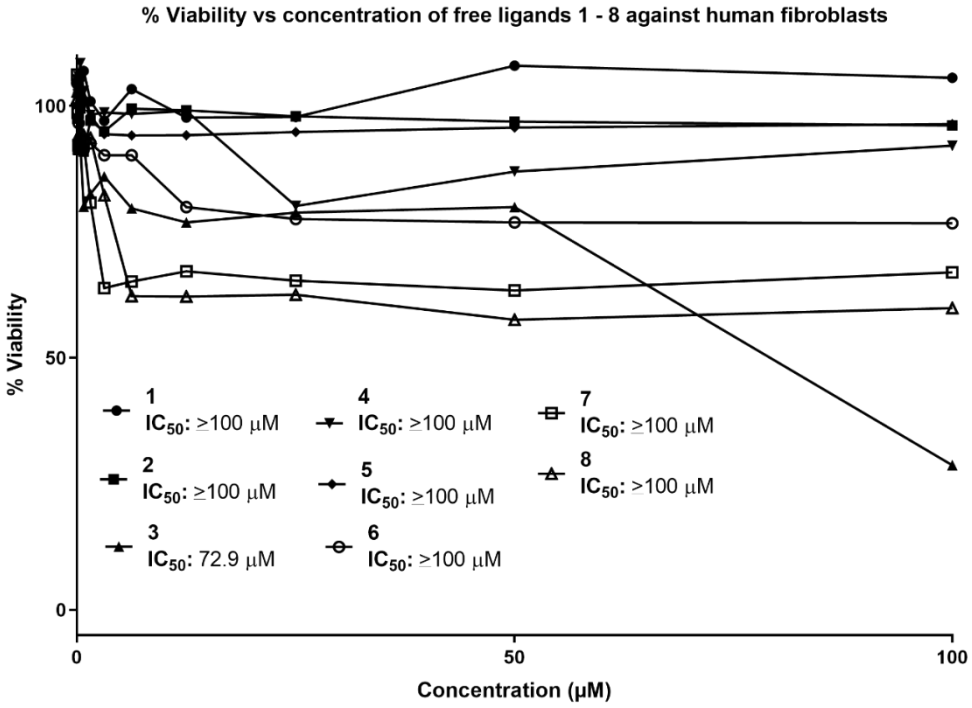

*Figure 2.1.33. % viability versus concentration of parent acids **1 – 8** against human fibroblasts.*

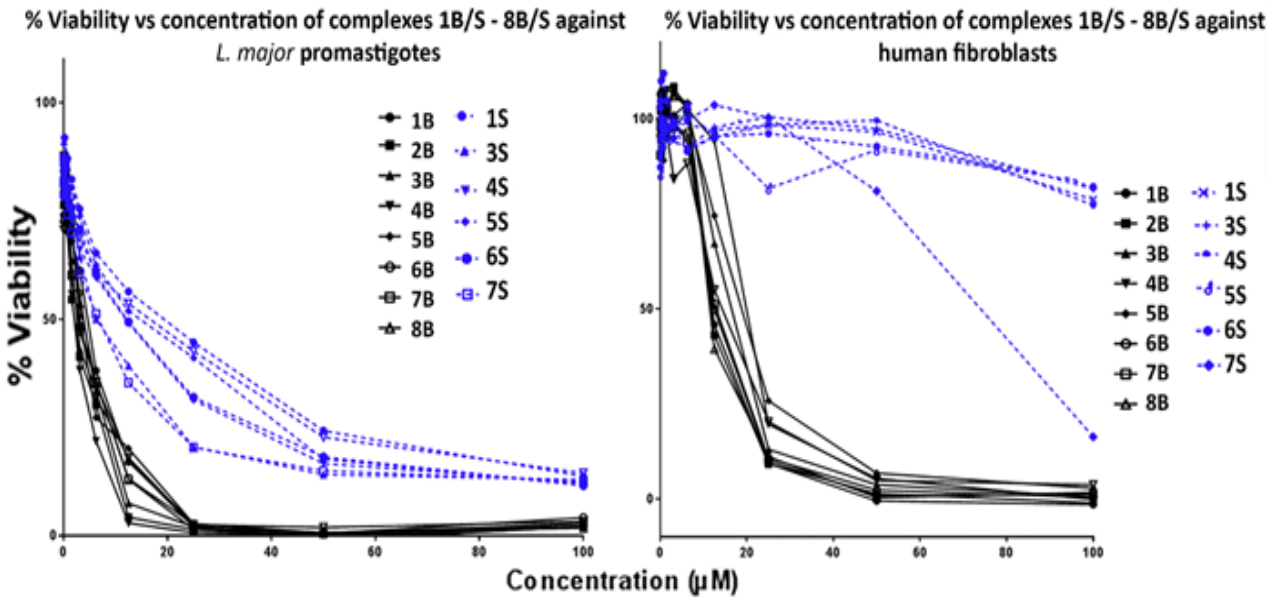

*Figure 2.1.34. Comparison of percentage cell viability after treatment with the Bi(V) complexes **1B – 8B (black)** and the Sb(V) complexes **1S – 8S (blue),** against L. major promastigotes and Human primary fibroblasts. Dose response curves were generated over a range of concentrations (48nM – 100µM in the appropriate culture media from 10mM DMSO stock solutions. All readings were compared spectroscopically to non-treated control and the percent growth inhibition calculated.*

Significantly better activity was observed for the bismuth complexes as opposed to antimony against the *L. major* promastigotes, with ranges of 2.06 µM – 4.63 µM and 6.18– 19.1 µM respectively. As the bismuth complexes presented with rapid and uncontrollable decomposition the actual concentration at which they exhibited activity could possibly be marginally lower than the calculated value, attesting to the potency of bismuth as an anti-parasitic. However due to the non-selective nature of the complexes, and with mammalian IC_{50} values within the ranges of 11.4 – 19.8 µM no further testing could be justified. In contrast to this, though not as potent as the bismuth complexes, the antimony complexes were selective in their activity, with mammalian IC_{50} values at $\geq$100 µM for all but one complex. The hydrolysis product **7S'** exhibited 50% cell death at 73.8 µM. Each complex and their corresponding activity has been tabulated below in tables 2.1.4 and 2.1.5.

Table 2.1.4. IC_{50} data of bismuth *complexes **1B** – **8B** against human fibroblasts and L. major promastigotes*

	1B	**2B**	**3B**	**4B**	**5B**	**6B**	**7B**	**8B**
Human Fibroblasts (IC_{50} µM)	11.8	12.1	16.4	19.8	18.7	12.9	12.4	11.4
***L. Major* promastigotes (IC_{50} µM)**	4.63	2.09	2.59	2.06	3.19	3.02	2.77	3.73

*Table 2.1.5. IC_{50} data of antimony complexes **1S** – **8S** against human fibroblasts and L. major promastigotes*

	1S	**3S**	**4S**	**5S**	**6S**	**7S'**
Human Fibroblasts (IC_{50} µM)	> 100	> 100	> 100	> 100	> 100	73.8
***L. Major* promastigotes (IC_{50} µM)**	19.1	6.18	11.8	14.4	12.1	6.62

2.1.5.2 Amastigote invasion assay

As the selectivity of the antimony complexes was found to greatly surpass that of the bismuth analogues, they qualified for the amastigote invasion assay. The parasites live, grow and replicate via a digenetic life-cycle. The form predominately found in the human vectors is the intercellular amastigote. Macrophages were cultured and infected with *L. major* promastigotes. These promastigotes were able to enter the macrophages and differentiate into amastigotes over a period of 24 – 48 hours depending on the level of infection. Complexes **1S,** $[SbPh_3(O_2CCH_2C_6H_4CH_3)_2]$, **3S,** $[SbPh_3(O_2CCH_2C_6H_4CH_3)_2]$, **4S,** $[SbPh_3(O_2CCH_2C_6H_4OCH_3)_2]$, **5S,** $[SbPh_3(O_2CCH_2C_6H_4OCH_3)_2]$, **6S,** $[SbPh_3(O_2CCH_2C_6H_4OCH_3)_2]$ and **7S',** $[SbPh_3(O_2CCH_2C_6H_4CH_3)_2]$ were added to each well at a concentration of 10 µM for a further 48 hours. After which, slides were washed, fixed and stained. An assessment of biological activity was determined by counting the infected cells versus non-infected (figure 2.1.35).

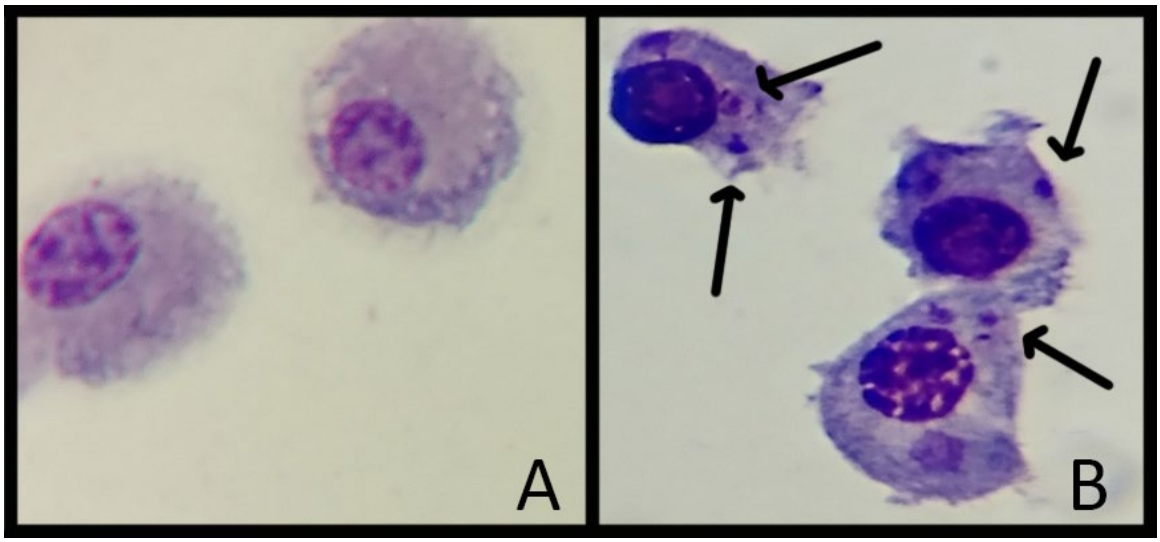

Figure 2.1.35. ***A)*** *Healthy non-infected macrophages;* ***B)*** *Heavily infected macrophages, amastigotes are labelled.*

All cells counts were compared against a positive control of untreated infected macrophages and were found to exhibit statically significant activity. This anti-amastigote activity ranged from mild to good. Only complex **7S'** was found to be unviable due to apparent cytotoxicity to both the mammalian cells and the parasites. This was concluded by the absence of viable cells (both macrophage and parasite) on either coverslip. In terms of activity, the percentage of infected cells ranged from 7.75 – 40.5 %, with complex **1S** presenting as the least effective and complex **6S** the most. A trend was observable after conclusion of the data work up, with the infection decreasing from **1S** – **6S**. This trend related not only to the functional group on the phenyl ring but the position of said functional group. **1S**, the *o*-tolylacetate, was the least effective of the tolylacetates, with *p*-tolylacetate the more effective (22.3 % $\pm$ 1.55). The methoxyphenyl acetates were more effective than either tolylacetate, and again a trend was observed with *o*-OMe $\leq$ *m*-OMe $\leq$ *p*-OMe, with values of 19.0 % $\pm$ 1.58, 14.5 % $\pm$ 2.63 and 7.75 % $\pm$ 1.18 **4S**, **5S** and **6S** respectively (figure 2.1.36).

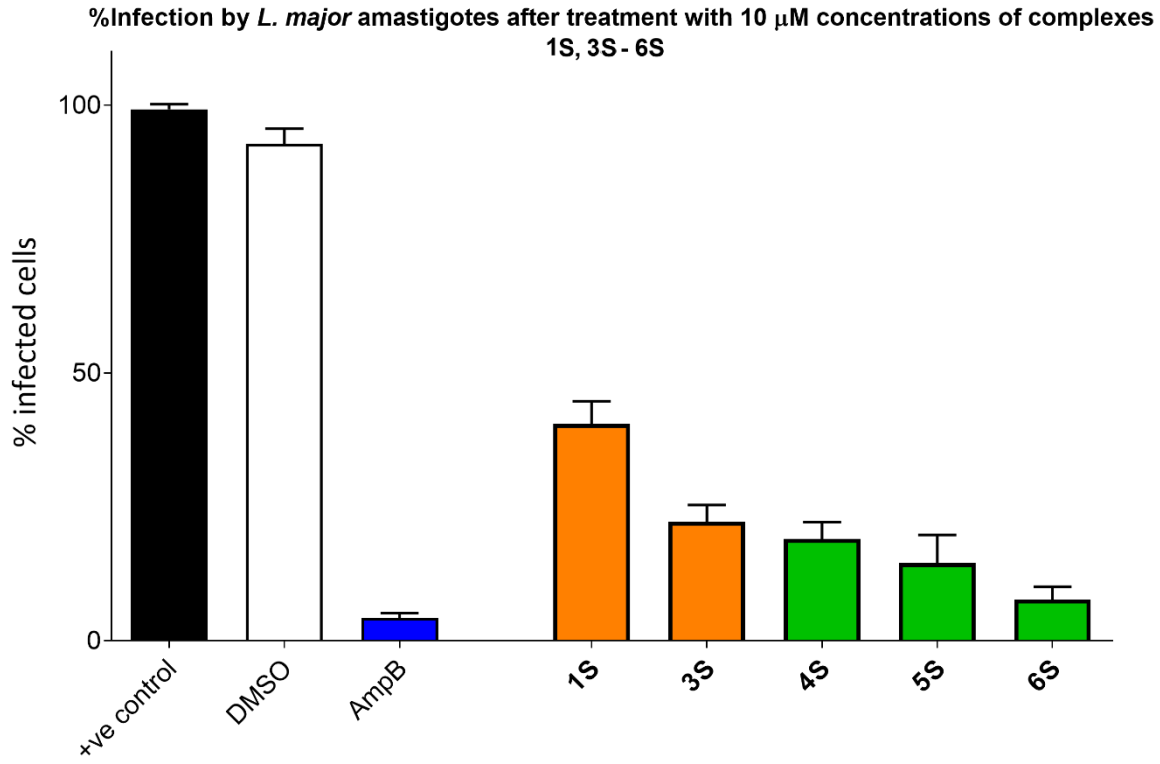

Figure 2.1.36. Infected macrophages after 48 hours. Number of infected macrophages was determined microscopically, in duplicate of fixed specimens. Amphotericin B (AmpB) was used as a positive control at 10 μM concentration. A DMSO control was also employed at a 1% concentration. Error bas indicate SEM, one-way ANOVA. Dunnett's multiple comparison test was used to determine the statistical significance between all test compounds and a positive control lacking treatment (+ve control).

Though these complexes showed some activity, they still lacked the excellent activity of previously synthesised Sb(V) carboxylates (percentage infection ranges of 0.5 – 3.5 μM).[18] Several of these reported complexes were able to completely eliminate infection of the macrophages, a feature that was not observed with this current class of Sb(V) carboxylates.[18] Still, the previous complexes exhibited a greater degree of mammalian toxicity, and were less selective. Due to a high degree of selectivity of this current class of Sb(V) carboxylates, an increase of the concentration in the amastigote invasion assay is possible. This would hopefully initiate a greater degree of activity, while remaining relatively non-toxic. For this reason, the complexes still present as potential drug candidates with further testing required.

2.1.6 Conclusions

This section highlights a series of triphenyl bismuth and triphenyl antimony carboxylates that were synthesised, characterised and their biological activity assessed. These complexes of the general formula $[MPh_3(O_2CR)_2]$ (excluding the oxido bridged **7S** of the formula $[(SbPh_3((O_2CCH_2OCO)Me))_2O]$), **1B** – **8B,** $[BiPh_3(O_2CCH_2C_6H_4CH_3)_2]$, $[BiPh_3(O_2CCH_2C_6H_4CH_3)_2]$, $[BiPh_3(O_2CCH_2C_6H_4CH_3)_2]$, $[BiPh_3(O_2CCH_2C_6H_4OCH_3)_2]$, $[BiPh_3(O_2CCH_2C_6H_4OCH_3)_2]$, $[BiPh_3(O_2CCH_2C_6H_4OCH_3)_2]$, $[BiPh_3(O_2CCH_2O_2CCH_3)_2]$, $[BiPh_3(O_2CCH_2OC_6H_5)_2]$ and **1S** – **6S** and **8S**, $[SbPh_3(O_2CCH_2C_6H_4CH_3)_2]$, $[SbPh_3(O_2CCH_2C_6H_4CH_3)_2]$, $[SbPh_3(O_2CCH_2C_6H_4CH_3)_2]$, $[SbPh_3(O_2CCH_2C_6H_4OCH_3)_2]$, $[SbPh_3(O_2CCH_2C_6H_4OCH_3)_2]$, $[SbPh_3(O_2CCH_2C_6H_4OCH_3)_2]$, $[SbPh_3(O_2CCH_2OC_6H_5)_2$ were obtained as crystalline compounds from a one-pot oxidative addition reaction, without the need for further purification. All the bismuth complexes were novel in nature as were four of the eight antimony complexes (**1S**, **3S**, **5S** and **7S**). Though complexes **4S**, **6S** and **8S** had been previously reported, their solid-state structures had not been elucidated. The only difference for complex **2S** was the synthetic method, Andrews *et al* had formerly used a salt metathesis of the carboxylate salt with $SbPh_3Cl_2$ to obtained the complex, here we employed a more efficient and cleaner oxidative addition with t-BuOOH was utilised. Analytical analysis of these complexes included ^{1}H and ^{13}C NMR, FT-IR, melting point, elemental analysis and X-ray analysis.

All complexes, excluding complex **2S**, were able to undergo analysis by single crystal X-ray diffraction to elucidate their solid-state structures. Similar to previously synthesised complexes, the bismuth analogues are seven coordinate and all but one antimony compounds five. The phenyl rings sit in the equatorial plane in a propeller like orientation whilst the acetates occupy the axial positions. Through IR spectroscopy in addition to the X-ray analysis, it was concluded the bismuth complexes had the acids bind in a *bi*dentate fashion, while the antimony complexes preferred a *mono*dentate binding mode. Complex **7S** was the only exception forming an oxido bridged

complex. This complex was also observed to have limited stability in aqueous/polar media, such as DMSO, undergoing hydrolysis into the *mono*-hydroxido complex, [$SbPh_3(O_2COCO_2CH_3)OH$], **7S'**.

Varying stability was observed for bismuth versus antimony, with emphasis on the reactivity with the mammalian tripeptide glutathione. The organometallic antimony complexes were found to reduce to the parent acid and $SbPh_3$ in a logarithmic decay, with a half-life of 54 minutes extrapolated from a ^1H NMR study over a period of eight hours. The presence of GSSG was observed though in excess due to the slow oxidation of GSH in D MSO.[43] It was hypothesised that the resulting reaction not only yielded the starting reagents but also the antimony – glutathione complex $Sb(GS)_3$. Unsurprisingly the bismuth complex **3B** underwent rapid reduction in a matter of minutes upon exposure to glutathione, further highlighting the large stability differences between itself and antimony. This increased reactivity too may potentially play a large role in the non-selective activity of these complexes.

All complexes were then assessed for their anti-Leishmanial activity and their mammalian cytotoxicity. Percentage viability assays were able to ascertain the difference in the biological activity of bismuth versus antimony. The bismuth complexes **1B** – **8B** were all found to be excellent anti-Leishmanials (to the promastigotes) but unfortunately also proved very cytotoxic to the mammalian fibroblast control. The antimony complexes however proved fruitful with complexes **1S, 3S** – **7S'** being selectively toxic to parasites with minimal to no cytotoxicity towards mammalian controls. Though less active than the bismuth complexes towards *L. major* promastigotes (2.06 µM – 4.63 µM versus 6.18– 19.1 µM for Bi/Sb respectively) the complexes were still significantly effective and therefore were screened for their anti-amastigote activity. Structure activity relationships were observed with the amastigote assay, with the percentage of infected cells increasing in the order of *o*-OMe $\leq$ *m*-OMe $\leq$ *p*-OMe for the methoxyphenyl antimony complexes **4S**– **6S**.

A similar trend was observed for the tolylacetates, with **3S**, the *p*-tolylacetate complex, exhibiting a higher degree of activity over the *o*-tolylacetate analogue. Overall **6S** presented as the most promising candidate, with a percentage infection value of 7.75% ± 1.18. Further analysis of these complexes *in vivo* would solidify their potential as lead compounds in the effort to eradicate the devastating disease *Leishmania.*

This study has highlighted the important differences between the group 15 metals antimony and bismuth, including major differences in reactivity, stability and biological activity when in the pentavalent state. The high reactivity of bismuth with sulfur containing moieties within biological systems is speculated to have greatly contributed to the non-selective activity we have observed. The use of antimony as metallodrugs in regards to *Leishmania* seems advantageous, with a high degree of stability in culture media and a superior degree of cell selectivity. Further analysis of these complexes in more clinically relevant *in vivo* settings is still required to conclude the full efficacy and activity of these complexes for further medicinal use. Future prospects for aryl Sb(V) carboxylates are promising, and are an area of study that should not go neglected.

2.1.7 References

1. H. Gilman and H. L. Yale, *J. Am. Chem. Soc.*, 1951, **73**, 4470-4471.
2. R. Goel and H. Prasad, *Can. J. Chem.*, 1970, **48**, 2488-2493.
3. R. Goel and H. Prasad, *J. Organomet. Chem.*, 1972, **36**, 323-332.
4. A. Ouchi, H. Honda and S. Kitazima, *J. Inorg. Nucl. Chem.*, 1975, **37**, 2559-2561.
5. U. Dittes, B. K. Keppler and B. Nuber, *Angew. Che. Int. Ed. Engl*, 1996, **35**, 67-68.
6. U. Dittes, E. Vogel and B. K. Keppler, *Coord. Chem. Rev.*, 1997, **163**, 345-364.
7. R. Agrawal, J. Sharma, D. Nandani, A. Batra and Y. Singh, *J. Coord. Chem.*, 2011, **64**, 554-563.
8. L. G. d. Oliveira, M. M. Silva, F. Paula, E. C. Pereira-Maia, C. L. Donnici, C. A. d. Simone, F. Frézard, E. N. Júnior and C. Demicheli, *Molecules*, 2011, **16**, 10314-10323.
9. T. Murafuji, Y. Miyoshi, M. Ishibashi, A. M. Rahman, Y. Sugihara, I. Miyakawa and H. Uno, *J. Inorg. Biochem.*, 2004, **98**, 547-552.
10. M. Khan, S. Gul, I. Hussain, M. A. Khan, M. Ashfaq, F. Ullah, G. F. Durrani, I. B. Baloch and R. Naz, *Org. Med. Chem. Lett.,* 2011, **1**, 2.
11. M.-X. Li, M. Yang, J.-Y. Niu, L.-Z. Zhang and S.-Q. Xie, *Inorg. Chem.*, 2012, **51**, 12521-12526.
12. P. J. Heard, *Prog. Inorg. Chem.*, 2005, **53**, 1-69.
13. G. Hogarth, *Mini Rev. Med. Chem.*, 2012, **12**, 1202-1215.
14. W. M. Haynes, *CRC handbook of chemistry and physics*, CRC press, 2014.
15. M. N. Rocha, P. M. Nogueira, C. Demicheli, L. G. de Oliveira, M. M. da Silva, F. Frézard, M. N. Melo and R. P. Soares, *Bioinorg. Chem. Appl.*, 2013, **2013**.
16. A. Islam, J. G. Da Silva, F. M. Berbet, S. M. da Silva, B. L. Rodrigues, H. Beraldo, M. N. Melo, F. Frézard and C. Demicheli, *Molecules*, 2014, **19**, 6009-6030.
17. R. N. Duffin, V. L. Blair, L. Kedzierski and P. C. Andrews, *Dalton Trans.*, 2018, **47**, 971-980.
18. M. I. Ali, M. K. Rauf, A. Badshah, I. Kumar, C. M. Forsyth, P. C. Junk, L. Kedzierski and P. C. Andrews, *Dalton Trans.*, 2013, **42**, 16733-16741.
19. Y. C. Ong, V. L. Blair, L. Kedzierski and P. C. Andrews, *Dalton Trans.*, 2014, **43**, 12904-12916.
20. Y. C. Ong, V. L. Blair, L. Kedzierski, K. L. Tuck and P. C. Andrews, *Dalton Trans.*, 2015, **44**, 18215-18226.
21. R. D. Hancock, *J. Chem. Educ*, 1992, **69**, 615.
22. Y. Kim, J.-Y. Cho, J.-H. Kuk, J.-H. Moon, J.-I. Cho, Y.-C. Kim and K.-H. Park, *Curr. Microbiol.*, 2004, **48**, 312-317.
23. R. Mushtaq, M. K. Rauf, M. Bolte, A. Nadhman, A. Badshah, M. N. Tahir, M. Yasinzai and K. M. Khan, *Appl. Organomet. Chem.*, 2017, **31**.
24. V. Sharutin, I. Egorova, O. Sharutina, T. Ivaneko, M. Pushilin and A. Gerasimenko, *Chem. Comput. Simul. Butlerov Commun*, 2002, **9**, 59-64.
25. D. V. Moiseev, Y. B. Malysheva, A. S. Shavyrin, Y. A. Kurskii and A. V. Gushchin, *J. Organomet. Chem.*, 2005, **690**, 3652-3663.
26. A. Gushchin, E. Dyomina and V. Dodonov, *Russ. Chem. Bull.*, 1995, **44**, 937-940.
27. V. Sharutin, O. Sharutina, E. Artem'eva and M. Makerova, *Russ. J. Gen. Chem.*, 2016, **86**, 2671-2676.
28. R. N. Duffin, V. L. Blair, L. Kedzierski and P. C. Andrews, *J. Inorg. Biochem.*, 2018, **189**, 151-162.
29. H. Barucki, S. J. Coles, J. F. Costello, T. Gelbrich and M. B. Hursthouse, *J. Chem. Soc. Dalton Trans.*, 2000, **14**, 2319-2325.
30. H. Barucki, S. J. Coles, J. F. Costello and M. B. Hursthouse, *J. Organomet. Chem.*, 2001, **622**, 265-273.

31. H. Barucki, S. J. Coles, J. F. Costello and M. B. Hursthouse, *Chem. Eur. J.*, 2003, **9**, 2877-2884.
32. N. N. Greenwood, *Spectroscopic properties of inorganic and organometallic compounds*, Royal Society of chemistry, 2007.
33. G. Deacon and R. Phillips, *Coord. Chem. Rev.*, 1980, **33**, 227-250.
34. N. C. Norman, *Chemistry of arsenic, antimony and* bismuth, Springer Science & Business Media, 1997.
35. V. K. Cherkasov, G. A. Abakumov, E. V. Grunova, A. I. Poddel'sky, G. K. Fukin, E. V. Baranov, Y. V. Kurskii and L. G. Abakumova, *Chem. Eur. J.*, 2006, **12**, 3916-3927.
36. I. Kumar, P. Bhattacharya and K. H. Whitmire, *Organometallics*, 2014, **33**, 2906-2909.
37. L. Quan, H. Yin and D. Wang, *Acta Crystallogr. Sect. Sect. E.*, 2009, **65**, 99.
38. L. Quan, H. Yin and D. Wang, *Acta Crystallogr. Sect. Sect. E.*, 2008, **64**, 349.
39. H. Preut, R. Rüther and F. Huber, *Acta Crystallogr. Sect. C.*, 1985, **41**, 358-360.
40. A. Meister and M. E. Anderson, *Annu. Rev. Biochem.*, 1983, **52**, 711-760.
41. F. Frézard, C. Demicheli, C. S. Ferreira and M. A. Costa, *Antimicrob. Agents Chemother.*, 2001, **45**, 913-916.
42. C. dos Santos Ferreira, P. S. Martins, C. Demicheli, C. Brochu, M. Ouellette and F. Frézard, *BioMetals*, 2003, **16**, 441-446.
43. H. Sun, *Biological chemistry of arsenic, antimony and* bismuth, Wiley Online Library, 2011.
44. N.Z. Homer, J. Reglinski, R. Sowden, C.M. Spickett, R. Wilson, J.J. Walker, *Cryobiology.*, 2005, **50,** 317-324
45. P. Escobar, S. Matu, C. Marques and S. L. Croft, *Acta Trop.*, 2002, **81**, 151-157.

2.2 Synthesis, characterisation and biological activity of Sb(V) *mono*-hydroxy quinolinolato complexes

2.2.1 Antimony in medicine

Antimony is a group 15 metalloid part of the pnictogen group, including nitrogen, phosphorus, arsenic and bismuth.[1] It has two naturally occurring stable isotopes and is commonly found in ores as either the sulfide, stibnite (Sb_2S_3) or the nitro-sulfide, Ullmanite (NiSbS). In contrast to the heavy metal bismuth, antimony is often described as a semi-metal, more closely related to arsenic. Antimony exist commonly in two stable oxidation states, +III and +V with ionic radii of 0.76 and 0.62 A respectively.[2] In the +III oxidation state, antimony forms complexes by means of a Lewis acid-base reaction with the valence orbitals of the metal centre. The lone $5s^2$ electron pair do not participate in bonding in the trivalent state.[3] The lone pair becomes active in the +V state and is able to participate in bonding, often leading to the formation of octahedral and/or distorted octahedral complexes.[4] Trigonal bipyramid coordination geometry is another often commonly observed configuration of Sb(V) complexes (Figure 2.2.1).[5]

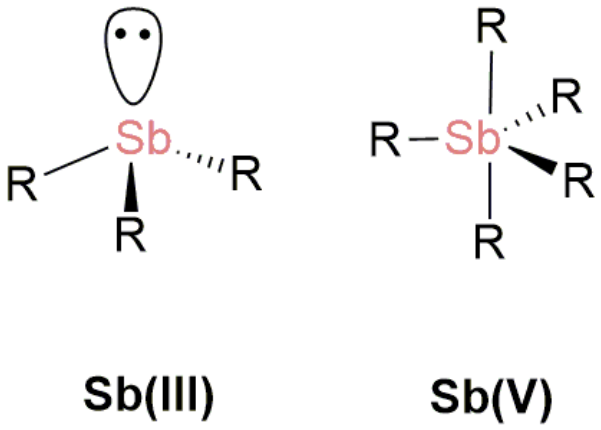

Figure 2.2.1. Common oxidation states and configurations of antimony

Antimony has been used medicinally for many years, stemming back centuries.[6] Historically, it was first used by the ancient Egyptians for the treatment of fevers and skin irritation. It was also

considered a great cosmetic due to the vivid colours the compounds could display.[7, 8] As discussed previously, antimony was first established as an anti-parasitic in the +III form as antimony potassium tartrate. Though an increase in parasitic death was observed, the increased risk to humans due to antimony toxicity lead to tatar emetic to be discontinued for use.[9, 10] Antimony complexes in the +V state were then investigated for their therapeutic activity. The pentavalent antimony complexes were found to be at least ten times less toxic to humans than the trivalent counterparts and exhibited a higher degree of activity.[11] As the complexes of antimony displayed excellent selectivity in section 2.1,[12, 13] an investigation into the activity of aryl Sb(V) complexes with a medically relevant ligand class was probed next.

2.2.2 Quinolinol

the heterocyclic 8-hydroxyquinoline, or 8-quinolinol (8QH) is an organic *N,O* donor (figure 2.2.2). It has been extensively studied in the literature in both medicinal and synthetic applications, where it is usually bound to a stabilising metal.

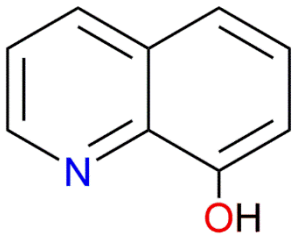

8-hydroxyquinoline, 8-quinolinol **(8QH)**

Figure 2.2.2. Structure of 8-hydroxyquinoline, known commonly as 8-quinolinol.

The biological application of quinolinol was extensively investigated by Albert *et al* in several studies which focused on anti-bacterial applications.[14,15] Interestingly, what Albert *et al* discovered was the biological activity of 8QH was directly affected by the presence of metal ions in the cell media. When the metal salts were removed a lower degree of activity was quantified. This

suggested that the chelate form is more bioactive.[14, 15] Expansion into the activity of 8QH and its derivatives on other strains of bacteria has been reported in the literature.[16] Bactericidal activity is not the only biological application that has been assessed. The anti-microbial applications of 8QH have been extended into the area of anti-parasitics. Excellent activity was observed for 8QH against three separate strains of *Leishmania* in both the promastigote (table 2.2.1) and the amastigote form (table 2.2.2). Initial animal studies utilising BALB/c mice infected with cutaneous strains of *Leishmania* exhibited a reduction in the lesion diameters, demonstrating the potential application both *in vitro* and *in vivo*.[17]

Table 2.2.1. MTT colorimetric assay results for 8QH versus three strains of Leishmania. Selectivity indices are also listed.

Strain	***L. amazonesis***	***L. infantum***	***L. braziliensis***
IC_{50} (μg mL^{-1})/Selectivity index	0.05 + 0.02 / 328.0	0.26 + 0.04 / 62.0	0.35 + 0.06 / 47.0

Table 2.2.2. Infectiveness reduction of Leishmania amastigotes in pre-infected macrophages.

Concentration (μg mL^{-1}/ μM)	**Infectiveness reduction (%)**		
	L. amazonesis	***L. infantum***	***L. braziliensis***
10.0/ 68.9	82.3 ± 3.3	86.1 ±2.2	70.6 ± 3.1
5.0/34.5	76.2 ± 2.4	82.6 ± 1.0	58.1 ± 1.7
2.5/17.2	68.0 ± 1.7	71.0 ± 3.3	48.4 ± 2.2

Several of the halido substituted quinolinols have also been previously investigated to treat a variety of ailments, including bacteria, fungi and protozoa. Figure 2.2.3 highlights the six 8-quinolinol derivatives utilised in this study.

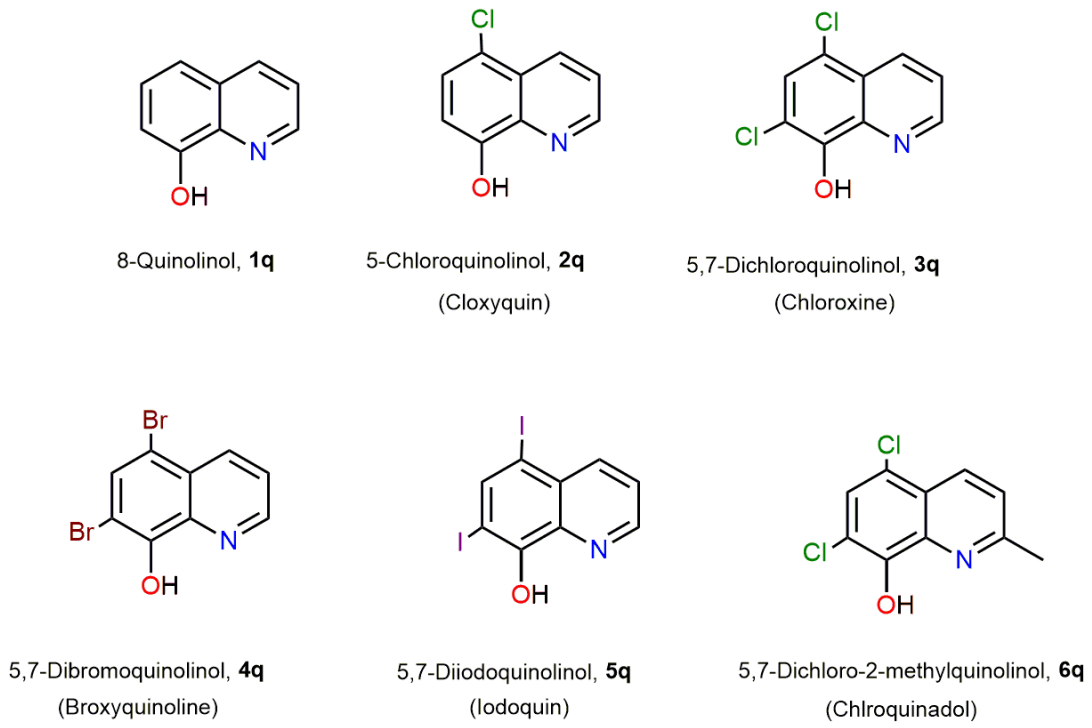

Figure 2.2.3. Structures of the six 8-quinolinol containing compounds utilised in this study. Common names are also listed.

5-chloroquinolinol, or cloxyquin, has been studied as both an anti-bacterial and anti-fungal complex. It has been shown to exhibit activity against *Mycobacterium tuberculosis,* including strains that are classified as resistant to common first line antibiotics.[18] Addition of another chloride in the seven position forms the 5,7-dichloroquinolinol, which is commonly known as chloroxine, an anti-fungal and anti-bacterial agent still widely used today.[19] The methyl substituted 5,7-dichloro-2-methyl-quinolinol (chlorquinaldol) has undergo strenuous testing of its medical properties, with literature dating back to the 1950s reporting topical effects on fungi.[20] More recent studies have also been published highlighting its biological activity.[21] Both the 5,7-dibromoquinolinol, broxyquinoline and 5,7-diiodoquinolinol, iodoquin, have also been studied as potential medicinals, though are less efficient than the chloro substituted analogues. Iodoquin was established as an anti-protozoan, however, was found to be toxic and cause potentially severe side-effects when used topically.[22-24] By chelating these compounds to a metal, it is anticipated

that the medicinal effects may be fine-tuned, leading to enhanced selectivity and diminished side-effects. The idea of using an aryl antimony is to mitigate the hydrophilicity of the front-line pentavalent antimony treatments for *Leishmania*, to potentially allow for oral consumption of the drugs. Therefore, it was theorised that by incorporating these medically active organics into the more lipophilic Sb(V) precursors, that a new class of anti-Leishmanial complexes could be produced. These differed from the conventional triaryl carboxylate, by utilising an *N,O* binding mode through a deprotonated alcoholic hydroxyl moiety. From this, six new novel complexes **1Sq,** $[SbPh_3(C_9H_6NO)(OH)]$, **2Sq,** $[SbPh_3(C_9H_5NOCl)(OH)]$, **3Sq,** $[SbPh_3(C_9H_5NOCl_2)(OH)]$, **4Sq,** $[SbPh_3(C_9H_4NOBr_2)(OH)]$, **5Sq,** $[SbPh_3(C_9H_4NOI_2)(OH)]$ and **6Sq**, $[SbPh_3(C_9H_3NOCl_2CH_3)(OH)]$, were synthesised, fully characterised and their anti-Leishmanial activity assessed. Complexes of this general formula were not previously known in the literature and are the first examples of Sb(V) triaryl *mono*-hydroxido quinolinolates (figure 2.2.4).

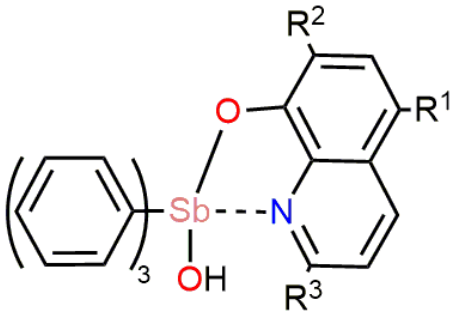

R¹= H, Cl, Cl, Br, I, Cl
R²= H, H, Cl, Br, I, Cl
R³= H, H, H, H, H, Me

*Figure 2.2.4. General formula of the complexes **1Sq** – **6Sq**.*

2.2.3 Synthesis and characterisation

2.2.3.1 Synthesis

Similar to the synthesis of the series of acetate complexes (section 2.1), the quinolinol complexes were formed via an oxidative addition of tertiary-butyl hydroperoxide to the triaryl antimony precursor (scheme 2.2.1). The initial approach was the addition of peroxide to two equivalents of the desired quinolinol to generate the *bis*-substituted complex similar to the formation of the common triaryl Sb(V) carboxylate complexes. However, it was found by ^{1}H NMR spectral analysis of the product of the 8-quinolinol complex, **1Sq**, that this was not the case. The synthetic route follows the initial oxidation to the $SbPh_3(OH)_2$ precursor, whereby condensation subsequently occurs at one hydroxyl, forming a *mono*-hydroxido quinolinolate complex (scheme 2.2.2). Even when heating the *mono*-hydroxido quinolinolate complex with an additional equivalent of the quinolinol, no formation of the *bis* complex is observed.

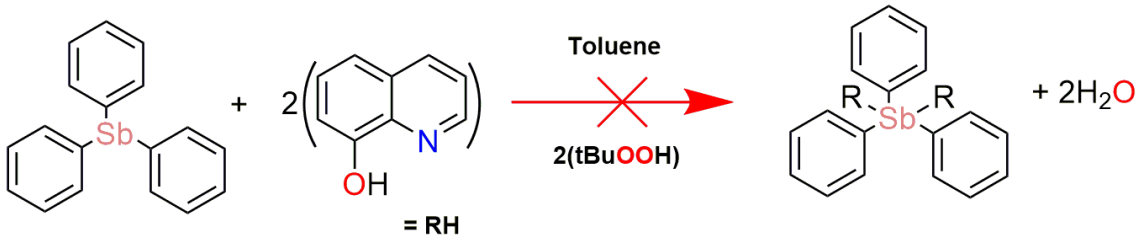

Scheme 2.2.1. Hypothesised pathway for formation of Sb(V) quinolinolate complexes.

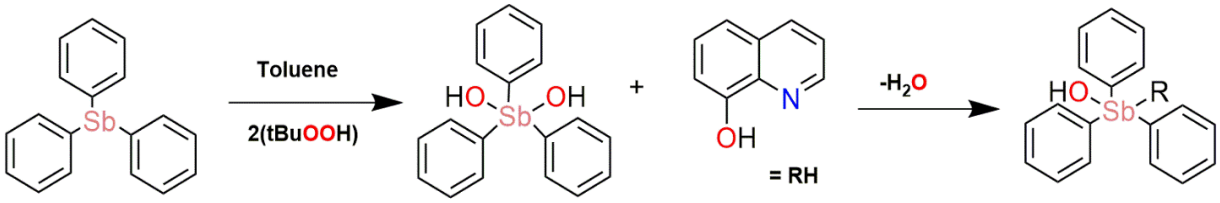

*Scheme 2.2.2. General scheme for the experimentally determined pathway for the formation of the mono-hydroxy quinolinolato Sb(V) complexes **1Sq – 6Sq**. All reaction conditions and biproducts are not listed.*

Therefore, an adjustment was made to the synthesis to isolate the desired Sb(V) complex in a higher yield, with minimal by-products. Only one equivalent of the quinolinol was added to the oxidised triaryl antimony precursors in the correct product stoichiometry. All reactions were performed in toluene or diethyl ether. Solubility of the quinolinol reagents decreased as the halide substitution increased, however, the solubility of $SbPh_3$ in both solvents ensured the heterogeneous reaction was still able to proceed. All the products were easily obtained by removal of the solvent, tBuOH and H_2O under reduced pressure. The initial crude product obtained was a yellow oil, however sonication in H_2O resulted in the isolation of each complex as a bright yellow powder. Complex **6Sq,** $[SbPh_3(C_9H_3NOCl_2CH_3)(OH)]$, differed, yielding a green solid. This variation in colour was the result of the quinolinol binding to the metal centre, as all the starting reagents, **1** – **6**, were off white or pale yellow. Yields for these complexes ranged from 72 – 90 %. All complexes synthesised are novel and the first of their kind, with the only marginally similar complex in the literature a triphenyl antimony(V) *mono*chloro 8-quinolinol complex synthesised in 1969.[25]

2.2.3.2. Characterisation

All complexes were characterised by ^1H and ^{13}C NMR, FT-IR, mp, elemental analysis and X-ray crystallography. The ^1H and ^{13}C NMR spectroscopic analysis was undertaken in d_6-DMSO for both carbon and hydrogen spectra. Binding was characterised by the lack of the hydroxyl proton of the parent quinolinol in the ranges of 9.78 ppm – 11.05 ppm. The shift to higher frequencies for the phenyl protons of the antimony reagent ($SbPh_3$) is characteristic of these triaryl Sb(V) complexes.[12, 13, 26] The ^1H NMR of an example complex **2Sq,** $[SbPh_3(C_9H_5NOCl)(OH)]$, is given below along with a comparison to the two parent reagents (figure 2.2.5).

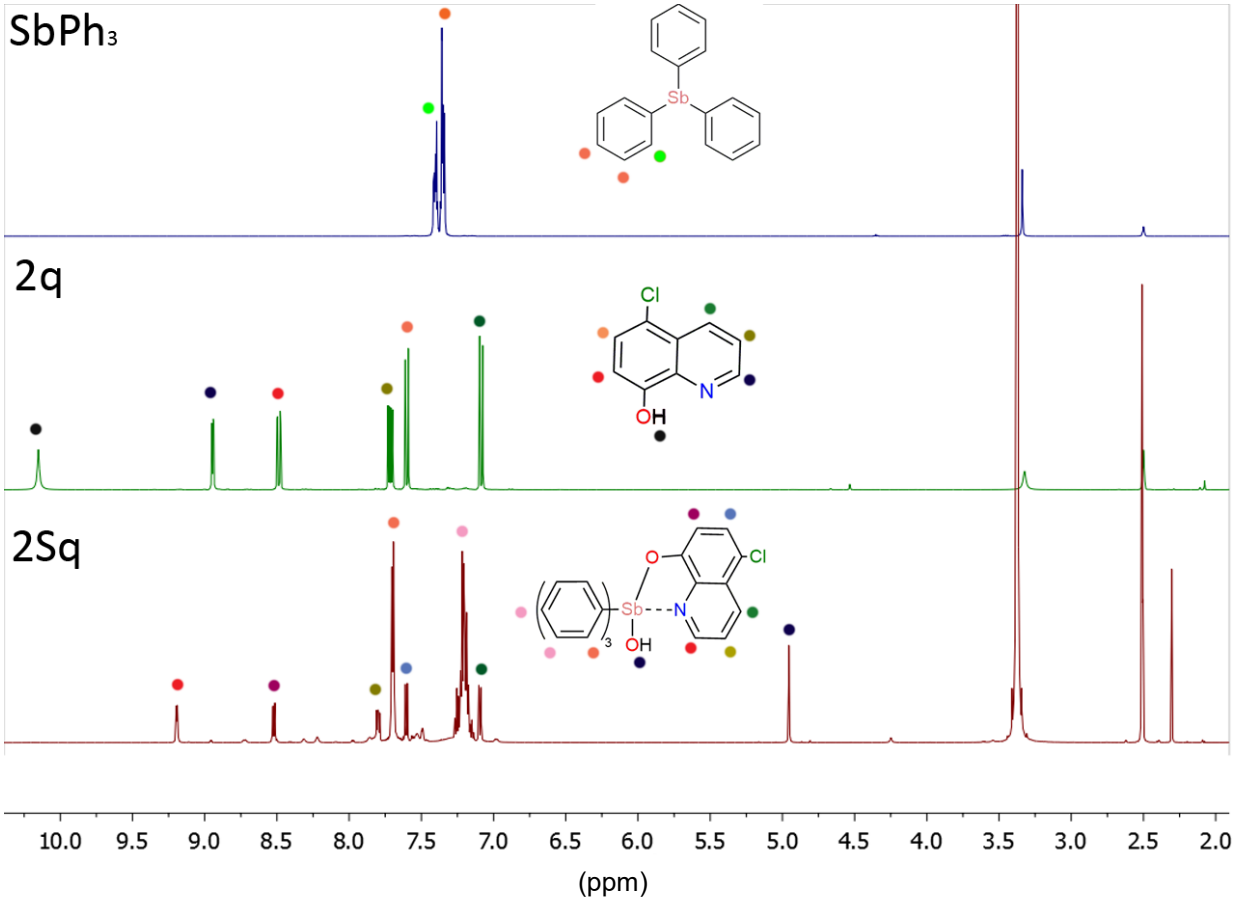

*Figure 2.2.5. Comparative ^{1}H NMR overlay of complex **2sq,** [$SbPh_3(C_9H_5NOCl)(OH)$], in d_6-DMSO, with $SbPh_3$ and free quinolinol, **2q,** cloxyquin. The water and d_6-DMSO signals appear at 3.33ppm and 2.50ppm respectively.*

The most distinct difference from the starting materials is the presence of the proton of the bound hydroxyl moiety, at 4.95 ppm. These covalently bound hydroxyls range from 4.78 ppm – 5.51 ppm in complexes **1Sq** – **6Sq.** It can be observed that upon oxidation and binding of a ligand, the phenyl protons of the triphenyl antimony become more resolved (figure 2.2.6). The *o*-Ph protons form the multiplet at 7.70 ppm in complex **2Sq**, whereas the *m*-Ph and *p*-Ph protons are found to be overlapping more upfield at approximately 7.21 ppm. As both the *para* and *meta* protons are further from the metal centre, the upfield shift compared to the *ortho* phenyl protons is expected. The *ortho* protons also become more downfield shifted upon oxidation and binding. This is most likely due to the presence of more electron de-shielding from the bound quinolinol and hydroxyl moiety, leading to the greater resolution of these aryl protons in the complexes. Shifting of the

aromatic signals of the free quinolinol is also present, with a greater degree of shifting observed for the protons closer to both the oxygen and nitrogen atoms in the quinolinolate moiety (figure 2.2.6).

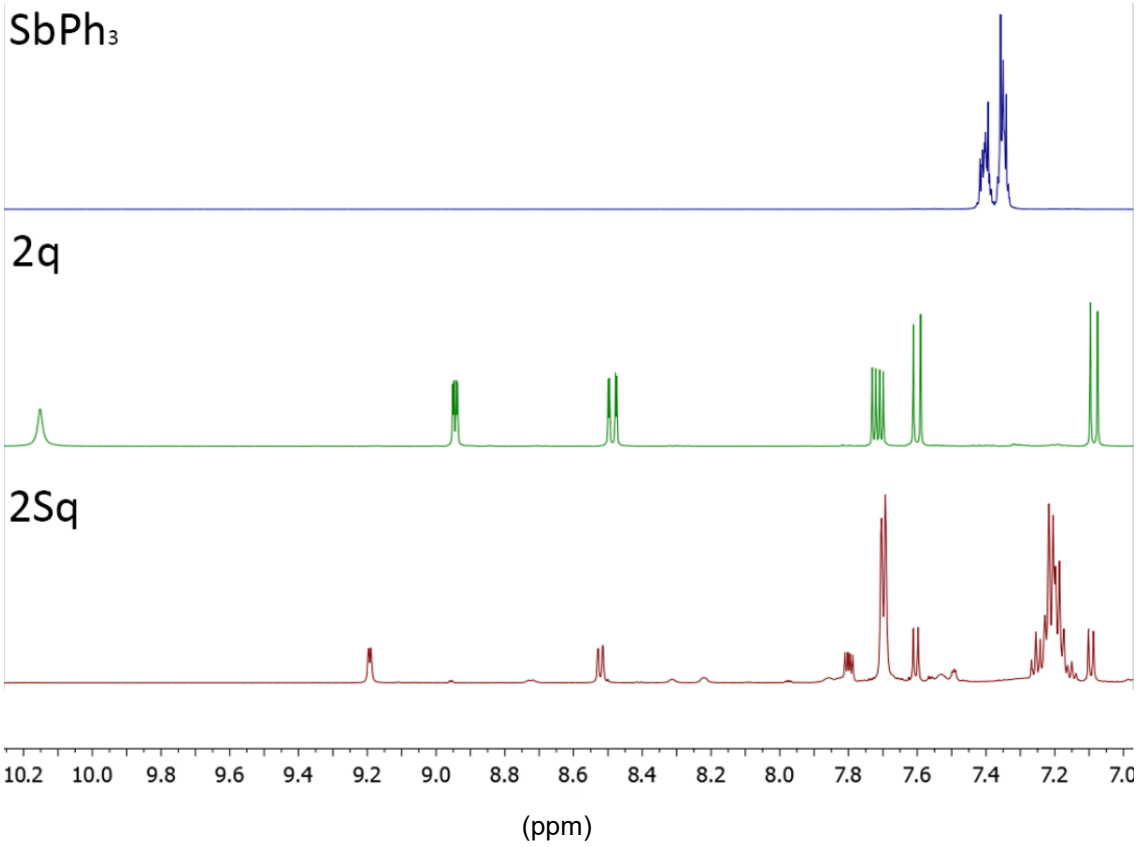

Figure 2.2.6. Insert of the aromatic region of complex ***2Sq****, [$SbPh_3(C_9H_5NOCl)(OH)$], free quinolinol* ***2q,*** *cloxyquin and* $SbPh_3$.

^{13}C NMR was difficult to obtain, with three distinctive signals of the phenyl groups visible, but failing to yield information on the quinolinol. This may possible be due to prototropic tautomerisation of the ligand in wet DMSO. Strong hydrogen bonding of the ligand to the solvent, coupled with this tautomerisation could lead to broadening or even disappearance of the carbon signals, which was observed for all complexes.[27] Nevertheless, ^{1}H NMR and other analytical techniques were able to be employed to determine with certainty the complex structure and purity. The three distinctive signals of the phenyl rings were found to be shifted upfield, which

correlates well to previous triphenyl antimony complexes.[12, 26] The quaternary carbon of the phenyl ring was also unobservable within the spectra. This tautomerisation of the quinolinol will be discussed in greater detail in section 2.3.

Infrared analysis of each of the complexes allowed for confirmation of the binding mode observed in the ^{1}H NMR spectra. The absence of the large and broad OH signal from the parent quinolinol was observed in all complexes at ranges of ~ 3300 – 2800 cm^{-1}. This signal was replaced by the presence of the covalently bound hydroxyl which was found to give a narrower range of the 3306 – 3241 cm^{-1}, and was found to be weaker than that of the alcoholic hydroxyl of the free quinolinol. A significant reduction of the strong C-N signal ranging from 1201 – 1290 cm^{-1} and OH bend ranging from 1331 – 1276 cm^{-1} present in the parent quinolinol was also noted upon complexation to the antimony. A comparison of the example complex, **2Sq,** $[SbPh_3(C_9H_5NOCl)(OH)]$, is given below against the parent ligand **2q,** cloxyquin (figure 2.2.7). The remaining significant hydroxyl shifts for the other complexes are listed in Table 2.2.3.

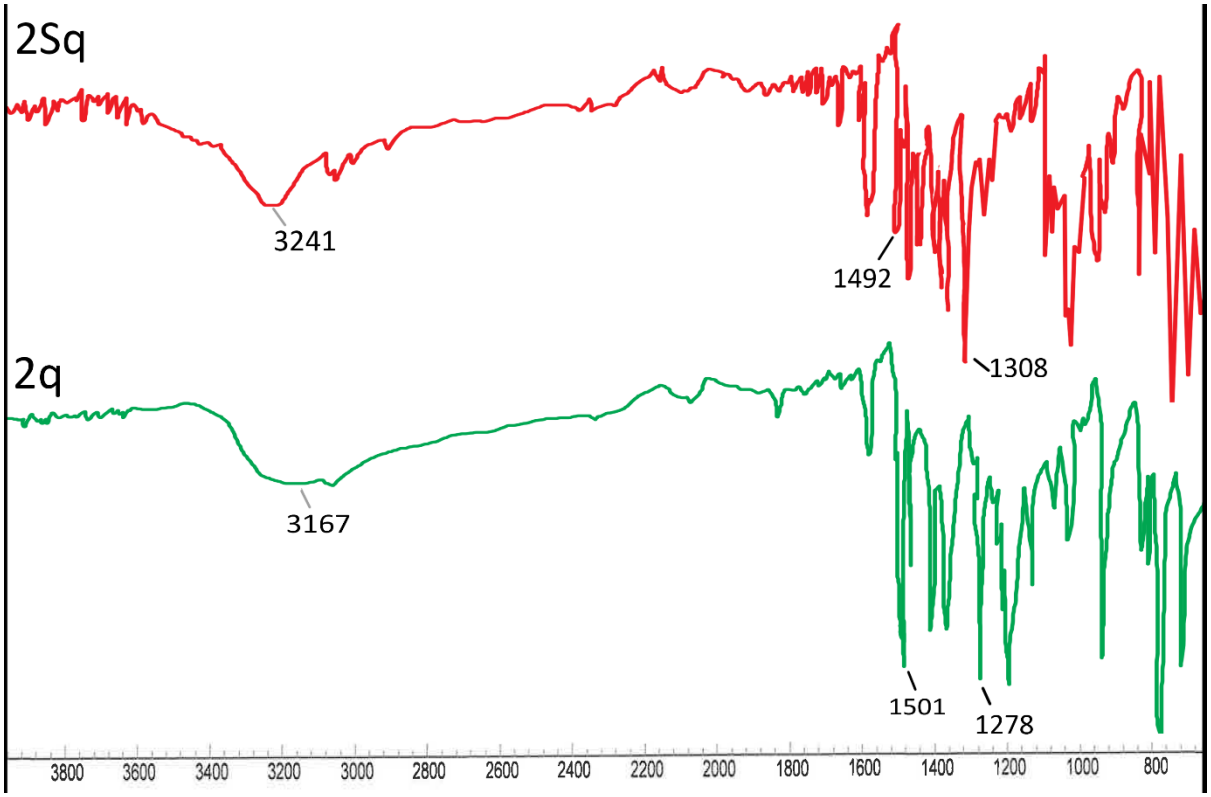

*Figure 2.2.7 Comparative IR spectrum of the complex **2Sq,** [$SbPh_3(C_9H_5NOCl)(OH)$], versus the free ligand **2q**. Significant signals have been labelled.*

Table 2.2.3. IR stretching and bending frequencies of the alcoholic quinolinol hydroxyl versus the covalently bound hydroxyl of the complex

Compound	**ν-(OH) (cm^{-1})**	**δ-(OH) (cm^{-1})**
1q	3106	1497
1Sq	3371	1469
3q	3067	1481
3Sq	3290	1429
4q	3070	1488
4Sq	3275	1430
5q	2950	1481
5Sq	3050	1430
6q	2763	1432
6Sq	3306	1430

2.2.3.3 X-ray crystallography

All complexes **1Sq** – **6Sq** were able to be structurally identified using X-ray diffraction. Single crystals of complexes **2Sq** – **6Sq** were obtained by dissolving a small amount of the pure powder into DMSO and allowing it to cool to room temperature. Complex **1Sq,** [$SbPh_3(C_9H_6NO)(OH)$], crystallised from the yellow toluene filtrate of the reaction mixture. All complexes excluding **1Sq** and **6Sq** exist in the monoclinic $P2_1/n$ space group.[28] Complexes **1Sq** and **6Sq** differ presenting as $P2_1/C$ and $Pna2_1$ respectively. The coordination number of the all the complexes is six, with the metal centre adopting a distorted octahedral geometry. This geometry is less common for triaryl Sb(V) complexes, with the usual coordination number of five in *bis*-carboxylates resulting in a trigonal bipyramidal geometry. However a similar configuration was observed in a *mono*-mandelate complex of the general formula ($SbPh_3L.DMSO$) due to the dative interaction with the solvent moleulce.[12] A series of triaryl antimony hydroximates also share this less common octahedral geometry and coordination number of six.[29] These complexes were all found to deviate from an ideal 180 ° angle along the axial plane orientation of the covalently bound hydroxyl and the deprotonated quinolinol, with ranges of 164.3 – 174.0 °. Complex **6Sq,** [$SbPh_3(C_9H_3NOCl_2CH_3)(OH)$], was found to exhibit the least distortion with a bond angle of 174.0(14) ° for O(1) – Sb(1) – O(2), whereas the cloxyquin analogue **2Sq,** [$SbPh_3(C_9H_5NOCl)(OH)$], deviated the most from the ideal 180 ° with an angle of 164.3(8) °. The phenyl rings sit in the usual propeller like conformation in the remaining equatorial positions.[12, 13, 26] Complexes **2Sq** – **6Sq** all incorporate a DMSO molecule within the lattice, hydrogen bonding to the covalently bound hydroxyl. A brief summary of each complex, disregarding example complex **2Sq**, is given below in figures 2.2.8 – 2.2.12. **2Sq** will be discussed in more detail. Selected bond lengths and angles are listed with all atoms at 50% probability.

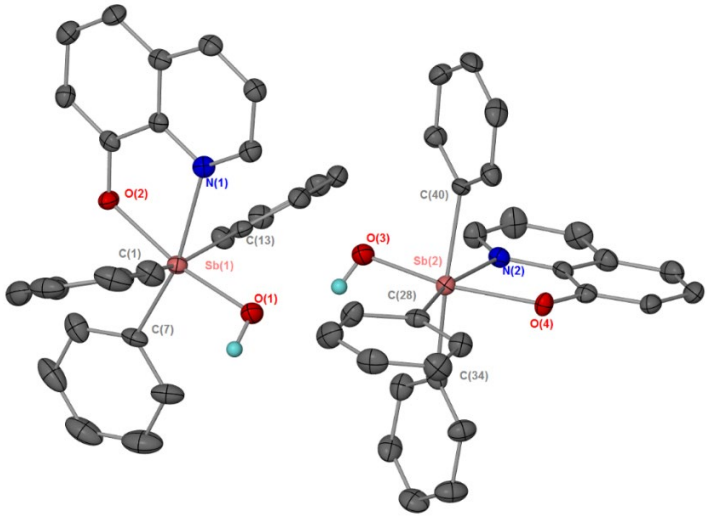

Figure 2.2.8. Solid-state structure of complex ***1sq,*** *[$SbPh_3(C_9H_6NO)(OH)$] thermal ellipsoids at 50% probability. Hydrogen atoms omitted for clarity, selected bond lengths (Å and angles (°). Sb(1) – O(1) 2.014(4), Sb(1) – O(2) 2.072(3), Sb(1) – N(1), 2.400(4), Sb(1) – C(1)2.167(5), Sb(2) – O(3) 1.984(4), Sb(2) – O(4) 2.115(3), Sb(2) – N(2), 2.329(4), Sb(2) – C(28), 2.135(4); O(1) – Sb(1) – O(2) 169.1(14), O(1) – Sb(1) – N(1) 94.13(14), O(2) – Sb(1) – N(1) 75.08(13), C(1) – Sb(1) – C(13) 164.0(19), C(1) – Sb(1) – C(7) 99.46(18).*

Figure 2.2.9.

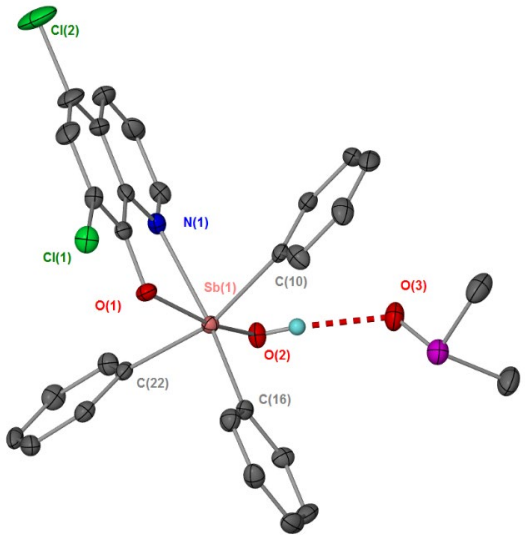

Solid-state structure of complex ***3sq,*** *[$SbPh_3(C_9H_4NOCl_2)(OH)$] thermal ellipsoids at 50% probability. Hydrogen atoms omitted for clarity, selected bond lengths (Å and angles (°). Sb(1) – O(1) 2.128(2), Sb(1) – O(2) 1.965(2), Sb(1) – N(1), 2.400(3), Sb(1) – C(10) 2.134(3), H(2) – O(3) 1.956; O(2) – Sb(1) – O(1) 164.9(10), O(2) – Sb(1) – N(1) 91.48(10), O(1) – Sb(1) – N(1) 73.51(9), C(10) – Sb(1) – C(22) 163.7(13), C(16) – Sb(1) – C(22) 96.90(13)*

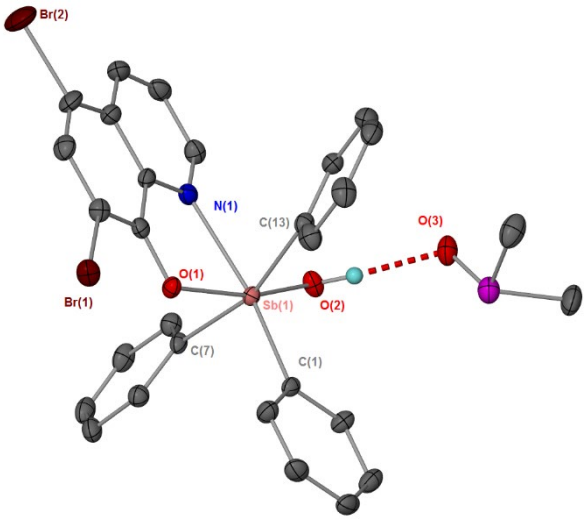

Figure 2.2.10. Solid-state structure of complex ***4sq,*** *[$SbPh_3(C_9H_4NOBr_2)(OH)$} thermal ellipsoids at 50% probability. Hydrogen atoms omitted for clarity, selected bond lengths (Å and angles (°). Sb(1) – O(1) 1.972(2), Sb(1) – O(2) 2.120(2), Sb(1) – N(1), 2.402(3), Sb(1) – C(1) 2.134(3), H(2) – O(3) 1.913; O(2) – Sb(1) – O(1) 165.4(9), O(2) – Sb(1) – N(1) 92.10(9), O(1) – Sb(1) – N(1) 73.37(9), C(7) – Sb(1) – C(13) 163.0(12), C(1) – Sb(1) – C(7) 97.89(12).*

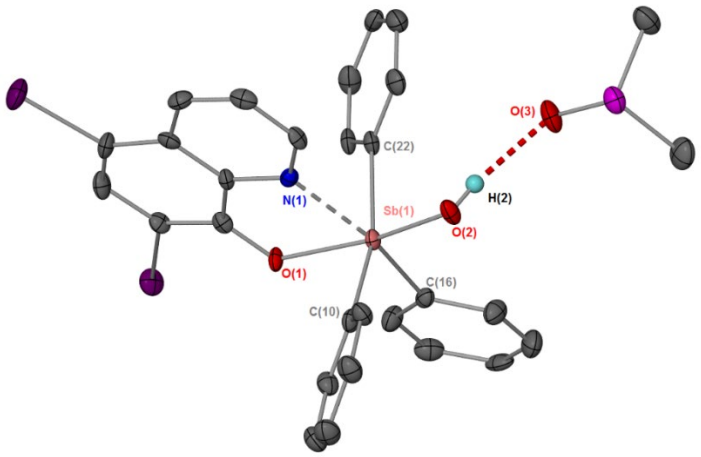

Figure 2.2.11. Solid-state structure of complex ***5sq,*** *[$SbPh_3(C_9H_4NOI_2)(OH)$] thermal ellipsoids at 50% probability. Hydrogen atoms omitted for clarity, selected bond lengths (Å) and angles (°). Sb(1) – O(1) 1.966(4), Sb(1) – O(2) 2.118(3), Sb(1) – N(1), 2.389(4), Sb(1) – C(1) 2.156(5), H(2) – O(3) 1.997; O(2) – Sb(1) – O(2) 167.0(15), O(2) – Sb(1) – N(1) 93.41(15), O(1) – Sb(1) – N(1) 73.81(14), C(1) – Sb(1) – C(15) 163.1(17), C(1) – Sb(1) – C(7) 96.20(2).*

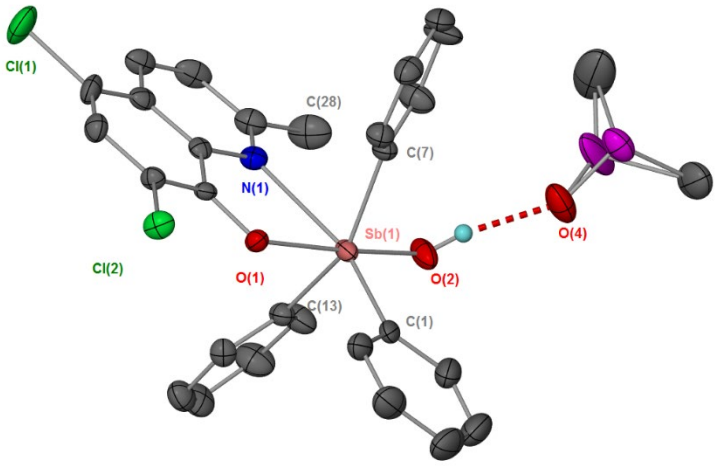

Figure 2.2.12. Solid-state structure of complex ***6sq,*** *[$SbPh_3(C_9H_3NOCl_2CH_3)(OH)$] thermal ellipsoids at 50% probability. Hydrogen atoms omitted for clarity, selected bond lengths (Å) and angles (°). Sb(1) – O(2) 1.977(3), Sb(1) – O(1) 2.115(3), Sb(1) – N(1), 2.597(4), Sb(1) – C(1) 2.140(6), H(2) – O(3) 1.881; O(2) – Sb(1) – O(1) 174.0(14), O(2) – Sb(1) – N(1) 103.3(14), O(1) – Sb(1) – N(1) 70.77(13), C(7) – Sb(1) – C(13) 152.8(2), C(1) – Sb(1) – C(7) 104.7(2).*

Example complex **2Sq** was found to be analogous to the remaining complexes, as all were found to exhibit the general formula of [$SbPh_3(C_9H_4NORR')(OH)$] (figure 2.2.13).

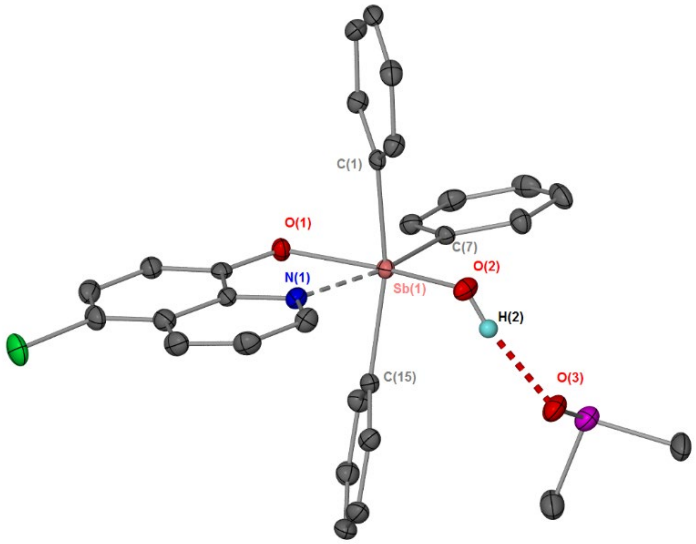

Figure 2.2.13. Solid-state structure of complex ***2sq,*** *[$SbPh_3(C_9H_5NOCl)(OH)$] thermal ellipsoids at 50% probability. Hydrogen atoms omitted for clarity, selected bond lengths (Å and angles (°). Sb(1) – O(1) 1.957(19), Sb(1) – O(2) 2.116(18), Sb(1) – N(1), 2.358(2), Sb(1) – C(1) 2.135(3), H(2) – O(3) 1.956; O(2) – Sb(1) – O(1) 164.3(8), O(2) – Sb(1) – N(1) 90.25(8), O(1) – Sb(1) – N(1) 74.27(7), C(1) – Sb(1) – C(15) 165.5(9), C(1) – Sb(1) – C(7) 95.17(10).*

The average bond lengths for the carbon to antimony of the phenyl rings was found to be 2.138 Å, which is well within the range for a covalent bond. Clarification of the covalent nature of the hydroxyl was also established by the bond length observed of 1.957(19) for Sb(1) – O(2). This length is well within the covalent radius of antimony and oxygen.[30-32] The coordinative behaviour of nitrogen was confirmed by the bond length of 2.358(2) Å for Sb(1) – N(1). This dative interaction is favourable as it forms a five-membered chelate ring to the antimony centre, which overall increases the stability of the complex.[33] Similar dative bond lengths for an antimony – nitrogen interaction was observed in the Sb(III) equivalent *bis*-quinolinolato complexes synthesised by Hoskins *et al,* of which were found to be 2.368(7) Å for Sb(1) – N(1) and 2.373(7) Å for Sb(1) – N(2).[34] The tetranuclear 8-hydroxyquinolinol Sb(III) complex synthesised by Jami and Basker also exhibited a similar, though slightly shorter, dative bond length of 2.238(2) Å.[35] Along with complexes **3Sq** – **6Sq**, **2Sq** was found to incorporate a hydrogen bonded DMSO solvent molecule

in the lattice, with a strong hydrogen – oxygen interaction length of 1.956 Å. A table summarising the crystallographic data of complexes **1Sq** – **6Sq** is given below in table 2.2.4.

*Table 2.2.4. Crystallographic data of triphenyl mono-*hydroxido *Sb(V) quinolinolates,* ***1Sq*** *–* ***6Sq***

	1Sq	**2Sq**	**3Sq**	**4Sq**	**5Sq**	**6Sq**
Chemical formula	2($C_{27}H_{22}NO_2Sb$)	$C_{27}H_{21}ClNO_2Sb$·DMSO	$C_{27}H_{20}Cl_2NO_2Sb$.DMSO	$C_{27}H_{20}Br_2NO_2Sb$·DMSO	$C_{27}H_{20}I_2NO_2Sb$.DMSO	$C_{28}H_{22}Cl_2NO_2Sb$·DMSO
M_r	1028.41	626.77	661.22	750.14	844.12	669.20
Crystal system, space group	Monoclinic, $P2_1/c$	Monoclinic, $P2_1/n$	Monoclinic, $P2_1/n$	Monoclinic, $P2_1/n$	Monoclinic, C2/c	Orthorhombic, $Pna2_1$
Temperature (K)	123	293	296	293	296	296
a, *b*, *c* (Å)	19.5772 (4), 13.9073 (2), 17.9336 (3)	15.280 (3), 9.940 (2), 17.950 (4)	16.1527 (10), 9.9269 (8), 17.8073 (15)	16.350 (3), 9.880 (2), 17.850 (4)	27.1171 (14), 9.8206 (4), 22.1552 (11)	17.1394 (3), 10.5124 (2), 16.0786 (4)
V (Å^3)	116.471 (2)	2586.2 (10)	2719.9 (4)	2754.9 (11)	5775.9 (5)	2896.98 (10)
Z	4	4	4	4	8	4
T_{min}, T_{max}	0.627, 1.000	0.386,0.434	0.688, 0.745	0.373 0.434	0.624, 0.745	0.695, 0.745
R_{int}	0.048	0.053	0.062	0.058	0.058	0.058
$(\sin\theta/\lambda)_{max}$ (Å^{-1})	0.634	0.633	0.610	0.641	0.610	0.617
$R[F^2 > 2\sigma(F^2)]$, $wR(F^2)$, *S*	0.042, 0.107, 1.05	0.031, 0.077, 1.06	0.034, 0.066, 1.02	0.034, 0.093, 1.05	0.036, 0.075, 1.02	0.028, 0.059, 1.04
No. of reflections	8327	5494	5147	6075	5465	5694
No. of parameters	561	330	337	339	339	342

2.2.4 Stability studies and biological activity

2.2.4.1. Stability studies

Like most triaryl Sb(V) complexes, **1Sq,** [$SbPh_3(C_9H_6NO)(OH)$], **2Sq,** [$SbPh_3(C_9H_5NOCl)(OH)$], **3Sq,** [$SbPh_3(C_9H_5NOCl_2)(OH)$], **4Sq,** [$SbPh_3(C_9H_4NOBr_2)(OH)$], **5Sq,** [$SbPh_3(C_9H_4NOI_2)(OH)$] and **6Sq**, [$SbPh_3(C_9H_3NOCl_2CH_3)(OH)$], exhibited a high degree of stability in the solid state as determined by melting point analysis over a long period of time, and further confirmed by elemental analysis of the samples. Even with repeated exposure to changing atmospheric conditions there was no observable degradation of any of the complexes. All complexes were examined for their solution

state stability in d_6-DMSO using ^{1}H NMR spectroscopy over a period of t = 0 hrs, t = 24 hrs and t = one week. Complex **2Sq** will be discussed as an example**.** After 24 hours there was no significant change in **2Sq**, however it was noted that after one week the solution colour changed from bright fluorescent yellow to colourless and a solid was present at the bottom of the tube. This solid was insoluble in the NMR solvent (d_6-DMSO) and the ^{1}H NMR spectra indicated the presence of no signals. Therefore, it can be concluded that the complexes are not stable in d_6-DMSO for extended periods of time.

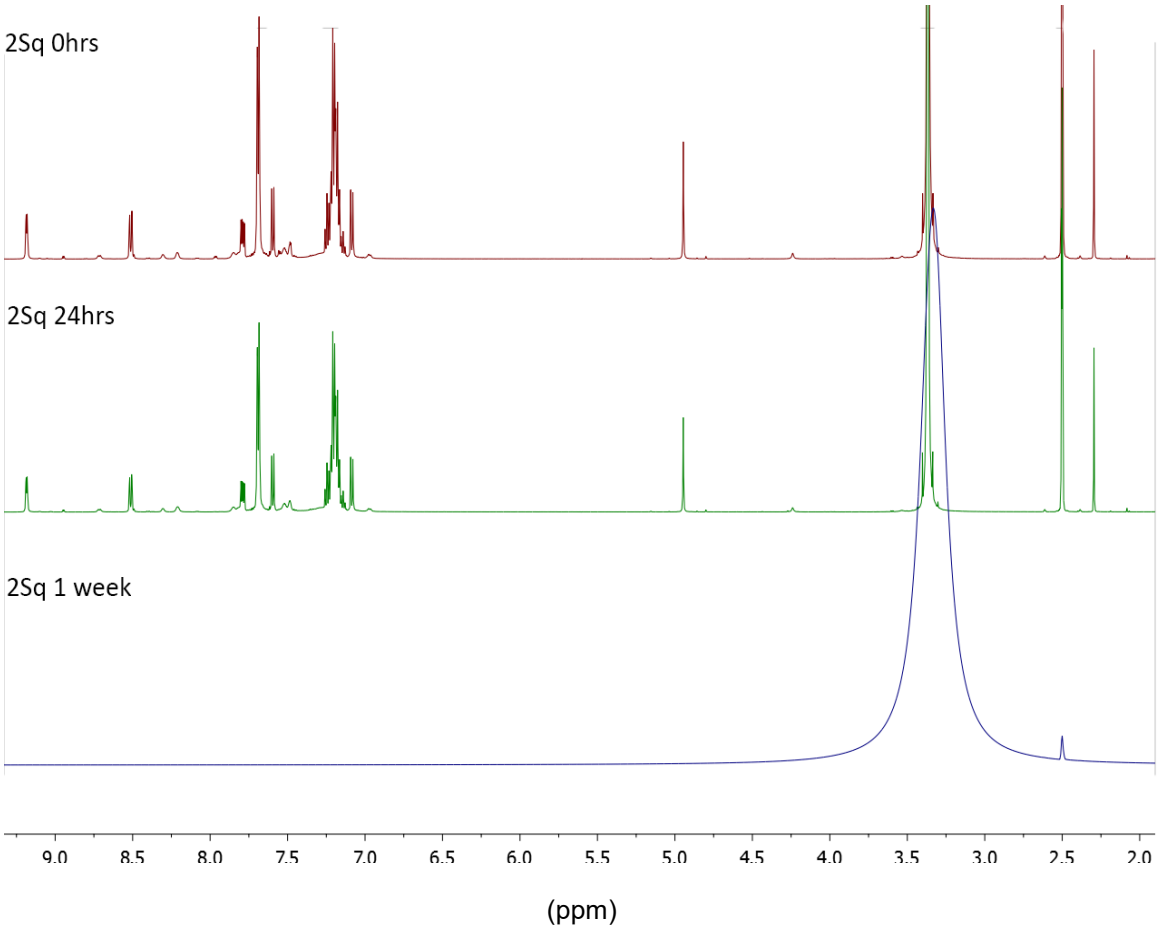

*Figure 2.2.14 ^{1}H NMR study if complex **2Sq,** [$SbPh_3(C_9H_5NOCl)(OH)$], in d_6-DMSO at times 0 hours, 24 hours and 1 week. Residual H_2O and DMSO signal are found at 3.33 ppm and 2.50 ppm respectively.*

2.2.4.2 Biological activity

All antimony complexes underwent both a mammalian cytotoxicity assay and an anti-promastigote assay to establish base-line activity. Initial studies on the anti-promastigote activity of complexes **1Sq,** $[SbPh_3(C_9H_6NO)(OH)]$, **2Sq,** $[SbPh_3(C_9H_5NOCl)(OH)]$, **3Sq,** $[SbPh_3(C_9H_5NOCl_2)(OH)]$, **4Sq,** $[SbPh_3(C_9H_4NOBr_2)(OH)]$, **5Sq,** $[SbPh_3(C_9H_4NOI_2)(OH)]$ and **6Sq**, $[SbPh_3(C_9H_3NOCl_2CH_3)(OH)]$, yielded highly potent results. The IC_{50} value range derived from the average of repeated experiments was within the values of 2.03 – 3.39 µM (figure 2.2.15).

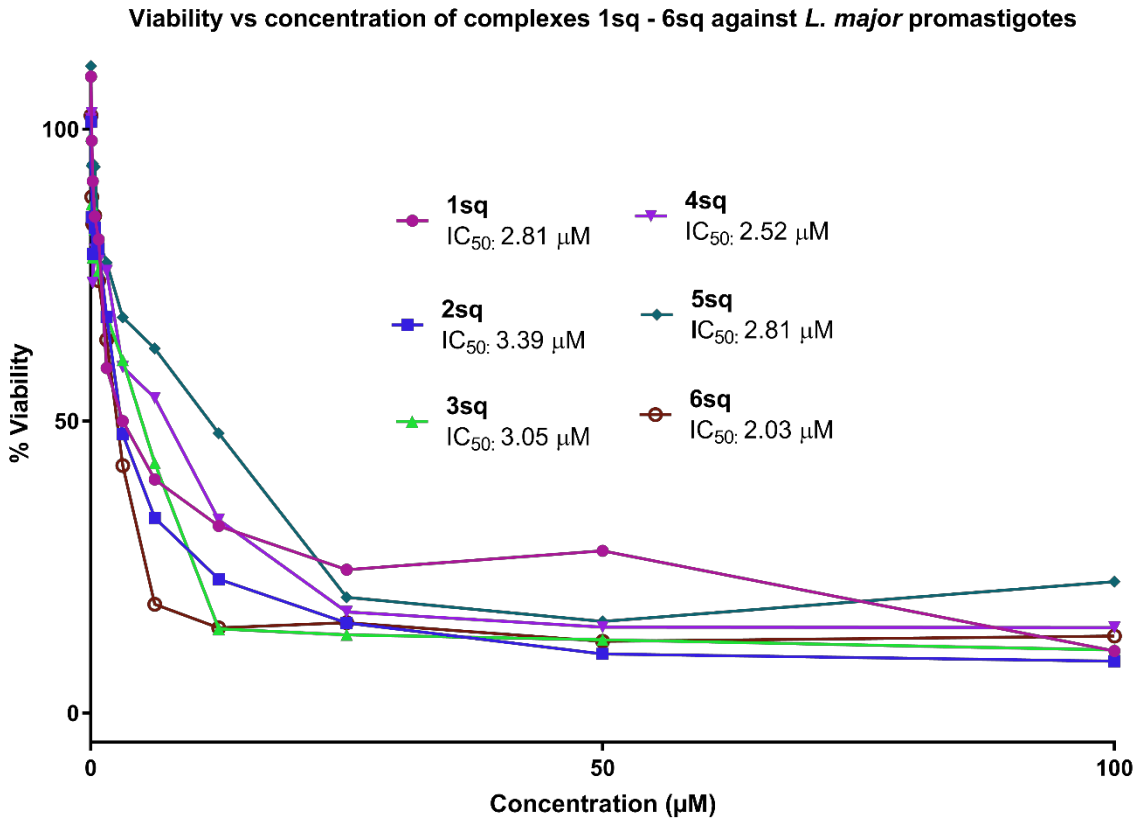

*Figure 2.2.15 Comparison of percentage cell viability after treatment with the Sb(V) complexes **1sq – 6sq,** against L. major promastigotes. Dose response curves were generated over a range of concentrations (48nM - 100µM in the appropriate culture media from 10mM DMSO stock solutions. All readings were compared spectroscopically to non-treated control and the percent growth inhibition calculated.*

Unfortunately the same selectivity that was observed for the triphenyl carboxylate complexes of section 2.1 was not retained with the Sb(V) *mono*hydroxido quinolinolates.[12, 13] The complexes varied in their cytotoxicity with a range of 12.7 µM – 46.9 µM obtained (figure 2.2.16).

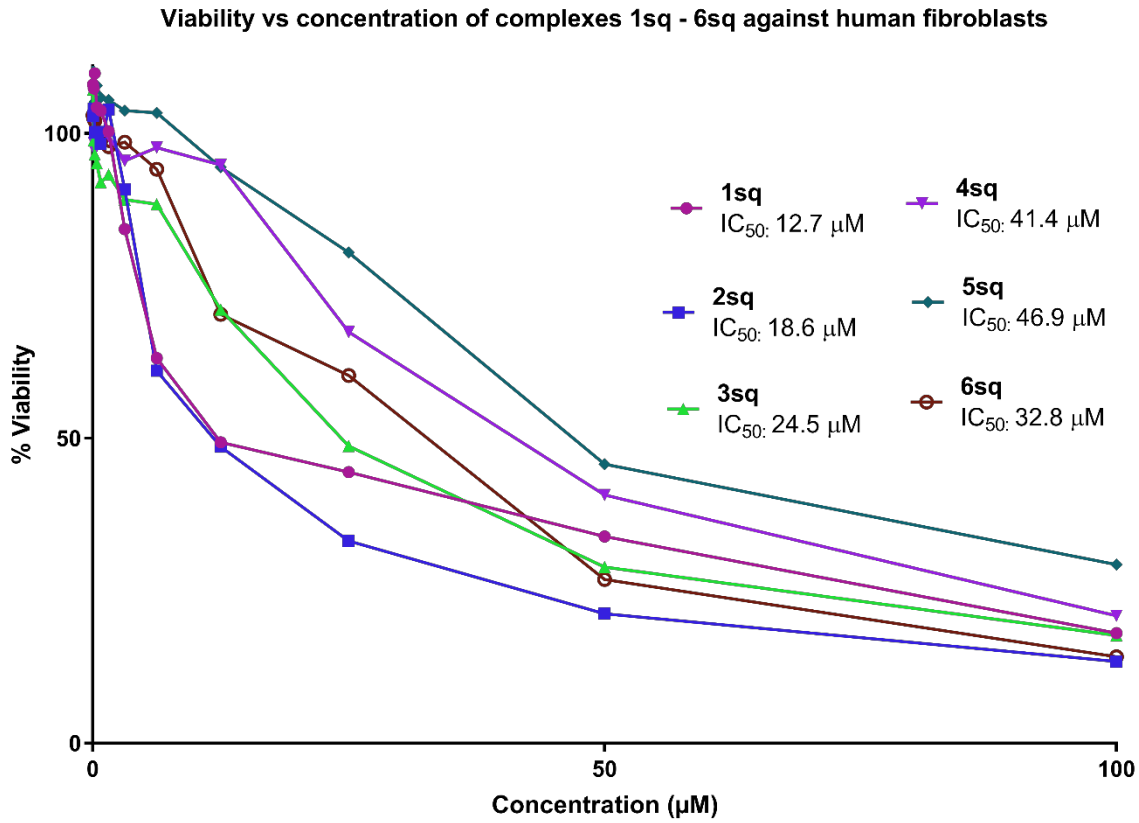

*Figure 2.2.16. Comparison of percentage cell viability after treatment with the Sb(V) complexes **1sq – 6sq,** against human fibroblasts. Dose response curves were generated over a range of concentrations (48nM - 100µM in the appropriate culture media from 10mM DMSO stock solutions. All readings were compared spectroscopically to non-treated control and the percent growth inhibition calculated*

The chelate of the 8-hydroxyquinolate, **1Sq,** $[SbPh_3(C_9H_6NO)(OH)]$, proved the most cytotoxic toward the human fibroblasts, with the least toxic complex found to be the iodoquin chelate, **5Sq,** $[SbPh_3(C_9H_4NOI_2)(OH)]$**.** This was surprising due to the previous studies on iodoquin exhibiting cytotoxic effects humans.[22, 36] A clear trend was observed which showed that the toxicity towards mammalian cells decreased with an increase in the halogen size on the R and R' positions (figure

2.2.4). From these values a selectivity index could be calculated by dividing the IC_{50} value of the fibroblast assay by the IC_{50} value obtained from the anti-promastigote assay. From this a range of 4.52 – 16.7 was calculated, with **5Sq** exhibited as the most selective out of the six triphenyl antimony *mono*-hydroxido quinolinolato complexes (table 2.2.5)

*Table 2.2.5. Selectivity indices of complexes **1sq** – **6sq**. Indices calculated based on IC_{50}(mammalian)/IC_{50}(parasite). Yellow highlights the least selective, with the values in green indicating a high degree of selectivity.*

Complex	**1Sq**	**2Sq**	**3Sq**	**4Sq**	**5Sq**	**6Sq**
IC_{50}(fibroblasts) µM	12.7	18.6	24.5	41.4	46.9	32.8
IC_{50}(promastigote) µM	2.81	3.39	3.05	2.52	2.81	2.03
Selectivity index	4.52	5.49	8.03	16.4	16.7	16.2

Despite the significant cytotoxicity of complexes **1Sq** and **2Sq**, the amastigote invasion assay was conducted at a concentration of 10 µM. Fibroblasts are considered a more fragile mammalian cell line and so it was theorised that the macrophages would be more resistant to the toxic effects of **1Sq** and **2Sq**.

Complexes **1Sq – 6Sq** were then assessed against the amastigote form, utilising the same assay as described in section 2.1. In contrast to the complexes described in section 2.1, the antimony *mono*-hydroxido quinolinolates exhibited excellent activity against the amastigote form, with percentage infection values ranging from 9.00 – 2.25 %. Similar to the cytotoxicity studies, a trend was observable for the antimony complexes, with better activity observed with the increase of halogen size on the 5 and 7 position of the halido-quinolinol (figures 2.2.17 and table 2.2.6).

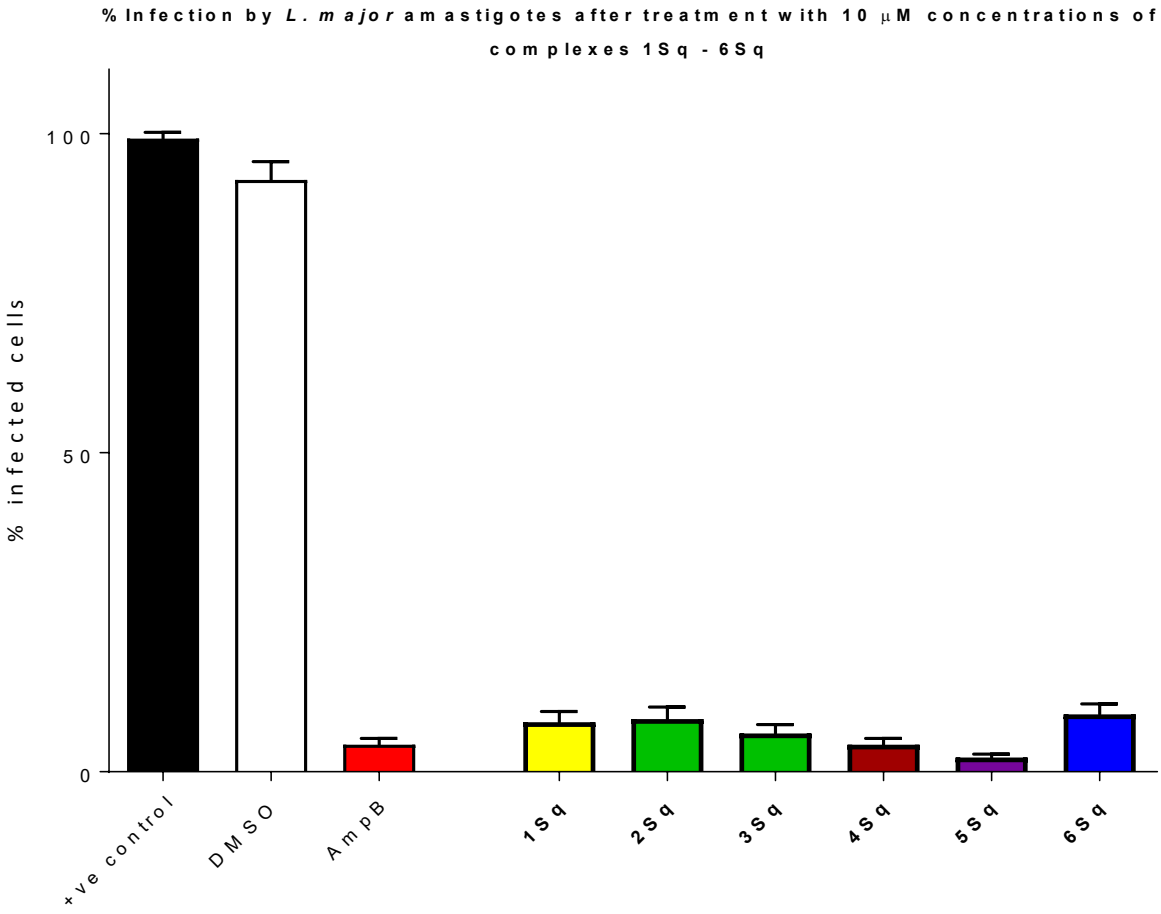

Figure 2.2.17. Infected macrophages after treatment of complexes 1Sq – 6Sq, after 48 hours. Number of infected macrophages was determined microscopically, in duplicate of fixed specimens. Amphotericin B (AmpB) was used as a positive control at 10 µM concentration. A DMSO control was also employed at a 1% concentration. Error bas indicate SEM, one-way ANOVA. Dunnett's multiple comparison test was used to determine the statistical significance between all test compounds and a positive control lacking treatment (+ve control)

*Table 2.2.6. Percentage Infection values for complexes **1Sq** – **6Sq**, all values are calculated by comparison to a positive control of untreated infected cells.*

Complex	**1Sq**	**2Sq**	**3Sq**	**4Sq**	**5Sq**	**6Sq**
% Infection	7.75 ± 0.85	8.25 ± 0.95	6.00 ± 0.71	4.25 ± 0.48	2.25 ± 0.25	9.00 ± 0.83

From the graph it can be seen that complex **5Sq**, $[SbPh_3(C_9H_4NOI_2)(OH)]$, the iodoquin complex, had the greatest degree of activity with the lowest value for percentage infected of 2.25 % ± 0.25. Whereas the compound that exhibited the least activity was the chlorquinaldol complex **6Sq**, $[SbPh_3(C_9H_3NOCl_2CH_3)(OH)]$, yielding a value of 9.00 % ± 0.83. Despite this, all six of the *mono*-hydroxido quinolinolates exhibited a higher degree of activity than the Sb(V) carboxylates of section 2.1. A trend was observed for the efficacy of the complexes, with the increase of halogen size on both the 5 and 7 position of the complexes resulting in an increase of anti-amastigote activity, with values of 6.00 % ± 0.71, 4.25 % ± 0.48 and 2.25 % ± 0.25 for complexes **3Sq**, $[SbPh_3(C_9H_4NOCl_2)(OH)]$, **4Sq,** $[SbPh_3(C_9H_6NOBr_2)(OH)]$ and **5Sq,** $[SbPh_3(C_9H_6NOI_2)(OH)]$, respectively. This difference in the halogen size and electronegativity may contribute to the difference in activity. Further investigations into halogen substitution is required to fully elucidate whether it plays a major role in the biological efficacy. The cloxyquin complex **2Sq,** $[SbPh_3(C_9H_4NOCl)(OH)]$ was found to be less active than the 5,7-halido substituted complexes of chloroxine, broxyquinoline and iodoquin, with a value of 8.25 % + 0.95. The complex of the simplest ligand, 8-quinolinol, **1Sq**, $[SbPh_3(C_9H_6NO)(OH)]$, followed after it with a percentage infection value of 7.75 % ± 0.85. Based on the previously calculated selectivity indices, complex **5Sq** was therefore found to be the best candidate for future *in vivo* testing, due to its 16-fold difference between mammalian and parasite IC_{50} and high degree of anti-amastigote activity.

Activity of the parent quinolinols were also assessed at 10 µM to identify whether binding to a metal enhanced the biological activity. All antimony complexes outclassed the parent quinolinols **1 – 6,** with percentage infection values in the range of 12.5 – 30.8 %. These are listed below in table 2.2.7. Though 8QH in particular has been proven to exert anti-leishmanial activity, it seems that by chelating it to a metal this activity is increased. Whether the metal acts synergistically or acts as a delivery system remains to be seen. Further mechanistic studies are required to elucidate the mechanism of action.

*Table 2.2.7. Percentage Infection values for parent quinolinols **1q** – **6q**, all values are calculated by comparison to a positive control of untreated infected cells.*

Complex	1q	2q	3q	4q	5q	6q
% Infection	15.3 ± 3.00	21.5 ± 5.13	30.8 ± 3.28	23.8 ± 4.86	16.0 ± 2.81	12.5 ± 2.92

In section 2.1, antimony complexes of acetates **1S** – **7S'**, were found to have percentage infection values ranging from 7.75 – 40.5 %, with only compound **6S**, the *p*-methoxyphenyl acetate, exhibiting a higher degree of activity than complexes **6Sq** and **2Sq**. Though these quinolinolate complexes are more toxic to the intracellular parasite, their selectivity when paralleled to the Sb(V) acetic acetates pales in comparison.[13] Selectivity is often a reoccurring issue when designing anti-Leishmanial complexes. Studies into complexes containing other metals such as gold, ruthenium and zinc, have incorporated a variety of mammalian cytotoxic controls to gauge the selectivity when compared to the activity against *Leishmania spp* and other microbes.[37-40] Several recent publications of effective anti-Leishmanial antimony(V) complexes tend to omit this important deduction with a lack of cytotoxicity assays performed on a variety of Sb(V) aryl carboxylates.[41-43] It is vital that cytotoxicity assays be performed on complexes to determine whether future testing is applicable.

All selectivity indices of the complexes **1Sq** – **6Sq** fall above the FDA guidelines for potential therapeutics, with the FDA defining a Narrow Therapeutic index (NTI) as anything that exhibits less than a two-fold difference between the LD_{50} (or IC_{50}) and ED_{50} (which in this case is the IC_{50} of the mammalian cells, also known as the CC_{50}).[44] In fact, complexes **4Sq** – **6Sq** actually proved to be fairly selective, all presenting with 16-fold differences when compared to complexes **1Sq** – **3Sq**, of which had selectivity indices in the ranges of 4.52 – 8.03.

2.2.6 Conclusion

Following on from our previous conclusions of the non-selective activity of Bi(V), the solo use of the group 15 metalloid antimony was employed. To further establish structure activity, six novel complexes that incorporated a medically active class of organic heterocycles and a covalent bound hydroxyl were synthesised. Complexes **1Sq,** [$SbPh_3(C_9H_6NO)(OH)$], **2Sq,** [$SbPh_3(C_9H_5NOCl)(OH)$], **3Sq,** [$SbPh_3(C_9H_5NOCl_2)(OH)$], **4Sq,** [$SbPh_3(C_9H_4NOBr_2)(OH)$], **5Sq,** [$SbPh_3(C_9H_4NOI_2)(OH)$] and **6Sq**, [$SbPh_3(C_9H_3NOCl_2CH_3)(OH)$], exhibited an overall coordination number of six.

These complexes, which presented with the general formula [$SbPh_3(C_9H_4NORR')(OH)$], were all synthesised by an oxidative addition of tert-butyl hydroperoxide to the triphenyl antimony precursor, before addition of one equivalent of the quinolinols **1** – **6**. All complexes were obtained in moderate to high yields of 72 – 90 % and were characterisation via ^{1}H and ^{13}C NMR, melting point, FT-IR, elemental analysis and single crystal X-ray crystallography.

Complexes **2Sq** – **6Sq**, were found to be analogous in structure, presenting as monomers, with **1Sq** found to exist in a dimeric aggregation state. This dimerisation was proposed to be due to the interaction of the hydroxyl moiety of one unit with the hydroxyl of the other. However, difficulties in modelling the hydrogen positions were unable to confirm this. The hydroxyl moiety in complexes **2Sq** – **6Sq** were found to be interacting with a solvent molecule of DMSO, which most likely promoted crystallisation. The phenyl rings of all complexes were found to occupy three of equatorial positions of the distorted octahedron, with the remaining position occupied by the dative interaction between antimony and the quinolinol nitrogen. The quinolinol oxygen and the hydroxyl moiety occupying the axial positions in an almost linear angle, with only very minor distortion about the O – Sb – O bond, ranging from 174.0 – 164.3 These complexes are the first examples of a triaryl antimony *mono*-hydroxido quinolinolato complexes.

Stability of the complexes was assessed by a ^{1}H NMR study over a period of 0 hours, 24 hours and one week. It was observed that the complexes were stable after dissolution into d_6-DMSO for the 24 hours period, however after one week the complexes were broken down into insoluble white crystalline products, with no soluble traces observed in the d_6-DMSO NMR.

Each complex underwent assessment of their mammalian cytotoxicity and their potential anti-Leishmanial activity. A cell viability assay was performed on *L. Major* promastigotes, with the mammalian control cell of human primary fibroblasts. Each complex exhibited excellent activity against the parasite, but did retain a moderate level of human cytotoxicity, with selectivity indices ranging from 4.52 - 16.7. The smaller indices of **1Sq** – **3Sq** however do still fall above the FDA approved range for a narrow therapeutic index, with complexes **4Sq** - **6Sq** proving to exhibit a greater degree of selectivity, each above a 16-fold difference between IC_{50} and CC_{50}. An observable trend was concluded, with the increase of halogen size resulting in a higher degree of selectivity. This trend was extended out into the anti-amastigote activity, with Cl $\leq$ Br $\leq$ I. Complex **5Sq**, the iodoquin complex, was determined to be the best candidate for future *in vivo* testing due to its higher degree of selectivity and anti-amastigote activity.

The addition of an alcoholic hydroxyl antimony – oxygen bond was explored over the conventional carboxylate binding moiety to establish whether this may induce a higher level of reactivity towards microbes. The use of an already established class of organic drugs molecules, the halido-8-quinolinols, was explored in the hope that the addition of bioactive molecules may also contribute to both activity and selectivity. Though the initial plan of *bis*-substitution by the 8-quinolinol derivatives was not obtainable, the addition of the covalent bound hydroxyl from the dihydroxido antimony intermediate was interesting nevertheless both structurally and biologically. This has highlighted the need for further testing of the group 15 complexes in a more

clinically relevant *in vivo* setting, exhibited by the moderate selectivity and high degree of bioactivity.

2.2.7 References

1. J. Emsley, *The elements*, Clarendon Press, Oxford, 1991.
2. W. M. Haynes, *CRC handbook of chemistry and physics*, CRC press, 2014.
3. N. C. Norman, *Chemistry of arsenic, antimony and* bismuth, Springer Science & Business Media, 1997.
4. W. Levason and G. Reid, in *Comprehensive Coordination Chemistry II*, Elsevier, 2003, 465-544.
5. N. C. Norman, *Phosphorus, Sulfur, and Silicon and the Related Elements*, 1994, **87**, 167-176.
6. H. Sun, L. Zhang and K.-Y. Szeto, *Met. Ions Biol. Syst.*, 2004, **41**, 333-378.
7. Wtl, *J. Chem. Educ.*, 1979, **56**, A352.
8. A. G. Debus, *Antimony in medical history: An account of the medical uses of antimony and its compounds since early times to the present*, Pentland Press, 2000, 362-364.
9. H. Schmidt and F. M. Peter, *Advances in the Therapeutics of Antimony.*, 1938.
10. B. Venugopal and T. D. Luckey, *Metal toxicity in mammals. Volume 2. Chemical toxicity of metals and metalloids*, Plenum Press., 1978.
11. P. Olliaro and A. Bryceson, *Parasitol. Today*, 1993, **9**, 323-328.
12. R. N. Duffin, V. L. Blair, L. Kedzierski and P. C. Andrews, *Dalton Trans.*, 2018, **47**, 971-980.
13. R. N. Duffin, V. L. Blair, L. Kedzierski and P. C. Andrews, *J. Inorg. Biochem.*, 2018.
14. A. Albert, S. Rubbo, R. Goldacre and B. Balfour, *Br. J. Exp. Pathol.*, 1947, **28**, 69.
15. A. Albert, M. Gibson and S. Rubbo, *Br. J. Exp. Pathol.*, 1953, **34**, 119.
16. J.-H. Jeon, C.-H. Lee and H.-S. Lee, *J. Korean. Soc. Appl. Biol. Chem.*, 2009, **52**, 202-205.
17. M. C. Duarte, L. M. dos Reis Lage, D. P. Lage, J. T. Mesquita, B. C. S. Salles, S. N. Lavorato, D. Menezes-Souza, B. M. Roatt, R. J. Alves and C. A. P. Tavares, *Vet. Parasitol.*, 2016, **217**, 81-88.
18. P. Hongmanee, K. Rukseree, B. Buabut, B. Somsri and P. Palittapongarnpim, *Antimicrob. Agents Chemother.*, 2007, **51**, 1105-1106.
19. W. Andrew, *Pharmaceutical Manufacturing Encyclopedia, 3rd Edition*, Elsevier Science, 2013, 305.
20. H. M. Robinson Jr and M. B. Hollander, *J. Investig. Dermatol.*, 1956, **26**, 143-147.
21. T. Agner and T. Menné, *Contact Dermatitis*, 1993, **29**, 163-163.
22. A. K. Fisher, F. G. Walter and S. Szabo, *J. Toxicol.: Clin. Toxicol.*, 1993, **31**, 113-120.
23. M. Khaw and C. B. Panosian, *Clin. Microbiol. Rev.*, 1995, **8**, 427-439.
24. R. Swain, J. Bapna, A. Das, S. Chandrasekar, R. Swaminathan, B. Bosco, S. Veliath and D. Thombre, *Hum. Toxicol.*, 1986, **5**, 35-41.
25. H. Meinema, E. Rivarola and J. Noltes, *J. Organomet. Chem.*, 1969, **17**, 71-81.
26. M. I. Ali, M. K. Rauf, A. Badshah, I. Kumar, C. M. Forsyth, P. C. Junk, L. Kedzierski and P. C. Andrews, *Dalton Trans.*, 2013, **42**, 16733-16741.
27. P. D. Woodgate, J. M. Herbert and W. A. Denny, *Magn. Reson. Chem.*, 1988, **26**, 191-196.
28. M. F. C. Ladd, R. A. Palmer and R. A. Palmer, *Structure determination by X-ray crystallography*, Springer, 1985.

29. G.-C. Wang, Y.-N. Lu, J. Xiao, L. Yu, H.-B. Song, J.-S. Li, J.-R. Cui, R.-Q. Wang and F.-X. Ran, *J. Organomet. Chem.*, 2005, **690**, 151-156.
30. H. Sun, *Biological chemistry of arsenic, antimony and* bismuth, Wiley Online Library, 2011.
31. T. Westhoff, F. Huber, R. Rüther and H. Preut, *J. Organomet. Chem.*, 1988, **352**, 107-113.
32. H. Preut, R. Rüther and F. Huber, *Acta. Crystallogr. C.*, 1985, **41**, 358-360.
33. R. D. Hancock, *J. Chem. Educ*, 1992, **69**, 615.
34. B. F. Hoskins, E. R. T. Tiekink and G. Winter, *Inorg. Chim. Acta*, 1985, **97**, 217-222.
35. M. Brinkmann, B. Fite, S. Pratontep and C. Chaumont, *Chem. Mater.*, 2004, **16**, 4627-4633.
36. G. Farruggia, S. Iotti, L. Prodi, M. Montalti, N. Zaccheroni, P. B. Savage, V. Trapani, P. Sale and F. I. Wolf, *J. Am. Chem. Soc.*, 2006, **128**, 344-350.
37. C. Zhang, S. B. Delmas, A. F. Alvarez, A. Valentin, C. Hemmert and H. Gornitzka, *Eur. J. Med. Chem.*, 2018, **143**, 1635-1643.
38. J. D. S. Chaves, L. G. Tunes, C. H. d. J. Franco, T. M. Francisco, C. C. Correa, S. M. Murta, R. L. Monte-Neto, H. Silva, A. P. S. Fontes and M. V. de Almeida, *Eur. J. Med. Chem.*, 2017, **127**, 727-739.
39. N. R. F. do Nascimento, F. L. N. de Aguiar, C. F. Santos, A. M. L. Costa, D. de Jesus Hardoim, K. da Silva Calabrese, F. Almeida-Souza, E. H. S. de Sousa, L. G. de França Lopes and M. J. Teixeira, *Acta Trop.*, 2019, **192**, 61-65.
40. M. S. Costa, Y. G. Gonçalves, D. C. Nunes, D. R. Napolitano, P. I. Maia, R. S. Rodrigues, V. M. Rodrigues, G. Von Poelhsitz and K. A. Yoneyama, *J. Inorg. Biochem.*, 2017, **175**, 225-231.
41. T. Iftikhar, M. K. Rauf, S. Sarwar, A. Badshah, D. Waseem, M. N. Tahir, A. Khan, K. M. Khan and G. M. Khan, *J. Organomet. Chem.*, 2017, **851**, 89-96.
42. L. Saleem, A. A. Altaf, A. Badshah, M. K. Rauf, A. Waseem, M. Danish, S. S. Azam, M. N. Arshad, A. M. Asiri and S. Ahmad, *Inorg. Chim. Acta*, 2018, **474**, 148-155.
43. S. Sarwar, T. Iftikhar, M. K. Rauf, A. Badshah, D. Waseem, M. N. Tahir, K. M. Khan and G. M. Khan, *Inorg. Chim. Acta*, 2018, **476**, 12-19.
44. R. D. Abughazaleh and T. S. Tracy, *Wiley StatsRef: Stat. Ref. Online.* 2007, doi:10.1002/9781118445112.stat07121

2.3 Synthesis, characterisation, photophysical properties and biological activity of alkyl gallium and indium quinolinolato complexes

2.3.1 Gallium and Indium

2.3.1.1 Group 13 complexes as medicinals: Gallium

As discussed previously in section 1.5, both gallium and indium compounds are predominately found in trivalent state.[1] The use of gallium as a medicinal complex has been well established. Some of the earliest uses of gallium are due to the discovery of the localisation of the radioactive ^{67}Ga in malignant cells (in the form of gallium citrate (figure 2.3.1)).[2] This led to the formulation of newer more stringently tested complexes for the detection of tumour cells for various forms of cancer.[3] It also was frequently incorporated as a detection drug for any residual cancerous growth and/or cells after a patient had undergone chemotherapy/radiotherapy. This allowed doctors to determine whether a relapse may occur in the near future.[4] Gallium complexes were found to not only be able to detect cancerous growth, but in certain instances were able to induce metabolic distress in these rapidly growing cells.[5, 6] Gallium nitrate (Ganite ™) is still used widely today for the treatment of cancer-associated hypercalcemia (figure 2.3.1).[7, 8]

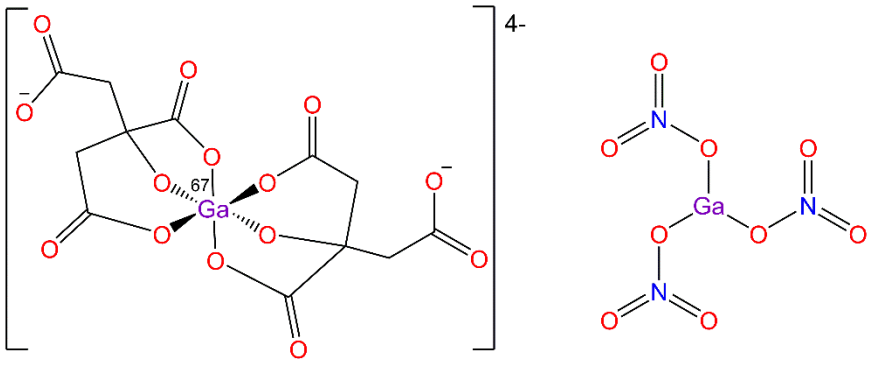

^{67}Gallium Citrate Gallium nitrate (Ganite ™)

Figure 2.3.1 Empirical structures of ^{67}Gallium citrate and commercial Gallium nitrate (Ganite ™).

Ganite ™ works via inhibition of oestoclast activity and calcium resorption from bone, exerting a hypocalcemic effect.[9] The use of gallium has been expanded upon from radiopharmaceuticals to anti-microbial and anti-cancer agents. As discussed previously, the theory behind gallium anti-microbial activity can be attributed to its pharmacological properties in the +III state, and its similarities to the physiologically essential Fe(III). Gallium is able to replace iron and block cellular homeostasis by its lack of a physiologically possible reductive pathway (Ga(III) – Ga(II)).[6, 10] There are multiple pathways that gallium is able to take in able to enter pathogenic organisms, including siderophores, ion channels and transferrin and lactoferrin, often at a higher efficacy than the external iron sources.[11-13]

2.3.2 Group 13 complexes as medicinals: Indium

Despite its electronic and chemical similarities to gallium, there is little in regards to the use of indium in a medicinal setting. Instead, a large emphasis has been placed on indium complexes as OLEDs (organic light emitting diode) and semi-conductors.[1] Indium has been shown to accumulate in bacteria, however the mechanism of uptake of indium is still unclear.[14] It has been proposed that the uptake of indium is related to the uptake of gallium in bacterial cells. The interaction of indium with *Pseudomonas fluorescens*, a bacterium notable for its studies of metal interactions, exhibited minimal influence on bacterial growth.[15] Indium nitrate has shown anti-microbial activity against the marine bacterium *V. Fischeri,* theorised to be induced by interactions with a bacterial oxidative phosphorylation mechanism.[16] Species of microalgae, including *Chlorella vulgaris* and *Dapnia magna* have also shown a high degree of susceptibility to indium nitrate. One hopeful study concluded that indium complexes of 1,4,8,11-tetraazacyclotetradecane (TETA) were an effective treatment against *Mycobacterium tuberculosis*, the pathogen responsible for

tuberculosis (figure 2.3.2).[17] Nevertheless, the studies into indium anti-microbials is currently limited and an area of study should be expanded upon in the future.

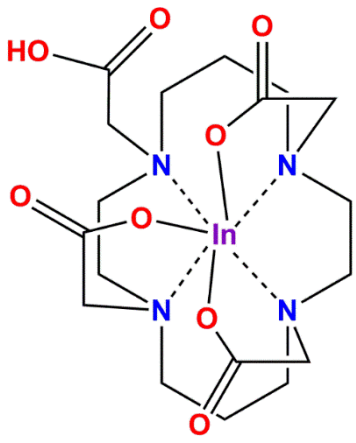

Indium TETA

Figure 2.3.2. Hypothesised structure of Indium TETA complex

2.3.3 *Leishmania* and iron acquisition

In section 1.1 the *Leishmania* parasite was introduced, a devastating and highly infectious protozoa.[18-21] The front-line treatments for *Leishmania* incorporate pentavalent antimony metallodrugs, as discussed in section 1.3. In order to grow and replicate *Leishmania,* like all eukaryotes, require iron, of which they obtain from exogenous sources. *Leishmania* are more sophisticated in their ability to acquire iron than prokaryotic organisms, able to uptake iron by multiple pathways. These pathways can be dependent on the species of *Leishmania* and its surrounding environment.[22] These change in acquisition are not only species dependant, but life cycle dependant, with different pathways observed for promastigote and amastigote. For example: *L. chagasis* promastigotes acquire iron from both transferrin and lactoferrin, essential iron transfer proteins, whereas *L. donavani* promastigotes obtain iron from saturable binding of haemoglobin (figure 2.3.3).[23-25] Promastigotes acquire iron predominately in the +II state (ferrous), with *L. chagsis* in particular utilising NADH-dependant reductases, which alludes to reductase-

dependant iron uptake from both lactoferrin and transferrin.[24] Amastigotes face a harsher environment, within the iron poor and low pH phagolysosome of mammalian macrophages.[26] In order to thrive, amastigotes possess a highly effective iron uptake system, which again can be species dependant. For example: *L. mexicana* develops characteristics of a late endosomal compartment, which potentially strips iron that is bound to the transferrin protein.[27] *L. amazonensis* however possess a family of ferrous iron transfer proteins, which are a requirement for cellular growth and development.[28]

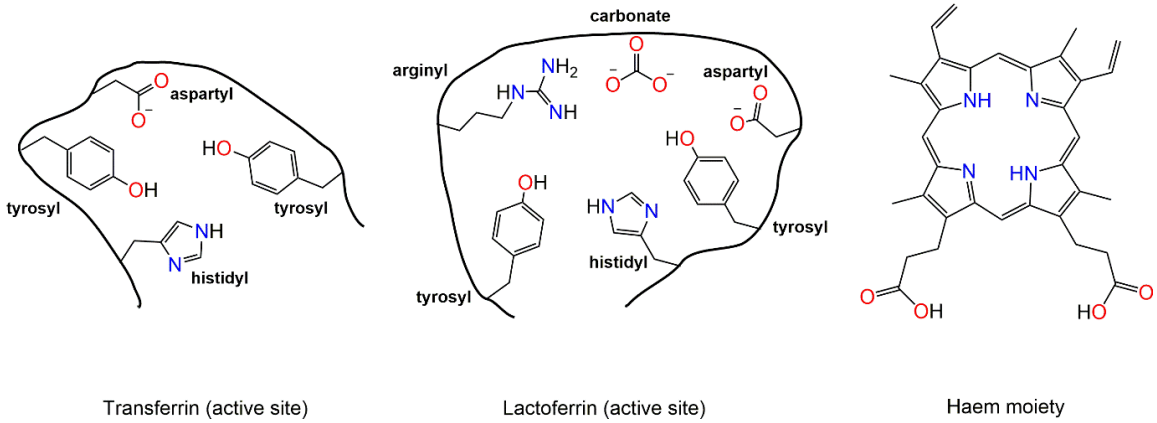

Figure 2.3.3. Iron transport proteins in biological systems

2.3.4. Alkyl gallium and indium quinolinolates

There is potential to exploit the exogenous iron acquisition of *Leishmania* by the introduction of gallium complexes. Gallium has been shown to bind competitively to the iron transport proteins lactoferrin and transferrin, leading to large influxes of gallium uptake intracellularly.[13] In some cases, gallium chelates can become too stable for any relevant activity to occur. This was observed in the tris-8-quinolinolato complex (KP46) (figure 2.3.4). Synthesised as an anti-cancer agent, it was found to be too thermodynamically and kinetically inert to elicit any anti-cancer activity. The hydrolytic stability of KP46 led to an inferred decrease of gallium release which in turn led to a decrease in gallium uptake, overall resulting in decreased biological activity.[29]

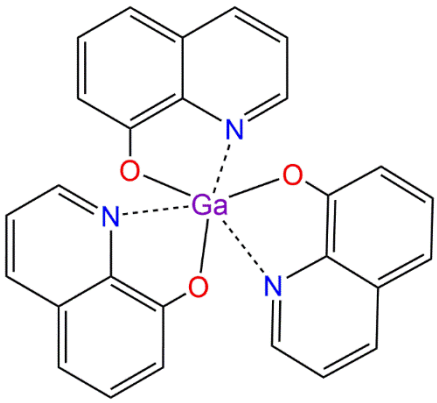

gallium tris-8-quinolinolate **(KP46)**

Figure 2.3.4. Structure of anti-cancer complex gallium tris-8-quinolinolate (KP46)

To strike a balance between reactivity and stability, heteroleptic *mono*-methyl and *bis*-methyl alkyl gallium quinolinolates were targeted. Due to the lack of activity of KP46, synthesis of the tris-substitution was not pursed. Hydrophilicity has been a major hurdle for anti-Leishmanials, therefore the additions of alkyl chains was hypothesised to increase complex lipophilicity. As previously discussed, quinolinol is an extensively studied *N,O* metal chelator, with its analogues exhibiting a variety of biological activities, including anti-Leishmanial activity.[30-35] The idea was to generate a class of complexes which would remain hydrolytically stable, but with the addition of reactive Ga – C bonds would also exhibited enough activity to exchange readily with iron in the presence of lactoferrin and transferrin. The effects of halide substitution of the quinolinols was addressed to gauge whether a biological correlation could be established (figure 2.3.5). The synthesis of the indium analogues was also attempted as a direct metal comparison to the more clinically relevant gallium complexes.

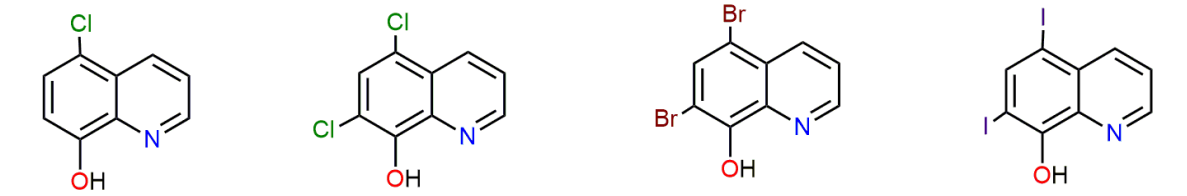

5-Chloroquinolinol, **1**
(Cloxyquin)

5,7-Dichloroquinolinol, **2**
(Chloroxine)

5,7-Dibromoquinolinol, **3**
(Broxyquinoline)

5,7-Diiodoquinolinol, **4**
(Iodoquin)

*Figure 2.3.5. Four 8-quinolinol derivatives explored in this study (**1** – **4**).*

2.3.5 Synthesis and characterisation.

2.3.5.1 Synthesis

In order to synthesise the complexes an inert and dry atmosphere was essential, due to the commercially available trimethyl gallium precursor being a highly reactive and pyrophoric liquid. The synthesis was straightforward and required only one pre-dried Schlenk vessel, via a modified procedure from Bakewell *et al*.[36] Prior to trimethyl gallium addition, the quinolinols **1** – **4** were dried under high vacuum to remove excess moisture from the solid pale yellow to off white compounds. Each quinolinol was suspended in either toluene or hexane, depending on the equivalency (summarised in Scheme 2.3.1), and cooled to -78 ^{o}C. Trimethyl gallium was transferred by a gas tight syringe to the pale yellow to off white suspension, giving an immediate colour change to bright yellow and the visible evolution of methane gas. To obtain the *mono*-methyl complexes, once warming to room temperature, the suspension was heated to reflux overnight.

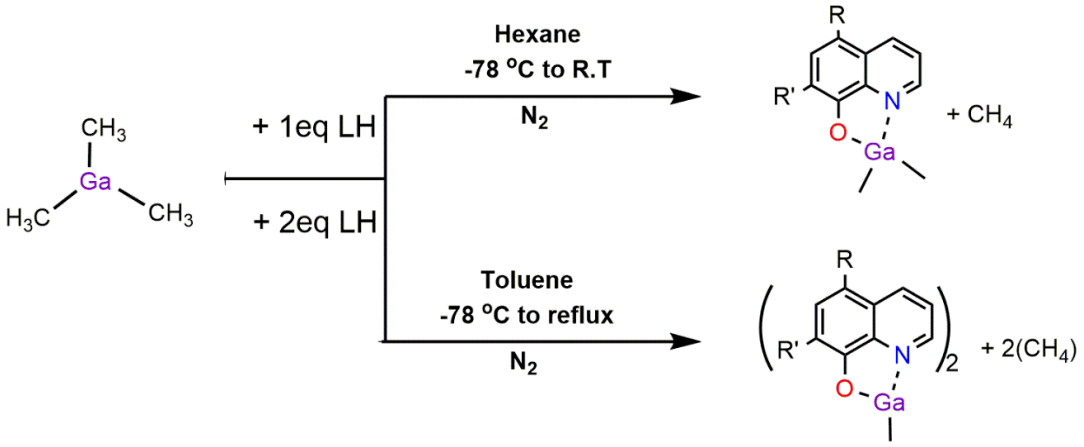

*Scheme 2.3.1. Synthetic approaches to bis-methyl and mono-*methyl *alkyl gallium quinolinolates.*

The air and moisture stable solids were then extracted by suspending any solids adhering to the sides of the flask, and collected via gravity filtration. Often the remaining filtrates were brightly coloured, and so were left to stand, yielding single crystals of all gallium complexes **1G/G'** – **4G/G'** by slow evaporation at room temperature (figure 2.3.6). Complexes were obtained in excellent yields of 89 - 97 % for complexes **1G,** $[Ga(Me)_2C_9H_5NOCl]$, **2G,** $[Ga(Me)_2C_9H_4NOCl_2]$, **3G,** $[Ga(Me)_2C_9H_4NOBr_2]$, and **4G**, $[Ga(Me)_2C_9H_4NOI_2]$ and 72 - 83 % for complexes **1G',** $[GaMe(C_9H_5NOCl)_2]$, **2G',** $[GaMe(C_9H_4NOCl_2)_2]$, **3G',** $[GaMe(C_9H_4NOBr_2)_2]$ and **4G',** $[GaMe(C_9H_4NOI_2)_2]$.

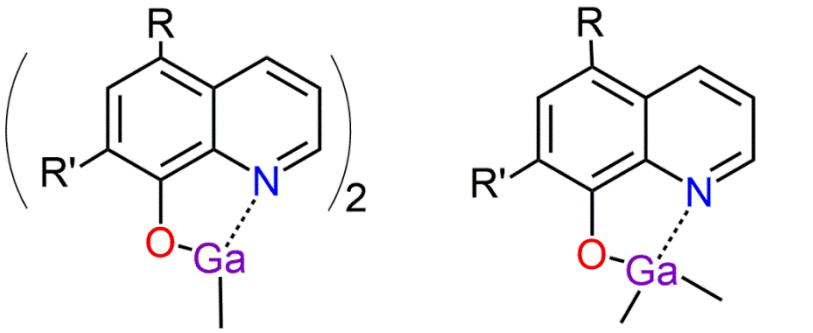

$[GaCH_3(L)_2]$, **(G')** $[Ga(CH_3)_2L]$, **(G)**

Figure 2.3.6. General formula of the synthesised gallium complexes ***1G – 4G,*** *$[Ga(Me)_2L]$ and* ***1G' – 4G',*** *$[GaMe(L)_2]$.*

The indium complexes required an additional step, the synthesis of trimethyl indium. This was performed by suspending anhydrous indium trichloride in hexane before the addition of three equivalents of methyl lithium at -78 °C. The soluble trimethyl indium was then extracted from the lithium chloride by-product by filter cannulation directly into a Schlenk flask containing the desired quinolinol, **1** – **4** (scheme 2.3.2). Only the *bis*-methyl indium complexes were successfully isolated and characterised fully. Complications with stability led to an inability to obtain all the *mono*-methyl complexes, which will be discussed further in the section (figure 2.3.7).

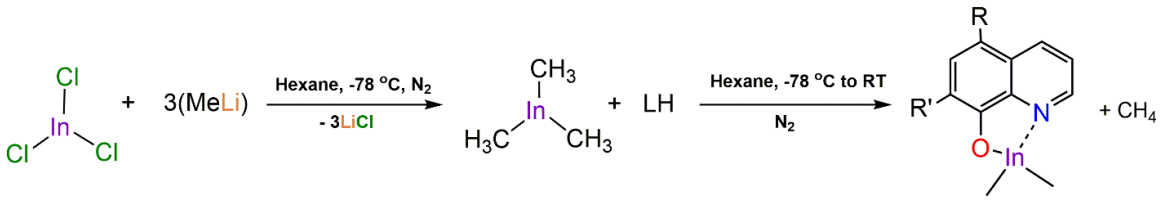

Scheme 2.3.2. Synthetic approach to bis-methyl indium quinolinolates, ***1I – 4I,*** *$[In(Me)_2L]$.*

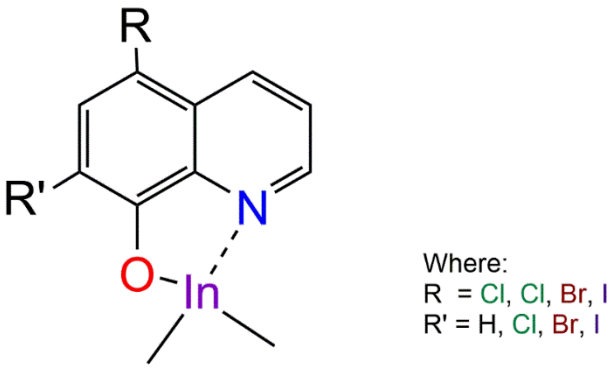

Figure 2.3.7. General formula of the bis-methyl indium quinolinolates synthesised, ***1I – 4I*** *, [In(Me)$_2$L].*

Despite the addition of another synthetic step, high yields were obtained for all indium complexes **1I,** [In(Me)$_2$C$_9$H$_5$NOCl], **2I,** [In(Me)$_2$C$_9$HNOCl$_2$], **3I,** [In(Me)$_2$C$_9$H$_5$NOBr$_2$], and **4I**, [In(Me)$_2$C$_9$H$_5$NOI$_2$] in the ranges of 73 - 86 %.

2.3.5.2. Characterisation

All complexes were characterised single crystal X-ray diffraction, FT-IR, elemental analysis, melting point, ^{1}H and ^{13}C NMR and MS (for complexes **1G** – **4G** and **1I** to **4I**). All *bis*-methyl complexes (**1G – 4G**, **1I – 4I**) and one *mono*-methyl complex (**1G'**) were completely soluble in d$_6$-DMSO and so were able to be analysed by ^{1}H and ^{13}C NMR. The *mono*-methyl complexes of gallium (**2G' – 4G')** were sparingly soluble with heating, limiting analysis to ^{1}H NMR, with ^{13}C NMR unachievable. As both trimethyl gallium and trimethyl indium are highly sensitive to both air and moisture, a reference NMR in d$_6$-DMSO was difficult to obtain, however ^{1}H NMR of each quinolinol precursor, **1** – **4**, was able to be acquired. For each complex, the main distinguishing signal to correlate to complex formation was the hydroxyl signal of the free alcohols (ranging from 10.15 – 10.95 ppm), which was absent in all of the gallium and indium complexes. To further validate alkyl gallium and indium complex formation, the addition of a methyl singlet was apparent in the ranges of - 0.345 to - 0.007 ppm for gallium (both *mono*-methyl and *bis*-methyl) and - 0.369 to - 0.332 ppm for the *bis*-methyl indium complexes. An example ^{1}H NMR of the broxyquinoline complexes **3G,**

$[Ga(Me)_2C_9H_4NOBr_2]$, and **3I,** $[In(Me)_2C_9H_4Br_2NOBr_2]$, is given below. An upfield shift of the aromatic proton on position two of the quinolinol is observed for both **3G** and **3I**. This upfield shift may be due to a number of reasons, the proximity to the metal – methyl interaction, of which methyl is a known electron donating group, or due to aromatic resonance from the lone pair of the nitrogen in the quinolinol pulling electron density from the ring towards the metal.

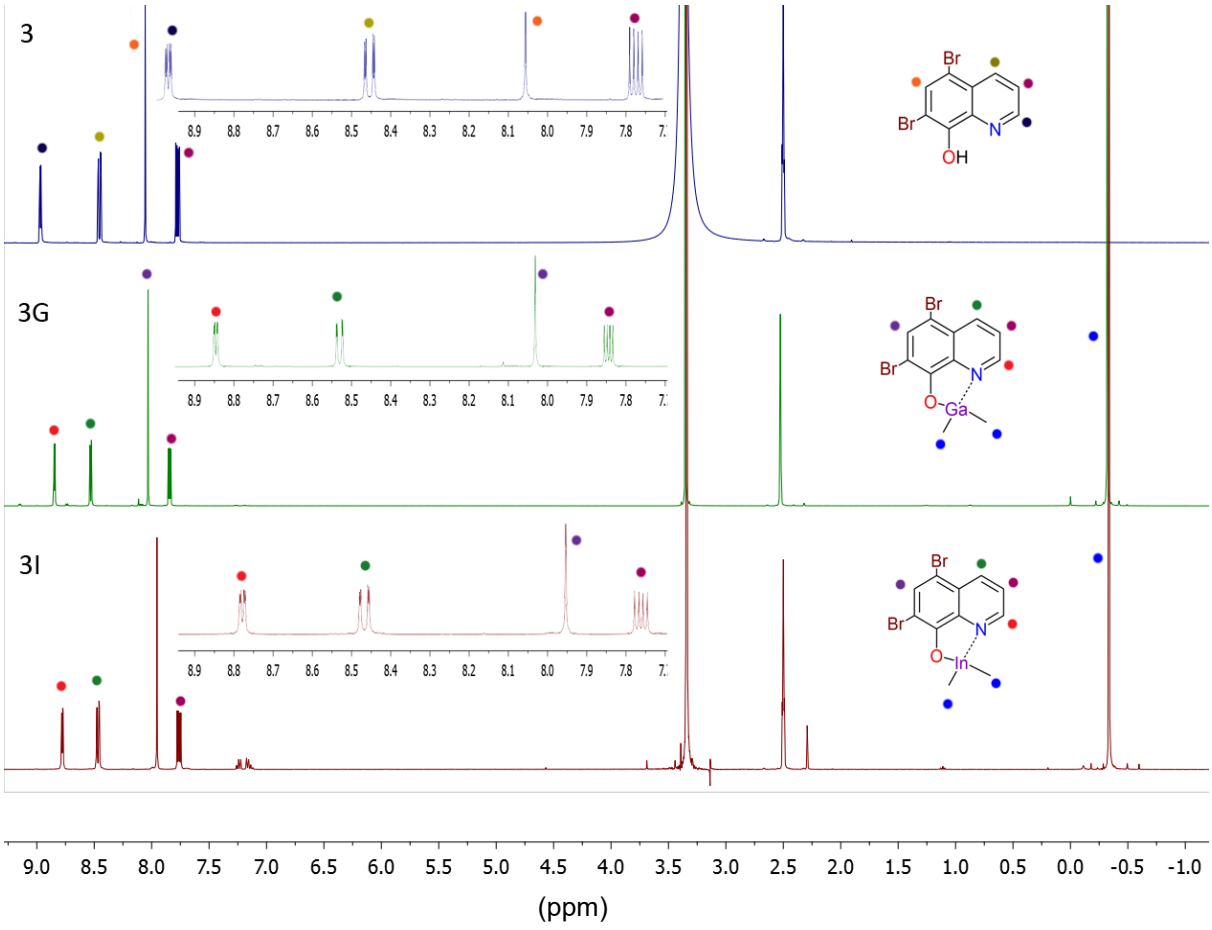

*Figure 2.3.8. ^1H NMR spectrum of complexes **3G,** $[Ga(Me)_2C_9H_4NOBr_2]$, and **3I,** $[In(Me)_2C_9H_4NOBr_2]$, against the parent alcohol, **3**, broxyquinoline, in d_6-DMSO, residual solvent signals are as followed: toluene (ar), water, DMSO and toluene (CH_3) at 7.20 ppm (**3I** spectra), 3.33 ppm, 2.50 ppm and 2.30 ppm (**3I** spectra).Insert of the expanded aromatic region given.*

The *bis*-methyl complexes of gallium (**1G – 4G**) differed from their corresponding *mono*-methyl counterparts, with only very slight shifts in the aromatic signals between the two classes

observed. Given below is an example comparative spectrum of **1G** versus **1G'**. This was the ideal comparison due the complete solubility of **1G',** [GaMe($C_9H_5NOCl)_2$], in d_6-DMSO.

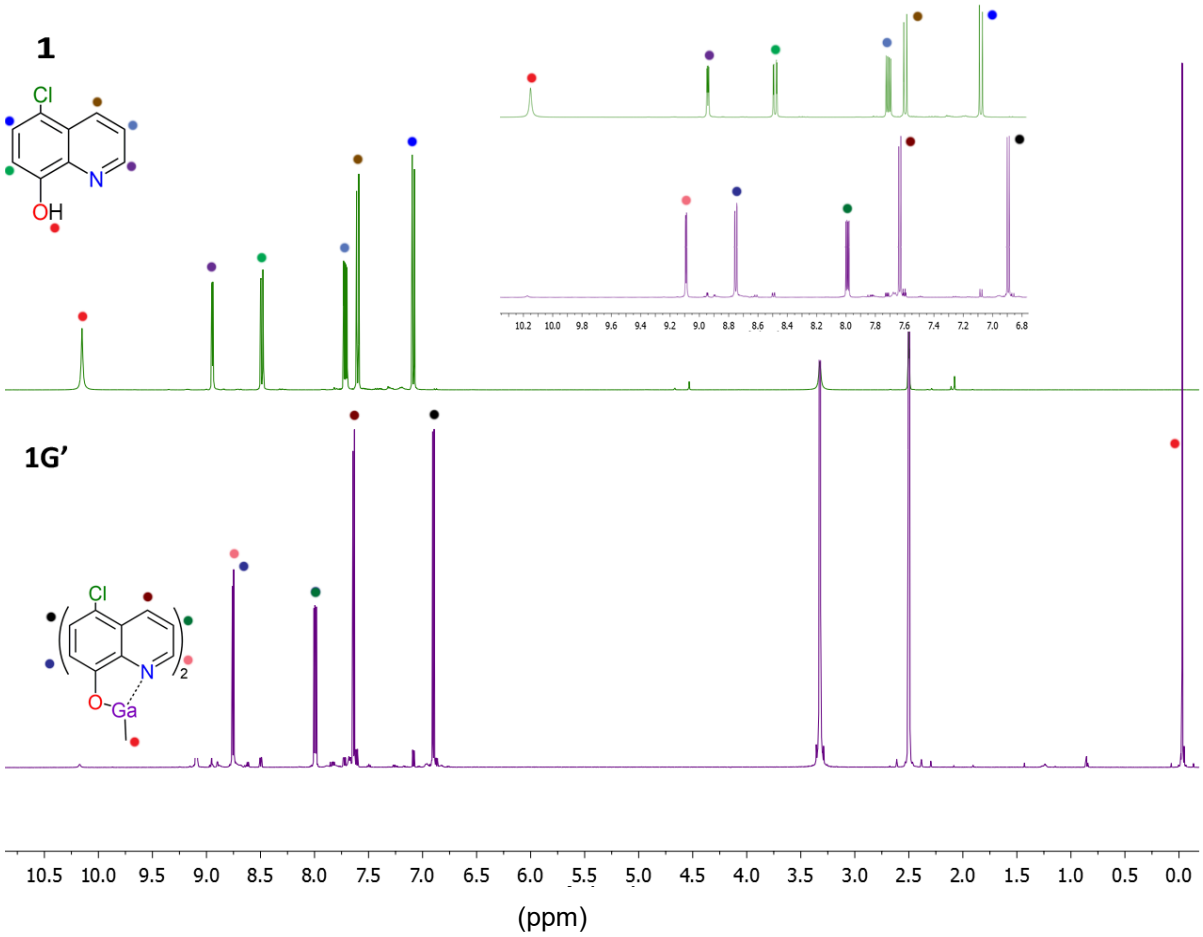

*Figure 2.3.9. ^{1}H NMR spectrum of complex **1G',** [GaMe($C_9H_5NOCl)_2$], against parent alcohol **1**, cloxyquin, in d_6-DMSO, residual solvent signal and H_2O signal at 2.50ppm and 3.33ppm respectively have not been labelled. Insert of the expanded aromatic region given.*

Complexation of the alkyl metal to the quinolinol was further clarified by infrared spectrum of each complex against the parent quinolinol. The appearance of several signals' indicative of C-H stretching (ν), asymmetric deformation (δ_{asym}) and symmetric deformation (δ_{sym}) of the methyl groups of the alkyl metal are observed along with the disappearance of the large hydroxyl stretches and hydroxyl bends (ρ) of the parent alcohol respectively. These signals and their corresponding compounds are listed below in table 2.3.1 and 2.3.2. A visual representation is also given in figure 2.3.10 and 2.3.11.

*Table 2.3.1. IR frequencies of the alkyl gallium quinolinolate complexes **1G – 4G, 1G' – 4G'** against major frequencies in ligands **1 – 4.***

Compound	CH_3-ν (cm^{-1})	CH_3-δ_{asym} (cm^{-1})	CH_3-δ_{sym} (cm^{-1})	OH-ν (cm^{-1})	OH-ρ (cm^{-1})
1	-	-	-	3167	1501
1G	2954	1458	1363	-	-
1G'	3054	1456	1366	-	-
2	-	-	-	3067	1481
2G	2961	1450	1368	-	-
2G'	3073	1459	1370	-	-
3	-	-	-	3070	1488
3G	2957	1449	1363	-	-
3G'	2958	1451	1367	-	-
4	-	-	-	2950	1481
4G	2960	1446	1367	-	-
4G'	2954	1451	1361	-	-

*Table 2.3.2. IR frequencies of the alkyl indium quinolinolate complexes **1I – 4I** against major frequencies in ligands **1 – 4.***

Compound	CH_3-ν	CH_3-δ_{asym}	CH_3-δ_{sym}	OH-ν	OH-ρ
1	-	-	-	3167	1501
1I	2963	1456	1363	-	-
2	-	-	-	3067	1481
2I	2973	1442	1358	-	-
3	-	-	-	3070	1488
3I	2920	1438	1368	-	-
4	-	-	-	2950	1481
4I	2906	1436	1368	-	-

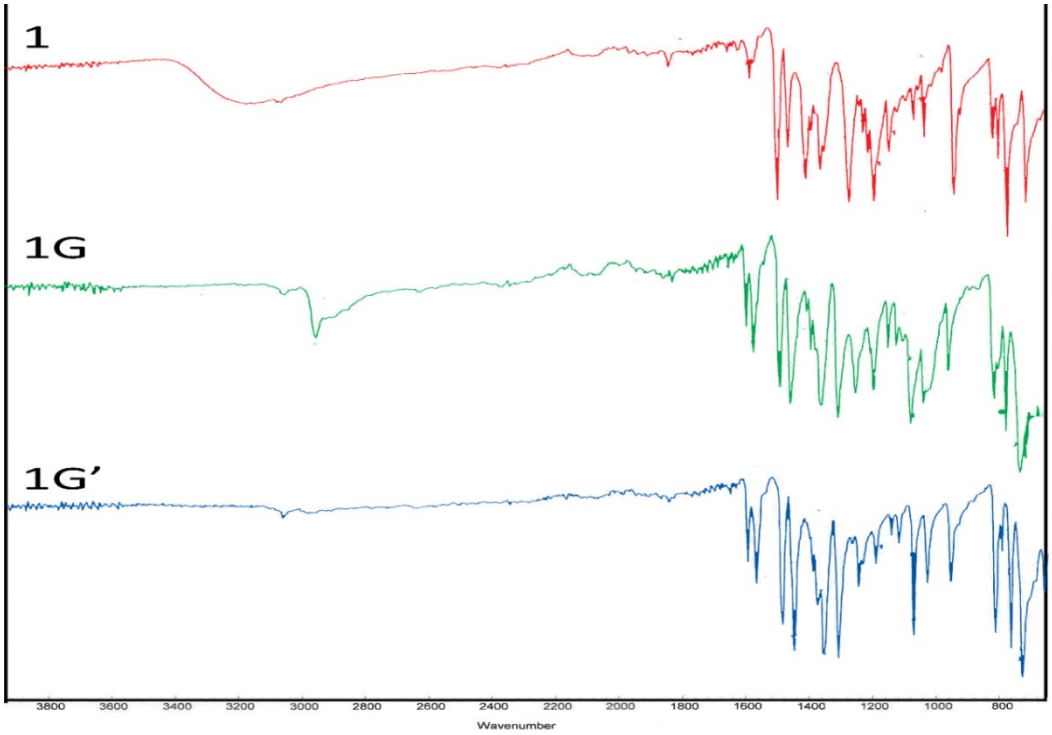

*Figure 2.3.10. Comparative IR spectrum of complexes **1G,** [Ga(Me)$_2$C$_9$H$_5$NOCl] and **1G',** [GaMe(C$_9$H$_5$NOCl)$_2$] versus parent alcohol, **1,** cloxyquin.*

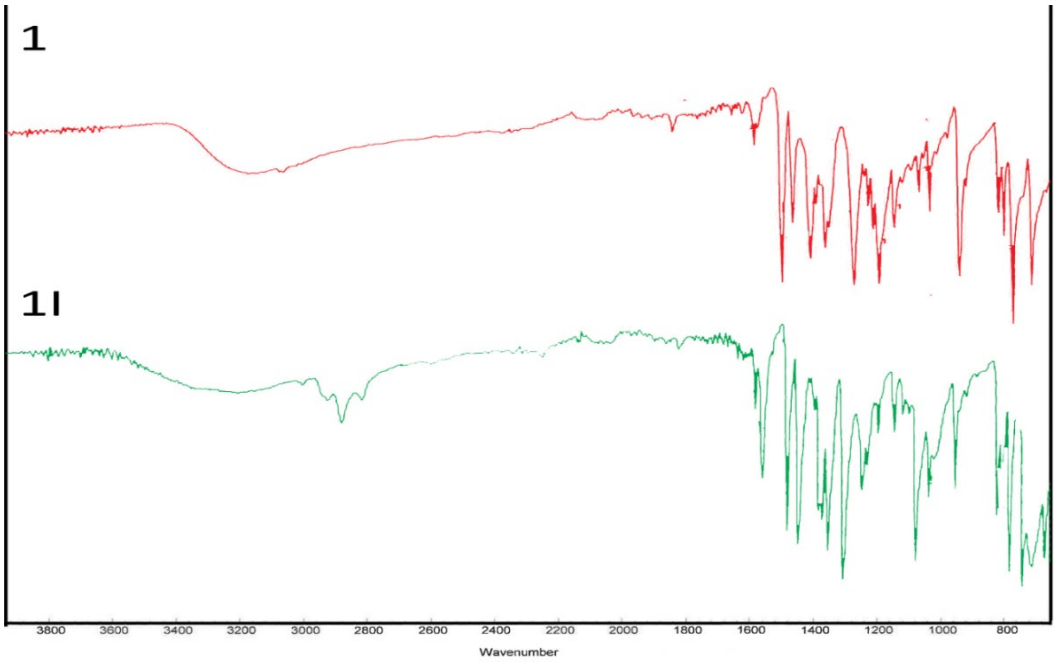

*Figure 2.3.11. Comparative IR spectrum of complexes **1I,** [In(Me)$_2$C$_9$H$_5$NOCl], versus parent alcohol, **1,** cloxyquin.*

Attempts to obtain the *mono*-methyl indium complexes in high yield proved difficult. Similar to the gallium complexes, attempts were made to react one equivalent of the *in-situ* produced $InMe_3$ with two equivalents of the free quinolinol. However, it was observed that the reactions with two equivalents of the parent alcohol led to the persistent formation of the *bis*-methyl complex, even with repeated refluxing under inert conditions in high boiling point solvents such as toluene. Despite this, the indium complexes **1I** – **4I** ($[In(Me)_2C_9H_5NOCl]$, $[In(Me)_2C_9H_4NOCl_2]$, $[In(Me)_2C_9H_4NOBr_2]$, $[In(Me)_2C_9H_4NOI_2]$), were found to be stable in the solid state (table 2.3.3), as determined by repeated elemental analysis of the complexes. Complex **1I** was repeatedly found to exist as the di-hydrate, $[In(Me)_2C_9H_4NOI_2].2H_2O$ in the solid-state. For complex **4I**, re-arrangement in solvent was rapid, and so crystals were only isolated as the complex $[(In(Me)_2(C_9H_4NOI_2)_2(In(Me)_2OH)]$, **4I-O**.

*Table 2.3.3. Elemental analysis results of complexes **1G – 4G, 1G' – 4G'** and **1I – 4I**, expected values are listed along with the duplicate averages obtained.*

Complex	EXPECTED C:H:N	FOUND C:H:N	Complex	EXPECTED C:H:N	FOUND C:H:N
1G	**C:** 47.46 **H:** 3.98 **N**: 5.03	**C:** 47.26 **H:** 3.89 **N:** 4.95	**1I**	**C:** 38.69 **H:** 3.83 **N:** 4.10	**C:** 39.05 **H:** 3.77 **N:**4.19
2G	**C:** 42.23 **H:** 3.22 **N:** 4.48	**C:** 42.35 **H:** 3.14 **N:** 4.48	**2I**	**C:**36.91 **H:** 2.82 **N:**3.91	**C:** 36.70 **H:** 2.91 **N:**3.85
3G	**C:** 32.89 **H:** 2.97 **N:** 6.34	**C:** 32.70 **H:** 2.47 **N:** 3.38	**3I**	**C:**29.57 **H :**2.26 **N:**3.13	**C:** 29.34 **H:** 2.38 **N:**3.23
4G	**C:** 26.65 **H:** 2.03 **N:** 2.83	**C:** 26.79 **H:** 1.92 **N:** 2.93	**4I**	**C:**24.43 **H:** 1.86 **N:**2.59	**C:** 24.60 **H:** 1.85 **N:** 2.66
1G'	**C:** 51.64 **H:** 2.97 **N:** 6.34	**C:** 51.84 **H:** 2.73 **N:** 6.49	-	-	-
2G'	**C:** 44.67 **H:** 2.17 **N:** 5.48	**C:** 44.57 **H:** 2.02 **N:** 5.58	-	-	-
3G'	**C:** 33.14 **H:** 1.61 **N:** 4.07	**C:** 33.28 **H:** 1.53 **N:** 4.14	-	-	-
4G'	**C:** 26.03 **H:** 1.26 **N:** 3.20	**C:** 26.19 **H:** 1.41 **N:** 3.30	-	-	-

Whist stable in the solid state, the complexes rapidly redistributed when solubilised, especially in solvents miscible with water. An example of this instability is given in figure 2.3.12 below. Complex **3l,** [$In(Me)_2(C_9H_4Br_2NO)$] was dissolved into d_6-DMSO and an ^1H NMR spectrum recorded. After one week, a second ^1H NMR taken. The formation of multiple products as seen by the several sets of both aromatic and methyl signals was observed. It is possibly a mix of decomposition products, methyl hydroxides and oxides; however, the overlap of signals and lack of reference material makes it difficult to ascertain. .

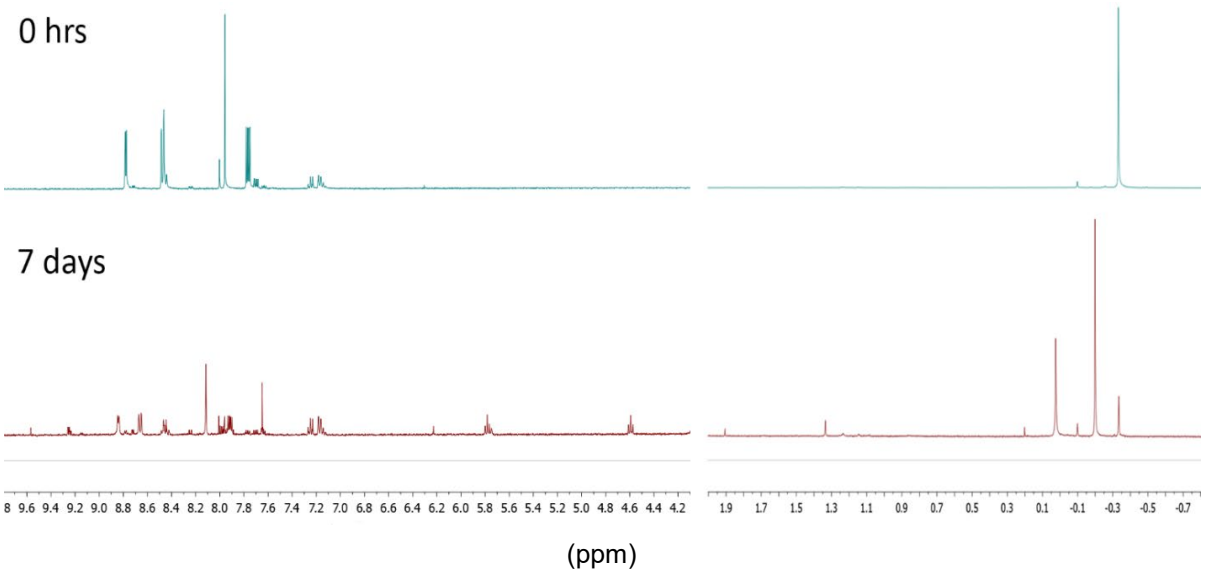

*Figure 2.3.12. ^1H NMR study of complex **3**l, [$In(Me)_2(C_9H_4Br_2NO)$], from 0 hours to seven days. Residual solvent signals have not been included for clarity.*

Although synthetically difficult to obtain, one *mono*-methyl complex was obtained in a reaction mixture of the *bis*-methyl complex that had been heated into acetone. The complex, **3l'**, [$InMe(C_9H_4NOBr_2)_2$], is the *mono*-methyl broxyquinoline indium analogue. These crystals were not easily isolated from the mixture of products, leading to difficulties in obtaining a clean NMR. Crystals of the *bis*-methyl complex **3l,** [$In(Me)_2C_9H_4NOBr_2$], were obtained by heating a small portion of the pure solid into acetone, it was filtered and then immediately placed into an ice bath causing a small crop of crystals to form. These crystals were isolated and the solid-state structure

for **3I** obtained. The same solution was left at room temperature and within a day a new set of similar shaped crystals had grown from the highly coloured solution. These crystals were then determined to be the redistribution product **3I'** (further discussion and visual representation given in the X-ray discussion below). When the solution was left to stand over a week, dark orange crystals were produced within the yellow residue left in the vial. These orange cubic crystals were removed from the yellow residue and a solid-state structure obtained. This turned out to be an indium cluster (**3I-C**, $[In_4(OH)_4(C_9H_5NOBr_2)_8]$), further discussion and visual representation given in the X-ray section), in which two methyl groups had been replaced by 5,7-dibromoquinolinol and the remaining methyl group hydrolysed to a hydroxide moiety. This hydroxide interacts with other indium centres to form the four indium cluster core. Similar to complex **3I'**, the cluster complex, **3I-C**, was difficult to purify due to solvent similarities and a very low yield (negligible). Though NMR data could not be obtained for **3I'** and **3I-C**, it is reasonable to assume that since they both formed from the heating of **3I** in acetone, some sort of redistribution and hydrolysis had occurred which was favourable in the presence of air and moisture. A COSY NMR was also performed on the reaction mixture in an attempt to identify the many products, however no discernible products could be easily identified. It is probable the mixture was comprised of multiple alkyl indium oxides, hydroxides, along with variations of the ligand containing complex. Though unable to be determined solidly through ^{1}H NMR, the use of single crystal X-ray diffraction assisted in alluding to the possible pathway (scheme 2.3.3).

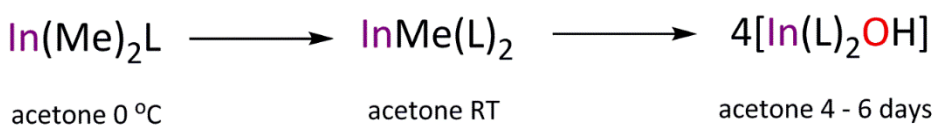

Scheme 2.3.3. Theoretical pathway as monitored by X-ray crystallography. No by-products, other reagents or solvents are listed.

Along with the broxyquinoline cluster, clusters of chloroxine and iodoquin were also obtained after leaving solutions of **2I,** [$In(Me)_2C_9H_4NOCl_2$], and **4I,** [$In(Me)_2C_9H_4NOI_2$)], at room temperature for upwards of a week. The cluster, **4I-C,** [$In_4(OH)_4(C_9H_5NOI_2)_8$], was obtained from toluene, and **2I-C,** [$In_4(OH)_4(C_9H_5NOCl_2)_8$], from acetone. As no concrete analytical data other than X-ray crystallography could be obtained on these clusters there will be no further discussion on their synthesis and characterisation.

All remaining complexes were able to undergo analysis via single crystal X-ray diffraction to elucidate their solid-state structure. All gallium complexes were obtained from the brightly coloured filtrates of the reaction mixture. The indium complexes proved more difficult. Complex **1I** and **2I** were obtained from reaction filtrates, however as discussed previously, complexes **3I** and **4I** had to be crystallised via a hot filtration in acetone, which caused issues with re-arrangement and instability of the indium complexes.

2.3.5.2 X-ray crystallography

All gallium complexes **1G,** [$Ga(Me)_2C_9H_5NOCl$], **2G,** [$Ga(Me)_2C_9H_4NOCl_2$], **3G,** [$Ga(Me)_2C_9H_4NOBr_2$], and **4G**, [$Ga(Me)_2C_9H_4NOI_2$] were analogous in structure presenting as four-coordinate tetrahedrons. Due to the symmetry of **1G**, it can form a dative interaction with the oxygen of a neighbouring **1G** molecule. This forms a dimer which is formally five-coordinate, trigonal bipyramidal about the gallium. The *bis*-substituted complexes **1G',** [$GaMe(C_9H_5NOCl)_2$], **2G',** [$GaMe(C_9H_4NOCl_2)_2$], **3G',** [$GaMe(C_9H_4NOBr_2)_2$] and **4G',** [$GaMe(C_9H_4NOI_2)_2$], are all five coordination through the chelation of two substituted quinolinols along with one covalent bound methyl group. Similar to the **1G** dimer, they are all distorted trigonal bipyramids.

Several complexes synthesised with an alkyl gallium carboxylate configuration exhibit dimerisation. The carboxylate allows for a covalent bond to one gallium centre with the

carboxylate hydroxyl, and a dative interaction from the carbonyl oxygen, forming a dimeric bridge complex. Complexes synthesised by Kaluderovic *et al*, of which were tested exclusively for their anti-cancer activity, highlight this carboxylate bridging dimerisation.[37, 38] Although dimerisation with itself is not an unknown phenomena with alkyl gallium complexes, little structural characterisation on both the *bis*-methyl and *mono*-methyl substituents utilising the halido-8-quinolinol class has been assessed. The only structures present in the literature that have been characterised by X-ray diffraction are that of the 8-quinolinol and the 5,7-dichloro-2-methyl-8-quinolinol, known commonly as chlorquinadol.[36] Complex **1G** was found to be analogous to the formerly synthesised 8QH complex, due to the formation of the dimer complex (figure 2.3.13).

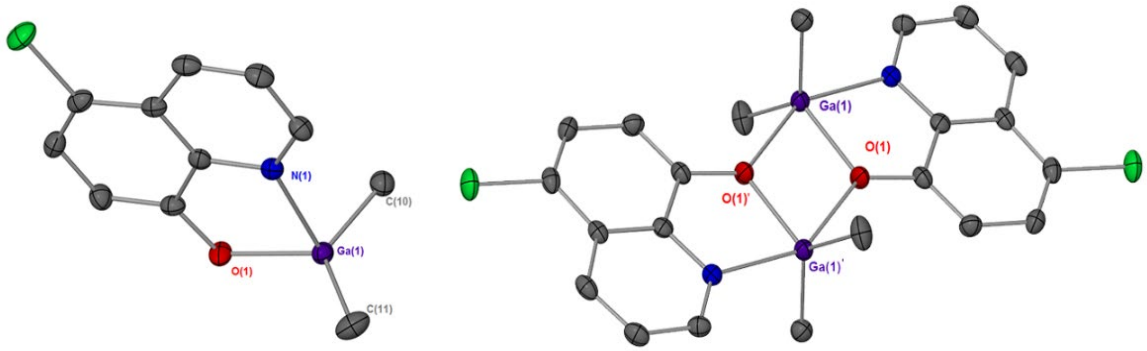

*Figure 2.3.13. Solid-state structure of the asymmetric unit and dimer of complex [Ga(Me)$_2$C$_9$H$_5$NOCl)], **1G**, thermal ellipsoids at 50% probability. Hydrogen atoms have been omitted for clarity. Selected bonds lengths (Å) and angles (o). Ga(1) – O(1), 1.953(16), Ga(1) – N(1), 2.204(19), Ga(1) – C(10), 1.963(2), Ga(1) – C(11), 1.969(3); O(1) – Ga(1) – N(1), 78.07(7), O(1) – Ga(1) – C(10), 111.3(9), O(1) – Ga(1) – C(11), 118.3(10), C(10) – Ga(1) – C(11), 130.1(14), N(1) – Ga(1) – O(1)', 149.8(7). Symmetry operator: 1 - x, -y, -z.*

The Ga – C bond for complex **1G** is similar to that of the 8QH complex synthesised and characterised by Onyitikua *et al*, with averaged bond lengths of 1.966 Å and 1.945 Å respectively. The discrepancy in the average lengths may be due in part to the halide substitution of the five position in complex **1G**. The resonance of the quinoline moiety deposits a stable positive charge

on the five position of the ring, which could allude to the shortening of the carbon – gallium bond in the 8QH structure. The combination of this resonance and the addition of a electronegative chlorine may exhibit both resonance and inductive effects on the ring, drawing electron density and allowing for a lengthening of the bond as observed in **1G**. Chlorine like other halogen (excluding fluorine) has both a resonance dipole and electronegativity dipole, however the effects of the electronegativity dipole exceeds that of the resonance dipole and so chlorine in ring systems acts largely as an electron withdrawing group.[39] the bond length for Ga – O can be determined as covalent, with bond length of a 1.953 Å, whereas the Ga – N bond was observed to be dative, with a length of 2.204 Å. These lengths are similar to those observed in the 8-quinolinol complex synthesised by Onyitikua *et al*, with lengths of 1.892 Å and 2.127 Å for Ga – O and Ga – N respectively. Like complex **1G**, the 8QH complex also presents as a distorted four coordinate tetrahedron in the asymmetric unit, but five coordination trigonal bipyramid in the dimeric state. This dimer complex is planar with regards to the quinolinol ligand, with the quinolinol sitting in the equatorial plane, central to the gallium. The oxygens in this unit occupy both axial and equatorial positions in regards to the gallium centres. One coordination site of the gallium centre is occupied by an oxygen in the axial position through a dative interaction, with the other sitting in the equatorial plane as the covalently bound substituent. A trigonal angle of 149.8(7) ° was exhibited for N(1) – Ga(1) – O(1)' for complex **1G,** of which was almost identical to the 8QH complex synthesised by Onyitikua *et al*, of 149.7 °. Both exhibit distortion along the trigonal angle from the ideal trigonal bipyramidal geometry of 120 °.[40]

The remaining complexes **2G – 4G,** $[Ga(Me)_2C_9H_4NOCl_2]$, $[Ga(Me)_2C_9H_4NOBr_2]$, $[Ga(Me)_2C_9H_4NOI_2]$, were found to exist exclusively as *mono*mers, forming four-coordinate distorted tetrahedrons. The Ga – C bond also seems to lengthen in comparison to the cloxyquin complex **1G,** for the chloroxine, broxyquinoline and iodoquin complexes **2G**, **3G** and **4G** respectively. This alludes to the size of the halides on the 5 and 7 positions of the ring having an

observable effect on the gallium – methyl bonds. A visual representation of complex **2G** is given below in figure 2.3.14.

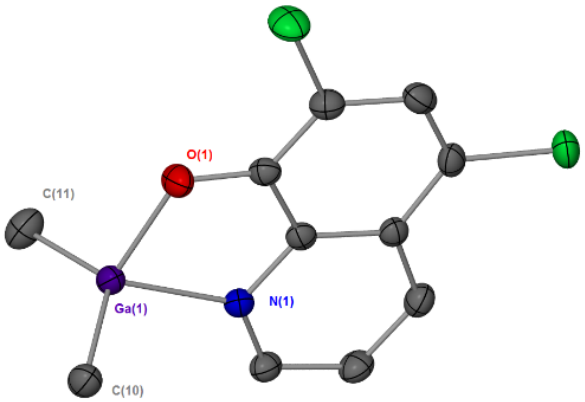

*Figure 2.3.14. Solid-state structure [Ga(Me)$_2$C$_9$H$_4$NOCl$_2$], **2G**, Thermal ellipsoids at 50% probability. Hydrogen atoms have been omitted for clarity. Selected bonds lengths (Å) and angles (o). Ga(1) – O(1), 1.929(17), Ga(1) – N(1), 2.064(2), Ga(1) – C(10), 1.954(2), Ga(1) – C(11), 1.958(3); O(1) – Ga(1) – N(1), 83.02(7), O(1) – Ga(1) – C(10), 109.10(10), O(1) – Ga(1) – C(11), 110.73(10), C(10) – Ga(1) – C(11), 126.99(12), N(1) – Ga(1) – C(11), 108.88(10)*

The major difference between the *mono*-methyl and *bis*-methyl complexes is the coordination number, due to the addition of a second *bi*-chelating quinolinolate ligand in place of a methyl group. All *mono*-methyl complexes **1G',** [GaMe(C$_9$H$_5$NOCl)$_2$], **2G',** [GaMe(C$_9$H$_4$NOCl$_2$)$_2$], **3G',** [GaMe(C$_9$H$_4$NOBr$_2$)$_2$] and **4G',** [GaMe(C$_9$H$_4$NOI$_2$)$_2$], exist as five coordinate complexes with distorted trigonal bipyramidal geometry. Although there is little literature on *mono*-methyl *bis*-quinolinolate complexes, structurally similar complexes which replace the methyl group with a chloride or a tert-butoxide are geometrically similar to the complexes **1G' – 4G'.** A *mono*chloro *bis*-quinolinolato complex [Ga(C$_9$H$_3$Cl$_2$CH$_3$)$_2$Cl] and a *mono-tert*butoxido *bis*-quinolinolato complex [Ga(C$_9$H$_3$Cl$_2$CH$_3$)$_2$O(CH$_3$)$_3$], synthesised by Bakewell *et al* exhibit the same geometry, with the distortion largely associated with the N – Ga – N bonds in the axial plane of the metal complexes.[36] Indeed this distortion from the ideal linear angle of 180 ° is also observed in the

mono-methyl complex of chloroxine, **2G'**, with a bond angle of 160.84 ° for N(1) – Ga(1) – N(2) (figure 2.3.15).

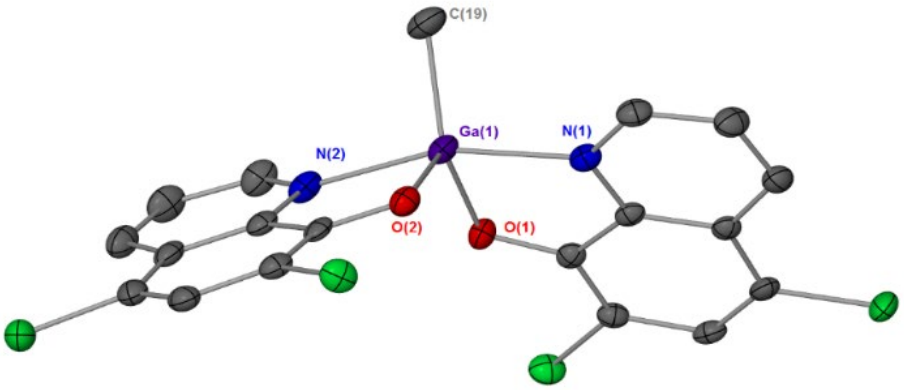

*Figure 2.3.15. Solid-state structure [GaMe($C_9H_4NOCl_2$)$_2$], **2G'**, Thermal ellipsoids at 50% probability. Hydrogen atoms have been omitted for clarity. Selected bonds lengths (Å) and angles (o). Ga(1) – O(1), 1.906(18), Ga(1) – O(2), 1.918(18), Ga(1) – N(1), 2.122(2), Ga(1) – N(2), 2.142(2), Ga(1) – C(19), 1.959(3); O(1) – Ga(1) – O(2), 112.40(8), O(1) – Ga(1) – N(1), 81.21(8), O(1) – Ga(1) – N(2), 85.16(8), C(10) – Ga(1) – O(1), 131.82(11).*

The gallium oxygen bonds of the quinolinolato ligand sit in two of the three equatorial positions of the complex and are formally covalent, with an average bond length of 1.918 Å. The elongated dative interactions of the Ga – N bonds was found to be dative (average: 2.132 Å). This correlates well with the structurally similar complexes from Bakewell *et al*, with a report of average lengths of 1.868 Å and 2.107 A for Ga – O and Ga – N respectively.[36] the methyl group of the complex sits in the equatorial plane, adjacent from the oxygen atoms of the quinolinolate. The bond length of 1.959(3) Å for Ga – C was observed and is indicative of a covalent interaction between carbon and gallium. The axial plane angle in the *mono*-methyl complexes was found to exhibit less distortion than the dimeric complexes of indium and the cloxyquin gallium complex **1G**. An axial angle along N(1) – Ga – N(2) for **2G'** was found to be 160.84(8) °, compared to the axial angle of 149.8(7) ° in complex **1G**. A difference in the extended packing of the dimeric **1G** versus the monomeric **2G** was also observed. The units of the **1G** dimer pack parallel to each other, forming interactions through slipped π - π stacking of the quinolinol of one unit, to the quinolinol of another (figure 2.3.16).

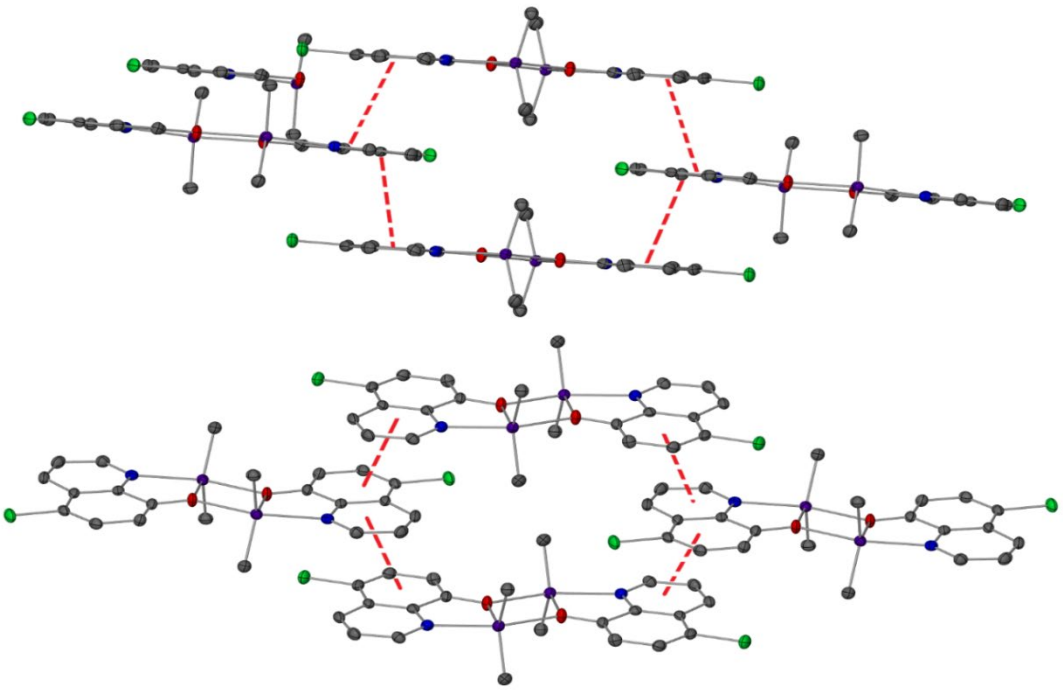

*Figure 2.3.16. Expanded cell of complex **1G**, [Ga(Me)$_2$C$_9$H$_5$NOCl)], highlighting the packing orientation. The slipped π centroid – centroid interactions are denoted by dashed red lines.*

The centroid – centroid distance of these interactions were found to be 3.532(2) Å. The quinolinol moieties are planar, whilst the methyl groups sit perpendicular to the ligands in the arrangement. Quinoline derivatives synthesised by Pena-Solorzano *et al* and Zhao *et al* were found to exhibit similar behaviour with π - π stacking of aromatic moieties within the packing diagram. The centroid distance of three *N*-(3-acetylphenyl)quinolone-2-carboxamides and one *N*-(2-benzoyl-5-ethylnylphenyl)quinoline-2-carboxamide synthesised by Pena-Solorzano *et al* were all found to have distances ranging from 3.577(1) Å – 3.780(1) Å.[41, 42] Similar to these, the 6-(4-Nitrobenzyloxy)quinoline synthesised by Zhao *et al* presented with a centroid – centroid distance of 3.663(2) Å.[43] **1G** has a slightly shorter centroid – centroid distance which indicates a higher level of stability and a more tightly bound interaction between the moieties. It is possible that being a metal complex as opposed to a free organic may contribute to this tighter interaction between units. The remaining complexes **2G** – **4G** all have a different packing orientation than that of **1G**.

The monomeric complexes tend to pack in an alternating parallel conformation, with a similar slipped π - π system through centroid – centroid interactions. Similar to **1G**, the quinolinols are planar with the methyl groups perpendicular to them. Complex **2G** was found to have a centroid – centroid distance of 3.879(10) Å, significantly longer than the dimeric **1G** but still within a reasonable distance for the crystallographic interaction (2.3.17).[41-43]

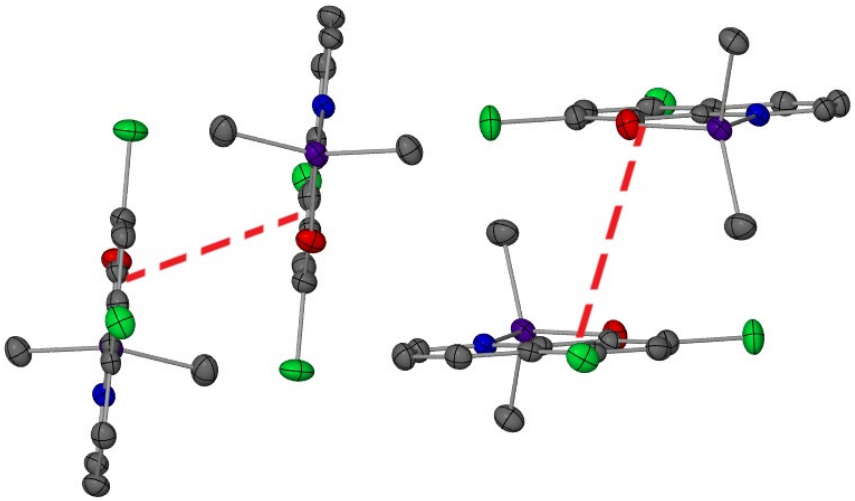

*Figure 2.3.17. Expanded cell of complex **2G**, [Ga(Me)$_2$C$_9$H$_4$NOBr$_2$], highlighting the packing orientation. The slipped pi centroid – centroid interactions are denoted by dashed red lines.*

The three *bis*-methyl indium complexes **1I**, [In(Me)$_2$C$_9$H$_5$NOCl], **2I,** [In(Me)$_2$C$_9$H$_4$NOCl$_2$] and **3I,** [In(Me)$_2$C$_9$H$_4$NOBr$_2$NO], were analogous in structure to complex **1G,** presenting as dimeric in the solid-state. Similar to gallium, dimerisation is common in alkyl indium complexes. Indium will readily form dative interactions with neighbouring atoms to fill its larger coordination sphere. This pushes the coordination number of the indium from four to five, giving it an overall distorted trigonal bipyramidal geometry. The only existing complex that incorporates this class of ligand is the tris-8-quinolinolate.[44] Reports of alkyl indium carboxylate complexes share a similar coordination, incorporating either five membered or six membered *N,O* chelates.[45-47] The dimer forms via an interaction of one indium with the covalently bound oxygen of the other indium in

the complex, forming a four membered chelate. Indium complexes that have an *O,O* chelate also tend to form the same four membered In_2-X_2 core, where X in this case is oxygen.[48-52] Example complex **3I** (figure 2.3.18) was found to have average In – C bond length of 2.137 Å.

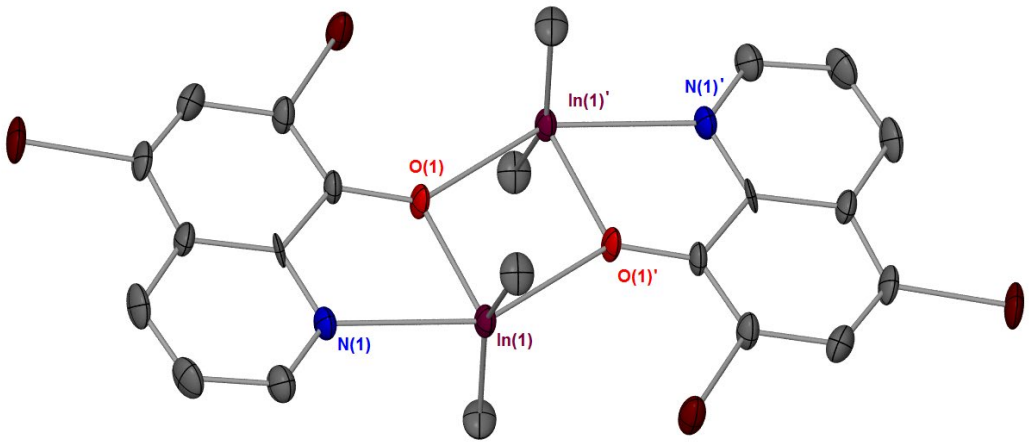

Figure 2.3.18. Solid-state structure $[In(Me)_2C_9H_4NOBr_2]$, ***3I****, Thermal ellipsoids at 50% probability. Hydrogen atoms have been omitted for clarity. Selected bonds lengths (Å) and angles (o). In(1) – O(1), 2.235(4), In(1) – N(1), 2.406(5), In(1) – C(10), 2.139(7), In(1) – C(11), 2.136(6); O(1) – In(1) – N(1), 71.32(18), O(1) – In(1) – C(10), 104.0(2), O(1) – In(1) – C(11), 91.60(2), C(10) – In(1) – C(11), 154.7(3), N(1) – In(1) – C(11), 95.90(2) O(1) – In – O(1)', 76.78(17), N(1) – In – O(1)', 148.07(17).*

These average lengths are similar to other alkyl indium *N,O* chelates. Complexes synthesised by Shen *et al*, Lewinski *et al* and Basharat *et al*, exhibited average In – C bond lengths of 2.144 Å, 2.135 Å and 2.155 Å, 2.156 Å and 2.148 Å respectively. Similar to the analogous gallium complex, the methyl groups sit in the equatorial plane of the molecule, with the ligand occupying the axial positions and the remaining equatorial positions. The In(1) – O(1) covalent length of **3I** 2.235(4) Å is almost 0.2 Å shorter than the corresponding dative interaction it forms with the quinolinol of the second indium centre, of 2.413(4) Å. The interaction between the quinolinol nitrogen and the indium to form the five-membered chelate is also dative in nature, with a bond length of 2.406(5) Å. This interaction is similar to those found in the *bis*-methyl indium *N,O* chelates synthesised by

Shen *et al* and Lewinski *et al* who observed dative interactions with bond lengths of 2.523(5) Å and 2.366(3) Å respectively.[46, 53] All bond lengths were found to be longer than the analogous gallium complex. As indium has larger radius than gallium this is not surprising (M^{3+}: 0.62 In Å versus 0.47 Ga Å).[1] Distortion along the axial plane of the O(1)' – In(1) – N(1) interaction was observed, deviating away from the ideal trigonal angle of 120 ° with an angle of 148.07(17) °. Deviation was also observed in the axial – equatorial planes with a large degree of distortion observed from the ideal 90 °, with bond angles of 71.32(18) ° and 76.78(17) ° for O(1) – In(1) – O(1)' and O(1) – In(1) – N(1) respectively. Similar deviations were observed in the complex, [$Me_2In(\mu$ –O–$CH_2CH_2(2$ –$C_5H_4N)_2$)], synthesised by Shen *et al*, which was observed to have equatorial – axial plane bond angles of 80.2(2) ° and 75.4(2) ° for O – In – N and O* – In – O respectively (where * = the dative oxygen interaction).[45]

3I', [$InMe(C_9H_4NOBr_2)_2$] is structurally analogous to **3G'**, [$GaMe(C_9H_4NOBr_2)_2$], a five-coordinate trigonal bipyramid incorporating the broxyquinoline ligand. *Mono*-methyl *bis*-substituted complexes of indium are lacking in the literature, with only scattered reports of *mono*-methyl and one *mono*-chloro indium complex with large tetradentate ligands.[54-57] Regardless of denticity, the complexes are still five coordinate and exist in a similar geometry to complex **3I'** (figure 2.3.19). The bond length of the indium carbon bond was found to be 2.109(7) Å, which was observed to be shorter than the *bis-methyl* analogue **3I**.

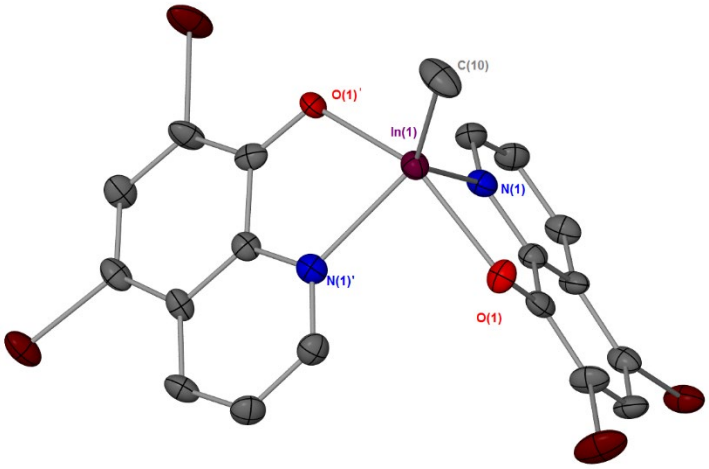

*Figure 2.3.19. Solid-state structure [InMe($C_9H_4NOBr_2$)$_2$], **3I'**, Thermal ellipsoids at 50% probability. Hydrogen atoms have been omitted for clarity. Selected bonds lengths (Å) and angles (o). In(1) – O(1), 2.172(3) , In(1) – N(1), 2.244(4), In(1) – C(10),2.109(7); O(1) – In(1) – O(1)', 147.20(16), O(1) – In(1) – N(1), 83.71(12), O(1) – In(1) – N(1)', 83.71(2), C(10) – In(1) – N(1), 130.91(1). Symmetry operator: 1-x, y, 1/2-z*

The In – O and In – N bonds were found to be shorter than those in the *bis*-methyl complexes **3I** (In(1) – O(1): 2.172(3) Å, In(1) – N(1): 2.244(4) Å). These lengths are similar to the *mono*-methyl salen indium complexes synthesised by Normand *et al* and Hyun *et al,* which observed average lengths of 2.101 Å, 2.087 Å and 2.239 Å, 2.249 Å for In – O and In – N respectively.[55] The distortion along the axial angle was observed to be more pronounced in the indium complex as opposed to the gallium, and to further distinguish the two, the axial positions in the indium complex are occupied by the oxygen atoms as opposed to the nitrogen. An axial angle of 147.20(16) ° was observed for O(1) – In – O(1)' of complex **3I'** as opposed to the 160.84(8) ° of the N(1) – Ga – N(2) angle of **2G'**.

Complex **3I-C,** [$In_4(OH)_4(C_9H_5NOBr_2)_8$], was obtained again from the same filtrate solution of **3I** and **3I'**, after a week-long crystallisation period. The orange crystals were found to be the indium cluster of the formula 4[In(L)$_2$OH] (figure 2.3.20).

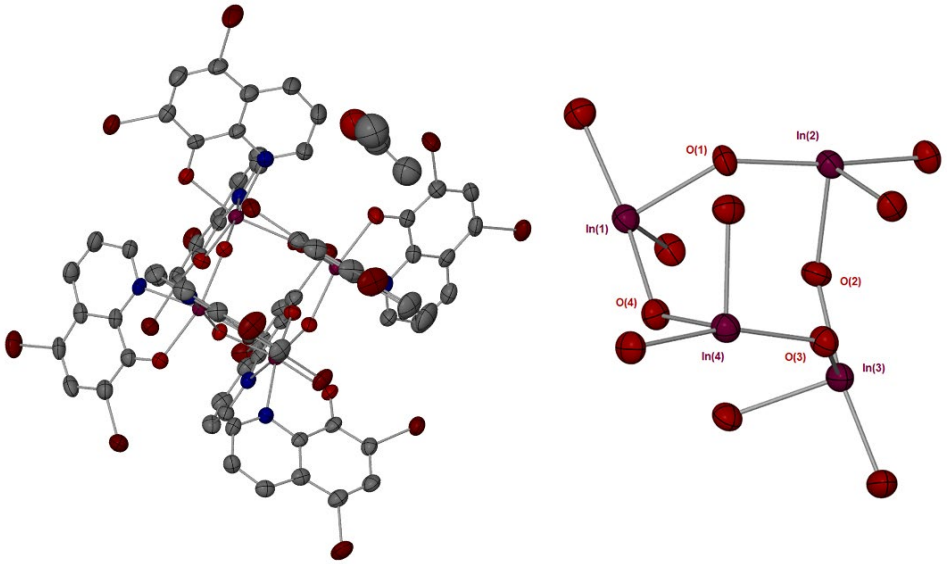

Figure 2.3.20. Solid-state structure $[In_4(OH)_4(C_9H_4NOBr_2)_8]$, ***3I-C,*** *$In_4$ – $(OH)_4$ cluster core has been included. Thermal ellipsoids at 50% probability. Hydrogen atoms have been omitted for clarity. Selected bonds lengths (Å) and angles (o). In(1) – O(1), 2.111(3) , In(1) – O(4), 2.129(3), In(2) – O(1), 2.114(3) , In(2) – O(2), 2.107(3), In(3) – O(3), 2.099(3), In(3) – O(4), 2.151(3) In(4) – O(3), 2.133(3) , In(4) – O(4), 2.128(3); O(1) – In(1) – O(2), 94.57(13), O(1) – In(2) – O(2), 99.58(13).*

The cluster core consisted of four indium atoms and four oxygen atoms in a repeated In – O – In – O fashion. Resonance throughout this cluster core was confirmed by the bond lengths observed between each indium and oxygen within the core. An average bond length of 2.114 Å was calculated. Despite the similar bond lengths between each oxygen and indium atom, it is assumed that the oxygen atoms must be hydroxides in order to balance the +III charge of the indium metal centre. This interaction differs from other indium-hydroxide clusters in the literature, with the cluster synthesised by Arif and Barron exhibiting clear differences between the covalent In – O bond and the dative interaction of a neighbouring indium (average lengths of 2.163 A and 2.287 Å respectively).[58] A similar situation was observed for indium clusters synthesised by Chamazi *et al*, with a distinct difference between the covalent and dative interactions within the cluster core.[59] Major differences between these complexes and **3I-C** are the size and angles of the cores themselves. While **3I-C** was found to be a $[In_4(OH)_4]$ core, the clusters synthesised by Arif and Barron and Chamazi *et al* were observed to be $[In_2P_2(OH)_4]$ and $[In_{10}(OR)_{12}O_2]$ cores respectively.

The bond angles for O – In – O were found to average 94.533 °, with only minimal distortion form the ideal 90 ° angles, whereas the average In – O – In angle was distorted from the ideal trigonal angle with an average value of 131.41 °. This angle was observed to be not dissimilar to the trigonal angles of the example *mono*-methyl complexes **2G'** and **3I'** (131.82(11) ° and 130.91(9) ° respectively). A larger degree of distortion and angle variation was observed in the indium cluster $[(MeIn)_{10}(O)_2(OEt)_{12}(OH)_4].2THF$ synthesised by Chamazi *et al*.[59]

All remaining crystal structures for complexes **3G, 4G, 1G', 3G', 4G', 1I, 2I, 3I** and **4I-O**, and selected bond lengths and angles are given below in figures 3.3.21 – 2.3.28. Crystallographic data for the complexes has also been listed in tables 2.3.4 - 2.3.6.

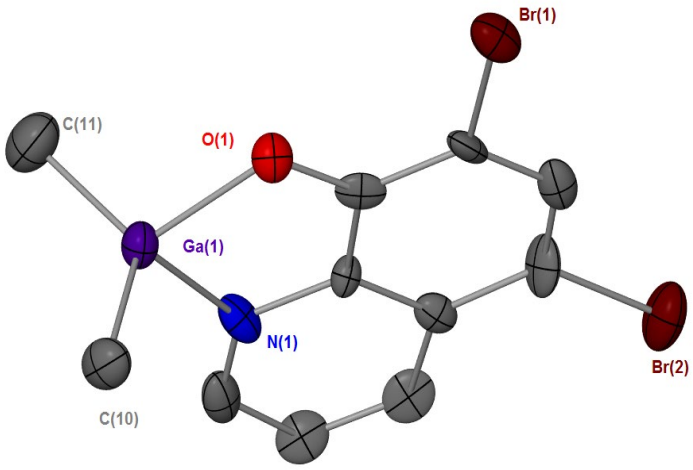

Figure 2.3. 21. Solid-state structure $[Ga(Me)_2C_9H_4NOBr_2]$, ***2G****, Thermal ellipsoids at 50% probability. Hydrogen atoms have been omitted for clarity. Selected bonds lengths (Å) and angles (o). Ga(1) – O(1), 1.913(9), Ga(1) – N(1), 2.066(12), Ga(1) – C(10), 1.948(12), Ga(1) – C(11), 1.950(13); O(1) – Ga(1) – N(1), 82.50(4), O(1) – Ga(1) – C(10), 109.5(5), O(1) – Ga(1) – C(11), 112.3(5), C(10) – Ga(1) – C(11), 126.99(12), N(1) – Ga(1) – C(11), 111.2(5).*

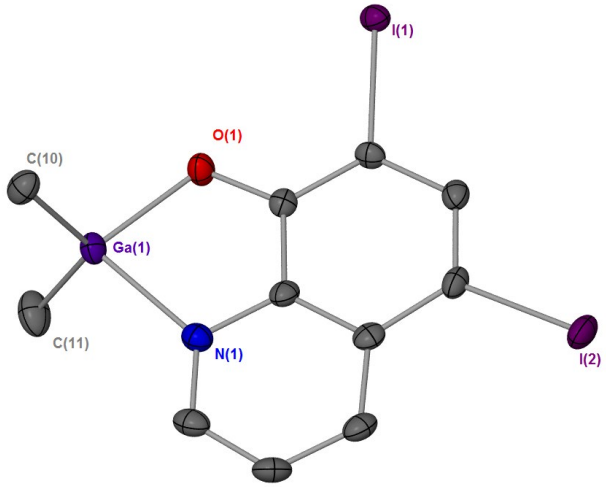

Figure 2.3.22. Solid-state structure $[Ga(Me)_2C_9H_4NOI_2]$, ***4G****, Thermal ellipsoids at 50% probability. Hydrogen atoms have been omitted for clarity. Selected bonds lengths (Å) and angles (o). Ga(1) – O(1), 1.927(3), Ga(1) – N(1), 2.055(3), Ga(1) – C(10), 1.958(4), Ga(1) – C(11), 1.969(4); O(1) – Ga(1) – N(1), 83.28(12), O(1) – Ga(1) – C(10), 109.0(16), O(1) – Ga(1) – C(11), 113.6(17), C(10) – Ga(1) – C(11), 125.5(19), N(1) – Ga(1) – C(11), 107.6(17).*

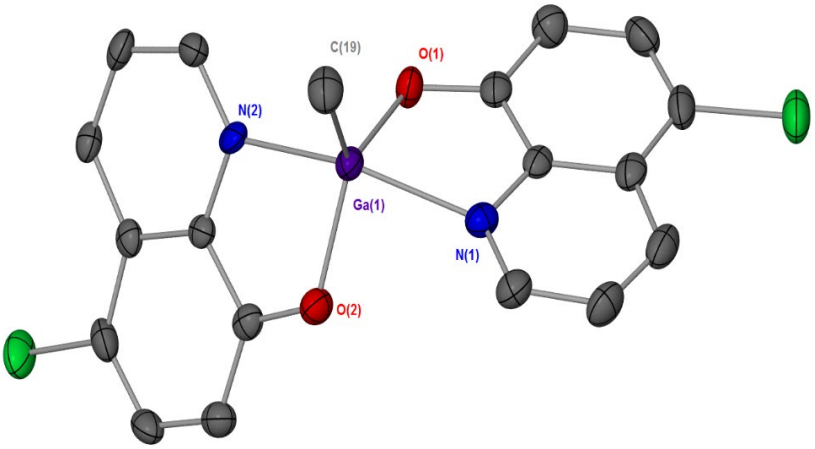

Figure 2.3.23. Solid-state structure $[GaMe(C_9H_5NOCl)_2]$, ***1G'****, Thermal ellipsoids at 50% probability. Hydrogen atoms have been omitted for clarity. Selected bonds lengths (Å) and angles (o). Ga(1) – O(1), 1.899(3), Ga(1) – O(2), 1.906(3), Ga(1) – N(1), 2.123(3), Ga(1) – N(2), 2.147(3), Ga(1) – C(19), 1.945(4); O(1) – Ga(1) – O(2), 119.6(11), O(1) – Ga(1) – N(1), 80.85(11), O(1) – Ga(1) – N(2), 87.41(11), C(10) – Ga(1) – O(1), 122.7(15).*

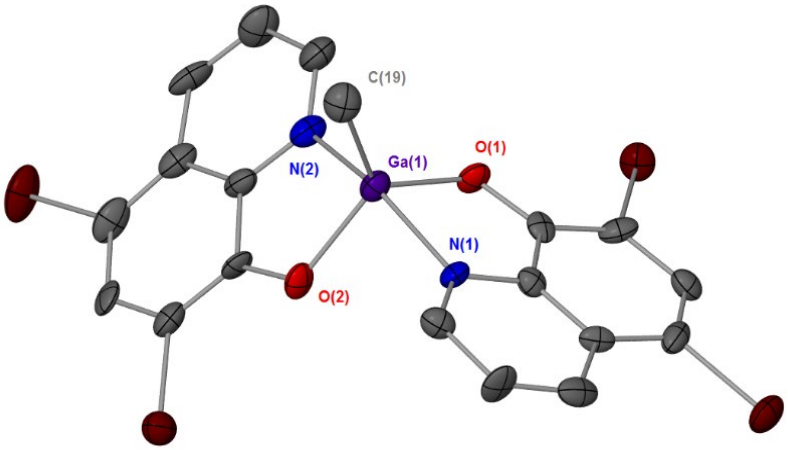

*Figure 2.3.24. Solid-state structure [GaMe($C_9H_4NOBr_2$)$_2$], **3G'**, Thermal ellipsoids at 50% probability. Hydrogen atoms have been omitted for clarity. Selected bonds lengths (Å) and angles (o). Ga(1) – O(1), 1.906(4), Ga(1) – O(2), 1.909(4), Ga(1) – N(1), 2.101(5), Ga(1) – N(2), 2.117(5), Ga(1) – C(19), 1.938(6); O(1) – Ga(1) – O(2), 116.3(18), O(1) – Ga(1) – N(1), 81.57(18), O(1) – Ga(1) – N(2), 86.42(18), C(10) – Ga(1) – O(1), 126.3(2)*

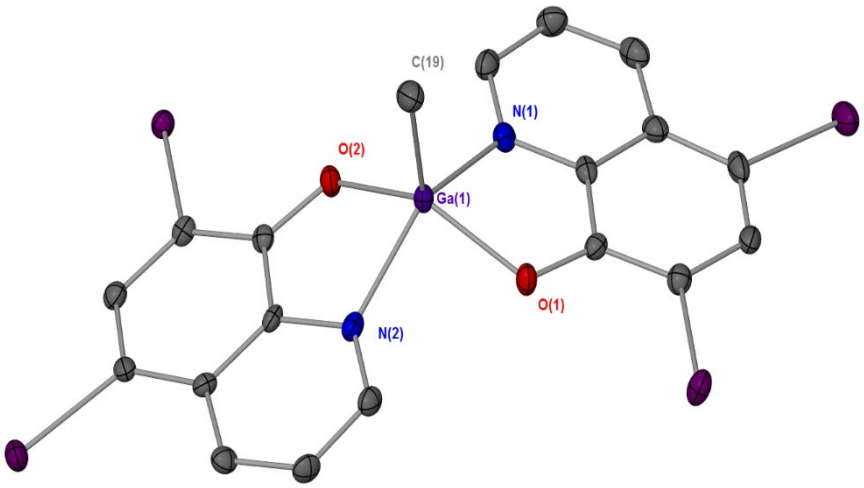

*Figure 2.3.25. Solid-state structure [GaMe($C_9H_4NOI_2$)$_2$], **4G'**, Thermal ellipsoids at 50% probability. Hydrogen atoms have been omitted for clarity. Selected bonds lengths (Å) and angles (o). Ga(1) – O(1), 1.947(3), Ga(1) – O(2), 1.958(3), Ga(1) – N(1), 2.063(4), Ga(1) – N(2), 2.091(4), Ga(1) – C(19), 1.959(5); O(1) – Ga(1) – O(2), 138.8(14), O(1) – Ga(1) – N(1), 80.53(14), O(1) – Ga(1) – N(2), 84.24(14), C(10) – Ga(1) – O(1), 110.8(18)*

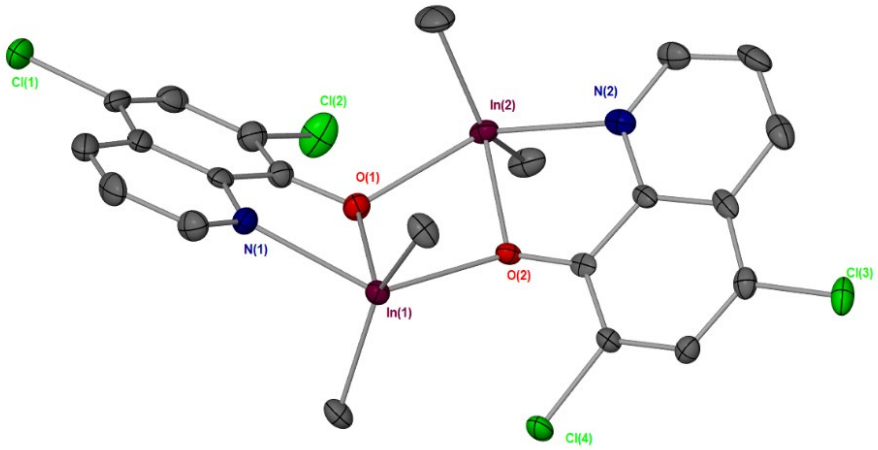

Figure 2.3.26. Solid-state structure $[In(Me)_2C_9H_5NOCl]$, ***1l****, Thermal ellipsoids at 50% probability. Hydrogen atoms have been omitted for clarity. Selected bonds lengths (Å) and angles (o). In(1) – O(1), 2.191(19), In(1) – O(2), 2.317(18), In(1) – N(1), 2.383(2), In(1) – C(1), 2.149(3), In(1) – C(2), 2.142(3); O(1) – In(1) – N(1), 71.17(7), O(1) – In(1) – C(1), 113.4(10), O(1) – In(1) – C(2), 96.79(10), C(1) – In(1) – C(2), 136.8(14), N(1) – In(1) – C(1), 95.47(9).*

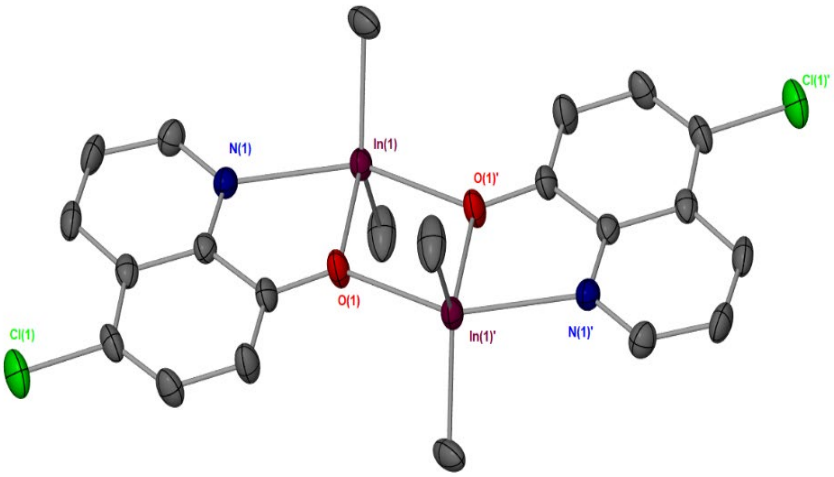

Figure 2.3.27. Solid-state structure $[In(Me)_2C_9H_4NOCl_2]$, ***2l****, Thermal ellipsoids at 50% probability. Hydrogen atoms have been omitted for clarity. Selected bonds lengths (Å) and angles (o). In(1) – O(1), 2.252(3), In(1) – O(2), 2.392(2), In(1) – N(1), 2.383(3), In(1) – C(1), 2.134(4), In(1) – C(2), 2.136(6); O(1) – In(1) – N(1), 71.03(10), O(1) – In(1) – C(1), 117.8(13), O(1) – In(1) – C(2), 96.01(13), C(1) – In(1) – C(2), 146.2(16), N(1) – In(1) – C(1), 99.45(14).*

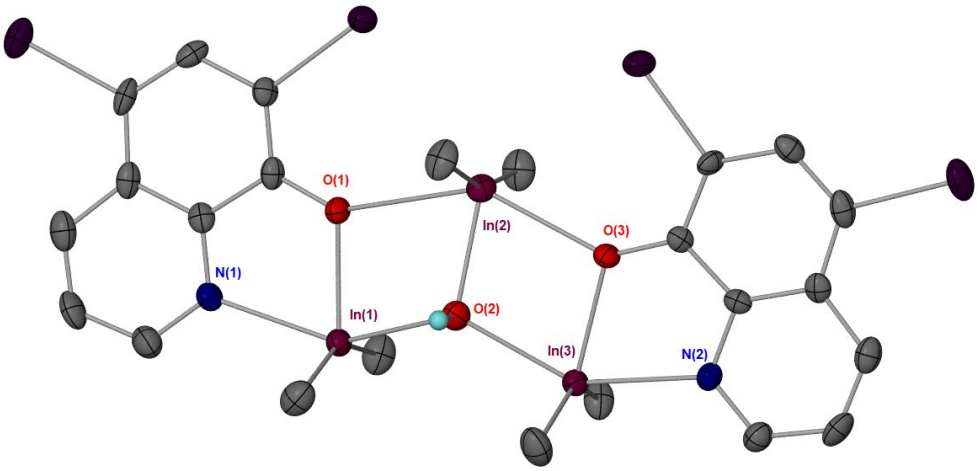

*Figure 2.3.28. Solid-state structure [(In(Me)$_2$C$_9$H$_4$NOI$_2$)$_2$In(Me)$_2$OH], **4I-O**, Thermal ellipsoids at 50% probability. Hydrogen atoms have been omitted for clarity. Selected bonds lengths (Å) and angles (o). In(1) – O(1), 2.252(4), In(1) – O(2), 2.318(4), In(1) – N(1), 2.362(5), In(1) – C(1), 2.137(8), In(1) – C(2), 2.153(7), In(2) – O(2), 2.200(5); O(1) – In(1) – N(1), 71.26(17), O(1) – In(1) – C(1), 113.6(3), O(1) – In(1) – C(2), 90.5(3), C(1) – In(1) – C(2), 140.9(3), N(1) – In(1) – C(1), 95.6(2.)*

*Table 2.3.4. Crystallographic data of complexes **1G – 4G***

	1G	**2G**	**3G**	**4G**
Chemical formula	($C_{22}H_{22}Cl_2Ga_2N_2O_2$)	$C_{11}H_{10}Cl_2GaNO$	2($C_{11}H_{10}Br_2GaNO$)	$C_{11}H_{10}GaI_2NO$
M_r	371.17	312.82	803.48	495.72
Crystal system, space group	Triclinic, *P*	Monoclinic, $P2_1/n$	Orthorhombic, $Pca2_1$	Monoclinic, *P*2/*c*
Temperature (K)	123	123	296	293
***a*, *b*, *c* (Å)**	7.4360 (3), 9.4490 (4), 16.2638 (8)	10.6614 (4), 10.3703 (3), 11.6311 (4)	13.9070 (6), 5.0939 (2), 35.9790 (17)	19.430 (4), 5.070 (1), 14.470 (3)
***V* (Å^3)**	1094.44 (9)	1231.74 (8)	2548.78 (19)	1350.6 (5)
Z	4	4	4	4
T_{min}, T_{max}	0.838, 1.000	0.624, 1.000	0.567, 0.745	0.593, 0.746
R_{int}	0.026	0.032	0.073	0.040
$(\sin\theta/\lambda)_{max}$ (Å^{-1})	0.596	0.596	0.626	0.649
$R[F^2 > 2\sigma(F^2)]$, $wR(F^2)$, *S*	0.027, 0.070, 1.06	0.027, 0.074, 1.06	0.043, 0.083, 0.99	0.029, 0.073, 1.10
No. of reflections	3860	2186	4644	3093
No. of parameters	275	147	293	147

*Table 2.3.5. Crystallographic data of complexes **1G' – 4G'***

	1G'	**1I**	**3G'**	**4G'**
Chemical formula	$C_{19}H_{13}Cl_2GaN_2O_2$	$C_{19}H_{11}Cl_4GaN_2O_2$	$C_{19}H_{11}Br_4GaN_2O_2$	$C_{19}H_{11}GaI_4N_2O_2$
M_r	441.93	510.82	688.66	876.62
Crystal system, space group	Monoclinic, *C*2/*c*	Monoclinic, *C*2/*c*	Monoclinic, *C*2/*c*	Triclinic, *P*
Temperature (K)	296	123	296	293
***a*, *b*, *c* (Å)**	23.899 (2), 12.2775 (12), 12.2071 (11)	15.8748 (5), 14.9556 (4), 17.9254 (5)	23.6635 (9), 24.2959 (9), 15.9270 (7)	9.3200 (19), 15.250 (3), 17.010 (3)
***V* (Å^3)**	3452.7 (6)	3873.7 (2)	8093.5 (6)	2185.7 (9)
Z	8	8	16	4
T_{min}, T_{max}	0.648, 0.746	0.718, 1.000	0.556, 0.746	0.651, 0.746
R_{int}	0.075	0.033	0.109	0.043
(sin θ/λ)$_{max}$ (Å^{-1})	0.649	0.597	0.658	0.625
R*[*F*^{2} > 2σ(*F*^{2})], *wR*(*F*^{2}), *S	0.044, 0.093, 1.01	0.032, 0.084, 1.04	0.045, 0.102, 1.02	0.028, 0.072, 1.06
No. of reflections	3963	3422	9656	8839
No. of parameters	236	254	508	507

*Table 2.3.6. Crystallographic data of complexes **1I** - **4I***

	1I	**2I**	**3I**	**4I-O**
Chemical formula	$C_{11}H_{11}ClInNO$	$C_{22}H_{20}Cl_4In_2N_2O_2$	$Br_4C_{22}In_2N_2O_2$	$C_{24}H_{27}I_4In_3N_2O_3$
M_r	323.48	715.84	873.52	1243.53
Crystal system, space group	Monoclinic, $P2_1/n$	Monoclinic, *C*2/*c*	Monoclinic, $P2_1/c$	Monoclinic, $P2_1/c$
Temperature (K)	293	296	123	123
***a*, *b*, *c* (Å)**	10.2515 (4), 11.9019 (4), 10.4303 (4)	35.085 (2), 10.6452 (4), 13.9213 (6)	9.0152 (3), 19.9814 (5), 7.5791 (3)	12.91523 (17), 13.2564 (2), 18.9035 (2)
***V* (Å^3)**	1184.74 (8)	4876.3 (4)	1251.93 (8)	3203.38 (8)
Z	4	8	2	4
T_{min}, T_{max}	0.652, 0.746	0.680, 0.746	0.457, 1.000	0.115, 1.000
R_{int}	0.029	0.044	0.069	0.058
(sin θ/λ)$_{max}$ (Å^{-1})	0.667	0.649	0.633	0.634
R*[*F*^{2} > 2σ(*F*^{2})], *wR*(*F*^{2}), *S	0.025, 0.058, 1.03	0.032, 0.065, 1.02	0.059, 0.163, 1.05	0.038, 0.106, 1.08
No. of reflections	2945	5560	2545	6666
No. of parameters	138	293	145	331

2.3.7 Stability and biological activity of the gallium complexes

As the indium complexes were observed to form multiple products in DMSO, they were excluded from biological assays. The gallium complexes conversely, proved to exhibit a good degree of stability in both solid and solution state as assessed by repeated elemental analysis and a ^{1}H NMR study in d_6-DMSO. An example complex **1G,** [$Ga(Me)_2C_9H_5NOCl$], was dissolved into d_6-DMSO and the ^{1}H NMR taken at both 0 hours and 24 hours, with no change observed (fig 2.3.29).

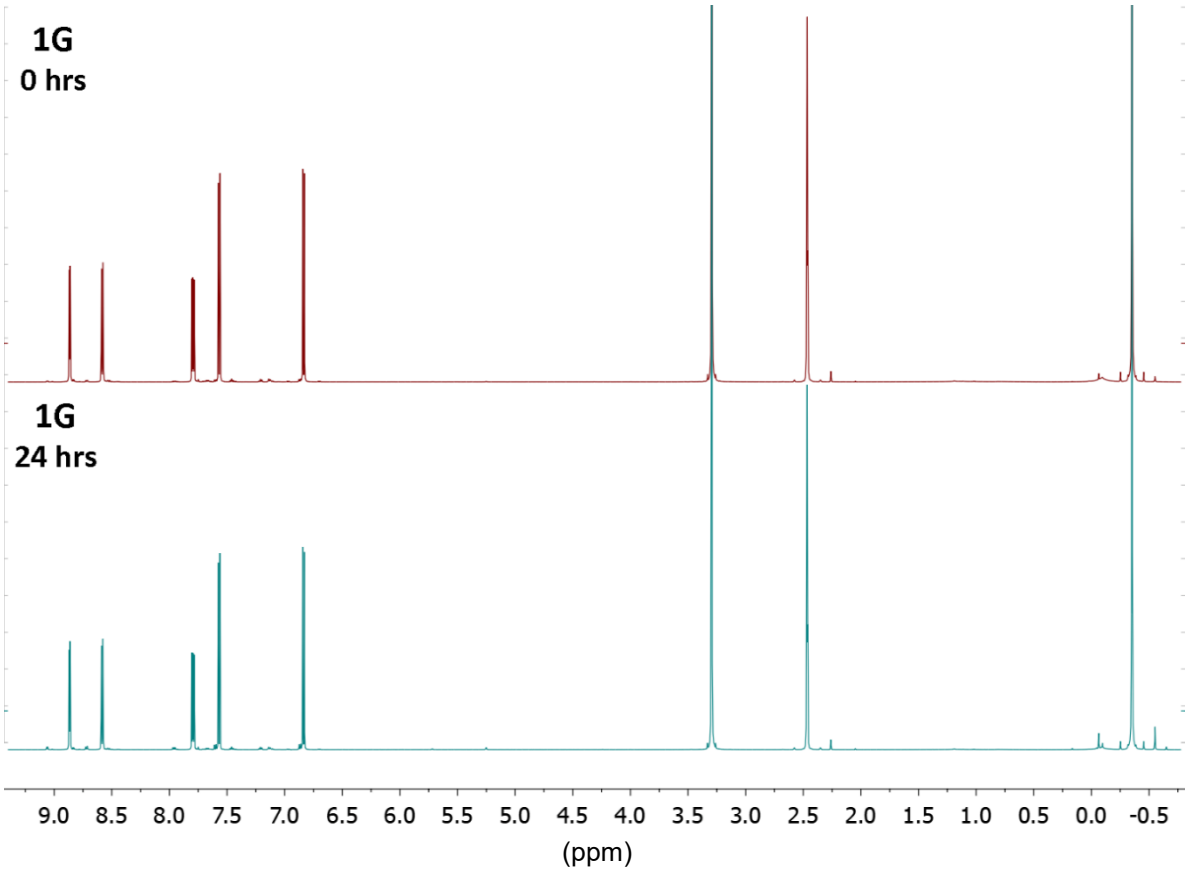

*Figure 2.3.29. ^{1}H NMR study of complex **1G,** [$Ga(Me)_2C_9H_5NOCl$], in d_6-DMSO, over a 24 hours period. Signals at 3.33ppm and 2.50ppm are representative of water and the residual solvent DMSO respectively.*

The remaining *bis*-methyl complexes **2G**, [$Ga(Me)_2C_9H_4NOCl_2$], **3G,** [$Ga(Me)_2C_9H_4NOBr_2$] and **4G,** [$Ga(Me)_2C_9H_4NOI_2$], also exhibited this degree of stability in d_6-DMSO. Unfortunately for the *mono*-methyl complexes only complex **1G',** [$GaMe(C_9H_5NOCl)_2$], was found to be completely

soluble in DMSO at the stock concentration of 10 mM. Complexes **2G',** [GaMe($C_9H_4NOCl_2$)$_2$], **3G'**, [GaMe($C_9H_4NOBr_2$)$_2$] and **4G',** [GaMe($C_9H_4NOI_2$)$_2$], were not sufficiently soluble in DMSO and were excluded from testing.

2.3.7.1 Mammalian cell testing

Prior to any biological application, mammalian cytotoxicity is assessed, therefore all five gallium complexes (**1G - 4G** and **1G',** [Ga(Me)$_2C_9H_5NOCl$], [Ga(Me)$_2C_9H_4NOCl_2$], [Ga(Me)$_2C_9H_4NOBr_2$], [Ga(Me)$_2C_9H_4NOI_2$], [GaMe(C_9H_5NOCl)$_2$]) underwent analysis for their cytotoxic activity against two separate mammalian control cells, Cos-7 and human fibroblasts. Cos-7 cells were selected as they are an immortal cell line and are simple to culture and maintain.[60] Human fibroblasts (skin cells) were selected as they present as the ideal control for the strain of *Leishmania* assessed, *L. major* V121, as *L. major* leads to the cutaneous form of the disease.[61] Initial results were promising, with the complexes **1G** – **4G** and **1G'** exhibiting little to no cytotoxic activity towards the Cos-7 control cells (fig 2.3.30).

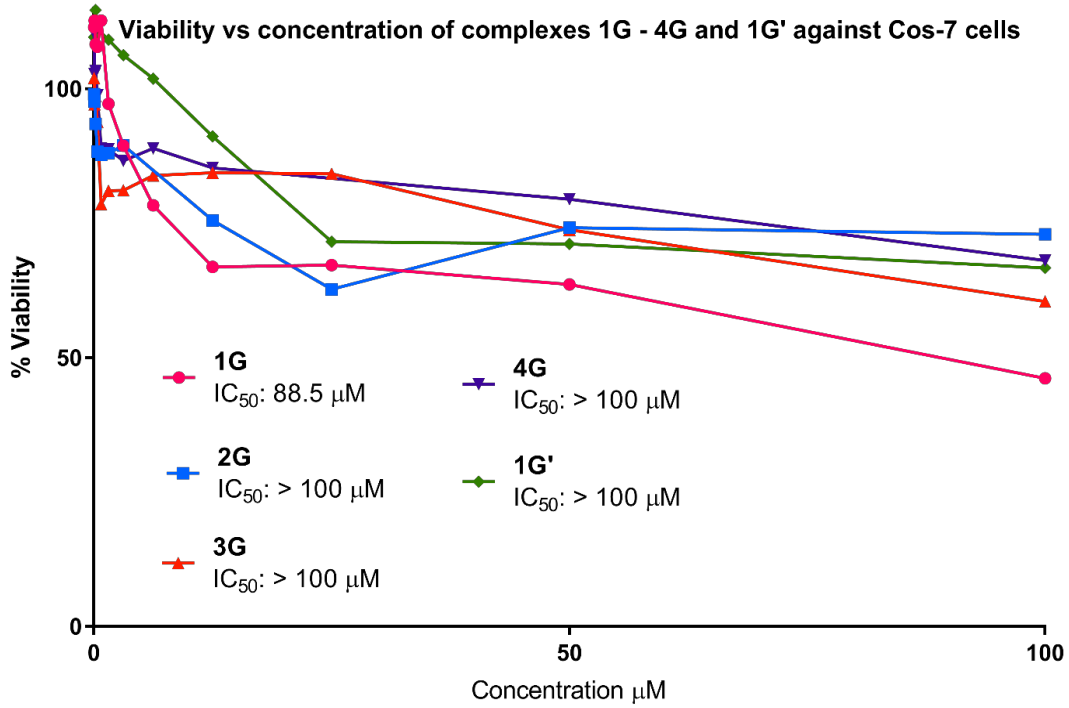

*Figure 2.3.30. Viability percentage of complexes **1G** – **4G** and **1G'** against Cos-7 cells. Dose response curves were generated over a range of concentrations (48nM - 100μM) in the appropriate culture media from 10mM DMSO stock solutions. All readings were compared spectroscopically to non-treated control and the percent growth inhibition calculated*

All complexes, excluding **1G**, were found to have IC_{50}: $\geq$ 100 μM**. 1G** exhibited some cytotoxicity with an IC_{50} of 88.5 μM. This low degree of activity was not observed however for the human fibroblasts (fig 2.3.31), with a small degree of toxicity observed for all complexes, excluding **3G** and **4G**. **1G** and **1G'** presented as the most cytotoxic towards fibroblasts with IC_{50} values of 16.2 μM and 52.2 μM respectively. Despite this, the complexes were assessed for their anti-bacterial, anti-cancer and anti-Leishmanial activity.

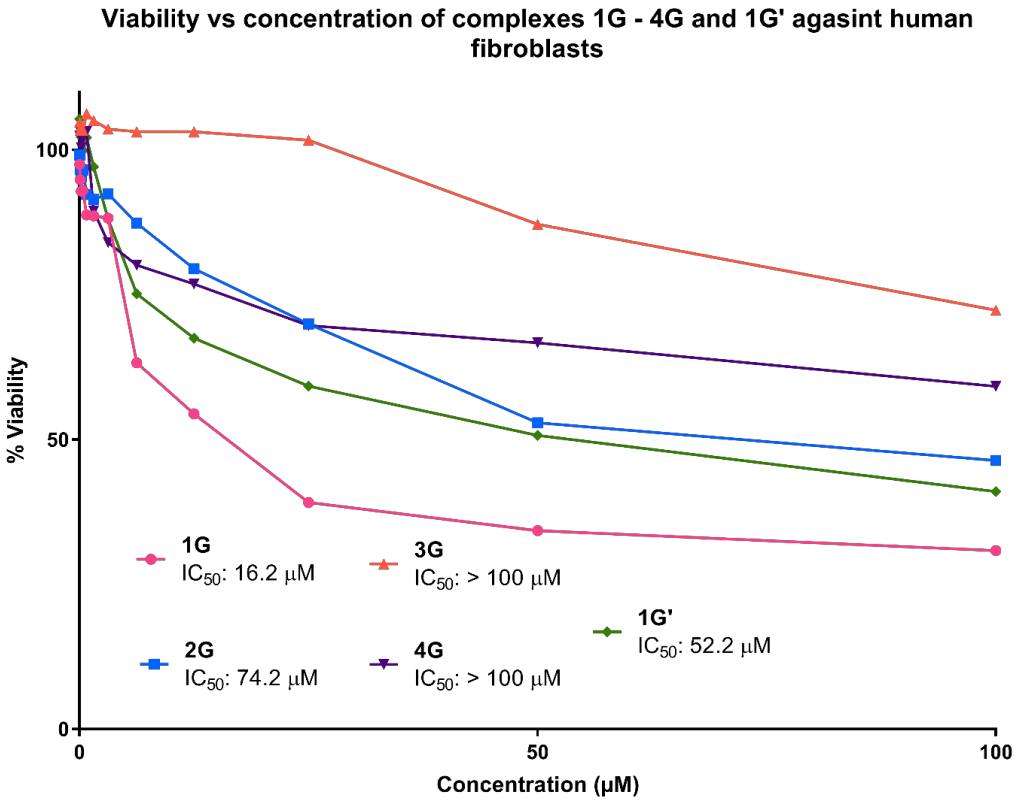

*Figure 2.3.31. Viability percentage of complexes **1G** – **4G** and **1G'** against Human fibroblasts. Dose response curves were generated over a range of concentrations (48nM - 100µM) in the appropriate culture media from 10 mM DMSO stock solutions. All readings were compared spectroscopically to non-treated control and the percent growth inhibition calculated.*

2.3.6.2 anti-cancer assessment

Gallium has long established itself as an anti-cancer metal.[62-64] The organic quinolinol ligand has also been associated with gallium anti-cancer complexes, with the tris-quinolinolate, KP46, reaching phase II clinical trials. However, it was at this phase that it was deemed unsuccessful for future testing.[29, 65] In an attempt to expand on the use of gallium as anti-cancer agents, and the biological significance of quinolinol, the five alkyl gallium quinolinolates, **1G** – **4G** and **1G'** were tested for their inhibitory activity against HeLa cervical cancer cells. It was theorised that the alkyl groups would helped to mitigate the increase hydrolytic stability of KP46, of which limited its exploration to phase II clinical trials. Unfortunately, it was noted that the complexes exhibited no activity and so no further anti-cancer activity was explored.

2.3.6.3 Anti-bacterial assessment

Tests into the anti-microbial activity were then pursued, with all complexes able to undergo a degree of qualitative anti-bacterial testing. The insoluble complexes, **2G'** – **4G**' were utilised in an agar solid-state zone of inhibition test. A small amount of the solid complex is stabbed into bacteria smeared agar plate and incubated, a protocol utilised in previous studies by Werrett *et al*.[66] The soluble complexes, **1G** – **4G** and **1G'** were qualitatively and quantitatively assessed at 5 mg/mL in DMSO. Similar to the cancer cells, little to no activity was observed for any of the complexes. Only very small zones of inhibition were observed for two of the soluble complexes. **2G,** $[Ga(Me)_2C_9H_5NOCl_2]$, exhibited a small degree of activity towards both *E. Coli* and *S. aureus,* with complex **4G,** $[Ga(Me)_2C_9H_5NOI_2]$, exhibiting minor activity against *S. aureus* alone. It was concluded from this that perhaps the hydrolytic stability of the complexes matched or exceeded that of KP46, alluding to their lack of activity.

2.3.6.4 Anti-Leishmanial *assessment*

A final set of tests was then carried out on the eukaryotic microbe *Leishmania,* specifically *L. major* V121, a cutaneous form of the parasite. Despite having little to no activity against both cancer cells and bacteria, all five gallium complexes exhibited excellent activity against the *L. major* promastigotes, with IC_{50} values ranging from 1.11 – 13.4 μM (figure 2.3.32).

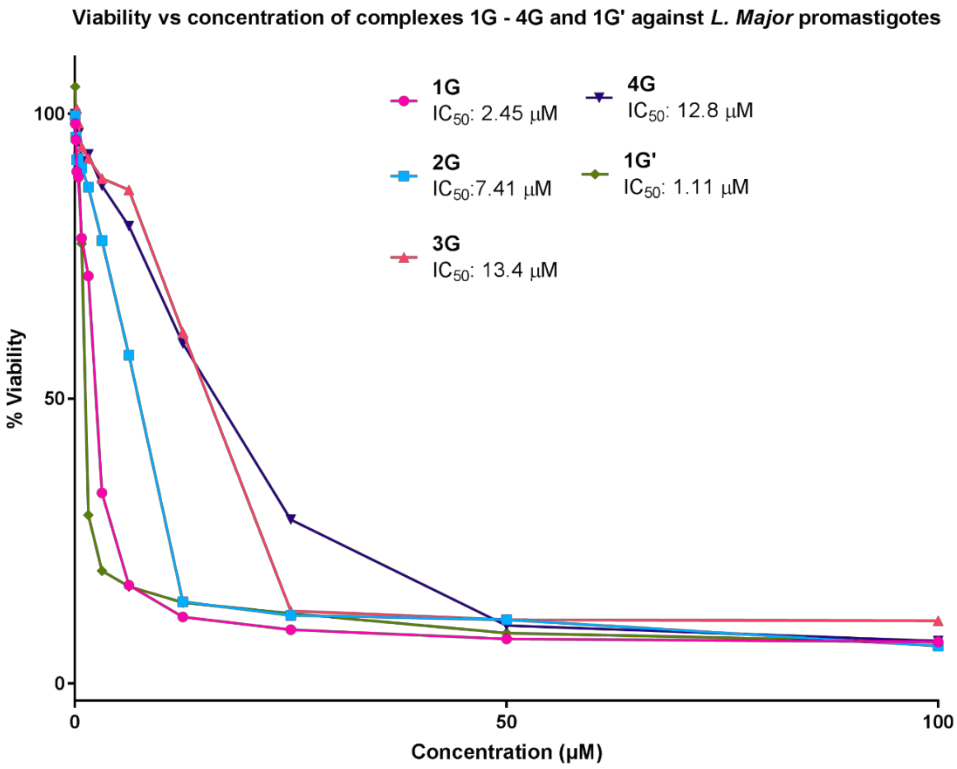

*Figure 2.3.32. Viability percentage of complexes **1G** – **4G** and **1G'** against L. major promastigotes. Dose response curves were generated over a range of concentrations (48nM - 100µM) in the appropriate culture media from 10mM DMSO stock solutions. All readings were compared spectroscopically to non-treated control and the percent growth inhibition calculated*

As previously determined, the mammalian cytotoxicity towards the human fibroblast controls also varied, with complexes **1G,** $[Ga(Me)_2C_9H_5NOCl]$, and **1G',** $[GaMe(C_9H_5NOCl)_2]$, proving to exhibit the greatest cytotoxicity (16.2 and 52.3 respectively). However, **1G** and **1G'** also proved the most effective anti-Leishmanial, and exhibited selectivity indices of 6.61 and 47.0 for **1G** and **1G'** respectively. **1G'** was found to be particularly selective (table 2.3.6). The human fibroblast IC_{50} values for complexes **3G,** $[Ga(Me)_2C_9H_5NOBr_2]$, and **4G,** $[Ga(Me)_2C_9H_5NOI_2]$, were extrapolated by fitting a trendline to the curve. From the graph, **4G** proved the most selective of all the complexes with an index of 64.6 (table 2.3.7).

*Table 2.3.7. Selectivity indices for complexes **1G** – **4G** and **1G'**. where SI = IC_{50}(fibroblasts)/IC_{50}(parasite). Yellow highlights the least selective, with the values in green indicating a high degree of selectivity.*

Complex	**1G**	**2G**	**3G**	**4G**	**1G'**
IC_{50} (Fibroblast) µM	16.2	74.2	170*	827*	52.2
IC_{50} (Promastigote) µM	2.45	7.41	13.4	12.8	1.11
Selectivity index	6.61	10.0	12.7	64.6	47.0

An amastigote invasion assay was then carried out. Complexes **1G** – **4G** and **1G'** were made into stock solution of 1mM in DMSO and added to infected macrophages at a final concentration of 10 µM. The 24-well plate was incubated for 48 hours to allow the drug to enter the macrophages and then the intracellular amastigote. After this 48-hour period the slides were stained as per the protocol in the experimental section (4.3.5). Approximately 200 cells were randomly counted per duplicate compound and the percentage of infected cells compared to a positive control (100% infection). The usual drug control, amphotericin B and DMSO were also utilised (figure 2.3.33). All complexes were found to display excellent anti-amastigote activity when compared to the drug control, with percentage infection values ranging from 3.5 % $\pm$ 0.65 – 11.5 % $\pm$ 0.65. As discussed in section 2.2, the parent quinolinols were also assessed for their anti-amastigote activity. All gallium complexes, similar to the antimony quinolinolates, were found to outclass the parent quinolinols (table 2.2.7, section 2.2.4.2.)

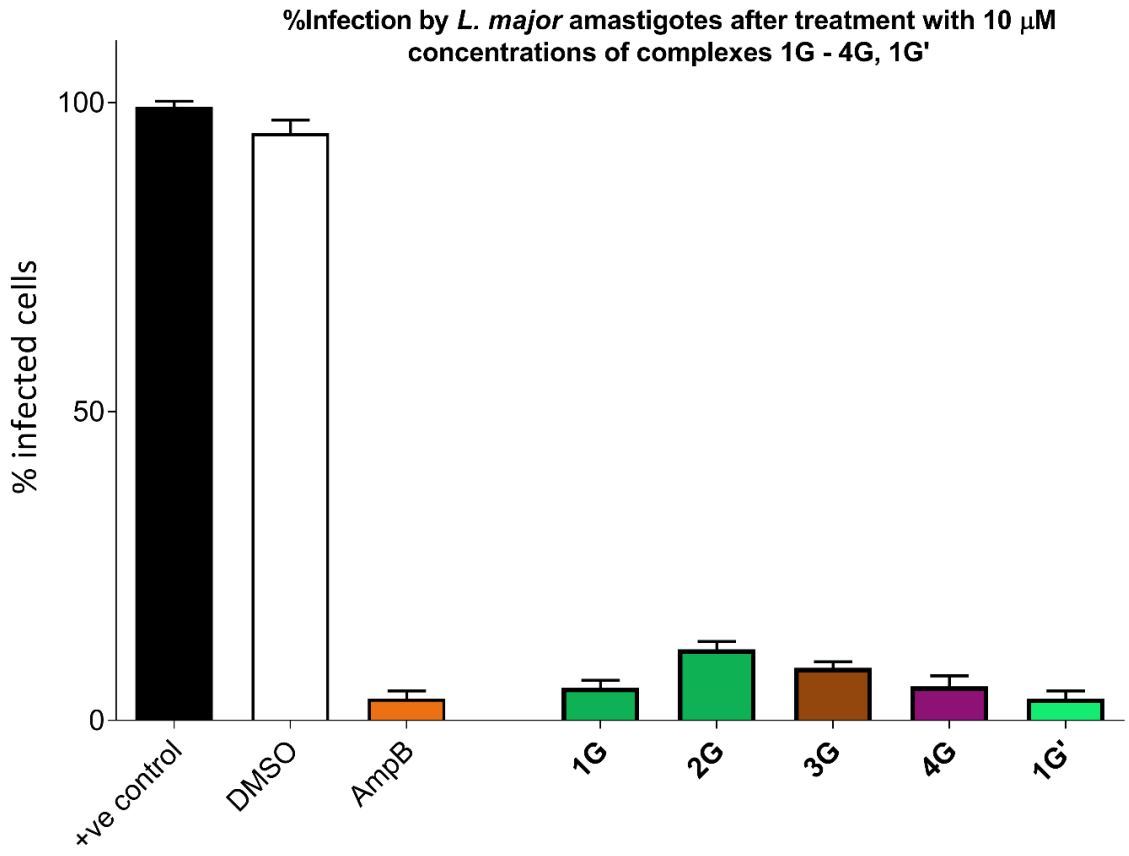

Figure 2.3.33. Infected macrophages after 48 hours. Number of infected macrophages was determined microscopically, in duplicate of fixed specimens. Amphotericin B (AmpB) was used as a positive control at 10 μM concentration. A DMSO control was also employed at a 1% concentration. Error bars indicate SEM, one-way ANOVA. Dunnett's multiple comparison test was used to determine the statistical significance between all test compounds and a positive control lacking treatment (+ve control)

The *mono*-methyl complex **1G',** [$GaMe(C_9H_5NOCl)_2$], presented with the lowest percentage of infection, therefore presents with the greatest activity of 3.5 % $\pm$ 0.65. The *bis*-methyl cloxyquin complex **1G,** [$Ga(Me)_2C_9H_5NOCl$], followed close behind with a percentage infection value of 5.3 % $\pm$ 0.63. For the remaining complexes with halide substitution in the 5 and 7 position of the quinolinol, a trend was observed. The rate of infection increased with a decrease in the halide size with values of 11.5 % $\pm$ 0.65, 8.5 % $\pm$ 0.50 and 5.5 % $\pm$ 0.86 for **2G**, [$Ga(Me)_2C_9H_5NOCl_2$], **3G,** [$Ga(Me)_2C_9H_5NOBr_2$] and **4G,** [$Ga(Me)_2C_9H_5NOI_2$], respectively. As percentage infected decreases

for **2G** > **3G** > **4G** the activity increases as the halide increases, therefore in terms of anti-Leishmanial activity: Cl < Br < I. What was also observed with the amastigote invasion assay was an increase of the number of bound quinolinol ligands also had an effect on activity, with the only soluble *bis*-substituted complex, **1G'**, [GaMe($C_9H_5NOCl)_2$], proving the most potent to the amastigotes. These activities are comparable to those explored with previously analysed Sb(V) a-hydroxy carboxylates.[67, 68] Even with **2G** and **3G** proving the least effective based solely on the percentage infection value, in terms of selectivity indices, **2G** and **3G** are still considered ideal candidates for future *in vivo* testing. When considering the selectivity index and anti-amastigote activity, the iodoquin complex, **4G**, presents as the top candidate for future testing out of the five complexes analysed. With a selectivity index of 64.6 and a percentage infection value of 5.5 + 0.86, complex **4G** has proven both an effective anti-amastigote complex, and non-toxic to mammalian cell controls. Therefore, **4G** is exceptionally selective, falling well above the FDA NTI with a 60 fold difference.[69] Complex **1G'** also proved exceptionally selective, with an index of 47.0 and a percentage infection value of 3.5 % $\pm$ 0.65.

2.3.6.5 Measurement of reactive oxygen species

Gallium has been well established as an iron mimic, with similarities between itself in the +III oxidation state and bioavailable Fe(III).[70] The most accepted theories of gallium-iron inhibition focus on the transport of gallium by iron sequestering proteins such as transferrin and lactoferrin often at greater binding efficacy than the exogenous iron itself.[12] Gallium generally inhibits ferric iron-dependant pathways by replacing the iron moieties within these transport proteins, disrupting microbial growth and maintenance.[6, 71, 72] As previously mentioned, *Leishmania spp.* require iron from exogenous sources and different species of *Leishmania* have developed unique ways in which to obtain iron, however all evolved around an iron sequestering protein.[22, 24-26] *Leishmania* amastigote in particular reside in the low iron environment of the phagolysosome of the mammalian macrophages. Amastigotes bypass the macrophages immunological response

(the production of superoxide radicals),[73, 74] by conversion of these radicals to low concentrations of H_2O_2 and O_2.[75, 76] To effectively convert the superoxide to harmless by-products, *Leishmania spp.* require enough exogenous iron to produce iron superoxide dismutase. When in the low iron environment of the phagolysosome, this scarcity of iron triggers the up-regulation of iron sequestering channels within the parasite and causes increased promastigote – amastigote transformation. This increased uptake of iron allows for greater balance and control of the iron superoxide dismutase (FeSOD) activity and hydrogen peroxide generation within the parasite.[28] A study by Mittra *et al* concluded that in these iron poor environments, FeSOD activity greatly increases initially, however after several days in iron-poor media this activity then dramatically drops to a point at which no detectable FeSOD activity is observed. This results in increased levels of superoxide and eventual death of the *Leishmania* population. Conversion of superoxide by FeSOD to H_2O_2 is a vital step in the differentiation and proliferation of *Leishmania.*[77]

A test was carried out to measure whether example complexes **1G,** [$Ga(Me)_2C_9H_5NOCl$] and **1G',** [$GaMe(C_9H_5NOCl)_2$], initiated the production of reactive oxygen species (ROS). The assay utilised a similar procedure by Wojtala *et al*, though modified to include prior infection of the macrophages.[78] The dye, dihydroethidium was used to measure the production of ROS spectroscopically, by the conversion of dihydroethidium (DHE) to the fluorescent 2-hydroxyeithidum. A negative control of cells without infection was used as baseline, and each were compared to the drug control amphotericin B. A more detail explanation of the assay can be found in the experimental section 4.3.3. The complexes and the DHE were added to the well-plate at time intervals of 6, 12 and 24 hours. Prior to all measurements, the plates were washed with PBS to remove any complex **1G**/**1G'** and DHE that had not passed through the cell membrane. At the six-hour interval a notable percentage increase of ROS was detected in both **1G** and **1G**' treated wells when measured against the negative control. This implies that addition of the complexes to the cells, allows generation of superoxide radicals. At the twelve-hour mark, this

production of ROS increased further still before dropping off at the 24-hour mark (fig 2.3.34). These values were compared to the product of ROS by amphotericin B. The mechanism of action of amphotericin B relates to changes in the permeability of the parasite cell membrane, allowing small metabolites and other small molecules to pass through, such as superoxide.[79] It has also been proposed recently that the amphotericin B can cause accumulation of ROS in other eukaryotes such as fungi, which may contribute to the increased signal observed upon treatment of AmpB to the parasites, which are also eukaryotic.[80] The percentage increase values of **1G**, **1G'** and AmpB are given below in table 2.7.8.

*Table 2.3.8 % Increase of ROS after treatment with **1G** and **1G'** and Amphotericin B. All values are compared to a negative control baseline of 100%*

	1G	**1G'**	**AmpB**
6 hours	135.4 % ± 8.1	175.7 % ± 11.7	125.0 % ± 7.7
12 hours	156.8 % ± 4.7	177.1 % ± 27.3	122.3 % ± 5.4
24 hours	119.6 % ± 1.5	141.6 % ± 14.8	125.1 % ± 2.7

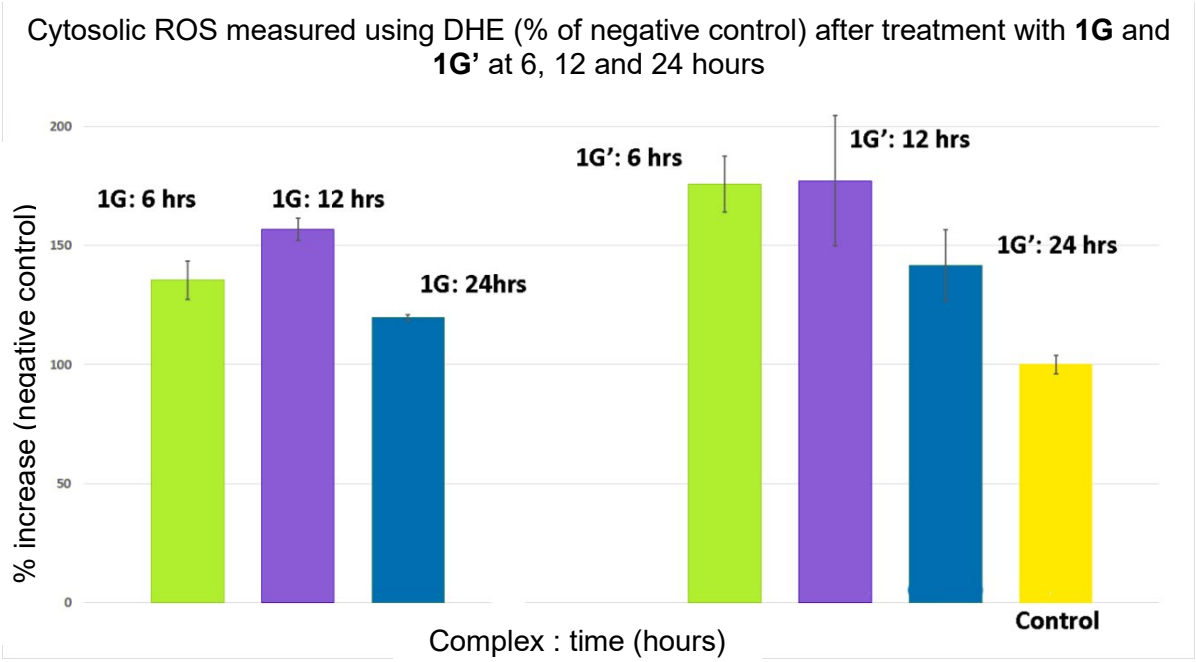

*Fig 2.3.34. % increase of Cytosolic ROS produced by infected macrophages after treatment with **1G** and **1G'** at 6 hours, 12 hours and 24 hours, against a negative control of no infection and no drug*

Whether this increased production of ROS in the presence of gallium complexes is directly or indirectly acting upon the parasite remains to be seen. As FeSOD plays an important role in the survival of the parasite within the macrophage, a decrease in FeSOD activity would result in an increase of ROS. Therefore, it is hypothesised that the gallium complex may be acting indirectly. The gallium complexes are preferentially taken up by the parasite in the low iron environment, where they inhibit the production of FeSOD, leading to the inability of the parasites to resist the superoxide radicals produced by the macrophages.

2.3.7 Photophysical properties of alkyl gallium and indium quinolinolates

The compound 8-quinolinol displays a bright yellow colour when exposed to UV-light. Therefore, there may be a possibility to exploit this. The heterocycle exhibits differing degrees of fluorescent activity in relation to solvent. In neutral water, at a pH of approximately 7, the quinolinol is nearly non-fluorescent, existing predominately in the enolic form, with a negligible quantum yield of 2 x

10^{-4}.[81] When the pH is decreased and the quinolinol placed in an acidic environment, the nitrogen of the ring becomes protonated forming the positively charged quinolinolium ion. Conversely, in basic solution of pH ~ 10, the hydroxyl becomes deprotonated, forming the quinolinolate (fig 2.3.35). The quinolinolate form has a 100-fold increase in its fluorescence intensity, which increases as the basicity of the solution increases. A similar increase in intensity is described for the quinolinolium ion also, however this highly fluorescent form exists only in concentrated acid solution such as sulfuric acid.[82]

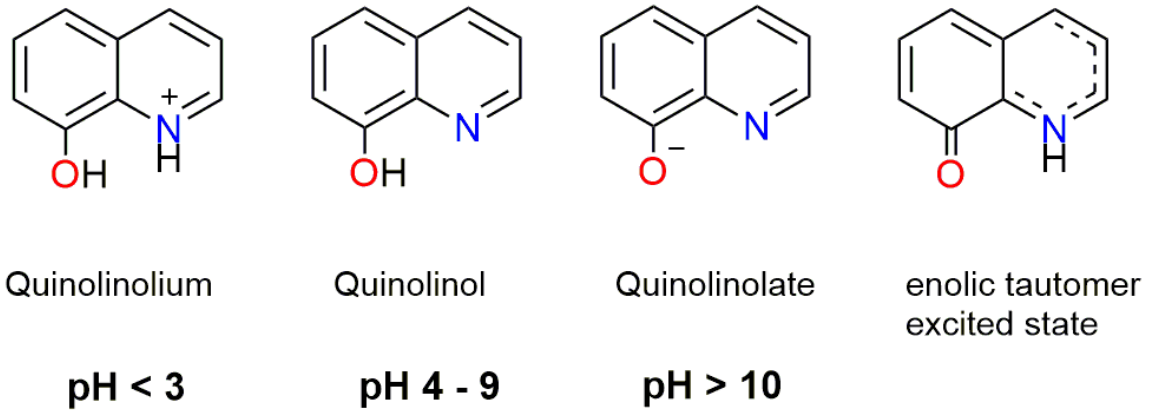

Figure 2.3.35. Enolic tautomer form and different configurations of the 8-quinolinol at differing pH ranges

The enolic tautomer state results from excitation of the photoproduct with a non-radiative de-excitation mechanism. This coupled with competitive simultaneous charge transfer from the prototropic site to the adjacent ring, results in the decrease of the quantum yield as observed in highly polar and water miscible solvents.[83]

As all gallium and indium complexes were purified as bright yellow powders, qualitative tests were conducted on complexes **1G,** $[Ga(Me)_2C_9H_5NOCl]$, **2G,** $[Ga(Me)_2C_9H_4NOCl_2]$, **3G,** $[Ga(Me)_2C_9H_4NOBr_2]$, **4G**, $[Ga(Me)_2C_9H_4NOI_2]$ **1G',** $[GaMe(C_9H_5NOCl)_2]$, **2G',** $[GaMe(C_9H_4NOCl_2)_2]$, **3G',** $[GaMe(C_9H_4NOBr_2)_2]$, **4G',** $[GaMe(C_9H_4NOI_2)_2]$, **1I,** $[In(Me)_2C_9H_5NOCl]$, **2I,** $[In(Me)_2C_9HNOCl_2]$, **3I,** $[In(Me)_2C_9H_5NOBr_2]$, and **4I**, $[In(Me)_2C_9H_5NOI_2]$, to gauge their fluorescent activity. The bright

yellow powder cloxyquin complexes of gallium (**1G**) and indium (**1I**) were exposed to UV-light (320 – 400 nm). Both solid exhibited brightly coloured fluorescence, with **1G** fluorescing bright yellow, whereas the indium complex **1I** presented as a more blue-shifted, lighter blue colour (fig 2.3.36). Though both appeared to be strongly fluorescing in the solid state, solid-state fluorescence analysis is incompatible with biological imaging and so no quantitative analysis on the solid-state fluorescence was required.

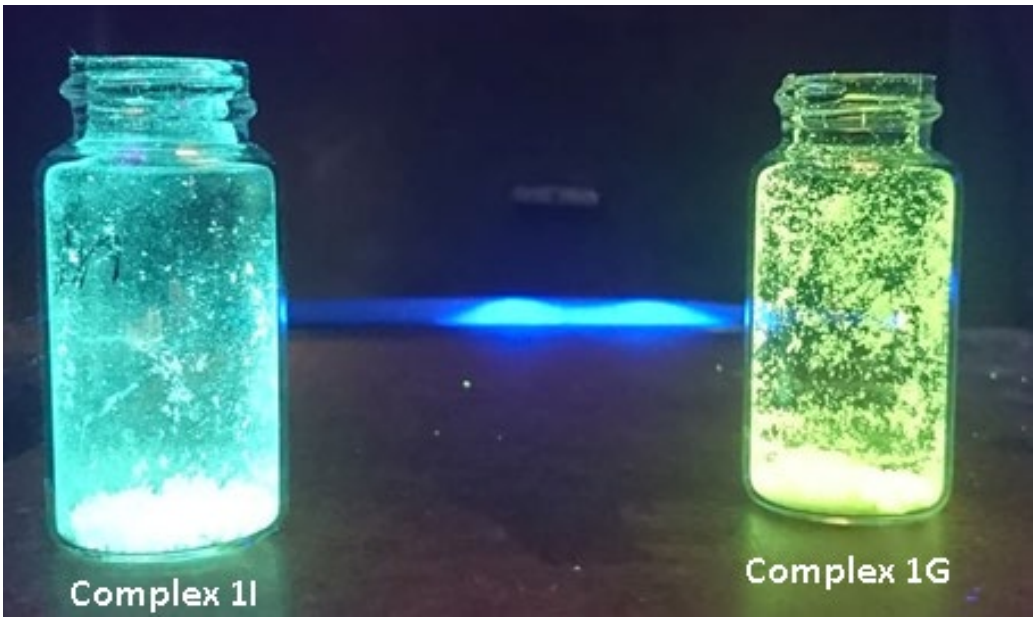

*Figure 2.3.36. Solid-state fluorescence of complexes **1I** and **1G** under exposure to a UV-lamp.*

Qualitative solution-state analysis was also conducted on the complexes in solvents of different polarities. Small masses of example complexes **1G** and **1I** were placed into separate vials and dissolved in toluene, acetone and DMSO. These solutions were all brightly coloured yellow solutions prior to UV-analysis. The complexes displayed a degree of solvatochromism. An increasing degree of red shifting occurred, going from the most non-polar solvent, toluene to the most polar, DMSO (fig2.3.37).

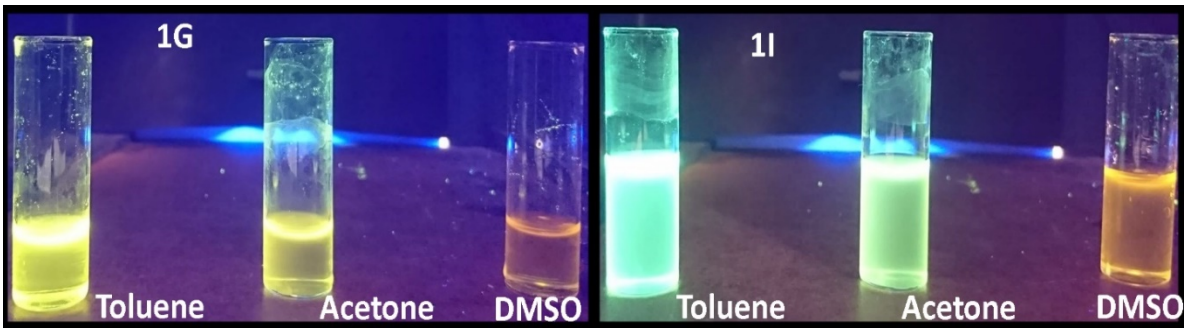

Fig 2.3.37. Solvatochromism of complexes ***1G,*** *$[Ga(Me)_2C_9H_5ClNO]$, and* ***1I,*** *$[In(Me)_2C_9H_5ClNO]$, in increasing polarity solvents: Toluene < Acetone < DMSO.*

DMSO is also known to absorb atmospheric moisture, therefore the quenching of the fluorescence may be due in part to the concentration of water within the solution.[83]

Though the significant fluorescence quenching in DMSO disqualified the complexes for any further analysis as potential biological trackers, fluorescence activity was still observed in the non-polar solvents. As the gallium complexes exhibited the greatest degree of qualitative fluorescence in toluene, preliminary UV-Visible spectroscopy was performed on all complexes at 10^{-4}M in order to locate the λ max of each complex. Graphs were constructed for each class, *bis*-methyl and *mono*-methyl, and the λ max values of each compared along with their relative nm shift (figures 2.3.38 and 2.3.39).

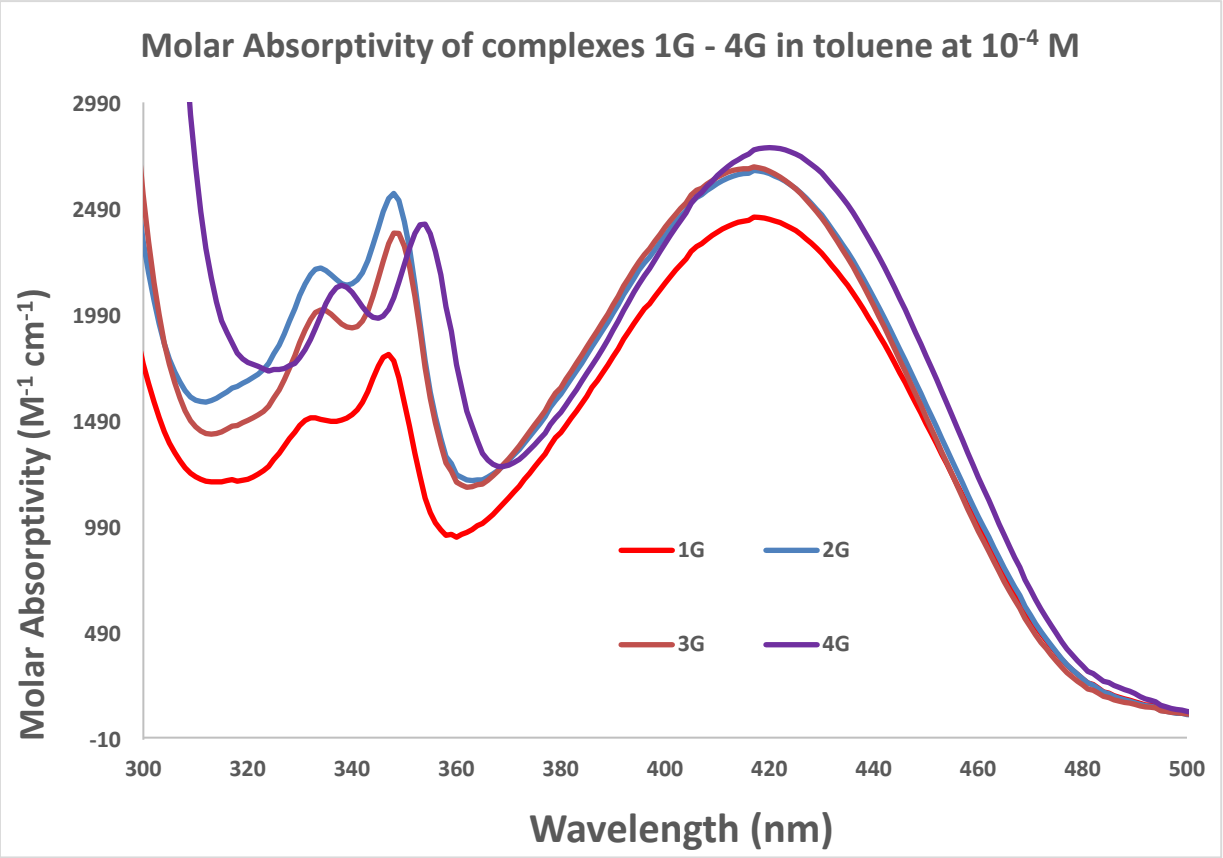

*Fig 2.3.38. UV-Visible spectrum of complexes **1G** – **4G** in toluene at 10 $^{-4}$M.*

All complexes exhibited the presence of multiple bands in the UV-visible spectrum, a phenomenon described by Moeller *et al* in the 1950s on the UV-visible spectrum of metal quinolinol chelates. The largest of these bands was generally found within 400 – 425 nm, of which matches to the spectrum in figure 2.3.28. The study also concluded that increasing the size of the metal caused an increase in the bathochromic shift of the λ max. Therefore, it could be assumed that increasing the halide size on the ligand could have a similar effect, though this is only noticeable with the iodoquin analogue **4G**.[84]

The cloxyquin complex **1G** presented as the weakest absorber and iodoquin complex **4G** the strongest, with ε values of 2458 $M^{-1}cm^{-1}$ and 2784 $M^{-1}cm^{-1}$ respectively, implying a small trend in

the change in halogen size. All values and the corresponding max are given below in table 2.3.9. The *mono*-methyl complexes **1G'** – **4G'** were observed to be stronger absorbers than the *bis-methyl* complexes, which was most likely attributed to the presence of two quinolinol moieties as opposed to one in the complete molecule (fig.2.3.39). The molar absorptivity of **1G'** – **4G'** were almost a two-fold increase when compared to the *bis*-methyl complexes **1G** – **4G**, further supporting the ligand addition theory.

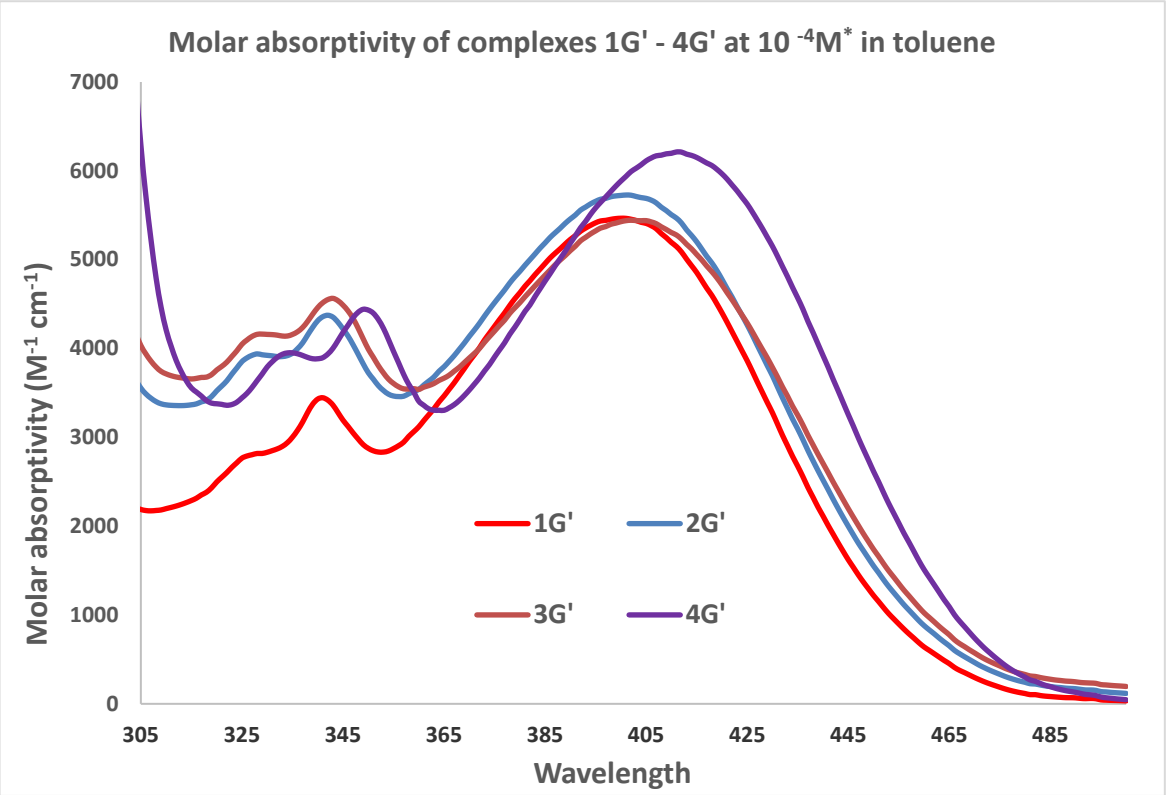

*Fig 2.3.39. UV-Visible spectrum of complexes **1G** – **4G** in toluene at 10 $^{-4}$M. *Complex concentration close to 10 $^{-4}$M, slight particulates observed for **2G'** and **3G'**.*

*Table 2.3.9. UV-visible λ max values and molar absorptivity values of complexes **1G** – **4G** and **1G'** – **4G'**.*

	1G	**2G**	**3G**	**4G**	**1G'**	**2G'**	**3G'**	**4G'**
λ max (nm)	417	417	418	421	401	400	405	412
ε (M^{-1} cm^{-1})	2458	2691	2678	2784	5439	5723	5439	6211

An attempt to gather information on the fluorescence intensity of the complexes was conducted, however, very little signal was observed when the complexes were excited (in both the solid and solution state) at the λ max values obtained from the UV-visible graphs. Due to this, no further analysis into the fluorescence activity was pursued.

Unlike highly polar solvents, in alkane solvents it has been observed that molecules of 8-quinolinol will self-associate to form stable dimers which are able to undergo biprotonic transfer in the excited state. The stability of these dimers affects the overall quantum yield of the molecule. Quenching of 8QH most often occurs via the attraction of the hydroxyl group to strong hydrogen acceptor solvents such as water and DMSO, which leads to deexcitation by internal conversion. However, in weakly interacting solvents such as toluene, intramolecular bonding between the hydroxyl and the nitrogen increase the dimer stability and lead to a similar quenching of the fluorescence.[81] Though the chelation of the quinolinol locks it in the ideal conformation and prevents formation of the excited state tautomer, fluorescence activity in metal chelates has been shown to be marginally lower when compared to conventional fluorophores, especially those used in a biological setting. Therefore, no further photophysical analysis on the complexes was required.

2.3.8 Conclusion

In this section the therapeutic potential of the group 13 metals gallium and indium was detailed. The medically active halido-quinolinol class was utilised. Reactive alkyl groups were incorporated in an attempt to decrease the hydrolytically stability and increase lipophilicity.

A total of 12 completely isolatable complexes were synthesised and characterised, four *bis*-methyl gallium quinolinolates, **1G,** $[Ga(Me)_2C_9H_5NOCl]$, **2G,** $[Ga(Me)_2C_9H_4NOCl_2]$, **3G,** $[Ga(Me)_2C_9H_4NOBr_2]$, **4G**, $[Ga(Me)_2C_9H_4NOI_2]$, four *mono*-methyl gallium quinolinolates, **1G',**

[GaMe($C_9H_5NOCl)_2$], **2G',** [GaMe($C_9H_4NOCl_2)_2$], **3G',** [GaMe($C_9H_4NOBr_2)_2$], **4G',** [GaMe($C_9H_4NOI_2)_2$], and four *bis*-methyl indium quinolinolates, **1I,** [In$(Me)_2C_9H_5NOCl$], **2I,** [In$(Me)_2C_9HNOCl_2$], **3I,** [In$(Me)_2C_9H_5NOBr_2$], and **4I**, [In$(Me)_2C_9H_5NOI_2$]. Three other indium products that were characterised solely by X-ray crystallography were also produced: **3I'**, [InMe($C_9H_4NOBr_2)_2$], **3I-C,** [$In_4(OH)_4(C_9H_4NOI_2)_8$], and **4I-O,** [$(In(Me)_2C_9H_4NOI_2)_2(In(Me)_2OH)$].

The complexes produced were isolated and characterised in the general formulae of [$M(Me)_2L$] for **1G** – **4G** and **1I** – **4I** and [$GaMe(L)_2$] for complexes **1G'** – **4G'**. The brightly coloured products obtained were all stable to air and moisture upon completion of the reaction. The yields for both the *bis*-methyl and *mono*-methyl equivalents were exceptional, ranging from 72 - 97%. All complexes were characterised by ^{1}H NMR, melting point, FT-IR, mass spectrometry, elemental analysis and single crystal X-ray diffraction. Complexes **1G** – **4G** and **1I** – **4I** were also analysed by ^{13}C NMR, complexes **1G'** – **4G'** faced issues with solubility and so definitive ^{13}C NMR data was unobtainable.

Complexes **2G** – **4G** were found to be analogous in structure, presenting as distorted tetrahedrons in the solid-state. **1G** and **1I** – **4I** presented as dimers in the solid-state, with a coordination number of five characterised as a distorted trigonal bipyramidal geometry. The quinolinol ligands sat planar in the solid-state, occupying the both the equatorial (O) axial plane (N) in respect to the metal with the methyl groups occupying two of the three equatorial positions. Distortion for the ideal trigonal angle of 120 ^{o} was observed for all complexes, along with lengthening of the carbon – gallium bond as the halogen size increased. The *mono*-methyl complexes **1G'** – **4G'** and **3I'** were all analogous in structure, similar to the dimeric **1G** and **1I** – **4I**, all were found to be five coordinate trigonal bipyramids. For these *bis*-substituted complexes, the covalently bound oxygen atoms are occupying two of the three equatorial planes, with the remaining site occupied by the methyl group. The nitrogen of the quinolinol ring was observed to be sitting the two axial positions of the

trigonal bipyramid. The indium complex **3I** was observed to undergo rearrangement in the solution state to **3I'** and then to the indium complex **3I-C**. This complex was characterised by X-ray alone and found to be the cluster complex of the general formula $4[In(L)_2OH]$. The cluster core comprised of four indium metal centres and four hydroxide moieties $[In_4(OH)_4]$. The complex was determined to contain hydroxide moieties as opposed to oxides to enable charge balance of the overall cluster, unfortunately due to the large degree of electron density within the core the hydrogens were unable to be modelled.

The indium complexes were observed to be unstable in the solution, resulting in re-arrangement of the initial *bis-methyl* complex to a variety of difficult to characterise by-products. The gallium complexes displayed good solution state stability, making them ideal candidates for biological testing. Complexes were dissolved into d_6-DMSO and monitored for 24 hours to observed if any changes to the signals would occur. Unfortunately complexes **2G'** – **4G'** proved only partially soluble in the biological solvent DMSO and so were disqualified from biological testing. Complexes **1G** – **4G** and **1G'** however proved to exhibit a high degree of solubility and hydrolytic stability and were prime candidate for biological assessment.

Complexes **1G** – **4G** and **1G'** were all tested for their biological activity against a variety of therapeutic targets including Gram positive/negative bacteria, HeLa cervical cancer cells and *L. major* promastigotes and amastigotes, as well as mammalian controls, Cos-7 cells and human fibroblasts. All five complexes were found to be non-toxic to the mammalian control cell Cos-7, with the only notable activity arising from complex **1G**, with an IC_{50} of 88.3 μM. The gallium complexes exhibited little to no activity against HeLa and no further assessment of their anti-cancer activity was necessary. Tests into their anti-microbial action were performed on both the soluble and insoluble complexes. Complexes **1G** – **4G** and **1G'** were analysed as 5 mg/mL solutions onto bacteria inoculated agar plates, whereas the insoluble **2G'** – **4G'** were qualitatively assessed

by means of a solid-state test. Similar to the HeLa assay, the complexes exhibited very little anti-bacterial activity and no further analysis was conducted. A final assay was conducted on the promastigote form of *Leishmania* specifically *L. major* V121. The gallium complexes exhibited excellent anti-promastigote activity in the ranges of 1.11 – 13.4 μM. Their selectivity was assessed by a comparative mammalian control cell line, human fibroblasts. An IC_{50} range of 16.2 – $\geq$ 100 μM was obtained, with complexes **1G** and **1G'** proving the most cytotoxic. Despite the small degree of cytotoxicity, all complexes exhibited an excellent degree of selectivity**.** All complexes were then assessed for their anti-amastigote activity at a standard concentration of 10 μM. Excellent anti-amastigote activity was observed across the board, with percentage infection values of 3.35 % $\pm$ 0.65 – 11.5 % $\pm$ 0.65. Complex **1G**' proved the most ideal candidate based on anti-amastigote activity alone, but when considering overall selectivity, the Iodoquin complex **4G** reigned supreme, with a percentage infection value of 5.5 % $\pm$ 0.86 and selectivity index of 64.6.

To gain insight into potential mechanistic action of the complexes an assay to detect the production of reactive oxygen species was assessed. Example complexes **1G** and **1G**' were observed to initiate a percentage increase of ROS when added to infected macrophages, insinuating that they perhaps limit the ability for the intracellular parasite to disrupt the normal immunological response of the macrophages, allowing for ROS production and eventual parasite elimination.

Qualitative analysis of the UV-visible absorbance and fluorescence activity of the complexes yielded little results. All gallium and indium complexes were emissive in the solid-state under a UV-lamp, but lacked any potent measurable fluorescence. UV-visible analysis did however enable the further clarification of chelation of the quinolinol, by the appearance of multiple bands within the spectra. Due to **1I** – **4I**'s instability in the solution state, no solution state photophysical analysis was conducted. Complexes **1G** – **4G** and **1G'** – **4G'** were all found to be weak absorbers

even in largely non-polar solvents, with molar absorptivities ranging from 2458 – 6211 M^{-1} cm^{-1}. A noticeable two-fold increase in ε was observed when going from the *mono-quinolinolate*s (**1G** – **4G**) to the *bis*-substituted **1G'** – **4G'**. As the fluorescence of the complexes were greatly quenched in DMSO:H_2O, no further investigation into their potential biological fluorescence was investigated.

This section has highlighted the exploration into a different class of anti-Leishmanial complexes deviating from the traditionally used bismuth and antimony to focus on metals of the triel group, indium and gallium. A similar class of medically active halido-quinolinols were selected for their previously established therapeutic potential in order to assess possible synergistic effects by the chelation to a metal centre. The addition of alkyl groups in the final complex was theorised to alleviate the high hydrolytic stability of a previously synthesised tris-quinolinolate gallium complex that hindered it from further therapeutic use. The use of gallium and indium in the medical field is a continuously growing area of research and shows potential in the treatment of devastating tropical parasites.

2.3.9 References

1. A. J. Downs, *Chemistry of aluminium, gallium, indium and thallium*, Springer Science & Business Media, 1993.
2. C. L. Edwards and R. Hayes, *J. Nucl. Med.,* 1969, **10**, 103-105.
3. G. S. Johnston, *Int. J. Nucl. Med. Biol.*, 1981, **8**, 249-255.
4. S. C. King, R. J. Reiman and L. R. Prosnitz, *J. Clin. Oncol.*, 1994, **12**, 306-311.
5. M. M. Hart and R. H. Adamson, *Proc. Natl. Sci. U.S.A.*, 1971, **68**, 1623-1626.
6. L. R. Bernstein, *Pharmacol. Rev.*, 1998, **50**, 665-682.
7. D. W. Hedley, E. H. Tripp, P. Slowiaczek and G. J. Mann, *Cancer Res.*, 1988, **48**, 3014-3018.
8. M. Gielen and E. R. Tiekink, *Metallotherapeutic drugs and metal-based diagnostic agents: the use of metals in medicine*, John Wiley & Sons, 2005.
9. T. Two, *Chem. Biol.*, 2002, **9**, 1051-1052.
10. R. Beriault, R. Hamel, D. Chenier, R. J. Mailloux, H. Joly and V. Appanna, *Biometals*, 2007, **20**, 165-176.
11. W. R. Harris and L. Messori, *Coord. Chem. Rev.*, 2002, **228**, 237-262.
12. W. R. Harris and V. L. Pecoraro, *Biochemistry (Mosc.)*, 1983, **22**, 292-299.
13. C. R. Chitambar and Z. Zivkovic, *Cancer Res.*, 1987, **47**, 3929-3934.
14. R. Ardehali and S. Mohammad, *J. Biomed. Mater. Res.*, 1993, **27**, 269-275.
15. S. Anderson and V. D. Appanna, *Environ. Pollut.*, 1993, **82**, 33-37.
16. J. L. Zurita, A. Jos, A. del Peso, M. Salguero, A. M. Cameán, M. López-Artíguez and G. Repetto, *Sci. Total Environ.*, 2007, **387**, 155-165.
17. V. Barros, S. David, C. Cruz and R. Delgado, *FEMS Microbiol. Lett.*, 2005, **251**, 119-124.
18. J. Alvar, I. D. Vélez, C. Bern, M. Herrero, P. Desjeux, J. Cano, J. Jannin, M. den Boer and W. L. C. Team, *PLoS One*, 2012, **7**, e35671.
19. M. Boelaert, F. Meheus, A. Sanchez, S. Singh, V. Vanlerberghe, A. Picado, B. Meessen and S. Sundar, *Trop. Med. Int. Health*, 2009, **14**, 639-644.
20. J. Alexander, A. R. Satoskar and D. G. Russell, *J. Cell Sci.*, 1999, **112**, 2993-3002.
21. E. Handman, *Adv. Parasitol.*, 1999, **44**, 1-39.
22. R. Sutak, E. Lesuisse, J. Tachezy and D. R. Richardson, *Trends Microbiol.*, 2008, **16**, 261-268.
23. S. Sengupta, J. Tripathi, R. Tandon, M. Raje, R. P. Roy, S. K. Basu and A. Mukhopadhyay, *J. Biol. Chem.*, 1999, **274**, 2758-2765.
24. M. E. Wilson, R. W. Vorhies, K. A. Andersen and B. E. Britigan, *Infect. Immun.*, 1994, **62**, 3262-3269.
25. M. E. Wilson, T. S. Lewis, M. A. Miller, M. L. McCormick and B. E. Britigan, *Exp. Parasitol.*, 2002, **100**, 196-207.
26. C. Huynh and N. W. Andrews, *Cell. Microbiol.*, 2008, **10**, 293-300.
27. C. S. Chang and K.-P. Chang, *Mol. Biochem. Parasitol.*, 1985, **16**, 267-276.
28. C. Huynh, D. L. Sacks and N. W. Andrews, *J. Exp. Med.*, 2006, **203**, 2363-2375.
29. É. A. Enyedy, O. Dömötör, K. Bali, A. Hetényi, T. Tuccinardi and B. K. Keppler,*J. Biol. Inorg. Chem.*, 2015, **20**, 77-88.
30. A. R. Timerbaev, *Metallomics*, 2009, **1**, 193-198.
31. P. Hongmanee, K. Rukseree, B. Buabut, B. Somsri and P. Palittapongarnpim, *Antimicrob. Agents Chemother.*, 2007, **51**, 1105-1106.
32. R. Swain, J. Bapna, A. Das, S. Chandrasekar, R. Swaminathan, B. Bosco, S. Veliath and D. Thombre, *Hum. Toxicol.*, 1986, **5**, 35-41.
33. A. K. Fisher, F. G. Walter and S. Szabo, *J. Toxicol.: Clin. Toxicol.*, 1993, **31**, 113-120.
34. H. M. Robinson Jr and M. B. Hollander, *J. Investig. Dermatol.*, 1956, **26**, 143-147.

35. M. C. Duarte, L. M. dos Reis Lage, D. P. Lage, J. T. Mesquita, B. C. S. Salles, S. N. Lavorato, D. Menezes-Souza, B. M. Roatt, R. J. Alves and C. A. P. Tavares, *Vet. Parasitol.*, 2016, **217**, 81-88.
36. C. Bakewell, A. J. White, N. J. Long and C. K. Williams, *Inorg. Chem.*, 2013, **52**, 12561-12567.
37. M. R. Kaluđerović, S. Gómez-Ruiz, B. Gallego, E. Hey-Hawkins, R. Paschke and G. N. Kaluđerović, *Eur. J. Med. Chem.*, 2010, **45**, 519-525.
38. S. Gómez-Ruiz, B. Gallego, M. R. Kaluđerović, H. Kommera, E. Hey-Hawkins, R. Paschke and G. N. Kaluđerović, *J. Organomet. Chem.*, 2009, **694**, 2191-2197.
39. V. M. Vlasov, *Russ. Chem. Rev.*, 2003, **72**, 681-703.
40. C. Barnes, *J. Chem. Educ.*, 2003, **80**, 747.
41. D. Peña-Solórzano, B. König, C. A. Sierra and C. Ochoa-Puentes, *Acta. Crystallogr. E.*, 2017, **73**, 602-605.
42. D. Peña-Solórzano, B. König, C. A. Sierra and C. Ochoa-Puentes, *Acta. Crystallogr. E.*, 2017, **73**, 804-808.
43. M. M. Zhao, Y. H. Li and Y. Zhang, *Acta. Crystallogr. E.*, 2009, **65**, 1795.
44. M.-M. Duvenhage, H. C. Swart, O. M. Ntwaeaborwa and H. G. Visser, *OptMa*, 2013, **35**, 2366-2371.
45. Y. Shen, Y. Pan, X. Jin, X. Xu, X. Sun and X. Huang, *Polyhedron*, 1999, **18**, 2423-2426.
46. J. Lewiński, J. Zachara, K. B. Starowieyski, Z. Ochal, I. Justyniak, T. Kopeć, P. Stolarzewicz and M. Dranka, *Organometallics*, 2003, **22**, 3773-3780.
47. S. Basharat, C. J. Carmalt, S. A. Barnett, D. A. Tocher and H. O. Davies, *Inorg. Chem.*, 2007, **46**, 9473-9480.
48. P. Horeglad, M. Cybularczyk, A. Litwińska, A. Dąbrowska, M. Dranka, G. Żukowska, M. Urbańczyk and M. Michalak, *Polymer Chemistry*, 2016, **7**, 2022-2036.
49. E. Hecht, T. Gelbrich, K.-H. Thiele and J. Sieler, *Main Group Chem.*, 2000, **3**, 109-116.
50. O. Beachley, D. J. MacRae, M. R. Churchill, A. Y. Kovalevsky and E. S. Robirds, *Organometallics*, 2003, **22**, 3991-4000.
51. N. Alcock, I. Degnan, S. Roe and M. Wallbridge, *J. Organomet. Chem.*, 1991, **414**, 285-293.
52. G. G. Briand, A. Decken and N. S. Hamilton, *Dalton Trans.*, 2010, **39**, 3833-3841.
53. R. García-Contreras, E. Lira-Silva, R. Jasso-Chávez, I. L. Hernández-González, T. Maeda, T. Hashimoto, F. C. Boogerd, L. Sheng, T. K. Wood and R. Moreno-Sánchez, *Int. J. Med. Microbiol.*, 2013, **303**, 574-582.
54. Y.-Z. Shen, Y. Pan, L.-Y. Wang, G. Dong, X.-P. Jin, X.-Y. Huang and H. Hu, *J. Organomet. Chem.*, 1999, **590**, 242-247.
55. M. Normand, E. Kirillov, T. Roisnel and J.-F. o. Carpentier, *Organometallics*, 2011, **31**, 1448-1457.
56. K. Hyun, H. Jin, W. H. Woo, H. Shin, J. H. Lee, H. Hwang, M. Kim, K. M. Lee, M. H. Park and Y. Kim, *Dyes Pigm.*, 2018, **158**, 285-294.
57. S. H. Lee, N. Shin, S. W. Kwak, K. Hyun, W. H. Woo, J. H. Lee, H. Hwang, M. Kim, J. Lee and Y. Kim, *Inorg. Chem.*, 2017, **56**, 2621-2626.
58. A. M. Arif and A. R. Barron, *Polyhedron*, 1988, **7**, 2091-2094.
59. N. N. Chamazi, M. M. Heravi and B. Neumüller, *ZAAC*, 2006, **632**, 2043-2048.
60. Y. Gluzman, *Cell*, 1981, **23**, 175-182.
61. Y. Dowlati, *Clin. Dermatol.*, 1996, **14**, 425-431.
62. C. R. Chitambar, *Expert Opin. Invest. Drugs*, 2004, **13**, 531-541.
63. T. E. Hughes and L. A. Hansen, *Ann. Pharmacother.*, 1992, **26**, 354-362.
64. R. Adamson, G. Canellos and S. Sieber, *Cancer. Chemother. Rep.*, 1975, **59**, 599-610.
65. S. M. Valiahdi, P. Heffeter, M. A. Jakupec, R. Marculescu, W. Berger, K. Rappersberger and B. K. Keppler, *Melanoma Res.*, 2009, **19**, 283.

66. P. C. Andrews, M. Werrett, M. Herdman, R. Brammananth, U. Garusinghe, W. Batchelor, P. Crellin and R. Coppel, *Chem. Eur. J.*, 2018.
67. R. N. Duffin, V. L. Blair, L. Kedzierski and P. C. Andrews, *Dalton Trans.*, 2018, **47**, 971-980.
68. R. N. Duffin, V. L. Blair, L. Kedzierski and P. C. Andrews, *J. Inorg. Biochem.*, 2018.
69. R. D. Abughazaleh and T. S. Tracy, *Wiley StatsRef: Stat. Ref. Online.* 2007, doi:10.1002/9781118445112.stat07121.
70. C. R. Chitambar, *Biochim. Biophys. Acta. Mol. Cell. Res.*, 2016, **1863**, 2044-2053.
71. S. Hijazi, D. Visaggio, M. Pirolo, E. Frangipani, L. Bernstein and P. Visca, *Front. Cell. Infect. Mi.*, 2018, **8**, 316.
72. C. R. Chitambar, *Int. J. Env. Res. Public Health*, 2010, **7**, 2337-2361.
73. J. A. Imlay, *EcoSal Plus*, 2009, **3**.
74. A. Anjem, S. Varghese and J. A. Imlay, *Mol. Microbiol.*, 2009, **72**, 844-858.
75. N. G. Tessarollo, J. M. Andrade, D. d. S. Moreira and S. M. F. Murta, *Parasitol. Int.*, 2015, **64**, 125-129.
76. T. Naderer and M. J. McConville, *Cell. Microbiol.*, 2008, **10**, 301-308.
77. B. Mittra, M. Cortez, A. Haydock, G. Ramasamy, P. J. Myler and N. W. Andrews, *J. Exp. Med.*, 2013, **210**, 401-416.
78. A. Wojtala, M. Bonora, D. Malinska, P. Pinton, J. Duszynski and M. R. Wieckowski, *Methods Enzymol.*, Elsevier, 2014, vol. 542, pp. 243-262.
79. A. Kumar Saha, T. Mukherjee and A. Bhaduri, *Mol. Biochem. Parasitol.*, 1986, **19**, 195-200.
80. G. Cuddihy, E. K. Wasan, Y. Di and K. M. Wasan, *Pharmaceutics*, 2019, **11**, 99.
81. M. Goldman and E. Wehry, *Anal. Chem.*, 1970, **42**, 1178-1185.
82. S. G. Schulman, *Anal. Chem.*, 1971, **43**, 285-287.
83. E. Bardez, I. Devol, B. Larrey and B. Valeur, *J. Phys. Chem. B.*, 1997, **101**, 7786-7793.
84. T. Moeller and A. J. Cohen, *J. Am. Chem. Soc.*, 1950, **72**, 3546-3548.

2.4. Synthesis, characterisation and biological activity of triaryl Sb(V) R/S-mandelate complexes

2.4.1 Mandelic acid

Mandelic acid, like many conventional organic compounds, was first extracted from a natural source.[1] As most discoveries were back then, mandelic acid was isolated serendipitously in 1909. Walker and Krieble extracted amygdalin, a cyanogenetic glycoside, from bitter almonds. When heated in dilute hydrochloric acid, they isolated a white crystalline solid which they named mandelic acid, after the German word for almond, Mandel.[1] Mandelic acid was structurally characterised as an aromatic α-hydroxy acid with the molecular formula $C_6H_5CH(OH)COOH$, more systematically known as α-hydroxyl benzene acetic acid. It has a chiral centre on the α-carbon and is found in both the *R* or *S* confirmations (figure 2.4.1).

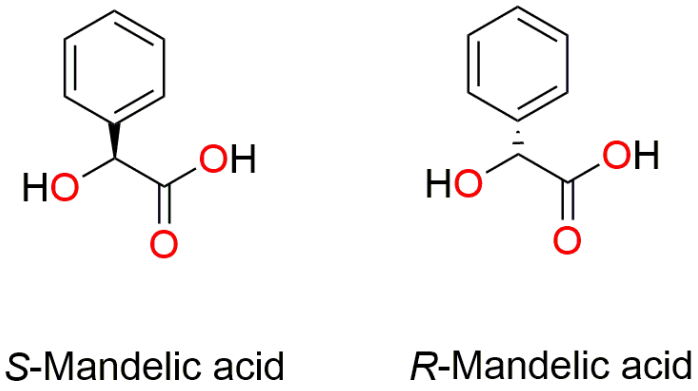

Figure 2.4.1. The two enantiomers of mandelic acid

Despite the aromatic group on the backbone of the acid, mandelic acid is freely soluble in water and other polar organic solvents.

2.4.1.1 Mandelic acid as biological detector.

Studies conducted in the early 1970s – 1980s found that mandelic acid levels in the urine of industrial workers could be used to determine the level of styrene exposure of the affected individuals.[2-6] In the human body, styrene is metabolised to styrene-7,8-oxide by cytochrome P-450 mediated monooxygenase systems and other biological mechanisms including lipoxynase-mediated enzymes and oxidation via oxyhaemoglobin and myoglobin.[7-10] Styrene-7,8-oxide then undergoes enzymatic hydrolysis to phenyl ethylene glycol which is further oxidised to mandelic acid and phenylglyoxylic acid (figure 2.4.2).[11]

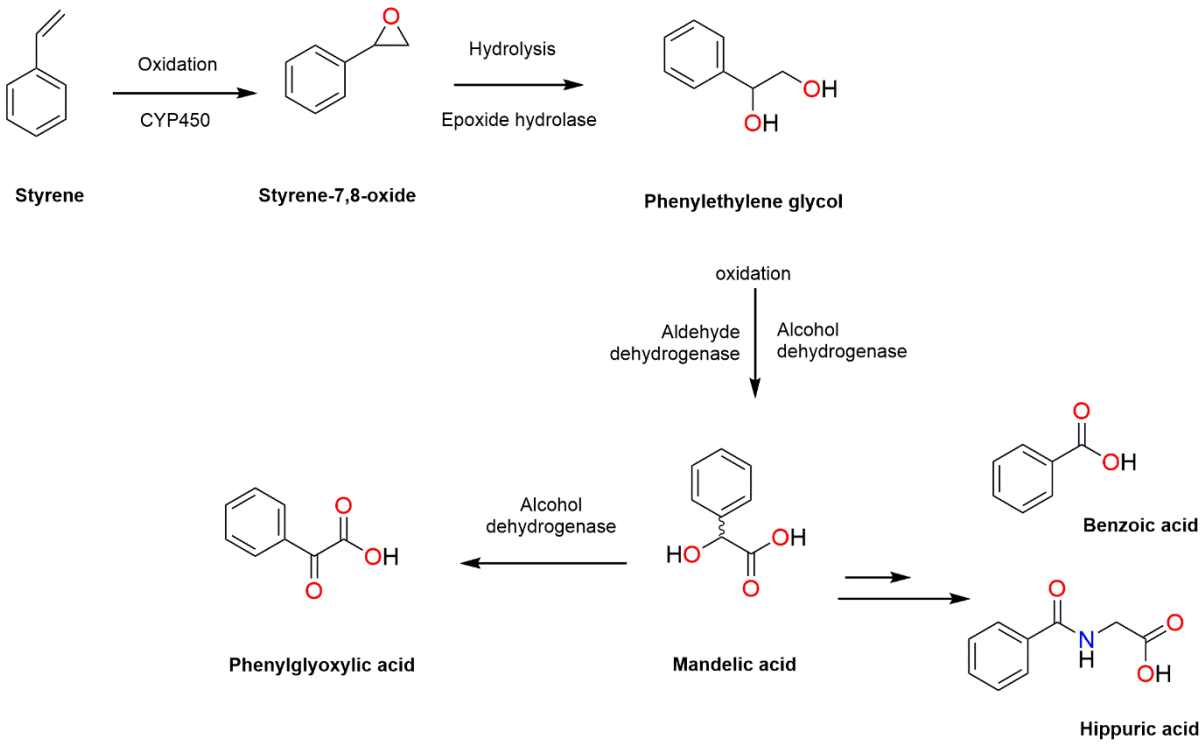

Figure 2.4.2. Major metabolic pathway of styrene in humans, several by-products have been excluded. CYP450: cytochrome P450.

The mandelic acid and phenylglyoxylic acid produced as a result of styrene exposure, exhibit a biphasic urinary excretion with a first phase half-life of 2.5 hours and a second phase half-life of 30 hours, allowing for accurate determination of the original styrene concentration.[12] This

mandelic acid quantification technique is still utilised today to quantify the exposure of plastic injection industrial workers to toxic gases and vapours, including styrene.[13]

2.4.1.2 Mandelic acid as an anti-microbial

Not only is mandelic acid a useful bio-detector for toxic vapour exposure, it has also been used for many years as a bladder irrigation fluid to prevent urinary tract infections. Solutions of 1% mandelic acid have a low pH of 2.4. This acidic solution is used to dissolve minerals that can form during urinary tract infections that lead to concernments and bladder stones.[14] The anti-bacterial activity of mandelic acid has been studied extensively, with research by Rosenhiem *et al* in the 1930s, assessing its viability as an anti-bacterial agent and its ability to remain unchanged during excretion.[15] The efficacy of mandelic acid relied heavily on the maintenance of a strictly acidic urine pH, without which its bacteriostatic abilities diminished. This limited its use against bacteria that produced basic compounds, such as ammonia, as metabolic by-products.[16]

Mandelic acids uses are still investigated today, it has been traditionally used in the cosmetics industry as a facial scrub and for the treatment of acne prone skin.[17] The large molecular size of mandelic acid allows for slower diffusion of the acid into the skin which results in less irritation of the lower dermis.[18] The anti-bacterial applications of mandelic acid focus on microbes that are localised in and around the skin as opposed to internal infection. Children with atopic dermatitis have been observed to house a significant reservoir of methicillin resistant *Staphylococcus aureus* (MRSA). Consequently, Motanmedifar *et al* demonstrated the promising effects of using mandelic acid as a combination therapy in the treatment of dermatitis and bacterial infections caused by MRSA.[19] Catalina *et al* also investigated activity based around topical treatments and dermatitis, analysing two mandelate derivatives as potential preservatives in topical.[20] The mandelate derivatives exhibited very good preservation of the topical ointments, even those exposed to *Pseudomonas aeruginosa* and *Candida albicans*.[20] Most recently a series of mandelate bromides

have been analysed for use in ionic liquids. These weakly coordinating salts showed low anti-microbial activity against thirteen different strains of bacteria and twelve fungal strains, with a trend of increasing activity as the alkyl ester chain increased.[21]

2.4.1.3 Metal complexes of mandelic acid

Mandelic acid has two potential deprotonation sites on its structure, the acidic carboxylate proton (pKa ~ 3.4) and the α-hydroxyl (pKa ~ 14.2).[22] This enables mandelic acid to bind to a metal through a monoanionic or dianionic binding mode, as a four membered or five membered chelate respectively (figure 2.4.3). The five membered chelate is commonly known as a cyclometallate due to its potential to redistribute back to the four membered monoanionic form. Most metal complexes tend to favour the binding through carboxylate with dative interactions through the carbonyl oxygen.

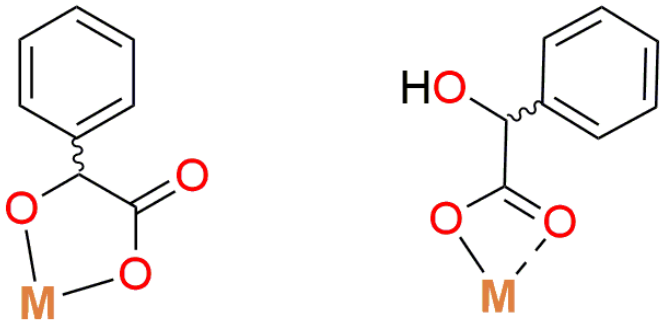

Figure 2.4.3. Metal binding modes of mandelic acid

Mandelate forms stable complexes with a variety of metals. Titrations of mandelic acid against a series of lanthanide complexes yielded changes in pH that were determined to be due the binding of the mandelate to the metal complex. Formation constants were calculated which showed a strong affinity of the acid to the metal centre.[23] Due to its two potential deprotonation sites, mandelate can form bridging complexes with a metal centre. Studies by Pruchnik *et al* back in the

1980s, characterised the binding of one mandelate to two separate rhodium centres, forming a mandelato bridge. The complex was observed to be both thermally and substitutionally stable in d_6-DMSO.[24] Spectroscopic studies on divalent transition metal complexes enabled insights into the structural stability of mandelate versus other conventional α-hydroxy acids such as glycolate and lactate. Mandelate was observed to be the most stable of the three in the spectrochemical series generated.[25] X-ray crystallographic studies into a copper mandelate complex observed binding of the copper through a double deprotonation of the mandelic acid, and interactions with adjacent copper centres through dative binding of the carbonyl oxygen.[26] Other metal complexes of mandelate include molybdenum, europium and silver.[27-29] The silver complex of mandelic acid was observed to differ from the transition metal complexes by binding of the carboxylate alone to one silver centre, and the interaction of the adjacent silver with the carbonyl oxygen. A five membered chelate was formed through both covalent and dative interactions of both hydroxyl groups to another silver centre, resulting in a polymeric structure.[29] This polymeric mandelate complex was also tested for its antimycobacterial properties. Though not extremely potent, they exhibited some anti-bacterial activity.[29]

Complexes of mandelate with group 15 metals, bismuth and antimony, have also been characterised. Initial studies by Zevaco and Postel *et al* on the Bi(III) complex, observed binding of the mandelates through a covalent interaction with the carboxylate hydroxyl, and a dative bond through the α-hydroxyl. The complex was also characterised to incorporate a Bi-O-Bi moiety, with two mandelates in the remaining coordination sites of the Bi(III) centres.[30] This oxide bridge complex found heavy use as a Bi mediated catalyst of aryl epoxides.[31] Mandelates have found use in the determination of the ratio of Sb(III) or Sb(V) ions in solution media.[32] More recently, investigations into the synthesise of the Bi(V) and Sb(V) aryl equivalents have been achieved, with Barucki *et al* focusing on the stereoselectivity of these complexes. The bismuth complexes were

observed to form *bis*-substituted complexes of the general formula [$BiPh_3(LH)_2$] whereas the antimony complexes were more stable as the cyclometallated ([$SbPh_3L$]).[33]

2.4.1.4 Mandelate anti-Leishmanials

Studies into to the potential anti-Leishmanial activity of triphenyl Bi(V) and Sb(V) mandelates were then conducted by Andrews *et al*.[34] The Bi(V) aryl mandelates complexes were disqualified from testing due to their lack of selectivity, but a high degree of selectivity from the analogous Sb(V) complexes made them ideal candidates. Due to the moderate activity observed by the Sb(V) complexes, a study into the structure activity was proposed, focusing on both the chirality, *R* or *S* mandelate, and changing of the aryl group from the original phenyl moiety.

2.4.2 Synthesis and characterisation

2.4.2.1 Synthesis

The synthesis of triaryl Sb(V) mandelates followed the same oxidative addition, though modified to encourage immediate formation of the cyclometallate complex. As opposed to two equivalents of acid, one equivalent was reacted with the triaryl antimony after oxidation to the dihydroxido intermediate. H_2O_2 was used in place of t-BuOOH, to encourage the formation of the cyclometallate by producing water, rather than t-BuOH as a by-product (figure 2.4.4). This was due to the similar *p*Ka of both t-BuOH and the α-hydroxy of mandelic.[35]

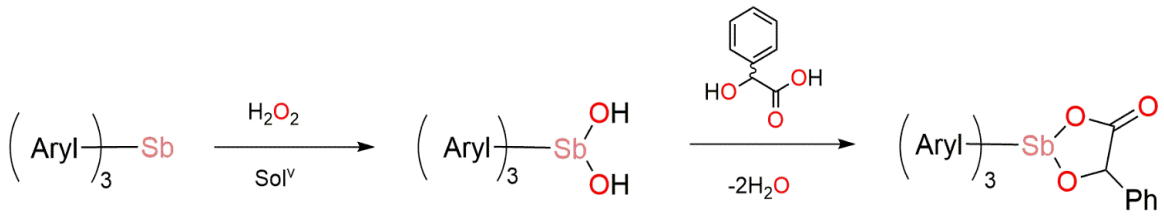

Aryl = *o*-tol, *m*-tol, *p*-tol, *o*-OMe, mesityl, *p-t*-butyl

Sol^V = Et_2O or Toluene

Figure 2.4.4. Synthetic pathway utilised in the synthesis of aryl Sb(V) R/S mandelates

The different aryl groups used in this study were *o, m, p*-tolyl, (*o,m,p*-tol*)* *o*-methoxyphenyl, (*o*-PhOMe*),* mesityl, (mes) and *p*-tertiary butyl-phenyl, (*p*-tBuPh) (figure 2.4.5). All starting aryls were produced easily from the salt metathesis reaction of $SbCl_3$ with the MgArBr under inert conditions in THF. The Grignard reagents were synthesised by the addition of the ArBr to Mg turnings prior to addition to antimony trichloride.[36] The synthesis of all starting Sb(III) aryls were high yielding (75 – 88%) and easily crystallised from either ethanol or acetone.

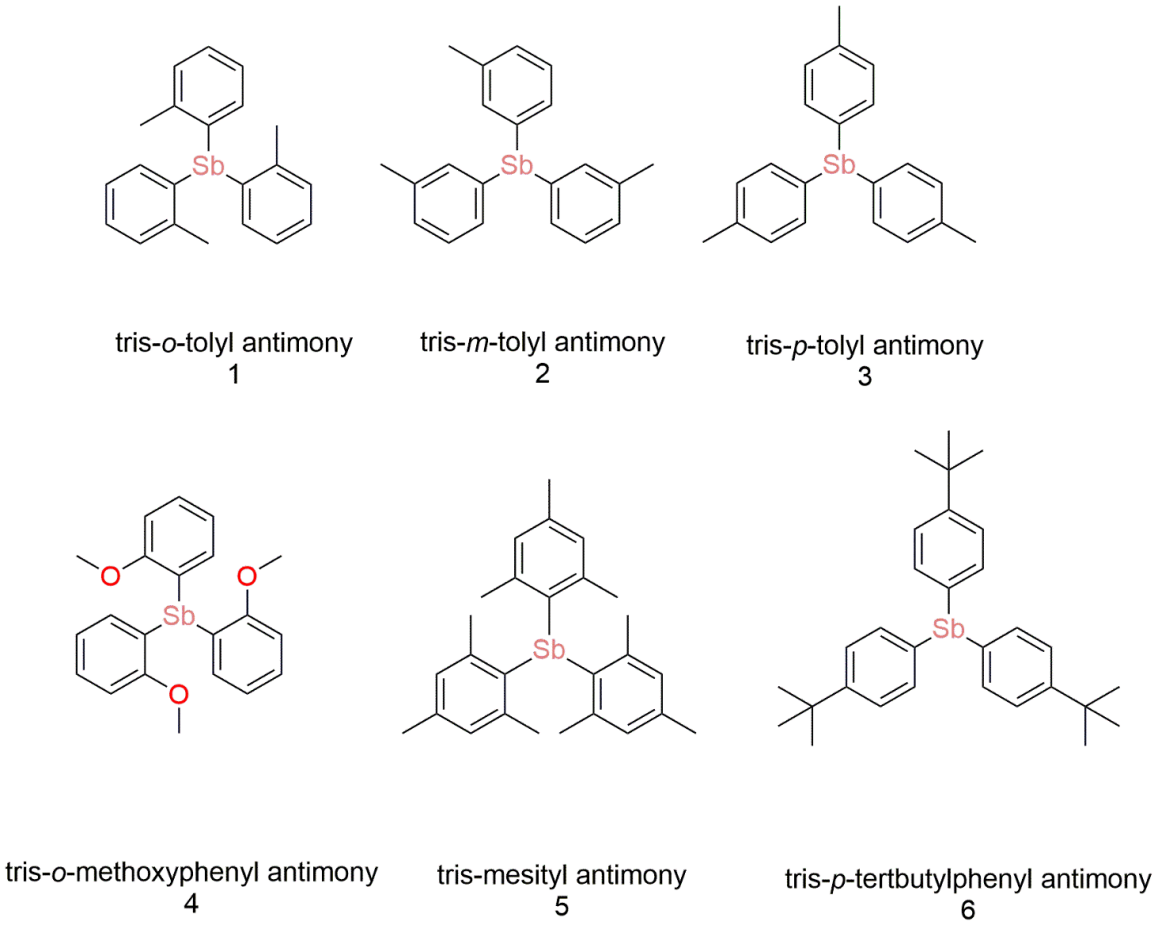

Figure 2.4.5. Aryl Sb(III) precursors explored in this study

Synthesis of the cyclometallate complexes of *R* or *S* mandelate, **1Sr/s,** $[Sb(o\text{-tol})_3O_2CCH(C_6H_5)O]$, **2Sr/s,** $[Sb(m\text{-tol})_3O_2CCH(C_6H_5)O]$, **3Sr/s,** $[(Sb(p\text{-tol})_3O_2CCH(C_6H_5)OH)_2O_2]$, **4Sr/s,** $[Sb(o\text{-phOMe})_3O_2CCH(C_6H_5)O]$, **5Sr/s,** $[Sb(mes)_3O_2CCH(C_6H_5)O]$ and **6Sr/s,** $[Sb(p\text{-tBuPh})_3O_2CCH(C_6H_5)O]$,

exhibited several issues. Despite the simple one-step oxidative addition, the products obtained often formed as oily residues. ^{1}H NMR studies on these residues revealed that the reactions had not gone to full completion. The reactions were given longer synthesis times but still produced impure oils. The oils were then sonicated in distilled water, which yielded solid white powders. Any mandelic acid left in the reaction mixture dissolved into the water upon sonication, and was subsequently filtered off. The products were dried and analysed to provide pure products. It was found that ether produced better yields and cleaner products than toluene, and so ether was predominantly used as the reaction solvent. It is not yet fully understood what the cause of the oil formation was, but may perhaps be due to the potential formation of triaryl antimony oxide bridged complexes.[37, 38]

2.4.2.2 Characterisation

All complexes were eventually synthesised and isolated in high yields (72 - 86%) and high purity. All were characterised by ^{1}H NMR, ^{13}C NMR, melting point analysis, FT-IR, elemental analysis and single crystal X-ray crystallography. Complexes of the *p*-tolyl antimony were the only complex to differ in their solid-state structure, complexes **1Ss/Sr**, **2Ss/Sr**, **4Ss/Sr** – **6Ss/Sr** were all characterised as cyclometallates, by both X-ray crystallography and IR spectroscopy. Complexes **3SS/Sr** however formed a perioxo bridged complex of the general formula [$(SbAr_3LH)_2O_2$], a structural representation is given below in figure 2.4.6. Unfortunately, repeated analysis by X-ray crystallography was unable to yield publishable data, but an idea on the connectivity was established. In the solution state however cyclometallation did occur forming complexes **3Sr'** and **3Ss'** (fig 2.4.5)**.**

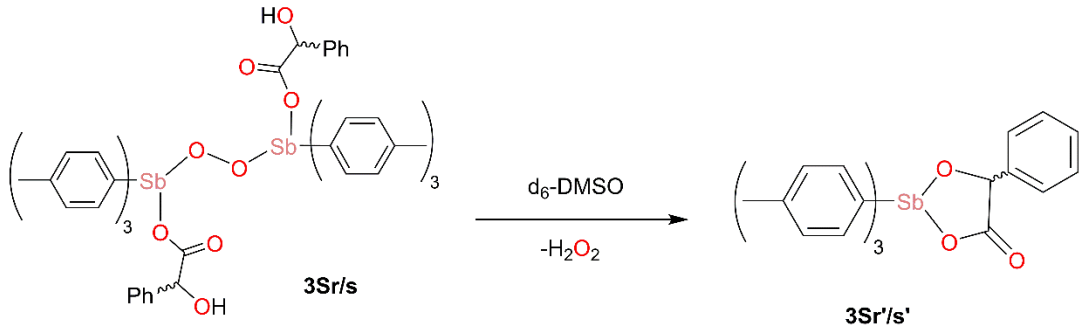

*Figure 2.4.6. General structures of complexes **3Sr/s,** [(Sb(p-tol)$_3$(manH)$_2$O$_2$] and the cyclometallate form **3Sr'/s'**, [Sb(p-tol)$_3$(man)].*

^{1}H NMR of complexes **3Ss** and **3Sr** highlighted the formation of the cyclometallate form **3Sr'/3Ss'** in the solution state. (figure 2.4.7). Cyclometallation was further confirmed by the presence of H_2O_2 at 0 hours of which degrades after 24 hours.

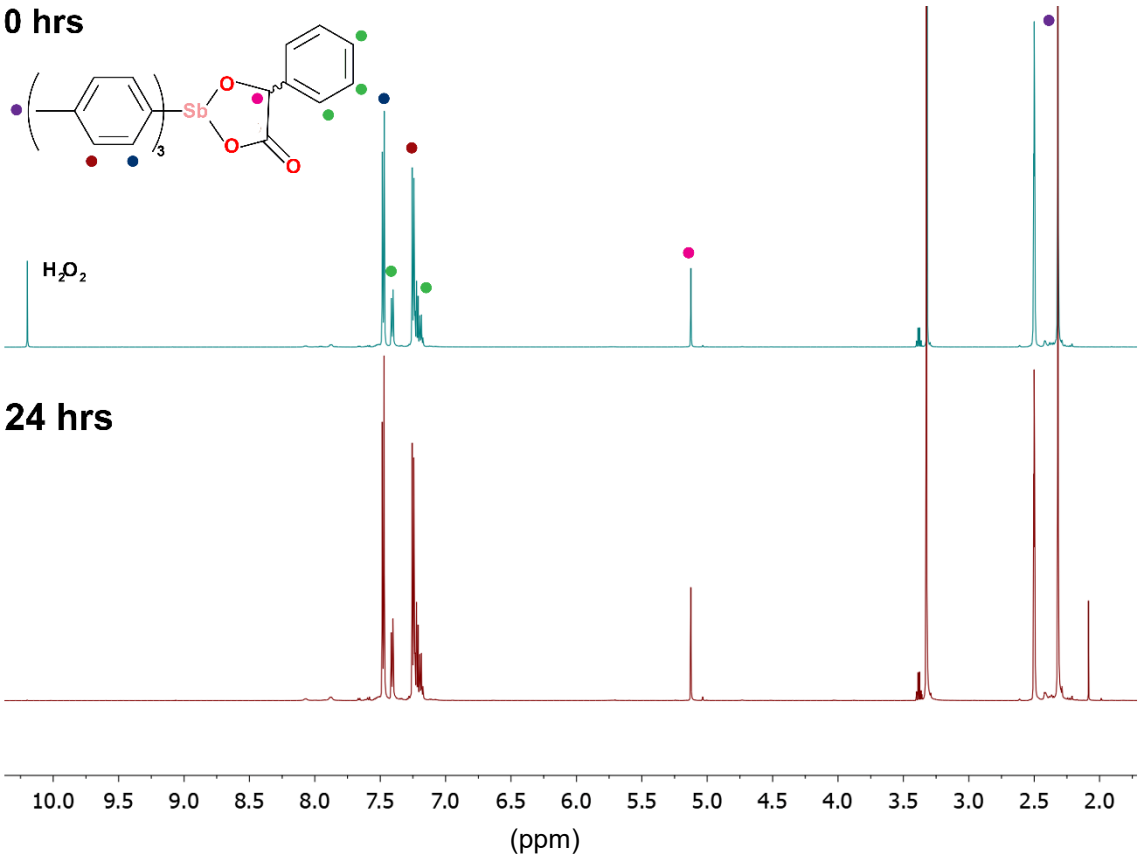

*Figure 2.4.7. ^{1}H NMR spectrum of complex **3Sr'**, [(Sb(p-tol)$_3$O$_2$CCH(C$_6$H$_5$)O], against precursor aryl, the residual solvent signal and H_2O signal can be found at 2.50ppm and 3.33ppm respectively. The presence of H_2O_2 at ~ 10 ppm can be observed.*

Similar to complex **3Sr'**, all remaining cyclometallates, be it *R* or *S*, are spectroscopically identical. An example ^{1}H NMR of complex **1Ss,** [(Sb(*o*-tol)$_3$O$_2$CCH(C$_6$H$_5$)O] and **1Sr,** [(Sb(*o*-tol)$_3$O$_2$CCH(C$_6$H$_5$)O], is given below (figure 2.4.8). Binding of the mandelate through both hydroxyls was identified by the lack of any hydroxyl signals in the ^{1}H NMR. The only definitive analytical technique utilised to distinguish between the two enantiomers was X-ray crystallography. Strangely, complexes **5Ss** and **5Sr**, the mesityl analogues, [Sb(mes)$_3$O$_2$CCH(C$_6$H$_5$)O], presented with unusual ^{1}H NMR data, despite being pure crystalline complexes. Polarimetry could be used but due to time constraints was not employed. The signals presented as quite broad, however for the most part the integrations were representative of the complex. This broadening of the signals could be related to the fluxionality of the mandelate, switching between the monodentate and bidentate binding mode. This could potentially be resolved by low temperature NMR studies, but as other analytical data correlated with the obtained X-ray structure this would have been an unnecessary step.

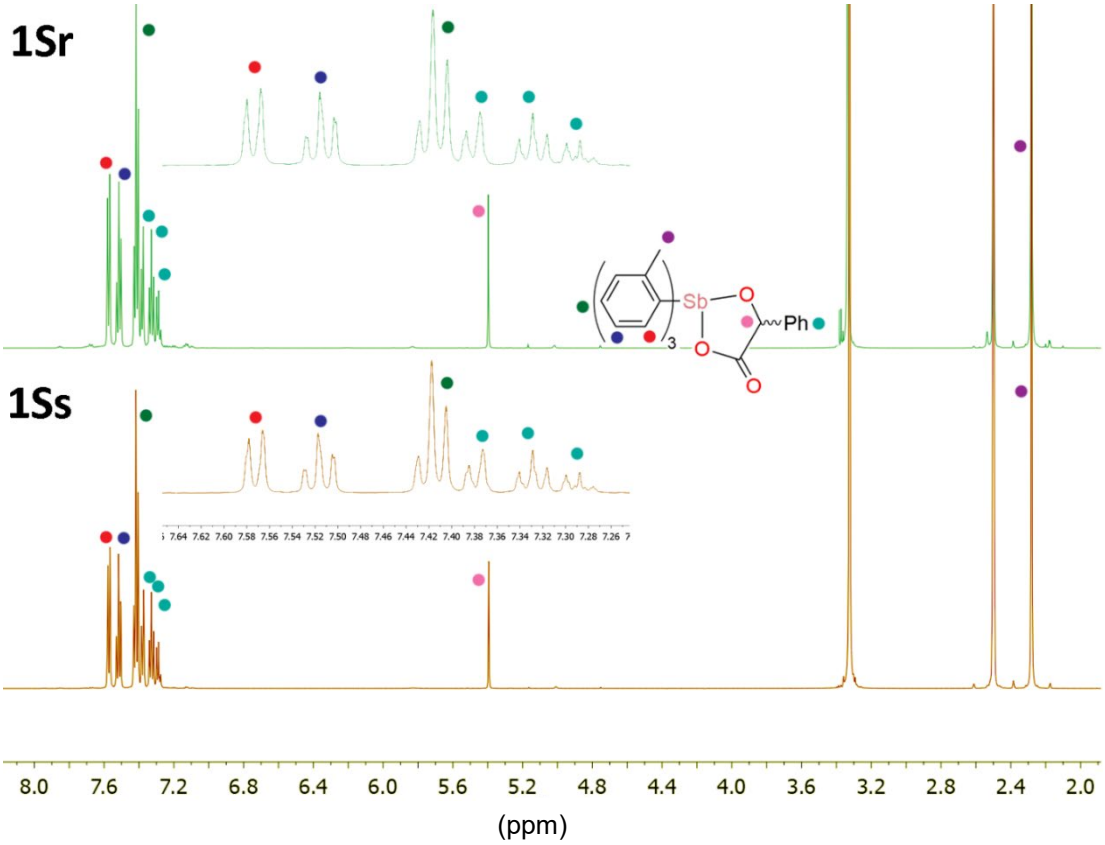

Figure 2.4.8. ^{1}H NMR of complexes ***1Sr/s,*** $[(Sb(o\text{-}tol)_3O_2CCH(C_6H_5)O]$, *in d_6-DMSO, the residual solvent signal and H_2O signal can be found at 2.50ppm and 3.33ppm respectively. Insert of the expanded aromatic region given.*

Similar to NMR spectra obtained, the IR spectrum of each complex was found to be the same, as was expected in a technique that yields information about the bonding of the complex only. Nevertheless, a list of the carboxylate stretching frequencies of all the complexes versus the free mandelic acid is given below in table 2.4.1.

*Table 2.4.1. IR stretching frequencies of free mandelic acid versus the cyclometallate (and peroxido) complexes **1Ss/Sr** – **6Ss/Sr***

Compound	v-COOH	v-COO
Mandelic acid (R/S)	1710 cm^{-1}	-
1Ss	-	1682 cm^{-1}
1Sr	-	1683 cm^{-1}
2Ss	-	1682 cm^{-1}
2Sr	-	1683 cm^{-1}
3Ss	-	1653 cm^{-1}
3Sr	-	1654 cm^{-1}
4Ss	-	1677 cm^{-1}
4Sr	-	1676 cm^{-1}
5Ss	-	1677 cm^{-1}
5Sr	-	1677 cm^{-1}
6Ss	-	1665 cm^{-1}
6Sr	-	1665 cm^{-1}

2.4.2.3 X-ray crystallography

Crystals of all complexes were obtained from either heating in a solvent (usually DMSO) or through slow evaporation of the filtered reaction mixture. The complexes that crystallised from DMSO, **6Ss** and **6Sr**, [Sb(*p*-tBuPh)$_3$O$_2$CCH(C$_6$H$_5$)O], both incorporated a datively bound DMSO. Complexes **1Ss** and **1Sr**, [Sb(*o*-tol)$_3$O$_2$CCH(C$_6$H$_5$)O], **2Ss** and **2Sr,** [Sb(*m*-tol)$_3$O$_2$CCH(C$_6$H$_5$)O], **4Sr** and **4Ss,** [Sb(*o*-PhOMe)$_3$O$_2$CCH(C$_6$H$_5$)O], **5Ss** and **5Sr,** [Sb(mes)$_3$O$_2$CCH(C$_6$H$_5$)O], all crystallised from the toluene or ether reaction mixture, without solvent molecules present. Complexes **2Sr** and **2Ss** differed

from the remaining structures through a dative interaction of the mandelate with the adjacent antimony centre. All complexes were solved in non-centrosymmetric space groups due to the pure enantiomeric chirality of the mandelic acid. All corresponding data can be found in tables 2.4.2 and 2.4.3. A visual representation of all complexes **2Ss/Sr**, **4Ss/Sr** – **6Ss/Sr** is given below in figures 2.4.9 – 2.4.16, a detailed description of complexes **1Ss** and **1Sr** will be discussed further.

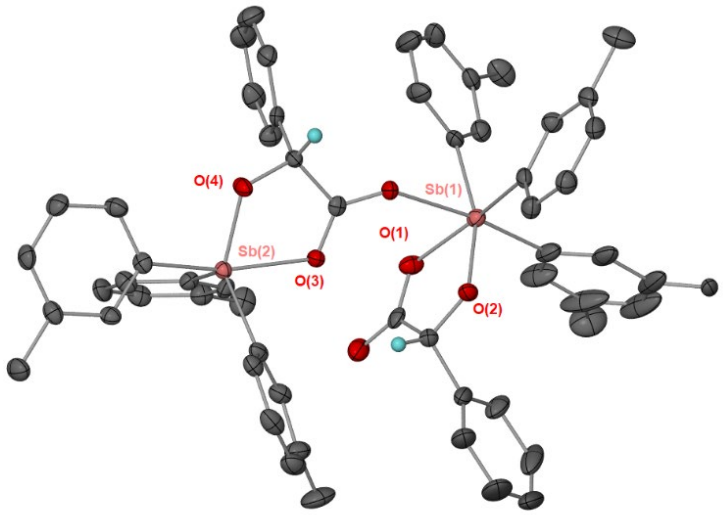

*Figure 2.1.9. Solid-state structure of 2[Sb($C_6H_4(CH_3)$)$_3O_2CCH(C_6H_5)O$], **2Sr**. Thermal ellipsoids at 50% probability. Hydrogen atoms have been omitted for clarity. Selected bonds lengths (Å) and angles (o). Sb(1) – O(1), 1.957(4), Sb(1) – O(2), 2.234(4), Sb(1) – C(1), 2.123(6), Sb(1) – C(7), 2.127(6), Sb(1) – C(15), 2.094(5); C(1) – Sb(1) – C(15), 101.0(2), C(1) – Sb(1) – C(7), 101.0(2), C(7) – Sb(1) – O(1), 129.9(19), O(1) – Sb(1) – O(2), 79.92(14). Disorder of the methyl group has been modelled over two positions.*

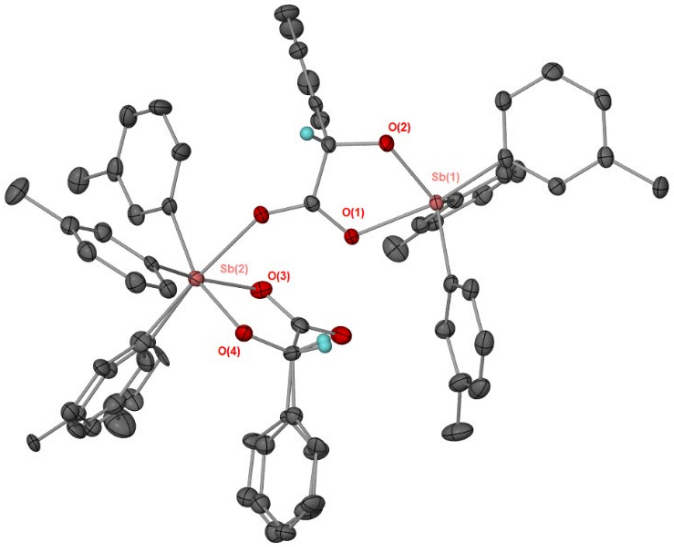

*Figure 2.1.10. Solid-state structure of 2[Sb($C_6H_4(CH_3)$)$_3O_2CCH(C_6H_5)O$], **2Ss**. Thermal ellipsoids at 50% probability. Hydrogen atoms have been omitted for clarity. Selected bonds lengths (Å) and angles (o). Sb(1) – O(1), 1.962(3), Sb(1) – O(2), 2.228(3), Sb(1) – C(1), 2.123(4), Sb(1) – C(7), 2.105(4), Sb(1) – C(15), 2.112(4); C(1) – Sb(1) – C(15), 100.5(17), C(1) – Sb(1) – C(7), 101.0(17), C(7) – Sb(1) – O(1), 129.9(14), O(1) – Sb(1) – O(2), 76.71(11). Disorder of the aryl groups has been modelled over two positions.*

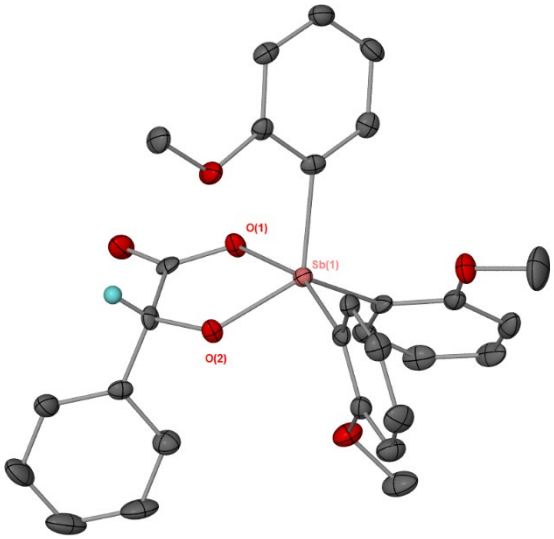

*Figure 2.1.11. Solid-state structure of [Sb($C_6H_4(OCH_3)$)$_3O_2CCH(C_6H_5)O$], **4Sr**. Thermal ellipsoids at 50% probability. Hydrogen atoms have been omitted for clarity. Selected bonds lengths (Å) and angles (o). Sb(1) – O(1), 1.956(3), Sb(1) – O(2), 2.162(3), Sb(1) – C(1), 2.118(5), Sb(1) – C(7), 2.103(4), Sb(1) – C(15), 2.100(5); C(1) – Sb(1) – C(15), 101.5(2), C(1) – Sb(1) – C(7), 108.1(2), C(7) – Sb(1) – O(1), 124.9(18), O(1) – Sb(1) – O(2), 77.00(14).*

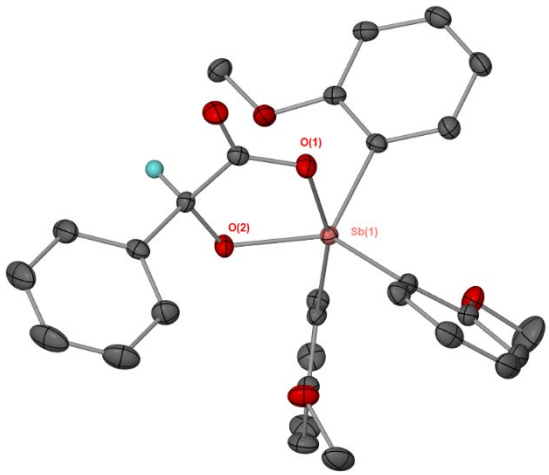

*Figure 2.1.12. Solid-state structure of [Sb($C_6H_4(OCH_3)$)$_3O_2CCH(C_6H_5)O$], **4Ss**. Thermal ellipsoids at 50% probability. Hydrogen atoms have been omitted for clarity. Selected bonds lengths (Å) and angles (o). Sb(1) – O(1), 1.961(12), Sb(1) – O(2), 2.165(13), Sb(1) – C(1), 2.108(18), Sb(1) – C(7), 2.104(17), Sb(1) – C(15), 2.127(17); C(1) – Sb(1) – C(15), 107.7(7), C(1) – Sb(1) – C(7), 101.5(7), C(7) – Sb(1) – O(1), 124.8(6), O(1) – Sb(1) – O(2), 76.99(5).*

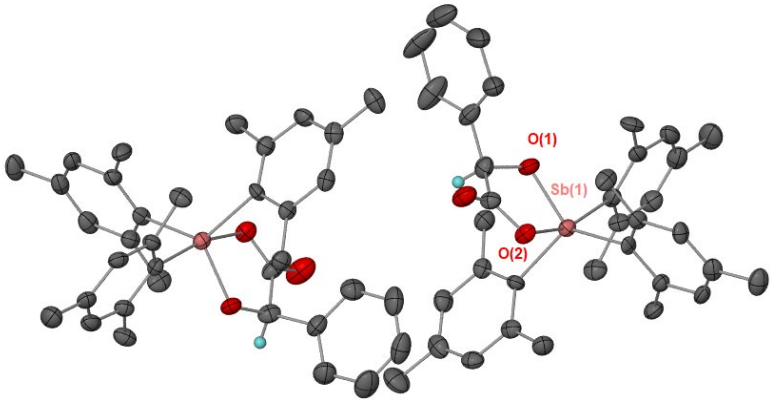

*Figure 2.1.13. Solid-state structure of [Sb($C_6H_2(CH_3)_3$)$_3O_2CCH(C_6H_5)O$], **5Sr**. Thermal ellipsoids at 50% probability. Hydrogen atoms have been omitted for clarity. Selected bonds lengths (Å) and angles (o). Sb(1) – O(1), 1.949(6), Sb(1) – O(2), 2.202(7), Sb(1) – C(1), 2.162(8), Sb(1) – C(7), 2.204(8), Sb(1) – C(15), 2.143(7); C(1) – Sb(1) – C(15), 123.6(3), C(1) – Sb(1) – C(7), 95.60(3), C(7) – Sb(1) – O(1), 121.1(3), O(1) – Sb(1) – O(2), 77.4(3).*

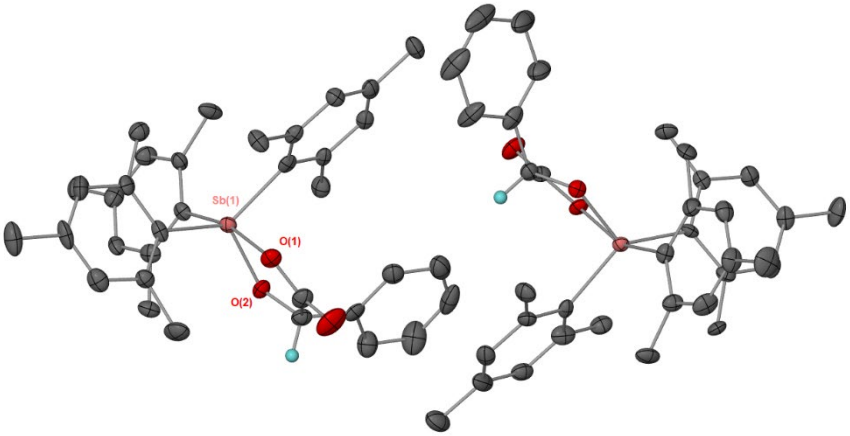

*Figure 2.1.14. Solid-state structure of [Sb($C_6H_2(CH_3)_3)_3O_2CCH(C_6H_5)O$], **5Ss**. Thermal ellipsoids at 50% probability. Hydrogen atoms have been omitted for clarity. Selected bonds lengths (Å) and angles (o). Sb(1) – O(1), 1.953(7), Sb(1) – O(2), 2.200(7), Sb(1) – C(1), 2.127(10), Sb(1) – C(7), 2.144(11), Sb(1) – C(15), 2.144(11); C(1) – Sb(1) – C(15), 112.7(4), C(1) – Sb(1) – C(7), 96.10(4), C(7) – Sb(1) – O(1), 126.2(3), O(1) – Sb(1) – O(2), 77.3(3).*

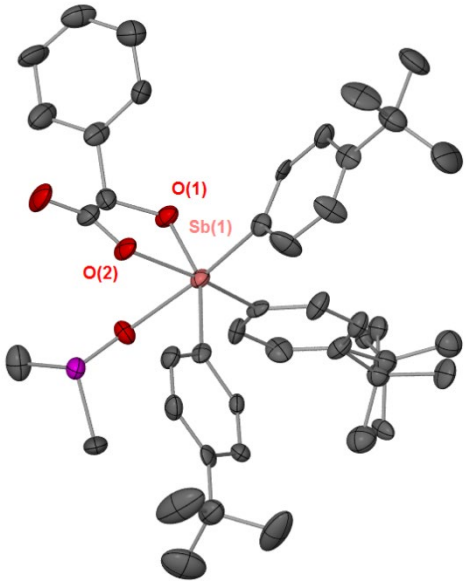

*Figure 2.1.15. Solid-state structure of [Sb($C_6H_4(C(CH_3)_3))_3O_2CCH(C_6H_5)O$], **6Sr**. Thermal ellipsoids at 50% probability. Hydrogen atoms have been omitted for clarity. Selected bonds lengths (Å) and angles (o). Sb(1) – O(1), 2.010(6), Sb(1) – O(2), 2.127(7), Sb(1) – C(1), 2.154(9), Sb(1) – C(7), 2.093(10), Sb(1) – C(15), 2.137(10); C(1) – Sb(1) – C(15), 100.1(4), C(1) – Sb(1) – C(7), 99.60(4), C(7) – Sb(1) – O(1), 91.80(3), O(1) – Sb(1) – O(2), 78.90(3). Disorder of the tert-butyl groups has been modelled over two positions. One of two complex moieties of the asymmetric unit is shown.*

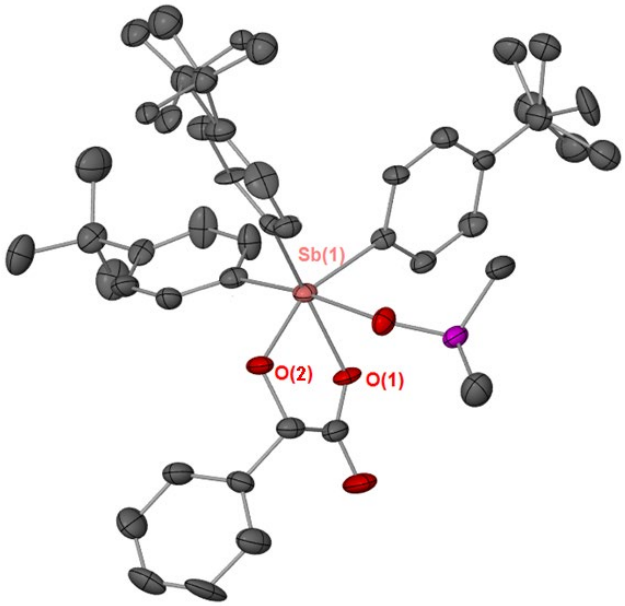

Figure 2.1.16. Solid-state structure of [Sb(C_6H_4(C(CH_3)$_3$))$_3$$O_2$CCH($C_6H_5$)O], ***6Ss****. Thermal ellipsoids at 50% probability. Hydrogen atoms have been omitted for clarity. Selected bonds lengths (Å) and angles (o). Sb(1) – O(1), 2.000(5), Sb(1) – O(2), 2.106(5), Sb(1) – C(1), 2.152(7), Sb(1) – C(7), 2.152(8), Sb(1) – C(15), 2.147(7); C(1) – Sb(1) – C(15), 100.5(3), C(1) – Sb(1) – C(7), 100.4(3), C(7) – Sb(1) – O(1), 93.40(3), O(1) – Sb(1) – O(2), 79.70(2). Disorder of the tert-butyl groups has been modelled over two positions. One of two complex moieties of the asymmetric unit is shown.*

Complexes **1Ss** and **1Sr** (figure 2.4.17 and 2.4.18) are analogous, with the only difference being the chirality of the mandelic acid. Hydrogen atoms have been included on the structure to demonstrate the different enantiomers.

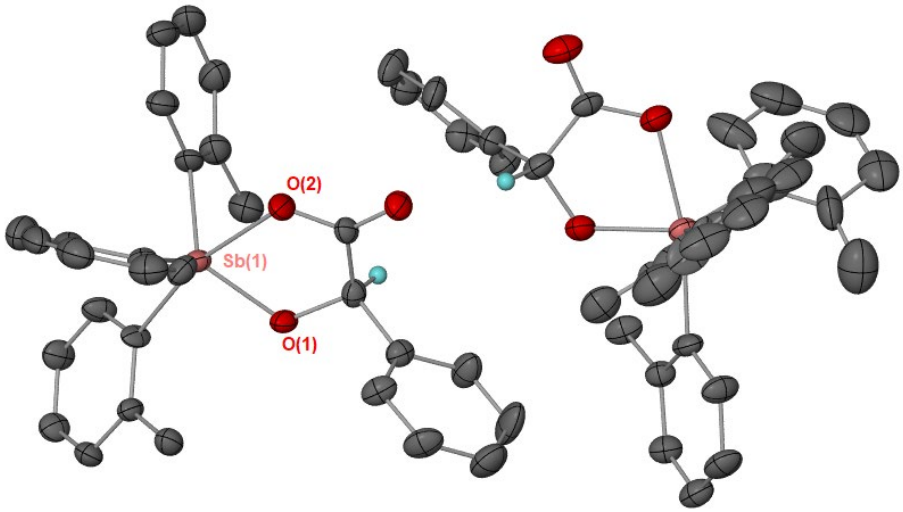

*Figure 2.1.17. Solid-state structure of [Sb(C$_6$H$_4$(CH$_3$))$_3$O$_2$CCH(C$_6$H$_5$)O], **1Sr**. Thermal ellipsoids at 50% probability. Hydrogen atoms have been omitted for clarity. Selected bonds lengths (Å) and angles (o). Sb(1) – O(1), 1.972(6), Sb(1) – O(2), 2.150(6), Sb(1) – C(1), 2.146(7), Sb(1) – C(7), 2.119(7), Sb(1) – C(15), 2.125(8); C(1) – Sb(1) – C(15), 105.5(3), C(1) – Sb(1) – C(7), 103.1(4), C(7) – Sb(1) – O(1), 123.2(3), O(1) – Sb(1) – O(2), 76.70(2).*

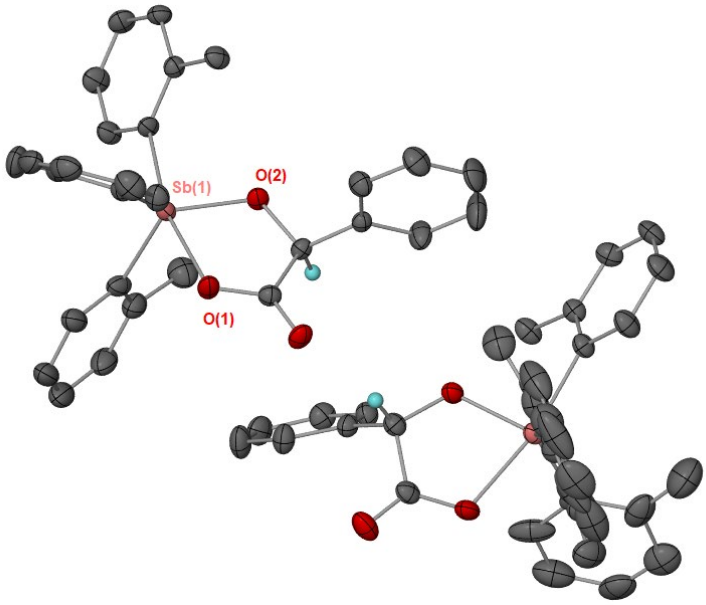

*Figure 2.1.18. Solid-state structure of [Sb(C$_6$H$_4$(CH$_3$))$_3$O$_2$CCH(C$_6$H$_5$)O], **1Ss**. Thermal ellipsoids at 50% probability. Hydrogen atoms have been omitted for clarity. Selected bonds lengths (Å) and angles (o). Sb(1) – O(1), 1.968(2), Sb(1) – O(2), 2.141(3), Sb(1) – C(1), 2.141(3), Sb(1) – C(7), 2.111(4), Sb(1) – C(15), 2.128(3); C(1) – Sb(1) – C(15), 105.5(14), C(1) – Sb(1) – C(7), 103.6(14), C(7) – Sb(1) – O(1), 123.1(12), O(1) – Sb(1) – O(2), 77.17(10).*

All complexes, except the *m*-tolyl and *p*-tertbutyl phenyl complexes, are five-coordinate in regards to the Sb(V) centre. Similar to previously synthesised aryl Sb(V) complexes, the equatorial

positions of the coordination sphere are occupied by the aryl groups, aligning in a propeller like orientation.[33, 34, 39-41] The mandelate oxygens occupy the two remaining axial positions of the trigonal bipyramids. Both **1Ss** and **1Sr** adopt this same trigonal bipyramidal configuration. This is a common geometrical preference for the antimony complexes. In terms of the cyclometallation, there is very little in the way of solid-state structures within the literature, with only two five-coordinate doubly deprotonated triaryl antimony complexes identified on the Cambridge Structural Database (accessed august 2019).[42, 43] One such cyclometallated product has been previously identified by X-ray crystallography by Barucki *et al*, with their α-hydroxy acid complex [$SbPh_3(O_2CC(O)CH_3(CH_2CH_3O)$]. The complex was found to be analogous in binding mode to **1Ss/Sr**, as five coordinate with covalent binding through both the carboxylate hydroxyl and the α-hydroxyl.[42] The Sb – C average bond length of 2.121 Å was observed to be similar to that of **1Ss** and **1Sr**, with average Sb – C lengths of 2.127 A and 2.130 Å respectively. The binding mode of the oxygens can be identified as covalent with average bond lengths of 1.968(2) Å, 2.141(3) Å, 1.972(6) Å and 2.150(6) Å for Sb(1) – O(1) and Sb(1) – O(2) for both **1Ss** and **1Sr** respectively. These lengths are similar to those observed by Coles *et al* with their unusual pinanediol complex [$SbPh_3(C_{10}H_{18}O_2)$], which had bond lengths of 2.008(2) Å and 1.989(2) Å for Sb(1) – O(1) and Sb(1) – O(2) respectively.[43] Widening of the trigonal angle for the complexes was observed from the ideal 120 °, as seen from the C(1) – Sb(1) – C(15), C(8) – Sb(1) – C(15) and C(1) – Sb(1) – C(8) angles of 103.1 °, 111.7 ° and 105.5 °, for **1Sr**, and 103.6 °, 111.8 ° and 105.5 ° for **1Ss**, respectively. These were observed to average as 106.7 ° and 107.0 °, exhibiting very little difference between the two, as was expected with analogous ligands with only a minute change in the position of one proton. Distortion along the trigonal angle was also observed for the two cyclometallate complexes synthesised by Barucki *et al* and Coles *et al*, with an average trigonal angle of 111.9 ° and 100.8 ° respectively.[42, 43]

Table 2.4.2. Crystallographic data of triaryl Sb(V) R-mandelates

	1Sr	2Sr	4Sr	5Sr	6Sr
Chemical formula	$2(C_{29}H_{27}O_3Sb)$	$C_{58}H_{53}O_6Sb_2$	$C_{29}H_{27}O_6Sb$	$2(C_{35}H_{39}O_3Sb)$	$2(C_{40}H_{51}O_4SSb)$
M_r	1091.52	1088.49	593.25	1258.82	1499.23
Crystal system, space group	Orthorhombic, $P2_12_12_1$	Tetragonal, $P4_3$	Orthorhombic, $P2_12_12_1$	Monoclinic, $P2_1$	Triclinic, $P1$
Temperature (K)	123	123	296	123	296
a, b, c (Å)	10.7025 (1), 11.2182 (1), 40.6305 (5)	10.3478 (2), 44.3125 (12)	8.9081 (2), 15.0477 (4), 19.4610 (5)	16.7298 (3), 10.6454 (2), 17.1552 (3)	11.8815 (5), 12.2367 (5), 14.7749 (6)
V (Å^3)	4878.21 (9)	4744.8 (2)	2608.68 (11)	3003.03 (10)	2037.91 (15)
Z	4	4	4	2	1
T_{min}, T_{max}	0.219, 1.000	0.837, 1.000	0.704, 0.746	0.611, 1.000	0.691, 0.745
R_{int}	0.097	0.070	0.100	0.121	0.049
$(\sin \theta/\lambda)_{max}$ (Å^{-1})	0.634	0.722	0.625	0.610	0.625
$R[F^2 > 2\sigma(F^2)]$, $wR(F^2)$, S	0.049, 0.122, 1.05	0.039, 0.071, 1.02	0.034, 0.060, 1.07	0.052, 0.139, 1.10	0.039, 0.086, 1.04
No. of reflections	10159	11655	5325	11383	16575
No. of parameters	663	611	328	721	954

Table 2.4.3. Crystallographic data of triaryl Sb(V) S-mandelates

	1Ss	**2Ss**	**4Ss**	**5Ss**	**6Ss**
Chemical formula	$2(C_{29}H_{27}O_3Sb)$	$C_{58}H_{54}O_6Sb_2$	$C_{29}H_{27}O_6Sb$	$2(C_{35}H_{39}O_3Sb)$	$C_{40}H_{51}O_4SSb \cdot C_{40}H_{50}O_4SSb$
M_r	1090.51	1090.51	594.26	1262.81	1499.23
Crystal system, space group	Orthorhombic, $P2_12_12_1$	Tetragonal, $P4_1$	Orthorhombic, $P2_12_12_1$	Monoclinic, $P2_1$	Triclinic, $P1$
Temperature (K)	123	123	123	123	123
a, b, c (Å)	10.6912 (2), 11.2340 (2), 40.5757 (7)	10.3411 (1), 44.2900 (9)	8.9216 (1), 15.0712 (1), 19.4861 (2)	16.7163 (6), 10.6351 (3), 17.1243 (6)	11.9041 (2), 12.2908 (2), 14.8301 (2)
V (Å^3)	4873.34 (15)	4736.30 (13)	2620.09 (4)	2993.27 (17)	2057.12 (6)
Z	4	4	4	2	1
T_{min}, T_{max}	0.553, 1.000	0.534, 1.000	0.483, 1.000	0.610, 1.000	0.845, 1.000
R_{int}	0.042	0.050	0.048	0.137	0.065
$(\sin \theta/\lambda)_{max}$ (Å^{-1})	0.774	0.717	0.777	0.617	0.721
$R[F^2 > 2\sigma(F^2)]$, $wR(F^2)$, S	0.035, 0.069, 1.01	0.029, 0.064, 0.99	0.020, 0.043, 1.01	0.061, 0.155, 1.01	0.036, 0.077, 1.01
No. of reflections	16097	11987	9563	11768	19663
No. of parameters	648	719	328	721	1035

2.4.3 Biological activity

2.4.3.1 Leishmania promastigote and fibroblast assay

All complexes **1Sr/s,** [Sb(*o*-tol)$_3$O$_2$CCH(C$_6$H$_5$)O], **2Sr/s,** [Sb(*m*-tol)$_3$O$_2$CCH(C$_6$H$_5$)O], **3Sr'/s',** [Sb(*p*-tol)$_3$O$_2$CCH(C$_6$H$_5$)O], **4Sr/s,** [Sb(*o*-phOMe)$_3$O$_2$CCH(C$_6$H$_5$)O], **5Sr/s,** [Sb(mes)$_3$O$_2$CCH(C$_6$H$_5$)O] and **6Sr/s,** [Sb(*p*-tBuPh)$_3$O$_2$CCH(C$_6$H$_5$)O], were dissolved into DMSO to make stocks of 10 mM. At this concentration, all complexes were readily soluble with no signs of precipitation. Complexes also exhibited solubility in the biological media M199 and DMEM at the concentration of 100 µM. Due to the cyclometalltion of complexes **3Sr/s** in DMSO, the active species examined would be the complexes **3Sr'/s'**.

Initial mammalian cell testing on human fibroblasts yielded varying results. A range of IC_{50} values of 2.07 – $\geq$ 100 µM was observed for the *R*-enantiomer complexes, **1Sr** – **6Sr** and a range of 2.90 – 93 µM for the analogous *S*-enantiomer complexes (figures 2.4.19 and 2.4.20). The toxicity varied dramatically for each class of aryl group but was within error for both *R* and *S* analogues. The most toxic of these were found to be the *p*-tertiary-butylphenyl complexes **6Sr** and **6Ss**, [Sb(*p*-tBuPh)$_3$O$_2$CCH(C$_6$H$_5$)O], with IC_{50} values of 2.07 µM and 2.90 µM respectively. The mesityl complexes, **5Ss** and **5Sr** followed close behind with IC_{50} values of 6.04 µM and 5.02 µM respectively. The least toxic of these were observed to be the *o*-methoxyphenyl complexes, **4Ss** and **4Sr**, [Sb(*o*-PhOme)$_3$O$_2$CH(C$_6$H$_5$)O], which exhibited little to no activity (93 µM and $\geq$ 100 µM respectively). All complexes were tested against the drug control amphotericin B. A DMSO control was unnecessary as it had been proven multiple times prior that DMSO has no effect on either fibroblasts or *L. major* promastigotes.[34, 39]

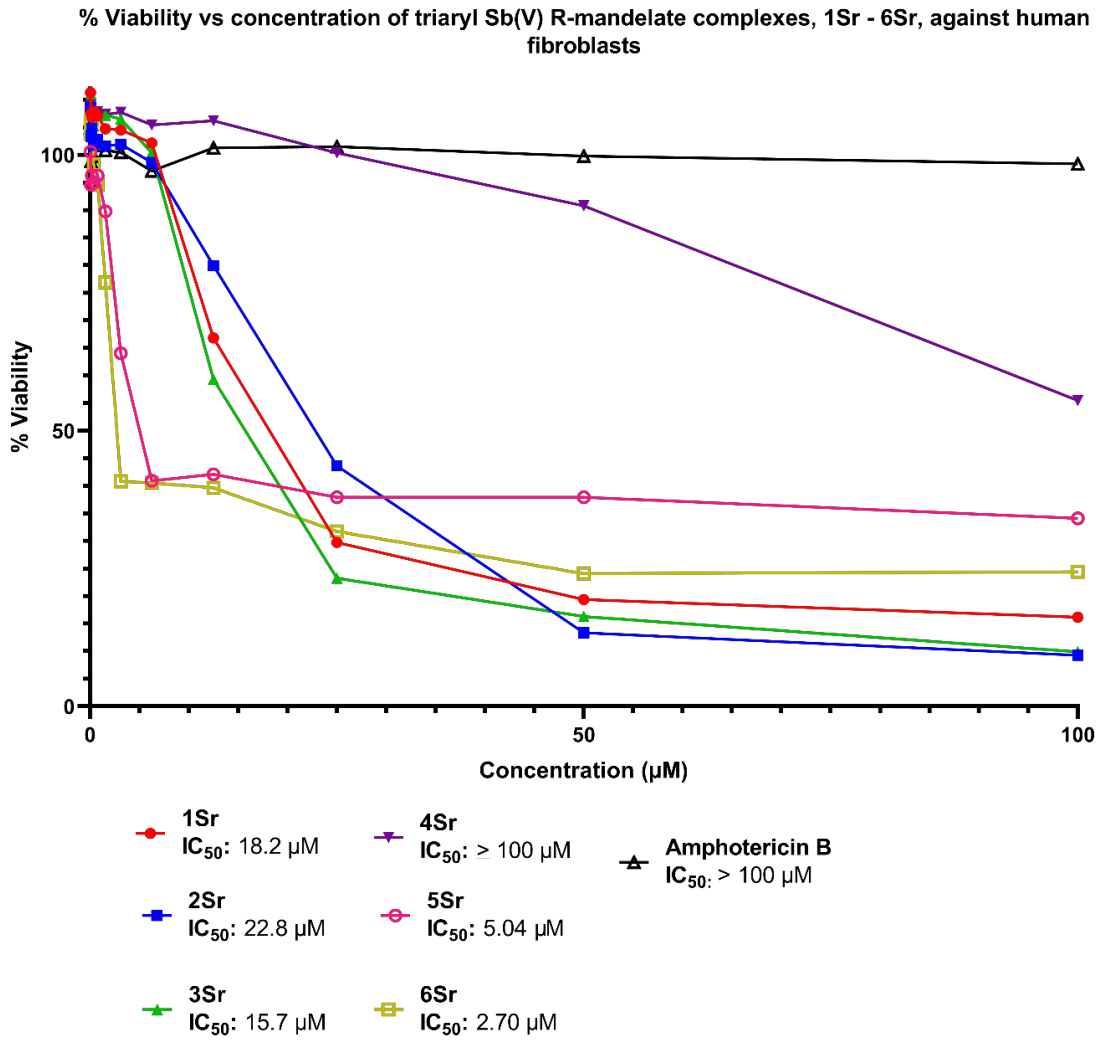

*Figure 2.4.19. Comparison of percentage cell viability after treatment with the Sb(V) complexes **1Sr – 6Sr,** against human fibroblasts. Dose response curves were generated over a range of concentrations (48 nM – 100 μM in the appropriate culture media from 10mM DMSO stock solutions. All readings were compared spectroscopically to non-treated control and the percent growth inhibition calculated.*

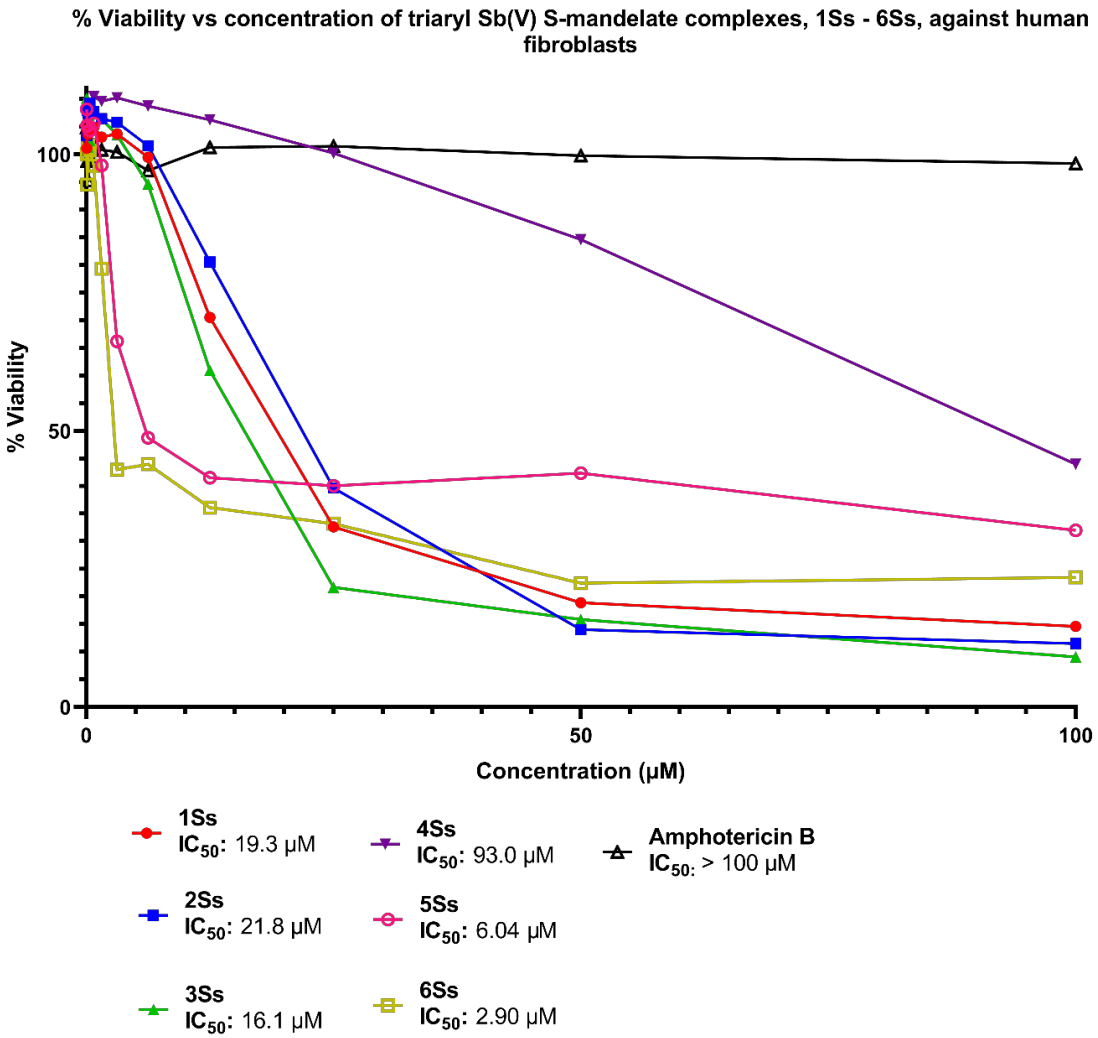

Figure 2.4.20. Comparison of percentage cell viability after treatment with the Sb(V) complexes ***1Ss – 6Ss,*** *against human fibroblasts. Dose response curves were generated over a range of concentrations (48 nM – 100 μM in the appropriate culture media from 10mM DMSO stock solutions. All readings were compared spectroscopically to non-treated control and the percent growth inhibition calculated.*

Despite this varied degree of mammalian cytotoxicity, all complexes still proceeded to the initial anti-promastigote assay to gauge the anti-Leishmanial capability. Surprisingly, complexes **4Ss** and **4Sr** exhibited no apparent anti-Leishmanial activity, with IC_{50} values $\geq$ 100 μM. The *o*-tolyl complexes **1Ss** and **1Sr,** $[Sb(o\text{-tol})_3O_2CCH(C_6H_5)O]$, also lacked a good degree of potency, with

values of 14.6 µM and 15.7 µM respectively. The *p*-tolyl complexes **3Ss'** and **3Sr'**, [Sb(*p*-tol)$_3$O$_2$CCH(C$_6$H$_5$)O], along with the *m*-tolyl complexes **2Ss** and **2Sr**, [Sb(*m*-tol)$_3$O$_2$CCH(C$_6$H$_5$)O], performed better, with IC_{50} values of 2.65 µM, 5.04 µM, 4.56 µM and 4.29 µM respectively. Despite presenting as the most cytotoxic complexes, the *p*-tertiary-butylphenyl and mesityl complexes **5Ss**, **5Sr, 6Ss** and **6Sr**, were extremely potent anti-promastigote complexes, with a 50% reduction of the parasites in the significantly lower ranges of 0.21 – 0.60 µM (figures 2.4.21 and figure 2.4.22).

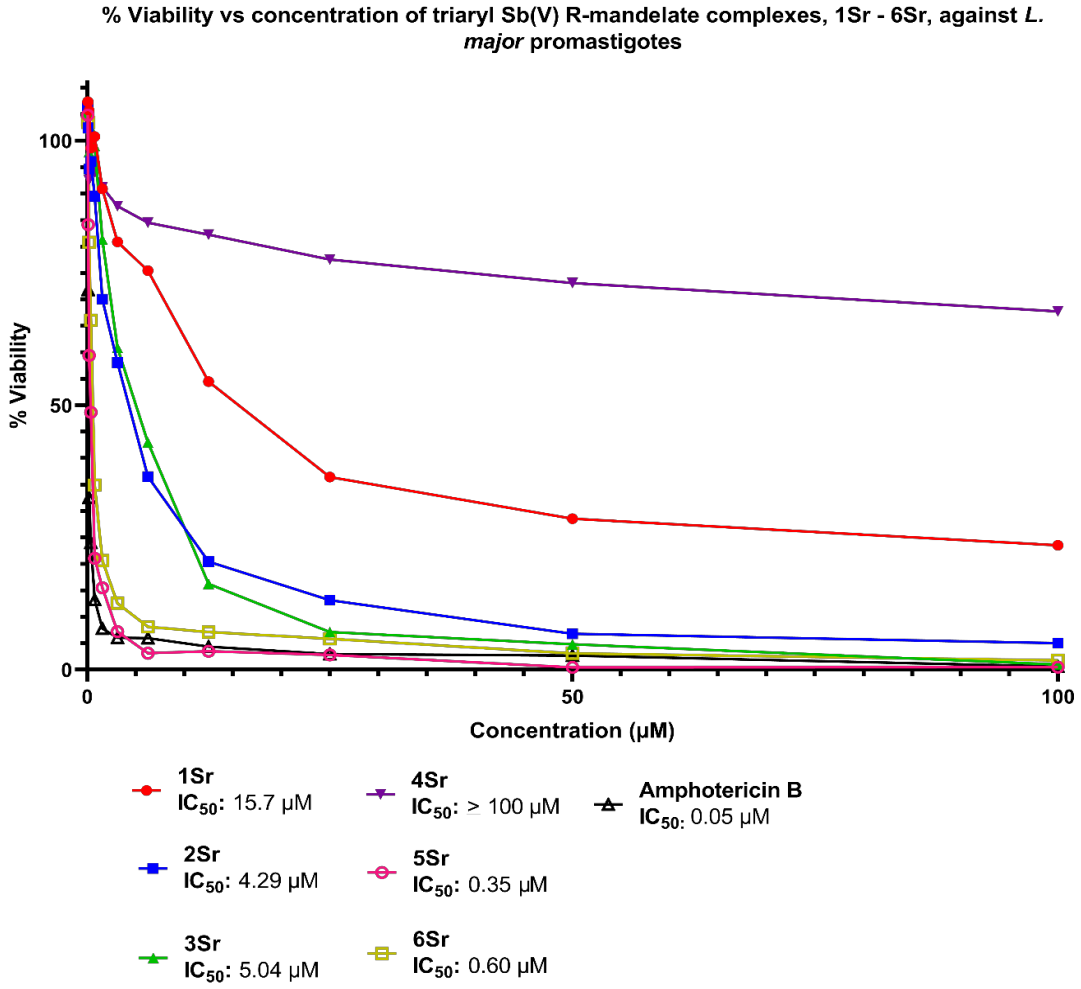

*Figure 2.4.21. Comparison of percentage cell viability after treatment with the Sb(V) complexes **1Sr – 6Sr,** against L. major promastigotes. Dose response curves were generated over a range of concentrations (48 nM – 100 µM in the appropriate culture media from 10mM DMSO stock solutions. All readings were compared spectroscopically to non-treated control and the percent growth inhibition calculated.*

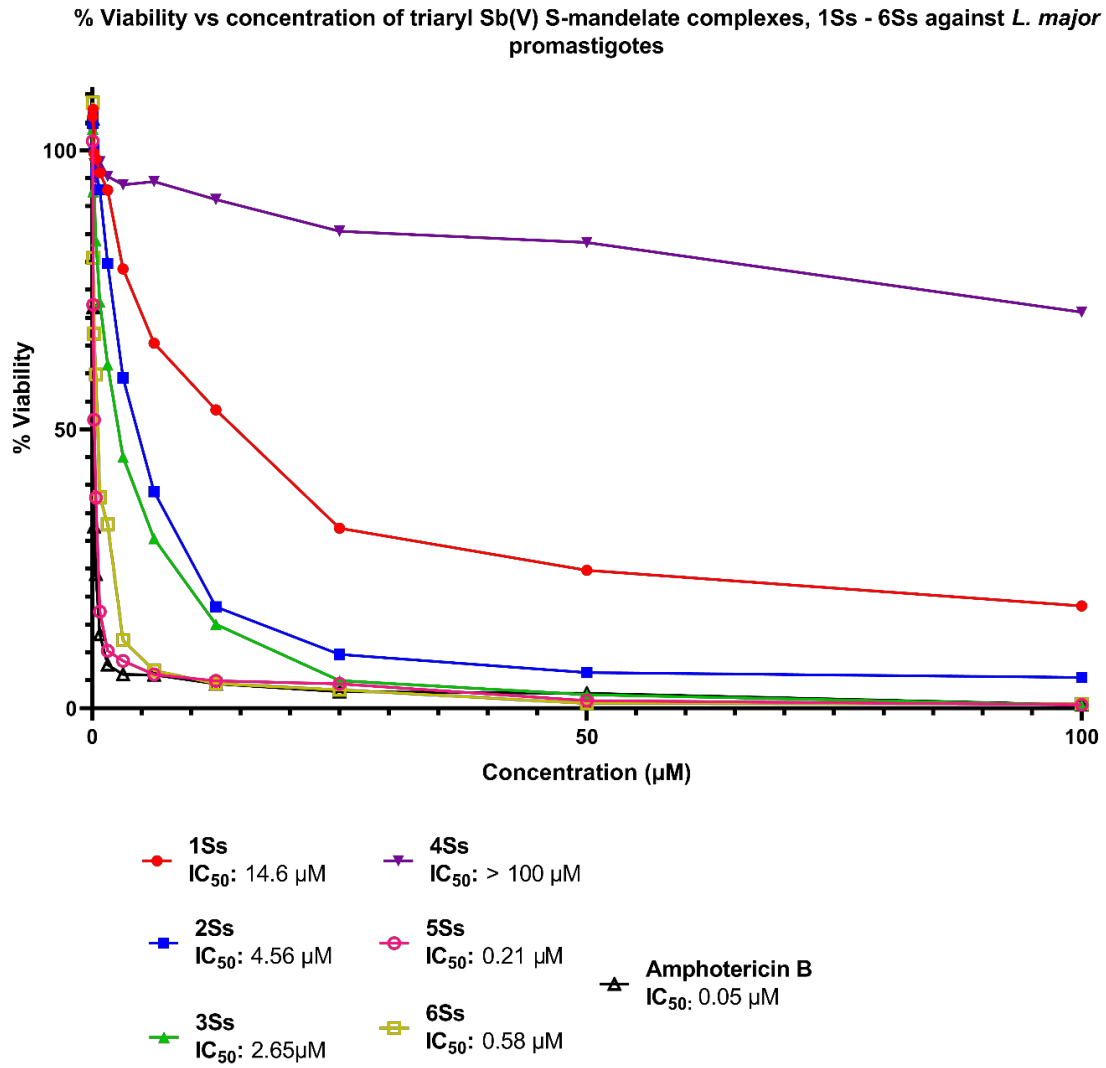

*Figure 2.4.22. Comparison of percentage cell viability after treatment with the Sb(V) complexes **1Ss – 6Ss,** against L. major promastigotes. Dose response curves were generated over a range of concentrations (48 nM – 100 μM in the appropriate culture media from 10mM DMSO stock solutions. All readings were compared spectroscopically to non-treated control and the percent growth inhibition calculated.*

All IC_{50} values for both fibroblasts and promastigote have been given, along with the selectivities indices below in tables 2.4.4 and 2.4.5.

*Table 2.4.4. Selectivity indices of complexes **1Sr – 6Sr**. Indices calculated based on IC_{50}(mammalian)/IC_{50}(parasite). Red denotes no selectivity, yellow = limited and green = good.*

Complex	**1Sr**	**2Sr**	**3Sr'**	**4Sr**	**5Sr**	**6Sr**
IC_{50}(fibroblasts) µM	16.2	22.8	15.7	$\geq$ 100	5.01	2.07
IC_{50}(promastigote) µM	15.7	4.29	5.04	$\geq$ 100	0.33	0.60
Selectivity index	1.03	5.31	3.16	-	15.2	3.45

*Table 2.4.5. Selectivity indices of complexes **1Ss – 6Ss**. Indices calculated based on IC_{50}(mammalian)/IC_{50}(parasite). Red denotes no selectivity, yellow = limited and green = good*

Complex	**1Ss**	**2Ss**	**3Ss'**	**4Ss**	**5Ss**	**6Ss**
IC_{50}(fibroblasts) µM	19.3	21.8	16.1	93	6.04	2.90
IC_{50}(promastigote) µM	14.6	4.56	2.65	$\geq$ 100	0.21	0.58
Selectivity index	1.32	4.78	6.08	-	28.8	5.00

Unfortunately, no real trend was able to drawn from the data obtained. However, the *ortho* substitution on the phenyl did tend to lead to a less active complex. The *o*-tolyl complexes **1Ss** and **1Sr** exhibited little selectivity, with fairly similar IC_{50} values for both fibroblasts and *L. major* promastigotes (indices: 1.32, 1.03). The *o*-methoxyphenyl complexes **4Ss** and **4Sr** proved worse, with little to no activity against either cell line. Conversely, the *m*-substituted tolyl complexes **2Ss** and **2Sr** proved to exhibit a good degree of selectivity and were less toxic to the fibroblasts than the *o*-substituted **1Ss** and **1Sr**, with selectivities of 4.78 and 5.31 respectively. Complexes **3Sr'/s'**, the *p*-tolyl complexes were exhibited to be the most selective of the tolyl series (for the S enantiomer). A trend of *p* > *m* > *o* was observed. Perhaps the positioning of the methyl group on the ring has a profound electronic effect on the complex and therefore biological effect. Both **6Ss**

and **6Sr** were very potent, perhaps alluding to the *para* position having a more profound effect on cytotoxicity. The mesitylene complexes were found to exhibit the greatest selectivity (**5Ss**: 28.8, **5Sr**: 15.2) which could be partially linked to the increased sterics of the mesityl ring when compared to the remaining aryls **1 – 4** and **6.** However, this structure activity relationship is still speculative in nature. It would seem that the averaged selectivity of the complexes seems to exist in the following trend: mes $\geq$ tBuPh $\geq$ *m*-Tol $\geq$ *p*-tol $\geq$ *o*-Tol $\geq$ *o*-OMePh. No real trend was observed for the difference in chirality, with all complexes exhibiting similar cytotoxicity and parasite toxicity values for either *R* or *S*. For the amastigote invasion assay, only the complexes that exhibited a selectivity index of 3 or higher were selected for the assay, disqualifying complexes **1Ss, 1Sr**, **4Ss** and **4Sr** from further biological assessment. Complexes **2Ss** and **2Sr**, [Sb(*m*-tol)$_3$O$_2$CCH(C$_6$H$_5$)O], **3Ss'** and **3S'r,** [Sb(*p*-tol)$_3$O$_2$CCH(C$_6$H$_5$)O], were all tested at the standard 10 μM employed in sections 2.1, 2.2 and 2.3, whereas, due to their increased cytotoxicity, complexes **5Ss** and **5Sr**, [(Sb(mes)$_3$O$_2$CCH(C$_6$H$_5$)O)], **6Ss** and **6Sr,** [(Sb(*p*-tBuPh)$_3$O$_2$CCH(C$_6$H$_5$)O)], were all tested at half that concentration (5 μM).

2.4.3.2 Amastigote invasion assay

J774 macrophages were plated onto glass slides in a 24 well plate, and the assay performed as described in previous sections and in more detail in the experimental section 4.3.5. After drug inoculation for 48 hours, the slides were washed with PBS, fixed with methanol and stained. Cells were counted per duplicate slide, with the number of infected versus non-infected cells analysed. All complexes exhibited excellent anti-amastigote activity, with percentage infection values in the ranges of 0.75 – 3.00 % for those tested at 10 μM and 0.25 – 2.50 % for the remaining 5 μM complexes (figures 2.4.22 and 2.4.23).

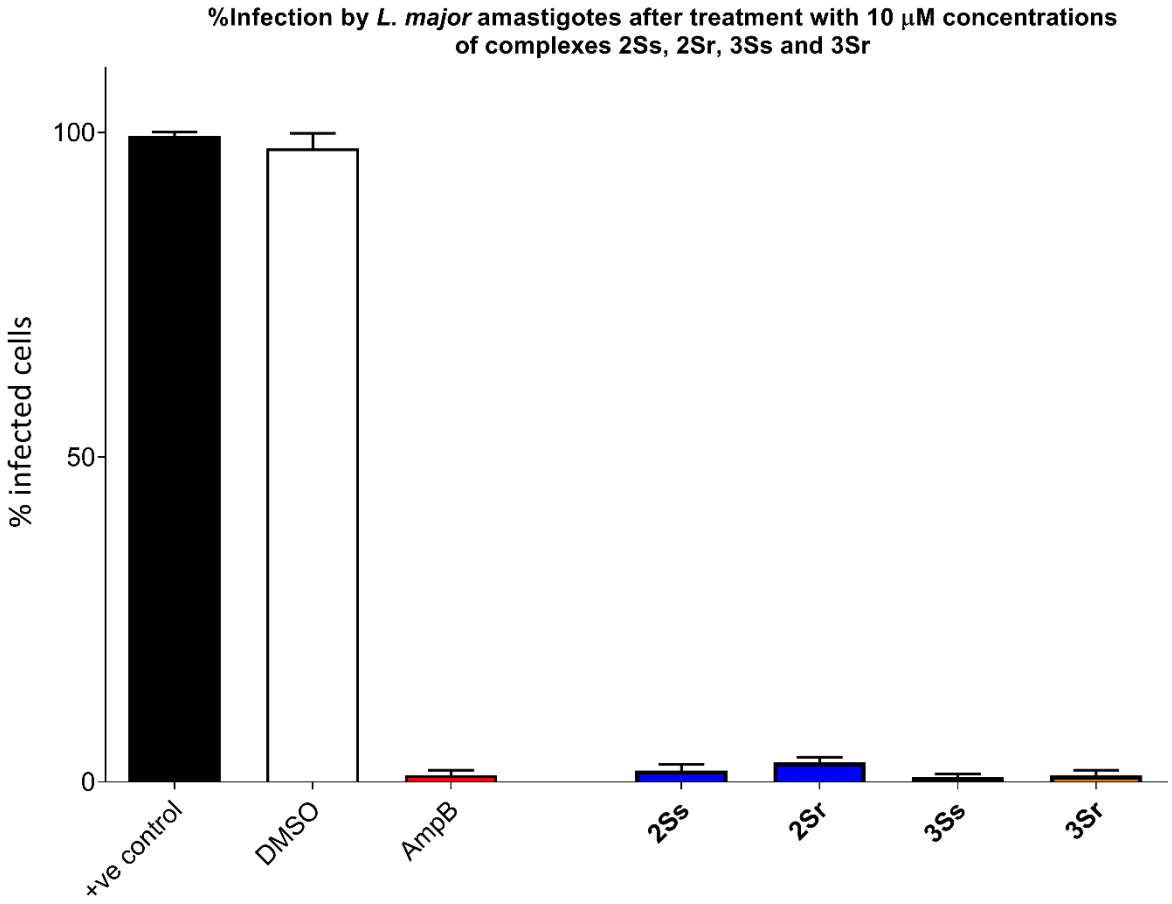

*Figure 2.4.22. Infected macrophages after treatment of complexes **2Ss, 2Sr**, **3Ss** and **2Sr**, after 48 hours. Number of infected macrophages was determined microscopically, in duplicate of fixed specimens. Amphotericin B (AmpB) was used as a positive control at 10 μM concentration. A DMSO control was also employed at a 1% concentration. Error bas indicate SEM, one-way ANOVA. Dunnett's multiple comparison test was used to determine the statistical significance between all test compounds and a positive control lacking treatment (+ve control)*

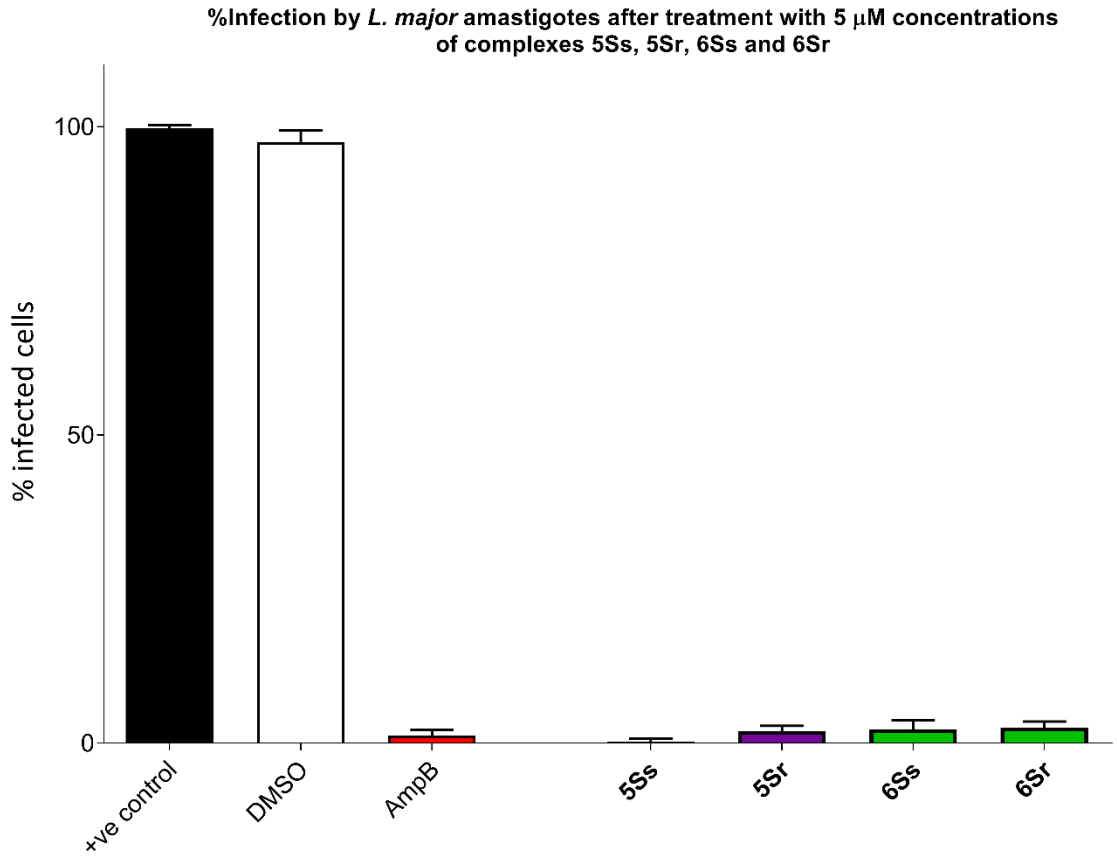

*Figure 2.4.23. Infected macrophages after treatment of complexes **5Ss, 5Sr**, **6Ss** and **6Sr**, after 48 hours. Number of infected macrophages was determined microscopically, in duplicate of fixed specimens. Amphotericin B (AmpB) was used as a positive control at 5 μM concentration. A DMSO control was also employed at a 1% concentration. Error bas indicate SEM, one-way ANOVA. Dunnett's multiple comparison test was used to determine the statistical significance between all test compounds and a positive control lacking treatment (+ve control)*

Although excellent activity was observed for all complexes, it did not come without consequences. For complexes **2Ss** and **2Sr**, [Sb(*m*-tol)$_3$O$_2$CCH(C$_6$H$_5$)O], **3Ss'** and **3Sr',** [Sb(*p*-tol)$_3$O$_2$CCH(C$_6$H$_5$)O], **5Ss** and **5Sr**, [(Sb(mes)$_3$O$_2$CCH(C$_6$H$_5$)O)], a high degree of macrophage stress was visually observed. Cell density was low in several of the aforementioned. For the mesityl complexes **5Ss** and **5Sr**, it is quite possible that the infection was completely eradicated, however it could not be ultimately

confirmed with the cellular stress observed. It may be possible to test the complexes at a less damaging concentration, such as 1 µM and still retain a good degree of anti-amastigote activity. All values can be found below in table 2.4.6.

*Table 2.4.6. Percentage infection values for complexes **2Ss, 2Sr, 3Ss, 3Sr, 6Ss, 6Sr, 7Ss** and **7Sr**. All values are calculated by comparison to a positive control of untreated infected cells.*

Complex	**2Ss**	**2Sr**	**3Ss**	**3Sr**	**5Ss**	**5Sr**	**6Ss**	**6Sr**
% infection	1.75 ± 0.56	3.00 ± 0.50	0.75 ± 0.83	1.00 ± 0.50	0.25 ± 0.35	2.00 ± 0.48	2.25 ± 0.79	2.50 ± 0.56

All complexes were shown to completely outclass the simpler phenyl substituted Sb(V) mandelates of our previous studies, confirming that changing the aryl group has a significant effect on the biological activity of the complex.[34] The trend obtained from the anti-amastigote assay found the mesityl complexes the most effective and the *m*-tolyl complexes the least, going from: mes > *p*-tol > *p*-tBuPh = *m*-tol (based on the average between *R* and *S*).

Chirality in biological systems has often proven to be an important factor to whether a complex is selective. The greatest example of this is the morning sickness drug thalidomide. Despite the *R*-enantiomer of this organic compound being an extremely effective sedative, the *S*-enantiomer is a potent teratogen. Unfortunately with thalidomide in particular, interconversion between R and S occurs, prohibiting fine chiral control of the drug.[44] Commercial ibuprofen is another great example of the racemisation effects of chiral drugs. The *S*-enantiomer is the bioactive form, inhibiting cyclooxygenase (COX) at clinically relevant concentrations, with the *R*-enantiomer at the same concentration producing no inhibitory effects. Similar to thalidomide, ibuprofen can undergo interconversion, however this only occurs from *R* to *S* (figure 2.4.24).[45] As both the *R* and *S* mandelates exhibited similar activity, it may be possible that reversible enantiomerisation could occur, as enolisation of the mandelic acid is possible in humans. This process however is

enzymatically catalysed at the acid hydroxyl of the organic acid.[46] Therefore, it is more likely that the mandelate is locked into its pure enantiomeric form *in vitro*, by the strong binding affinity of the Sb(V).[47] Chiral HPLC could be potentially explored as a method for conclusively determining the chirality of the complex in future *in vitro* studies.[48] CD spectroscopy and polarimetry ma also provide insight into the potential racemisation. However, with the limited data obtained, no real answer on the differences of chirality was concluded.

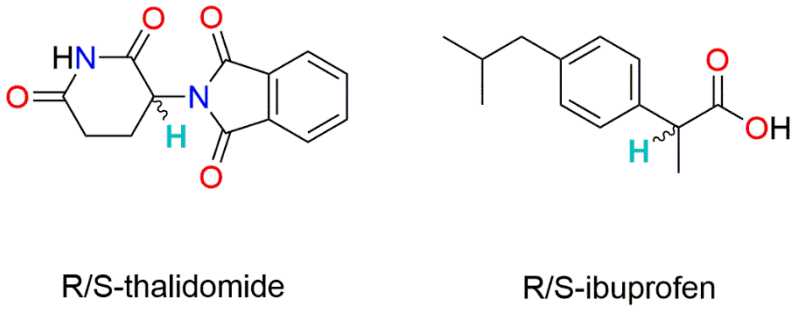

Figure 2.4.24. R/S-thalidomide and R/S-Ibuprofen. The chiral centre has been denoted by the addition of the hydrogen atom.

2.4.8 Conclusions

As an extension into previous research on α-hydroxy acid complexes of antimony and bismuth, a library of Sb(V) aryl *R/S*-mandelates that incorporated differing aryl groups were synthesised and characterised. The aims to distinguish a structure activity relationship between changing of the aryl group and changing of the chirality were met with a varying degree of successes. Firstly, no discernible trend was obtained from the initial biological analysis in relation to the change in aryl group, nor the differences in chirality. Though chirality can often have major biological affects, in the case of mandelic acid this does not seem to be the case.

The complexes **1Sr** and **1Ss,** [Sb(*o*-tol)$_3$O$_2$CCH(C$_6$H$_5$)O], **2Sr** and **2Ss,** [Sb(*m*-tol)$_3$O$_2$CCH(C$_6$H$_5$)O], **3Sr** and **3Ss,** [(Sb(*p*-tol)$_3$O$_2$CCH(C$_6$H$_5$)OH)$_2$O$_2$], **3Sr'** and **3Ss',** [Sb(*p*-tol)$_3$O$_2$CCH(C$_6$H$_5$)O], **4Sr** and **4Ss,** [Sb(*o*-phOMe)$_3$O$_2$CCH(C$_6$H$_5$)O], **5Sr** and **5Ss,** [Sb(mes)$_3$O$_2$CCH(C$_6$H$_5$)O] and **6Sr** and **6Ss,** [Sb(*p*-

tBuPh)$_3$O$_2$CCH(C$_6$H$_5$)O], were synthesised by an oxidative addition of the triaryl antimony with one equivalent of either *R* or *S* mandelic acid. Complexes were high yielding, ranging from 72 - 86%. All complexes were analysed by FT-IR, ^{1}H NMR, ^{13}C NMR, melting point and elemental analysis. All but the peroxide bridged complexes, **3Ss** and **3Sr** were successfully analysed by X-ray crystallography. Though several crystalline samples of **3Ss** and **3Sr** were grown, repeated measurements of different crystals resulted in poor data. Nevertheless, connectivity was established leading to the clarification of the binding mode of both the mandelate and the peroxide bridge. The complex was observed to undergo cyclometallation in DMSO, liberating H_2O_2.

Complexes **1Sr/s, 4Sr/s, 5Sr/s** and **6Sr/s** were five-coordinate distorted trigonal bipyramids in the solid-state, incorporating one double deprotonated mandelic acid moiety as opposed to the usual *bis*-carboxylato substitution observed in previous research.[34, 39, 40] This cyclometallate has the advantage of being a more thermodynamically stable five-membered chelate through both hydroxyls as a opposed to a four-membered chelate from a covalent and dative carboxylate binding.[49] Complexes **3Ss** and **3Sr** differed from the remaining complexes by incorporation of a peroxido bridge between two antimony centres, the mandelates also bound through the carboxylate hydroxyl only, so no cyclometallation occurred. The mandelate ligands occupy the axial positions of the coordination sphere with the aryl groups in the equatorial plane in a propeller like orientation. The *m*-tolyl complexes incorporated two moieties in the asymmetric unit, with one of these moieties datively interacting with the carbonyl of the other, pushing its coordination number to six, forming a distorted octahedron.

Initial biological studies into the complexes revealed little to no clear trend in terms of both cytotoxicity and anti-Leishmanial activity. Despite a high degree of mammalian cytotoxicity, complexes **5Ss**, **5Sr**, **6Ss** and **6Sr** proved to be extremely potent anti-promastigote complexes, giving them a high degree of selectivity within their cytotoxic ranges. Complexes **2Ss**, **2Sr**, **3Ss'** and

3Sr' were less effective anti-Leishmanials, but did exhibit less toxicity towards the mammalian controls. Complexes **1Ss, 1Sr**, **4Ss** and **4Sr** had limited selectivity and so were disqualified from the amastigote invasion assay. Due to the higher degree of toxicity, complexes **5Ss**, **5Sr**, **6Ss** and **6Sr** were tested at concentrations of 5 μM against *L. major* amastigote infected macrophages, whilst complexes **2Ss**, **2Sr**, **3Ss'** and **3Sr'** were analysed at the conventional 10 μM.

All complexes were found to exhibit excellent activity against the clinically relevant amastigote form. Ranges of 0.75 – 3.00 % for those tested at 10 μM and 0.25 – 2.50 % for the remaining 5 μM complexes were obtained from the amastigote invasion assay. These complexes constitute the best anti-amastigote complexes of all sections, though their mammalian cell toxicity was of some concern. The mesityl complexes **5Ss** and **5Sr** potentially cleared the infection from the cells, however causes a substantial amount of cellular stress on the macrophages. Complexes **2Ss**, **2Sr**, **3Ss'** and **3Sr'** exhibited a similar degree of cellular stress on the mammalian cells despite their lower mammalian cytotoxicity during the fibroblast control assay. Percentage infection of complexes **6Ss** and **6Sr** were found to be conclusively determined due to increased cellular health and density. Though no real clear trend was obtained, position of the functional group on the aryl ring did seem to affect the structure activity relationship, with aryls that included a *para* position functional group often exhibiting a greater degree of biological activity.

When comparing these results to previous research, no solid trend was able to be obtained, with the selectivity of the complexes found to decrease in the following order: mes $\geq$ *p*-tBuPh $\geq$ *m*-Tol $\geq$ *p*-tol $\geq$ *o*-Tol $\geq$ *o*-OMePh.

Though chirality can often lead to drastic changes in biological activity, we have concluded that this is most likely not an effect of the organometallic complexes of antimony. An extension into this may lead to more information on the effects of aryl groups on the antimony, and how

changing the electronics of the ring with the addition of electron withdrawing versus electron donating groups may impact the overall biological activity. Nonetheless, this study has highlighted the effects of changing both chirality and precursor aryl groups and how it affects the structure, reactivity and biological activity of the simple α-hydroxy acid.

2.4.9 References

1. J. W. Walker and V. K. Krieble, *J. Chem. Soc. Trans.*, 1909, **95**, 1369-1377.
2. K. Engström and J. Rantanen, *Int. Arch. Arbeitsmed.*, 1974, **33**, 163-167.
3. M. Ikeda, T. Imamura, M. Hayashi, T. Tabuchi and I. Hara, *Int. Arch. Arbeitsmed.*, 1974, **32**, 93-101.
4. H. Ohtsuji and M. Ikeda, *Occup. Environ. Med.*, 1970, **27**, 150-154.
5. A. Slob, *Occup. Environ. Med.*, 1973, **30**, 390-393.
6. J. Gromiec and J. Piotrowski, *Int. Arch. Occup. Environ. Health*, 1984, **55**, 61-72.
7. T. Nakajima, E. Elovaara, F. J. Gonzalez, H. V. Gelboin, H. Raunio, O. Pelkonen, H. Vainio and T. Aoyama, *Chem. Res. Toxicol.*, 1994, **7**, 891-896.
8. T. Beveridge, *Can. J. Microbiol.*, 1978, **24**, 89-104.
9. F. Tursi, M. Samaia, M. Salmona and G. Belvedere, *Experientia*, 1983, **39**, 593-594.
10. P. O. De Montellano and C. Catalano, *J. Biol. Chem.*, 1985, **260**, 9265-9271.
11. S. J. Sumner and T. R. Fennell, *Crit. Rev. Toxicol.*, 1994, **24**, S11-S33.
12. H. Wieczorek and J. Piotrowski, *Int. Arch. Occup. Environ. Health*, 1988, **61**, 107-113.
13. M. Mohamadyan, M. Moosazadeh, A. Borji, N. Khanjani and S. R. Moghadam, *Environ. Monit. Assess.*, 2019, **191**, 62.
14. P. Putten, *Antonie Leeuwenhoek*, 1979, **45**, 622-623.
15. M. L. Rosenheim, *The Lancet*, 1935, **225**, 1032-1037.
16. D. P. Zangwill, L. P. J. Porter, A. L. Kaitz, R. S. Cotran, P. T. Bodel and E. H. Kass, *JAMA Intern. Med.*, 1962, **110**, 801-817.
17. M. B. Taylor, *Cosmet Dermatol*, 1999, **12**, 26-28.
18. G. Kontochristopoulos and E. Platsidaki, *Clin. Dermatol.*, 2017, **35**, 179-182.
19. M. Motamedifar, A. Bazargani, M. R. Namazi and H. S. E. Sarai, *World Appl Sci J*, 2014, **31**, 925-929.
20. C. D. Stan, A. Ştefanache, G. Tătărîngă, M. Drăgan and C. Tuchiluş, *Farmacia*, 2015, **63**, 577-580.
21. H. Prydderch, A. Haiβ, M. Spulak, B. Quilty, K. Kümmerer, A. Heise and N. Gathergood, *RSC Advances*, 2017, **7**, 2115-2126.
22. P.-Y. Liu, Y.-H. Lin, C. H. Feng and Y.-L. Chen, *Electrophoresis*, 2012, **33**, 3079-3086.
23. H. Thun, F. Verbeek and W. Vanderleen, *J. lnorg. Nucl. Chem.*, 1966, **28**, 1949-1954.
24. F. Pruchnik, B. R. James and P. Kvintovics, *Can. J. Chem.*, 1986, **64**, 936-939.
25. A. Fischinger, A. Sarapu and A. Companion, *Can. J. Chem.*, 1969, **47**, 2629-2637.
26. A. Beghidja, S. Hallynck, R. Welter and P. Rabu, *Eur. J. Inorg. Chem.*, 2005, **2005**, 662-669.
27. A. Cuin and A. C. Massabni, *J. Coord. Chem.*, 2007, **60**, 1933-1940.
28. M. Babij and A. Mondry, *Journal of Rare Earths*, 2011, **29**, 1188-1191.
29. A. Cuin, A. C. Massabni, C. Q. Leite, D. N. Sato, A. Neves, B. Szpoganicz, M. S. Silva and A. J. Bortoluzzi, *J. Inorg. Biochem.*, 2007, **101**, 291-296.
30. T. Zevaco and M. Postel, *Synth. React. Inorg. Met.-Org. Chem.*, 1992, **22**, 289-297.
31. V. Le Boisselier, E. Duñach and M. Postel, *J. Organomet. Chem.*, 1994, **482**, 119-123.
32. S. Sato, *Talanta*, 1985, **32**, 341-344.
33. H. Barucki, S. J. Coles, J. F. Costello and M. B. Hursthouse, *Chem. Eur. J.,* 2003, **9**, 2877-2884.
34. R. N. Duffin, V. L. Blair, L. Kedzierski and P. C. Andrews, *Dalton Trans.*, 2018, **47**, 971-980.
35. W. Reeve, C. M. Erikson and P. F. Aluotto, *Can. J. Chem.*, 1979, **57**, 2747-2754.
36. J. P. Finet, *Chem. Rev.*, 1989, **89**, 1487-1501.
37. R. Kather, T. Svoboda, M. Wehrhahn, E. Rychagova, E. Lork, L. Dostál, S. Ketkov and J. Beckmann, *Chem. Commun.*, 2015, **51**, 5932-5935.
38. G. Ferguson, C. Glidewell, B. Kaitner, D. Lloyd and S. Metcalfe, *Acta. Crystallogr. C.*, 1987, **43**, 824-826.

39. R. N. Duffin, V. L. Blair, L. Kedzierski and P. C. Andrews, *J. Inorg. Biochem.*, 2018. **189**, 151-162.
40. M. I. Ali, M. K. Rauf, A. Badshah, I. Kumar, C. M. Forsyth, P. C. Junk, L. Kedzierski and P. C. Andrews, *Dalton Trans.*, 2013, **42**, 16733-16741.
41. H. Barucki, S. J. Coles, J. F. Costello, T. Gelbrich and M. B. Hursthouse, *J. Chem. Soc. Dalton. Trans*., 2000, 2319-2325.
42. H. Barucki, S. J. Coles, J. F. Costello and M. B. Hursthouse, *J. Organomet. Chem.*, 2001, **622**, 265-273.
43. S. J. Coles, J. F. Costello, M. B. Hursthouse and S. Smith, *J. Organomet. Chem.*, 2002, **662**, 98-104.
44. M. E. Franks, G. R. Macpherson and W. D. Figg, *The Lancet*, 2004, **363**, 1802-1811.
45. A. M. Evans, *Clin. Rheumatol.*, 2001, **20**, 9-14.
46. M. Yevglevskis, C. R. Bowskill, C. C. Y. Chan, J. H. J. Heng, M. D. Threadgill, T. J. Woodman and M. D. Lloyd, *Org. Biomol. Chem.*, 2014, **12**, 6737-6744.
47. H. Sun, *Biological chemistry of arsenic, antimony and* bismuth, Wiley Online Library, 2011.
48. Y. Okamoto and T. Ikai, *Chem. Soc. Rev.*, 2008, **37**, 2593-2608.
49. R. D. Hancock and A. E. Martell, *Comments Inorg. Chem.*, 1988, **6**, 237-284.

3. Conclusions and future work

Leishmaniasis remains a persistent and deadly tropical disease, with the need for further research a given. In chapter 2.1, 17 complexes were synthesised and characterised, of which eight bismuth analogues and five of the nine antimony complexes were novel. The complexes were all able to be structurally elucidated by single-crystal X-ray crystallography to give insight into the binding mode of Bi(V) versus Sb(V). Comparatively, the Sb(V) complexes presented as the more stable and biologically selective class, with the Bi(V) analogues presenting as both unstable in culture media and non-selectively toxic.

Chapter 2.2. aimed to investigate a different class of triaryl organometallic antimonials, by the incorporation of an alcoholic bond as opposed to the conventional carboxylate. All six complexes were structurally elucidated, allowing confirmation as a novel class of *mono*-hydroxido, *mono*quinolinolato complexes. The difference in activity was noted, with these six triphenyl antimony *mono*-hydroxido quinolinolates exhibiting a higher degree of mammalian toxicity than the acetates from 2.1. Despite this, the complexes were selective and so ideal candidates to further *in vitro* analysis. All complexes also yielded promising results as anti-amastigote complexes.

Chapter 2.3. deviated from the usual class of anti-Leishmanial metals, aiming to investigate whether the group 13 metals, gallium and indium, could be utilised as anti-parasitics. Gallium's similarities to iron(III) made it an ideal candidate, as *Leishmania* acquires iron from its intracellular surroundings. Both *bis-methyl* gallium and *bis-methyl* indium *mono-quinolinolate*s, and *mono*-methyl gallium *bis*-quinolinolate complexes were synthesised, incorporating four of the six quinolinols explored in chapter 2.2. Both solid state and solution state stability of these novel complexes was assessed, leading to the conclusion that the indium analogues were unstable in the solution state and therefore unable to be biologically assessed. Solid-state structures were

obtained for all complexes, with several of these structures alluding to the re-arrangement of the indium complexes in the solution state. There were differences in solubility between the *bis-methyl* gallium and *mono*-methyl gallium complexes, with only one of the four *mono*-methyl complexes able to be solubilised in the biological solvent DMSO. The five soluble gallium complexes were tested for both their cytotoxicity and anti-parasitic activity. All complexes were observed to exhibit excellent anti-parasitic activity, while remaining highly selective. The gallium complexes were found to be the most selective of any complexes tested within this study, leading to a potentially whole new area of research for anti-Leishmanial complexes.

Chapter 2.4. Expanded on previous research on the α-hydroxy acid mandelic acid, with a change in both chirality of the mandelic acid and a change in the aryl group of the antimony precursor. Similar to chapters 2.1, 2.2 and 2.3, most of the complexes were able to be structurally elucidated. The complexes of the *p*-tolyl antimony differed from the others, forming a perioxo-bridge complex as opposed to a cyclometallate. For this acid, a change in chirality had little effect on the biological activity, with similar activity noted for both *R* and *S*. Despite a high degree of mammalian toxicity, several of the complexes displayed extremely potent anti-promastigote activity, therefore presenting within an acceptable selectivity range. Their anti-amastigote activity was found to be exceptional despite a high degree of mammalian cytotoxicity.

This study focused on the synthesised of organometallic complexes of the metal's antimony, bismuth, gallium and indium, with a significant emphasis on the classic anti-Leishmanial metal antimony.

One major conclusion drawn from this study is bismuths lack of selectivity in the +V oxidation state, due to a high reductive potential and lack of stability. Though a large emphasis has been placed on bismuth in the literature, it mainly reflects its potential in the +III oxidation state as

opposed to the +V. This study has concluded that the oxidation state plays a heavy role on the stability and reactivity of bismuth, therefore there is little precedent to continue to pursue the +V state. Focus should be placed back onto the +III state, in particular, studies into the metallomics of bismuth's biological mechanism. Antimony however, continues to prove that a toxic perception does not equal a toxic compound, with this study concluding that more research needs to be placed on the biological relevance of Sb(V) complexes in the fight to successfully and sustainably treat Leishmaniasis. Similar to bismuth, more studies into the actual mechanistic pathways of the antimony complexes is imperative.

The alkyl gallium complexes yielded exceptional results, with Ga(III) proving just as effective as the Sb(V) complexes. The group 13 metal has proven to be more selective in the classes examined, with little to no cytotoxicity and a high degree of parasite activity. Though research into antimony complexes should not be neglected, there is room for a new class of metal complexes featuring gallium as the centrepiece.

Future studies should incorporate the synthesis of other classes of alkyl gallium complexes with different *O,O* or *N,O* chelators, and an assessment of their activity. For the antimony complexes, the next natural progression would be to examine the change in aryl group on the best *mono*-hydroxido quinolinolate complexes to determine whether this change would induce greater or lesser biological activity. Lastly a greater understanding of the mechanism of action of these complexes needs to be established. If more was understood about how these complexes interact with the parasite, there would be more information available to fine tune the structural chemistry of these complexes. Overall, this study has highlighted the importance of continued chemical research into neglected tropical diseases and has alluded to the potential to expand the ever-growing library of anti-Leishmanial complexes to main group metal other than the historically used group 15.

4. Experimental Section

4.1 General

All compounds have been named using the nomenclature of organic and metal compounds in agreement with the IUPAC convention. For practical reasons, the appropriate numbering system classified in the schemes of each substance was not used in agreement with the IUPAC convention.

4.2 Instrumentation

Proton nuclear magnetic resonance (^{1}H NMR) spectra were recorded on either a Bruker Avance DRX400 spectrometer (400 MHz) or Bruker Avance DRX600 spectrophotometer (600 MHz). All chemical shifts were referenced to the appropriate deuterated solvent (d_1-chloroform δ = 7.26 ppm and d_6-*bis-methyl*sulfoxide δ = 2.50 ppm). Chemical shifts (δ) were recorded on the parts per million scale (ppm). Signals were reported using the following format: chemical shift (δ ppm) [Integration, multiplicity, coupling constant and assignment]. Multiplicities have been designated as singlet (s), broad singlet (br.s), doublet (d), doublet of doublets (dd), triplet (t) or multiplet (m). Coupling constants, J, are given in Hertz (Hz). Deficiencies of 0.5 Hz for coupling constants and 0.1 ppm for chemical shifts was considered. All reported NMR data was auto generated on the MestreLab Research, MestReNova v.14 software, using the automatic multiplicity tool.[1]

^{13}C NMR spectra were recorded on either a Bruker Avance DRX400 spectrometer (100 MHz), or a Bruker Avance DRX600 spectrometer (600 MHz) referenced to the appropriate deuterated solvent (d_1-chloroform δ = 77.00 ppm and d_6-*bis-methyl*sulfoxide δ = 39.52 ppm). Chemical shifts (δ) were recorded on the parts per million scale (ppm). A deficiency of 0.1 ppm for the chemical shifts was considered. All reported NMR data was auto generated on the MestreLab Research, MestReNova v.14 software, using the automatic multiplicity tool.[1]

Melting points were analysed in open end capillary tubes on a digital Stuart Scientific melting point apparatus SMP10.

Infrared Spectra were recorded on an Agilent Technologies Cary 630 FTIR spectrometer, using a range of 4000 – 500 cm^{-1}, with the frequencies reported in cm^{-1}.

Mass spectrometry (ESI) was obtained by Mr. Scott Blundell, utilising a Micromass Platform QMS spectrometer, with an electrospray source and a cone voltage of 35 eV.

CHNS elemental analysis (EA) was obtained from one of: The Campbell Microanalytical Laboratory, Department of Chemistry, *University of Otago*, Dunedin New Zealand.
School of Human Sciences, Science Centre at *London Metropolitan University*, United Kingdom.
The Department of Chemistry, *Monash University*, Australia.

UV-visible wavelength scan from 300 nm – 700 nm was obtained on an Agilent Cary-60 UV-Visible spectrophotometer to determine the λ_{max} and therefore fluorescence excitation wavelength in toluene. Fluorescence emission spectrum in both the solution state and solid state were obtained using an Agilent Cary Eclipse Fluorimeter. All graphs were produced using Microsoft excel.

Crystallographic data on all appropriate complexes were collected myself on one of the following: Bruker X8 APEXII CCD diffractometer, equipped with an OXFORD Cryosystem 700 Cryostream and cooled to 123(2) K. Data collection occurred using *mono*chromatic (graphite) MoK_{α} radiation (λ = 0.71070 Å) and was processed using the Bruker Apex2 v2014.7-1 software.[2] polarisation, Lorentz and absorption corrections (multi-scan-SADBABS) were applied.[3] OXFORD Gemini Ultra equipped with an OXFORD Cryosystems 700 Cryostream and cooled to 173(2) K. Data was collected with *mono*chromatic (graphite) CuK/α radiation (λ = 0.71073 Å) and processed using the CrysAlisPro v

1.171.34.36 software.[4] OXFORD XtaLAB Synergy, Dualflex, HyPix diffractometer equipped with an OXFORD Cryosystems 700 Cryostream and cooled to 173(2) K. Data was collected with *mono*chromatic (graphite) CuK/α radiation (λ = 0.71073 Å) or MoK_α radiation (λ = 0.71070 Å) and processed using the CrysAlisPro v 1.171.40.49a software.[5] MX1 beamline at the Australian Synchrotron, Melbourne, Victoria, Australia, operating at 17.4 KeV, with λ= 0.7073 Å, using an open flow N_2 cryostream cooled to 100(2) K. The data collection and reduction was obtained using BlueIce[6] and XDS. Each compound was solved and refined using SHELX-97 utilising the graphical interface X-Seed or Olex2.[7, 8] Refinement was achieved by using the full matrix least-squares technique on F^2, which minimises the function given by $(F_o-F_c)^2$, where F_o and F_c are the observed and calculated structure amplitudes respectively, given that the weight is defined as $4F_0^2/2F_o^2$. Unless otherwise indicated, all non-hydrogen atoms were refined with anisotropic thermal parameters. Hydrogen atoms were placed in calculated positions using a riding model with C-H = 0.95 – 0.98 Å and $U_{iso}(H) = xU_{iso}(C)$, x = 1.2 or 1.5 unless otherwise indicated. Dr. Craig M. Forsyth and Dr. Victoria L. Blair provided advice and assistance during the refinement process of structures.

4.3 Biological Testing

4.3.1. Bacteria preparation and assay.

Vancomycin resistant E. faecalis (VRE, M846910) and Methicillin resistance S. aureus (MRSA, M118979) were cultured in Brain-heart infusion broth media (Oxiod), S. epidermidis (A130/ATCC14990) and S. aureus (A134/ATCC6538) were grown in nutrient agar and Luria-Bertani (LB) broth. E. coli (G102) was grown in LB broth and LB agar. Bacteria were streaked onto agar overnight from glycerol stocks and incubated at 37 ^oC before inoculation of a single colony into broth. 100 µL of suspended cell culture was then spread onto fresh agar plates and allowed to grown overnight. For soluble complexes, solutions were made up to 5 mg/mL in DMSO and the

solution soaked into small circles of filter paper before placing onto the agar plates. For the insoluble compounds, using a 10 µL pipette tip, a small amount ~ 1 mg, was pierced into the agar. The plates were incubated overnight and the zones of inhibition measured. Each was performed in triplicate.[9]

4.3.2. Cell culture.

Leishmania major virulent clone V121 was derived from the LRC-L137 L. major isolate and maintained at 26 °C in supplemented M199 media (10% (v/v) heat inactivated FBS, 1% Pen-Strep) and Hemin, purchased from Gibco ™. Human primary fibroblasts, Cervical cancer HeLa and Cos-7 cells were cultured and maintained in Dulbecco's Modified Eagles Medium (DMEM) supplemented with 10% FBS, 1% Pen-Strep and 1% Glutamax (purchased from Gibco ™) at 37 °C in a 5% CO_2 incubator.[10]

4.3.3. Measurement of reactive oxygen species.

Measurement of ROS was achieved by a modified assay from Wojtala et al.[11] J774 macrophages were plated into 24-well plates at 30,000 cells per well. Cells were given 24 hours to adhere before infection with L. major promastigotes a ratio of 1:5 in plain DMEM. The L. major promastigotes were incubated for six hours to infect and differentiate into amastigotes before excess promastigotes were washed away with PBS. The cells were incubated for a further 24 hours to allow complete infection. At each interval, 10 µM of the complexes were added in plain DMEM along with 1 µM of dihydroethidium, in triplicate. A drug control of amphotericin B and a negative control of non-infected cells without drug treatment was included. At intervals of 6, 12 and 24 hours, the cells were washed with PBS and a fluorescence reading taken in the measurement buffer of 5 mM of glucose in PBS at excitation of 535 nm and emission of 635 nm. Treated wells were compared to the negative control and the % increase calculated.

4.3.4. In vitro testing of L. major, HeLa, Cos-7 and human fibroblasts.

Celltiter Blue Cell Viability Assay was purchased from Promega™, and used for the determination of percentage viability of the parasite and human fibroblasts. Compounds **1G – 4G** and **1G'** were dissolved in DMSO to make up a 10mM working stock and sequentially diluted out in the appropriate culture media (100 µM to 48 nM). Assays were set up in duplicate in 96-well Falcon plates. Volumes of 10^6 promastigotes/mL, 10^5 Cos-7/mL, 10^5 HeLa/mL and 10^5 fibroblasts/mL were used. All cell assays were measured spectroscopically using fluorescence excitation at 544nm and emission at 590nm. Fibroblasts and L. major were measured after 48hrs, Cos-7 and HeLa were measured after 24hrs. The compounds were compared to a no drug negative control and the percent inhibition calculated.[12] Fluorescence measurements were conducted on either a BMG-Labtech FluoStar Omega microplate reader or BMG-Labtech ClarioStar microplate reader.[13, 14]

4.3.5. Amastigote invasion assay.

Macrophage invasion assays were performed as previously described.[15, 16] Briefly, bone marrow-derived mouse macrophages were plated onto coverslips in a 24 well plate and allowed to adhere for 48hrs. The cells were exposed to L. major promastigotes at a 1:10 ratio and incubated for a further 24hrs to allow for amastigote formation in vitro. The slides were then washed thoroughly with PBS to remove any excess extracellular promastigotes, and exposed to compounds for 48hrs before washing, fixation and cellular staining with a commercial Hema Color kit purchased from Merck. Following Giemsa staining, 200 cells per duplicate slide were then counted microscopically and the percentage of infected cells calculated against a positive control.

4.4 Reagents and solvents

Diethyl ether (Et_2O), ethanol, tetrahydrofuran (THF), toluene, *bis-methyl* sulfoxide (DMSO), and acetone were purchased from Merck. For the synthesis of all triaryl metal precursors the solvents

were dried prior to use and obtained from an MBruan-SPS-800 and stored over molecular sieves (4Å) in a Schlenk flash under a dry nitrogen atmosphere. Trimethyl indium was synthesised in situ in hexane under anhydrous conditions using anhydrous indium trichloride and and excess of 3.2 equivalents of a 3.1M methyllithium solution in diethoxyethane. All other required reagents were purchased from Sigma-Aldrich, Chem Supply and BioScineitific.

4.5 Schlenk protocol

Reactions requiring anhydrous conditions were completed with oven dried glassware under a dry nitrogen environment, utilising a vacuum/nitrogen line and Schlenk techniques. All glassware was dried at 100 ^{o}C for approximately 24 hrs prior, and allowed to cool under vacuum to reduce moisture content. The Schlenk apparatus was placed under high vacuum to purge air/moisture and backfilled with nitrogen in triplicate. Solvents and reagents were transferred through suba-seals using oven dried/nitrogen purged syringes. Filtering of solutions proceeded using oven dried/nitrogen purged cannulas with glass microfiber filters (GF/A, circles ø 42.5 mm, Whatman®) fixed via Teflon tape, through suba-seals.

4.6. Precursor Synthesis

4.6.1 Synthesis of triphenylbismuth, [$Bi(C_6H_5)_3$)] and triphenylantimony, [$Sb(C_6H_5)_3$)]

The reaction was conducted using anhydrous conditions. $BiCl_3$ (7 g, 22 mmol) was weighed into a 500 ml three-neck flask, equipped with a magnetic stirrer bar, dropping funnel and Schlenk tap, in a high purity nitrogen recirculating dry box. Dry THF (125 ml) was added and the $BiCl_3$ suspended. The suspension was cooled over an ice-bath to 0 ^{o}C. Phenylmagnesium bromide (66 ml, 1.0 M solution in THF) was transferred to the dropping funnel and added dropwise to the suspension over an hour. The mixture was allowed to stir overnight before quenching over ice. The resultant

precipitate was recrystallised from hot ethanol. The synthesis was repeated when required, giving an average yield of 60%.

Triphenylantimony was prepared using the same method for triphenylbismuth, with the exception of $SbCl_3$ in place of $BiCl_3$. An average yield of 75% was obtained.

*4.6.1.1. Triphenyl*bismuth*: m.p: 77 – 79 °C (Lit. 78 – 80 °C).[17] H NMR (400 MHz, DMSO-d_6) δ 7.78 – 7.68 (m, 6H, CH_{ar}), 7.43 – 7.34 (m, 6H, CH_{ar}), 7.39 – 7.26 (m, 3H, CH_{ar}); ^{13}C NMR (101 MHz, DMSO-d_6) δ 157.00 (BiC), 137.26 (C_{ar}), 130.25, 127.44 (C_{ar}).*

4.6.1.2 Triphenylantimony: m.p: 52 – 54 °C (Lit. 52 – 54 °C).[18] ^{1}H NMR (400 MHz, DMSO-d_6) δ 7.45 – 7.28 (m, 15H, CH_{ar}); ^{13}C NMR (101 MHz, DMSO-d_6) δ 138.18 (SbC), 135.81 (C_{ar}), 128.90 (C_{ar}), 128.62 (C_{ar}).

4.6.2 Synthesis of tris-*o*-tolyl antimony *o*-[$Sb(C_7H_7)_3$] Tris-m-tolyl antimony *m*-[$Sb(C_7H_7)_3$], tris-*p*-tolylantimony *p*-[$Sb(C_7H_7)_3$], tris-mesityl-antimony [$Sb(C_9H_{11})_3$] and tris-*p*-tertbutylphenyl antimony [$Sb(C_{10}H_{13})_3$]

The reaction was conducted using anhydrous conditions. Magnesium metal (3.2g, 3.1 equivalents) was added to a three-neck round bottom flask, equipped with a stirring bead, dropping funnel, condenser and Schlenk tap. The apparatus was evacuated and backfilled with nitrogen in triplicate before the addition of ~ 70 mL of dry THF. 19 mL, 19 mL, 24.2 g, 22.2 mL, 23 mL of 2-bromotoluene, 3-bromotoluene, 4-bromotoluene, bromomesitylene and 4-bromotertbutyphenyl respectively, were added to the dropping funnel and ~ 20 mL of dry THF added to either dissolve or homogenise the brominated aryl. The solution was added dropwise to the stirring magnesium turnings until self-reflux occurred. The solution was stirred for approximately 4 – 6 hours, forming a dark

coloured Grignard solution. The Grignard was filtered cannulated over to a prior prepared solution of 10 g of $SbCl_3$ in a three-neck flask (4.6.1). The solution was kept over ice during the filtration. After 24 hours, the dark grey solution was quenched over ice, yielding an off-white solid of the crude aryl antimony. Each was re-crystallised in hot ethanol, removing impurities. An average yield of 75% - 85% was obtained for all aryls respectively.

4.6.2.1 Tris-o-tolyl antimony: *m.p: 108 – 110 °C, 82% ^{1}H NMR (400 MHz, DMSO-d_6) δ 7.35 – 7.24 (m, 2H, CH_{ar}), 7.07 (ddd, J = 8.7, 5.1, 2.5 Hz, 1H, CH_{ar}), 6.91 – 6.82 (m, 1H, CH_{ar}), 2.40 (s, 3H); ^{13}C NMR (101 MHz, DMSO) δ 143.49 (SbC), 135.19 (C_{ar}), 129.76 (C_{ar}), 126.58 (C_{ar}), 24.17 (CH_3).*

4.6.2.2 Tris-m-tolyl antimony: m.p: 70 – 72 °C, 76%; ^{1}H NMR (400 MHz, DMSO-d_6) δ = 7.29 – 7.19 (m, 6H, CH_{ar}), 7.15 (dd, J = 10.5, 7.6 Hz, 6H, CH_{ar}), 2.24 (s, 9H, CH_3); ^{13}C NMR (101 MHz, DMSO-d_6) δ = 138.33 (SbC), 133.22 (C_{ar}), 129.84 (C_{ar}), 21.49 (CH_3).

4.6.2.3 Tris-p-tolyl antimony: m.p: 130 – 132 °C, 75%; ^{1}H NMR (400 MHz, DMSO-d_6) δ = 7.26 (d, J = 7.6 Hz, 6H, CH_{ar}), 7.16 (d, J = 7.6 Hz, 6H, CH_{ar}), 2.28 (s, 9H, CH_3); ^{13}C NMR (101 MHz, DMSO-d_6) δ = 138.45 (SbC), 136.23 (C_{ar}), 134.92 (C_{ar}), 130.10 (C_{ar}), 21.42 (CH_3).

4.6.2.4 Tris-mesityl antimony: m.p: 136 – 138 °C, 85%; ^{1}H NMR (400 MHz, DMSO-d_6) δ = 6.82 (s, 9H, CH_{ar}), 2.19 (d, J = 4.0 Hz, 18H, CH_3), 2.13 (d, J = 18.2 Hz, 9H, CH_3); ^{13}C NMR (101 MHz, DMSO-d_6) δ = 144.45 (SbC), 129.29 (C_{ar}), 25.24 (CH_3).

4.6.2.5 Tris-p-tertbutylphenyl antimony: m.p: 278 – 280 °C, 83%, ^{1}H NMR (400 MHz, Chloroform-d) δ 7.44 – 7.31 (m, 5H, CH_{ar}), 1.32 (s, 27H, tBu-CH). ^{13}C NMR (101 MHz, $CDCl_3$) δ 151.38 (SbC), 136.02 (C_{ar}), 134.80 (C_{ar}), 128.24 (C_{ar}), 125.83 (C_{ar}), 34.64 (tBu-C), 31.30 (tBu-C), 31.15 (tBu-C).

4.6.3. Synthesis of tris-*o*-methoxyphenyl antimony, [$Sb(C_7H_7O)_3$]

The reaction was carried out under anhydrous conditions. 7.2 mL of anhydrous anisole was transferred into a Schlenk flask and suspended in dry THF. Three equivalents (41 mL) of 1.6M n-butyllithium solution in hexane, was added dropwise at 0 °C. The lithiated solution was then added to a pre-purged dropping funnel in a pre-urged three-neck RBF, with 5 g of $SbCl_3$, set-up as per 4.6.1. The solution was added dropwise to the SCl_3 solution in THF, maintaining a temperature of 0 °C. The solution was quenched over ice to remove the LiCl produced and precipitate out the triaryl antimony. The crude product was recrystallised from hot ethanol, yielding a crystalline white solid of 69% yield.

4.6.3.1 Tris-o-methoxyphenyl antimony: m.p.: 180 – 182 °, 69%; ^{1}H NMR (400 MHz, DMSO-d_6) δ = 7.35 (ddd, J = 8.2, 7.3, 1.7 Hz, 3H, CH_{ar}), 7.03 (dd, J = 8.3, 1.0 Hz, 3H, CH_{ar}), 6.82 (td, J = 7.3, 1.0 Hz, 3H, CH_{ar}), 6.68 (dd, J = 7.2, 1.7 Hz, 3H, CH_{ar}), 3.72 (s, 9H, OCH_3); ^{13}C NMR (101 MHz, DMSO-d_6) δ = 162.28 (SbC), 130.50 (C_{ar}), 121.75 (C_{ar}), 110.20 (C_{ar}), 55.63 (OCH_3).

4.7. Compound synthesis

4.7.1 General procedure 1 (GP1)

One equivalent of the desired triphenyl metal was placed into a glass vial, equipped with a stirrer bead and dissolved into either toluene or diethyl ether. To this, a slight excess of 2.2 equivalents of 70% tertbutyl hydroperoxide solution in water was added. After approximately five minutes, two equivalents of the desired acid were added and the reaction stirred for 30 minutes to an hour before filtration into a fresh vial. The vial was left to stand, yielding the complexes **1S** – **8S** and **1B** – **8B** as crystalline solids.

4.7.1.1. Triphenylantimony bis(o-tolylacetic acetate), ***1S****. $SbPh_3$ (0.176 g, 0.5 mmol), o-tolylacetic acid (0.150 g, 1.0 mmol) and 70% t-BuOOH (150 µL, 1.1 mmol) were reacted as per GP1. Yield: 89% 0.289 g; m.p: 129 – 131 °C; ^{1}H NMR (400 MHz, $CDCl_3$): δ = 7.73 (6H, m, CH_{ar}) 7.44 (3H, m, CH_{ar}) 7.36 (6H, m, CH_{ar}) 7.11 (2H, m, CH_{ar}) 7.06 (4H, m, CH_{ar}) 6.96 (2H, m, CH_{ar}) 4.51 (4H, s, CH_2) 1.93 (6H, s, CH_3); ^{13}C NMR (100 MHz, $CDCl_3$, 25 °C): 174.5 (COO), 137.3 (SbC), 134.3 (C_{ar}), 133.8 (C_{ar}), 130.9 (C_{ar}) 130.1 (C_{ar}), 129.9 (C_{ar}), 129.1 (C_{ar}), 126.7 (C_{ar}), 125.7 (C_{ar}), 41.1 (CH_2), 19.3 (CH_3); FT-IR [cm $^{-1}$]: 3063 (w), 3013 (w), 2995 (w), 2909 (w), 1651 (sh), 1576 (w), 1481 (m), 1437 (m), 1342 (sh), 1301 (m), 1244 (sh), 1211 (sh), 1172 (m), 1069 (m), 1022 (m), 996 (m), 853 (w), 731 (sh), 689 (sh); Elemental analysis, expected: %C66.38 %H5.11 found: %C66.14 %H5.00 CCDC 1578382*

*4.7.1.2. Triphenyl*bismuth *bis(o-tolylacetic acetate),* ***1B****. $BiPh_3$ (0.221 g, 0.5 mmol), o-tolylacetic acid (0.150 g, 1.0 mmol) and 70% t-BuOOH (150 µL, 1.1 mmol) were reacted as per GP1. Yield: 81% 0.299 g; m.p: 143 - 144 °C; ^{1}H NMR (400 MHz, $CDCl_3$): δ = 7.98 (6H, m, CH_{ar}) 7.49 (3H, m, CH_{ar}) 7.43 (6H, m, CH_{ar}) 7.07 (2H, m, CH_{ar}) 6.99 (4H, m, CH_{ar}) 6.90 (2H, m, CH_{ar}) 3.40 (4H, s, CH_2) 1.94 (6H, s, CH_3); ^{13}C NMR (100 MHz, $CDCl_3$): 177.1 (COO), 159.5 (BiC), 136.7 (C_{ar}), 134.0 (C_{ar}), 131.0 (C_{ar}) 130.6 (C_{ar}), 129.9 (C_{ar}), 126.4 (C_{ar}), 126.7 (C_{ar}), 125.7 (C_{ar}), 40.7 (CH_2), 19.3 (CH_3)); FT-IR [cm $^{-1}$]: 3061 (w), 3020 (w), 2912 (w), 1601 (m), 1560 (sh), 1470 (m), 1437 (m), 1349 (sh), 1325 (m), 1258 (m), 1217 (m), 1190 (m), 1052 (w), 1009 (m), 986 (sh), 852 (w), 728 (sh), 680 (sh); Elemental analysis, Expected: C:58.54 H:4.45 found: C:58.47 H:4.47 CCDC 1578385*

4.7.1.3. Triphenylantimony bis(m-tolylacetic acetate), ***2S****. $SbPh_3$ (0.176 g, 0.5 mmol), m-tolylacetic acid (0.150 g, 1.0 mmol) and 70% t-BuOOH (150 µL, 1.1 mmol) were reacted as per GP1. Yield: 79% 0.257 g; ^{1}H NMR and ^{13}C NMR consistent with previously synthesised.*[15]

*4.7.1.4. Triphenyl*bismuth *bis(m-tolylacetic acetate),* ***2B****. $BiPh_3$ (0.220 g, 0.5 mmol), m-tolylacetic acid (0.151 g, 1.0 mmol) and 70% t-BuOOH (150 µL, 1.1 mmol) were reacted as per GP1. Yield: 77%*

0.284 g; m.p: 124 – 126 °C; ^{1}H NMR (400 MHz, $CDCl_3$): δ = 8.03 (6H, m, CH_{ar}) 7.50 (6H, m, CH_{ar}) 7.46 (3H, m, CH_{ar}) 7.06 (2H, m, CH_{ar}) 6.98 (2H, m, CH_{ar}) 6.82 (4H, m, CH_{ar}) 3.40 (4H, s, CH_2) 2.24 (6H, s, CH_3); ^{13}C NMR (100 MHz, $CDCl_3$): 159.6 (BiC), 133.9 (C_{ar}), 131.0 (C_{ar}), 130.6 (C_{ar}) 129.8 (C_{ar}), 128.0 (C_{ar}), 126.9 (C_{ar}), 126.0 (C_{ar}), 42.8 (CH_2), 20.1 (CH_3); FT-IR [cm $^{-1}$]: 3051 (w), 2918 (w), 1602 (sh), 1570 (sh), 1559 (sh), 1490 (m) 1435 (sh), 1364 (m) 1348 (sh), 1238 (w) 1150 (m), 1101 (m), 984 (sh), 948 (w), 771 (m), 728 (sh) 666 (sh); Elemental analysis, Expected: C:58.45 H:4.45 Found: C:58.24 H:4.46 CCDC 1578380

4.7.1.5. Triphenylantimony bis(p-tolylacetic acetate), ***3S****. $SbPh_3$ (0.175 g, 0.5 mmol), p-tolylacetic acid (0.150 g, 1.0 mmol) and 70% t-BuOOH (150 µL, 1.1 mmol) were reacted as per GP1. Yield: 91% 0.295 g; m.p: 144 – 146 °C; ^{1}H NMR (400 MHz, $CDCl_3$): δ = 7.77 (6H, m, CH_{ar}) 7.44 (3H, m, CH_{ar}) 7.35 (6H, m, CH_{ar}) 7.01 (4H, m, CH_{ar}) 6.90 (4H, m, CH_{ar}) 3.36 (4H, s, CH_2) 2.32 (6H, s, CH_3); ^{13}C NMR (100 MHz, $CDCl_3$): 175.0 (COO), 137.4 (SbC), 135.8 (C_{ar}), 133.9 (C_{ar}), 132.4 (C_{ar}) 130.9 (C_{ar}), 129.1 (C_{ar}), 128.9 (C_{ar}), 42.8 (CH_2), 21.1 (CH_3); FT-IR [cm $^{-1}$]: 3056 (w), 2939 (w), 1644 (sh), 1574 (w), 1479 (m), 1434 (m), 1305 (sh), 1267 (sh), 1192 (m), 1131 (sh), 1066 (m), 939 (m), 863 (w), 782 (m) 734 (sh), 687 (sh); Elemental analysis, Expected: C:66.38 H:5.11 Found: C:66.31 H:5.09 CCDC 1578609*

*4.7.1.6. Triphenyl*bismuth *bis(p-tolylacetic acetate),* ***3B****. $BiPh_3$ (0.220 g, 0.5 mmol), p-tolylacetic acid (0.151 g, 1.0 mmol) and 70% t-BuOOH (150 µL, 1.1 mmol) were reacted as per GP1. Yield: 69% 0.255 g; m.p: 150 - 153 °C; ^{1}H NMR (400 MHz, $CDCl_3$): δ = 8.00 (6H, m, CH_{ar}) 7.56 (3H, m, CH_{ar}) 7.48 (6H, m, CH_{ar}) 6.94 (4H, m, CH_{ar}) 6.86 (4H, m, CH_{ar}) 3.37 (4H, s, CH_2) 2.29 (6H, s, CH_3); ^{13}C NMR (100 MHz, $CDCl_3$): 162.2 (BiC), 133.9 (C_{ar}), 133.7 (C_{ar}), 131.0 (C_{ar}) 130.5 (C_{ar}), 128.8 (C_{ar}), 128.9 (C_{ar}), 42.8 (CH_2), 21.1 (CH_3); FT-IR [cm $^{-1}$]: 3051 (w), 2916 (w), 1600 (sh), 1560 (w), 1468 (m), 1434 (m), 1371 (sh), 1260 (sh), 1010 (m), 984 (s), 790 (m), 763 (m) 728 (sh), 679 (sh); Elemental analysis, Expected: C:58.45 H:4.45 Found: C:58.43 H:4.51 CCDC 1578384*

4.7.1.7. Triphenylantimony bis(2-methoxyphenylacetic acetate), ***4S****. $SbPh_3$ (0.176 g, 0.5 mmol), 2-methoxyphenylacetic acid (0.166 g, 1.0 mmol) and 70% t-BuOOH (150 µL, 1.1 mmol) were reacted as per GP1. Yield: 89% 0.307 g; ^{1}H NMR and ^{13}C NMR consistent with previously synthesised.[19] CCDC 1578602*

*4.7.1.8. Triphenyl*bismuth *bis(2-methoxyphenylacetic acetate),* ***4B****. $BiPh_3$ (0.220 g, 0.5 mmol), 2-methoxyphenylacetic acid (0.166 g, 1.0 mmol) and 70% t-BuOOH (150 µL, 1.1 mmol) were reacted as per GP1. Yield: 80% 0.302 g m.p: 148 – 150 °C; ^{1}H NMR (400 MHz, d_6-DMSO): δ = 7.93 (6H, m, CH_{ar}) 7.65 (6H, m, CH_{ar}) 7.57 (3H, m, CH_{ar}) 7.16 (2H, m, CH_{ar}) 6.86 (2H, m, CH_{ar}) 6.74 (2H, m, CH_{ar}) 3.53 (6H, s, CH_3) 2.09 (4H, s, CH_2); ^{13}C NMR (100 MHz, d_6-DMSO): 177.1 (COO), 159.7 (BiC), 137.1 (C_{ar}), 133.8 (C_{ar}), 131.9 (C_{ar}) 131.4 (C_{ar}), 130.8 (C_{ar}), 128.2 (C_{ar}), 120.3 (C_{ar}), 110.8 (C_{ar}), 55.9 (OCH_3), 31.5 (CH_2); FT-IR [cm $^{-1}$]: 3063 (w), 2952 (w), 1599 (sh), 1570 (m), 1490 (m), 1467 (m), 1359 (sh), 1291 (m) 1238 (sh), 1113 (m), 1027 (m) 983 (m), 733 (sh), 689 (sh); Elemental analysis, Expected: C:56.11 H:4.32 Found: C:56.14 H:4.23 CCDC 1578381*

4.7.1.9. Triphenylantimony bis(3-methoxyphenylacetic acetate), ***5S****. $SbPh_3$ (0.176 g, 0.5 mmol), 3-methoxyphenylacetic acid (0.167 g, 1.0 mmol) and 70% t-BuOOH (150 µL, 1.1 mmol) were reacted as per GP1. Yield: 91% 0.315 g; m.p: 103 – 105 °C; ^{1}H NMR (400 MHz, $CDCl_3$): δ = 7.78 (6H, m, CH_{ar}) 7.46 (3H, m, CH_{ar}) 7.38 (6H, m, CH_{ar}) 7.15 (2H, m, CH_{ar}) 6.78 (2H, m, CH_{ar}) 6.65 (4H, m, CH_{ar}) 3.72 (6H, s, CH_3) 3.40 (4H, s, CH_2); ^{13}C NMR (100 MHz, $CDCl_3$): 174.5 (COO), 159.5 (SbC), 137.2 (C_{ar}), 136.9 (C_{ar}), 133.8 (C_{ar}) 131.0 (C_{ar}), 129.2 (C_{ar}), 121.7 (C_{ar}), 114.5 (C_{ar}), 112.4 (C_{ar}), 55.1 (OCH_3), 43.5 (CH_2); FT-IR [cm $^{-1}$]: 3062 (w), 2951 (w), 1619 (sh), 1593 (sh), 1481 (m), 1433 (m), 1413 (m), 1367 (sh), 1263 (m) 1237 (sh), 1165 (m), 1039 (m) 996 (m), 738 (sh), 690 (sh); Elemental analysis, Expected: C:63.27 H:4.87 Found: C:63.22 H:5.15 CCDC 1578603*

*4.7.1.10. Triphenyl*bismuth *bis(3-methoxyphenylacetic acetate),* ***5B****. $BiPh_3$ (0.221 g, 0.5 mmol), 3-methoxyphenylacetic acid (0.166 g, 1.0 mmol) and 70% t-BuOOH (150 µL, 1.1 mmol) were reacted as per GP1. Yield: 75% 0.289 g; m.p: 121 – 123 °C; ^{1}H NMR (400 MHz, $CDCl_3$): δ = 8.02 (6H, m, CH_{ar}) 7.51 (6H, m, CH_{ar}) 7.44 (3H, m, CH_{ar}) 7.08 (2H, m, CH_{ar}) 6.73 (2H, m, CH_{ar}) 6.62 (4H, m, CH_{ar}) 3.71 (6H, s, CH_3) 3.41 (4H, s, CH_2); ^{13}C NMR (100 MHz, $CDCl_3$, 25 °C): 175.9 (COO), 159.5 (BiC), 133.9 (C_{ar}), 131.5 (C_{ar}), 131.0 (C_{ar}) 131.0 (C_{ar}), 129.0 (C_{ar}), 126.8 (C_{ar}), 121.5 (C_{ar}), 112.2 (C_{ar}), 55.1 (OCH_3), 43.0 (CH_2); FT-IR [cm $^{-1}$]: 3052 (w), 2964 (w), 1605 (sh), 1555 (sh), 1489 (m), 1466 (m), 1434 (m), 1371 (sh), 1267 (sh) 1223 (sh), 1157 (m), 1037 (m) 980 (m), 730 (sh), 691 (sh); Elemental analysis, Expected: C:56.11 H:4.32 Found: C:63.35 H:4.84 CCDC 1578377*

4.7.1.11. Triphenylantimony bis(4-methoxyphenylacetic acetate), ***6S****. $SbPh_3$ (0.177 g, 0.5 mmol), 4-methoxyphenylacetic acid (0.166 g, 1.0 mmol) and 70% t-BuOOH (150 µL, 1.1 mmol) were reacted as per GP1. Yield: 91% 0.313 g; ^{1}H NMR and ^{13}C NMR consistent with previously synthesised.[19] CCDC 1578379*

*4.7.1.12. Triphenyl*bismuth *bis(4-methoxyphenylacetic acetate),* ***6B****. $BiPh_3$ (0.221 g, 0.5 mmol), 4-methoxyphenylacetic acid (0.165 g, 1.0 mmol) and 70% t-BuOOH (150 µL, 1.1 mmol) were reacted as per GP1. Yield: 75% 0.285g; m.p: 140 – 141 °C; ^{1}H NMR (400 MHz, d_6-DMSO): δ = 7.91 (6H, m, CH_{ar}) 7.63 (6H, m, CH_{ar}) 7.55 (3H, m, CH_{ar}) 6.86 (2H, m, CH_{ar}) 6.74 (2H, m, CH_{ar}) 3.70 (6H, s, CH_3) 2.08 (4H, s, CH_2); ^{13}C NMR (100 MHz, d_6-DMSO): 172.1 (COO), 158.2 (BiC), 134.3 (C_{ar}), 133.7 (C_{ar}), 131.9 (C_{ar}) 131.5 (C_{ar}), 130.3 (C_{ar}), 128.2 (C_{ar}), 123.1 (C_{ar}), 114.0 (C_{ar}), 55.6 (OCH_3), 31.2 (CH_2); FT-IR [cm $^{-1}$]: 3055 (w), 2934 (w), 1596 (sh), 1556 (m), 1510 (sh), 1466 (m), 1435 (m), 1350 (sh), 1239 (sh), 1176 (m), 1037 (m) 981 (m), 738 (sh), 681 (m); Elemental analysis, Expected: C:56.11 H:4.32 Found: C:56.38 H:4.18 CCDC 1578383*

4.7.1.13. (µ2-Oxo)-bis((acetoxyacetato)-triphenylantimony(v))), ***7S****. $SbPh_3$ (0.353 g, 1.0 mmol), acetoxyacetic acid (0.118 g, 1.0 mmol) and 70% t-BuOOH (300 µL, 2.2 mmol) were reacted as per*

GP1. Yield: 86% 0.411 g; m.p: 184 – 185 °C. ; ^{1}H NMR (400 MHz, $CDCl_3$): δ = 7.96 (4H, m, CH_{ar}) 7.38 (10H, m, CH_{ar}) 7.25 (16H, m, CH_{ar}) 4.45 (4H, br(s), CH_2) 2.05 (6H, br(s), CH_3); FT-IR [cm $^{-1}$]: 3057 (w), 2955 (w), 1741 (m) 1732 (m) 1653 (sh), 1480 (m), 1434 (m), 1352 (m), 1336 (sh), 1269 (m) 1231 (sh), 1061 (m) 919 (m), 737 (sh), 691 (sh); Elemental analysis, Expected: C:55.26 H:4.22 Found: C:55.11 H:4.30 CCDC 1578606

4.7.1.14. Triphenylantimony mono-hydroxy-(monoacetoxyacetate), ***7S'****. 7aS was dissolved in d_6-DMSO with quantitative conversion to 7aS' observed. ; ^{1}H NMR (400 MHz, d_6-DMSO): δ = 8.02 (6H, m, CH_{ar}) 7.55 (9H, m, CH_{ar}) 4.80 (1H, s, OH) 4.39 (2H, s, CH_2) 2.50 (3H, s, CH_3);*

*4.7.1.15. Triphenyl*bismuth *bis(acetoxy acetate),* ***7B****. $BiPh_3$ (0.220 g, 0.5 mmol), acetoxyacetic acid (0.117 g, 1.0 mmol) and 70% t-BuOOH (150 µL, 1.1 mmol) were reacted as per GP1. Yield: 66% 0.222 g; m.p: 136 – 138 °C; ^{1}H NMR (400 MHz, $CDCl_3$): δ = 8.11 (6H, m, CH_{ar}) 7.63 (6H, m, CH_{ar}) 7.51 (3H, m, CH_{ar}) 4.39 (4H, s, CH_2) 2.06 (6H, s, CH_3); ^{13}C NMR (100 MHz, $CDCl_3$, 25 °C): 170.4 (COO), 157.9 (BiC), 134.1 (C_{ar}), 131.6 (C_{ar}), 131.3 (C_{ar}), 36.4 (CH_2), 20.7 (CH_3); FT-IR [cm $^{-1}$]: 3049 (w), 1744 (sh), 1629 (sh), 1576 (m), 1470 (m), 1436 (m), 1393 (sh), 1267 (m) 1217 (sh), 1066 (sh) 982 (m), 730 (sh), 678 (sh); Elemental analysis, Expected: C:46.30 H:3.74 Found: C:46.01 H:3.88 CCDC 1578370*

4.7.1.16. Triphenylantimony bis(phenoxyacetic acetate), ***8S****. $SbPh_3$ (0.177 g, 0.5 mmol), phenoxyacetic acid (0.152 g, 1.0 mmol) and 70% t-BuOOH (150 µL, 1.1 mmol) were reacted as per GP1. Yield: 78% 0.255 g; ^{1}H NMR and ^{13}C NMR consistent with previously synthesised.[15] CCDC 1578378*

*4.7.1.17. Triphenyl*bismuth *bis(phenoxyacetic acetate),* ***8B****. $BiPh_3$ (0.220 g, 0.5 mmol), phenoxyacetic acid (0.152 g, 1.0 mmol) and 70% t-BuOOH (150 µL, 1.1 mmol) were reacted as per*

GP1. Yield: 65% 0.241 g; m.p: 144 – 146 °C; ^{1}H NMR (400 MHz, d_6-DMSO): δ = 7.97 (6H, m, CH_{ar}) 7.72 (6H, m, CH_{ar}) 7.63 (3H, m, CH_{ar}) 7.14 (4H, m, CH_{ar}) 6.88 (2H, m, CH_{ar}) 6.58 (4H, m, CH_{ar}) 4.49 (4H, s, CH_2); ^{13}C NMR (100 MHz, d_6-DMSO): 174.5 (COO), 159.5 (BiC), 137.2 (C_{ar}), 136.9 (C_{ar}), 133.8 (C_{ar}) 131.0 (C_{ar}), 129.1 (C_{ar}), 121.7 (C_{ar}), 114.6 (C_{ar}), 112.4 (C_{ar}), 55.1 (CH_2); FT-IR [cm $^{-1}$]: 3059 (w), 2929 (w), 1624 (sh), 1598 (sh), 1557 (m), 1495 (sh), 1469 (m), 1436 (sh) 1353 (sh), 1261 (m) 1218 (sh), 1174 (m), 1071 (m) 984 (m), 735 (sh), 691 (sh); Elemental analysis, Expected: C:54.99 H:3.94 Found: C:54.69 H:3.86 CCDC 1578608

4.7.2 General procedure 2 (GP2):

One equivalent of triphenyl antimony was added to a 100 mL RBF, equipped with stirrer bead and dissolved in toluene. To this, a slight excess of 2.2 mmol of a 70% tertbutyl hydroperoxide solution in water was added. After approximately 5 minutes, 1 mmol of the desired quinolinol was added and the reaction stirred overnight. The solvent and tBuOH/H_2O biproducts were removed under vacuum yielding oily solids. The oily substance was sonicated in H_2O, precipitating out a solid. The solids were collected via filtration, yielding complexes **1Sq** – **6Sq**. Complexes were crystallised from either toluene or DMSO.

*4.7.2.1. Triphenylantimony mono-hydroxy 8-quinolinolate, **1Sq**. $SbPh_3$ (0.353 g, 1 mmol) was reacted with t-BuOOH (140 µL, 2 mmol) before addition of 8-quinolinol (0.145 g, 1 mmol) according to GP2. Yellow solid (.427 g, 83%). m.p: 161 – 162 °C; ^{1}H NMR (400 MHz, DMSO-d_6) δ = 9.10 (dd, J = 4.6, 1.4 Hz, 1H), 8.40 (dd, J = 8.4, 1.4 Hz, 1H, CH_{ar}), 7.73 – 7.65 (m, 6H, CH_{ar}), 7.65 – 7.57 (m, 1H, CH_{ar}), 7.52 – 7.43 (m, 1H, CH_{ar}), 7.23 – 7.14 (m, 9H, CH_{ar}), 7.11 (ddd, J = 12.8, 8.0, 1.2 Hz, 2H, CH_{ar}), 4.78 (s, 1H, OH). ^{13}C NMR (101 MHz, DMSO-d_6) δ = 156.44 (SbC), 142.08 (C_{ar}), 139.30 (C_{ar}), 130.02 (C_{ar}), 129.73 (C_{ar}), 128.91 (C_{ar}), 128.38 (C_{ar}), 127.93 (C_{ar}), 121.17 (C_{ar}), 113.86 (C_{ar}), 104.53 (C_{ar}); FT-IR [cm $^{-1}$]: 3571 (w), 2109 (w), 1575 (m), 1495 (m), 1460 (sh), 1429 (m), 1390 (m), 1319 (sh), 1279*

(m), 1239 (w), 1103 (sh), 1064 (m), 824 (m), 735 (sh). 692 (sh); Elemental analysis, Expected: C:63.06 H:4.31 N:2.72 Found: C:63.35 H:4.48 N:2.71 CCDC: 1942091

4.7.2.2. Triphenylantimony mono-hydroxy 5-chloro-8-quinolinolate, ***2Sq****. $SbPh_3$ (0.353 g, 1 mmol) was reacted with t-BuOOH (140 µL, 2 mmol) before addition of 5-chloro-8-quinolinol (0.179 g, 1 mmol) according to GP2. Yellow solid (0.448 g, 81%). m.p: 128 – 130 °C; ^{1}H NMR (600 MHz, DMSO-d_6) δ = 9.18 (dd, J = 4.6, 1.4 Hz, 1H, CH_{ar}), 8.51 (dd, J = 8.5, 1.4 Hz, 1H, CH_{ar}), 7.79 (dd, J = 8.5, 4.6 Hz, 1H, CH_{ar}), 7.71 – 7.66 (m, 6H, CH_{ar}), 7.60 (d, J = 8.4 Hz, 1H, CH_{ar}), 7.27 – 7.13 (m, 9H, CH_{ar}), 7.09 (d, J = 8.5 Hz, 1H, CH_{ar}), 4.95 (s, 1H, OH); ^{13}C NMR (101 MHz, DMSO-d_6) δ = 156.38 (SbC), 151.22 (C_{ar}), 143.31 (C_{ar}), 135.85 (C_{ar}), 132.99 (C_{ar}), 130.14 (C_{ar}), 128.52 (C_{ar}), 126.96 (C_{ar}), 123.31 (C_{ar}), 114.53 (C_{ar}); FT-IR [cm $^{-1}$]: 3241 (br), 3052 (w), 2109 (w), 1571 (m), 1492 (m), 1452 (sh), 1429 (m), 1379 (m), 1362 (s) 1308 (sh), 1256 (m), 1084 (w), 1022 (sh), 826 (m), 740 (sh), 697 (sh); Elemental analysis (2sq.dmso), Expected: C:55.57 H:4.34 N:2.23 S:5.11 Found: C:55.40 H:4.38 N:2.22 S:5.02. CCDC: 1901551*

4.7.2.3 Triphenylantimony mono-hydroxy 5,7-dichloro-8-quinolinolate, ***3Sq****. $SbPh_3$ (0.353 g, 1 mmol) was reacted with t-BuOOH (140 µL, 2 mmol) before addition of 5,7-dichloro8-quinolinol (0.214 g, 1 mmol) according to GP2. Yellow solid (0.594 g, 89%). m.p: 95 – 97 °C; ^{1}H NMR (600 MHz, DMSO-d_6) δ = 9.20 (dd, J = 4.6, 1.4 Hz, 1H, CH_{ar}), 8.49 (dd, J = 8.5, 1.4 Hz, 1H, CH_{ar}), 7.83 (s, 1H, 7.77 (dd, J = 6.2, 4.4 Hz, 6H, CH_{ar}), 7.31 – 7.10 (m, 10H, CH_{ar}), 5.16 (s, 1H, OH^{13}C NMR (101 MHz, DMSO) δ 152.22 (SbC), 151.92 (C_{ar}), 144.46 (C_{ar}), 136.11 (C_{ar}), 135.62 (C_{ar}), 132.62 (C_{ar}), 129.46 (C_{ar}), 128.84 (C_{ar}), 128.26 (C_{ar}), 128.26 (C_{ar}), 125.68 (C_{ar}), 123.07 (C_{ar}), 118.06 (C_{ar}), 114.69 (C_{ar}); FT-IR [cm $^{-1}$]: 3244 (w), 3053 (w), 2165 (w), 1571 (m), 1494 (m), 1450 (sh), 1429 (m), 1397 (m), 1308 (sh), 1256 (w), 1084 (m), 1025 (sh), 958 (sh), 826 (m), 740 (sh), 697 (sh); Elemental analysis (****3Sq.2H$_2$O****) Expected: C:52.38 H:3.91 N:2.26 Found C:52.61 H:4.06 N: 2.27. CCDC: 1938022*

4.7.2.4. Triphenylantimony mono-hydroxy 5,7-dibromo-8-quinolinolate, ***4Sq****. $SbPh_3$ (0.353 g, 1 mmol) was reacted with t-BuOOH (140 µL, 2 mmol) before addition of 5,7-dibromo-8-quinolinol (0.303 g, 1 mmol) according to GP2. Yellow solid (0.540 g, 72%). m.p: 121 -123 ^oC; ^1H NMR (600 MHz, DMSO-d_6) δ = 9.17 (dd, J = 4.6, 1.4 Hz, 1H, CH_{ar}), 8.41 (dd, J = 8.5, 1.4 Hz, 1H, CH_{ar}), 8.05 (s, 1H, CH_{ar}), 7.82 – 7.71 (m, 6H, CH_{ar}), 7.29 – 7.12 (m, 10H, CH_{ar}), 5.16 (s, 1H, OH); ^{13}C NMR (101 MHz, DMSO-d_6) δ = 132.56 (C_{ph}), 128.80 (C_{ph}), 128.22 (C_{ph}); FT-IR [cm $^{-1}$]: 3275 (w), 3065 (w), 2081 (w), 1560 (m), 1481 (m), 1430 (sh), 1390 (m), 1357 (sh), 1309 (m), 1242 (w), 1103 (m), 1022 (sh), 943 (m), 864 (w), 743 (sh), 690 (sh); Elemental analysis (4sq.dmso), Expected: C:46.43 H:3.49 N:2.03 S:4.27 Found: C:46.30 H:3.49 N:1.87 S:4.42. CCDC: 1938252*

4.7.2.5. Triphenylantimony mono-hydroxy 5,7-diiodo-8-quinolinolate, ***5Sq****. $SbPh_3$ (0.353 g, 1 mmol) was reacted with t-BuOOH (140 µL, 2 mmol) before addition of 5,7-diiodo-8-quinolinol (0.397 g, 1 mmo). Yellow solid (0.598 g, 78%) according to GP2. m.p: 179 -181 ^oC; ^1H NMR (400 MHz, DMSO-d_6) δ = 9.10 (dd, J = 4.6, 1.4 Hz, 1H, CH_{ar}), 8.31 (s, 1H, CH_{ar}), 8.27 (dd, J = 8.5, 1.3 Hz, 1H, CH_{ar}), 7.75 (dd, J = 8.5, 4.5 Hz, 6H, CH_{ar}), 7.21 (m, 10H, CH_{ar}), 5.12 (s, 1H, OH); ^{13}C NMR (101 MHz, DMSO-d_6) δ = 132.53 (C_{ph}), 128.71 (C_{ph}), 128.18 (C_{ph}); FT-IR [cm $^{-1}$]: 3050 (w), 2115 (w), 1545 (m), 1475 (m), 1430 (sh), 1385 (m), 1353 (sh), 1307 (w), 1243 (m), 1102 (m), 1063 (m), 846 (m), 733 (sh), 692 (sh); Elemental analysis, Expected: C:41.47 H: 2.54 N:1.86 Found: C:41.38 H:2.75 N:1.89. CCDC: 1938021*

4.7.2.6. Triphenylantimony mono-hydroxy 5,7-dichloro-2-methyl-8-quinolinolate, ***6Sq****. $SbPh_3$ (0.353 g, 1 mmol) was reacted with t-BuOOH (140 µL, 2 mmol) before addition of 5,7-dichloro-2-methyl-8-quinolinol (0.229 g, 1 mmol) according to GP2. Yellow solid (.449 g, 75%). m.p: 150 -153 ^oC; ^1H NMR (600 MHz, DMSO-d_6) δ = 8.23 (d, J = 8.6 Hz, 1H, CH_{ar}), 7.88 (dt, J = 6.3, 1.4 Hz, 6H, CH_{ar}), 7.71 (s, 1H, CH_{ar}), 7.42 (d, J = 8.6 Hz, 1H, CH_{ar}), 7.31 – 7.21 (m, 10H, CH_{ar}), 4.93 (s, 1H, OH), 2.91 (s, 3H, CH_3). ^{13}C NMR (101 MHz, DMSO-d_6) δ = 132.59 (C_{ph}), 129.18 (C_{ph}), 129.39 (C_{ph}); FT-IR [cm $^{-1}$]: 3599 (w), 3048 (w), 2973 (w), 1573 (w), 1548 (w), 1480 (w), 1423 (sh), 1357 (m), 1326 (m), 1251*

*(w), 1107 (m), 1021 (w), 829 (m), 732 (sh). 690 (sh); Elemental analysis (**6sq.tBuOH**), Expected: C:57.26 H:4.84 N:2.17 Found: C:57.48 H:447 N:2.30. CCDC: 1938023*

4.7.3. General procedure 3 (GP3)

1 mmol of the desired quinolinol was placed into a Schlenk flask under vacuum for approximately 3 – 4 hours to remove any excess moisture. The quinolinol was then suspended in hexane and placed into an isopropanol/N_2 bath at -78 °C. 1 mmol of neat trimethyl gallium was added by pre-purged syringe to the flask, yielding an immediate colour change. The reaction was allowed to warm to room temperature before the solid produced was filtered, yielding compunds **1G** – **4G**. The coloured filtrate was left to stand, yielding crystalline solid over time.

*4.7.3.1. Bis-methyl gallium mono-5-chloro-quinolinolate, **1G**. 5-chloroquinolinol (0.179 g, 1 mmol) was reacted with trimethyl gallium (0.1 mL, 1 mmol) according to GP3. Yellow solid, (0.250 g, 89%), m.p: 215 – 216 °C; ^{1}H NMR (600 MHz, DMSO-d_6) δ = 8.90 (dd, J = 4.6, 1.4 Hz, 1H, CH_{ar}), 8.62 (dd, J = 8.5, 1.3 Hz, H, CH_{ar}), 7.83 (dd, J = 8.5, 4.5 Hz, 1H, CH_{ar}), 7.60 (d, J = 8.4 Hz, 1H, CH_{ar}), 6.87 (d, J = 8.4 Hz, 1H, CH_{ar}), -0.32 (s, 6H, CH_3). ^{13}C NMR (600 MHz, DMSO-d_6) δ = 162.9 (C_{ar}) 148.1 (C_{ar}), 141.9 (C_{ar}), 138.3 (C_{ar}), 132.9 (C_{ar}), 129.3 (C_{ar}), 126.4 (C_{ar}) 115.3 (C_{ar}), 115.1 (C_{ar}), -0.514 (CH_3). FT-IR [cm^{-1}]: 3053 (w), 2954 (w), 1599 (m), 1576 (w), 1493 (m), 1363 (m), 1310(sh), 1254 (m), 1152 (m), 1081 (sh), 780 (sh), 734 (sh), 669 (sh); MS (ESI)$^+$ m/z = 180.0 [LH_2^+], 99.0 [$Ga(CH_3)_2^+$] 68.9 [Ga]. ESI$^-$: 100.9 [$Ga(CH_3)_2H_2^-$]. Elemental analysis, Expected: C:47.46 H:3.98 N:5.03 Found: C:47.26 H:3.89 N:4.95. CCDC 1898525*

*4.7.3.2. Bis-methyl gallium mono-5,7-dichloro-quinolinolate, **2G.** 5,7-dichloroquinolinol (0.214 g, 1 mmol) was reacted with trimethyl gallium (0.1 mL, 1 mmol) according to GP3. Yellow solid, (0.280 g, 90%), m.p: 127 -129 °C; ^{1}H NMR (600 MHz, DMSO-d_6) δ = 8.85 (dd, J = 4.5, 1.4 Hz, 1H, CH_{ar}), 8.57 (dd, J = 8.5, 1.4 Hz, 1H, CH_{ar}), 7.79 (m, 1H CH_{ar}), 7.78 (s, 1H, CH_{ar}), -0.35 (s, 6H, CH_3). ^{13}C NMR (600*

MHz, DMSO-d_6) δ = 157.8 (C_{ar}) 148.0 (C_{ar}), 141.1 (C_{ar}), 137.1 (C_{ar}), 131.5 (C_{ar}), 127.3 (C_{ar}), 125.5 (C_{ar}), 117.5 (C_{ar}), 114.6 (C_{ar}), -0.514 (CH_3). FT-IR [cm $^{-1}$]: 2961 (w), 1567 (m), 1491 (w), 1456 (m), 1399 (m), 1368(sh), 1259 (w), 1196 (w), 1057 (w), 811 (sh), 782 (sh), 651 (sh); MS (ESI)$^+$ m/z = 214.0 [LH_2^+], 99.0 [$Ga(CH_3)_2^+$], 68.9 [Ga]. ESI $^-$: 100.9 [$Ga(CH_3)_2H_2^-$]. Elemental analysis, Expected: C:42.23 H:3.22 N:4.48 Found: C:42.35 H:3.14 N:4.48. CCDC 1898522

*4.7.3.3. Bis-methyl gallium mono-5,7-dibromo-quinolinolate, **3G.** 5,7-dibromoquinolinol (0.303 g, 1 mmol) was reacted with trimethyl gallium (0.1 mL, 1 mmol) according to GP3. Yellow solid, (0.391 g, 97%), m.p: 136 - 138 °C; ^{1}H NMR (600 MHz, DMSO-d_6) δ = 8.85 (dd, J = 4.5, 1.4 Hz, 1H, CH_{ar}), 8.53 (dd, J = 8.5, 1.4 Hz, 1H, CH_{ar}), 8.03 (s, 1H, CH_{ar}), 7.84 (dd, J = 8.5, 4.5 Hz, 1H, CH_{ar}), -0.32 (s, 6H, CH_3). ^{13}C NMR (600 MHz, DMSO-d_6) δ = 159.6 (C_{ar}) 147.9 (C_{ar}), 141.0 (C_{ar}), 139.5 (C_{ar}), 136.7 (C_{ar}), 129.0 (C_{ar}), 125.9 (C_{ar}), 107.5 (C_{ar}), 103.8 (C_{ar}), -0.512 (CH_3). FT-IR [cm $^{-1}$]: 2957 (w), 1547 (m), 1478 (w), 1451 (m), 1363 (sh), 1233 (w), 1221 (w), 1191 (w), 850 (m), 750 (sh), 707 (m); MS (ESI)$^+$ m/z = 303.9 [LH_2^+], 99.0 [$Ga(CH_3)_2^+$], 68.9 [Ga]. ESI $^-$: 101.0 [$Ga(CH_3)_2H_2^-$]. Elemental analysis, Expected: C:32.89 H:2.51 N:3.79 Found: C:32.70 H:2.47 N:3.38. CCDC 1898528*

*4.7.3.4. Bis-methyl gallium mono-5,7-diiodo-quinolinolate, **4G.** 5,7-diiodoquinolinol (0.397 g, 1 mmol) was reacted with trimethyl gallium (0.1 mL, 1 mmol) according to GP3. Yellow solid, (0.425 g, 91%), m.p: 165 - 167 °C; ^{1}H NMR (600 MHz, DMSO-d_6) δ 8.75 (dd, J = 4.5, 1.3 Hz, 1H, CH_{ar}), 8.36 (dd, J = 8.5, 1.4 Hz, 1H, CH_{ar}), 8.28 (s, 1H, CH_{ar}), 7.79 (dd, J = 8.5, 4.5 Hz, 1H, CH_{ar}), -0.35 (s, 6H, CH_3). ^{13}C NMR (600 MHz, DMSO-d_6) δ = 163.5 (C_{ar}), 147.9 (C_{ar}), 147.8 (C_{ar}), 144.1 (C_{ar}), 139.8 (C_{ar}), 132.2 (C_{ar}), 126.4 (C_{ar}), 84.3 (C_{ar}), 78.9 (C_{ar}), -0.490 (CH_3). FT-IR [cm $^{-1}$]: 2960 (w), 1560 (m), 1485 (m), 1451 (sh), 1367 (sh), 1261 (w), 1191 (w), 1112 (m), 1055 (w), 809 (m), 781 (m), 686 (sh); MS (ESI)$^+$ m/z = 397.8 [LH_2^+], 99.0 [$Ga(CH_3)_2^+$], 68.9 [Ga]. ESI $^-$: 100.9 [$Ga(CH_3)_2H_2^-$]. Elemental analysis, Expected: C:26.65 H:2.03 N:2.83 Found: C:26.79 H:1.92 N:2.93. CCDC 1898524*

4.7.4. General procedure 4 (GP4)

1 mmol of anhydrous indium trichloride was added to a Schlenk flask and suspended in dry hexane. The solution was cooled to -78 ^{o}C using an isopropanol/N_2 bath before the addition of 3.2 mmol of methyllithium in diethoxymethane solution via a pre-purged syringe. The solution was left to stir for ~ three hours. The solution was added via filter cannulation to remove the LiCl produced, to a pre-dried suspension of 1 mmol of the desired quinolinol in hexane, at -78 ^{o}C. The reaction was allowed to warm to room temperature before the solid produced was filtered yielding compounds **1l** – **4l**. Compounds were recrystallised from acetone.

*4.7.4.1. Bis-methyl indium mono-5-chloro-quinolinolate, **1l**, 5-chloroquinolinol (0.179 g, 1 mmol) was reacted with previous prepared trimethyl indium (~ 1 mmol) according to GP4. Yellow solid, (0.236 g, 73%) m.p: 250 – 253 ^{o}C decomp; ^{1}H NMR (600 MHz, DMSO-d_6) δ 8.77 – 8.72 (m, 1H, CH_{ar}), 8.54 – 8.49 (m, 1H, CH_{ar}), 7.72 (dd, J = 8.5, 4.4 Hz, 1H, CH_{ar}), 7.51 (d, J = 8.5 Hz, 1H, CH_{ar}), 6.76 (t, J = 8.2 Hz, 1H, CH_{ar}), -0.35 (s, 6H, CH_3); ^{13}C NMR (151 MHz, DMSO-d_6) δ = 161.71 (C_{ar}), 160.36 (C_{ar}), 145.25 (C_{ar}), 144.90 (C_{ar}), 140.12 (C_{ar}), 134.63 (C_{ar}), 129.65 (C_{ar}), 126.77 (C_{ar}), 125.31 (C_{ar}), 122.86 (C_{ar}), 113.03 (C_{ar}), 110.43 (C_{ar}), -4.03 (CH_3); FT-IR [cm $^{-1}$] 2917 (w), 2280 (w), 1599 (m), 1574 (m), 1495 (sh), 1456 (sh), 1393 (sh), 1363 (sh). 1255 (m), 1083 (sh), 1043 (sh), 958 (m), 822 (m), 782 (sh), 737 (sh); MS (ESI)$^{+}$ m/z = 292.9 [In(L)$^{+}$], 144.9 [In$(CH_3)_2^{+}$], 114.9 [In]. ESI $^{-}$: 292.9 [In(L)$^{-}$], 178.0 [L – H^{-}], 146.9 [In$(CH_3)_2H_2^{-}$], 112.9 [^{113}In]; Elemental analysis (**1l.2H_2O)**, Expected: C:38.69 H:3.83 N:4.10 Found: C:39.05 H:3.77 N:4.19. CCDC: 1938266*

*4.7.4.2. Bis-methyl indium mono-5,7-dichloro-quinolinolate, **2l**, 5,7-dichloroquinolinol (0.214 g, 1 mmol) was reacted with previous prepared trimethyl indium (~ 1 mmol) according to GP4 Yellow solid, (0.273 g, 79%) m.p: 254 – 257 ^{o}C decomp; ^{1}H NMR (600 MHz, DMSO-d_6) δ 8.81 (d, J = 4.1 Hz, 1H, CH_{ar}), 8.53 (dd, J = 8.5, 1.5 Hz, 1H, CH_{ar}), 7.75 (dd, J = 8.5, 4.4 Hz, 1H, CH_{ar}), 7.72 (s, 1H), -0.33 (s, 6H, CH_3); ^{13}C NMR (151 MHz, DMSO-d_6) δ = 157.60 (C_{ar}), 146.34 (C_{ar}), 140.00 (C_{ar}), 134.90 (C_{ar}),*

129.22 (C_{ar}), 125.73 (C_{ar}), 122.88 (C_{ar}), 116.27 (C_{ar}), 110.45 (C_{ar}), -3.78 (CH_3); FT-IR [cm $^{-1}$] 2973 (w), 2922 (w), 2371 (w), 1595 (w), 1560 (m), 1489 (sh), 1442 (sh), 1390 (sh), 1358 (sh), 1228 (m), 1103 (m), 1053 (m), 963 (m), 884 (sh), 736 (sh), 714 (sh); MS (ESI)$^+$ m/z = 144.9 [$In(CH_3)_2^+$], 114.9 [In]. ESI $^-$: 211.9 [L – H^-], 146.9 [$In(CH_3)_2H_2^-$], 112.9 [^{113}In]; Elemental analysis, Expected: C:36.91 H:2.82 N:3.91 Found: C:36.70 H:2.91 N:3.85. CCDC: 1938263

*4.7.4.3. Bis-methyl indium mono-5,7-bromo-quinolinolate, **3l**, 5,7-dibromoquinolinol (0.303 g, 1 mmol) was reacted with previous prepared trimethyl indium (~ 1 mmol) according to GP4 Yellow solid, (0.321 g, 74%) m.p 225 – 228 ^{o}C decomp; ^{1}H NMR (400 MHz, DMSO-d_6) δ 8.78 (dd, J = 4.4, 1.5 Hz, 1H, CH_{ar}), 8.47 (dd, J = 8.6, 1.5 Hz, 1H, CH_{ar}), 7.96 (s, 1H, CH_{ar}), 7.77 (dd, J = 8.5, 4.4 Hz, 1H, CH_{ar}), -0.33 (s, 6H, CH_3); ^{13}C NMR (151 MHz, DMSO-d_6) δ = 146.27 (C_{ar}), 136.94 (C_{ar}), 134.48 (C_{ar}), 127.45 (C_{ar}), 123.07 (C_{ar}), 106.62 (C_{ar}), -3.51 (CH_3); FT-IR [cm $^{-1}$] 2920 (w), 2296 (w), 1592 (w), 1556 (m), 1483 (sh), 1438 (sh), 1385 (sh), 1367 (sh), 1350 (sh), 1235 (m), 1099 (sh), 1050 (w), 940 (m), 859 (m), 725 (sh), 685 (sh); MS (ESI)$^+$ m/z = 144.9 [$In(CH_3)_2^+$], 114.9 [In]. ESI $^-$: 301.9 [L – H^-], 146.9 [$In(CH_3)_2H_2^-$], 112.9 [^{113}In]; Elemental analysis, Expected: C:29.57 H:2.26 N:3.13 Found: C:29.34 H:2.38 N:3.23. CCDC: 1938265*

*4.7.4.4. Bis-methyl indium mono-5,7-diiodo-quinolinolate, **4l**, 5,7-dichloroquinolinol (0.397 g, 1 mmol) was reacted with previous prepared trimethyl indium (~ 1 mmol) according to GP4. Yellow solid, (0.454 g, 86%), m.p: 239 – 242 ^{o}C decomp; ^{1}H NMR (600 MHz, DMSO-d_6) δ 8.69 (dd, J = 4.4, 1.4 Hz, 1H, CH_{ar}), 8.32 (dd, J = 8.5, 1.4 Hz, 1H, CH_{ar}), 8.25 (s, 1H, CH_{ar}), 7.73 (dd, J = 8.5, 4.4 Hz, 1H, CH_{ar}), -0.34 (s, 6H, CH_3); ^{13}C NMR (151 MHz, DMSO-d_6) δ = 146.69 (C_{ar}), 145.12 (C_{ar}), 144.60 (C_{ar}), 140.34 (C_{ar}), 130.41 (C_{ar}), 123.20 (C_{ar}), 118.05 (C_{ar}), 83.03 (C_{ar}), -3.21 (CH_3); FT-IR [cm $^{-1}$] 2906 (w), 2289 (w), 1541 (m), 1476 (m), 1436 (sh), 1381 (sh), 1368 (sh), 1350 (sh), 1247 (w), 1102 (m), 1050 (w), 927 (w), 804 (m), 736 (sh), 691 (sh); MS (ESI)$^+$ m/z = 144.9 [$In(CH_3)_2^+$], 114.9 [In]. ESI $^-$: 395.9 [L*

– H^-], 146.9 [$In(CH_3)_2H_2^-$], 112.9 [^{113}In]; Elemental analysis, Expected: C:24.43 H:1.86 N:2.59 Found: C:24.60 H:1.85 N:2.66. CCDC: 1942090 [$(In(Me)_2L)_2(In(Me)_2OH)$].

4.7.4.5. Methyl indium bis-5,7-dibromoquinolinolate, ***3I'****.* ***3I'*** *was isolated as a small crop of crystal from the reaction mixture of complex* ***3I*** *after 24 hours****.*** *Yellow blocks (> 5%). CCDC: 1938264*

*4.7.4.6. 4[Indium mono-*hydroxido *bis-5,7-dibromoquinolinolate],* ***3I-C.*** **3I-C** *was isolated from the reaction mixture of complex* ***3I*** *and* ***3I'*** *after several days. Orange blocks, (> 5%). CCDC: 1938267*

4.7.5. General procedure 5 (GP5)

2 mmol of the desired quinolinol was placed into a Schlenk flask under vacuum for approximately 3 – 4 hours to remove any excess moisture. The quinolinol was then either dissolved or suspended in toluene and placed into an isopropanol/N_2 bath at -78 °C. 1 mmol of neat trimethyl gallium was added by pre-purged syringe to the flask, yielding an immediate colour change. The reaction was allowed to warm to room temperature before refluxing at 110 °C the solid produced was filtered, yielding complexes **1G'** – **4G'.** The coloured filtrate was left to stand, yielding crystalline solid over time

4.7.5.1. Methyl gallium bis-5-chloro-quinolinolate, ***1G'.*** *5-chloroquinolinol (0.358 g, 2 mmol) was reacted with trimethyl gallium (0.1 mL, 1 mmol) according to GP5. Yellow solid, (0.315 g, 72%), m.p: 225 - 227 °C decomp; ^{1}H NMR (600 MHz, DMSO-d_6) δ = 9.09 (dd, J = 4.6, 1.4 Hz, 2H, CH_{ar}), 8.75 (dd, J = 8.6, 1.3 Hz, 2H, CH_{ar}), 7.99 (dd, J = 8.6, 4.6 Hz, 2H, CH_{ar}), 7.64 (d, J = 8.4 Hz, 2H, CH_{ar}), 6.90 (d, J = 8.4 Hz, 2H, CH_{ar}), -0.03 (s, 3H, CH_3). δ = 157.8 (C_{ar}) 146.2 (C_{ar}), 138.5 (C_{ar}), 136.4 (C_{ar}), 130.8 (C_{ar}), 126.5 (C_{ar}), 124.4 (C_{ar}), 114.3 (C_{ar}),112.5 (C_{ar}), -4.82 (CH_3). FT-IR [cm $^{-1}$]: 3054 (w), 1601 (m), 11575 (m), 1494 (sh), 1458 (sh), 1320 (sh), 1256 (w), 1085 (sh), 829 (m), 780 (sh), 744 (sh). Elemental analysis, Expected: C:51.64 H:2.97 N:6.34 Found: C:51.84 H:2.73 N:6.49. CCDC 1898523*

4.7.5.2. Methyl gallium bis-5,7-dichloro-quinolinolate, ***2G'.*** *5,7-dichloroquinolinol (0.428 g, 2 mmol) was reacted with trimethyl gallium (0.1 mL, 1 mmol) according to GP5. Yellow solid, (0.422 g, 81%), m.p: > 300 °C decomp; ^{1}H NMR (600 MHz, DMSO-d_6), residual toluene and acetone are not labelled. δ = 9.17 (dd, J = 4.7, 1.3 Hz, 2H, CH_{ar}), 8.81 (dd, J = 8.5, 1.3 Hz, 2H, CH_{ar}), 8.06 (dd, J = 8.5, 4.6 Hz, 2H, CH_{ar}), 7.87 (s, 1H CH_{ar}), -0.00 (s, 3H, CH_3). FT-IR [cm $^{-1}$]: 3073 (w), 1566 (m), 1488 (sh), 1450 (sh), 1370 (sh), 1235 (w), 1235 (w), 1114 (m), 1053 (w), 892 (m), 752 (sh), 660 (sh). Elemental analysis, Expected: C:33.14 H:1.61 N:4.07 Found: C:33.28 H:1.53 N:4.14. CCDC 1898526*

4.7.5.3. Methyl gallium bis-5,7-dibromo-quinolinolate, ***3G'.*** *5,7-bromoquinolinol (0.606 g, 2 mmol) was reacted with trimethyl gallium (0.1 mL, 1 mmol) according to GP5. Yellow solid, (0.616 g, 80%), m.p: 165 - 167 °C; ^{1}H NMR (600 MHz, DMSO-d_6) δ = 9.14 (d, J = 4.7 Hz, 2H, CH_{ar}), 8.75 (d, J = 8.6 Hz, 2H, CH_{ar}), 8.20 – 7.97 (m, 4H, CH_{ar}), 0.00 (s, 3H, CH_3). FT-IR [cm $^{-1}$]: 2958 (w), 1560 (m), 1483 (m), 1449 (sh), 1367 (sh), 1221 (w), 1203 (w), 1110 (m), 1051 (w), 869 (m), 748 (sh), 690 (sh). Elemental analysis, Expected: C:33.14 H:1.61 N:4.07 Found: C:33.28 H:1.53 N:4.14. CCDC 1898529*

4.7.5.4. Methyl gallium bis-5,7-diiodo-quinolinolate, ***4G'.*** *5,7-diiodoquinolinol (0.784 g, 2 mmol) was reacted with trimethyl gallium (0.1 mL, 1 mmol) according to GP5. Yellow solid, (0.666 g, 81%), m.p: > 300 °C decomp; ^{1}H NMR (600 MHz, DMSO-d_6) δ = 9.10 (dd, J = 4.6, 1.3 Hz, 2H, CH_{ar}), 8.62 (dd, J = 8.5, 1.3 Hz, 2H, CH_{ar}), 8.41 (s, 2H, CH_{ar}), 8.10 (dd, J = 8.5, 4.7 Hz, 2H, CH_{ar}), 0.00 (s, 3H, CH_3). FT-IR [cm $^{-1}$]: 2954 (w), 1545 (m), 1474 (sh), 1446 (sh), 1361 (sh), 1246 (w), 1218 (w), 1113 (m), 1050 (w), 851 (m), 747 (sh), 720 (m). Elemental analysis, Expected: C:26.03 H:1.26 N:3.20 Found: C:26.19 H:1.41 N:3.30. CCDC 1898527*

4.7.6. General procedure (GP6)

0.5 mmol of the desired triaryl antimony (0.176 g) was added to a 100 mL RBF, equipped with stirrer bead and dissolved in diethyl ether. To this, a slight excess of 1.2 mmol of a 30% hydrogen

peroxide solution in water was added. After approximately 5 minutes, 0.5 mmol of the either R or S mandelic acid (0.076g) was added and the reaction stirred overnight. The solvent and tBuOH/H_2O biproducts were removed under vacuum yielding oily solids. The oily substance was sonicated in H_2O, precipitating out a solid. The solids were collected via filtration, yielding complexes **1S** – **6S**, **1R** – **6R.** Complexes were crystallised from the ether filtrate, or by heating the solid in DMSO.

*4.7.6.1. Tris-o-tolyl antimony R-mandelate, **1Sr**. Tris-o-tolyl antimony (0.197 g, 0.5 mmol) was reacted with R-mandelic acid (0.071 g, 0.5 mmol) according to GP6. White solid (0.226 g, 83%), m.p: 136 – 139 °C; ^{1}H NMR (600 MHz, DMSO-d_6) δ = 7.58 – 7.56 (m, 3H, CH_{ar}), 7.52 – 7.49 (m, 3H, CH_{ar}), 7.42 (t, J = 7.2 Hz, 6H, CH_{ar}), 7.37 (d, J = 1.2 Hz, 2H, CH_{ar}), 7.34 – 7.31 (m, 2H, CH_{ar}), 7.30 – 7.26 (m, 1H, CH_{ar}), 5.40 (s, 1H, CCH), 2.28 (s, 9H, CH_3); ^{13}C NMR (151 MHz, DMSO-d_6) δ = 173.10 (COOH), 141.76 (SbC), 139.81 (C_{ar}), 138.13 (C_{ar}), 133.61 (C_{ar}), 131.90 (C_{ar}), 131.67 (C_{ar}), 128.15 (C_{ar}), 127.62 (C_{ar}), 127.12 (C_{ar}), 126.98 (C_{ar}), 73.57 (COH), 64.92 (CCH), 22.92 (CH_3); FT-IR [cm $^{-1}$]: 3055 (w), 2922 (w), 1682 (sh), 1450 (m), 1309 (m), 1286 (sh), 1045(m), 1026 (m), 797 (w), 747 (sh), 697 (sh). Elemental Analysis, Expected: C:63.88 H:4.99, Found: C63.63 H:5.11. CCDC: 1938254*

*4.7.6.1 Tris-o-tolyl antimony S-mandelate, **1Ss**. Tris-o-tolyl antimony (0.197 g, 0.5 mmol) was reacted with S-mandelic acid (0.071 g, 0.5 mmol) according to GP6. White solid (0.280 g, 80%), m.p: 137 – 140 °C; ^{1}H NMR (600 MHz, DMSO-d_6) δ = 7.58 – 7.56 (m, 3H, CH_{ar}), 7.52 – 7.49 (m, 3H, CH_{ar}), 7.42 (t, J = 7.2 Hz, 6H, CH_{ar}), 7.37 (d, J = 1.2 Hz, 2H, CH_{ar}), 7.34 – 7.31 (m, 2H, CH_{ar}), 7.30 – 7.26 (m, 1H, CH_{ar}), 5.40 (s, 1H, CCH), 2.28 (s, 9H, CH_3); ^{13}C NMR (151 MHz, DMSO-d_6) δ = 173.10 (COOH), 141.76 (SbC), 139.81 (C_{ar}), 138.13 (C_{ar}), 133.61 (C_{ar}), 131.90 (C_{ar}), 131.67 (C_{ar}), 128.15 (C_{ar}), 127.62 (C_{ar}), 127.12 (C_{ar}), 126.98 (C_{ar}), 73.57 (COH), 64.92 (CCH), 22.92 (CH_3); FT-IR [cm $^{-1}$]: 3057 (w), 2922 (w), 1683 (sh), 1450 (m), 1310 (m), 1286 (sh), 1045(m), 1027 (m), 797 (w), 753 (sh), 697 (sh). Elemental Analysis, Expected: C:63.88 H:4.99, Found: C63.43 H:4.98. CCDC: 1938260*

4.7.6.3. Tris-m-tolyl antimony R-mandelate, ***2Sr****. Tris-m-tolyl antimony (0.197 g, 0.5 mmol) was reacted with R-mandelic acid (0.071 g, 0.5 mmol) according to GP6. White solid (0.224 g, 86%), m.p: 130 – 133 °C; ^{1}H NMR (600 MHz, DMSO-d_6) δ = 7.49 – 7.43 (m, 3H, CH_{ar}), , 7.43 – 7.37 (m, 3H, CH_{ar}), 7.36 – 7.30 (m, 6H, CH_{ar}), 7.28 – 7.25 (m, 2H, CH_{ar}), 7.25 – 7.21 (m, 2H, CH_{ar}), 7.21 (m, 1H, CH_{ar}), 5.16 (s, 1H, CH), 2.27 (s, 9H, CH_3); ^{13}C NMR (101 MHz, DMSO) δ = 174.60 (COOH), 142.70 (SbC), 141.38 (C_{ar}), 137.70 (C_{ar}), 134.69 (C_{ar}), 131.28 (C_{ar}), 130.51 (C_{ar}), 128.37 (C_{ar}), 127.45 (C_{ar}), 127.40 (C_{ar}), 126.73 (C_{ar}), 74.07 (COH), 21.30 (CH_3).FT-IR [cm $^{-1}$]: 2919 (w), 1683 (sh), 1619 (sh), 1450 (m), 1361 (m), 1278 (sh), 1070(m), 1038 (m), 791 (m), 763 (sh), 691 (sh). Elemental Analysis, Expected: C:63.88 H:4.99, Found: C63.56 H:5.10. CCDC: 1938259*

4.7.6.4. Tris-m-tolyl antimony S-mandelate, ***2Ss.*** *Tris-m-tolyl antimony (0.197 g, 0.5 mmol) was reacted with S-mandelic acid (0.071 g, 0.5 mmol) according to GP6. White solid (0.196 g, 72%), m.p: 129 – 131 °C; ^{1}H NMR (600 MHz, DMSO-d_6) δ = 7.49 – 7.43 (m, 3H, CH_{ar}), , 7.43 – 7.37 (m, 3H, CH_{ar}), 7.36 – 7.30 (m, 6H, CH_{ar}), 7.28 – 7.25 (m, 2H, CH_{ar}), 7.25 – 7.21 (m, 2H, CH_{ar}), 7.21 (m, 1H, CH_{ar}), 5.16 (s, 1H, CH), 2.27 (s, 9H, CH_3); ^{13}C NMR (101 MHz, DMSO) δ = 174.62 (COOH), 142.71 (SbC), 141.39 (C_{ar}), 137.70 (C_{ar}), 134.69 (C_{ar}), 131.29 (C_{ar}), 130.51 (C_{ar}), 128.36 (C_{ar}), 127.45 (C_{ar}), 127.40 (C_{ar}), 126.72 (C_{ar}), 74.09 (COH), 21.30 (CH_3); FT-IR [cm $^{-1}$]: 2918 (w), 1682 (sh), 1618 (sh), 1450 (m), 1362 (m), 1276 (sh), 1070(m), 1038 (m), 778 (m), 763 (sh), 690 (sh). Elemental Analysis, Expected: C:63.88 H:4.99, Found: C63.87 H:5.24. CCDC: 1938255*

4.7.6.5. Peroxybis(tris-p-tolyl antimony R-mandelate), ***3Sr****. Tris-p-tolyl antimony (0.197 g, 0.5 mmol) was reacted with R-mandelic acid (0.071 g, 0.5 mmol) according to GP6. White solid (0.227 g, 81%), m.p: 145 – 147 °C; FT-IR [cm $^{-1}$]: 3026 (w) 2920 (w), 1653 (sh), 1493 (sh), 1451 (m), 1314 (m), 1283 (sh), 1059 (m), 1015 (m), 797 (sh), 732 (sh), 696 (sh). Elemental Analysis, Expected: C:61.95 H:5.02, Found: C61.84 H:5.24.*

4.7.6.6. Tris-p-tolyl antimony R-mandelate, ***3Sr'****. Complex* ***3Sr*** *was placed into d_6-DMSO, liberating H_2O_2 and forming the solution state cyclometallate. ^{1}H NMR (600 MHz, DMSO-d_6) δ = 10.20 (s, 1H, OH), 7.49 – 7.46 (m, 6H, CH_{ar}), 7.43 – 7.40 (m, 2H, CH_{ar}), 7.26 – 7.24 (m, 6H, CH_{ar}), 7.22 – 7.20 (m, 2H, CH_{ar}), 7.20 – 7.17 (m, 1H, CH_{ar}), 5.12 (s, 1H, CCH), 2.32 (s, 9H, CH_3); ^{13}C NMR (151 MHz, DMSO-d_6) δ = 174.5 (COOH), 141.4 (SbC), 139.4 (C_{ar}), 139.3 (C_{ar}), 134.2 (C_{ar}), 129.2 (C_{ar}), 127.4 (C_{ar}), 127.3 (C_{ar}), 126.6 (C_{ar}), 73.9 (COH) , 64.9 (CCH), 21.0 (CH_3).*

4.7.6.7. Peroxybis(tris-p-tolyl antimony S-mandelate, ***3Ss****. Tris-p-tolyl antimony (0.197 g, 0.5 mmol) was reacted with S-mandelic acid (0.071 g, 0.5 mmol) according to GP6. White solid (0.222 g,79%), m.p: 144 – 146 °C. FT-IR [cm $^{-1}$]: 3024 (w) 2919 (w), 1654 (sh), 1492 (sh), 1450 (m), 1312 (m), 1283 (sh), 1059 (m), 1015 (m), 796 (sh), 732 (sh), 696 (sh). Elemental Analysis, Expected: C:61.95 H:5.02, Found: C61.90 H:4.82.*

4.7.6.8. Tris-p-tolyl antimony S-mandelate, ***3Ss'****. Complex* ***3Ss*** *was placed into d_6-DMSO, liberating H_2O_2 and forming the solution state cyclometallate. ^{1}H NMR (600 MHz, DMSO-d_6) δ = 10.20 (s, 1H, OH), 7.49 – 7.46 (m, 6H, CH_{ar}), 7.43 – 7.40 (m, 2H, CH_{ar}), 7.26 – 7.24 (m, 6H, CH_{ar}), 7.22 – 7.20 (m, 2H, CH_{ar}), 7.20 – 7.17 (m, 1H, CH_{ar}), 5.12 (s, 1H, CCH), 2.32 (s, 9H, CH_3); ^{13}C NMR (151 MHz, DMSO-d_6) δ = 174.5 (COOH), 141.4 (SbC), 139.4 (C_{ar}), 139.3 (C_{ar}), 134.2 (C_{ar}), 129.2 (C_{ar}), 127.4 (C_{ar}), 127.3 (C_{ar}), 126.6 (C_{ar}), 73.9 (COH) , 64.9 (CCH), 21.0 (CH_3).*

4.7.6.9. Tris-o-methoxypheny antimony R-mandelate, ***4Sr****. Tris-o-methoxyphenyl antimony (0.221 g, 0.5 mmol) was reacted with R-mandelic acid (0.071 g, 0.5 mmol) according to GP6. White solid (0.213 g, 72%), m.p: 195 – 197 °C; ^{1}H NMR (600 MHz, DMSO-d_6) δ = 7.56 – 7.48 (m, 8H, CH_{ar}), 7.37 – 7.28 (m, 2H, CH_{ar}), 7.28 – 7.24 (m, 1H, CH_{ar}), 7.17 – 7.08 (m, 6H, CH_{ar}), 5.23 (s, 1H, CH), 3.56 (s, 9H, OCH_3); ^{13}C NMR (151 MHz, DMSO-d_6) δ = 173.45 (COOH), 160.21 ($COCH_3$), 140.89 (SbC), 133.14 (C_{ar}), 132.47 (C_{ar}), 128.95 (C_{ar}), 127.76 (C_{ar}), 127.07 (C_{ar}), 126.49 (C_{ar}), 121.81 (C_{ar}), 111.94 (OCH_3),*

72.86 (COH), 55.77 (CCH); FT-IR [cm $^{-1}$]: 3063 (w) 2941 (w), 1677 (sh), 1577 (sh), 1470 (m), 1431 (m), 1297 (sh), 1242 (m), 1009 (m), 790 (sh), 756 (sh), 705 (m). Elemental Analysis, Expected: C:59.07 H:5.12, Found: C59.37 H:4.84. CCDC: 1938261

4.7.6.10. Tris-o-methoxyphenyl antimony S-mandelate, ***4Ss****. Tris-o-methoxyphenyl antimony (0.221 g, 0.5 mmol) was reacted with S-mandelic acid (0.071 g, 0.5 mmol) according to GP6. White solid (0.231 g. 78%), m.p: 196 – 198 °C; δ = 7.56 – 7.48 (m, 8H, CH_{ar}), 7.37 – 7.28 (m, 2H, CH_{ar}), 7.28 – 7.24 (m, 1H, CH_{ar}), 7.17 – 7.08 (m, 6H, CH_{ar}), 5.23 (s, 1H, CH), 3.56 (s, 9H, OCH_3); ^{13}C NMR (151 MHz, DMSO-d_6) δ = 173.45 (COOH), 160.21 ($COCH_3$), 140.89 (SbC), 133.14 (C_{ar}), 132.47 (C_{ar}), 128.95 (C_{ar}), 127.76 (C_{ar}), 127.07 (C_{ar}), 126.49 (C_{ar}), 121.81 (C_{ar}), 111.94 (OCH_3), 72.86 (COH), 55.77 (CCH); FT-IR [cm $^{-1}$]: 3063 (w) 2941 (w), 1677 (sh), 1577 (sh), 1470 (m), 1431 (m), 1297 (sh), 1242 (m), 1009 (m), 790 (sh), 756 (sh), 705 (m). Elemental Analysis,* ***4Ss.0.5Et$_2$O*** *Expected: C:59.07 H:5.12, Found: C59.45 H:4.91. CCDC: 1938262*

4.6.7.11. Tris-mesityl antimony R-mandelate, ***5Sr****. Tris-mesityl antimony (0.238 g, 0.5 mmol) was reacted with R-mandelic acid (0.071 g, 0.5 mmol) according to GP6. White solid (0.297 g, 78%), m.p: 230 – 232 °C; ^{1}H NMR (600 MHz, DMSO-d_6) δ = 7.30 – 7.25 (m, 3H, CH_{ar}), 7.11 (m, 2H, CH_{ar}), 7.02 (m, 3H, CH_{ar}), 6.88 – 6.81 (m, 3H, CH_{ar}), 5.02 (s, 1H, CH), 2.38 (s, 9H, CH_3), 2.30 – 2.26 (m, 9H, CH_3), 2.21 – 2.12 (m, 9H, CH_3); ^{13}C NMR (151 MHz, DMSO-d_6) δ = 143.66 (SbC), 141.42 (C_{ar}), 140.77 (C_{ar}), 139.30 (C_{ar}), 139.16 (C_{ar}), 130.45 (C_{ar}), 129.90 (C_{ar}), 127.92 (C_{ar}), 127.48 (C_{ar}), 74.22 (COH), 23.53f (CH_3), 22.32 (CH_3), 20.46 (CH_3); FT-IR [cm $^{-1}$]: 3017 (w) 2921 (w), 1677 (sh), 1449 (m), 1311 (sh), 1291 (m), 1256 (sh), 1017 (sh), 945 (m), 785 (m), 765 (sh), 697 (m). Elemental Analysis, Expected: C:66.79 H:6.25, Found: C66.87 H:6.57. CCDC: 1938256*

4.6.7.12. Tris-mesityl antimony S-mandelate, ***5Ss****. Tris-mesityl antimony (0.238 g, 0.5 mmol) was reacted with S-mandelic acid (0.071 g, 0.5 mmol) according to GP6. White solid (0.300 g, 82%),*

m.p: 230 – 232 °C; ^{1}H NMR (600 MHz, DMSO-d_6) δ = 7.30 – 7.25 (m, 3H, CH_{ar}), 7.11 (m, 2H, CH_{ar}), 7.02 (m, 3H, CH_{ar}), 6.88 – 6.81 (m, 3H, CH_{ar}), 5.02 (s, 1H, CH), 2.38 (s, 9H, CH_3), 2.30 – 2.26 (m, 9H, CH_3), 2.21 – 2.12 (m, 9H, CH_3); ^{13}C NMR (151 MHz, DMSO-d_6) δ = 143.66 (SbC), 141.42 (C_{ar}), 140.77 (C_{ar}), 139.30 (C_{ar}), 139.16 (C_{ar}), 130.45 (C_{ar}), 129.90 (C_{ar}), 127.92 (C_{ar}), 127.48 (C_{ar}), 74.22 (COH), 23.53f (CH_3), 22.32 (CH_3), 20.46 (CH_3); FT-IR [cm $^{-1}$]: 3021 (w) 2919 (w), 1677 (sh), 1448 (m), 1311 (sh), 1291 (m), 1255 (sh), 1017 (sh), 945 (m), 785 (m), 765 (sh), 697 (m). Elemental Analysis, Expected: C:66.79 H:6.25, Found: C66.97 H:6.52. CCDC: 1938258

4.6.7.13. Tris-p-tert-butylphenyl antimony R-mandelate, ***6Sr****. Tris-p-tertbutylphenyl antimony (0.260 g, 0.5 mmol) was reacted with R-mandelic acid (0.071 g, 0.5 mmol) according to GP6. White solid (0.252 g, 75%), m.p: 196 – 198 °C; ^{1}H NMR (600 MHz, DMSO-d_6) δ = 7.61 – 7.50 (m, 6H, CH_{ar}), 7.49 – 7.43 (m, 6H, CH_{ar}), 7.41 – 7.33 (m, 2H, CH_{ar}), 7.21 – 7.16 (m, 3H, CH_{ar}), 5.14 (s, 1H, CH), 1.28 (s, 27H, CH_3); ^{13}C NMR (151 MHz, DMSO-d_6) δ = 174.52 (COOH), 152.46 (SbC), 139.76 (C_{ar}), 134.16 (C_{ar}), 127.45 (C_{ar}), 127.35 (C_{ar}), 125.58 (C_{ar}), 74.05 (COH), 56.16 (CCH), 34.65 (CH_3), 31.14 (CH_3), 18.70 (CH_3); FT-IR [cm $^{-1}$]: 3059 (w) 2957 (sh), 2902 (m), 1665 (sh), 1491 (m), 1311 (sh), 1267 (m), 1200 (m), 1064 (sh), 947 (w), 818 (sh), 800 (w), 698 (m). Elemental Analysis (****6R.1.5H₂O****), Expected: C:65.34 H6.93, Found: C65.47 H:7.10. CCDC: 1938257*

4.7.6.14. Tris-p-tert-butylphenyl antimony S-mandelate, ***6Ss****. Tris-p-tertbutylphenyl antimony (0.260 g, 0.5 mmol) was reacted with S-mandelic acid (0.071 g, 0.5 mmol) according to GP6. White solid (0.241 g, 73%), m.p: 197 – 199 °C; ^{1}H NMR (600 MHz, DMSO-d_6) δ = 7.61 – 7.50 (m, 6H, CH_{ar}), 7.49 – 7.43 (m, 6H, CH_{ar}), 7.41 – 7.33 (m, 2H, CH_{ar}), 7.21 – 7.16 (m, 3H, CH_{ar}), 5.14 (s, 1H, CH), 1.28 (s, 27H, CH_3); ^{13}C NMR (151 MHz, DMSO-d_6) δ = 174.52 (COOH), 152.46 (SbC), 139.76 (C_{ar}), 134.16 (C_{ar}), 127.45 (C_{ar}), 127.35 (C_{ar}), 125.58 (C_{ar}), 74.05 (COH), 56.16 (CCH), 34.65 (CH_3), 31.14 (CH_3), 18.70 (CH_3); FT-IR [cm $^{-1}$]: 3058 (w) 29575(sh), 2902 (m), 1665 (sh), 1491 (m), 1311 (sh), 1267 (m),*

*1200 (m), 1064 (sh), 949 (w), 818 (sh), 798 (w), 697 (m). Elemental Analysis (**6S.1.5H$_2$O**), Expected:*

C:65.34 H6.93, Found: C65.30 H:7.12. CCDC: 1938253

4.8 References

1. M. R. Willcott, *J. Am. Chem. Soc.*, 2009, **131**, 13180-13180.
2. Bruker-Nonius, Apex-II. SAINT-plus (version 7.06a) Bruker AXS Inc, *Wisconsin USA,* 2004.
3. G. Sheldrick, Bruker AXS Inc*., Madison, WI*, 2002.
4. CrysAlisPro version 1.171.34.36, Oxford Diffraction Ltd, *Yarton England,* 2010.
5. CrysAlisPro version 1.171.40.49a, Rigaku Oxford Diffraction Ltd*, Oxfordshire England,* 2015.
6. T. M. McPhillips, S. E. McPhillips, H.-J. Chiu, A. E. Cohen, A. M. Deacon, P. J. Ellis, E. Garman, A. Gonzalez, N. K. Sauter and R. P. Phizackerley, *J. Synchrotron. Radiat.*, 2002, **9**, 401-406.
7. G. M. Sheldrick, *Acta Crystallogr. A.,* 2008, **64**, 112-122.
8. O. V. Dolomanov, L. J. Bourhis, R. J. Gildea, J. A. Howard and H. Puschmann, *J. Appl. Crystallogr.*, 2009, **42**, 339-341.
9. P. C. Andrews, M. Werrett, M. Herdman, R. Brammananth, U. Garusinghe, W. Batchelor, P. Crellin and R. Coppel, *Chem. Eur. J.*, 2018.
10. Y. C. Ong, V. L. Blair, L. Kedzierski and P. C. Andrews, *Dalton Trans.*, 2014, **43**, 12904-12916.
11. A. Wojtala, M. Bonora, D. Malinska, P. Pinton, J. Duszynski and M. R. Wieckowski, in *Methods Enzymol.*, Elsevier, 2014, vol. 542, pp. 243-262.
12. A. Pathak, V. L. Blair, R. L. Ferrero, L. Kedzierski and P. C. Andrews, *J. Inorg. Biochem.*, 2017.
13. R. N. Duffin, V. L. Blair, L. Kedzierski and P. C. Andrews, *J. Inorg. Biochem.*, 2018, **189**, 151-162.
14. R. N. Duffin, V. L. Blair, L. Kedzierski and P. C. Andrews, *Dalton Trans.*, 2018, **47**, 971-980.
15. M. I. Ali, M. K. Rauf, A. Badshah, I. Kumar, C. M. Forsyth, P. C. Junk, L. Kedzierski and P. C. Andrews, *Dalton Trans.*, 2013, **42**, 16733-16741.
16. K. Lackovic, J. P. Parisot, N. Sleebs, J. B. Baell, L. Debien, K. G. Watson, J. M. Curtis, E. Handman, I. P. Street and L. Kedzierski, *Antimicrob. Agents Chemother.*, 2010, **54**, 1712-1719.
17. R. Goel and H. Prasad, *Can. J. Chem.*, 1970, **48**, 2488-2493.
18. F. C. Whitmore, *Organic Syntheses, Vol: VII*, John Wiley and Sons, 1927.
19. R. Mushtaq, M. K. Rauf, M. Bolte, A. Nadhman, A. Badshah, M. N. Tahir, M. Yasinzai and K. M. Khan, *Appl. Organomet. Chem.*, 2017, **31,** e3606.

Dalton Transactions

PAPER

View Article Online
View Journal | View Issue

Cite this: *Dalton Trans.*, 2018, **47**, 971

Comparative stability, toxicity and anti-leishmanial activity of triphenyl antimony(v) and bismuth(v) α-hydroxy carboxylato complexes†

Rebekah N. Duffin,[a] Victoria L. Blair,[a] Lukasz Kedzierski[b] and Philip C. Andrews *[a]

Received 6th November 2017,
Accepted 12th December 2017

DOI: 10.1039/c7dt04171c

rsc.li/dalton

A series of triphenyl Sb(v) and Bi(v) α-hydroxy carboxylato complexes of the general formula $[MPh_3(O_2CROH)_2]$ and $[MPh_3(O_2CRO)]$ have been successfully synthesised and characterised, and subsequently assayed for their comparative activity towards Leishmania parasites and human fibroblast cells. Four complexes are novel; $[SbPh_3Gly]$, $[BiPh_3(GlyH)_2]$, $[SbPh_3(R\text{-}ManH)_2]$ and $[SbPh_3(S\text{-}ManH)_2]$, and have been structurally characterised through X-ray diffraction. These were combined in the study with the known complexes; ($[SbPh_3(R\text{-}Man)]$, $[SbPh_3(S\text{-}Man)]$, $[BiPh_3(R\text{-}ManH)_2]$, $[BiPh_3(R\text{-}ManH)_2]$, $[SbPh_3(BenzH)_2]$, $[BiPh_3(BenzH)_2]$, for which the crystal structures of $[BiPh_3(S\text{-}ManH)_2]$ and $[BiPh_3(R\text{-}Man)_2]$ have now been authenticated ($GlyH_2$ = glycolic acid, $R/S\text{-}ManH_2$ = mandelic acid, $BenzH_2$ = benzilic acid). The complexes adopt a typical bipyramidal 7-coordinate geometry with the phenyl rings occupying the equatorial plane, and the ligands on the axial. In contrast to previous studies the Bi(v) compounds show a relatively high degree of stability in DMEM culture media. Promastigote and human fibroblast cell assays showed the Bi(v) analogues to be non-selectively toxic with a respective IC_{50} range of 3.58–6.33 μM and 5.83–7.01 μM. In contrast, the Sb(v) analogues provided much greater selectivity (promastigotes 12.5–20.7; fibroblasts 72.8–≥100 μM). Assessment of the Sb(v) complexes against amastigotes at 10 μM showed them to be effective with % infection values ranging from 9.5 ± 0.5–30 ± 1.3.

Introduction

Leishmaniasis is classified by the World Health Organisation as a severely neglected tropical parasitic disease, affecting approximately 350 million people across 88 tropical and subtropical countries.[1] The parasite is spread by the bite of an infected female sandfly (genus *Phlebotomus* and *Lutzomyia*) with the threat of infection being greater in lower socio-economic communities.[2,3] Approximately 200 000–400 000 incidences are a result of the deadlier visceral parasite, with 10% of these cases resulting in death.[4] Visceral Leishmaniasis (VL) arises from infection by the sub-species *Leishmania donovani*, with 70% of the recorded cases occurring in Bihar, a state of the Indian subcontinent.[5] Without immediate treatment the infection can become lethal.[6]

The front-line treatment of VL relies heavily on the use of pentavalent antimonials, notably sodium stibogluconate (SSG, Pentostam™) and meglumine antimoniate (Glucantime™).[7] These Sb(v) compounds have been theorised to act as pro-drugs, reducing *in vivo* to Sb(III) through interactions with cysteine rich glutathione and trypanothione,[8] while other studies suggest a direct role for SSG in inhibiting protein phosphatase pathways prior to reduction both *in vitro* and *in vivo*.[9] Despite their success and efficacy the front-line Sb(v) treatments present unavoidable side-effects, including joint and muscle pain, elevation of hepatocellular enzymes and in serious cases, cardiotoxicity and pancreatitis.[8] The inherent hydrophilicity and rapid renal clearance of the drugs means they are administered daily by injection over 28 days, under medical supervision, leading to significant non-compliance.[6,10,11] Resistance to the drugs has also appeared, predominately in Bihar, India, where high levels of exposure to arsenic in drinking water has resulted in a leishmanial As(v) reductase that can act upon the Sb(v) compounds.[12,13] Alternative second-line therapeutics, such as miltefosine, are expensive and harbour their own potentially debilitating side-effects.[10,11,14]

To improve compliance and ease of treatment it would be preferable to have orally active drugs. However, the strong

[a]*School of Chemistry, Monash University, Clayton, Melbourne, VIC 3800, Australia. E-mail: phil.andrews@monash.edu; Tel: +61 (03) 9905 5509*
[b]*Faculty of Veterinary and Agricultural Sciences at The Peter Doherty Institute for Infection and Immunity, 792 Elizabeth Street, Melbourne 3000, Victoria, Australia*

† Electronic supplementary information (ESI) available. CCDC 1578595–1578597 and 1580805. For ESI and crystallographic data in CIF or other electronic format see DOI: 10.1039/c7dt04171c

aqueous solubility of both sodium stibogluconate and meglumine antimoniate mean they have very low absorption in the stomach and are inactive if taken orally. In attempting to increase hydrophobicity and the possibility of absorption through the gastric mucosa we, and others, have targeted and assessed heteroleptic Sb(v) complexes of the general formula $[SbAr_3(O_2CR)_2]$, incorporating both aryl and carboxylato ligands. We have demonstrated that these complexes show significant activity against both the promastigote and amastigote form of the leishmania parasite with minimum inhibitory concentrations (MIC) in the range 0.5–3.5 μM, while demonstrating little toxicity toward human fibroblast cells below 25 μM.[15] These provide good lead compounds.

In attempting to ameliorate the inherent toxicity of Sb(III) in the treatment regimen we also investigated the potential use of Bi(III) and Bi(V) complexes as anti-leishmanials, predicated on the generally recognised understanding that bismuth has a much lower systemic toxicity in mammals than antimony.[16] Bismuth(III) carboxylate and thioxoketonate complexes exhibit excellent activity towards *Leishmania* promastigotes, but also showed significant toxicity towards human fibroblasts.[17,18] One class of ligand which provided greater promise was the α-hydroxy carboxylates.[26] From this study, the glycolate complexes [Bi(gly)(H-gly)] and [Bi(gly)$(NO_3)(H_2O)$] showed good activity toward amastigotes at 50 μM (% viability 7.5 ± 3.8 and 1.8 ± 0.9 respectively), with no observable toxicity on human fibroblasts at the same concentration, providing a reasonable degree of selectivity.

Our initial studies into Bi(V) analogues, $[BiAr_3(O_2CR)_2]$ (Ar = Ph; *o*-, *m*-, and *p*-Tol), of the promising organo-antimony(V) dicarboxylato complexes involved benzoate ligands drawn from a range of non-steroidal anti-inflammatory drugs (NSAIDs).[19] While the range of IC_{50} values for the series of complexes towards promastigotes proved promising (Ar = Ph, 0.71–2.50 μM; Ar = Tol, 0.57–1.77), the complexes proved chemically unstable in culture media, undergoing reduction and precipitating $BiAr_3$, and were mostly non-selective in their toxicity to human fibroblasts. However, two complexes based on diflunisal (Ar = *o*-Tol) and aspirin (Ar = *m*-Tol) demonstrated some potential with selectivity indices ≤100 (fibroblast/promastigote) at 6.12 μM.

In our current study, the target was to directly compare the stability, anti-leishmanial activity and mammalian cell toxicity of related organometallic Bi(V) and Sb(V) complexes incorporating ligands derived from the α-hydroxy acids; glycolic acid ($GlyH_2$), *R*,*S*-mandelic acid (*R*,*S*-$ManH_2$), and benzilic acid ($BenzH_2$), shown in Fig. 1. In so doing, four novel complexes have been successfully synthesised and characterised; ([$SbPh_3Gly$] **1S**, $[BiPh_3(GlyH)_2]$ **1B**, $[SbPh_3(R\text{-}ManH)_2]$ **2Sr**, $[SbPh_3(S\text{-}ManH)_2]$ **2Ss**) and assessed alongside four previously recorded complexes ([$SbPh_3$(*R*-Man)] **2Sr′**, $[SbPh_3(S\text{-}Man)]$ **2Ss′**, $[BiPh_3(R\text{-}ManH)_2]$ **2Br**, $[BiPh_3(S\text{-}ManH)_2]$ **2Bs**, $[SbPh_3(BenzH)_2]$ **3S**, $[BiPh_3(BenzH)_2]$ **3B**) (Fig. 2).[20–22]

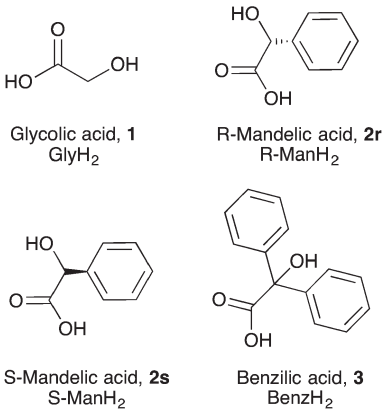

Fig. 1 Four α-hydroxy carboxylic acids used in the formation of a series of $[MPh_3(O_2CR)_2]$ complexes (M = Bi or Sb).

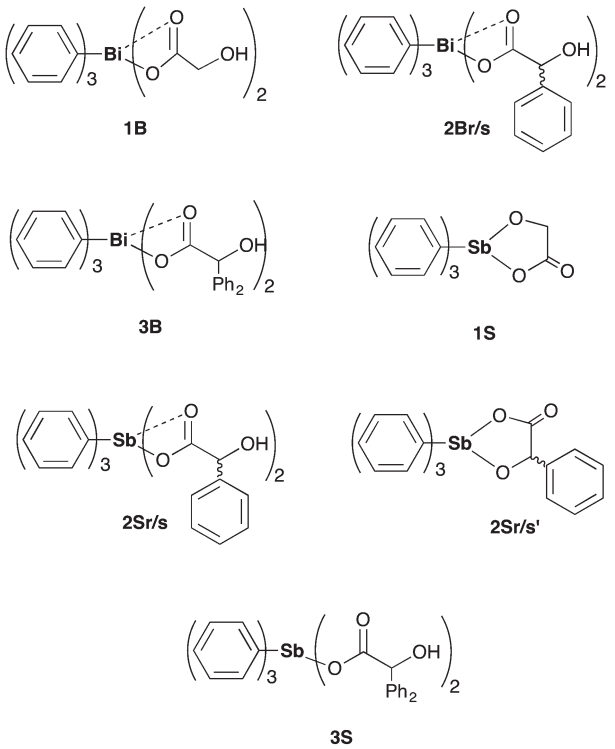

Fig. 2 Composition of the Bi(V); **1B–3B**, and Sb(V); **1S**, **2Sr/s**, **2Sr/s′**, **3S**, complexes.

Results and discussion

Synthesis and characterisation

Bismuth complexes $[BiPh_3(GlyH)_2]$, **1B**, $[BiPh_3(ManH)_2]$, **2Br**/**2Bs**, $[BiPh_3(BenzH)_2]$, **3B**, and antimony complexes [$SbPh_3Gly$], **1S**, $[SbPh_3(ManH)_2]$, **2Sr**/**2Ss**, and $[SbPh_3(BenzH)_2]$, **3S**, were synthesised *via* an oxidative addition reaction in which MPh_3 (M = Sb or Bi) was treated with two equivalent of *t*-BuOOH followed by two equivalents of the chosen α-hydroxy carboxylic acid (Scheme 1).[23] The *t*-BuOOH oxidises the metal from the +III to +V state in forming $[MPh_3(OH)_2]$ and subsequently

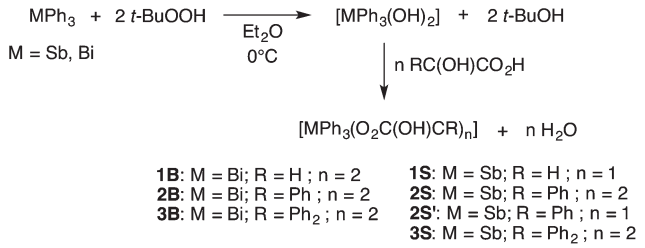

Scheme 1 Oxidative addition pathway for the synthesis of Sb(v) and Bi(v) complexes.

undergoes a condensation reaction on treatment with the acid to give the target complex, $[MPh_3(O_2C(OH)CHR)_2]$.[24] The by-products, H_2O and *t*-BuOH, are easily removed under vacuum. The resultant solid was crystallised from hot solvent and the resulting crystals collected by filtration and washed with cold diethyl ether to remove any excess acid and/or MPh_3.[25] Moderate to good yields were obtained without the need for further purification. Crystals of **1S** when grown from DMSO solution incorporate a single molecule of DMSO as a co-ligand on the Sb centre and so is more properly represented as [**1S·DMSO**]. These crystals have a melting point (161–162 °C) lower than the microcrystalline solid **1S** obtained from toluene (191–192 °C).

When **2Sr** and **2Ss** were dissolved in polar solvents a proton shift occurred liberating one molecule of mandelic acid while simultaneously forming the cyclometallate complex [$SbPh_3$(*R*, *S*-Man)].

This mono-substituted complex has been isolated previously by Barucki *et al.* through a salt metathesis route involving the silver salt of mandelic acid and $SbPh_3Cl_2$. They reported that this mono-substituted form could not be an intermediate to the di-ester as an excess of silver salt failed to produce the di-substituted mandelate.[22] Through the oxidative addition route in toluene, the di-substituted form was able to be isolated as a pure crystalline compound. Though stable in the solid-state, as confirmed by elemental analysis, the complex readily undergoes cyclometallation to the mono-substituted chelate form in solution. Presumably water mediates the dissociative and protonation sequence resulting in the formation of the mono-substituted cyclometallate. This rearrangement of complex **2Sr** and **2Ss** to complex **2Sr′** and **2Ss′** is both thermodynamically and entropically favourable (Fig. 3).[26,27]

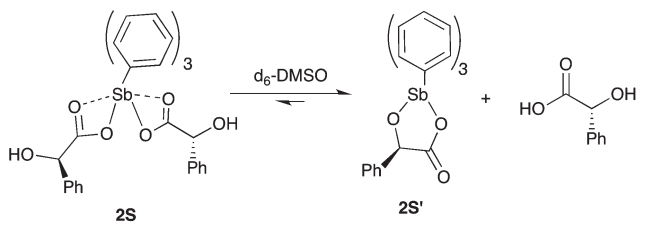

Fig. 3 Cyclometallation of complex **2S** to complex **2S′** in d_6-DMSO.

The novel complexes **1B**, **1S**, **2Sr** and **2Ss** were characterised by ^{1}H NMR, ^{13}C NMR, FT-IR spectroscopy, melting point, mass spectrometry, and elemental analysis. Solid-state structure of complexes **2Br**, **2Bs**, **2Sr** and **2Ss** were obtained through X-ray diffraction.

The composition of the previously described complexes **2Br**, **2Bs**, **2Sr′**, **2Ss′**, **3B** and **3S** were confirmed by their characteristic ^{1}H NMR and ^{13}C NMR spectra and where appropriate, unit cell analysis.[20] Full analytical details on each complex is given in the Experimental section.

^{1}H and ^{13}C NMR spectroscopy was conducted on all complexes in both d_6-DMSO and $CDCl_3$ solutions. Complexation of the carboxylate to the metal centre was indicated by the absence of the carboxylic O*H* signal of the parent acid normally found between 12.14 ppm and 12.52 ppm, but only in d_6-DMSO as this proton in the acid itself was not observed in $CDCl_3$. Complex formation was also accompanied by a general shift to higher frequency of the *o*-, *m*-, and *p*-H signals of the M*Ph* groups in contrast to those of MPh_3. This is consistent with proton shifts observed in the ^{1}H NMR spectra of previously synthesised triaryl carboxylato complexes of Sb(v) and Bi(v).[19,25]

When attempting to obtain the ^{1}H NMR of the di-substituted complexes **2Sr** and **2Ss** in d_6-DMSO it was found that cyclometallation occurred, liberating free mandelic acid and the mono-substituted complex previously reported.[22] The cyclometallate was isolated by extraction from DMSO with water, when analysed *via* ^{1}H and ^{13}C NMR it was found to be the pure mono-substituted complexes **2Sr′** and **2Ss′**. Similar to complex **1S**, a molecule of DMSO was found to be coordinating to the complex. The ^{1}H NMR analysis of the di-substituted complexes was analysed using a dry deuterated solvent (C_6D_6). No free mandelate was observed however the signals appeared as broad multiplets with no clear splitting. Though definitive ^{1}H NMR analysis was difficult to obtain on the complex, elemental confirmed di-substitution of the bulk sample for both **2Sr** and **2Ss**.

In the FT-IR spectra of all complexes a shift in the wavenumber of the carboxylic acid carbonyl was observed for each complex from the parent acid range of 1705–1715 cm^{-1}. Each shifted to a lower wavenumber, corresponding to both the asymmetric and symmetric carboxylate carbonyl stretches within the ranges of 1556–1690 and 1432–1557 cm^{-1} respectively. This is indicative of deprotonation of the carboxylic acid and subsequent binding to the metal centre through a carboxylate anion forming the $[MPh_3(O_2CC(OH)R)_2]$ or $[MPh_3(O_2CC(O)R)]$ complexes. For the Sb complexes **2S** and **3S**, the difference in the asymmetric and symmetric stretches were found to be greater than 200 cm^{-1}, with the opposite effect seen for the analogous Bi complexes. **1B** and **2B**. According to Deacon and Phillips, a difference of greater than 200 cm^{-1} is indicative of monodentate binding, whereas a difference less than 200 cm^{-1} is attributed to bidentate binding of the carboxylic acid functionality to the metal centre.[28] This trend was further observed by analysis of the solid state structures of the novel complexes **1S**, **1B**, **2Sr**, **2Ss**. For the previously synthesised complexes **2Br**,

2Bs, **3S** and **3B**, a similar binding mode was also observed.[20,21] For complexes **1S** and **2S′** the binding occurs through the carboxyl hydroxyl and α-hydroxyl giving a bidentate chelation mode, however in terms of the carboxylate it is monodentate as coordinate interactions with the carbonyl oxygen are not observed, this is supported by the IR data. A summary of the shifts in wavelengths is given in the ESI.†

Mass spectral studies were also conducted in DMSO as further confirmation of complex formation. As DMSO was the solvent of choice it can be assumed the complexes **2Sr** and **2Ss** are found as the previously characterised **2Sr′** and **2Ss′**, nevertheless the mass spectral data was included in the Experimental section. Typical ion peaks corresponding to the metal were observed for the bismuth complexes (Bi, 208.9), along with the $[MPh_2^+ + 6H_2O]^+$ fragments for complexes **1S**, **2Sr′**, **2Ss′**, **1B** and the previously synthesised **2Br** and **2Bs** [Bi (471.0) Sb (382.9)]. The high water content in DMSO can be attributed to the presence of the hydrated metal fragment. The mandelate ligand was observed in the ESI^- for both **2Sr′** and **2B**, as $[LH - H]^-$ with a fragment mass of 150.9. For the novel complex **1B**, a peak at 515.0 in the ESI^+ was observed to be the fragment $[BiPh_3L]^+$. Further mass spectral data is given in the Experimental section.

X-ray crystallography

The four novel complexes, $[Sb(Ph)_3Gly]$ **1S**, $[Bi(Ph)_3(GlyH)_2]$ **1B**, $[Sb(Ph)_3(R\text{-ManH})_2]$ **2Sr**, and $[Sb(Ph)_3(S\text{-ManH})_2]$ **2Ss**, and the previously characterised **2Br** and **2Bs**, were able to undergo analysis *via* single crystal X-ray diffraction. Unfortunately for complexes **1S** and **1B** a recurring problem of twinning was observed despite multiple X-ray data collection of separate crystalline samples. Due to the twinning of the complexes, pertinent bond angles and lengths cannot be discussed in detail. The connectivity of each complex could however be established, the structures can be found in the ESI.† Representative complexes **2Sr** and **2Br** were found to be analogous in terms of molecular geometry. A discussion of both complexes is provided. The *S*-enantiomers **2Bs** and **2Ss** were analogous in structure and so were not discussed. Crystals suitable for analysis were obtained for both complexes by slow evaporation of toluene. Both complexes adopt a trigonal bipyramidal geometry, with a greater degree of distortion observed in the bismuth analogue in contrast to the antimony complex. The only major difference between the complexes observed was found to be the chelation mode of the carboxylate functionality of the mandelate (Fig. 4 and 5). The carboxylates were found to occupy the axial plane, with the phenyl groups found in the equatorial plane. This structural configuration has been commonly observed in Sb(v) and Bi(v) tri-aryl complexes.[15,19,25] The M–C bond lengths for both complexes are similar to those observed in previously synthesised complexes of the general formula $[MPh_3(O_2CR)_2]$.

The bond M–C bond lengths observed in **2Br**, were found to be; Bi(1)–C(1) 2.200(4) Å, Bi(1)–C(7) 2.203(5) Å, Bi(1)–C(13) 2.213(5) Å. Ong *et al.* reported complexes of the general formula $[BiPh_3(O_2CR)_2]$ to share a similar range of Bi–C bond lengths, ranging from 2.177(4) Å–2.210(6) Å, and giving an overall average length of 2.196 Å.[19] Due to proximity effects from the carbonyl functionality, a bidentate binding mode of the mandelate was observed, pushing the coordination number of the bismuth centre from five to seven which can be

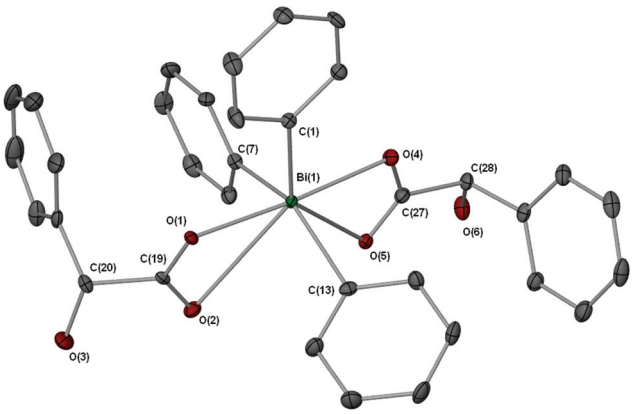

Fig. 4 Molecular structure of $[BiPh_3(R\text{-ManH})_2]$ **2Br** showing thermal ellipsoids at 40% probability. Hydrogen atoms have been omitted for clarity. Selected bond lengths (Å) and angles (°). Bi(1)–C(1), 2.200(4); Bi(1)–C(7), 2.203(5); Bi(1)–C(13), 2.213(5); Bi(1)–O(1), 2.284(3); Bi(1)–O(4), 2.327(3); Bi(1)–O(5), 2.806(3); Bi(1)–O(2), 3.040(4); C(1)–Bi(1)–C(7), 104.51(18); C(7)–Bi(1)–C(13), 145.35(17); C(1)–Bi(1)–O(1), 87.60(15); C(13)–Bi(1)–O(1), 93.75(14); C(7)Bi(1)–O(4), 90.57(15); O(1)–Bi(1)–O(4), 176.31(12); O(1)–Bi(1)–O(5), 132.06(10); O(4)–Bi(1)–O(5), 50.50(11).

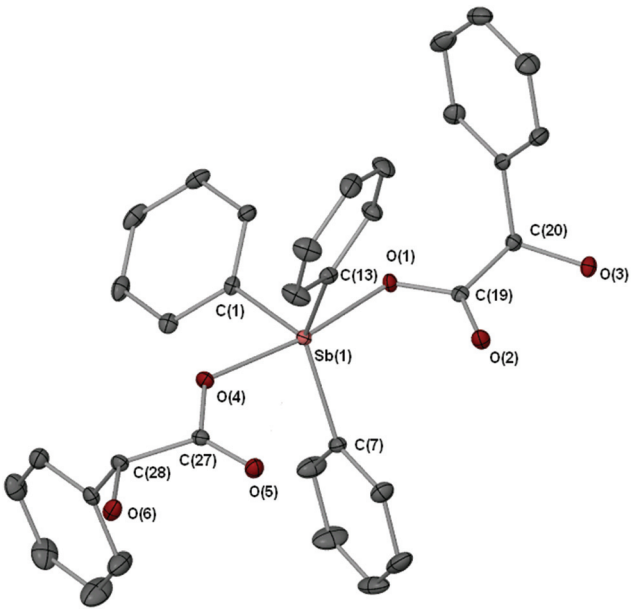

Fig. 5 Molecular structure of $[Sb(Ph)_3(R\text{-ManH})_2]$ **2Sr** showing thermal ellipsoids at 40% probability. Hydrogen atoms have been omitted for clarity. Selected bond lengths (Å) and angles (°). Sb(1)–C(1), 2.094(2); Sb(1)–C(7), 2.103(2); Sb(1)–O(4), 2.1036(16); Sb(1)–O(1), 2.1077(17); Sb(1)–C(13), 2.112(2); C(1)–Sb(1)–C(7), 111.94(9); C(1)–Sb(1)–O(4), 85.00(8); C(7)–Sb(1)–O(4), 92.06(8); O(4)–Sb(1)–O(1), 169.73(7); C(7)–Sb(1)–C(13), 131.94(10); O(4)–Sb(1)–C(13), 91.28(9).

said to give an overall pentagonal bipyramidal geometry. The average bond length observed for the Bi(1)–O(1), Bi(1)–O(4) (2.301(3) Å) suggests they are covalent in character and the direct result of deprotonation of the carboxylic hydroxyl. Coordinate bonding interactions between Bi(1)–O(2) and Bi(1)–O(5) were then characterised by their increased bond lengths of 3.040(4) Å and 2.804(3) Å respectively. A similar set of lengths were observed by Egorova *et al.*, with the average Bi–O covalent and coordinate bond lengths of 2.303 Å and 2.892 Å respectively. A coordination geometry of seven was also observed in complexes synthesised by Egorova *et al.* and Ong *et al.*[19,29] This was further confirmed by the $\Delta\nu$ observed in the IR spectrum. The bidentate coordination of the carboxylic functionality causes distortion of the trigonal angles in complex **2Br**, as observed by the deviation of the ideal bond angle of 120° in the equatorial plane to 145.35(17)°, 110.14(18)° and 104.51(18)° for C(7)–Bi(1)–C(13), C(1)–Bi(1)–C(13) and C(1)–Bi(1)–C(7) respectively. This deviation of the bond angles may be attributed to the *cis* conformation of the acetate ligands around the central Bi(v) atom and can be said to push the geometry towards a pentagonal square pyramidal configuration. **1B** was found to be similar to complexes previously synthesised by Ali *et al.*, with an overall coordination number of five observed, giving a trigonal bipyramidal conformation.[15] **1B** was found to have formally monodentate carboxylate functionalities in contrast to the bidenate binding observed in the analogous **2Br**.

This monodentate binding mode was further supported by the IR spectrum. The average bond length between Sb–O covalent interactions in **1B**, were found to be shorter than those observed in **2Br**, 2.103(16) Å and 2.327(3) Å respectively. This was expected due to the higher bond energy associated with the Sb–O bond.[30] Though IR data suggests monodentate binding of the carboxylate, the oxygens may potentially exhibit long, weak coordinate bonding interactions. Distortion toward a square pyramidal geometry is observed due to a widening of the trigonal angle of C(7)–Sb(1)–C(13) to 131.94°. This distortion could therefore allow coordinate interactions to occur. A major difference was observed in the solid state structures of **1S** and **2Sr**, with **1S** found to encompass one doubly-deprotonated glycolate dianion around its centre as opposed to **2Sr** which was found to have two monoanionic glycolate ligands and share a similar suggested geometry to **2Br**. The glycolate in **1S** was found to have deprotonated at the carboxylate hydroxyl (O(2)) and the alpha hydroxyl (O(1)) before chelation to the antimony centre. A solvent molecule (DMSO) was also found to be interacting with the centre, pushing the coordination number from five to six, suggesting a distorted octahedral geometry. This geometry has been observed in previously synthesised complexes of the structurally related Sb(v) triaryl hydroximates I.[31]

Stability studies

In order to assess the viability of the complexes for antiparasitic activity the stability of the compounds in the solution and solid state was studied. All complexes were exposed to atmospheric conditions and screened *via* melting point over a period of eight months, yielding no change. This is indicative of a high degree of stability in the solid-state. Assessment of solution stability was conducted by comparing ^{1}H NMR spectra taken in deuterated solvents over a set time period. Each complex was dissolved in either d_6-DMSO or $CDCl_3$ and the ^{1}H NMR spectrum taken at t = 0 and 48 h. There was no observable change in the chemical shifts of complexes **1S**, **2Sr′**, **2Ss′**, **3S**, **1B**, **2Br**, **2Bs** and **3B**, supporting high stability in the solution state. As complexes **2Sr** and **2Ss** undergo proton shifting to the cyclometallate form they can be assumed to be unstable in DMSO.

Our previous studies have shown that $[BiAr_3(LH)_2]$ (Ar = Ph, Tol) complexes can be stable in water and DMSO but will decompose readily when in DMEM culture medium, resulting in reduction of the Bi(v) complex and liberation of the reduced $BiAr_3$ species.[25] This decomposition normally occurs over a period of several hours, and though the exact mechanism by which it occurs is still unknown the Bi(v) complexes are able to exert a strong toxic effect on the parasite within that short timeframe.

In consideration of this, the rate of decomposition of complexes **1B–3B**, **1S**, **2Sr′**, **2Ss′**, **3S** in culture medium was determined by collecting ^{1}H NMR data on the complexes (50 μM) dissolved in DMEM (1 mL) every 60 minutes. The culture medium was initially freeze dried and resuspended in D_2O to minimise the signal from H_2O prior to the study. The integration ratio of an unchanging signal from the culture medium against the *ortho* protons of the complexes was then compared every hour for upwards of 50 h. An unchanging signal in the culture media at 5.07 ppm for the representative mandelate complex **2Br** was selected due to the overlap of the aromatic signals of the complex with the culture media. For **1B** the unchanging culture media signal at 7.01 ppm was used as it was clear of any overlap.

In contrast to our previous study on the decomposition of $[Bi(o\text{-Tol})_3(dif)_2]$, which exhibited a one-phase exponential decay with a half-life of 1.2 h.[25] complexes **1B** and **2Br** were found to be significantly more stable and exhibited a linear decomposition (R^2 = 0.9986 and 0.9990 respectively) over many hours, shown in Fig. 6. It is not yet known why these α-hydroxy carboxylato complexes exhibit such an increased stability in the culture medium. The decay graph of **2Br** is given below as a representation of the stability. The graph of **1B** can be found in the ESI.†

Our previous study on $[Bi(o\text{-Tol})_3(dif)_2]$ seemingly ruled out reactions with other anions (incl. phosphate) and the various amino acids in the culture medium. One contributing factor could be glucose, which is present in high concentration. However, a separate NMR study on the interaction of $[Bi(m\text{-Tol})_3(asp)_2]$ (where asp = aspirin) with glucose showed a reduction of the Bi(v) species but only slowly and over the period of a week, substantially longer than the calculated half-life in culture medium.[25] Our attempts to fully understand this process are ongoing.

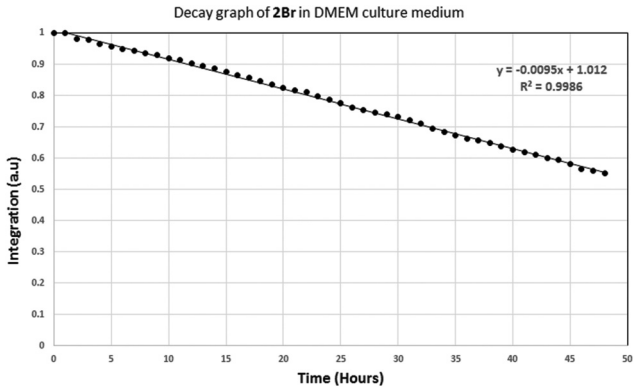

Fig. 6 Decomposition curve of $[BiPh_3(ManH)_2]$, **2Br**, in DMEM culture media at 25 °C *vs.* time.

Biological activity

Complexes **1S–3S** and **1B–3B** were assessed for their activity against *L. major* and for toxicity towards human primary fibroblast cells. We have previously tested both the parent α-hydroxy carboxylic acids and MPh_3 against both cell types and reported that no toxicity is observed at concentrations of ≤100 μM for human primary fibroblasts and *L. major* promastigotes, and upwards of 50 μM for bone-marrow derived macrophages and *L. major* amastigotes.[15,32] DMSO and amphotericin B (AmpB) were also tested as the reference anti-leishmanial agents under the same set of experimental conditions.

Cell viability assay. Each complex underwent a duplicate biological assay with the parasitic strain *L. major* v121 and human primary fibroblasts. The antimony complexes showed a high degree of solubility in the culture media, however the bismuth analogues, though soluble in DMSO, often formed opaque solutions upon injection into the media. Having complete solubility of the complexes in the culture medium is important in accurately determining the minimum inhibitory concentration (MIC) of a particular complex, and the observed cloudiness, which presumably is slow precipitation in a high water content environment, thus made it difficult to determine the exact concentration at which the bismuth complexes exhibited activity. Nevertheless, they did show significant activity and at least provided data that allows a comparison with the Sb(v) complexes (Fig. 7).

It should be noted that for complexes **2Sr** and **2Ss** the form assayed would most likely be that of the mono-substituted **2Sr′** and **2Ss′** as the complexes are first dissolved into DMSO.

All eight complexes exhibited moderate activity towards the parasite with IC_{50} values from a range of 3.58 μM–20.7 μM observed. The bismuth complexes in particular showed the highest potential toxicity (IC_{50} range 3.58–6.33 μM), with the lowest IC_{50} observed for the *S*-mandelate complex **2Bs**. Unfortunately, all four of the bismuth complexes were found to be non-selectively toxic at significant levels to human fibroblasts, IC_{50} range 5.83 μM–7.01 μM (Fig. 8). The antimony complexes were found not only to be toxic to the parasite (IC_{50} 12.5–20.7 μM) but selectively toxic, showing little to no activity towards fibroblasts at concentrations ranging from 72.8–≥100 μM (Fig. 8). We have observed a similar trend with Sb(v) carboxylate complexes exhibiting a high degree of selectivity and the bismuth counterparts presenting with a lower degree of selectivity.[15,19] With selectivity indices of over 30 for complexes **1S**, **2Sr′**, **2Ss′** and **3S**, further studies on the *in vivo* activity against the clinically relevant amastigote form of the complex were then assessed. For complexes **1B–3B**, a low selectivity index and troubles with solubility disqualify the need for further testing. Individual graphs of each complex against both fibroblast and *L. major* promastigotes is given in Fig. 8 below, IC_{50} value are also listed.

Amastigote invasion assay. Due to the high selectivity of the antimony complexes further an assay was conducted on amastigotes, the more clinically relevant form of the parasite. Bone-marrow derived macrophages were infected with *L. major* pro-

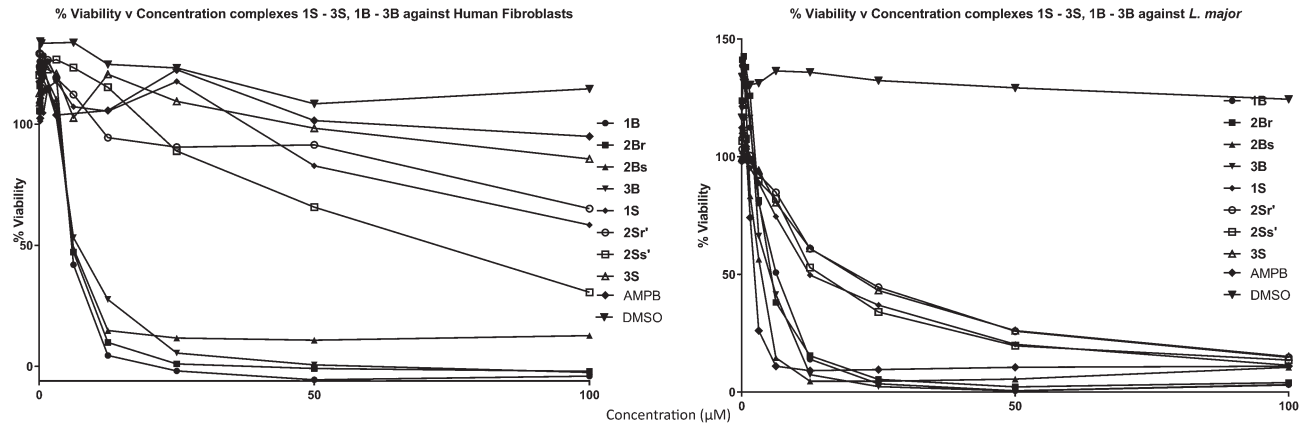

Fig. 7 Comparison of %cell viability of complexes **1S**, **2Sr′**, **2Ss′**, **3S**, **1B–3B**, against *L. major* promastigotes and human primary fibroblasts. Dose response curves were generated over a range of concentrations (48 nm–100 μM) in the appropriate culture media from 10 mM DMSO stock solutions. All readings were compared spectroscopically to non-treated control and the percent growth inhibition calculated. A DMSO control and positive drug control (Amp B) were also included at the same range of concentrations.

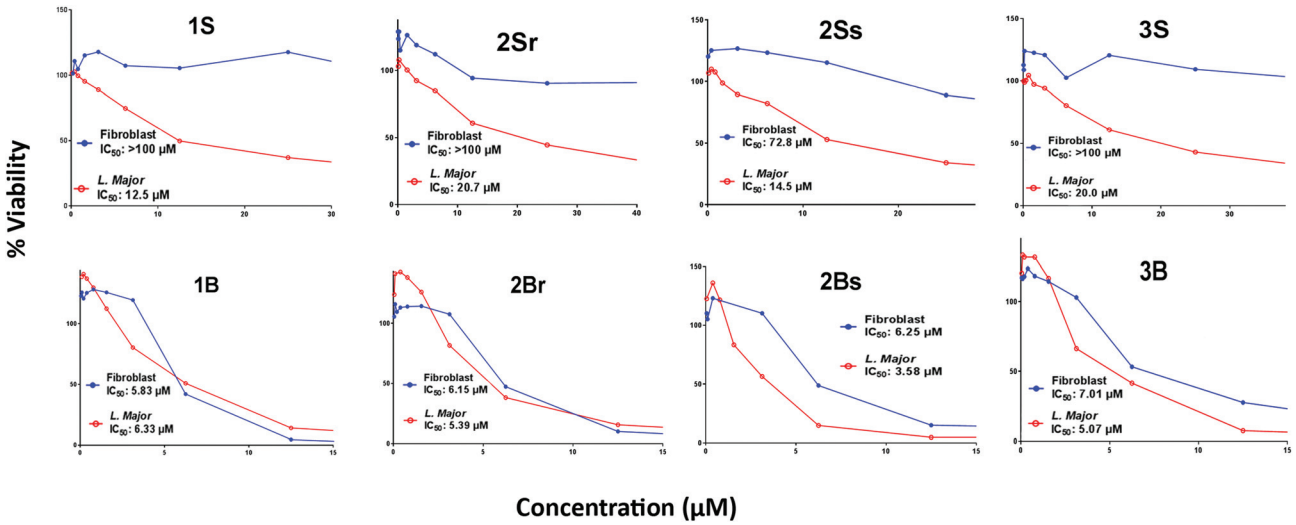

Fig. 8 Individual activity of complexes **1S**, **2Sr′**, **2Ss′**, **3S**, **1B–3B** after 48 hours incubation, with IC50 values listed for both *L. major* promastigotes and human primary fibroblasts. Dose response curves were generated over a range of concentrations (48 nm–100 μM) in the appropriate culture media from 10 mM DMSO stock solutions.

mastigotes and incubated for 48 h. After differentiation into amastigotes, the cells were washed and incubated for a further 48 h with 10 μM concentrations of the complexes **1S–3S**. Biologically the environment of a macrophages is much more demanding than that of a primary fibroblast, which can have a drastic effect on the complexes activity. To enter the macrophage the complexes have to traverse two membranes and still retain biological activity in the acidic environment of phagolysosomes.[25] All four compounds exhibited activity against the *L. major* amastigotes at statistically significant different levels when compared to the positive control (Fig. 9). Surprisingly the two cyclometallate mandelate complexes showed the highest activity with % infected cells of 21 ± 0.72 for the *R*-enantiomer and 9.5 ± 0.50 for the *S*. The *R*-enantiomer, **2Sr′**, was found to exhibit the highest IC_{50} value for *L. major* promastigotes of 20.7 μM, this suggest that the activity of the complexes cannot be accurately assessed on promastigotes assays alone.[33] It is unknown as to why the *S*-enantiomer is the more biologically active, though it may elude to the effects of chirality. Good activity towards promastigotes doesn't reflected the potential activity against the clinically relevant amastigote form. The di-substituted benzilate complexes showed the least activity giving a % infection of 30 ± 1.3. Though significant activity was observed for all four complexes, none exhibited greater activity in comparison to the drug control amphotericin B (% infected 4.3). The complexes were also found to be less biologically active when compared to the previously synthesised Sb(v) carboxylate complexes, several of which yielded nearly 0% observable infection at 10 μM.[15] However as the complexes are selectivity toxic they may still yet have potential as anti-leishmanial drug candidates. As the cell viability of the human fibroblasts was found to be 72.8–100 μM, it may be viable to increase the concentration of the complexes to 15–20 μM to see if any significant difference in infection occurs at slightly higher concentrations.

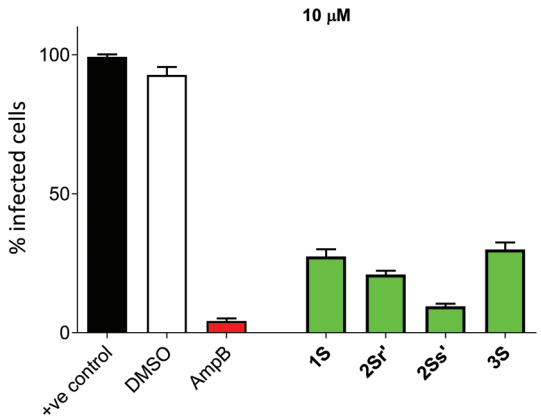

Fig. 9 Infected macrophages after 48 hours. Number of infected macrophage was determined microscopically, in duplicate of fixed specimens. Amphotericin B (AmpB) was used as a positive control at 10 μM concentration. A DMSO control was also employed at a 1% concentration. Error bas indicate SEM, one-way ANOVA. Dunnett's multiple comparison test was used to determine the statistical significance between all test compounds and a positive control lacking treatment (+ve control).

Conclusions

Eight α-hydroxy carboxylate complexes of bismuth and antimony have been successfully synthesised by a one-pot oxidative addition reaction, four of which are novel. Each complex, **1S**, [$SbPh_3Gly$], **1B**, [$BiPh_3(GlyH)_2$], **2Sr**, [$SbPh_3$(*R*-$ManH)_2$] **2Ss**, [$SbPh_3$(*S*-$ManH)_2$], **2Br**, [$BiPh_3$(*R*-$ManH)_2$] **2Bs**, [$BiPh_3$(*S*-$ManH)_2$] **3S**, [$SbPh_3(BenzH)_2$], **3B**, [$BiPh_3(BenzH)_2$] and the cyclometallate complexes **2Sr′**, [$SbPh_3$(*R*-Man)], and

2Ss′, [$SbPh_3$(*S*-Man)], was fully characterised by a range of techniques. Differences in the binding mode of the $GlyH_2$ and $ManH_2$ moiety was observed by the calculated $\Delta\nu$ of each complex and further supported by the solid-state structures. The bismuth complexes **1B–3B** were found to support a bidentate chelation mode of the carbonyl functionality of the carboxylate ligands. The antimony complex **1S** incorporated one doubly-deprotonated glycolate ligand forming a more stable five membered chelate ring. A solvent molecule was also found to be coordinating in the solid-state structure. The antimony complex **2S** was found to exhibit proton shifting behaviour in DMSO as described by the ^{1}H NMR in d_6-DMSO, incorporating a doubly-deprotonated mandelate ligand, while retaining bis-substitution in the solid state when grown from toluene. Complex **2S′** was successfully isolated as a pure derivative of complex **2S** from aqueous extraction from DMSO. The bismuth complexes were found to adopt the typical trigonal bipyramidal geometry common for substituted triaryl Bi(v) complexes. All complexes were assessed for their anti-parasitic activity against *L. major* promastigotes and toxicity towards human fibroblast cells. The four bismuth complexes were found to be non-selectively toxic towards human fibroblast. This degree of toxicity and problems with solubility disqualified them from further testing. In contrast, the three antimony complexes were found to have excellent selectivity with IC_{50} values of $\geq$100 μM observed for human fibroblasts. Macrophage invasion assays performed on the four antimony complexes at 10 μM yielded viable results, with each complex exhibiting some degree of activity against the amastigotes with % infection values ranging from 9.5 ± 0.5–30 ± 1.3. Though not as effective as previously synthesised Sb(v) triaryl carboxlyates, the compounds still exhibited clinically relevant activity, whilst remaining non-toxic toward mammalian cells. Therefore, it is concluded the high selectivity of the Sb(v) complexes make them much more viable candidates for further *in vivo* studies in contrast to their Bi(v) counterparts.

Experimental section

Both $BiPh_3$ and $SbPh_3$ were synthesised according to literature procedures.[34] High purity MPh_3 were obtained from recrystallisation from hot ethanol. All α-hydroxy acids were purchased from Sigma-Aldrich or Alfa Aesar, without the need for further purification. All remaining reagents and solvents were purchased from Sigma-Aldrich and Merck. Dried solvents were obtained from a MBruan-SPS-800 and stored over molecular sieves (4 Å) under a dry nitrogen atmosphere. All reactions requiring anhydrous conditions were performed with oven-dried glassware under an inert atmosphere of nitrogen, utilising a Schlenk manifold. ^{1}H NMR and ^{13}C NMR spectra were recorded on a Bruker Avance DRX400 spectrometer (400 MHz) with the chemical shifts referenced to the appropriate deuterated solvent (d_6-DMSO or $CDCl_3$). Multiplicities are denoted as singlet (s), doublet (d), triplet (t), multiplet (m) and broad (b), or a combination where necessary. Melting points were analysed in open end capillary tubes on a digital Stuart Scientific melting point apparatus SMP10. Infrared Spectra were recorded on an Agilent Technologies Cary 630 FTIR spectrometer, using a range of 4000–500 cm^{-1}. Mass spectrometry (ESI) was obtained utilising a Micromass Platform QMS spectrometer, with an electrospray source and a cone voltage of 35 eV. CHS elemental analysis (EA) was obtained from The Campbell Microanalytical Laboratory, Department of Chemistry, University of Otago, Dunedin New Zealand.

Biological assays

Cell culture. *Leishmania major* virulent clone v121 was derived from the LRC-L137 *L. major* isolate and maintained at 26 °C in supplement M199 media (10% (v/v) heat inactivated FBS, 1% pen–strep), purchased from Gibco ™. Human primary fibroblasts were cultured and maintained in Dulbecco's Modified Eagles Medium (DMEM) supplemented with 10% FBS and 1% pen–strep (purchased from Gibco ™) at 37 °C in a 5% CO_2 incubator.[19]

***In vitro* testing of *L. major* and human fibroblasts.** Celltiter Blue Cell Viability Assay was purchased from Promega™, and used for the determination of percentage viability of the parasite and human fibroblasts. Compounds **1S–3S** and **1B–3B** were dissolved in DMSO to make up a 10 mM working stock and sequentially diluted out in the appropriate culture media (100 μM to 48 nM). Assays were set up in duplicate in 96-well Falcon plates. Volumes of 10^6 promastigotes per mL and 10^5 fibrolasts per mL were used. Cell viability for human fibroblasts was measured spectroscopically at 550 nm.[35] Cell titre Blue dye was added to the samples at $T = 0$, and subsequently subtracted from all readings at 600 nm as background interference. *L. Major* assay viability was measured spectroscopically using fluorescence excitation at 544 nm and emission at 590. The compounds were compared to a negative control of no drug and the percent inhibition calculated.[36] All absorbance plate readings were conducted on a BMG-Labtech Spectrostar Nano UV-Vis microplate reader. Fluorescence measurements were conducted on a BMG-Labtech FluoStar Omega microplate reader.

Macrophage invasion assays were performed as previously described.[15,37] Briefly, bone marrow-derived mouse macrophages were plated onto coverslips in a 24 well plate and allowed to adhere for 48 h. The cells were exposed to *L. major* promastigotes at a 1 : 10 ratio and incubated for a further 48 h to allow for amastigote formation *in vitro*. The slides were then washed to remove any excess promastigotes and exposed to compounds for 48 h before washing and fixation with methanol. Following Giemsa staining, the cells were then counted microscopically and the percentage of infected cells analysed.

Synthesis and characterisation

General procedure, GP. MPh_3 and α-hydroxy acid (1 : 2 or 1 : 1) were dissolved in 10 mL of diethyl ether or toluene at 0 °C and stirred. An excess of 2.2 equivalents of *t*-BuOOH was added and the mixture stirred for approximately one hour.[23] The mixtures were left to stand for 24–48 h before the com-

pounds were obtained. The compounds either crystallised straight from the ether filtrate, or required crystallisation in hot solvent.

Synthesis of triphenylantimony mono(glycolate), 1S. $SbPh_3$ (0.176 g, 0.5 mmol), glycolic acid (0.038 g, 0.5 mmol) and 70% *t*-BuOOH (150 μL, 1.1 mmol) were reacted in diethyl ether as per **GP**. Yield: 82% [(microcrystalline, no solvent coordinated) (0.176 g, 0.82 mmol)]; m.p.: 191–192 °C, **1S**, 161–162 °C, **1S·DMSO**; solubility: hot THF, DMSO, chloroform. ^{1}H NMR (400 MHz, $(CD_3)_2SO$, 25 °C): δ = 7.54 (6H, m, *o*-CH_{ar}) 7.43 (6H, m, *m*-CH_{ar}) 7.41 (3H, m, *p*-CH_{ar}) 4.07 (2H, s, CH_2) 2.55 (6H, s, DMSO); ^{13}C{^{1}H} NMR (100 MHz, $CDCl_3$, 25 °C): 174.2 (*C*OO), 142.9 (Sb*C*), 134.0 (*o*-*C*H$_{ar}$), 129.6 (*m*-*C*H$_{ar}$), 128.5 (*p*-*C*H$_{ar}$), 62.3 (*C*H$_2$), 40.3 (DMSO). IR [cm^{-1}]: 3045 (w), 2993 (w), 2883 (w), 2837 (w), 2091 (w), 1690 (s), 1577 (w), 1478 (m), 1428 (s), 1333 (m), 1293 (b), 1183 (w), 1072 (s), 1036 (w), 1020 (w), 987 (s), 928 (sh), 729 (sh), 693 (sh), 659 (m). MS (ESI)$^+$ *m*/*z* = 382.9 [$SbPh_2$ + $6H_2O$]$^+$, 424.3 [$SbPh_3$ + $4H_2O$], 464.2 [$SbPh_2L$ + $2H_2O$]$^+$; (ESI)$^-$ *m*/*z* = 444.5 [$SbPh_3L$ − H_2O]$^-$; $C_{22}H_{23}O_4SSb$ (504.04) calculated: %C 52.30, %H 4.59, %S 6.35, found: %C 52.30, %H 4.60, %S6.27.

Synthesis of triphenylbismuth bis(glycolate), 1B. $BiPh_3$ (0.220 g, 0.5 mmol), glycolic acid (0.076 g, 1.0 mmol) and 70% *t*-BuOOH (150 μL, 1.1 mmol) were in diethyl ether reacted as per **GP**. Yield: 61% (0.184 g, 0.30 mmol); m.p.: 182–184 °C; ^{1}H NMR (400 MHz, $CDCl_3$, 25 °C): δ = 8.12 (6H, d, ^3J = 8.6 Hz, *o*-CH_{ar}), 7.64 (6H, t, ^3J = 7.6 Hz, *m*-C-H_{ar}), 7.18 (3H, t, ^3J = 7.4 Hz, *p*-C-H_{ar}), 3.86 (4H, s, CH_2), 2.41 (2H, s, O*H*); ^{13}C{^{1}H} NMR (100 MHz, $CDCl_3$, 25 °C): δ = 178.2 (*C*OO), 158.7 (Bi*C*), 134.2 (*o*-*C*H$_{ar}$), 131.8 (*m*-*C*H$_{ar}$), 131.6 (*p*-*C*H$_{ar}$), 61.7 (*C*H$_2$). IR [cm^{-1}]: 3487 (b), 3093 (w), 3050 (w), 2889 (w), 2107 (w), 1602 (s), 1586 (s), 1558 (s), 1468 (s), 1432 (s), 1408 (m), 1320 (b), 1289 (b), 1174 (m), 1081 (sh), 1010 (sh), 984 (sh), 921 (s), 726 (sh), 678 (sh). MS (ESI)$^+$ *m*/*z* = 152.1 [BiPh + H_2O]$^{2+}$, 208.9 [Bi], 363.0 [$BiPh_2$]$^+$, 471.0 [$BiPh_2$ + $6H_2O$]$^+$, 515.0 [$BiPh_3L$]; (ESI)$^-$ *m*/*z* = 437.0 [$BiPh_2L$ − H]$^-$, 513.0 [$BiPh_3L$ − H], 589.0 [$BiPh_3LL$ − H]$^-$; $C_{22}H_{21}BiO_6$ (590.11) calculated: %C 44.76, %H 3.59, found: %C 44.83, %H 3.61.

Synthesis of triphenylantimony bis(*R*-mandelate), 2Sr. $SbPh_3$ (0.353 g, 1.0 mmol), mandelic acid (0.306 g, 2.0 mmol) and 70% *t*-BuOOH (300 μL, 2.2 mmol) were reacted in toluene as per **GP**. **2S**: Yield: 71% (0.466 g, 0.71 mmol); m.p.: 151–152 °C; **2S**: FT-IR [cm^{-1}]: 3405 (m), 3060 (w), 3209 (w), 2924 (w), 1663 (sh), 1577 (w), 1481 (m), 1438 (m), 1404 (w), 1304 (sh), 1257 (w), 1228 (m), 1181 (s), 1089 (sh), 1071 (s), 996 (m), 858 (w), 785 (w), 733 (sh), 687 (sh). $C_{34}H_{29}SbO_6$ (655.31) calculated: %C 62.31, %H 4.46, found: %C 62.21, %H 4.60; CCDC 1578596.†

Synthesis of triphenylantimony bis(*S*-mandelate), 2Ss. $SbPh_3$ (0.353 g, 1.0 mmol), mandelic acid (0.306 g, 2.0 mmol) and 70% *t*-BuOOH (300 μL, 2.2 mmol) were reacted in toluene as per **GP**. **2S**: Yield: 81% (0.531 g, 0.81 mmol); m.p.: 151–152 °C; **2S**: FT-IR [cm^{-1}]: 3405 (m), 3060 (w), 3209 (w), 2924 (w), 1663(sh), 1577 (w), 1481 (m), 1438 (m), 1404 (w), 1304 (sh), 1257 (w), 1228 (m), 1181 (s), 1089 (sh), 1071 (s), 996 (m), 858 (w), 785 (w), 733 (sh), 687 (sh). $C_{34}H_{29}SbO_6$ (655.31) calculated: %C 62.31, %H 4.46, found: %C 62.23, %H 4.55; CCDC 1578595.†

Synthesis of triphenylantimony mono(*R*-mandelate), 2Sr′. 0.5 mmol (0.328 g) $SbPh_3$(*R*-ManH)$_2$ was dissolved into 5 mL of DMSO, 10 mL of H_2O was added and the white solid extracted *via* filtration. Conversion: 95% (0.311 g, 0.47 mmol) m.p. 87–89 °C; ^{1}H NMR (400 MHz, $(CD_3)_2SO$, 25 °C) δ = 7.61 (6H, m, *o*-SbCH_{ar}), 7.45 (9H, m, *m*-SbCH_{ar}, *p*-SbCH_{ar}), 7.40 (2H, m, *o*-CH_{ar}), 7.21 (3H, m, *m*-CH_{ar}, *p*-CH_{ar}), 5.18 (1H, s, H^6) 5.18 (1H, s, CH_2), 2.54 (6H, s, DMSO); ^{13}C{^{1}H} NMR (100 MHz, $(CD_3)_2SO$, 25 °C): δ = 163.9 (*C*OO), 142.9 (*o*-*C*H$_{ar}$), 134.2 (*m*-*C*H$_{ar}$), 127.4 (*p*-*C*H$_{ar}$), 129.8 (*C*H$_{ar}$), 128.6 (*C*H$_{ar}$), 127.2 (*C*H$_{ar}$), 104.5 (*C*H), 39.5 (DMSO). Analytical data consistent with that previously reported.[22] MS (ESI)$^+$ *m*/*z* = 382.9 [$SbPh_2$ + $6H_2O$]$^+$, 390.9 [$SbPh_3$ + K]$^+$, 524.9 [$SbPh_3L$ − H + Na]$^+$, 753 [$SbPh_3LL$ − H + 2Na + $3H_2O$]$^+$; (ESI)$^-$ *m*/*z* = 107.0 [L − COOH]$^-$, 151.0 [L − H]$^-$, 325.0 [2L − 2H + Na]$^-$, 493 [SbL_2 − 2H + $4H_2O$]$^-$.

Synthesis of triphenylantimony mono(*S*-mandelate), 2Ss′. Compound was prepared using a similar procedure to **2Sr′** using the di-substituted *S*-enantiomer **2Ss**. 0.5 mmol (0.328 g) $SbPh_3$(*R*-ManH)$_2$ was dissolved into 5 mL of DMSO, 10 mL of H_2O was added and the white solid extracted *via* filtration. Conversion: 96% (0.313 g, 0.48 mmol) m.p. 89–92 °C; ^{1}H and ^{13}C NMR consistent with previously reported.[22] MS (ESI)$^+$ *m*/*z* = 382.9 [$SbPh_2$ + $6H_2O$]$^+$, 390.9 [$SbPh_3$ + K]$^+$, 524.9 [$SbPh_3L$ − H + Na]$^+$, 753 [$SbPh_3LL$ − H + 2Na + $3H_2O$]$^+$; (ESI)$^-$ *m*/*z* = 107.0 [L − COOH]$^-$, 151.0 [L − H]$^-$, 325.0 [2L − 2H + Na]$^-$, 493 [SbL_2 − 2H + $4H_2O$]$^-$.

Synthesis of triphenylbismuth bis(*R*-mandelate), 2Br. $BiPh_3$ (0.441 g, 1.0 mmol), mandelic acid (0.306 g, 2.0 mmol) and 70% *t*-BuOOH (300 μL, 2.2 mmol) were reacted in diethyl ether as per **GP**. Yield: 80% (0.596 g, 0.80 mmol) m.p. 158–159 °C; IR [cm^{-1}]: ^{1}H and ^{13}C NMR consistent with previously reported.[21] CCDC 1578597.†

Synthesis of triphenylbismuth bis(*S*-mandelate), 2Bs. $BiPh_3$ (0.441 g, 1.0 mmol), mandelic acid (0.306 g, 2.0 mmol) and 70% *t*-BuOOH (300 μL, 2.2 mmol) were reacted in diethyl ether as per **GP**. Yield: 72% (0.538 g, 0.72 mmol) m.p. 160–161 °C; ^{1}H and ^{13}C NMR consistent with previously reported.[21] CCDC 1580805.†

Synthesis of triphenylantimony bis(benzilate), 3S. $SbPh_3$ (0.177 g, 0.5 mmol), benzilic acid (0.228 g, 1.0 mmol) and 70% *t*-BuOOH (150 μL, 1.1 mmol) were reacted in diethyl ether as per **GP**. Yield: 72% (0.292 g, 0.80 mmol) m.p. 158–159 °C; ^{1}H and ^{13}C NMR consistent with previously reported.[20]

Synthesis of triphenylbismuth bis(benzilate), 3B. $BiPh_3$ (0.220 g, 0.5 mmol), benzilic acid (0.228 g, 0.5 mmol) and 70% *t*-BuOOH (150 μL, 1.1 mmol) were reacted in diethyl ether as per **GP**. Yield: 87% (0.325 g, 0.80 mmol) m.p. 168–169 °C; ^{1}H and ^{13}C NMR consistent with previously reported.[20]

Conflicts of interest

There are no conflicts to declare.

Acknowledgements

The authors would like to extend their thanks to the Australian Research Council and Monash University. We would also like to thank Dr Lukasz Kedzierski for supplying the *L. major* parasites and human primary fibroblasts and subsequent training in culturing and biological cell assays.

References

1 W. H. Organization, *World Health Organ. Tech. Rep. Ser.*, 2010, xii.
2 J. A. R. Postigo, *Int. J. Antimicrob. Agents*, 2010, **36**, S62–S65.
3 S. M. Gossage, M. E. Rogers and P. A. Bates, *Int. J. Parasitol.*, 2003, **33**, 1027–1034.
4 W. H. Organization, *World health statistics 2015*, World Health Organization, 2015.
5 J. Alvar, I. D. Vélez, C. Bern, M. Herrero, P. Desjeux, J. Cano, J. Jannin, M. den Boer and W. L. C. Team, *PLoS One*, 2012, **7**, e35671.
6 A. Stauch, H.-P. Duerr, J.-C. Dujardin, M. Vanaerschot, S. Sundar and M. Eichner, *PLoS Neglected Trop. Dis.*, 2012, **6**, e1973.
7 J. van Griensven, M. Balasegaram, F. Meheus, J. Alvar, L. Lynen and M. Boelaert, *Lancet Infect. Dis.*, 2010, **10**, 184–194.
8 H. Sun, *Biological chemistry of arsenic, antimony and bismuth*, Wiley Online Library, 2011.
9 M. K. Pathak and T. Yi, *J. Immunol.*, 2001, **167**, 3391–3397.
10 S. Sundar, K. Kumar, J. Chakravarty, D. Agrawal, S. Agrawal, A. Chhabra and V. Singh, *Trans. R. Soc. Trop. Med. Hyg.*, 2006, **100**, 698–700.
11 S. L. Croft and J. Engel, *Trans. R. Soc. Trop. Med. Hyg.*, 2006, **100**, S4–S8.
12 M. Ouellette, J. Drummelsmith and B. Papadopoulou, *Drug Resist. Updates*, 2004, **7**, 257–266.
13 G. Mandal, V. Govindarajan, M. Sharma, H. Bhattacharjee and R. Mukhopadhyay, in *Antimicrob. Drug. Resist*, Springer, 2017, pp. 649–665.
14 S. Sundar, T. K. Jha, C. P. Thakur, S. K. Bhattacharya and M. Rai, *Trans. R. Soc. Trop. Med. Hyg.*, 2006, **100**(Supplement 1), S26–S33.
15 M. I. Ali, M. K. Rauf, A. Badshah, I. Kumar, C. M. Forsyth, P. C. Junk, L. Kedzierski and P. C. Andrews, *Dalton Trans.*, 2013, **42**, 16733–16741.
16 J. A. Salvador, S. A. Figueiredo, R. M. Pinto and S. M. Silvestre, *Future Med. Chem.*, 2012, **4**, 1495–1523.
17 P. C. Andrews, V. L. Blair, R. L. Ferrero, P. C. Junk, L. Kedzierski and R. M. Peiris, *Dalton Trans.*, 2014, **43**, 1279–1291.
18 P. C. Andrews, R. Frank, P. C. Junk, L. Kedzierski, I. Kumar and J. G. MacLellan, *J. Inorg. Biochem.*, 2011, **105**, 454–461.
19 Y. C. Ong, V. L. Blair, L. Kedzierski and P. C. Andrews, *Dalton Trans.*, 2014, **43**, 12904–12916.
20 H. Barucki, S. J. Coles, J. F. Costello, T. Gelbrich and M. B. Hursthouse, *J. Chem. Soc., Dalton Trans.*, 2000, 2319–2325.
21 H. Barucki, S. J. Coles, J. F. Costello and M. B. Hursthouse, *Chem. – Eur. J.*, 2003, **9**, 2877–2884.
22 H. Barucki, S. J. Coles, J. F. Costello and M. B. Hursthouse, *J. Organomet. Chem.*, 2001, **622**, 265–273.
23 D. V. Moiseev, Y. B. Malysheva, A. S. Shavyrin, Y. A. Kurskii and A. V. Gushchin, *J. Organomet. Chem.*, 2005, **690**, 3652–3663.
24 V. Sharutin, I. Egorova, O. Sharutina, T. Ivaneko, M. Pushilin and A. Gerasimenko, *Chem. Comput. Simul. Butlerov Commun.*, 2002, **9**, 59–64.
25 Y. C. Ong, V. L. Blair, L. Kedzierski, K. L. Tuck and P. C. Andrews, *Dalton Trans.*, 2015, **44**, 18215–18226.
26 C.-S. Chung, *J. Chem. Educ.*, 1984, **61**, 1062.
27 R. D. Hancock and A. E. Martell, *Comments Inorg. Chem.*, 1988, **6**, 237–284.
28 G. Deacon and R. Phillips, *Coord. Chem. Rev.*, 1980, **33**, 227–250.
29 I. Egorova, V. Sharutin, T. Ivanenko, N. Nikolaeva, A. Molokov and G. Fukin, *Russ. J. Coord. Chem.*, 2006, **32**, 644–651.
30 W. M. Haynes, *CRC handbook of chemistry and physics*, CRC press, 2014.
31 G.-C. Wang, Y.-N. Lu, J. Xiao, L. Yu, H.-B. Song, J.-S. Li, J.-R. Cui, R.-Q. Wang and F.-X. Ran, *J. Organomet. Chem.*, 2005, **690**, 151–156.
32 A. Loh, Y. C. Ong, V. L. Blair, L. Kedzierski and P. C. Andrews, *J. Biol. Inorg. Chem.*, 2015, **20**, 1193–1203.
33 M. Vermeersch, R. I. da Luz, K. Toté, J.-P. Timmermans, P. Cos and L. Maes, *Antimicrob. Agents Chemother.*, 2009, **53**, 3855–3859.
34 D. H. Barton, N. Y. Bhatnagar, J.-P. Finet and W. B. Motherwell, *Tetrahedron*, 1986, **42**, 3111–3122.
35 L. Kedzierski, J. M. Curtis, M. Kaminska, J. Jodynis-Liebert and M. Murias, *Parasitol. Res.*, 2007, **102**, 91–97.
36 A. Pathak, V. L. Blair, R. L. Ferrero, L. Kedzierski and P. C. Andrews, *J. Inorg. Biochem.*, 2017, DOI: 10.1016/j.jinorgbio.2017.05.014.
37 K. Lackovic, J. P. Parisot, N. Sleebs, J. B. Baell, L. Debien, K. G. Watson, J. M. Curtis, E. Handman, I. P. Street and L. Kedzierski, *Antimicrob. Agents Chemother.*, 2010, **54**, 1712–1719.

Journal of Inorganic Biochemistry 189 (2018) 151–162

Contents lists available at ScienceDirect

Journal of Inorganic Biochemistry

journal homepage: www.elsevier.com/locate/jinorgbio

Comparative stability, cytotoxicity and anti-leishmanial activity of analogous organometallic Sb(V) and Bi(V) acetato complexes: Sb confirms potential while Bi fails the test

Rebekah N. Duffin[a], Victoria L. Blair[a], Lukasz Kedzierski[b], Philip C. Andrews[a,*]

[a] School of Chemistry, Monash University, Clayton, Melbourne, VIC 3800, Australia
[b] Department of Microbiology and Immunology and Faculty of Veterinary and Agricultural Sciences, The Peter Doherty Institute for Infection and Immunity, 792 Elizabeth Street, Melbourne 3000, Victoria, Australia

ABSTRACT

A series of sixteen triphenyl Bi(V) and Sb(V) acetato complexes of general formula $[MPh_3(O_2CCR)_2]$ and one oxido-bridge antimony complex $[(SbPh_3(O_2C{-}O{-}C(=O)Me))_2O]$, have been synthesised and characterised, thirteen of which are novel. The solid-state structures of fifteen of the complexes have been successfully authenticated by single crystal X-ray diffraction. All structures, excluding the oxido-bridge antimony complex, adopt a typical trigonal bipyramidal confirmation with the phenyl rings in a propeller-like orientation in the equatorial plane. Fourteen of the complexes were screened for their anti-leishmanial activity and cytotoxicity towards mammalian cells. The Bi(V) complexes were found to be unstable in DMEM culture media and to be severely toxic towards mammalian cells, with IC_{50} values in the range 11.4 μM–19.8 μM. In contrast, the Sb(V) complexes demonstrated a high degree of stability and selectivity, with IC_{50} values 6.18–19.1 μM for the promastigote assay, and of 73.8–≤100 μM for the human fibroblasts. Assessment of the Sb(V) complexes against the clinically relevant amastigote form of these parasites at 10 μM showed all but the oxido-bridged complex to be effective, with % infection values ranging from 7.0 ± 1.7–40.5 ± 2.0.

1. Introduction

Leishmaniasis is classified by the World Health Organisation (WHO) as a '*neglected tropical disease*' since while being highly prevalent it is ranked low on the political and research agenda of many countries and is of minimal interest to major pharmaceutical companies, due mainly to its localisation in lower socioeconomic areas [1]. A spike in the prevalence of leishmaniasis has appeared in the last decade along with an expansion of endemic regions [2]. The WHO has estimated 0.2–0.4 million new cases of potentially fatal visceral leishmaniasis (VL) occurring every year in the 98 countries the protozoan is found [3,4]. Approximately 10% of VL infections result in a fatality within 2 years of contracting the disease [2,5].

For many decades, the frontline treatment of VL has relied heavily on the use of the pentavalent antimony complexes sodium stibogluconate (Pentosam ™) and meglumine antimoniate (Glucantime ™) [6]. Current consensus is that Sb(V) is reduced *in vivo* to the more active +III form, making the parent +V complexes pro-drugs [7]. Some studies though have shown that the Sb(V) complexes may also inhibit parasite function in the +V state prior to reduction via the inhibition of protein phosphatases, causing cellular cascade and eventual apoptosis, thus targeting the parasite both directly and indirectly [8]. However, these two common antimonial drugs have serious draw backs since antimony is inherently toxic and side-effects ranging from mild nausea to severe cardiotoxicity can occur [7]. Drug resistance is now another major problem, arising in part because of poor treatment compliance in part from the challenging treatment regimen, which involves daily intramuscular/intravascular injections since the drugs are highly hydrophilic [9,10], and also evolution of a leishmanial As(V) reductase, arising from exposure of humans to high levels of arsenic in drinking water, which can also act on the Sb(V) drugs [2,11,12].

The organic alternatives to antimonials for the treatment of leishmaniasis; pentamidine, miltefosine, and liposomal formulations of amphotericin B (Fig. 1), were originally developed as anti-trypanosomal [13], anti-cancer [14] and anti-fungal [15] agents respectively. Unfortunately, as with the antimonial drugs, they each have debilitating draw-backs: Miltefosine has a narrow therapeutic window and is tetratogenic, pentamidine salts induce serious cardiac and gastro toxicity, and amphotericin B, though the most effective of all current treatments, is expensive and can cause numerous side effects, including renal failure [16]. Resistance to the orally available amphotericin B derivative (AmBisome ™) has also become an issue having been recently observed in clinical isolates of *L. donavani*, both *in vitro* and *in vivo* [17]. This resistance is thought to be associated with an increase in specific leishmanial sterols, which alter the fluidity of the cell membrane resulting in the potential inhibition of the movement of drugs into the

* Corresponding author.
E-mail address: phil.andrews@monash.edu (P.C. Andrews).

https://doi.org/10.1016/j.jinorgbio.2018.08.015
Received 30 July 2018; Received in revised form 21 August 2018; Accepted 24 August 2018
Available online 01 September 2018
0162-0134/

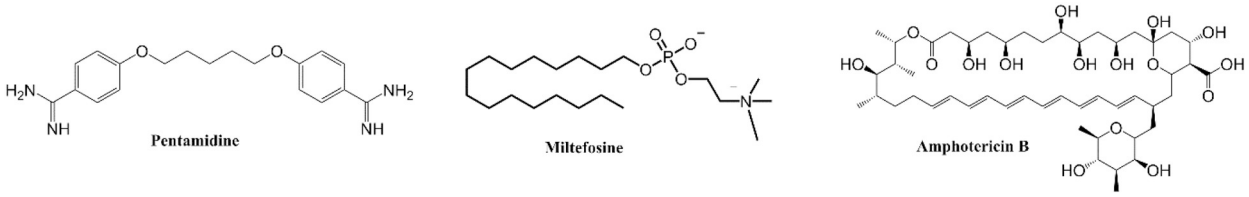

Fig. 1. Non-antimony based compounds used to treat leishmaniasis.

parasites [18].

Both cost and administration remain the major hurdles in the advancement of potential anti-leishmanial drugs. In terms of ease of administration, the current pentavalent antimonials are too hydrophilic to be absorbed in the stomach and so cannot be taken orally. The only orally administered drugs, Miltefosine and liposomal amphotericin B (AmBisome ™) are expensive and already facing resistance [17,19]. The development of cheap, oral treatments would be a major advance and hence a key research target is the design and synthesis of lipophilic organometallic complexes of the group 15 metals as new metallo-drugs. The move from Sb(V) to Bi(V) is an attempt to reduce the significant toxic load on the body while undergoing treatment. Despite being classified as a heavy metal, bismuth has a reported low systematic toxicity in humans, mainly due to low solubility of the compounds in biological fluids, while showing effective antimicrobial activity at low concentrations. However this reported non-toxicity is mainly limited to the +III oxidation state, with little information available on the +V state [20].

In our previous studies, we have shown that complexes of the general formula $[SbAr_3(O_2CR)_2]$ can show significant activity towards both the promastigote and clinically relevant amastigote forms of the parasite at concentrations between 0.5 and 3.5 μM. They can also show good selectivity, with concentrations of > 25 μM needed for toxicity to be observed towards human fibroblast cells [21]. The analogous bismuth complexes have also been examined [22], and though significant activity towards the parasite was observed they unfortunately proved to be chemically unstable in the culture medium [21]. Non-selective toxicity of the bismuth complexes on human fibroblasts was also observed, often at low μM concentrations [22,23].

The key challenge therefore is whether this class of organometallic Bi(V) complex can be designed to improve both solution stability and therapeutic selectivity. Our recent study on Bi(V) α-hydroxy carboxylates showed that as a class they exhibit unusually high stability when compared with previous similar carboxylate complexes [24], we believe predicated on the additional thermodynamic stability provided by the chelating nature of the ligands. A second common structural feature of this class of ligand is the two-carbon chain backbone. To determine whether this structural feature was a contributing factor in the toxicity of the Bi(V) complexes we have now examined a range of Bi(V) and Sb (V) complexes incorporating a family of substituted acetates.

The simplest aryl acetate, $PhCH_2CO_2^-$, has been shown to display effective antimicrobial activity, and hence prompted further analysis of the biological and chemical effects of ring substitution [25]. In this study, we have synthesised and characterised thirteen novel complexes, and four reported previously, [21,26] incorporating anionic ligands derived from the acids shown in Fig. 2 using an oxidative addition route with MPh_3.

2. Experimental section

Both $BiPh_3$ and $SbPh_3$ were synthesised according to literature procedures [27]. Crystalline high purity MPh_3 were obtained from recrystallisation from hot ethanol. $SbPh_3$ was also purchased as a 99% purity powder from Sigma Aldrich. All carboxylic acids were purchased from Sigma-Aldrich or Alfa Aesar, without the need for further purification. Dried solvents were obtained from an MBruan-SPS-800 and stored under a dry nitrogen environment over molecular sieves (4 Å. All remaining reagents and solvents were purchased from Sigma-Aldrich and Merck. All reactions requiring anhydrous conditions were performed with oven-dried glassware under an inert atmosphere of nitrogen, utilising a Schlenk manifold and technique. ^{1}H NMR and ^{13}C NMR spectra were recorded on a Bruker Avance DRX400 spectrometer (400 MHz) with the chemical shifts referenced to the appropriate residual protiated solvent (d_6-DMSO or $CDCl_3$). Multiplicities are denoted as singlet (s), doublet (d), triplet (t), multiplet (m) and broad (b), or a combination where necessary. Melting points were analysed in open end capillary tubes on a digital Stuart Scientific melting point apparatus SMP10. Infrared Spectra were recorded on an Agilent Technologies Cary 630 FTIR spectrometer, using a range of 4000–500 cm^{-1}. CH elemental analysis (EA) was obtained from The Campbell Microanalytical Laboratory, Department of Chemistry, University of Otago, Dunedin New Zealand.

2.1. Biological assays

2.1.1. Cell culture

Leishmania major virulent clone v121 was derived from the LRC-L137 *L. major* isolate and maintained at 26 °C in Gibco ™ supplemented M199 media (10% (v/v) heat inactivated FBS, 1% Pen-Strep). Human primary fibroblasts were cultured and maintained in Dulbecco's Modified Eagles Medium (DMEM) supplemented with 10% FBS and 1% Pen-Strep (purchased from Gibco ™) at 37 °C in a 5% CO_2 incubator [22].

2.1.2. In vitro testing of L. major and human fibroblasts

Celltiter Blue Cell Viability Assay was purchased from Promega ™, and used for the determination of percentage viability of the parasite and human fibroblasts. Compounds **1S**, **3S–7S** and **1B–8B** were dissolved in DMSO to a 10 mM working stock and serially diluted in 96-well plate rows in the appropriate culture media (100 μM to 48 nM). Assays were set up in duplicate in 96-well Falcon plates. Volumes of 10^6 promastigotes/mL and 10^5 fibroblasts/mL were used. Cell viability for human fibroblasts was measured spectroscopically at 550 nm [28]. Cell titre Blue dye was added to the samples at T = 0, and subsequently subtracted from all readings at 600 nm as background interference. *L. major* assay viability was measured spectroscopically using fluorescence excitation at 544 nm and emission at 590. The compounds were compared to a negative control (no drug) and the percent inhibition calculated [29]. All absorbance plate readings were conducted on a BMG-Labtech Spectrostar Nano UV–Vis microplate reader. Fluorescence measurements were conducted on a BMG-Labtech FluoStar Omega microplate reader.

2.1.3. Amastigote assay

Macrophage invasion assays were performed as previously described [21,30]. Briefly, bone marrow-derived mouse macrophages were plated onto coverslips in a 24 well plate and allowed to adhere for 48 h. The cells were exposed to *L. major* promastigotes at a 1:10 ratio and incubated for a further 48 h to allow for amastigote formation *in vitro*. The slides were then washed to remove any excess promastigotes and exposed to compounds for 48 h before washing and fixation with methanol. Following Giemsa staining, the cells were then counted

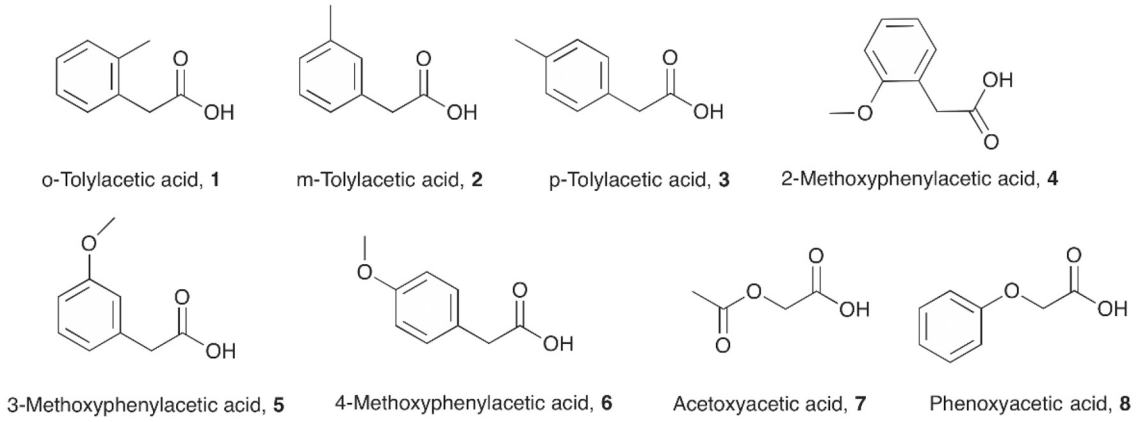

Fig. 2. Composition of the carboxylic acids **1–8** used in this study.

microscopically and the percentage of infected cells analysed.

2.2. X-ray crystallography

Crystallographic data on complexes **1B–8B**, **1S**, **3S–8S** were collected on a Bruker ×8 APEXII CCD diffractometer, equipped with an OXFORD Crysosystem 700 cryostream and cooled to 123(2) K. Data collection occurred using monochromatic (graphite) MoK_α radiation ($\lambda = 0.71070$ Å) and was processed using the Bruker Apex2 v2014.7-1 software [31], polarisation, Lorentz and absorption corrections (multi-scan-SADBABS) were applied [32]. Each compound was solved and refined using SHELX-97 on X-seed or Olex2 [33,34]. Unless otherwise indicated, all non-hydrogen atoms were refined with anisoptropic thermal parameters. Hydrogen atoms were placed in calculated positions using a riding model with C-H = 0.95–0.98 Å and $U_{iso}(H) = x$U-iso(C), x = 1.2 or 1.5 unless otherwise indicated. A summary of the X-ray data can be found in the ESI, Tables S1/S2.

2.3. Synthesis and characterisation

2.3.1. General procedure, GP

MPh_3 and acetic acid (1:2 or 1:1) were dissolved in 10 mL of diethyl ether, toluene or THF at room temperature and stirred. An excess of 2.2 equivalents of t-BuOOH was added and the mixture stirred for approximately one hour [35]. The compounds either crystallised straight from the solvent filtrate, or required crystallisation in hot solvent.

2.3.1.1. Triphenylantimony bis(o-tolylacetate), ***1S***. $SbPh_3$ (0.176 g, 0.5 mmol), *o*-tolylacetic acid (0.150 g, 1.0 mmol) and 70% t-BuOOH (150 µL, 1.1 mmol) were reacted as per **GP**. Yield: 89% 0.289 g; m.p: 129–131 °C; ^{1}H NMR (400 MHz, ($CDCl_3$, 25 °C): δ = 7.73 (6H, m, *o*-CH_{ar}) 7.44 (3H, m, *p*-CH_{ar}) 7.36 (6H, m, *m*-CH_{ar}) 7.11 (2H, m, CH_{ar}) 7.06 (4H, m, CH_{ar}) 6.96 (2H, m, CH_{ar}) 4.51 (4H, s, CH_2) 1.93 (6H, s, CH_3); ^{13}C{^{1}H} NMR (100 MHz, $CDCl_3$, 25 °C): 174.5 (*C*OO), 137.3 (Sb*C*), 134.3 (*C*H$_{ar}$), 133.8 (*C*H$_{ar}$), 130.9 (*C*H$_{ar}$) 130.1 (*C*H$_{ar}$), 129.9 (*C*H$_{ar}$), 129.1 (*C*H$_{ar}$), 126.7 (*C*H$_{ar}$), 125.7 (*C*H$_{ar}$), 41.1 (*C*H$_2$), 19.3 (*C*H$_3$); FT-IR [cm^{-1}]: 3063 (w), 3013 (w), 2995 (w), 2909 (w), 1651 (sh), 1576 (w), 1481 (m), 1437 (m), 1342 (sh), 1301 (m), 1244 (sh), 1211 (sh), 1172 (m), 1069 (m), 1022 (m), 996 (m), 853 (w), 731 (sh), 689 (sh); Elemental analysis, expected: %C 66.38%H 5.11 found: %C 66.14%H 5.00. CCDC 1578382.

2.3.1.2. Triphenylbismuth bis(o-tolylacetate), ***1B***. $BiPh_3$ (0.221 g, 0.5 mmol), *o*-tolylacetic acid (0.150 g, 1.0 mmol) and 70% t-BuOOH (150 µL, 1.1 mmol) were reacted as per **GP**. Yield: 81% 0.299 g; m.p: 143–144 °C; ^{1}H NMR (400 MHz, ($CDCl_3$, 25 °C): δ = 7.98 (6H, m, *o*-CH_{ar}) 7.49 (3H, m, *p*-CH_{ar}) 7.43 (6H, m, *m*-CH_{ar}) 7.07 (2H, m, CH_{ar}) 6.99 (4H, m, CH_{ar}) 6.90 (2H, m, CH_{ar}) 3.40 (4H, s, CH_2) 1.94 (6H, s, CH_3); ^{13}C{^{1}H} NMR (100 MHz, $CDCl_3$, 25 °C): 177.1 (*C*OO), 159.5 (Bi*C*), 136.7 (*C*H$_{ar}$), 134.0 (*C*H$_{ar}$), 131.0 (*C*H$_{ar}$) 130.6 (*C*H$_{ar}$), 129.9 (*C*H$_{ar}$), 126.4 (*C*H$_{ar}$), 126.7 (*C*H$_{ar}$), 125.7 (*C*H$_{ar}$), 40.7 (*C*H$_2$), 19.3 (*C*H$_3$)); FT-IR [cm^{-1}]: 3061 (w), 3020 (w), 2912 (w), 1601 (m), 1560 (sh), 1470 (m), 1437 (m), 1349 (sh), 1325 (m), 1258 (m), 1217 (m), 1190 (m), 1052 (w), 1009 (m), 986 (sh), 852 (w), 728 (sh), 680 (sh); Elemental analysis, expected: %C 58.54%H 4.45 found: %C 58.47%H 4.47. CCDC 1578385.

2.3.1.3. Triphenylantimony bis(m-tolylacetate), ***2S***. $SbPh_3$ (0.176 g, 0.5 mmol), *m*-tolylacetic acid (0.150 g, 1.0 mmol) and 70% t-BuOOH (150 µL, 1.1 mmol) were reacted as per **GP**. Yield: 79% 0.257 g; ^{1}H NMR and ^{13}C NMR consistent with previously synthesised [21].

2.3.1.4. Triphenylbismuth bis(m-tolylacetate), ***2B***. $BiPh_3$ (0.220 g, 0.5 mmol), *m*-tolylacetic acid (0.151 g, 1.0 mmol) and 70% t-BuOOH (150 µL, 1.1 mmol) were reacted as per **GP**. Yield: 77% 0.284 g; m.p: 124–126 °C; ^{1}H NMR (400 MHz, ($CDCl_3$, 25 °C): δ = 8.03 (6H, m, *o*-CH_{ar}) 7.50 (6H, m, *m*-CH_{ar}) 7.46 (3H, m, *p*-CH_{ar}) 7.06 (2H, m, CH_{ar}) 6.98 (2H, m, CH_{ar}) 6.82 (4H, m, CH_{ar}) 3.40 (4H, s, CH_2) 2.24 (6H, s, CH_3); ^{13}C{^{1}H} NMR (100 MHz, $CDCl_3$, 25 °C): 159.6 (Bi*C*), 133.9 (*C*H$_{ar}$), 131.0 (*C*H$_{ar}$), 130.6 (*C*H$_{ar}$) 129.8 (*C*H$_{ar}$), 128.0 (*C*H$_{ar}$), 126.9 (*C*H$_{ar}$), 126.0 (*C*H$_{ar}$), 42.8 (*C*H$_2$), 20.1 (*C*H$_3$); FT-IR [cm^{-1}]: 3051 (w), 2918 (w), 1602 (sh), 1570 (sh), 1559 (sh), 1490 (m) 1435 (sh), 1364 (m) 1348 (sh), 1238 (w) 1150 (m), 1101 (m), 984 (sh), 948 (w), 771 (m), 728 (sh) 666 (sh); Elemental analysis, expected: %C 58.45%H 4.45 found: %C 58.24%H 4.46. CCDC 1578380.

2.3.1.5. Triphenylantimony bis(p-tolylacetate), ***3S***. $SbPh_3$ (0.175 g, 0.5 mmol), *p*-tolylacetic acid (0.150 g, 1.0 mmol) and 70% t-BuOOH (150 µL, 1.1 mmol) were reacted as per **GP**. Yield: 91% 0.295 g; m.p: 144–146 °C; ^{1}H NMR (400 MHz, ($CDCl_3$, 25 °C): δ = 7.77 (6H, m, *o*-CH_{ar}) 7.44 (3H, m, *p*-CH_{ar}) 7.35 (6H, m, *m*-CH_{ar}) 7.01 (4H, m, CH_{ar}) 6.90 (4H, m, CH_{ar}) 3.36 (4H, s, CH_2) 2.32 (6H, s, CH_3); ^{13}C{^{1}H} NMR (100 MHz, $CDCl_3$, 25 °C): 175.0 (*C*OO), 137.4 (Sb*C*), 135.8 (*C*H$_{ar}$), 133.9 (*C*H$_{ar}$), 132.4 (*C*H$_{ar}$) 130.9 (*C*H$_{ar}$), 129.1 (*C*H$_{ar}$), 128.9 (*C*H$_{ar}$), 42.8 (*C*H$_2$), 21.1 (*C*H$_3$); FT-IR [cm^{-1}]: 3056 (w), 2939 (w), 1644 (sh), 1574 (w), 1479 (m), 1434 (m), 1305 (sh), 1267 (sh), 1192 (m), 1131 (sh), 1066 (m), 939 (m), 863 (w), 782 (m) 734 (sh), 687 (sh); Elemental analysis, expected: %C 66.38%H 5.11 found: %C 66.31%H 5.09. CCDC 1578609.

2.3.1.6. Triphenylbismuth bis(p-tolylacetate), ***3B***. $BiPh_3$ (0.220 g, 0.5 mmol), *p*-tolylacetic acid (0.151 g, 1.0 mmol) and 70% t-BuOOH (150 µL, 1.1 mmol) were reacted as per **GP**. Yield: 69% 0.255 g; m.p: 150–153 °C; ^{1}H NMR (400 MHz, ($CDCl_3$, 25 °C): δ = 8.00 (6H, m, *o*-CH_{ar}) 7.56 (3H, m, *p*-CH_{ar}) 7.48 (6H, m, *m*-CH_{ar}) 6.94 (4H, m, CH_{ar}) 6.86 (4H, m, CH_{ar}) 3.37 (4H, s, CH_2) 2.29 (6H, s, CH_3); ^{13}C{^{1}H} NMR

(100 MHz, $CDCl_3$, 25 °C): 162.2 (Bi*C*), 133.9 (*C*H$_{ar}$), 133.7 (*C*H$_{ar}$), 131.0 (*C*H$_{ar}$) 130.5 (*C*H$_{ar}$), 128.8 (*C*H$_{ar}$), 128.9 (*C*H$_{ar}$), 42.8 (*C*H$_2$), 21.1 (*C*H$_3$); FT-IR [cm^{-1}]: 3051 (w), 2916 (w), 1600 (sh), 1560 (w), 1468 (m), 1434 (m), 1371 (sh), 1260 (sh), 1010 (m), 984 (s), 790 (m), 763 (m) 728 (sh), 679 (sh); Elemental analysis, expected: %C 58.45%H 4.45 found: %C 58.43%H 4.51. CCDC 1578384.

2.3.1.7. Triphenylantimony bis(2-methoxyphenylacetate), ***4S***. $SbPh_3$ (0.176 g, 0.5 mmol), 2-methoxyphenylacetic acid (0.166 g, 1.0 mmol) and 70% t-BuOOH (150 μL, 1.1 mmol) were reacted as per **GP**. Yield: 89% 0.307 g; ^{1}H NMR and ^{13}C NMR consistent with previously synthesised [26]. CCDC 1578602.

2.3.1.8. Triphenylbismuth bis(2-methoxyphenylacetate), ***4B***. $BiPh_3$ (0.220 g, 0.5 mmol), 2-methoxyphenylacetic acid (0.166 g, 1.0 mmol) and 70% t-BuOOH (150 μL, 1.1 mmol) were reacted as per **GP**. Yield: 80% 0.302 g m.p: 148–150 °C; ^{1}H NMR (400 MHz, (d_6-DMSO, 25 °C): δ = 7.93 (6H, m, *o*-C*H*$_{ar}$) 7.65 (6H, m, *m*-C*H*$_{ar}$) 7.57 (3H, m, *p*-C*H*$_{ar}$) 7.16 (2H, m, C*H*$_{ar}$) 6.86 (2H, m, C*H*$_{ar}$) 6.74 (2H, m, C*H*$_{ar}$) 3.53 (6H, s, C*H*$_3$) 2.09 (4H, s, C*H*$_2$); ^{13}C{^{1}H} NMR (100 MHz, d_6-DMSO, 25 °C): 177.1 (*C*OO), 159.7 (Bi*C*), 137.1 (*C*H$_{ar}$), 133.8 (*C*H$_{ar}$), 131.9 (*C*H$_{ar}$) 131.4 (*C*H$_{ar}$), 130.8 (*C*H$_{ar}$), 128.2 (*C*H$_{ar}$), 120.3 (*C*H$_{ar}$), 110.8 (*C*H$_a$), 55.9 (O*C*H$_3$), 31.5 (*C*H$_2$); FT-IR [cm^{-1}]: 3063 (w), 2952 (w), 1599 (sh), 1570 (m), 1490 (m), 1467 (m), 1359 (sh), 1291 (m) 1238 (sh), 1113 (m), 1027 (m) 983 (m), 733 (sh), 689 (sh); Elemental analysis, expected: %C 56.11%H 4.32 found: %C 56.14%H 4.23. CCDC 1578381.

2.3.1.9. Triphenylantimony bis(3-methoxyphenylacetate), ***5S***. $SbPh_3$ (0.176 g, 0.5 mmol), 3-methoxyphenylacetic acid (0.167 g, 1.0 mmol) and 70% t-BuOOH (150 μL, 1.1 mmol) were reacted as per **GP**. Yield: 91% 0.315 g; m.p: 103–105 °C; ^{1}H NMR (400 MHz, ($CDCl_3$, 25 °C): δ = 7.78 (6H, m, *o*-C*H*$_{ar}$) 7.46 (3H, m, *p*-C*H*$_{ar}$) 7.38 (6H, m, *m*-C*H*$_{ar}$) 7.15 (2H, m, C*H*$_{ar}$) 6.78 (2H, m, C*H*$_{ar}$) 6.65 (4H, m, C*H*$_{ar}$) 3.72 (6H, s, C*H*$_3$) 3.40 (4H, s, C*H*$_2$); ^{13}C{^{1}H} NMR (100 MHz, $CDCl_3$, 25 °C): 174.5 (*C*OO), 159.5 (Sb*C*), 137.2 (*C*H$_{ar}$), 136.9 (*C*H$_{ar}$), 133.8 (*C*H$_{ar}$) 131.0 (*C*H$_{ar}$), 129.2 (*C*H$_{ar}$), 121.7 (*C*H$_{ar}$), 114.5 (*C*H$_{ar}$), 112.4 (*C*H$_{ar}$), 55.1 (O*C*H$_3$), 43.5 (*C*H$_2$); FT-IR [cm^{-1}]: 3062 (w), 2951 (w), 1619 (sh), 1593 (sh), 1481 (m), 1433 (m), 1413 (m), 1367 (sh), 1263 (m) 1237 (sh), 1165 (m), 1039 (m) 996 (m), 738 (sh), 690 (sh); Elemental analysis, expected: %C 63.27%H 4.87 found: %C 63.22%H 5.15. CCDC 1578603.

2.3.1.10. Triphenylbismuth bis(3-methoxyphenylacetate), ***5B***. $BiPh_3$ (0.221 g, 0.5 mmol), 3-methoxyphenylacetic acid (0.166 g, 1.0 mmol) and 70% t-BuOOH (150 μL, 1.1 mmol) were reacted as per **GP**. Yield: 75% 0.289 g; m.p: 121–123 °C; ^{1}H NMR (400 MHz, ($CDCl_3$, 25 °C): δ = 8.02 (6H, m, *o*-C*H*$_{ar}$) 7.51 (6H, m, *m*-C*H*$_{ar}$) 7.44 (3H, m, *p*-C*H*$_{ar}$) 7.08 (2H, m, C*H*$_{ar}$) 6.73 (2H, m, C*H*$_{ar}$) 6.62 (4H, m, C*H*$_{ar}$) 3.71 (6H, s, C*H*$_3$) 3.41 (4H, s, C*H*$_2$); ^{13}C{^{1}H} NMR (100 MHz, $CDCl_3$, 25 °C): 175.9 (*C*OO), 159.5 (Bi*C*), 133.9 (*C*H$_{ar}$), 131.5 (*C*H$_{ar}$), 131.0 (*C*H$_{ar}$) 131.0 (*C*H$_{ar}$), 129.0 (*C*H$_{ar}$), 126.8 (*C*H$_{ar}$), 121.5 (*C*H$_{ar}$), 112.2 (*C*H$_{ar}$), 55.1 (O*C*H$_3$), 43.0 (*C*H$_2$); FT-IR [cm^{-1}]: 3052 (w), 2964 (w), 1605 (sh), 1555 (sh), 1489 (m), 1466 (m), 1434 (m), 1371 (sh), 1267 (sh) 1223 (sh), 1157 (m), 1037 (m) 980 (m), 730 (sh), 691 (sh); Elemental analysis, expected: %C 56.11%H 4.32 found: %C 56.05%H 4.33. CCDC 1578377.

2.3.1.11. Triphenylantimony bis(4-methoxyphenylacetate), ***6S***. $SbPh_3$ (0.177 g, 0.5 mmol), 4-methoxyphenylacetic acid (0.166 g, 1.0 mmol) and 70% t-BuOOH (150 μL, 1.1 mmol) were reacted as per **GP**. Yield: 91% 0.313 g; ^{1}H NMR and ^{13}C NMR consistent with previously synthesised [26]. CCDC 1578379.

2.3.1.12. Triphenylbismuth bis(4-methoxyphenylacetate), ***6B***. $BiPh_3$ (0.221 g, 0.5 mmol), 4-methoxyphenylacetic acid (0.165 g, 1.0 mmol) and 70% t-BuOOH (150 μL, 1.1 mmol) were reacted as per **GP**. Yield: 75% 0.285 g; m.p: 140–141 °C; ^{1}H NMR (400 MHz, (d_6-DMSO, 25 °C): δ = 7.91 (6H, m, *o*-C*H*$_{ar}$) 7.63 (6H, m, *m*-C*H*$_{ar}$) 7.55 (3H, m, *p*-C*H*$_{ar}$) 6.86 (2H, m, C*H*$_{ar}$) 6.74 (2H, m, C*H*$_{ar}$) 3.70 (6H, s, C*H*$_3$) 2.08 (4H, s, C*H*$_2$); ^{13}C{^{1}H} NMR (100 MHz, d_6-DMSO, 25 °C): 172.1 (*C*OO), 158.2 (Bi*C*), 134.3 (*C*H$_{ar}$), 133.7 (*C*H$_{ar}$), 131.9 (*C*H$_{ar}$) 131.5 (*C*H$_{ar}$), 130.3 (*C*H$_{ar}$), 128.2 (*C*H$_{ar}$), 123.1 (*C*H$_{ar}$), 114.0 (*C*H$_a$), 55.6 (O*C*H$_3$), 31.2 (*C*H$_2$); FT-IR [cm^{-1}]: 3055 (w), 2934 (w), 1596 (sh), 1556 (m), 1510 (sh), 1466 (m), 1435 (m), 1350 (sh), 1239 (sh), 1176 (m), 1037 (m) 981 (m), 738 (sh), 681 (m); Elemental analysis, expected: %C 56.11%H 4.32 found: %C 56.38%H 4.18 CCDC 1578383.

2.3.1.13. Triphenylantimony (μ^2-oxido)(acetoxyacetato), ***7S***. $SbPh_3$ (0.353 g, 1.0 mmol), acetoxyacetic acid (0.118 g, 1.0 mmol) and 70% t-BuOOH (300 μL, 2.2 mmol) were reacted as per **GP**. Yield: 86% 0.411 g; m.p: 184–185 °C; ^{1}H NMR (400 MHz, ($CDCl_3$, 25 °C): δ = 7.96 (4H, m, C*H*$_{ar}$) 7.38 (10H, m, C*H*$_{ar}$) 7.25 (16H, m, C*H*$_{ar}$) 4.45 (4H, br(s), C*H*$_2$) 2.05 (6H, br(s), C*H*$_3$); FT-IR [cm^{-1}]: 3057 (w), 2955 (w), 1741 (m) 1732 (m) 1653 (sh), 1480 (m), 1434 (m), 1352 (m), 1336 (sh), 1269 (m) 1231 (sh), 1061 (m) 919 (m), 737 (sh), 691 (sh); Elemental analysis, expected: %C55.26%H4.22 found: %C 55.11%H 4.30. CCDC 1578606.

2.3.1.14. Triphenylantimony hydroxido-(acetoxyacetate), ***7S′***. **7S** was dissolved in d_6-DMSO with quantitative conversion to ***7S′*** observed; ^{1}H NMR (400 MHz, (d_6-DMSO, 25 °C): δ = 8.02 (6H, m, *o*-C*H*$_{ar}$) 7.55 (9H, m, *m,p*-C*H*$_{ar}$) 4.80 (1H, s, O*H*) 4.39 (2H, s, C*H*$_2$) 2.50 (3H, s, C*H*$_3$);

2.3.1.15. Triphenylbismuth bis(acetoxy acetate), ***7B***. $BiPh_3$ (0.220 g, 0.5 mmol), acetoxyacetic acid (0.117 g, 1.0 mmol) and 70% t-BuOOH (150 μL, 1.1 mmol) were reacted as per **GP**. Yield: 66% 0.222 g; m.p: 136–138 °C; ^{1}H NMR (400 MHz, ($CDCl_3$, 25 °C): δ = 8.11 (6H, m, *o*-C*H*$_{ar}$) 7.63 (6H, m, *m*-C*H*$_{ar}$) 7.51 (3H, m, *p*-C*H*$_{ar}$) 4.39 (4H, s, C*H*$_2$) 2.06 (6H, s, C*H*$_3$); ^{13}C{^{1}H} NMR (100 MHz, $CDCl_3$, 25 °C): 170.4 (*C*OO), 157.9 (Bi*C*), 134.1 (*C*H$_{ar}$), 131.6 (*C*H$_{ar}$), 131.3 (*C*H$_{ar}$), 36.4 (*C*H$_2$), 20.7 (*C*H$_3$); FT-IR [cm^{-1}]: 3049 (w), 1744 (sh), 1629 (sh), 1576 (m), 1470 (m), 1436 (m), 1393 (sh), 1267 (m) 1217 (sh), 1066 (sh) 982 (m), 730 (sh), 678 (sh); Elemental analysis, expected: %C46.30%H3.74 found: %C 46.01%H 3.88. CCDC 1578370.

2.3.1.16. Triphenylantimony bis(phenoxyacetic acetate), ***8S***. $SbPh_3$ (0.177 g, 0.5 mmol), phenoxyacetic acid (0.152 g, 1.0 mmol) and 70% t-BuOOH (150 μL, 1.1 mmol) were reacted as per **GP**. Yield: 78% 0.255 g; ^{1}H NMR and ^{13}C NMR consistent with previously synthesised [21]. CCDC 1578378.

2.3.1.17. Triphenylbismuth bis(phenoxyacetic acetate), ***8B***. $BiPh_3$ (0.220 g, 0.5 mmol), phenoxyacetic acid (0.152 g, 1.0 mmol) and 70% t-BuOOH (150 μL, 1.1 mmol) were reacted as per **GP**. Yield: 65% 0.241 g; m.p: 144–146 °C; ^{1}H NMR (400 MHz, (d_6-DMSO, 25 °C): δ = 7.97 (6H, m, *o*-C*H*$_{ar}$) 7.72 (6H, m, *m*-C*H*$_{ar}$) 7.63 (3H, m, *p*-C*H*$_{ar}$) 7.14 (4H, m, C*H*$_{ar}$) 6.88 (2H, m, C*H*$_{ar}$) 6.58 (4H, m, C*H*$_{ar}$) 4.49 (4H, s, C*H*$_2$); ^{13}C{^{1}H} NMR (100 MHz, d_6-DMSO, 25 °C): 174.5 (*C*OO), 159.5 (Bi*C*), 137.2 (*C*H$_{ar}$), 136.9 (*C*H$_{ar}$), 133.8 (*C*H$_{ar}$) 131.0 (*C*H$_{ar}$), 129.1 (*C*H$_{ar}$), 121.7 (*C*H$_{ar}$), 114.6 (*C*H$_{ar}$), 112.4 (*C*H$_a$), 55.1 (*C*H$_2$); FT-IR [cm^{-1}]: 3059 (w), 2929 (w), 1624 (sh), 1598 (sh), 1557 (m), 1495 (sh), 1469 (m), 1436 (sh) 1353 (sh), 1261 (m) 1218 (sh), 1174 (m), 1071 (m) 984 (m), 735 (sh), 691 (sh); Elemental analysis, expected: %C 54.99%H 3.94 found: %C 54.69%H 3.86. CCDC 1578608.

3. Results and discussion

3.1. Synthesis

All sixteen complexes (Fig. 3) were synthesised via an oxidative addition pathway involving treatment of one equivalent of MPh_3 (M = Sb or Bi) with two equivalents of t-BuOOH followed by addition

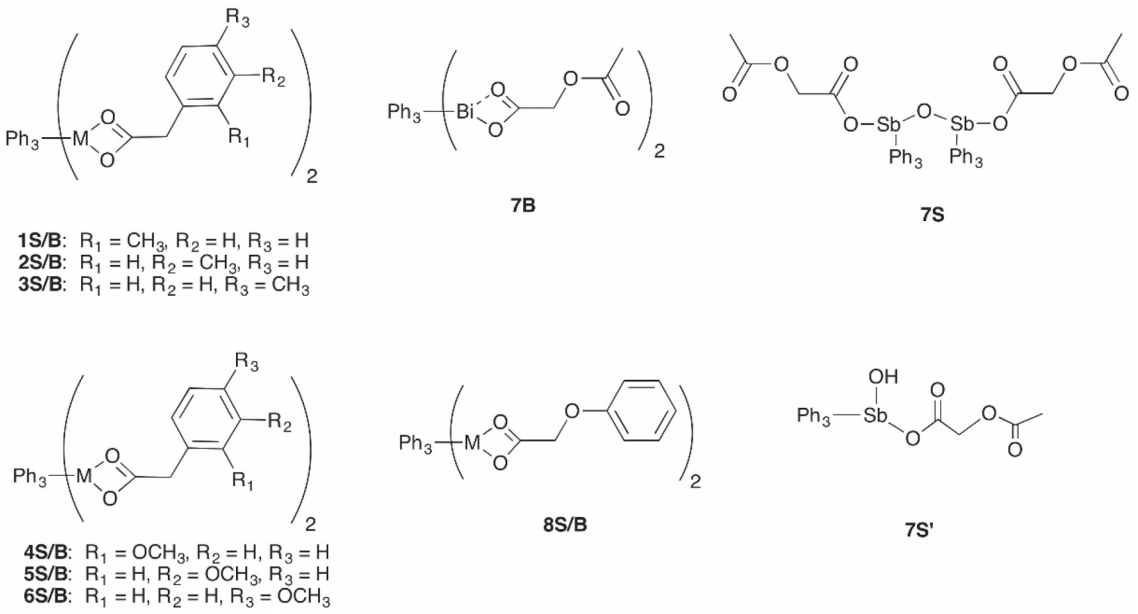

Fig. 3. Composition of the Bi(V) complexes **1B–8B**, and the Sb(V) complexes, **1S–8S**.

of two equivalents of the chosen carboxylic acid [35].

Oxidation of the metal from +III to +V results in the formation of the dihydroxido intermediate $[MPh_3(OH)_2]$ which then undergoes a facile condensation with the acid to generate the desired complex, $[MPh_3(O_2CR)_2]$ [36]. The H_2O and t-BuOH by-products are easily removed under vacuum prior to recrystallization of the complex from a hot solvent, either toluene or THF, making the overall reaction process clean and efficient. In contrast, we found the other possible synthetic route of salt metathesis involving $[MPh_3Cl_2]$ and the Na or K carboxylate results in mixed products and lower yields. Crystalline products were washed with cold diethyl ether to remove any unreacted material with good to excellent isolated yields obtained (64–91%). In terms of complex composition, **7S** is the exception being an oxido-bridged bimetallic $[(SbPh_3(O_2C{-}O{-}C(=O)Me))_2O]$, presumably through self-condensation. A rational synthesis using a 1:1 ratio of MPh_3 to carboxylate was employed to maximise the yield. In polar protic solvents **7S** undergoes a potentially reversible hydrolysis to form $[SbPh_3(O_2C{-}O{-}C(=O)Me)OH]$, **7S′**, as identified by ^{1}H NMR. This differs from the solid-state structure obtained from toluene, which was also confirmed by elemental analysis (Fig. 4).

We have described previously the synthesis, characterisation, and biological activity of complexes **2S** and **8S** towards *L. major* [21]. The solid-state structure of **2S** had been confirmed by single crystal X-ray diffraction but that of **8S** was not and so to complete this work, crystals of **8S** were grown and the crystal structure determined. Complexes **4S** and **6S** have been previously tested against a separate strain of *Leishmania*, so were able to undergo analysis via cell inhibition assays to determine their activity against *L. major* [26]. For this study, complexes **4S** and **6S** were also synthesized and their solid-state structures determined by single crystal X-ray diffraction.

3.2. NMR spectroscopy

All novel complexes (**1B–8B**, **1S**, **3S**, **5S**, **7S** and **7S′**) were characterised by ^{1}H and ^{13}C NMR spectroscopy, FT-IR, melting point, and elemental analysis. The solid-state structure of each complex, with the exception of **2S**, was authenticated by X-ray diffraction studies. The composition of the previously characterised complexes **2S**, **4S**, **6S** and **8S** were each confirmed by NMR spectroscopy and elemental analysis. Full analytical details on each complex are given in the Experimental section.

NMR spectra of all the complexes were obtained in $CDCl_3$, and also in d_6-DMSO for complexes **4B**, **6B** and **8B**. Binding of the carboxylate moiety to the metal centre was evidenced by the absence of the broad singlet of the carboxylic acid proton at 12.10–13.25 ppm in d_6-DMSO. In $CDCl_3$ the carboxylic acid proton is observed as a very broad signal close to the baseline, this large broad signal disappears upon complexation. A shift in the proton and carbon signals of the phenyl ring is also observed upon complexation, with a move to higher frequency observed for the *o*-, *m*-, *p*-H signals compared with those in MPh_3. As previously reported, these shifts are consistent with the formation of triaryl carboxylato complexes of both Sb(V) and Bi(V) [21–23]. The conversion of **7S** to **7S′** was observed in the ^{1}H NMR spectrum collected in 'wet' d_6-DMSO. In the presence of water the bridging oxygen of complex **7S** breaks forming two equivalents of the mono-hydroxido complex $[SbPh_3(O_2C{-}O{-}C(=O)Me)OH]$. The hydrolysis of the bridging oxygen is facile being quantitative in only 30 min. The process is slower in $CDCl_3$ due the lower concentration of water. Fluxionality of the hydroxyl and terminal methyl signal of **7S** are observed by the presence of the broad and sharp singlets at 2.1 ppm and 4.4 ppm (Figs. 5 and 6).

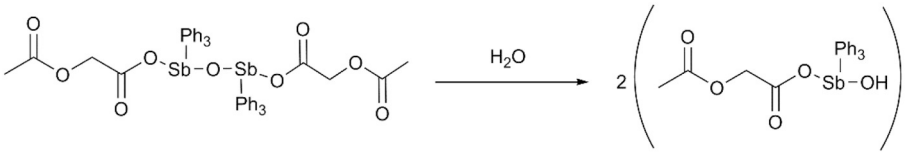

Fig. 4. Hydrolysis product of complex $[(SbPh_3(O_2C{-}O{-}C(=O)Me)_2O]$ **7S** to $[SbPh_3(O_2C{-}O{-}C(=O)Me)OH]$ **7S′**.

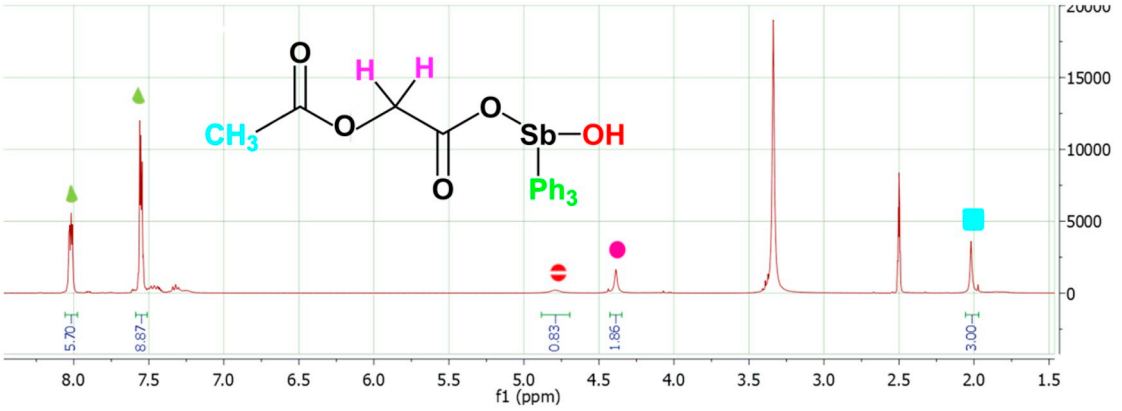

Fig. 5. ^{1}H NMR spectrum of quantitative conversion to **7S′** in d_6-DMSO, DMSO signal at 2.5 ppm and H_2O at 3.33 ppm.

3.3. Infrared spectroscopy

Formation of the metal carboxylates was further confirmed by FT-IR through the appearance of the asymmetric and symmetric carboxylate signals in the ranges of 1696–1703 cm^{-1} and 1435–1510 cm^{-1} respectively. These differ from the parent carboxylic acids for which the carbonyl stretching frequencies are found in the ranges of 1686–1731 cm^{-1} and 1408–1595 cm^{-1}. The difference in the symmetric and asymmetric stretches ($\Delta\nu$) were calculated for each complex and used to predict the binding mode of the carboxylate to the metal, i.e. whether it is mono- or didentate. Deacon and Phillips observed that a difference of > 200 cm^{-1} is generally indicative of a monodentate bonding mode, while < 200 cm^{-1} indicates a didentate chelate involving both O atoms of the carboxylate moiety [37]. A comparison of the structures founded on the FT-IR absorbance and those obtained from X-ray diffraction is given in the Supporting information, Table S3. In summary, the two methods correlate closely.

3.4. X-ray crystallography

Crystals of the twelve novel complexes (**1B**–**8B**, **1S**, **3S**, **5S** and **7S′**), and the three previously synthesised Sb(V) complexes, **4S**, **6S a**nd **8S**, were studied by single crystal X-ray diffraction, and the solid-state structure of each determined. Crystals suitable for analysis were obtained from toluene solutions on slow evaporation. Each complex, with the exception of **7S′**, adopts a trigonal bipyramidal geometry, as commonly observed for complexes of the general formula $[MPh_3(O_2CR)_2]$. To illustrate the structural types the authenticated structures of **1B** and **1S** are given in Figs. 7 and 8. The carboxylate ligands are found to occupy the axial plane, with the phenyl rings arranged in a propeller orientation in the equatorial plane [21,22,24]. In contrast to the Sb(V) complexes, which adopt a five coordinate configuration, the Bi(V) analogues are seven coordinate [24]. A greater degree of distortion of the bipyramidal geometry is observed in the Bi(V) analogues, which may allow for easier access of the carbonyl oxygen for dative interactions, pushing the coordination number from five to seven. The greater size in coordination sphere of Bi(V) compared to Sb(V) also contributes to the preferred difference in coordination number (0.74 Å v 0.62 Å) [7].

A detailed description of structural features of complexes **1B** and **1S** (Figs. 7 and 8) along with a summary of the crystallographic data on all remaining complexes can be found in the Supplementary Information Table S1.

7S is the only complex which was found to adopt a different structural chemistry, incorporating a bridging oxide between two Sb(V) centres (Fig. 9). The structure is centrosymmetric, with the asymmetric unit incorporating one Sb(V) unit, with the second being symmetry generated. The geometry about each Sb(V) centre can be considered as trigonal bipyramidal with a coordination number at the metal of five. The Sb – C^{Ph} bonds are similar to those in the more typical Sb(V) triaryl di-carboxylato complexes, with bond lengths of 2.110(4) Å (Sb(1) – C(1)), 2.108(5) Å (Sb(1) – C(7)), and 2.106(4) Å (Sb(1) – C(13)). All phenyl ligands occupy the equatorial plane in the distinctive propeller orientation. The covalent bond between Sb(1) and the bridging oxygen O(5) was found to be shorter than the covalent interaction with the

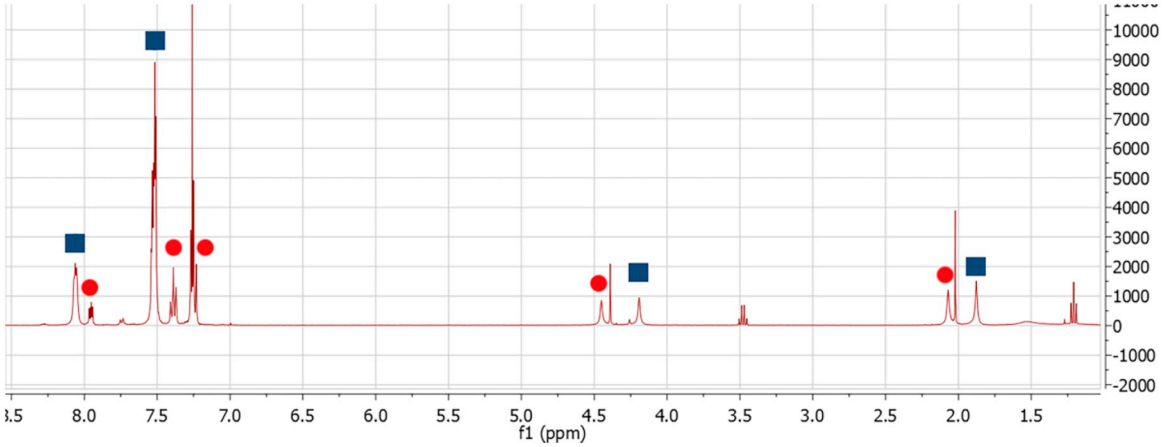

Fig. 6. ^{1}H NMR spectrum of **7S** (circle) and hydrolysis product **7S′** (square) in $CDCl_3$, the residual solvent signal and ether signal retained from synthesis has not been labelled (t, 1.2 ppm, q, 3.4 ppm).

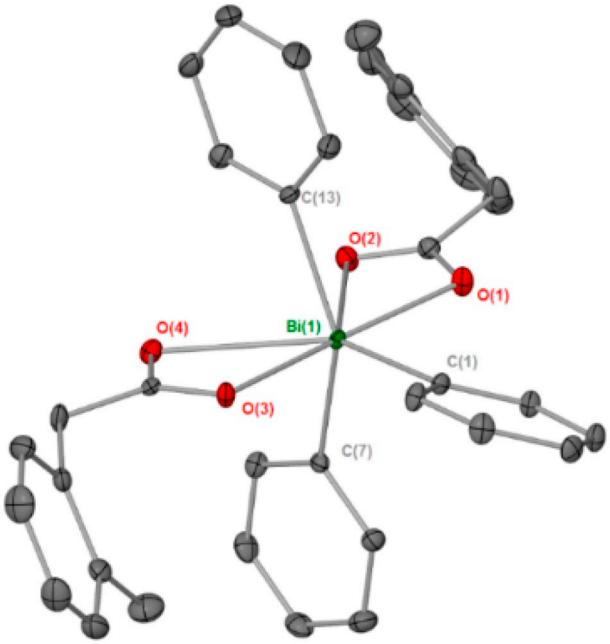

Fig. 7. Solid-state structure of $[Bi(C_6H_5)_3((O_2CCH_2C_6H_4CH_3)_2]$, **1B**. Thermal ellipsoids at 50% probability. Hydrogen atoms have been omitted for clarity. Selected bonds lengths (Å) and angles (°). Bi(1) – O(1), 2.278(14), Bi(1) – O(2), Bi(1) – O(3), 2.308(14), Bi(1) – O(4), 2.703(15), 2.815(14), Bi(1) – C(1), 2.205(19), Bi(1) – C(7), 2.186(2), Bi(1) – C(13), 2.195(2); C(7) – Bi(1) – C(13), 143.6(8), C1 – Bi(1) – C(7), 104.5(7), C7 – Bi(1) – O(1), 95.15(6), C(7) – Bi(1) – O(4), 75.93(6), O(1) – Bi(1) – O(3), 170.3(5).

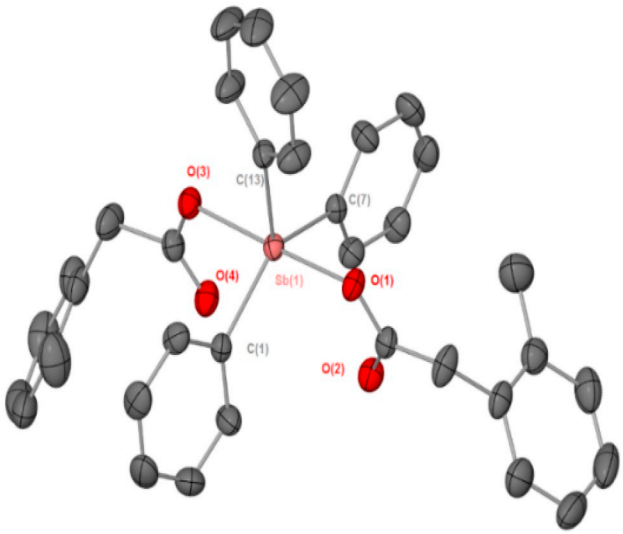

Fig. 8. Solid state structure of $[Sb(C_6H_5)_3((O_2CCH_2C_6H_4CH_3)_2]$, **1S**. Thermal ellipsoids at 50% probability. Hydrogen atoms have been omitted for clarity. Selected bonds lengths (Å) and angles (°). Sb(1) – O(1), 2.110(14), Sb(1) – O(3), 2.131(14), Sb(1) – C(1), 2.108(19), Sb(1) – C(7), 2.104(19), Sb(1) – C(13), 2.116(18); C(7) – Sb(1) – C(1), 139.1(7), C1 – Sb(1) – C(13), 113.5(7), C1 – Sb (1) – O(1), 90.71(6), O(1) – Sb(1) – O(3), 174.0(5).

carboxylate oxygen O(1), with comparative lengths of 1.901(5) Å versus 2.147(3) Å. This shorter bond distance has been observed previously in oxido bridge Sb(V) complexes. Quan et al., Abakumov et al. and Preut et al., all reported Sb—O bond lengths of 1.950(4) Å, 1.968(6) Å and 1.936(1) Å respectively [38–40]. Each carboxylate ligand occupies the remaining axial position, forming an almost linear angle for O (1) – Sb(1) – O(5) of 175.2(8)°. The angle of the oxido bridge in **7S** (Sb (1) – O(5) – Sb(1)′, 179.9(18)°) is linear with respect to the two Sb(V)

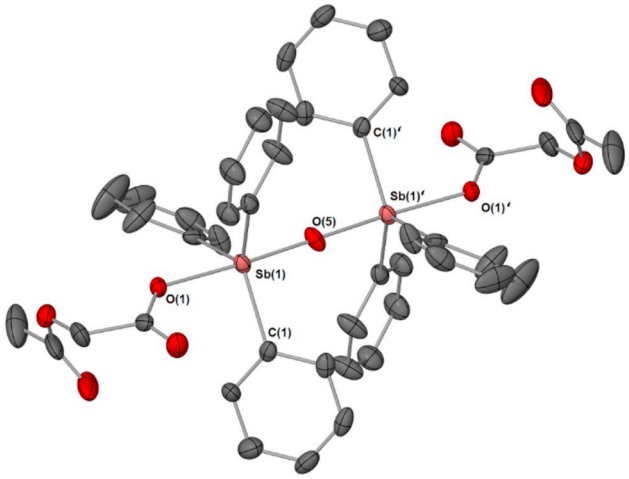

Fig. 9. Solid state structure of $[(SbPh_3(O_2CCR))_2O]$, **7S**. Thermal ellipsoids at 50% probability. Hydrogen atoms have been omitted for clarity. Selected bonds lengths (Å) and angles (°). Sb(1) – O(1), 2.147(3), Sb(1) – O(5), 1.951(5), Sb(1) – C(1), 2.110(4), Sb(1) – C(7), 2.108(5), Sb(1) – C(13), 2.106(4); C(7) – Sb(1) – C(1), 126.5(17), C(1) – Sb(1) – C(13), 115.9(17), C1 – Sb(1) – O(1), 90.46(16), O(1) – Sb(1) – O(5), 175.2(8), Sb(1) – O(5) – Sb(1)', 179.9(18). Symmetry operator′ = 1 − x, 1 − y, 1 − z.

centres on the axial plane. Similar linearity was observed in the complex {$[SbPh_3(C_2H_2ClO_2)_2]O$} characterised by Quan et al. with a formal angle of 180° for the Sb—O—Sb bond [38]. These oxido bridges are not always found to be linear, as a second triaryl carboxylato complex, {$[SbPh_3(C_6H_3ClNO_2)_2]O$} later characterised by Quan et al. exhibited distortion of the oxido bridge angle from the ideal 180° with an angle of 165.1(4)° obtained. This was characterised as a bent geometry about the Sb – O – Sb angle [41].

3.5. Stability studies

For complexes to exhibit viable anti-parasitic activity and to be considered as potential drugs a high degree of stability is required. As such, studies of all complexes in both the solid and solution state were conducted. Melting point analysis over several months on all the complexes showed them to be stable to atmospheric conditions in the solid-state. Assessment of solution stability was conducted through ^1H NMR spectral data in either $CDCl_3$ or d_6-DMSO over the period of one week. The NMR spectrum of each complex was recorded at room temperature (*ca* 24 °C) at t = 0 and 48 h and at t = 7 days. No changes in the expected chemical shifts and integral values were observed, confirming stability of the compounds in solution over that time. Complex **7S** was the exception undergoing hydrolysis at the oxido bridge to form two equivalents of a new hydroxido complex **7S′**, as previously described. Thus, it is established that complex **7S** is unstable in polar protic solvents while the thermodynamically favoured product of the equilibrium **7S′** is. **7S′** was isolated as a pure complex from a mixture of DMSO:H_2O and when re-dissolved in d_6-DMSO remained in solution as **7S′** with no formation of the original complex **7S** observed.

Previously, we have found that while complexes of the general formula $[BiAr_3(O_2CR)_2]$) are stable in water and DMSO (Ar = Ph, Tol) they readily undergo decomposition in DMEM culture media, decomposing to half their original concentration within 2 h [22,23]. From our more recent studies, complexes with chelating α-hydroxy carboxylate ligands show higher stability in the culture media with half-lives of 50 + h. The current study sought to establish whether the two carbon structural backbone contributed to this improved stability [24], but unfortunately for the new Bi(V) complexes the decomposition process was found to take between 5 and 6 h, though significant activity was still observed on both the parasite and the mammalian cells within the

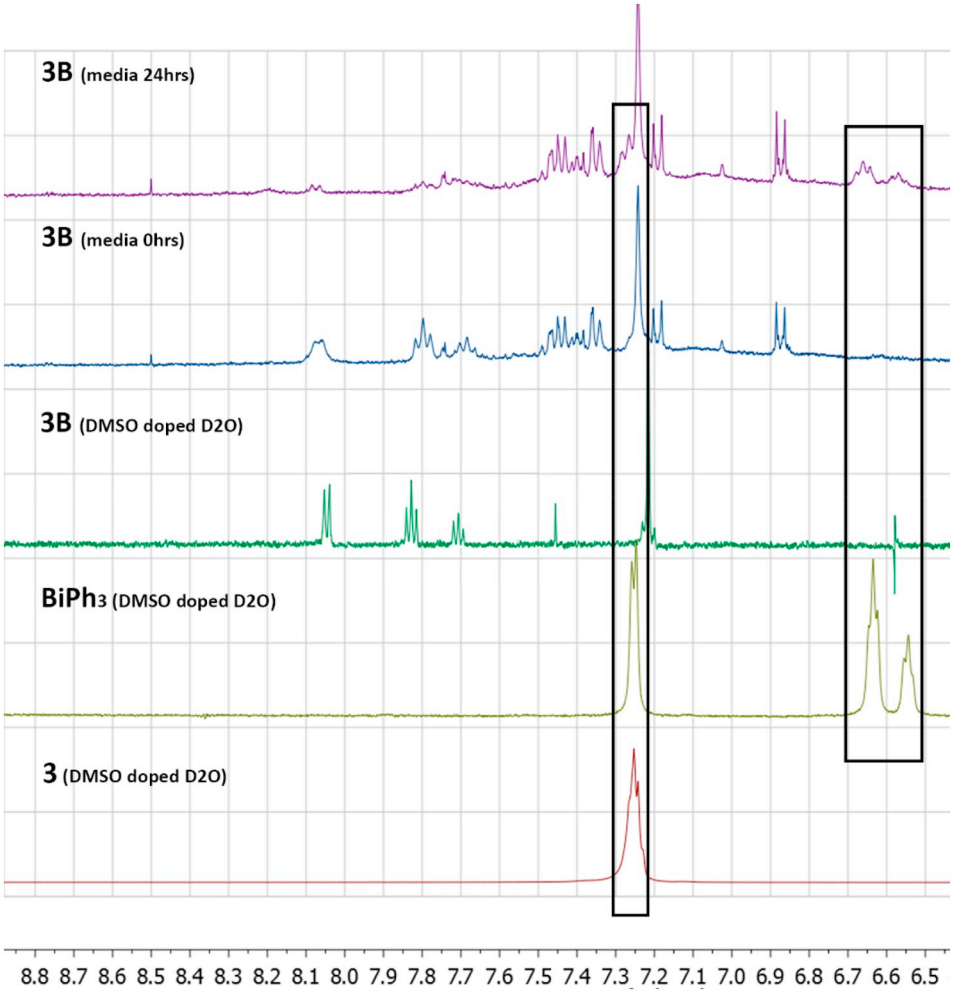

Fig. 10. ^{1}H NMR decomposition of complex **3B** in d_6-DMSO doped freeze dried D_2O DMEM culture medium, at 25 °C at 0 and 24 h, references of the complex, **3B**, $BiPh_3$ and free ligand **3** in d_6-DMSO:D_2O given.

short timeframe. The implication from this is that it is the chelating nature of the α-hydroxy carboxylate ligands which is the main contributing factor to the increased stability in the culture medium.

In this study **3B**, $[BiPh_3(O_2CCH_2C_6H_4CH_3)_2]$ (from *p*-tolylacetic acid), was selected as the test compound since its stability in d_6-DMSO and structure are representative of all the other Bi(V) complexes. The complex was placed in 1 mL of DMEM media which was previously freeze dried and resuspended into D_2O, thus minimising the NMR signal from H_2O. A small degree of precipitation was observed for two of the eight Bi(V) compounds (**7B** and **8B**). Initial studies on **3B** at t = 0 and 24 h showed that after 24 h the complex had almost completely dissociated into the parent $BiPh_3$ and *p*-tolylacetic acid, with only traces of **3B** remaining. This reflects and confirms our previous study on the decomposition of such Bi(V) complexes in culture medium.

The decomposition into $BiPh_3$ can be observed at 7.2, 6.6 and 6.5 ppm, however the *ortho* and *meta* aromatic signals for the acid, **3a**, overlap with those from both the culture media and $BiPh_3$ at 7.2 ppm (Fig. 10). However, the appearance of a multiplet beside the large singlet can be seen at 7.2 ppm as **3B** undergoes decomposition into the parent acid, **3**, and $BiPh_3$, along with the characteristic signals of the *para* and *meta* aromatics of $BiPh_3$ at 6.6 and 6.5 ppm (Fig. 10).

A 12 × 1 hr study was then conducted to elucidate the half-life of the complex, along with a corresponding study on the antimony analogue **3S**. The signal corresponding to the *p*-CH of the phenyl group of the complex was compared over time to a constant signal from the culture media at 5 ppm. Though complex **3B** decays rapidly, it shares a

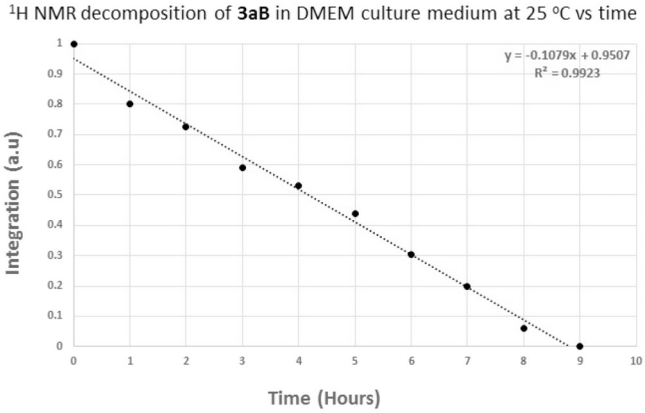

Fig. 11. ^{1}H NMR decomposition curve of $[BiPh_3((O_2CCH_2C_6H_4CH_3)_2]$, **3B** at 10 mM, in DMEM culture medium at 25 °C *vs* time. Half-life = 5.2 h, rate constant = 48 μM/h.

linear decomposition with the previously synthesised α-hydroxy complexes (Fig. 11). This zero-order decay was found to have a rate constant of approximately 59.5 μM/h, decaying to half the original 500 μM concentration after 4.2 h.

The NMR study conducted on the analogous antimony complex **3S** exhibited unsurprising results, with no decomposition in the media observed. No significant changes in the integration of the *o*-CH protons

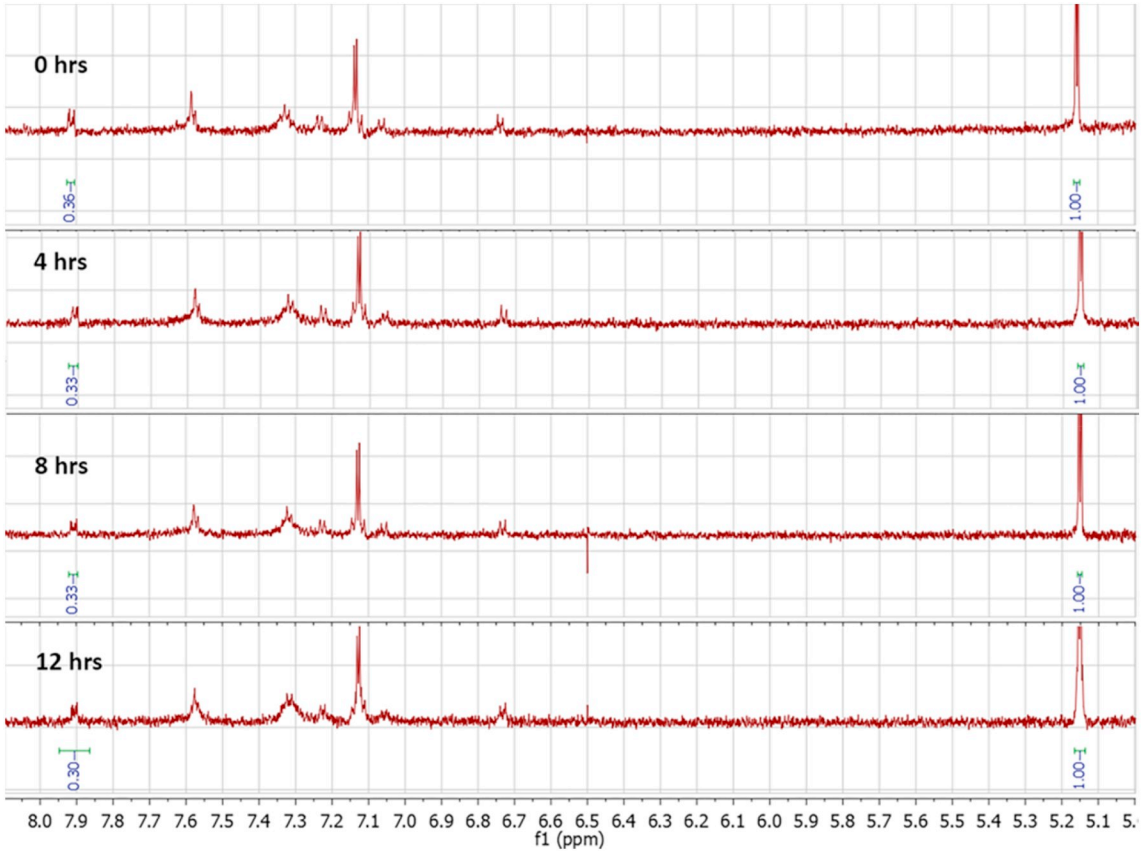

Fig. 12. ^{1}H NMR spectral study of complex [$SbPh_3((O_2CCH_2C_6H_4CH_3)_2$], **3S** at 10 mM, in DMEM culture medium, at 25 °C at 0, 4, 8 and 12 h.

of the phenyl ring relative to the same signal of the media at 5 ppm was observed over the 12 h period (Fig. 12).

3.6. Biological activity

Despite the instability of the Bi(V) complexes in the culture medium they were still included in the initial assays against both human fibroblasts and *L. major* promastigotes so that an assessment of their toxicity could be made and compared with their Sb(V) analogues. As expected, the Sb(V) complexes exhibited a high degree of solubility in the culture medium, while two of the Bi(V) complexes (**7B** and **8B**) formed partially opaque solutions, indicating a small degree of precipitation. Without completely soluble components it is not possible to have the known concentration gradient which a requirement for establishing an accurate assessment of toxicity. As complexes **2S** and **8S** have been tested previously on *L. major* and human fibroblasts, no further assays were conducted [21]. Complexes **4S** and **6S** have been previously tested on *L. tropica*, giving IC_{50} values of 18.3 and 20.9 μM respectively [26]. Because of physiological differences with *L. major* it was considered appropriate to include them is this study. *L. major* compared to several other species was observed to be more resilient to the commercial drugs currently on the market and therefore a more difficult vector to combat [42]. All eight ligands were also assessed for their potential toxicity towards mammalian cells and found to exhibit little to no activity at concentration of ≥100 μM, with the exception of **3** which shows some minor toxicity, with an IC_{50} of 72.9 μM. Ligands **6**, **7**, and **8** exhibited a small degree of activity, with a slight drop in the viability at concentrations ≥12.5 μM, though this change in %viability was insignificant in comparison to the complexed Bi(V) and Sb(V) analogues as all three ligands still retained an IC_{50} of ≥100 μM. The viability graphs of the ligands can be found in the ESI.

The Bi(V) complexes exhibited non-selective toxicity towards both *L. major* and mammalian cells, illustrated in Fig. 12. In contrast, the Sb (V) complexes, with the exception of **7S**, were all found to stable and soluble and to be significantly more toxic towards *L. major* than the fibroblast cells, thereby providing a good selectivity index for each complex [24].

For the bismuth complexes **1B–8B** the IC_{50} values for *L. major* were found in the range of 2.06 μM–4.63 μM while the antimony complexes **1S–8S** gave were in the range of 6.18–19.1 μM (Fig. 13). This attests to the potency of the bismuth complexes towards the parasite cells as they are present in a reduced concentration because of their rapid decomposition. However, the IC_{50} values for the human primary fibroblasts were between 11.4 and 19.8 μM. As such, no further assays were conducted with the Bi(V) complexes. This further supports the high reduction potential of Bi(V) playing a primary role in the non-selective toxicity rather than stability and ligand class effects.

In contrast, the Sb(V) complexes exhibited a much lower toxicity to the human fibroblast cells, with complex **7S′** presenting with the lowest IC_{50} value of 73.8 μM. The six remaining Sb(V) complexes all gave an IC_{50} value of > 100 μM. A table of the IC_{50} values can be found in the ESI (Tables S4 and S5). The Sb(V) complexes were therefore taken forward into an amastigote invasion assay.

3.7. Selectivity of Bi(V) versus Sb(V)

This trend in stability and selectivity supports our previous observations and reports. In almost all cases, the Bi(V) analogues are non-selective, exhibiting high levels of toxicity towards both human fibroblasts and *L. major* parasites. In contrast, the Sb(V) analogues are selective, targeting only the parasite. This somewhat contradicts the common assumption that bismuth is a less toxic alternative to antimony, but the difference in toxicity can be attributed to the oxidation state and the difference in reduction potentials of Sb(V) and Bi(V)

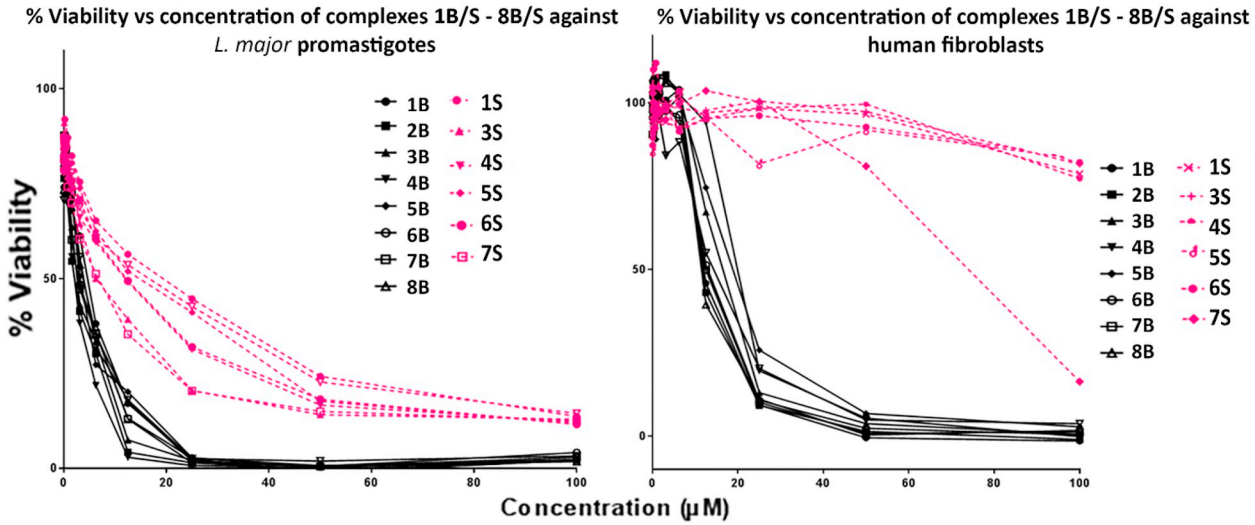

Fig. 13. Comparison of percentage cell viability after treatment with the Bi(V) complexes **1B–8B** (black) and the Sb(V) complexes **1S–8S** (pink), against *L. major* promastigotes and Human primary fibroblasts. Dose response curves were generated over a range of concentrations (48 nm–100 μM in the appropriate culture media from 10 mM DMSO stock solutions. All readings were compared spectroscopically to non-treated control and the percent growth inhibition calculated. A DMSO control and positive drug control (Amp B) were also included at the same range of concentrations which can be found in the ESI. Numerical data for each curve is given in the Supplementary information. (For interpretation of the references to color in this figure legend, the reader is referred to the web version of this article.)

(E^o = +V/+III = 0.59 and 2.03 V respectively) [7].

Both mammalian cells and *L. major* parasites are rich in sulfur containing proteins, such as trypanothione (parasite specific, TPH) and glutathione (parasite and mammalian cells, GSH), which, as reductants, are theorised to play an important role in maintaining pH and reducing oxidative stress in the cell, as well as having a key determining role in the mechanism of action of the metallodrugs [43,44]. Interactions of Sb (III) with leishmanial TPH have been identified by protein crystallography, disclosing the actual mechanism of action in the trivalent state. The Sb(III) binds to the protein active site with high affinity, interacting directly with two cysteine moieties and one threonine and histidine, blocking hydride transfer and trypanthione reduction [45]. This interaction with the sulfur rich moieties, such as cysteine and methionine side chains of proteins, is consistent with the thiophilic nature of the group 15 metals/metalloids [26]. Bismuth is a highly thiophilic metal, preferring sulfur bonds over oxygen. In the +III state bismuth readily exchanges carboxylate ligands for S containing moieties, so it can be inferred that in the more reactive +V state, it will readily reduce in the presence of sulfur rich proteins where the redox-based thiol/disulfide pair plays a key function [46]. The high reduction potential of Bi(V) could possibly induce redox chemistry within the cell, reducing Bi(V) to Bi(III) and subsequently oxidising sulfur rich proteins in the process, rendering them inactive. This could then cause a cascade effect in which the cells undergo oxidative stress and finally apoptosis, similar to processes observed with the trivalent Sb(III). Biological reduction of an unstable oxidation state metal in both intracellular and extracellular processes is commonly observed with major contributing metals being chromium +VI and manganese +IV. Reduction of Cr(VI) and Mn(IV), similar to Bi(V), is believed to occur in part with interactions with low molecular weight thiols such as GSH and cysteine after crossing the cellular membrane [47,48]. The reduction potential of both Cr(VI)/Cr(III) and Mn(IV)/Mn(III) are significantly large (1.36 V and 1.22 V respectively) leading to facile intracellular reduction, and hence generalised oxidative stress and damage [7,49]. As previously mentioned, the reduction of potential of Bi(V)/Bi(III) is significantly larger still at 2.03 V, inferring a potential high level of reactivity [7].

3.8. Amastigote invasion assay

Given the good selectivity indices (promastigote *vs* human fibroblast) established for the Sb(V) compounds, they were then taken forward to be assessed in an amastigote invasion assay - the more clinically relevant form of the parasite. In order for the promastigotes to differentiate into the amastigote form, bone-marrow derived macrophages (BMDM) were infected with promastigotes for 48 h. BMDMs were then washed, resuspended in media and 10 μM solutions of complexes **1S** and **3S–7S** added. The plates were further incubated for a further 48 h. Assessment of the complex activity was determined by counting infected versus non-infected cells. Infected macrophages are distinguished by the presence of amastigotes within the cytosol (Fig. 14).

Statistically significant activity, when compared to the positive control, was observed for all complexes, ranging from mild to good activity (Fig. 15). Complex ***7S′***, however, was found to be cytotoxic to the mammalian macrophages as well as the parasite, as concluded by

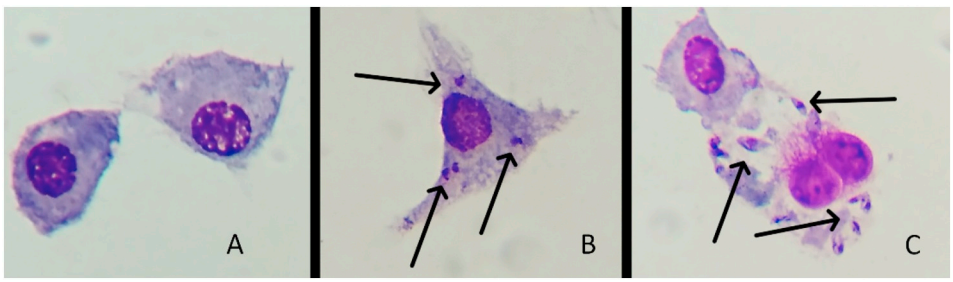

Fig. 14. A) Non-infected macrophages; **B**) infected macrophage; **C**) macrophage under apoptotic stress following treatment with *tri*phenylantimony *bis*(*o*-tolylacetate), **1S**. Amastigotes are labelled with arrows. Images taken at 100× magnification oil immersion.

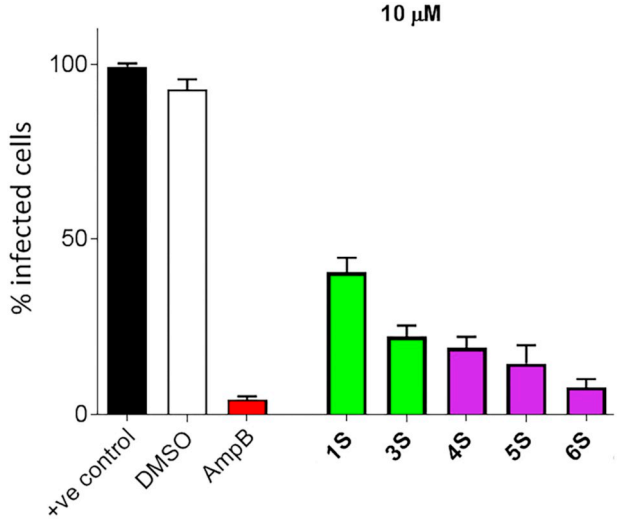

Fig. 15. Infected macrophages after 48 h. Number of infected macrophage was determined microscopically, in duplicate of fixed specimens. Amphotericin B (AmpB) was used as a positive control at 10 μM concentration. A DMSO control was also employed at a 1% concentration. Error bas indicate SEM, one-way ANOVA. Dunnett's multiple comparison test was used to determine the statistical significance between all test compounds and a positive control lacking treatment (+ve control).

the presence of no viable cells on either slide tested. Though active, the % infected cells for the tolylacetates were found to be the highest, with **1S** and **3S** presenting with values of 40.5% ± 2.01 and 22.3% ± 1.55 respectively. The methoxyphenylacetates **4S**, **5S** and **6S** proved more effective than the tolyacetates, with a trend correlating to the position of the methoxy functionality, with efficiency increasing in the order *o*-OMe ≥ *m*-OMe ≥ *p*-OMe. A similar trend is also observed for the tolylacetates, **1S** and **3S**, with efficiency increasing from *o*-Tol to *p*-Tol. Complex **6S** exhibited notable activity, with a value of 7.75% ± 1.18, while **4S** and **5S** were also moderately effective with values of 19.0% ± 1.58 and 14.5% ± 2.63 respectively.

Though the methoxyphenylacetate in particular was significantly effective, the complexes tested still lacked the potent activity of previously synthesised Sb(V) triaryl dicarboxylato complexes which were found to exhibit significant activity at concentrations of 0.5–3.5 μM. The toxicity of the previous complexes toward human fibroblast was considerably higher though with the minimum IC_{50} of 25 μM observed [21,24]. As these newly synthesised Sb(V) complexes are significantly less toxic and their amastigote activity within clinically relevant concentrations, they present as potential drug candidates.

4. Conclusions

Eight Bi(V) and nine Sb(V) heteroleptic organometallic carboxylate complexes have been successfully synthesised, characterised, and assessed for their potential as anti-leishmanial agents. Twelve of the complexes are novel (1B–8B, 1S, 3S, 7S and 7S′) while four; 2S, 4S, 6S and 8S, have been synthesised previously, albeit it by a different synthetic route. The solid-state structures of all complexes, with the exception of 2S, were obtained through single crystal X-ray diffraction. As found in previous studies, the carboxylate moieties bind in a didentate chelating mode in the Bi(V) while they are monodentate in the Sb(V) complexes. All complexes except 7S adopt a trigonal bipyramidal geometry, common for complexes of general formula $[MAr_3(O_2CR)_2]$. The dinuclear Sb(V) oxido-bridged complex 7S $[(SbPh_3(O_2C{-}O{-}C(=O)Me))_2O]$, adopts a distorted octahedral geometry. In solution, this complex undergoes hydrolysis giving two equivalents of the complementary mono-nuclear hydroxido Sb(V) complex $[SbPh_3(O_2C{-}O{-}C(=O)Me)OH]$, **7S′**.

All complexes, with the exception of **2S** and **8S**, were assessed for their anti-leishmanial activity with the Sb(V) complexes being significantly more selective in their toxicity towards the parasite cells and human fibroblast cells than their Bi(V) counterparts. The Bi(V) complexes demonstrate high levels of toxicity to both cell types showing generalised non-selective toxicity. An amastigote invasion assay on the Sb(V) complexes revealed some structure-activity relationships determined by the positioning of the functional group on the aryl ring of the carboxylate ligands.

There is an increase in activity following the order *o*-OMe > *m*-OMe > *p*-OMe, and a similar trend for the tolylacetates with *o*-Tol > *p*-Tol. Complex **6S**, derived from 4-methoxyphenylacetic acid, in particular is a potential lead compound. In conclusion, the high oxidising ability and low stability of the Bi(V) complexes leads to non-specific toxicity and low selectivity. The triaryl Sb(V) complexes are far superior anti-parasitic activity and are currently better candidates for lead compounds and anti-leishmanial agents.

Conflicts of interest

There are no conflicts to declare.

Acknowledgements

The authors would like to thank the Australian Research Council (DP170103624) and Monash University for financial support. We would also like to thank Dr. Craig Forsyth (Monash) for assistance with X-ray crystallography.

Appendix A. Supplementary data

Supplementary data to this article can be found online at https://doi.org/10.1016/j.jinorgbio.2018.08.015.

References

[1] M. Boelaert, F. Meheus, A. Sanchez, S. Singh, V. Vanlerberghe, A. Picado, B. Meessen, S. Sundar, Tropical Med. Int. Health 14 (2009) 639–644.
[2] G. Mandal, V. Govindarajan, M. Sharma, H. Bhattacharjee, R. Mukhopadhyay, Antimicrob. Drug. Resist, Springer, 2017, pp. 649–665.
[3] J. Alvar, I.D. Vélez, C. Bern, M. Herrero, P. Desjeux, J. Cano, J. Jannin, M. den Boer, W.L.C. Team, PLoS One 7 (2012) e35671.
[4] W.H. Organization, 1990.
[5] S.M. Gossage, M.E. Rogers, P.A. Bates, Int. J. Parasitol. 33 (2003) 1027–1034.
[6] J. van Griensven, M. Balasegaram, F. Meheus, J. Alvar, L. Lynen, M. Boelaert, Lancet Infect. Dis. 10 (2010) 184–194.
[7] H. Sun, Biological Chemistry of Arsenic, Antimony and Bismuth, Wiley Online Library, 2011.
[8] M.K. Pathak, T. Yi, J. Immunol. 167 (2001) 3391–3397.
[9] A. Stauch, H.-P. Duerr, J.-C. Dujardin, M. Vanaerschot, S. Sundar, M. Eichner, PLoS Negl. Trop. Dis. 6 (2012) e1973.
[10] D. Légaré, M. Ouellette, Antimicrob. Resist. (2017) 313–341.
[11] M. Ouellette, J. Drummelsmith, B. Papadopoulou, Drug Resist. Updat. 7 (2004) 257–266.
[12] S. Sundar, T.K. Jha, C.P. Thakur, S.K. Bhattacharya, M. Rai, Trans. R. Soc. Trop. Med. Hyg. 100 (Supplement 1) (2006) S26–S33.
[13] N. Baker, H.P. de Koning, P. Mäser, D. Horn, Trends Parasitol. 29 (2013) 110–118.
[14] K. Seifert, M. Duchêne, W.H. Wernsdorfer, H. Kollaritsch, O. Scheiner, G. Wiedermann, T. Hottkowitz, H. Eibl, Antimicrob. Agents Chemother. 45 (2001) 1505–1510.
[15] L.H. Freitas-Junior, E. Chatelain, H.A. Kim, J.L. Siqueira-Neto, Int. J. Parasitol. Drugs Drug Resist. 2 (2012) 11–19.
[16] N. Tiwari, M.R. Gedda, V.K. Tiwari, S.P. Singh, R.K. Singh, Mini-Rev. Med. Chem. 18 (2018) 26–41.
[17] B. Purkait, A. Kumar, N. Nandi, A.H. Sardar, S. Das, S. Kumar, K. Pandey, V. Ravidas, M. Kumar, T. De, Antimicrob. Agents Chemother. 56 (2012) 1031–1041.
[18] R.A. Demel, B. De Kruyff, Biochim. Biophys. Acta Rev. Biomembr. 457 (1976) 109–132.
[19] A. Ponte-Sucre, F. Gamarro, J.-C. Dujardin, M.P. Barrett, R. López-Vélez, R. García-Hernández, A.W. Pountain, R. Mwenechanya, B. Papadopoulou, PLoS Negl. Trop. Dis. 11 (2017) e0006052.
[20] J.A. Salvador, S.A. Figueiredo, R.M. Pinto, S.M. Silvestre, Future Med. Chem. 4 (2012) 1495–1523.
[21] M.I. Ali, M.K. Rauf, A. Badshah, I. Kumar, C.M. Forsyth, P.C. Junk, L. Kedzierski,

P.C. Andrews, Dalton Trans. 42 (2013) 16733–16741.
[22] Y.C. Ong, V.L. Blair, L. Kedzierski, P.C. Andrews, Dalton Trans. 43 (2014) 12904–12916.
[23] Y.C. Ong, V.L. Blair, L. Kedzierski, K.L. Tuck, P.C. Andrews, Dalton Trans. 44 (2015) 18215–18226.
[24] R.N. Duffin, V.L. Blair, L. Kedzierski, P.C. Andrews, Dalton Trans. 47 (3) (2018) 971–980.
[25] Y. Kim, J.-Y. Cho, J.-H. Kuk, J.-H. Moon, J.-I. Cho, Y.-C. Kim, K.-H. Park, Curr. Microbiol. 48 (2004) 312–317.
[26] R. Mushtaq, M.K. Rauf, M. Bolte, A. Nadhman, A. Badshah, M.N. Tahir, M. Yasinzai, K.M. Khan, Appl. Organomet. Chem. 31 (2017).
[27] D.H. Barton, N.Y. Bhatnagar, J.-P. Finet, W.B. Motherwell, Tetrahedron 42 (1986) 3111–3122.
[28] L. Kedzierski, J.M. Curtis, M. Kaminska, J. Jodynis-Liebert, M. Murias, Parasitol. Res. 102 (2007) 91–97.
[29] A. Pathak, V.L. Blair, R.L. Ferrero, L. Kedzierski, P.C. Andrews, J. Inorg. Biochem. 177 (2017) 266–275.
[30] K. Lackovic, J.P. Parisot, N. Sleebs, J.B. Baell, L. Debien, K.G. Watson, J.M. Curtis, E. Handman, I.P. Street, L. Kedzierski, Antimicrob. Agents Chemother. 54 (2010) 1712–1719.
[31] B. AXS, Madison, vol. US, 2014.
[32] G. Sheldrick, Bruker AXS Inc., Madison, WI, 2002.
[33] G.M. Sheldrick, Acta Crystallogr. Sect. A: Found. Crystallogr. 64 (2008) 112–122.
[34] O.V. Dolomanov, L.J. Bourhis, R.J. Gildea, J.A. Howard, H. Puschmann, J. Appl. Crystallogr. 42 (2009) 339–341.
[35] D.V. Moiseev, Y.B. Malysheva, A.S. Shavyrin, Y.A. Kurskii, A.V. Gushchin, J. Organomet. Chem. 690 (2005) 3652–3663.
[36] V. Sharutin, I. Egorova, O. Sharutina, T. Ivaneko, M. Pushilin, A. Gerasimenko, Chem. Comput. Simul. Butlerov Commun, 9 (2002), pp. 59–64.
[37] G. Deacon, R. Phillips, Coord. Chem. Rev. 33 (1980) 227–250.
[38] L. Quan, H. Yin, D. Wang, Acta Crystallogr. Sect. Sect. E: Struct. Rep. Online 64 (2008) m349.
[39] G. Abakumov, N. Vavilina, Y.A. Kurskii, L. Abakumova, G. Fukin, V. Cherkasov, A. Shavyrin, E. Baranov, Russ. Chem. Bull. 56 (2007) 1813–1820.
[40] H. Preut, R. Rüther, F. Huber, Acta Crystallogr. Sect. C: Cryst. Struct. Commun. 41 (1985) 358–360.
[41] L. Quan, H. Yin, D. Wang, Acta Crystallogr. Sect. Sect. E: Struct. Rep. Online 65 (2009) m99.
[42] P. Escobar, S. Matu, C. Marques, S.L. Croft, Acta Trop. 81 (2002) 151–157.
[43] J. Walker, J.-J. Vasquez, M.A. Gomez, J. Drummelsmith, R. Burchmore, I. Girard, M. Ouellette, Mol. Biochem. Parasitol. 147 (2006) 64–73.
[44] A.B. Prowse, L.R. McQuade, K.J. Bryant, D.D. Van Dyk, B.E. Tuch, P.P. Gray, Proteomics 5 (2005) 978–989.
[45] P. Baiocco, G. Colotti, S. Franceschini, A. Ilari, J. Med. Chem. 52 (2009) 2603–2612.
[46] H.A. Phillips, M.D. Eelman, N. Burford, J. Inorg. Biochem. 101 (2007) 736–739.
[47] A. Zhitkovich, Chem. Res. Toxicol. 18 (2005) 3–11.
[48] H. Eriksson, K. Mägiste, L.-O. Plantin, F. Fonnum, K.-G. Hedström, E. Theodorsson-Norheim, K. Kristensson, E. Stålberg, E. Heilbronn, Arch. Toxicol. 61 (1987) 46–52.
[49] P. Vanýsek, Handbook of Chemistry and Physics, CRC, 1977.

European Journal of Medicinal Chemistry xxx (xxxx) xxx

Contents lists available at ScienceDirect

European Journal of Medicinal Chemistry

journal homepage: http://www.elsevier.com/locate/ejmech

Research paper

Alkyl gallium(III) quinolinolates: A new class of highly selective anti-leishmanial agents

Rebekah N. Duffin [a], Victoria L. Blair [a], Lukasz Kedzierski [b], Philip C. Andrews [a, *]

[a] School of Chemistry, Monash University, Clayton, Melbourne, VIC, 3800, Australia
[b] Faculty of Veterinary and Agricultural Sciences at the Peter Doherty Institute for Infection and Immunity, 792 Elizabeth Street, Melbourne, 3000, Victoria, Australia

ARTICLE INFO

Article history:
Received 10 September 2019
Received in revised form
15 November 2019
Accepted 15 November 2019
Available online xxx

Keywords:
Gallium
Quinolinol
Bacteria
Leishmania
Structure

ABSTRACT

A series of eight alkyl gallium complexes of general formulae [$GaMe_2(L)$] and [$Ga(Me)_2L$] have been synthesised, characterised and their antimicrobial activity against bacteria, cancer cells and *Leishmania* assessed. All eight complexes are novel, with the solid-state structures of all complexes successfully authenticated by single crystal X-ray diffraction. The dimethyl complexes all adopt a four-coordinate tetrahedral confirmation, while the monomethyl complexes are five-coordinate trigonal bipyramidal. All complexes were screened for their anti-bacterial activity either by solution state diffusion, or a solid-state stab test. The five soluble complexes underwent testing against two differing mammalian cell controls, with excellent selectivity observed against COS-7 cells, with an IC_{50} range of 88.5 μM to ≥100 μM. Each soluble complex was also tested for their anti-cancer capabilities, with no significant activity observed. Excellent activity was exhibited against the protozoan parasite *Leishmania major* (strain: V121) in both the promastigote and amastigote forms, with IC_{50} values ranging from 1.11 μM −13.4 μM for their anti-promastigote activity and % infection values of 3.5% ± 0.65−11.5% ± 0.65 for the more clinically relevant amastigote. Selectivity indices for each were found to be in the ranges of 6.61 −64.7, with significant selectivity noted for two of the complexes. At minimum, the gallium complexes show a 3-fold enhancement in activity towards the *Leishmania*amastigotes over the parent quinolinols alone.

1. Introduction

Neglected tropical diseases continue to be a growing worldwide problem, impacting not only on the health and wellbeing of millions of people but having a large negative impact on economic development in the affected countries [1]. Leishmaniasis is of particular concern owing to its distribution and prevalence in low socio-economic areas of the planet [2]. The World Health Organisation (WHO) estimates that in the 98 countries where the parasite resides there are between 0.2 and 0.4 million new cases of the potentially fatal visceral Leishmaniasis (VL) every year, of which around 10% of result in death [3–5]. The current front-line treatments remain the pentavalent antimonials; antimony stibogluconate (Pentostam ™) and meglumine antimoniate (Glucantime ™). However, they place a high toxic load on the body and require daily intravascular delivery under clinical conditions, often resulting in unwanted side-effects and poor compliance [6]. Also, through a lack of proper hygiene and improper use of conventional medications, drug resistance is becoming a major hurdle in the treatment of Leishmaniasis [7]. Mostly due to exposure of infected communities to increased levels of As(V) in drinking water. Native strains of *Leishmania* have evolved an arsenic reductase enzymes that are able to act upon the Sb(V) drugs, further contributing to an increase in parasite resistance [8–10]. It is not yet known whether new Sb(V) complexes will also be impacted by the resistance pathways that act upon the current front-line drugs. Though many metals, including transition metals, have been utilised for the synthesis of anti-leishmanials, antimony remains the number one choice of metal, with a varying degree of activity noted for complexes of both Sb(V) and Sb(III) [11–17].

Antimony can be a toxic metalloid and this proved difficult to overcome in researching existing and future medicinal applications. Most of the pentavalent antimony complexes studied exhibit a high degree of anti-parasitic activity, but mammalian cell toxicity

* Corresponding author.
E-mail address: phil.andrews@monash.edu (P.C. Andrews).

https://doi.org/10.1016/j.ejmech.2019.111895
0223-5234/

remains a challenge. A large degree of variation has been observed in the selectivity with some proving to be cytotoxic at levels similar to their anti-parasitic activity [11–14,16,18]. Antimony complexes exhibit a reliance on redox active pathways within the parasites in order to function to their full potential. The most widely accepted theory of the mechanism of action is based on the reduction of Sb(V) to Sb(III) intracellularly, inhibiting essential sulfur rich proteins by competitive binding [17]. This redox reliance has been a contributing factor to the increased resistance to the conventional treatments, alluding to the potential formation of parasitic resilience to future Sb(V) compounds synthesised [3,9,19].

Unlike antimony, gallium is not limited by its redox chemistry existing largely in its stable 0 and + III oxidation states. It has long been utilised in the synthesis and evaluation of medicinal complexes, as diagnostics, anti-microbials and most notably in the treatment of cancers [20–22]. The anti-microbial and anti-cancer activity is theorised to be due to the pharmacological properties of Ga^{3+}. The properties of Ga(III) are similar to those of Fe(III), having similar electronegativities (1.70 V and 1.96 V respectively), ionic radius (0.76 and 0.63 respectively) and a preference for a six coordinate geometry [23,24]. It is postulated that Ga(III) can replace and/or mimic Fe(III) in biological systems, substituting into important metalloprotein and enzymes. Microbial and proliferative cells uptake the Ga(III) via transport enzymes such as lactoferrin and transferrin [25,26], once inside Ga(III) inhibits cellular function by inhibition of iron pathways due to its inability to be reduced under physiological conditions [27,28], This is particularly prominent, though not limited to fast growing cells such as cancerous cells [29,30].

In order to grow and reproduce, both bacteria and parasites such as *Leishmania* require iron. In most cases, bacteria and *Leishmania* must obtain iron from exogenous sources. Bacteria have evolved differing methods to acquire iron from their surroundings, including high iron affinity siderophores, and surface receptors that specifically bind transferrin or lactoferrin [31,32]. Eukaryotes are a little more sophisticated in their iron acquisition, with subtle changes present in the different strains of *Leishmania*. For example, *L. chagasi* utilises a transferrin-binding protein on its cellular surface to harvest iron from its immediate environment inside mammalian macrophages, whereas *L. donavani*, another VL causing parasite, acquires iron through a saturable binding of haem [33–36]. By exploiting these mechanisms for iron uptake, it may be possible to substitute the iron for gallium, thereby causing cellular stress due to the inability for redox active pathways to commence. Gallium has previously been observed to inhibit iron pathways in several bacterial strains, such as *Mycobacterium avium* localised inside and outside of mammalian macrophages [37]. Though traditionally synthesised as anti-cancer agents, there is potential application of gallium chelates as microbial iron inhibitors due to competitive binding to transferrin leading to a large amount of cellular gallium uptake [38]. Though a potent inhibitor of bacterial and cancerous cell iron pathways, there is a paucity of studies on gallium as an anti-Leishmanial, with only one recent study from 2013 using curcumin derivatives. However, this study provided no insights into the activity against the clinically relevant amastigote form of the parasite, and neglected to assess the overall selectivity of the complexes [39].

Not only is the metal centre an important aspect in the biological activity of the overall complex, but so is the ligand class. Gallium is readily stabilised by organic chelates [37], such as the *N,O* donor 8-quinolinol (8-hydroxyquinoline, 8QH). The biological activity of unsubstituted 8-quinolinol stems from an initial study by Albert et al., in which they concluded that the bioactivity of 8QH was influenced by the presence of metals within the cellular media [40]. The biological potential of 8QH and its metal chelates has been extensively study against a large variety of ailments, including *Leishmania*, with promising results [41,42]. Gallium *tris*-8-quinolinolate, KP46, has reached phase II clinical trials as an anti-cancer agent. It was found to possess a high degree of thermodynamic stability ($\log\beta_3 = 40.7$), however, its high hydrolytic stability ($4.8 + 0.9 \times 10^{-5}\ s^{-1}$) means that it does not rapidly release gallium to transfer proteins such as transferrin, leading to a less effective anti-microbial [37,43]. Calculations on plasma models of KP46 concluded that the complex stays intact after traversing the gastrointestinal tract. This differed from other phase II gallium anti-cancer agents such as gallium maltolate, which releases Ga^{3+} into the bloodstream after absorption [44]. Therefore, it is essential to explore the fine line between a reactive and a stable compound, when contemplating the synthesis of a new class of metallodrugs.

In order to produce a complex that still exhibits cellular media stability, but is also labile enough to function as an iron mimic, we turned to alkyl gallium complexes. Trimethylgallium is a versatile and highly reactive precursor, which is notably pyrophoric. The idea was to generate dimethyl and monomethyl gallium quinolinols with the hope that the inclusion of Ga–C bonds would allow for increased activity with transferrin and lactoferrin. We also investigated the effect of halide substitution on the 8-quinolinol and whether there was a correlation between halide size and bioactivity. Therefore, four different halido substituted quinolinols; 5-chloroquinolinol (**1**), 5,7-dichloroquinolinol (**2**), 5,7-dibromoquinolinol (**3**) and 5,7-diiodoquinolinol (**4**), were selected for this study (Fig. 1). Each of these halido-quinolinols have been extensively studied against various microbes, with varying degrees of activity and selectivity [45–50]. Substitution on the 5 and 7 positions of the 8-quinolinol has previously shown to increase both lipid solubility and chelating ability, and markedly lower toxicity in higher animals [51]. Complexes of general formulae $[Ga(CH_3)L]$ and $[GaCH_3(L)_2]$ (Fig. 2) were synthesised, characterised and their activity against several strains of gram negative and gram-positive bacteria, cervical cancer, *L. major* promastigotes and amastigotes, and their cytotoxicity against two mammalian cell lines investigated as controls.

2. Results and discussion

2.1. Synthesis and characterisation

Synthesis of the alkyl gallium complexes; $[Ga(Me)_2C_9H_5NOCl]$ **1G**, $[Ga(Me)_2C_9H_4NOCl_2]$ **2G**, $[Ga(Me)_2C_9H_4NOBr_2]$, **3G** $[Ga(Me)_2C_9H_4NOI_2]$ **4G**, $[GaMe(C_9H_5NOCl)_2]$ **1G′**, $[GaMe(C_9H_4NOCl_2)_2]$ **2G′**, $[GaMe(C_9H_4NOBr_2)_2]$ **3G′**, $[GaMe(C_9H_4NOI_2)_2]$ **4G′**, was performed under an inert atmosphere, in the absence of air and moisture, following the addition of $Ga(CH_3)_3$ to either one or two equivalents of the quinolinols **1**–**4**, in either hexane or toluene at −78 °C [52]. This resulted in an immediate colour change to bright yellow solutions (**1G** - **4G**) or suspensions (**1G′**- **4G′**), dependant on stoichiometry. To obtain exclusively the monomethyl complexes the reaction mixture was allowed to warm to room temperature and then heated to reflux (Fig. 3). All the dimethyl complexes **1G** – **4G** were soluble in toluene but only sparingly in hexane. The monomethyl analogues (**1G′**- **4G′**) precipitated in both toluene and hexane. The filtrate of each though exhibited a yellow colouration, and when left to stand crystals of each respective complex formed over a period of one to three days.

The reaction involves deprotonation of the hydroxyl group at the 8 position and displacement of a methyl group, forming methane as the by-product. This provides a clean and highly favourable reaction process, and any excess quinolinol can be washed away with a polar solvent, such as ethanol or methanol. Each complex was obtained in excellent yields of between 89-97 %

Please cite this article as: R.N. Duffin et al., Alkyl gallium(III) quinolinolates: A new class of highly selective anti-leishmanial agents, European Journal of Medicinal Chemistry, https://doi.org/10.1016/j.ejmech.2019.111895

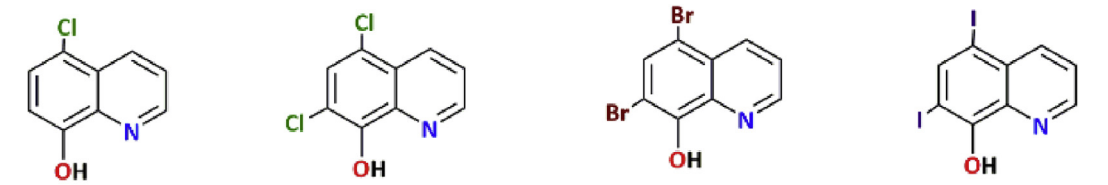

Fig. 1. Four halido substituted 8-quinolinols, C_9H_6NOCl, **1**, $C_9H_5NOCl_2$, **2**, $C_9H_5NOBr_2$, **3** and $C_9H_5NOI_2$, **4** used in this study.

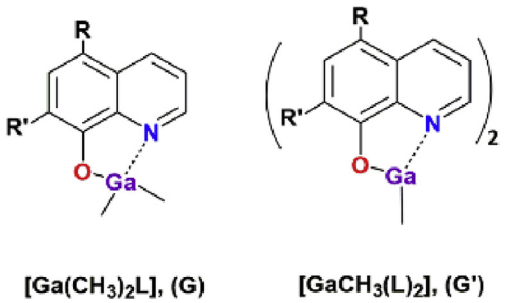

Fig. 2. General formulae of the alkyl gallium quinolinolato complexes (**1G** – **4G**; **1G′** – **4G′**) synthesised and characterised.

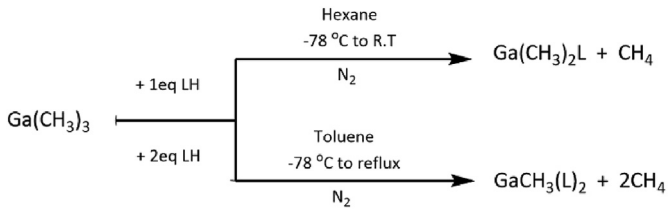

Fig. 3. Synthetic route used in the synthesis of **1G**, $[Ga(Me)_2C_9H_5NOCl]$, **2G**, $[Ga(Me)_2C_9H_4NOCl_2]$, **3G**, $[Ga(Me)_2C_9H_4NOBr_2]$, **4G**, $[Ga(Me)_2C_9H_4NOI_2]$ and **1G′**, $[GaMe(C_9H_5NOCl)_2]$, **2G′**, $[GaMe(C_9H_4NOCl_2)_2]$, **3G′**, $[GaMe(C_9H_4NOBr_2)_2]$ **4G′**, $[GaMe(C_9H_4NOI_2)_2]$.

for the dimethyl complexes and 72–83 % for the monomethyl complexes. Unfortunately, complexes **2G'** – **4G′** were found to have limited solubility in DMSO, and so biological testing was limited to using a simple 'stab-test' of the solid on bacterial agar plates. The remaining complexes **1G** – **4G** and **1G′** all exhibited reasonable solubility in DMSO and so were able to be tested against various bacteria, *Leishmanial* promastigotes and amastigotes, and towards mammalian cells in order to determine their cytotoxicity.

The solid-state structure of each complex was structurally authenticated through single crystal X-ray diffraction. The solution state composition of each complex, **1G** – **4G** and **1G'** – **4G′,** was established through ^{1}H NMR spectroscopy in DMSO-d_6, however due to solubility issues with **2G'** – **4G′**, only complexes **1G** – **4G** and **1G'** were able to be assessed by ^{13}C NMR and ESI mass spectroscopy. Physical and chemical analysis was completed using infrared spectroscopy (FT-IR), melting point (mp), and elemental analysis. Full analytical details on each complex is given in the Experimental section, and all spectra provided in the Supporting Information (ESI).

The dimethyl complexes, **1G** – **4G**, and one of the monomethyl analogues (**1G′**), were readily soluble in DMSO-d_6. The remaining monomethyl complexes, **2G'** – **4G′**, were only sparingly soluble with heating, however their presence could be distinguished on the baseline. Complex formation was indicated by disappearance of the hydroxyl proton of the quinolinols, normally observed between 10.15 and 10.95 ppm, and by shifts in the aromatic signals. The appearance of a methyl singlet due to residual $GaMe_x$ in the low frequency region of −0.345 and −0.007 ppm was also observed, typical of methyl gallium complexes [53–55]. As an illustration, the ^{1}H NMR spectra of complexes **1G** and **1G′** are given relative to the free quinolinol in Figs. S1 and S2 in the ESI. ^{13}C NMR spectra were obtained for the soluble complexes **1G** – **4G** and **1G′**, however inconclusive data were obtained for the poorly soluble monomethyl complexes **2G'** - **4G'.** The structure of these complexes, however, was confirmed by X-ray and elemental analysis.

Crystals suitable for X-ray diffraction were obtained from slow evaporation of the reaction filtrate, from either toluene or hexane. The asymmetric unit of each complex, **1G** – **4G**, is similar, and all adopt a 4-coordinate distorted tetrahedral geometry around the gallium centre comprising the two covalently bound methyl groups (Ga–C), the covalent deprotonated hydroxyl (Ga–O), and a single dative interaction between the quinolinol nitrogen (Ga–N). Complex **1G**, however, is the only one to form a dimer which lifts the coordination geometry to five with a largely distorted trigonal bipyramidal geometry (Fig. 4).

Because of the different composition complexes **1G'** – **4G′** are five-coordinate through chelation of two substituted quinolinol ligands and the single covalently bound methyl group. The geometry at the gallium centre is also distorted trigonal bipyramidal. A discussion of the 5,7-dichloroquinolinol derivatives, **2G** and **2G'** is given below (Figs. 5 and 6), remaining data can be found in the ESI (Table S1).

The crystal structure of the simplest alkyl gallium quinolinol, 8-hydroxyquinolinol, has been previously characterised by X-ray diffraction and found to form a structure analogous to the 5-chloroquinolinolate derivative **1G**. The average bond length of 1.966 Å is typical for a Ga–C bond in a dimethyl complex. The Ga–C bond tends to shorten with more electron withdrawing groups such as a carboxylate, as observed in the solid-state structure of dimethyl gallium carboxylates synthesised by Kaluderovic et al., with average bond lengths of 1.942 Å.[50,51] The analogous 8QH complex synthesised by Onyitiuka et al. had an observed average length of 1.945 Å for the Ga–C bond, indicating that the presence of the halide on the quinolinol ligand may influence the metal – carbon bond. The bond length observed for the Ga–O bond is representative of a covalent interaction with a bond length of 1.953 Å, whereas the Ga–N bond is typical of a dative bond (2.204 Å) [56]. The quinolinolate ligand sits in the equatorial plane, central to the gallium through the formation of a four membered Ga_2O_2 unit. Each asymmetrically bridged oxygen occupies one coordination site in the equatorial plane of one gallium atom, whilst occupying the axial coordination site of the other. For the complex synthesised by Onyitiuka et al. it was found that the dimeric unit exhibited a bond angle of 149.7° for the N(1)–Ga(1)–O(1)',

Please cite this article as: R.N. Duffin et al., Alkyl gallium(III) quinolinolates: A new class of highly selective anti-leishmanial agents, European Journal of Medicinal Chemistry, https://doi.org/10.1016/j.ejmech.2019.111895

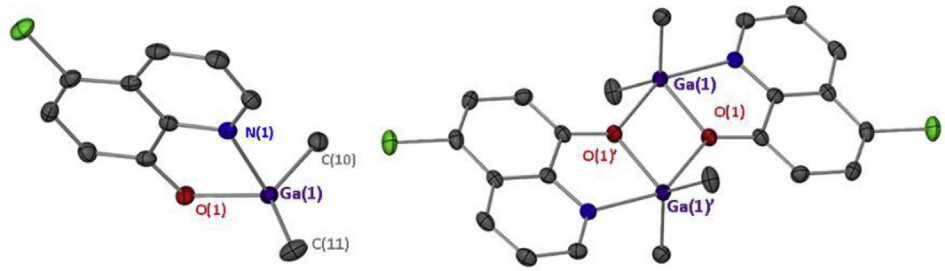

Fig. 4. Solid-state structure of the asymmetric unit and dimer of complex [$Ga(CH_3)_2(C_9H_5ClNO)$], **1G**, thermal ellipsoids at 50% probability. Hydrogen atoms have been omitted for clarity. Selected bonds lengths (Å) and angles (°). Ga(1)–O(1), 1.953(16), Ga(1)–N(1), 2.204(19), Ga(1)–C(10), 1.963(2), Ga(1)–C(11), 1.969(3); O(1)–Ga(1)–N(1), 78.07(7), O(1)–Ga(1)–C(10), 111.3(9), O(1)–Ga(1)–C(11), 118.3(10), C(10)–Ga(1)–C(11), 130.1(14), N(1)–Ga(1)–O(1)', 149.8(7). Symmetry operator' = 1 - x, -y, -z.

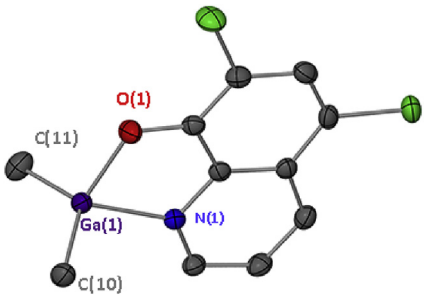

Fig. 5. Solid-state structure [$Ga(Me_2)C_9H_4Cl_2NO$], **2G**, Thermal ellipsoids at 50% probability. Hydrogen atoms have been omitted for clarity. Selected bonds lengths (Å) and angles (°). Ga(1)–O(1), 1.929(17), Ga(1)–N(1), 2.064(2), Ga(1)–C(10), 1.954(2), Ga(1)–C(11), 1.958(3); O(1)–Ga(1)–N(1), 83.02(7), O(1)–Ga(1)–C(10), 109.10(10), O(1)–Ga(1)–C(11), 110.73(10), C(10)–Ga(1)–C(11), 126.99(12), N(1)–Ga(1)–C(11), 108.88(10).

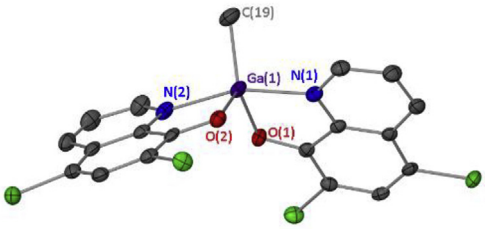

Fig. 6. Solid-state structure [$GaMe(C_9H_4Cl_2NO)_2$], **2G′**, Thermal ellipsoids at 50% probability. Hydrogen atoms have been omitted for clarity. Selected bonds lengths (Å) and angles (°). Ga(1)–O(1), 1.906(18), Ga(1)–O(2), 1.918(18), Ga(1)–N(1), 2.122(2), Ga(1)–N(2), 2.142(2), Ga(1)–C(19), 1.959(3); O(1)–Ga(1)–O(2), 112.40(8), O(1)–Ga(1)–N(1), 81.21(8), O(1)–Ga(1)–N(2), 85.16(8), C(1)–Ga(1)–C(19), 131.82(11).

complex **1G** had an almost identical angle of 149.8(7), exhibiting the distortion from the ideal trigonal bipyramidal geometry.

Similar to the asymmetric unit of **1G**, that of **2G** (Fig. 5.) can be described as a distorted tetrahedron, with a coordination number of four. This complex and the two remaining complexes **3G** and **4G** all exist as monomers in the solid-state. Lengthening of the Ga–C bond is observed in comparison to the mono-chlorido substituted quinolinol, further indicating that the halide substituent may influence the Ga–C bond. The major difference between the monomethyl and dimethyl quinolinolato complexes is the coordination number. The addition of a second chelate in place of the methyl group boosts the coordination from 4 to 5. Complex **2G'** (Fig. 6.), along with the remaining three complexes **1G′**, **3G′** and **4G′**, adopt a distorted trigonal bipyramidal geometry. There are few examples of structurally authenticated monomethyl bis-substituted gallium complexes, however there are geometrically similar complexes

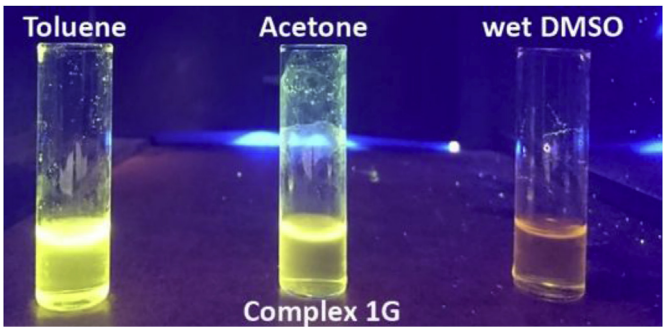

Fig. 7. Solvatochromism of complex **1G** in toluene, acetone and DMSO.

identified by Bakewell et al., a mono-chlorido bis-quinolinolato complex [$Ga(C_9H_3Cl_2CH_3)_2Cl$] and a mono-*tert*-butoxido *bis*-quinolinolato complex [$Ga(C_9H_3Cl_2CH_3)_2O(CH_3)_3$] [52]. Similar to complex **2G′**, these complexes are distorted trigonal bipyramids, with the distortion largely in the N–Ga – N bond in the axial plane. Complex **2G'** exhibits distortion from the ideal angle of 180°, with an axial angle of 160.84° for N(1)–Ga(1)–N(2). The methyl group sits in the equatorial plane, adjacent to the oxygens of the quinolinol. These Ga–O bonds can be said to be covalent with a formal average bond length of 1.918 Å, with the nitrogen atoms acting as dative donor atoms (average length: 2.132 Å). The complexes synthesised by Bakewell et al. share largely similar average covalent and dative bond lengths with an average of 1.868 Å for Ga–O and 2.107 Å for Ga–N [52]. A bond length of 1.959 Å for Ga(1)–C(1) is indicative of a covalent interaction.

2.2. Photophysical properties

The effects of metal chelation on the fluorescent activity of the 8-quinolinol has been well established. Ohnesorge et al. observed that with an increase in the atomic number of the central atom, there was a red-shift of the maximum absorbance [57,58]. For all complexes 1G – 4G and 1G' – 4G' a varying degree of solvatochromatism was observed. When going from the least polar toluene to the most polar DMSO (with acetone as the median) a visual colour change under UV exposure was noticeable, with DMSO fluorescing weakly (Fig. 7).

Complexes **1G** – **4G** exhibited the presence of multiple bands in the UV–visible spectrum, with the largest of these between 400 and 425 nm (ESI Fig. S6). Studies found that by increasing the size of the metal the bathochromic shift of the λ_{max} also increases, therefore it could be assumed that by increasing the halogen size on the ligand, an increase in shift could be observed [59]. A trend in absorbance was observed with increasing halogen. **1G** was the

weakest absorber and **4G** the strongest (ε = 2458 and 2784 respectively). The difference between monomethyl versus dimethyl was the former were found to be stronger absorbers, which would most likely be attributed to the presence of two quinolinols in the complete molecule (Fig. S7).

Fluorescence intensities of each complex was then conducted at the λ_{max} values derived from the UV–visible spectrum. Graphs of the normalised solution state fluorescence can be found in the ESI (Figs. S8 and S9). Unsurprisingly each complex exhibited weak fluorescence in both the solid and solution. Due to the weak fluorescence activity observed, there was no further need for quantum yield analysis therefore the fluorescence imaging discussed is qualitative in nature.

In alkane solvents, 8QH molecules self-associate to form stable dimers which are able to undergo biprotonic transfer in the excited state [60]. Previous studies indicate the quantum yield of the metal chelates are marginally low when compare to conventional fluorophores such as fluorescein. As the complexes were nearly non-fluorescent in DMSO the possibility of utilising these compounds as potential biological fluorophores was dismissed.

2.3. Stability and biological activity

The stability of compounds as solids under atmospheric conditions and in solution with conventional solvents is an important property of potential medicinal agents. Therefore, an assessment of the stability of each complex in both the solid and solution state was performed. Complexes **1G** – **4G** and **1G′** all had reasonable melting points of between 125 and 230 °C (full detail on each complex is given in the Experimental section), and so could be monitored by melting point analysis over a period of several months. Complexes **2G'** – **4G'**, however, have decomposition points >300 °C making analysis by melting point difficult and unreliable. As such, elemental analysis was performed twice within a period of a month with no changes in elemental composition observed.

Solution state stability of each complex was assessed in DMSO. Complexes **2G'** – **4G'** were found to be poorly soluble in DMSO and were therefore unsuitable for the biological assays, so a detailed assessment of their long-term stability was unnecessary. The soluble complexes were able to be analysed (^{1}H NMR in DMSO-d_6, 0–24 h), with a good degree of solution state stability overall. Example complex **1G** can be found in the ESI at 0, 24 and 48 h intervals in DMSO-d_6, with no changes to the signals observed (ESI Fig. S1).

The pH of the mammalian phagolysosome sits in the range of 4–5 [61,62]. Therefore, to determine whether the complexes are stable at this low pH, or undergo ligand exchange processes releasing the quinolinol, a solution of the complex was titrated with HCl and any changes in complex composition monitored using UV–visible spectroscopy. Complex **1G**, [Ga(Me$_2$)C$_9$H$_5$ClNO], was dissolved into ethanol at a concentration of 10^{-4} M. The parent quinolinol, cloxyquin, was used as a control at the same concentration. A weak HCl solution was added dropwise to the ethanolic solution of **1G**, monitored by a pH metre. Aliquots were taken at pH values of 8.5 (starting pH), 6.5 and 4.5. The absorbance was measured, noting a decrease in the complex signal and an increase of the parent quinolinol as pH decreased (Fig. 8). The final reading at pH of 4.5 was compared to the parent quinolinol at the same pH to accurately determine if the formation of the free quinolinol was occurring (ESI Fig. S2). At acidic pH the quinolinol dissociates from the gallium complex, differing from the *tris*-quinolinolate, KP46 [43,44,63,64]. This, however, is similar to the mode of action of the anti-cancer complex gallium *tris*-maltolate, which liberates gallium to transferrin proteins prior to crossing the intestinal epithelium [63,65,66]. This dissociation would allow the gallium a free coordination site to interact and inhibit iron transfer proteins, while simultaneously delivering a potentially biologically active ligand into the cell.

Before testing against any microbes was commenced a mammalian cell assay was conducted to determine their cytotoxicity. COS-7 cells were selected for the assay as they are an easily cultured immortal cell line [67]. As complexes **2G'** – **4G′** were limited in their DMSO solubility only complexes **1G** – **4G** and **1G'** were able to undergo testing. These complexes exhibited no reasonable toxicity towards the COS-7 control cells with IC$_{50}$ values exceeding ≥100 μM. Only complex **1G** showed moderate cytotoxicity with an IC$_{50}$ of 88.3 μM (Fig. 9).

Initial analysis of biological activity involved a qualitative assessment against bacterial agar plates. Complexes **1G** – **4G** and **1G′** were dissolved at approximately 5 mg/mL. Due to the

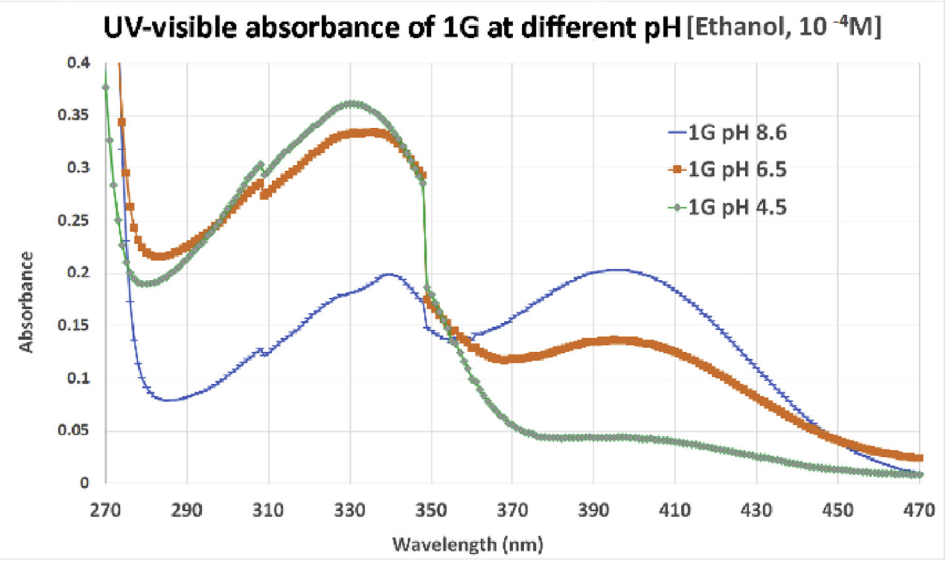

Fig. 8. UV–visible graph of complex **1G** at changing pH. The signal of the bound quinolinol complex at 397 nm decreases as pH decreases. The signal of the dissociated quinolinol at 332 nm increases as pH decreases.

Please cite this article as: R.N. Duffin et al., Alkyl gallium(III) quinolinolates: A new class of highly selective anti-leishmanial agents, European Journal of Medicinal Chemistry, https://doi.org/10.1016/j.ejmech.2019.111895

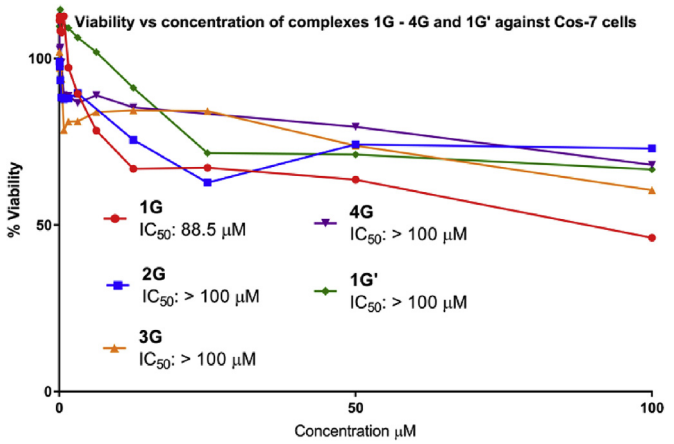

Fig. 9. Viability percentage of complexes **1G** − **4G** and **1G′** against COS-7 cells. Dose response curves were generated over a range of concentrations (48 nm−100 μM) in the appropriate culture media from 10 mM DMSO stock solutions. All readings were compared spectroscopically to non-treated control and the percent growth inhibition calculated.

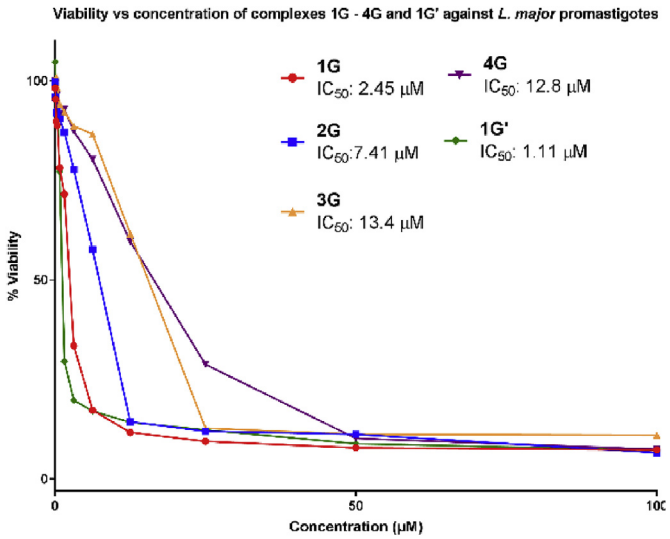

Fig. 10. Viability percentage of complexes **1G** − **4G** and **1G′** against *L. major* promastigotes Dose response curves were generated over a range of concentrations (48 nm - 100 μM) in the appropriate culture media from 10 mM DMSO stock solutions. All readings were compared spectroscopically to non-treated control and the percent growth inhibition calculated.

insolubility of complexes **2G'** − **4G′** only a qualitative "stab" test of each solid could be performed. Bacteria were prepared as described in the Experimental section. The solids were then analysed using a protocol utilised by Werrett et al. where a solid plug is gently pierced into the agar using sterile pipette tips at approximately 1 mg [68]. All solid complexes exhibited no activity against the five bacterial strains assayed. The soluble complexes fared no better with only a small zone of inhibition observed for *E. coli* for complex **2G**, and against *S. aureus* for complexes **2G** and **1G'**. One possible reason for this lack of activity could be the poor solubility of the complexes in aqueous media thereby limiting leeching of the gallium complex into the agar medium and into contact with the bacteria.

As many of the dimethyl gallium complexes have been traditionally tested against cancer cell lines [53–55], the soluble complexes **1G** − **4G** and **1G'** were then assessed for their anti-cancer activity towards the cervical cancer cell line HeLa. The results showed little activity against the HeLa cells (ESI, Fig. S3).

A final set of tests against the eukaryotic microbe *L. major* was then performed. Complexes **1G** − **4G** and **1G'** all exhibited excellent activity against the promastigote form of the parasite, with IC_{50} values ranging from 1.11 μM−13.4 μM (Fig. 10). As mentioned previously parasites require iron from exogenous sources and so it is possible the gallium is being taken up by the parasites within the culture media [34,35]. 8QH has also shown to exhibit a high degree of biological activity, which is greatly increased in the presence of metals within the media, thus is it possible that complexation to the gallium is enhancing the activity of the quinolinols **1**–**4**, against the *L. major* parasites [40,42].

Studies were undertaken on human primary fibroblasts to establish the selectivity of the complexes and their potential as therapeutic agents. Fibroblasts were chosen for the mammalian cell cytotoxicity assays since the species of *Leishmania* being investigated here, *L. major*, causes the cutaneous form of the disease which is characterised by lesion of the skin [69]. IC_{50} values ranging from 16.2 μM to ≥100 μM were obtained, with the most effective anti-promastigote complexes, **1G** and **1G′**, presenting as the most potent, with IC_{50} values of 16.2 μM and 52.2 μM respectively (Fig. 11). As the IC_{50} against the parasites is reasonably lower than that of the mammalian cells both complexes **1G** and **1G'** were tested further. Graphs and selectivity indices for each complex are given in Figs. 11 and 12 and Table 1.

With a good range of selectivities observed for complexes **1G** − **4G** and **1G′**, each complex then underwent analysis in the amastigote invasion assay described in the experimental section. Each complex was found to exhibit excellent activity when compared to the known drug control Amphotericin B (Fig. 12). Complex **1G′**, the monomethyl complex was found to exhibit the lowest rate of % infection, and therefore presents the greatest activity, with a value of 3.5% ± 0.65. The analogous dimethyl complex **1G**, followed close behind with a value of 5.3 ± 0.63. When going from the cloxyquin analogue to the chloroxine, it was found that activity decreased, with an increase of percentage of infection for complex **2G** of 11.5 ± 0.65, a notable trend was observed for these complexes, with the increase in halogen size on the 5 and 7 position of the quinolinol resulting in increased activity and therefore decreased infection rate. **3G** presented with an infection value of 8.5 ± 0.50 and **4G** with 5.5 ± 0.86. Excluding **1G**, which is substituted only on the 5 position, the complex activity follows the trend of **2G** < **3G** < **4G**, which correlates with Cl < Br < I substitution of the quinolinol. It seems that increasing the number of bound quinolinol ligands also contributes to an increase in activity, as complex **1G'**, the monomethyl bis-cloxyquin complex, exhibited the greatest activity of the five gallium complexes trialled. These values are comparable and, in most cases, more effective than our most recent class of Sb(V) aryl carboxylates, and the current drug control, amphotericin B (percentage infection 3.5% ± 0.80) [11,14].

Each parent quinolinol was also assessed for their anti-amastigote activity. The simplest 8QH has previously been shown to exhibit activity towards *L. amazonensis, L. infantum* and *L. braziliensis* amastigotes at concentrations of ~68.0, 34.0 and 17.0 μM (percentage infectivity ranges: 1.2–2.4, 5.2–54.9 and 21.8–72.3% respectively) [42]. For this study, each parent quinolinol was tested at the lower concentration of 10 μM, corresponding to the concentration used for the gallium complexes. The parent halido-quinolinols were found to have a percentage infection range of 16.0–30.8% against *L. major* amastigotes (ESI Fig. S4). The activity of the gallium complexes was found to be greater than that of the parent quinolinols which indicates that the metal plays an important role in the biological activity. A comparison of the percentage infection of each quinolinol (**1**–**4**) and the corresponding gallium

Please cite this article as: R.N. Duffin et al., Alkyl gallium(III) quinolinolates: A new class of highly selective anti-leishmanial agents, European Journal of Medicinal Chemistry, https://doi.org/10.1016/j.ejmech.2019.111895

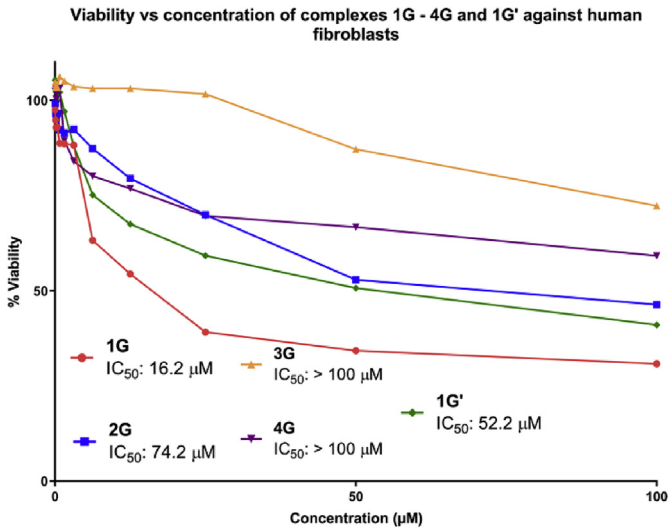

Fig. 11. Viability percentage of complexes **1G** – **4G** and **1G**′ against Human fibroblasts. Dose response curves were generated over a range of concentrations (48 nm - 100 μM) in the appropriate culture media from 10 mM DMSO stock solutions. All readings were compared spectroscopically to non-treated control and the percent growth inhibition calculated.

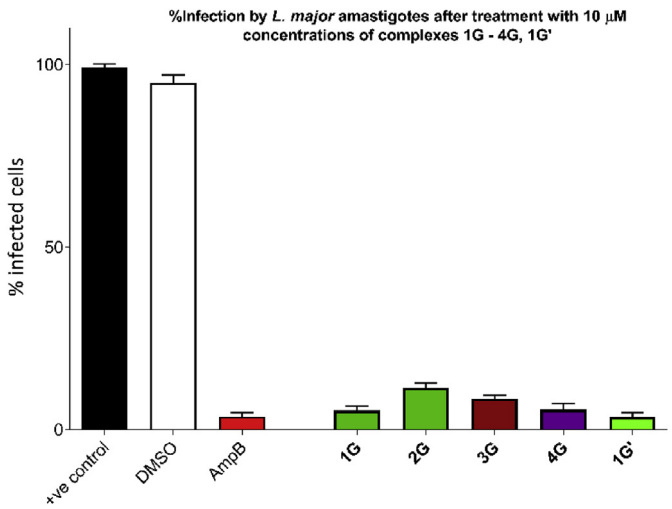

Fig. 12. Infected macrophages after 48 h. Number of infected macrophage was determined microscopically, in duplicate of fixed specimens. Amphotericin B (AmpB) was used as a positive control at 10 μM concentration. A DMSO control was also employed at a 1% concentration. Error bars indicate SEM, one-way ANOVA. Dunnett's multiple comparison test was used to determine the statistical significance between all test compounds and a positive control lacking treatment (+ve control).

complex are given in Table 2 below. A visual representation of infected cells in the positive control (untreated) versus treatment by example complex **1G** can be seen in Fig. 13. Several other examples can be found in the ESI (section 7).

Though complexes **2G** and **3G** did not exhibit the same level of activity as complexes **1G** and **1G**′, their increased selectivity and decreased cytotoxicity towards mammalian cells make them ideal candidates for future evaluation. Overall, with an IC_{50} of $\geq$100 μM against human fibroblasts for complex **4G**, and a rate of infection comparable to **1G** and **1G'**, **4G**, the iodoquin complex was found to be the most effective anti-Leishmanial alkyl gallium quinolinolate and therefore the most promising lead candidate. Though these complexes lack the potent activity of former Sb(V) aryl carboxylates they do exhibit better mammalian selectivity and are the first examples of heteroleptic gallium complexes to undergo anti-Leishmanial testing [70].

To probe a possible mechanism of action, a study was conducted to observe whether the gallium complexes initiated oxidative stress on the macrophages and intracellular amastigotes using a modified assay to measure the production of reactive oxygen species [71]. Reactive oxygen species (ROS) were measured spectroscopically by the addition of a non-fluorescent dye, dihydroethidium (DHE) at intervals of 6, 12 and 24 h to drug treated wells, containing amastigote infected macrophages. At each time interval, the plate was washed with PBS and re-inoculated with both the drug and the dye. Before each reading, a measurement buffer of 5 mM of glucose in PBS was added to each well. If the cells undergo oxidative stress, the DHE becomes the oxidised 2-hydroxyethidium upon reactions with superoxide and enables measurement via fluorescence. The % increase of ROS was calculated by comparing the increase to a control of the dye added to cells with no prior infection or drug inoculation (negative control) (Fig. 14 and Table 3). At the 6-h interval an increase in the production of ROS was observed for both complexes **1G** and **1G'** indicating that the complexes were able to initiate oxidative stress on the cells.

Macrophages generate superoxide in response to infection in what is known as an oxidative burst [72,73], *Leishmania* amastigotes however are able to bypass this by hiding within the phagolysosome of the macrophages and producing enzymes that convert superoxide to H_2O_2 and O_2 [74,75]. Addition of the gallium complexes is shown to initiate an ROS response within the macrophages, which may contribute to effectiveness of the complexes.

At the 12-h interval a slight increase was observed for **1G** and **1G'**, though minimal. After 24 h the production of ROS began to drop, indicating that it may take less than 24 h for the parasite to be successfully eliminated from the macrophages. Each was compared to a drug control of amphotericin B, exhibiting a greater increase of ROS (Table 3).

Though it has been theorised that gallium inhibits iron redox pathway, therefore causing cell death, the production of ROS does not discount this theory. Inhibition of important iron pathway leads to oxidative stress within a cell, which would lead to the production of reactive oxygen species. For complete differentiation to occur, *Leishmania* promastigotes require iron from extracellular sources. In iron poor environments such as the macrophage, regulation of iron transporters are increased. An increase in iron uptake by the parasite triggers physiological change into the amastigote. The iron is converted to iron superoxide dismutase, which causes the production of H_2O_2 within the parasite [76]. Therefore, it is possible the gallium complexes are inhibiting iron uptake and subsequent conversion to superoxide dismutase, which then allows the superoxide radicals produced by the macrophages to successfully eliminate the infection.

Other hypotheses can be related to a recent study by Costa et al. Their studies into the mechanism of action of ruthenium (II) complexes against *L. amazonensis* determined that an increase of ROS by the complexes led to the depolarisation of mitochondrial membrane, DNA cleavage and alterations to the parasite morphology. All these factors were thought to contribute to increased apoptosis of the parasites [77]. It has been demonstrated previously that apoptosis of *L. donavani* promastigotes has been attributed to respiratory chain inhibitors and therefore an increase in ROS [78]. Therefore, these ROS induced changes to the parasite morphology may also be a potential mechanism of action of the gallium complexes.

Nitric oxide is another small molecule produced by macrophages when fighting infection [79]. NO plays an important role in the control of parasitic infection [80]. Similar to the inhibition of

Table 1
Selectivity indices for complexes **1G** – **4G** and **1G'**, where SI = IC_{50}(fibroblasts)/IC_{50}(parasite).

	IC_{50} (μM) *L. major*	IC_{50} (μM) Fibroblasts	Selectivity Index (SI)
$[Ga(Me)_2C_9H_5NOCl]$ **1G**	2.45	16.2	6.61
$[Ga(Me)_2C_9H_4NOCl_2]$ **2G**	7.41	74.2	10.0
$[Ga(Me)_2C_9H_4NOBr_2]$ **3G**	13.4	170*	12.7
$[Ga(Me)_2C_9H_4NOI_2]$ **4G**	12.8	827*	64.6
$[GaMe(C_9H_5NOCl)_2]$ **1G'**	1.11	52.2	47.0

*values extrapolated by applying a trendline to the curve.

Table 2
Percentage infection value of the parent quinolinols at 10 μM and the gallium complexes **1G** – **4G** and **1G'** at 10 μM. The control Amphotericin B presented with a percentage infection of 3.5 ± 0.80

Quinolinol	1 $[C_9H_6NOCl]$	2 $[C_9H_5NOCl_2]$	3 $[C_9H_5NOBr_2]$	4 $[C_9H_5NOI_2]$	-
% infection	21.5 ± 5.13	30.8 ± 3.29	23.8 ± 4.86	16.0 ± 2.81	-
Complex	**1G** $[Ga(Me)_2C_9H_5NOCl]$	**2G** $[Ga(Me)_2C_9H_4NOCl_2]$	**3G** $[Ga(Me)_2C_9H_4NOBr_2]$	**4G** $[Ga(Me)_2C_9H_4NOI_2]$	**1G'** $[GaMe(C_9H_5NOCl)_2]$
% infection	5.30 ± 0.63	11.5 ± 0.65	8.50 ± 0.50	5.50 ± 0.86	3.50 ± 0.65

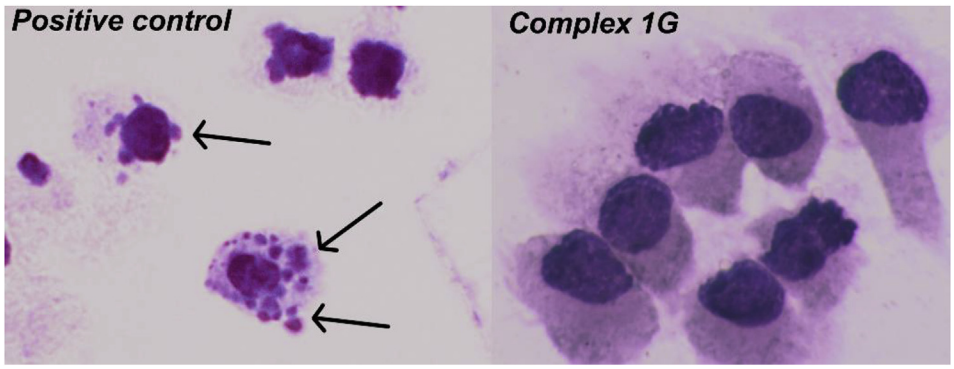

Fig. 13. Visual representation of amastigote infected cells in the untreated positive control (indicated by arrows) and non-infected cells after treatment with complex **1G**. Contrast and colour has been adjusted using adobe photoshop to improve clarity. (For interpretation of the references to colour in this figure legend, the reader is referred to the Web version of this article.)

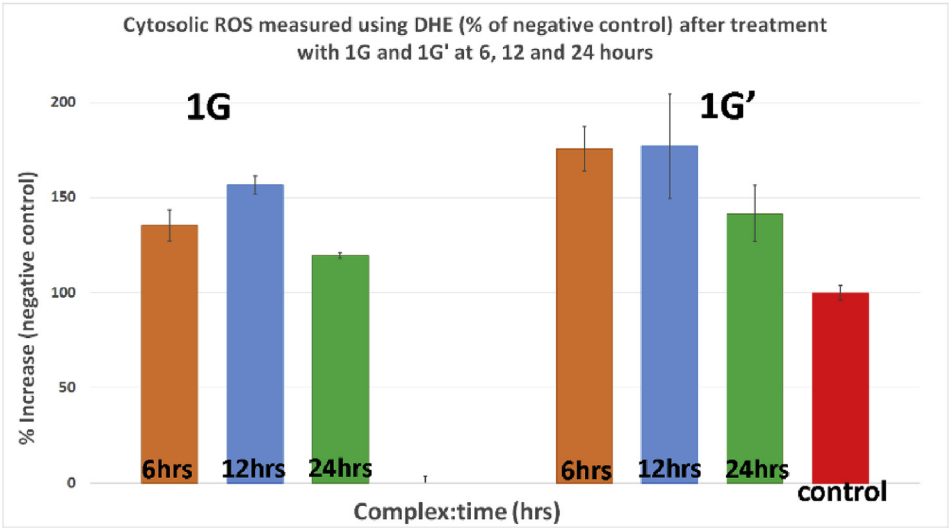

Fig 14. % Increase of cytosolic ROS produced by infected macrophages after treatment with **1G** and **1G'** at 6 h, 12 h and 24 h, against a negative control of no infection and no drug.

ROS, *Leishmania* spp. are able to further avoid host immunity by decreasing the production of NO [81,82]. Studies by Nascimento et al. showcased increased NO levels by the addition of organometallic Ru(II) complexes to the intracellular parasite [83]. The study highlighted this increase of NO as a potential mechanism of the complexes antileishmanial effect [83]. To determine whether the production of NO played an important role in the mechansim of action of the gallium complexes, a Griess assay was then performed

Table 3
% Increase of ROS after treatment with **1G**, **1G'** and AmpB with respect to time (hr). All values calculated by a comparison with the negative control baseline of 100%.

	1G	1G′	AmpB
6 h	135.4% ± 8.1	175.7% ± 11.7	125.0 ± 7.7
12 h	156.8% ± 4.7	177.1% ± 27.3	122.3 ± 5.4
24 h	119.6% ± 1.5	141.6% ± 14.8	125.1 ± 2.7

[84]. Macrophages were plated into a 24-well plate and infected as per the amastigote protocol. Colourless DMEM was added to each plate along with the example complexes **1G** and **1G'** at 10 μM. The infected cells were incubated for 6 h before the assay was conducted on the supernatant. A control of amphotericin B was also employed. The absorbance response was compared to a calibration curve of nitrite concentrations. The results showed no significant increase of NO. This suggests that the mechansim of the metallodrugs is unaffected by the production of NO and relies more so on the production of ROS and potential inhibition of iron-pathways (ESI S5 and Table S2).

3. Conclusions

Eight novel alkyl gallium quinolinolato complexes have been successfully synthesised and fully characterised; four dimethyl complexes [$Ga(CH_3)_2L$], and four analogous monomethyl complexes [$GaCH_3(L)_2$]. Five of the eight complexes were suitable for *in vitro* biological testing (**1G** − **4G**, **1G**′), with three (**2G'** − **4G'**) proving poorly soluble in water and DMSO. The solid-state structure of each of the eight complexes was determined through single crystal X-ray diffraction with the monomethyl complexes adopting a trigonal bipyramidal geometry and three of the dimethyl complexes a distorted tetrahedral geometry. Complex **1G** differed from the other three dimethyl complexes in presenting as a dimer in the solid-state with trigonal bipyramidal geometry. UV−visible and fluorescence analysis concluded that the complexes exhibited weak fluorescence in both the solution and solid state. Further fluorescence quenching by DMSO disqualified their future use as potential biological trackers.

Solution and solid-state studies conducted over a period of days to months revealed highly stable complexes resistant to both hydrolysis and atmospheric decomposition. Complexes **1G** − **4G** and **1G**′ were relatively soluble in a range of organic solvents, whereas the monomethyl complexes **2G** − **4G** exhibited a low degree of solubility in organic solvents, including DMSO. Therefore, only five of the eight novel complexes were able to undergo a full qualitative and quantitative assessment of biological activity, with complexes **2G'** − **4G**′ only able to be tested qualitatively as a solid "stab" test. None of the complexes exhibited any significant activity against five different bacterial strains, with only minimal activity against *E. coli* observed for complex **2G** and *S. aureus* for complexes **2G** and **1G'**. The five soluble complexes were found to be largely non-toxic towards mammalian COS-7 cells, with **1G** registering the lowest IC_{50} value of 88.3 μM. The complexes also exhibited little to no activity against the cervical cancer cell line HeLa.

Importantly though the complexes exhibited excellent activity against the motile promastigote form of *L. major* with IC_{50} values ranging from 1.11 μM−13.4 μM. Complexes **2G** − **4G** exhibited no toxicity towards the mammalian fibroblast control (IC_{50} 74.2 μM - ≥ 100 μM), with complexes **1G** and **1G**′ exhibiting limited toxicity with IC_{50} values of 16.2 μM and 52.2 μM respectively. All complexes exhibited excellent activity towards the clinically relevant, intracellular amastigote form of the parasite at the reasonably low concentration of 10 μM, with infection rates ranging from 3.5 ± 0.65−11.5 ± 0.65. The complexes were shown to exhibit better activity than the parent quinolinols. When considering substitution on both the 5 and 7 position of the quinolinol, a minor trend was observed, with an increase of activity corresponding to an increase in halogen size (**2G** < **3G** < **4G**: Cl < Br < I). Studies into the production of ROS and NO allowed for further elucidation into the potential mechanism of action. Further in-depth studies may provide even greater insight into the mechanistic pathway of these organometallic complexes and the ability to potentially fine-tune their anti-parasitic activity. Overall, the monomethyl complex **1G'** proved to be the most effective based on percentage infection value. However, **4G** exhibits the highest degree of selectivity based on the calculated selectivity index (SI), These two complexes are the most promising candidates for future invasive assays and for the development of possible drug candidates.

4. Experimental

4.1. Synthesis and characterisation

4.1.1. General

Trimethyl gallium was purchased from Merck and stored in a recirculated nitrogen glove box as a neat liquid canister with no further need for purification. All halido-quinolinols were purchased from sigma Aldrich as powders of 95−99% purity. 5-Chloroquinolinol was recrystallised from a hot toluene solution to increase purity. All reaction requiring inert conditions were performed under an atmosphere of nitrogen, using over dried glassware and utilising a Schlenk manifold and technique. All dried solvents were obtained from an MBruan-SPS-800 and stored under nitrogen over 4A molecular sieves, in flasks equipped with Youngs taps. ^{1}H NMR and ^{13}C NMR were recorded on a Bruker Avance DRX600 spectrophotometer (600 MHz), chemical shifts were references to the appropriate protiated solvent, DMSO-d_6. Melting point analysis was conducted in open end capillary tubes, on a digital Stuart Scientific melting point apparatus SMP10. Infrared Spectra were recorded on an Agilent Technologies Cary 630 FTIR spectrometer, using a range of 4000−500 cm^{-1}. Mass spectrometry (ESI) was obtained utilising a Micromass Platform QMS spectrometer, with an electrospray source and a cone voltage of 35 eV. Elemental analysis was obtained from the School of Human Sciences, Science Centre at London Metropolitan University, United Kingdom.

4.1.2. General procedure: GP1: synthesis of dimethyl complexes

1 mmol of the desired quinolinol was placed into a Schlenk flask under vacuum for approximately 3−4 h to remove any excess moisture. The quinolinol was then suspended in hexane and placed into an isopropanol/N_2 bath at −78 °C. 1 mmol of neat trimethyl gallium was added by pre-purged syringe to the flask, yielding an immediate colour change. The reaction was allowed to warm to room temperature before the solid produced was filtered. The coloured filtrate was left to stand, yielding crystalline solid over time.

4.1.2.1. Dimethyl gallium mono-5-chloro-quinolinolate, ***1G.*** 5-chloroquinolinol (0.179 g, 1 mmol) was reacted with trimethyl gallium (0.1 mL, 1 mmol) according to GP1. Yellow solid, (0.250 g, 89%), m.p: 215−216 °C. ^{1}H NMR (600 MHz, DMSO-d_6) δ = 8.90 (dd, *J* = 4.6, 1.4 Hz, 1H, ar-*H*), 8.62 (dd, *J* = 8.5, 1.3 Hz, H, ar-*H*), 7.83 (dd, *J* = 8.5, 4.5 Hz, 1H, ar-*H*), 7.60 (d, *J* = 8.4 Hz, 1H, ar-*H*), 6.87 (d, *J* = 8.4 Hz, 1H, ar-*H*), −0.32 (s, 6H). ^{13}C NMR (600 MHz, DMSO-d_6) δ = 162.9 (*C*-ar) 148.1 (*C*-ar), 141.9 (*C*-ar), 138.3 (*C*-ar), 132.9 (*C*-ar), 129.3 (*C*-ar), 126.4 (*C*-ar) 115.3 (*C*-ar), 115.1 (*C*-ar)fz −0.514 (CH_3). FT-IR [cm^{-1}]: 3053 (w), 2954 (w), 1599 (m), 1576 (w), 1493 (m), 1363 (m), 1310(sh), 1254 (m), 1152 (m), 1081 (sh), 780 (sh), 734 (sh),

Please cite this article as: R.N. Duffin et al., Alkyl gallium(III) quinolinolates: A new class of highly selective anti-leishmanial agents, European Journal of Medicinal Chemistry, https://doi.org/10.1016/j.ejmech.2019.111895

669 (sh); MS (ESI)$^+$ *m/z* = 180.0 [LH_2^+], 99.0 [$Ga(CH_3)_2^+$] 68.9 [Ga]. ESI: 100.9 [$Ga(CH_3)_2H_2^-$]. Elemental analysis, expected: %C 47.46 %H 3.98 %N 5.03 found: %C 47.26 %H 3.89 %N 4.95. CCDC 1898525.

4.1.2.2. Dimethyl gallium mono-5,7-dichloro-quinolinolate, ***2G.*** 5,7-dichloroquinolinol (0.214 g, 1 mmol) was reacted with trimethyl gallium (0.1 mL, 1 mmol) according to GP1. Yellow solid, (0.280 g, 90%), m.p: 127–129 °C. ^{1}H NMR (600 MHz, DMSO-d_6) δ = 8.85 (dd, *J* = 4.5, 1.4 Hz, 1H, ar-*H*), 8.57 (dd, *J* = 8.5, 1.4 Hz, 1H, ar-*H*), 7.79 (m, 1H ar-*H*), 7.78 (s, 1H, ar-*H*), −0.35 (s, 6H, CH_3). ^{13}C NMR (600 MHz, DMSO-d_6) δ = 157.8 (*C*-ar) 148.0 (*C*-ar), 141.1 (*C*-ar), 137.1 (*C*-ar), 131.5 (*C*-ar), 127.3 (*C*-ar), 125.5 (*C*-ar), 117.5 (*C*-ar), 114.6 (*C*-ar), −0.514 (*C*H_3). FT-IR [cm $^{-1}$]: 2961 (w), 1567 (m), 1491 (w), 1456 (m), 1399 (m), 1368(sh), 1259 (w), 1196 (w), 1057 (w), 811 (sh), 782 (sh), 651 (sh); MS (ESI)$^+$ *m/z* = 214.0 [LH_2^+], 99.0 [$Ga(CH_3)_2^+$], 68.9 [Ga]. ESI: 100.9 [$Ga(CH_3)_2H_2^-$]. Elemental analysis, expected: %C 42.23 %H 3.22 %N 4.48 found: %C 42.35 %H 3.14 %N 4.48. CCDC 1898522.

4.1.2.3. Dimethyl gallium mono-5,7-dibromo-quinolinolate, ***3G.*** 5,7-dibromoquinolinol (0.303 g, 1 mmol) was reacted with trimethyl gallium (0.1 mL, 1 mmol) according to GP1. Yellow solid, (0.391 g, 97%), m.p: 136–138 °C. ^{1}H NMR (600 MHz, DMSO-d_6) δ = 8.85 (dd, *J* = 4.5, 1.4 Hz, 1H, ar-*H*), 8.53 (dd, *J* = 8.5, 1.4 Hz, 1H, ar-*H*), 8.03 (s, 1H, ar-*H*), 7.84 (dd, *J* = 8.5, 4.5 Hz, 1H, ar-*H*), −0.32 (s, 6H, CH_3). ^{13}C NMR (600 MHz, DMSO-d_6) δ = 159.6 (*C*-ar) 147.9 (*C*-ar), 141.0 (*C*-ar), 139.5 (*C*-ar), 136.7 (*C*-ar), 129.0 (*C*-ar), 125.9 (*C*-ar), 107.5 (*C*-ar), 103.8 (*C*-ar), −0.512 (*C*H_3). FT-IR [cm $^{-1}$]: 2957 (w), 1547 (m), 1478 (w), 1451 (m), 1363 (sh), 1233 (w), 1221 (w), 1191 (w), 850 (m), 750 (sh), 707 (m); MS (ESI)$^+$ *m/z* = 303.9 [LH_2^+], 99.0 [$Ga(CH_3)_2^+$], 68.9 [Ga]. ESI: 101.0 [$Ga(CH_3)_2H_2^-$]. Elemental analysis, expected: %C 32.89 %H 2.51 %N 3.79 found: %C 32.70 %H 2.47 %N 3.38. CCDC 1898528.

4.1.2.4. Dimethyl gallium mono-5,7-diiodo-quinolinolate, ***4G.*** 5,7-dichloroquinolinol (0.397 g, 1 mmol) was reacted with trimethyl gallium (0.1 mL, 1 mmol) according to GP1. Yellow solid, (0.425 g, 91%), m.p: 165–167 °C. ^{1}H NMR (600 MHz, DMSO-d_6) δ 8.75 (dd, *J* = 4.5, 1.3 Hz, 1H, ar-*H*), 8.36 (dd, *J* = 8.5, 1.4 Hz, 1H, ar-*H*), 8.28 (s, 1H, ar-*H*), 7.79 (dd, *J* = 8.5, 4.5 Hz, 1H, ar-*H*), −0.35 (s, 6H, CH_3). ^{13}C NMR (600 MHz, DMSO-d_6) δ = 163.5(*C*-ar) 147.9 (*C*-ar), 147.8 (*C*-ar), 144.1 (*C*-ar), 139.8 (*C*-ar), 132.2 (*C*-ar), 126.4 (*C*-ar), 84.3 (*C*-ar), 78.9 (*C*-ar), −0.490 (*C*H_3). FT-IR [cm $^{-1}$]: 2960 (w), 1560 (m), 1485 (m), 1451 (sh), 1367 (sh), 1261 (w), 1191 (w), 1112 (m), 1055 (w), 809 (m), 781 (m), 686 (sh); MS (ESI)$^+$ *m/z* = 397.8 [LH_2^+], 99.0 [$Ga(CH_3)_2^+$], 68.9 [Ga]. ESI: 100.9 [$Ga(CH_3)_2H_2^-$]. Elemental analysis, expected: %C 26.65 %H 2.03 %N 2.83 found: %C 26.79 %H 1.92 %N 2.93. CCDC 1898524.

4.1.3. GP2: synthesis of monomethyl complexes

2 mmol of the desired quinolinol was placed into a Schlenk flask under vacuum for approximately 3–4 h to remove any excess moisture. The quinolinol was then either dissolved or suspended in toluene and placed into an isopropanol/N_2 bath at −78 °C. 1 mmol of neat trimethyl gallium was added by pre-purged syringe to the flask, yielding an immediate colour change. The reaction was allowed to warm to room temperature before refluxing at 110 °C the solid produced was filtered. The coloured filtrate was left to stand, yielding crystalline solid over time.

4.1.3.1. Methyl gallium bis-5-chloro-quinolinolate, ***1G'.*** 5-chloroquinolinol (0.358 g, 2 mmol) was reacted with trimethyl gallium (0.1 mL, 1 mmol) according to GP2. Yellow solid, (0.315 g, 72%), m.p: 225–227 °C decomp. ^{1}H NMR (600 MHz, DMSO-d_6) δ = 9.09 (dd, *J* = 4.6, 1.4 Hz, 2H, ar-*H*), 8.75 (dd, *J* = 8.6, 1.3 Hz, 2H, ar-*H*), 7.99 (dd, *J* = 8.6, 4.6 Hz, 2H, ar-*H*), 7.64 (d, *J* = 8.4 Hz, 2H, ar-*H*), 6.90 (d, *J* = 8.4 Hz, 2H, ar-*H*), −0.03 (s, 3H, CH_3). δ = 157.8 (*C*-ar) 146.2 (*C*-ar), 138.5 (*C*-ar), 136.4 (*C*-ar), 130.8 (*C*-ar), 126.5 (*C*-ar), 124.4 (*C*-ar), 114.3 (*C*-ar),112.5 (*C*-ar), −4.82 (*C*H_3). FT-IR [cm $^{-1}$]: 3054 (w), 1601 (m), 11575 (m), 1494 (sh), 1458 (sh), 1320 (sh), 1256 (w), 1085 (sh), 829 (m), 780 (sh), 744 (sh). Elemental analysis, expected: %C 51.64 %H 2.97 %N 6.34 found: %C 51.84 %H 2.73 %N 6.49. CCDC 1898523.

4.1.3.2. Methyl gallium bis-5,7-dichloro-quinolinolate, ***2G'.*** 5,7-dichloroquinolinol (0.428 g, 2 mmol) was reacted with trimethyl gallium (0.1 mL, 1 mmol) according to GP2. Yellow solid, (0.422 g, 81%), m.p: > 300 °C decomp. ^{1}H NMR (600 MHz, DMSO-d_6), residual toluene and acetone are not labelled. δ = 9.17 (dd, *J* = 4.7, 1.3 Hz, 2H, ar-*H*), 8.81 (dd, *J* = 8.5, 1.3 Hz, 2H, ar-*H*), 8.06 (dd, *J* = 8.5, 4.6 Hz, 2H, ar-*H*), 7.87 (s, 1H ar-*H*), −0.00 (s, 3H, CH_3). FT-IR [cm $^{-1}$]: 3073 (w), 1566 (m), 1488 (sh), 1450 (sh), 1370 (sh), 1235 (w), 1235 (w), 1114 (m), 1053 (w), 892 (m), 752 (sh), 660 (sh). Elemental analysis, expected: %C 33.14 %H 1.61 %N 4.07 found: %C 33.28 %H 1.53 %N 4.14. CCDC 1898526.

4.1.3.3. Methyl gallium bis-5,7-dibromo-quinolinolate, ***3G'.*** 5,7-bromoquinolinol (0.606 g, 2 mmol) was reacted with trimethyl gallium (0.1 mL, 1 mmol) according to GP2. Yellow solid, (0.616 g, 80%), m.p: 165–167 °C. ^{1}H NMR (600 MHz, DMSO-d_6) δ 9.14 (d, *J* = 4.7 Hz, 2H, ar-*H*), 8.75 (d, *J* = 8.6 Hz, 2H, ar-*H*), 8.20–7.97 (m, 4H, ar-*H*), 0.00 (s, 3H, CH_3). FT-IR [cm $^{-1}$]: 2958 (w), 1560 (m), 1483 (m), 1449 (sh), 1367 (sh), 1221 (w), 1203 (w), 1110 (m), 1051 (w), 869 (m), 748 (sh), 690 (sh). Elemental analysis, expected: %C 33.14 %H 1.61 % N 4.07 found: %C 33.28 %H 1.53 %N 4.14. CCDC 1898529.

4.1.3.4. Methyl gallium bis-5,7-diiodo-quinolinolate, ***4G'.*** 5,7-diiodoquinolinol (0.784 g, 2 mmol) was reacted with trimethyl gallium (0.1 mL, 1 mmol) according to GP2. Yellow solid, (0.666 g, 81%), m.p: > 300 °C decomp. ^{1}H NMR (600 MHz, DMSO-d_6) δ 9.10 (dd, *J* = 4.6, 1.3 Hz, 2H, ar-*H*), 8.62 (dd, *J* = 8.5, 1.3 Hz, 2H, ar-*H*), 8.41 (s, 2H, ar-*H*), 8.10 (dd, *J* = 8.5, 4.7 Hz, 2H, ar-*H*), 0.00 (s, 3H, CH_3). FT-IR [cm $^{-1}$]: 2954 (w), 1545 (m), 1474 (sh), 1446 (sh), 1361 (sh), 1246 (w), 1218 (w), 1113 (m), 1050 (w), 851 (m), 747 (sh), 720 (m). Elemental analysis, expected: %C 26.03 %H 1.26 %N 3.20 found: %C 26.19 %H 1.41 %N 3.30. CCDC 1898527.

4.1.4. UV–visible and fluorescence spectrophotometry

Samples **1G** – **4G** and **1G'** – **4G'** were dissolved into toluene at 10 $^{-4}$M. A UV–visible wavelength scan from 300 nm–700 nm was obtained on an Agilent Cary-60 UV–Visible spectrophotometer to determine the λ_{max} and therefore fluorescence excitation wavelength in toluene. Fluorescence emission spectrum in both the solution state and solid state were obtained using an Agilent Cary Eclipse Fluorimeter. All graphs were produced using Microsoft excel.

4.1.5. X-ray crystallography

Crystallographic data on complexes **3G**, **1G′** and **3G′** were collected on a Bruker X8 APEXII CCD diffractometer, equipped with an OXFORD Crysosystem 700 cryostream and cooled to 123(2) K. Data collection occurred using monochromatic (graphite) MoK_α radiation (λ = 0.71070 Å) and was processed using the Bruker Apex2 v2014.7–1 software [85], polarisation, Lorentz and absorption corrections (multi-scan-SADBABS) were applied [86]. Crystallographic data for compound **1G**, **2G** and **2G′** was collected on an OXFORD Gemini Ultra equipped with an OXFORD Cryosystems 700 Cryostream and cooled to 173(2) K. Data was collected with monochromatic (graphite) CuK/α radiation (λ = 0.71073 Å) and processed using the CrysAlisPro v 1.171.34.36 software [87,88].

Compounds **4G** and **4G'** were collected at the MX1 beamline at the Australian Synchrotron, Melbourne, Victoria, Australia, operating at 17.4 KeV, with $\lambda = 0.7073$ Å, using an open flow N_2 cryostream cooled to 100(2) K. The data collection and reduction was obtained using BlueIce [89] and XDS [90]. Each compound was solved and refined using SHELX-97 on X-seed or Olex2 [91,92]. Unless otherwise indicated, all non-hydrogen atoms were refined with anisotropic thermal parameters. Hydrogen atoms were placed in calculated positions using a riding model with C–H = 0.95–0.98 Å and $U_{iso}(H) = xU_{\neg iso\neg}(C)$, $x = 1.2$ or 1.5 unless otherwise indicated. A summary of the X-ray data can be found in the ESI.

4.2. Biological assays

4.2.1. Bacteria preparation and assay

Vancomycin resistant *E. faecalis* (VRE, M846910) and Methicillin resistance *S. aureus* (MRSA, M118979) were cultured in Brain-heart infusion broth media (Oxiod), *S. epidermidis* (A130/ATCC14990) and *S. aureus* (A134/ATCC6538) were grown in nutrient agar and Luria-Bertani (LB) broth. *E. coli* (G102) was grown in LB broth and LB agar. Bacteria were streaked onto agar overnight from glycerol stocks and incubated at 37 °C before inoculation of a single colony into broth. 100 μL of suspended cell culture was then spread onto fresh agar plates and allowed to grown overnight. For soluble complexes, solutions were made up to 5 mg/mL in DMSO and the solution soaked into small circles of filter paper before placing onto the agar plates. For the insoluble compounds, using a 10 μL pipette tip, a small amount ~1 mg, was pierced into the agar. The plates were incubated overnight and the zones of inhibition measured. Each was performed in triplicate.

4.2.2. Cell culture

Leishmania major virulent clone V121 was derived from the LRC-L137 *L. major* isolate and maintained at 26 °C in supplemented M199 media (10% (v/v) heat inactivated FBS, 1% Pen-Strep), purchased from Gibco ™. Human primary fibroblasts, Cervical cancer HeLa, J774 macrophages and COS-7 cells were cultured and maintained in Dulbecco's Modified Eagles Medium (DMEM) supplemented with 10% FBS and 1% Pen-Strep and 1% Glutamax (purchased from Gibco ™) at 37 °C in a 5% CO_2 incubator [93].

4.2.3. Measurement of reactive oxygen species

Measurement of ROS was achieved by a modified assay from Wojtala et al. [71]. J774 macrophages were plated into 24-well plates at 30,000 cells per well. Cells were given 24 h to adhere before infection with *L. major* promastigotes a ratio of 1:5 in plain DMEM. The *L. major* promastigotes were incubated for 6 h to infect and differentiate into amastigotes before excess promastigotes were washed away with PBS. The cells were incubated for a further 24 h to allow complete infection. At each interval, 10 μM of the complexes were added in plain DMEM along with 1 μM of dihydroethidium, in triplicate. A drug control of amphotericin B and a negative control of non-infected cells without drug treatment was included. At intervals of 6, 12 and 24 h, the cells were washed with PBS and a fluorescence reading taken in the measurement buffer of 5 mM of glucose in PBS at excitation of 535 nm and emission of 635 nm. Treated wells were compared to the negative control and the % increase calculated.

4.2.4. In vitro testing of L. major, HeLa, COS-7 and human fibroblasts

Celltiter Blue Cell Viability Assay was purchased from Promega ™, and used for the determination of percentage viability of the parasite and human fibroblasts. Compounds **1G** – **4G** and **1G'** were dissolved in DMSO to make up a 10 mM working stock and sequentially diluted out in the appropriate culture media (100 μM–48 nM). Assays were set up in duplicate in 96-well Falcon plates. Volumes of 10^6 promastigotes/mL, 10^5 COS-7/mL, 10^5 HeLa/mL and 10^5 fibroblasts/mL were used. All cell assays were measured spectroscopically using fluorescence excitation at 544 nm and emission at 590 nm. Fibroblasts and *L. major* were measured after 48hrs, COS-7 and HeLa were measured after 24hrs. The compounds were compared to a no drug negative control and the percent inhibition calculated [94]. Fluorescence measurements were conducted on a BMG-Labtech FluoStar Omega microplate reader [11,14].

4.2.5. Macrophage invasion assays

The assays were performed as previously described [70, 95]. Briefly, J774 macrophages were plated onto coverslips in a 24 well plate and allowed to adhere for 48hrs. The cells were exposed to *L. major* promastigotes at a 1:10 ratio and incubated for a further 24hrs to allow for amastigote formation *in vitro*. The slides were then washed to remove any excess extracellular promastigotes and exposed to compounds for 48hrs before washing, fixation and cellular staining with a commercial Hema Color kit purchased from Merck. Following Giemsa staining, 200 cells per duplicate slide were then counted microscopically and the percentage of infected cells calculated.

4.2.6. Griess assay

J774 macrophages were seeded at 10,000 cells per well in a 24-well plate. The cells were given 24 h to adhere to the plate before infection with 5x the amount of *L. major* promastigotes. The parasites were given 6 h to enter the cells before washing of any excess parasites with PBS. Parasites were given 24 h to differentiate into amastigote. The plate was washed again with PBS to remove any free-floating parasites. Compounds **1G** and **1G'** along with amphotericin B were added in triplicate at a concentration of 10 μM in colourless DMEM. The plate was incubated for a further 6 h. The DMEM was removed and the solution centrifuged to remove particulates. The supernatant was then plated into a 96-well plate and analysed as per the Griess assay protocol [84]. The absorbance was read at 530 nm and the values compared to a standard curve of nitrite to determine the increase percentage of nitric oxide.

Declaration of competing interest

The authors declare that they have no known competing financial interests or personal relationships that could have appeared to influence the work reported in this paper.

Acknowledgements

The authors would like to thank the Australian Research Council (DP170103624) and Monash University for financial support. We would also like to thank Dr. Craig Forsyth (Monash) for assistance with X-ray crystallography and Professor Louise Bennet (Monash) for use of the plate reader and Associate Professor Kellie Tuck (Monash) for the use of the Fluorimeter. The authors would also like to acknowledge the Australian Synchrotron for use of the MX1 beamline at the Australian Synchrotron, part of ANSTO.

Appendix A. Supplementary data

Supplementary data to this article can be found online at https://doi.org/10.1016/j.ejmech.2019.111895.

References

[1] P.J. Hotez, N.C. Lo, 27 - neglected tropical diseases: public health control programs and mass drug administration, in: E.T. Ryan, D.R. Hill, T. Solomon, N.E. Aronson, T.P. Endy (Eds.), Hunter's Tropical Medicine and Emerging Infectious Diseases, Tenth Edition, London, 2019, pp. 209–213.
[2] M. Boelaert, F. Meheus, A. Sanchez, S. Singh, V. Vanlerberghe, A. Picado, B. Meessen, S. Sundar, The poorest of the poor: a poverty appraisal of households affected by visceral leishmaniasis in Bihar, India, Trop. Med. Int. Health 14 (2009) 639–644.
[3] G. Mandal, V. Govindarajan, M. Sharma, H. Bhattacharjee, R. Mukhopadhyay, Drug resistance in Leishmania, in: Antimicrobial Drug Resistance, Springer, 2017, pp. 649–665.
[4] J. Alvar, I.D. Vélez, C. Bern, M. Herrero, P. Desjeux, J. Cano, J. Jannin, M. den Boer, W.L.C. Team, Leishmaniasis worldwide and global estimates of its incidence, PLoS One 7 (2012), e35671.
[5] S.M. Gossage, M.E. Rogers, P.A. Bates, Two separate growth phases during the development of Leishmania in sand flies: implications for understanding the life cycle, Int. J. Parasitol. 33 (2003) 1027–1034.
[6] A. Stauch, H.-P. Duerr, J.-C. Dujardin, M. Vanaerschot, S. Sundar, M. Eichner, Treatment of visceral leishmaniasis: model-based analyses on the spread of antimony-resistant L. donovani in Bihar, India, PLoS Neglected Trop. Dis. 6 (2012), e1973.
[7] J. van Griensven, M. Balasegaram, F. Meheus, J. Alvar, L. Lynen, M. Boelaert, Combination therapy for visceral leishmaniasis, Lancet Infect. Dis. 10 (2010) 184–194.
[8] M. Ouellette, J. Drummelsmith, B. Papadopoulou, Leishmaniasis: drugs in the clinic, resistance and new developments, Drug Resist. Updates 7 (2004) 257–266.
[9] D. Légaré, M. Ouellette, Drug Resistance in Leishmania, Handbook of Antimicrobial Resistance, 2017, pp. 313–341.
[10] S. Sundar, K. Kumar, J. Chakravarty, D. Agrawal, S. Agrawal, A. Chhabra, V. Singh, Cure of antimony-unresponsive Indian post-kala-azar dermal leishmaniasis with oral miltefosine, Trans. R. Soc. Trop. Med. Hyg. 100 (2006) 698–700.
[11] R.N. Duffin, V.L. Blair, L. Kedzierski, P.C. Andrews, Comparative stability, toxicity and anti-leishmanial activity of triphenyl antimony (v) and bismuth (v) α-hydroxy carboxylato complexes, Dalton Trans. 47 (2018) 971–980.
[12] A. Islam, J.G. Da Silva, F.M. Berbet, S.M. da Silva, B.L. Rodrigues, H. Beraldo, M.N. Melo, F. Frézard, C. Demicheli, Novel triphenylantimony (V) and triphenylbismuth (V) complexes with benzoic acid derivatives: structural characterization, in vitro antileishmanial and antibacterial activities and cytotoxicity against macrophages, Molecules 19 (2014) 6009–6030.
[13] S. Yan, L. Jin, H. Sun, 51Sb antimony in medicine, in: Metallotherapeutic Drugs and Metal-Based Diagnostic Agents: The Use of Metals in Medicine, 2005, pp. 441–461.
[14] R.N. Duffin, V.L. Blair, L. Kedzierski, P.C. Andrews, Comparative stability, cytotoxicity and anti-leishmanial activity of analogous organometallic Sb (V) and Bi (V) acetato complexes: Sb confirms potential while Bi fails the test, J. Inorg. Biochem. 189 (2018) 151–162.
[15] M. Khan, S. Gul, I. Hussain, M.A. Khan, M. Ashfaq, F. Ullah, G.F. Durrani, I.B. Baloch, R. Naz, In vitro anti-leishmanial and anti-fungal effects of new Sb III carboxylates, Org, Med. Chem. Lett. 1 (2011) 2.
[16] R. Mushtaq, M.K. Rauf, M. Bolte, A. Nadhman, A. Badshah, M.N. Tahir, M. Yasinzai, K.M. Khan, Synthesis, characterization and antileishmanial studies of some bioactive heteroleptic pentavalent antimonials, Appl. Organomet. Chem. 31 (2017), e3606.
[17] Y.C. Ong, S. Roy, P.C. Andrews, G. Gasser, Metal compounds against neglected tropical diseases, Chem. Rev. 119 (2018) 730–796.
[18] T. Iftikhar, M.K. Rauf, S. Sarwar, A. Badshah, D. Waseem, M.N. Tahir, A. Khan, K.M. Khan, G.M. Khan, Structural elucidation and bioassays of newly synthesized pentavalent antimony complexes, J. Organomet. Chem. 851 (2017) 89–96.
[19] P.L. Olliaro, T.A. Shamsuzzaman, B. Marasini, A. Dhariwal, A. Be-Nazir, D. Mondal, M.R. Banjara, P. Das, S. Sundar, S. Rijal, Investments in Research and surveillance are needed to go beyond elimination and stop transmission of Leishmania in the Indian subcontinent, PLoS Neglected Trop. Dis. 11 (2017), e0005190.
[20] R. Adamson, G. Canellos, S. Sieber, Studies on the antitumor activity of gallium nitrate (NSC-15200) and other group IIIa metal salts, Cancer Chemother. Rep. 59 (1975) 599–610.
[21] C.L. Edwards, R. Hayes, Tumour scanning with 67 Ga citrate, J. Nucl. Med. 10 (1969) 103–105.
[22] R.L. Littenberg, R.M. Taketa, N.P. Alazraki, S.E. Halpern, W.L. Ashburn, Gallium-67 for localization of septic lesions, Ann. Intern. Med. 79 (1973) 403–406.
[23] A.J. Downs, Chemistry of Aluminium, Gallium, Indium and Thallium, Springer Science & Business Media, 1993.
[24] I.B. Bersuker, Electronic Structure and Properties of Transition Metal Compounds: Introduction to the Theory, John Wiley & Sons, 2010.
[25] W.R. Harris, Thermodynamics of gallium complexation by human lactoferrin, Biochemistry (Mosc.) 25 (1986) 803–808.
[26] W.R. Harris, V.L. Pecoraro, Thermodynamic binding constants for gallium transferrin, Biochemistry (Mosc.) 22 (1983) 292–299.
[27] R. Beriault, R. Hamel, D. Chenier, R.J. Mailloux, H. Joly, V. Appanna, The overexpression of NADPH-producing enzymes counters the oxidative stress evoked by gallium, an iron mimetic, Biometals 20 (2007) 165–176.
[28] R. García-Contreras, E. Lira-Silva, R. Jasso-Chávez, I.L. Hernández-González, T. Maeda, T. Hashimoto, F.C. Boogerd, L. Sheng, T.K. Wood, R. Moreno-Sánchez, Isolation and characterization of gallium resistant Pseudomonas aeruginosa mutants, Int. J. Med. Microbiol. 303 (2013) 574–582.
[29] D.W. Hedley, E.H. Tripp, P. Slowiaczek, G.J. Mann, Effect of gallium on DNA synthesis by human T-cell lymphoblasts, Cancer Res. 48 (1988) 3014–3018.
[30] M.M. Berggren, L.A. Burns, R.T. Abraham, G. Powis, Inhibition of protein tyrosine phosphatase by the antitumor agent gallium nitrate, Cancer Res. 53 (1993) 1862–1866.
[31] V. Braun, H. Killmann, Bacterial solutions to the iron-supply problem, Trends Biochem. Sci. 24 (1999) 104–109.
[32] K. Blanton, G. Biswas, J. Tsai, J. Adams, D. Dyer, S. Davis, G. Koch, P. Sen, P. Sparling, Genetic evidence that Neisseria gonorrhoeae produces specific receptors for transferrin and lactoferrin, J. Bacteriol. 172 (1990) 5225–5235.
[33] M.E. Wilson, T.S. Lewis, M.A. Miller, M.L. McCormick, B.E. Britigan, Leishmania chagasi: uptake of iron bound to lactoferrin or transferrin requires an iron reductase, Exp. Parasitol. 100 (2002) 196–207.
[34] M.E. Wilson, R.W. Vorhies, K.A. Andersen, B.E. Britigan, Acquisition of iron from transferrin and lactoferrin by the protozoan Leishmania chagasi, Infect. Immun. 62 (1994) 3262–3269.
[35] C. Huynh, N.W. Andrews, Iron acquisition within host cells and the pathogenicity of Leishmania, Cell Microbiol. 10 (2008) 293–300.
[36] R. Sutak, E. Lesuisse, J. Tachezy, D.R. Richardson, Crusade for iron: iron uptake in unicellular eukaryotes and its significance for virulence, Trends Microbiol. 16 (2008) 261–268.
[37] C.R. Chitambar, Gallium and its competing roles with iron in biological systems, Biochim. Biophys. Acta 1863 (2016) 2044–2053.
[38] C.R. Chitambar, Z. Zivkovic, Uptake of gallium-67 by human leukemic cells: demonstration of transferrin receptor-dependent and transferrin-independent mechanisms, Cancer Res. 47 (1987) 3929–3934.
[39] R. Tahmasebi, A. Barazesh, M. Fouladvand, Evaluation of in vitro anti-leishmanial activity of curcumin and its derivatives "gallium curcumin, indium curcumin and diacethyle curcumin", Eur. Rev. Med. Pharmacol. Sci. 17 (2013) 3306–3308.
[40] A. Albert, M. Gibson, S. Rubbo, The influence of chemical constitution on antibacterial activity. Part VI: the bactericidal action of 8-hydroxyquinoline (oxine), Br. J. Exp. Pathol. 34 (1953) 119.
[41] V. Prachayasittikul, S. Prachayasittikul, S. Ruchirawat, V. Prachayasittikul, 8-Hydroxyquinolines: a review of their metal chelating properties and medicinal applications, Drug Des. Dev. Ther. 7 (2013) 1157.
[42] M.C. Duarte, L.M. dos Reis Lage, D.P. Lage, J.T. Mesquita, B.C.S. Salles, S.N. Lavorato, D. Menezes-Souza, B.M. Roatt, R.J. Alves, C.A.P. Tavares, An effective in vitro and in vivo antileishmanial activity and mechanism of action of 8-hydroxyquinoline against Leishmania species causing visceral and tegumentary leishmaniasis, Vet. Parasitol. 217 (2016) 81–88.
[43] É.A. Enyedy, O. Dömötör, K. Bali, A. Hetényi, T. Tuccinardi, B.K. Keppler, Interaction of the anticancer gallium(III) complexes of 8-hydroxyquinoline and maltol with human serum proteins, J. Biol. Inorg. Chem. 20 (2015) 77–88.
[44] I. Riddell, S.J. Lippard, V. Brabec, J. Kasparkova, Vi Menon, N.P. Farrell, V. Venkatesh, et al., Metallo-drugs: Development and Action of Anticancer Agents, vol. 18, Walter de Gruyter GmbH & Co KG, 2018.
[45] P. Hongmanee, K. Rukseree, B. Buabut, B. Somsri, P. Palittapongarnpim, In vitro activities of cloxyquin (5-chloroquinolin-8-ol) against Mycobacterium tuberculosis, Antimicrob. Agents Chemother. 51 (2007) 1105–1106.
[46] R. Swain, J. Bapna, A. Das, S. Chandrasekar, R. Swaminathan, B. Bosco, S. Veliath, D. Thombre, A study on the neurotoxicity of broxyquinoline and brobenzoxaldine combination in therapeutic doses, Hum. Toxicol. 5 (1986) 35–41.
[47] D. Caglič, M.C. Krutein, K.M. Bompiani, D.J. Barlow, G. Benoni, J.C. Pelletier, A.B. Reitz, L.L. Lairson, K.L. Houseknecht, G.R. Smith, T.J. Dickerson, Identification of clinically viable quinolinol inhibitors of botulinum neurotoxin A light chain, J. Med. Chem. 57 (2014) 669–676.
[48] D. Abrahams, W.D. Brown, Evaluation of fungicides for Haliphthoros milfordensis and their toxicity to juvenile European lobsters, Aquaculture 12 (1977) 31–40.
[49] L. Ejim, M.A. Farha, S.B. Falconer, J. Wildenhain, B.K. Coombes, M. Tyers, E.D. Brown, G.D. Wright, Combinations of antibiotics and nonantibiotic drugs enhance antimicrobial efficacy, Nat. Chem. Biol. 7 (2011) 348.
[50] A.K. Fisher, F.G. Walter, S. Szabo, Iodoquinol associated seizures and radiopacity, J. Toxicol. Clin. Toxicol. 31 (1993) 113–120.
[51] L. Scheibel, A. Adler, Antimalarial activity of selected aromatic chelators. III. 8-Hydroxyquinolines (oxines) substituted in positions 5 and 7, and oxines annelated in position 5, 6 by an aromatic ring, Mol. Pharmacol. 22 (1982) 140–144.
[52] C. Bakewell, A.J. White, N.J. Long, C.K. Williams, 8-Quinolinolato gallium complexes: iso-selective initiators for rac-lactide polymerization, Inorg. Chem. 52 (2013) 12561–12567.
[53] S. Gómez-Ruiz, B. Gallego, M.R. Kaluđerović, H. Kommera, E. Hey-Hawkins, R. Paschke, G.N. Kaluđerović, Novel gallium (III) complexes containing phthaloyl derivatives of neutral aminoacids with apoptotic activity in cancer cells, J. Organomet. Chem. 694 (2009) 2191–2197.
[54] B. Gallego, M.R. Kaluđerović, H. Kommera, R. Paschke, E. Hey-Hawkins, T.W. Remmerbach, G.N. Kaluđerović, S. Gómez-Ruiz, Cytotoxicity, apoptosis

Please cite this article as: R.N. Duffin et al., Alkyl gallium(III) quinolinolates: A new class of highly selective anti-leishmanial agents, European Journal of Medicinal Chemistry, https://doi.org/10.1016/j.ejmech.2019.111895

and study of the DNA-binding properties of bi-and tetranuclear gallium (III) complexes with heterocyclic thiolato ligands, Investig. New Drugs 29 (2011) 932–944.
[55] M.R. Kaluđerović, S. Gómez-Ruiz, B. Gallego, E. Hey-Hawkins, R. Paschke, G.N. Kaluđerović, Anticancer activity of dinuclear gallium (III) carboxylate complexes, Eur. J. Med. Chem. 45 (2010) 519–525.
[56] E.C. Onyiriuka, S.J. Rettig, A. Storr, J. Trotter, Synthesis, characterization, and crystal and molecular structures of the coordination compounds, [Me2Ga-•O(C5H3N)CH2NMe2] and [Me2Ga•O(C9H6N)]2, Can. J. Chem. 65 (1987) 782–788.
[57] W. Ohnesorge, L. Rogers, Fluorescence of some metal chelate compounds of 8-quinolinol—I: effect of metallic ion and solvent on spectrum and quantum yield, AcSpe 15 (1959) 27–40.
[58] S.D. Dowling, W.R. Seitz, Effect of metal—ligand ratio on polarization of fluorescence from metal-8-quinolinol complexes, Spectrochim. Acta A Mol. Spectrosc 40 (1984) 991–993.
[59] T. Moeller, A.J. Cohen, Relationships among the ultraviolet absorption spectra of the 8-quinolinol chelates of the group III-B elements, J. Am. Chem. Soc. 72 (1950) 3546–3548.
[60] M. Goldman, E. Wehry, Environmental effects upon fluorescence of 5-and 8-hydroxyquinoline, Anal. Chem. 42 (1970) 1178–1185.
[61] C. Bogdan, M. Röllinghoff, How do Protozoan parasites survive inside macrophages? Parasitol. Today 15 (1999) 22–28.
[62] J.-C. Antoine, E. Prina, T. Lang, N. Courret, The biogenesis and properties of the parasitophorous vacuoles that harbour Leishmania in murine macrophages, Trends Microbiol. 6 (1998) 392–401.
[63] A.R. Timerbaev, Advances in developing tris (8-quinolinolato) gallium (III) as an anticancer drug: critical appraisal and prospects, Metallomics 1 (2009) 193–198.
[64] A.V. Rudnev, L.S. Foteeva, C. Kowol, R. Berger, M.A. Jakupec, V.B. Arion, A.R. Timerbaev, B.K. Keppler, Preclinical characterization of anticancer gallium (III) complexes: solubility, stability, lipophilicity and binding to serum proteins, J. Inorg. Biochem. 100 (2006) 1819–1826.
[65] C.R. Chitambar, D.P. Purpi, J. Woodliff, M. Yang, J.P. Wereley, Development of gallium compounds for treatment of lymphoma: gallium maltolate, a novel hydroxypyrone gallium compound, induces apoptosis and circumvents lymphoma cell resistance to gallium nitrate, J. Pharmacol. Exp. Ther. 322 (2007) 1228–1236.
[66] C.R. Chitambar, Medical applications and toxicities of gallium compounds, Int. J. Environ. Res. Public Health 7 (2010) 2337–2361.
[67] Y. Gluzman, SV40-transformed simian cells support the replication of early SV40 mutants, Cell 23 (1981) 175–182.
[68] P.C. Andrews, M. Werrett, M. Herdman, R. Brammananth, U. Garusinghe, W. Batchelor, P. Crellin, R. Coppel, Bismuth phosphinates in Bi-nanocellulose composites and their efficacy towards multi-drug resistant bacteria, Chem. Eur J. 49 (2018) 12938–12949.
[69] J. Alexander, A.R. Satoskar, D.G. Russell, Leishmania species: models of intracellular parasitism, J. Cell Sci. 112 (1999) 2993–3002.
[70] M.I. Ali, M.K. Rauf, A. Badshah, I. Kumar, C.M. Forsyth, P.C. Junk, L. Kedzierski, P.C. Andrews, Anti-leishmanial activity of heteroleptic organometallic Sb (V) compounds, Dalton Trans. 42 (2013) 16733–16741.
[71] A. Wojtala, M. Bonora, D. Malinska, P. Pinton, J. Duszynski, M.R. Wieckowski, Methods to monitor ROS production by fluorescence microscopy and fluorometry, in: Methods in Enzymology, Elsevier, 2014, pp. 243–262.
[72] J.A. Imlay, Oxidative Stress vol. 3, EcoSal Plus, 2009.
[73] A. Anjem, S. Varghese, J.A. Imlay, Manganese import is a key element of the OxyR response to hydrogen peroxide in Escherichia coli, Mol. Microbiol. 72 (2009) 844–858.
[74] T. Naderer, M.J. McConville, The Leishmania–macrophage interaction: a metabolic perspective, Cell Microbiol. 10 (2008) 301–308.
[75] N.G. Tessarollo, J.M. Andrade, D.d.S. Moreira, S.M.F. Murta, Functional analysis of iron superoxide dismutase-A in wild-type and antimony-resistant Leishmania braziliensis and Leishmania infantum lines, Parasitol. Int. 64 (2015) 125–129.
[76] B. Mittra, M. Cortez, A. Haydock, G. Ramasamy, P.J. Myler, N.W. Andrews, Iron uptake controls the generation of Leishmania infective forms through regulation of ROS levels, J. Exp. Med. 210 (2013) 401–416.
[77] M.S. Costa, Y.G. Gonçalves, S.C. Teixeira, D.C. de Oliveira Nunes, D.S. Lopes, C.V. da Silva, M.S. da Silva, B.C. Borges, M.J.B. Silva, R.S. Rodrigues, Increased ROS generation causes apoptosis-like death: mechanistic insights into the anti-Leishmania activity of a potent ruthenium (II) complex, J. Inorg. Biochem. 195 (2019) 1–12.
[78] A. Mehta, C. Shaha, Apoptotic death in Leishmania donovani promastigotes in response to respiratory chain inhibition complex II inhibition results in increased pentamidine cytotoxicity, J. Biol. Chem. 279 (2004) 11798–11813.
[79] John MacMicking, Q.-w Xie, C. Nathan, Nitric oxide and macrophage function, Annu. Rev. Immunol. 15 (1997) 323–350.
[80] R. Olekhnovitch, P. Bousso, Induction, propagation, and activity of host nitric oxide: lessons from Leishmania infection, Trends Parasitol. 31 (2015) 653–664.
[81] M.F. Horta, B.P. Mendes, E.H. Roma, F.S.M. Noronha, J.P. Macêdo, L.S. Oliveira, M.M. Duarte, L.Q. Vieira, Reactive oxygen species and nitric oxide in cutaneous leishmaniasis, J. Parasitol. Res. (2012) 2012.
[82] M. Lee, J.C. Choy, Positive feedback regulation of human inducible nitric-oxide synthase expression by Ras protein S-nitrosylation, J. Biol. Chem. 288 (2013) 15677–15686.
[83] N.R.F. do Nascimento, F.L.N. de Aguiar, C.F. Santos, A.M.L. Costa, D. de Jesus Hardoim, K. da Silva Calabrese, F. Almeida-Souza, E.H.S. de Sousa, L.G. de França Lopes, M.J. Teixeira, In vitro and in vivo leishmanicidal activity of a ruthenium nitrosyl complex against Leishmania (Viannia) braziliensis, Acta Trop. 192 (2019) 61–65.
[84] Kenneth Hensley, S. Mou, Q.N. Pye, Nitrite determination by colorimetric and fluorometric griess diazotization assays, in: Methods in Biological Oxidative Stress, Springer, 2003, pp. 185–193.
[85] B. AXS, Bruker Apex2 V2014, vols. 7–1, 2014. Madison, US.
[86] G. Sheldrick, SAINT (Version 6.02), SADABS (Version 2.03), Bruker AXS Inc., Madison, WI, 2002.
[87] R. CrysAlisPro 34.36, Oxford Diffraction Ltd., Oxford, UK, 2010, version 1.171.
[88] O. Rigaku, P. CrysAlis, Rigaku Oxford Diffraction, 2015.
[89] T.M. McPhillips, S.E. McPhillips, H.-J. Chiu, A.E. Cohen, A.M. Deacon, P.J. Ellis, E. Garman, A. Gonzalez, N.K. Sauter, R.P. Phizackerley, Blu-Ice and the Distributed Control System: software for data acquisition and instrument control at macromolecular crystallography beamlines, J. Synchrotron Radiat. 9 (2002) 401–406.
[90] W. Kabsch, Automatic processing of rotation diffraction data from crystals of initially unknown symmetry and cell constants, J. Appl. Crystallogr. 26 (1993) 795–800.
[91] G.M. Sheldrick, A short history of SHELX, Acta Crystallogr. A: Found. Crystallogr. 64 (2008) 112–122.
[92] O.V. Dolomanov, L.J. Bourhis, R.J. Gildea, J.A. Howard, H. Puschmann, OLEX2: a complete structure solution, refinement and analysis program, J. Appl. Crystallogr. 42 (2009) 339–341.
[93] Y.C. Ong, V.L. Blair, L. Kedzierski, P.C. Andrews, Stability and toxicity of heteroleptic organometallic Bi (v) complexes towards Leishmania major, Dalton Trans. 43 (2014) 12904–12916.
[94] A. Pathak, V.L. Blair, R.L. Ferrero, L. Kedzierski, P.C. Andrews, Structural influences on the activity of bismuth (III) indole-carboxylato complexes towards Helicobacter pylori and Leishmania, J. Inorg. Biochem. 177 (2017) 266–275.
[95] K. Lackovic, J.P. Parisot, N. Sleebs, J.B. Baell, L. Debien, K.G. Watson, J.M. Curtis, E. Handman, I.P. Street, L. Kedzierski, Inhibitors of Leishmania GDP-mannose pyrophosphorylase identified by high-throughput screening of small-molecule chemical library, Antimicrob. Agents Chemother. 54 (2010) 1712–1719.

Please cite this article as: R.N. Duffin et al., Alkyl gallium(III) quinolinolates: A new class of highly selective anti-leishmanial agents, European Journal of Medicinal Chemistry, https://doi.org/10.1016/j.ejmech.2019.111895

Journal of Inorganic Biochemistry 203 (2020) 110932

Contents lists available at ScienceDirect

Journal of Inorganic Biochemistry

journal homepage: www.elsevier.com/locate/jinorgbio

Anti-leishmanial activity and cytotoxicity of a series of *tris*-aryl Sb(*V*) mandelate cyclometallate complexes

Rebekah N. Duffin[a], Victoria L. Blair[a], Lukasz Kedzierski[b], Philip C. Andrews[a,*]

[a] School of Chemistry, Monash University, Clayton, Melbourne, VIC 3800, Australia
[b] Faculty of Veterinary and Agricultural Sciences at The Peter Doherty Institute for Infection and Immunity, 792 Elizabeth Street, Melbourne 3000, Victoria, Australia

ARTICLE INFO

Keywords:
Leishmaniasis
Antimony
Organometallic
Mandelic acid
Aryl
Cyclometallate

ABSTRACT

A series of ten cyclometallates and two μ^2-peroxo bridged *tris*-aryl Sb(*V*) complexes derived from *R/S*-mandelic acid (= *R/S*-ManH_2) were synthesised and characterised. As confirmed by X-ray crystallography the complexes **1Sr/s**, [Sb(*o*-tol)$_3$(man)], **2Sr/s,** [Sb(*m*-tol)$_3$(man)], **4Sr/s**, [Sb(*o*-PhOMe)$_3$(man)], **5Sr/s,** [Sb(Mes)$_3$(man)] and **6Sr/s**, [Sb(*p-tert*-BuPh)$_3$(man)] are all cyclometallates. Complexes **3Sr/s**, [(Sb(*p*-tol)$_3$(manH)$_2$O$_2$], contain a bridging O_2^{2-} anion in the solid-state but convert to the cyclometallates in DMSO solution with concomitant release of H_2O_2 and formation of complexes [Sb(*p*-tol)$_3$(man)], **3Sr'/s'**. All complexes underwent initial testing against both human fibroblasts and L. *major* V121 promastigotes. IC_{50} values were found to range from 2.07 (**6Sr**) to > 100 (**4Sr**) μM and 0.21 (**5Ss**) to > 100 (**4Ss**) μM for fibroblasts and parasites respectively. Two of the complexes were found to be ineffective, displaying no toxicity (**4S/r**). Despite the degree of mammalian toxicity, the selectivity of most complexes exceeded an SI of three and so were assessed for their anti-amastigote activity. Excellent anti-amastigote activity was observed for complexes at both 10 μM and 5 μM, with percentage infection value ranging from 0.15–3.00% for those tested at 10 μM and 0.25–2.50% for those at 5 μM.

1. Introduction

The fight against neglected tropical diseases (NTD) is an ongoing effort. Leishmania is among these NTDs, with millions of individuals affected globally each year. The World Health Organisation (WHO) estimates there were approximately 1.5 million new cases of Leishmaniasis in 2018, with those numbers set to rise if the disease burden remains untreated [1]. The fatal visceral form of the infection (VL) is on the rise, with an estimated 0.2–0.4 million new cases each year [2]. Of those up to 40,000 people die from the disease due to lack of adequate treatment [3,4]. Though highly effective, the current front-line treatments, sodium stibogluconate (Pentostam™) and antimony meglumine (Glucantime™), have well known problems associated with delivery and toxicity, and more recently a significant increase in resistance, now affecting most of the Indian sub-continent [5–7]. These pentavalent antimonials are highly hydrophilic, leading to a high renal clearance, and therefore oral administration is ineffective and treatment requires daily intravenous injections for approximately 28 days [8–10]. Even the alternative treatments, amphotericin B and miltefosine harbour their owns problems with toxicity, expense and parasitic resistance (Fig. 1) [11–13]. Despite all this, drug development from major pharma companies remains limited, primarily due to the prevalence of Leishmania in lower socio-economic countries. [1,14].

The mechanism of action of the current pentavalent antimonial treatments is still not fully understood. However, current consensus seems to coalesce around observations that it is the *in vivo* reduction of Sb(*V*) to Sb(III) which is the key important step, making the Sb(V) compounds pro-drugs and the protein-bound Sb(III) form the active agent [9]. Reduction occurs through interactions with trypanothione, a thiol-rich protein based on glutathione and exclusive to the parasite, which then inhibits its primary function as an oxidative stress mediator [15,16]. An alternative and less developed hypothesis is that Sb(*V*) acts directly on the parasite by inhibition of phosphatases, leading to a cascade effect and eventual cell death [17].

Over the past 30 years a number of alternative metals (e.g. Cu, Zn, Ru, Sn, Pd, Au, Ag) and their complexes have been studied as possible replacements for Pentostam™ and Glucantime™, with little progress [18]. Our recent research has focused on families of organometallic Bi (*V*) and Sb(V) carboxylates as more lipophilic complexes with the possibility of having lower toxicity [19–23]. Unfortunately, bismuth complexes of the type [$BiAr_3(O_2CR)_2$] have proven to be unstable and non-selectively toxic to both parasite and mammalian cells [19,20]. Analogous Sb(*V*) complexes have proven to be more robust and more selective, and remain the most likely leads [19,20].

* Corresponding author.
E-mail address: phil.andrews@monash.edu (P.C. Andrews).

https://doi.org/10.1016/j.jinorgbio.2019.110932
Received 26 September 2019; Received in revised form 15 November 2019; Accepted 17 November 2019
Available online 23 November 2019
0162-0134/

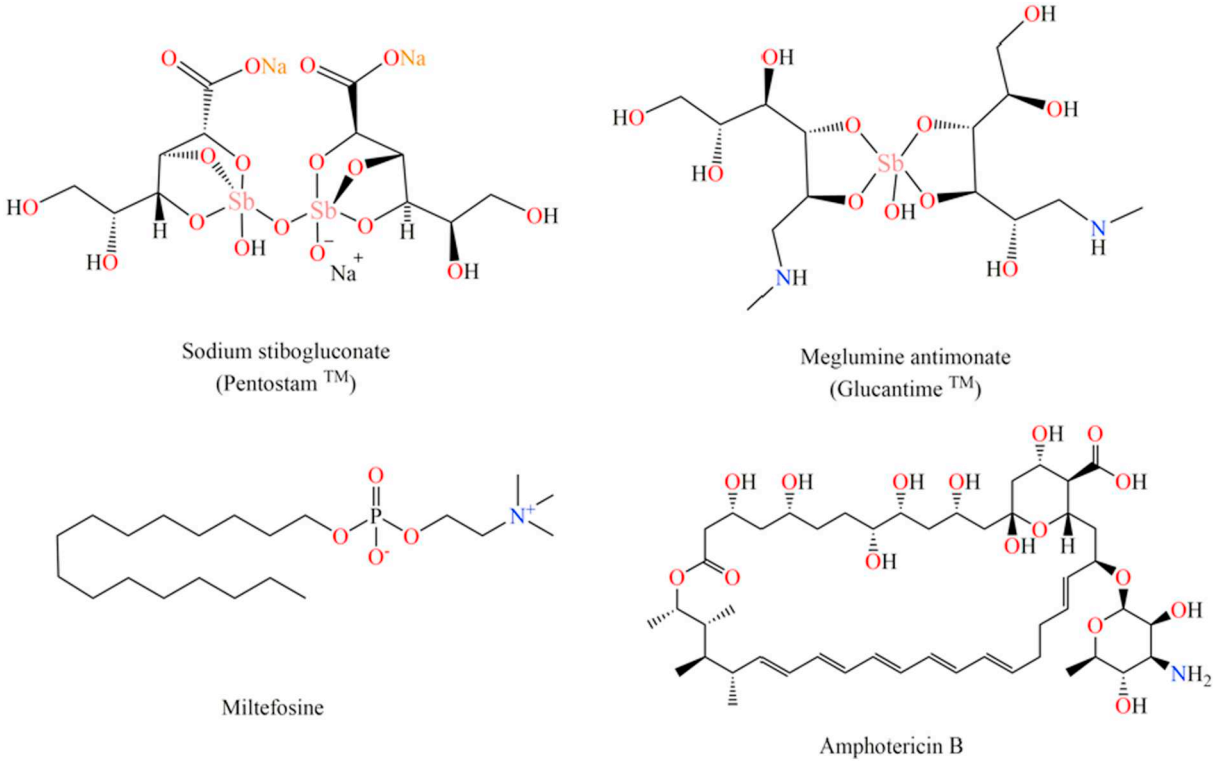

Fig. 1. Current pentavalent antimonial and organically derived anti-leishmanial treatments.

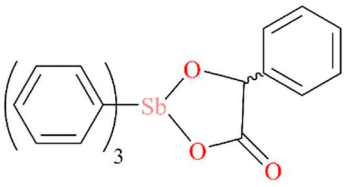

Fig. 2. Structure of the cyclometallate complex [$SbPh_3$(*R*/S-man)] [19].

One complex which combined excellent activity towards amastigotes (% infected cells. 21 ± 0.72) and low toxicity towards human fibroblasts (≥100 μM) was the *tris*-phenyl antimony(v) mandelate [$SbPh_3$(man)], in which mandelic acid (Man-H_2), an alpha-hydroxy acid, had undergone double deprotonation and formed a cyclometallate (Fig. 2).

This was the case whether the *R* or *S* enantiomer of mandelic acid was used, though there was some slight variation in the bioactivity [19,24,25]. Mandelic acid itself has been used medicinally as a biological detector for toxic vapour exposure and as a bladder irrigation fluid for urinary tract infections [26–31]. Mandelic acids anti-bacterial potential has also been assessed, with promising results in dermatological treatments [32,33].

Our previous studies on a large range of *tris*-aryl antimony(*V*) *bis*-carboxylate complexes, [$SbAr_3(O_2CR)_2$] (Ar = Ph or tolyl), have shown that the simple change from Ph to tolyl and then in the substitution pattern of the tolyl group (*o*-, *m*- or *p*-) can have a significant effect on both the activity and selectivity of the Sb(*V*) complexes [21,23]. Specifically, the most active and selective compounds were either *p*-tolyl or *m*-tolyl substituted, with the *m*-tolyl compounds being overall marginally better. The *o*-tolyl and Ph substituted compounds proved to be generally less selective. In a subsequent study on Bi(*V*) analogues it was noted that the tolyl derivatives were again more selective than their Ph counterparts [20]. From these studies, it was concluded that the tolyl groups not only improve selectivity but were largely responsible for mediating the mammalian cell toxicity, while the carboxylate groups affected activity towards the parasite.

With this information on hand, and being aware of the good activity and selectivity of the [$SbPh_3$(man)] complexes, we sought to improve the overall selectivity through a reduction in mammalian cell toxicity by replacing the three Ph groups with tolyl (*o*-, *m*- and *p*-), and three other substituted aryl groups (*o*-MeO-, mesityl, and *p*-*tert*-Bu), shown in Fig. 3.

In all six different aryl groups were assessed along with the different enantiomers of mandelic acid, to determine any structure – activity relationships dependant on the aryl group or the chirality of the carboxylate. We aimed to investigate whether these cyclometallate carboxylates may prove more effective than the conventional *bis*-substituted carboxylate complexes [$SbAr_3(manH)_2$]. As such, twelve novel complexes of general formulae [$SbAr_3$(man)] and [$(SbAr_3(manH)_2O_2$], were synthesised and characterised and their anti-leishmanial activity and cytotoxicity assessed.

2. Experimental

2.1. General

Mandelic acid (*R* or *S*) was purchased from Sigma Aldrich without the need for purification. All bromo-aryls were purchased from either Sigma Aldrich or Oakwood. Any remaining reagents were purchased from Sigma Aldrich and Alfa Aesar. Solvents were purchased from Merck. All reaction requiring inert conditions were performed under an atmosphere of nitrogen, using over dried glassware and utilising a Schlenk manifold and technique. All dried solvents were obtained from an MBraun-SPS-800 and stored under nitrogen over 4A molecular sieves, in flasks equipped with Youngs taps. ^{1}H NMR and ^{13}C NMR were recorded on a Bruker Avance DRX600 spectrophotometer (600 MHz), chemical shifts were references to the appropriate protiated solvent, d_6-DMSO. Melting point analysis was conducted in open end capillary tubes, on a digital Stuart Scientific melting point apparatus SMP10. Infrared Spectra were recorded on an Agilent Technologies Cary 630 FTIR spectrometer, using a range of 4000–500 cm^{-1}. Elemental

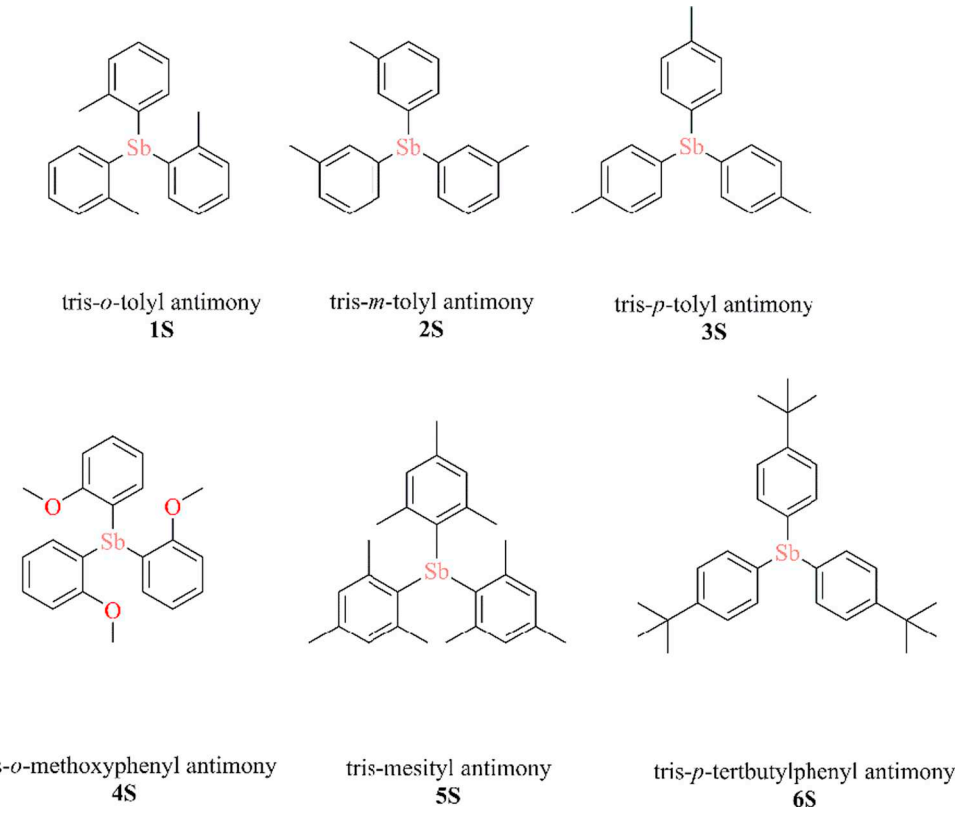

Fig. 3. $SbAr_3$ precursors used in this study: [Sb(*o*-tol)$_3$], **1S** [Sb(*m*-tol)$_3$], **2S** [Sb(*p*-tol)$_3$], **3S** [Sb(*o*-PhOMe)$_3$], **4S** [Sb(Mes)$_3$], **5S** [Sb(*p*-*tert*-BuPh)$_3$], **6S**.

analysis was obtained from either the School of Human Sciences, Science Centre at *London Metropolitan University, United Kingdom, or the School of Chemistry, Monash University*.

2.2. X-ray crystallography

Crystallographic data on all appropriate complexes were collected on an OXFORD XtaLAB Synergy, Dualflex, HyPix diffractometer equipped with an OXFORD Cryosystems 700 Cryostream and cooled to 173(2) K. Data was collected with monochromatic (graphite) CuK/α radiation (λ = 0.71073 Å) or MoK_α radiation (λ = 0.71070 Å) and processed using the CrysAlisPro *ν* 1.171.40.49a software [34]. Each compound was solved and refined using SHELX-97 utilising the graphical interface X-Seed or Olex2 [35,36]. Refinement was achieved by using the full matrix least-squares technique on F^2, which minimises the function given by $(F_o\text{-}F_c)^2$, where F_o and F_c are the observed and calculated structure amplitudes respectively, given that the weight is defined as $4F_0^2/2F_o^2$. Unless otherwise indicated, all non-hydrogen atoms were refined with anisotropic thermal parameters. Hydrogen atoms were placed in calculated positions using a riding model with C-H = 0.95–0.98 Å and $U_{iso}(H) = xU_{iso}(C)$, x = 1.2 or 1.5 unless otherwise indicated. Dr. Craig M. Forsyth and Dr. Victoria L. Blair provided advice and assistance during the refinement process of structures.

2.3. Cell culture

Leishmania major virulent clone V121 was derived from the LRC-L137 *L. major* isolate and maintained at 26 °C in supplemented M199 media (10% (*v*/v) heat inactivated FBS, 1% Pen-Strep), purchased from Gibco ™. Human primary fibroblasts and J774 macrophages were cultured and maintained in Dulbecco's Modified Eagles Medium (DMEM) supplemented with 10% FBS and 1% Pen-Strep and 1% Glutamax (purchased from Gibco ™) at 37 °C in a 5% CO_2 incubator [22].

2.4. In vitro testing of L. major and human fibroblasts

Celltiter Blue Cell Viability Assay was purchased from Promega ™, and used for the determination of percentage viability of the parasite and human fibroblasts. All compounds were dissolved in DMSO to make up a 10 mM working stock and sequentially diluted out in the appropriate culture media (100 μM to 48 nM). Assays were set up in duplicate in 96-well Falcon plates. Volumes of 10^6 promastigotes/mL and 10^5 fibroblasts/mL were used. All cell assays were measured spectroscopically using fluorescence excitation at 544 nm and emission at 590 nm. Fibroblasts and L. *major* were measured after 48 h, Cos-7 and HeLa were measured after 24 h. The compounds were compared to a no drug negative control and the percent inhibition calculated [37]. Fluorescence measurements were conducted on a BMG-Labtech FluoStar Omega microplate reader [19,20].

Macrophage invasion assays were performed as previously described [23,38]. Briefly, J774 macrophages were plated onto coverslips in a 24 well plate and allowed to adhere for 48 h. The cells were exposed to L. *major* promastigotes at a 1:10 ratio and incubated for a further 24 h to allow for amastigote formation *in vitro*. The slides were then washed to remove any excess extracellular promastigotes and exposed to compounds for 48 h before washing, fixation and cellular staining with a commercial Hema Color kit purchased from Merck. Following Giemsa staining, 200 cells per duplicate slide were then counted microscopically and the percentage of infected cells calculated.

2.5. Precursors synthesis

The reaction was conducted using anhydrous conditions. Magnesium metal (3.2 g, 3.1 equivalents) was added to a three-neck round bottom flask, equipped with a stirring bead, dropping funnel, condenser and Schlenk tap. The apparatus was evacuated and backfilled with nitrogen in triplicate before the addition of ~ 70 mL of dry THF. Either 19 mL, 19 mL, 24.2 g, 22.2 mL and 23 mL of 2-bromotoluene, 3-

bromotoluene, 4-bromotoluene, bromomesitylene and 4-bromotertbutyphenyl respectively, were added to the dropping funnel and ~ 20 mL of dry THF added to either dissolve or homogenise the brominated aryl. The solution was added dropwise to the stirring magnesium turnings until self-reflux occurred. If no reflux occurred, the solution was heated with a heat gun to initiate the reaction. The solution was stirred for approximately 4–6 h, forming a dark coloured Grignard. The Grignard was filtered cannulated over to a prior prepared solution of 10 g of $SbCl_3$ in a three-neck flask. The solution was kept over ice during the filtration. After 24 h, the dark grey solution was quenched over ice, yielding an off-white solid of the crude aryl antimony. Each was recrystallised in hot ethanol, removing impurities. An average yield of 75% - 85% was obtained for all aryls respectively. A different method was employed for the *o*-methoxyphenyl antimony. Approximately 7.2 mL of anhydrous anisole was transferred into a Schlenk flask and suspended in dry THF. Three equivalents (41 mL) of 1.6 M n-butyllithium solution in hexane, was added dropwise at 0 °C. The lithiated solution was then added to a pre-purged dropping funnel in a pre-urged three-neck RBF, with 5 g of $SbCl_3$. The solution was added dropwise to the $SbCl_3$ solution in THF, maintaining a temperature of 0 °C. The solution was quenched over ice to remove the LiCl produced and precipitate out the *tris*-aryl antimony. The crude product was recrystallised from hot ethanol, yielding a crystalline white solid of 69% yield.

2.5.1. Tris-o-tolyl antimony

m.p: 108–110 °C, 82% ^{1}H NMR (400 MHz, DMSO-d_6) δ 7.35–7.24 (m, 2H, CH_{ar}), 7.07 (ddd, J = 8.7, 5.1, 2.5 Hz, 1H, CH_{ar}), 6.91–6.82 (m, 1H, CH_{ar}), 2.40 (s, 3H); ^{13}C NMR (101 MHz, DMSO) δ 143.5 (SbC), 135.2 (C_{ar}), 129.8 (C_{ar}), 126.6 (C_{ar}), 24.2 (CH_3).

2.5.2. Tris-m-tolyl antimony

m.p: 70–72 °C, 76%; ^{1}H NMR (400 MHz, DMSO-d_6) δ = 7.29–7.19 (m, 6H, CH_{ar}), 7.15 (dd, J = 10.5, 7.6 Hz, 6H, CH_{ar}), 2.24 (s, 9H, CH_3); ^{13}C NMR (101 MHz, DMSO-d_6) δ = 138.3 (SbC), 133.2 (C_{ar}), 129.8 (C_{ar}), 21.5 (CH_3).

2.5.3. Tris-p-tolyl antimony

m.p: 130–132 °C, 75%; ^{1}H NMR (400 MHz, DMSO-d_6) δ = 7.26 (d, J = 7.6 Hz, 6H, CH_{ar}), 7.16 (d, J = 7.6 Hz, 6H, CH_{ar}), 2.28 (s, 9H, CH_3); ^{13}C NMR (101 MHz, DMSO-d_6) δ = 138.5 (SbC), 136.2 (C_{ar}), 134.9 (C_{ar}), 130.1 (C_{ar}), 21.4 (CH_3).

2.5.4. Tris-mesityl antimony

m.p: 136–138 °C, 85%; ^{1}H NMR (400 MHz, DMSO-d_6) δ = 6.82 (s, 9H, CH_{ar}), 2.19 (d, J = 4.0 Hz, 18H, CH_3), 2.13 (d, J = 18.2 Hz, 9H, CH_3); ^{13}C NMR (101 MHz, DMSO-d_6) δ = 144.5 (SbC), 129.3 (C_{ar}), 25.2 (CH_3).

2.5.5. Tris-p-tertbutylphenyl antimony

m.p: 278–280 °C, 83%, ^{1}H NMR (400 MHz, Chloroform-*d*) δ 7.44–7.31 (m, 5H, CH_{ar}), 1.32 (s, 27H, tert-Bu-CH). ^{13}C NMR (101 MHz, $CDCl_3$) δ 151.38 (SbC), 136.0 (C_{ar}), 134.8 (C_{ar}), 128.2 (C_{ar}), 125.8 (C_{ar}), 34.6 (tert-Bu-C), 31.3 (tert-Bu-C), 31.2 (tert-Bu-C).

2.5.6. Tris-o-methoxyphenyl antimony

m.p.: 180–182 °, 69%; ^{1}H NMR (400 MHz, DMSO-d_6) δ = 7.35 (ddd, J = 8.2, 7.3, 1.7 Hz, 3H, CH_{ar}), 7.03 (dd, J = 8.3, 1.0 Hz, 3H, CH_{ar}), 6.82 (td, J = 7.3, 1.0 Hz, 3H, CH_{ar}), 6.68 (dd, J = 7.2, 1.7 Hz, 3H, CH_{ar}), 3.72 (s, 9H, OCH_3); ^{13}C NMR (101 MHz, DMSO-d_6) δ = 162.3 (SbC), 130.5 (C_{ar}), 121.8 (C_{ar}), 110.2 (C_{ar}), 55.6 (OCH_3).

2.6. General procedure

Approximately 0.5 mmol of the desired *tris*-aryl antimony (0.176 g) was added to a 100 mL RBF, equipped with stirrer bead and dissolved in diethyl ether. To this, a slight excess of 1.2 mmol of a 30% hydrogen peroxide solution in water was added. After approximately 5 min, 0.5 mmol of the either *R* or *S* mandelic acid (0.076 g) was added and the reaction stirred overnight. The solvent and H_2O by-products were removed under vacuum yielding oily solids. The oily substances were sonicated in H_2O, precipitating out a solid. The solids were collected *via* filtration, yielding complexes **1Sr – 6Sr**, **1Rs – 6Rs.** Complexes were crystallised from the ether filtrate, or by heating the solid in DMSO.

2.6.1. Tris-o-tolyl antimony R-mandelate, ***1Sr***

Tris-o-tolyl antimony (0.197 g, 0.5 mmol) was reacted with R-mandelic acid (0.071 g, 0.5 mmol) according to GP. White solid (0.226 g, 83%), m.p: 136–139 °C; ^{1}H NMR (600 MHz, DMSO-d_6) δ = 7.58–7.56 (m, 3H, CH_{ar}), 7.52–7.49 (m, 3H, CH_{ar}), 7.42 (t, J = 7.2 Hz, 6H, CH_{ar}), 7.37 (d, J = 1.2 Hz, 2H, CH_{ar}), 7.34–7.31 (m, 2H, CH_{ar}), 7.30–7.26 (m, 1H, CH_{ar}), 5.40 (s, 1H, CCH), 2.28 (s, 9H, CH_3); ^{13}C NMR (151 MHz, DMSO-d_6) δ = 173.1 (COOH), 141.8 (SbC), 139.8 (C_{ar}), 138.1 (C_{ar}), 133.6 (C_{ar}), 131.9 (C_{ar}), 131.7 (C_{ar}), 128.2 (C_{ar}), 127.6 (C_{ar}), 127.1 (C_{ar}), 127.0 (C_{ar}), 73.6 (COH), 64.9 (CCH), 22.9 (CH_3); FT-IR [cm $^{-1}$]: 3055 (w), 2922 (w), 1682 (sh), 1450 (m), 1309 (m), 1286 (sh), 1045(m), 1026 (m), 797 (w), 747 (sh), 697 (sh). Elemental Analysis, Expected: C:63.88H:4.99, Found: C63.63H:5.11. CCDC: 1938254.

2.6.2. Tris-o-tolyl antimony S-mandelate, ***1Ss***

Tris-o-tolyl antimony (0.197 g, 0.5 mmol) was reacted with S-mandelic acid (0.071 g, 0.5 mmol) according to GP. White solid (0.280 g, 80%), m.p: 137–140 °C; ^{1}H NMR (600 MHz, DMSO-d_6) δ = 7.58–7.56 (m, 3H, CH_{ar}), 7.52–7.49 (m, 3H, CH_{ar}), 7.42 (t, J = 7.2 Hz, 6H, CH_{ar}), 7.37 (d, J = 1.2 Hz, 2H, CH_{ar}), 7.34–7.31 (m, 2H, CH_{ar}), 7.30–7.26 (m, 1H, CH_{ar}), 5.40 (s, 1H, CCH), 2.28 (s, 9H, CH_3); ^{13}C NMR (151 MHz, DMSO-d_6) δ = 173.1 (COOH), 141.8 (SbC), 139.8 (C_{ar}), 138.1 (C_{ar}), 133.6 (C_{ar}), 131.9 (C_{ar}), 131.7 (C_{ar}), 128.2 (C_{ar}), 127.6 (C_{ar}), 127.1 (C_{ar}), 127.0 (C_{ar}), 73.6 (COH), 64.9 (CCH), 22.9 (CH_3); FT-IR [cm $^{-1}$]: 3057 (w), 2922 (w), 1683 (sh), 1450 (m), 1310 (m), 1286 (sh), 1045(m), 1027 (m), 797 (w), 753 (sh), 697 (sh). Elemental Analysis, Expected: C:63.88H:4.99, Found: C63.69H:5.08. CCDC: 1938260.

2.6.3. Tris-m-tolyl antimony R-mandelate, ***2Sr***

Tris-m-tolyl antimony (0.197 g, 0.5 mmol) was reacted with R-mandelic acid (0.071 g, 0.5 mmol) according to GP. White solid (0.224 g, 86%), m.p: 130–133 °C; ^{1}H NMR (600 MHz, DMSO-d_6) δ = 7.49–7.43 (m, 3H, CH_{ar}), 7.43–7.37 (m, 3H, CH_{ar}), 7.36–7.30 (m, 6H, CH_{ar}), 7.28–7.25 (m, 2H, CH_{ar}), 7.25–7.21 (m, 2H, CH_{ar}), 7.21 (m, 1H, CH_{ar}), 5.16 (s, 1H, CH), 2.27 (s, 9H, CH_3); ^{13}C NMR (101 MHz, DMSO) δ = 174.6 (COOH), 142.7 (SbC), 141.4 (C_{ar}), 137.7 (C_{ar}), 134.7 (C_{ar}), 131.3 (C_{ar}), 130.5 (C_{ar}), 128.4 (C_{ar}), 127.5 (C_{ar}), 127.4 (C_{ar}), 126.7 (C_{ar}), 74.1 (COH), 21.3 (CH_3).FT-IR [cm^{-1}]: 2919 (w), 1683 (sh), 1619 (sh), 1450 (m), 1361 (m), 1278 (sh), 1070(m), 1038 (m), 791 (m), 763 (sh), 691 (sh). Elemental Analysis, Expected: C:63.88H:4.99, Found: C63.56H:5.10. CCDC: 1938259.

2.6.4. Tris-m-tolyl antimony S-mandelate, ***2Ss***

Tris-m-tolyl antimony (0.197 g, 0.5 mmol) was reacted with S-mandelic acid (0.071 g, 0.5 mmol) according to GP. White solid (0.196 g, 72%), m.p: 129–131 °C; ^{1}H NMR (600 MHz, DMSO-d_6) δ = 7.49–7.43 (m, 3H, CH_{ar}), 7.43–7.37 (m, 3H, CH_{ar}), 7.36–7.30 (m, 6H, CH_{ar}), 7.28–7.25 (m, 2H, CH_{ar}), 7.25–7.21 (m, 2H, CH_{ar}), 7.21 (m, 1H, CH_{ar}), 5.16 (s, 1H, CH), 2.27 (s, 9H, CH_3); ^{13}C NMR (101 MHz, DMSO) δ = 174.6 (COOH), 142.7 (SbC), 141.4 (C_{ar}), 137.7 (C_{ar}), 134.7 (C_{ar}), 131.3 (C_{ar}), 130.5 (C_{ar}), 128.4 (C_{ar}), 127.5 (C_{ar}), 127.4 (C_{ar}), 126.7 (C_{ar}), 74.1 (COH), 21.3 (CH_3); FT-IR [cm $^{-1}$]: 2918 (w), 1682 (sh), 1618 (sh), 1450 (m), 1362 (m), 1276 (sh), 1070(m), 1038 (m), 778 (m), 763 (sh), 690 (sh). Elemental Analysis, Expected: C:63.88H:4.99, Found: C63.87H:5.24. CCDC: 1938255.

2.6.5. Peroxybis(tris-p-tolyl antimony R-mandelate), ***3Sr***

Tris-p-tolyl antimony (0.197 g, 0.5 mmol) was reacted with R-mandelic acid (0.071 g, 0.5 mmol) according to GP. White solid (0.227 g, 81%), m.p: 145–147 °C; FT-IR [cm $^{-1}$]: 3600 (w), 3026 (w) 2920 (w), 1653 (sh), 1493 (sh), 1451 (m), 1314 (m), 1283 (sh), 1187 (sh)1059 (m), 1015 (m), 797 (sh), 732 (sh), 696 (sh). Elemental Analysis, Expected: C:61.95H:5.02, Found: C61.24H:5.24.

2.6.6. Tris-p-tolyl antimony R-mandelate, ***3Sr'***

Complex **3Sr** was placed into d_6-DMSO, liberating H_2O_2 and forming the solution state cyclometallate. ^{1}H NMR (600 MHz, DMSO-d_6) δ = 10.20 (s, 1H, OH), 7.49–7.46 (m, 6H, CH_{ar}), 7.43–7.40 (m, 2H, CH_{ar}), 7.26–7.24 (m, 6H, CH_{ar}), 7.22–7.20 (m, 2H, CH_{ar}), 7.20–7.17 (m, 1H, CH_{ar}), 5.12 (s, 1H, CCH), 2.32 (s, 9H, CH_3); ^{13}C NMR (151 MHz, DMSO-d_6) δ = 174.5 (COOH), 141.4 (SbC), 139.4 (C_{ar}), 139.3 (C_{ar}), 134.2 (C_{ar}), 129.2 (C_{ar}), 127.4 (C_{ar}), 127.3 (C_{ar}), 126.6 (C_{ar}), 73.9 (COH), 64.9 (CCH), 21.0 (CH_3).

2.6.7. Peroxybis(tris-p-tolyl antimony S-mandelate, ***3Ss***

Tris-p-tolyl antimony (0.197 g, 0.5 mmol) was reacted with S-mandelic acid (0.071 g, 0.5 mmol) according to GP. White solid (0.222 g,79%), m.p: 144–146 °C; FT-IR [cm $^{-1}$]: 3600 (w), 3024 (w) 2919 (w), 1654 (sh), 1492 (sh), 1450 (m), 1312 (m), 1283 (sh), 1187 (sh) 1059 (m), 1015 (m), 796 (sh), 732 (sh), 696 (sh). Elemental Analysis, Expected: C:61.95H:5.02, Found: C61.90H:4.82.

2.6.8. Tris-p-tolyl antimony S-mandelate, ***3Ss'***

Complex **3Ss** was placed into d_6-DMSO, liberating H_2O_2 and forming the solution state cyclometallate. ^{1}H NMR (600 MHz, DMSO-d_6) δ = 10.20 (s, 1H, OH), 7.49–7.46 (m, 6H, CH_{ar}), 7.43–7.40 (m, 2H, CH_{ar}), 7.26–7.24 (m, 6H, CH_{ar}), 7.22–7.20 (m, 2H, CH_{ar}), 7.20–7.17 (m, 1H, CH_{ar}), 5.12 (s, 1H, CCH), 2.32 (s, 9H, CH_3); ^{13}C NMR (151 MHz, DMSO-d_6) δ = 174.5 (COOH), 141.4 (SbC), 139.4 (C_{ar}), 139.3 (C_{ar}), 134.2 (C_{ar}), 129.2 (C_{ar}), 127.4 (C_{ar}), 127.3 (C_{ar}), 126.6 (C_{ar}), 73.9 (COH), 64.9 (CCH), 21.0 (CH_3).

2.6.9. Tris-o-methoxypheny antimony R-mandelate, ***4Sr***

Tris-*o*-methoxyphenyl antimony (0.221 g, 0.5 mmol) was reacted with R-mandelic acid (0.071 g, 0.5 mmol) according to GP. White solid (0.213 g, 72%), m.p: 195–197 °C; ^{1}H NMR (600 MHz, DMSO-d_6) δ = 7.56–7.48 (m, 8H, CH_{ar}), 7.37–7.28 (m, 2H, CH_{ar}), 7.28–7.24 (m, 1H, CH_{ar}), 7.17–7.08 (m, 6H, CH_{ar}), 5.23 (s, 1H, CH), 3.56 (s, 9H, OCH_3); ^{13}C NMR (151 MHz, DMSO-d_6) δ = 173.5 (COOH), 160.2 ($COCH_3$), 140.9 (SbC), 133.1 (C_{ar}), 132.5 (C_{ar}), 129.0 (C_{ar}), 127.8 (C_{ar}), 127.1 (C_{ar}), 126.5 (C_{ar}), 121.8 (C_{ar}), 111.9 (OCH_3), 72.9 (COH), 55.8 (CCH); FT-IR [cm $^{-1}$]: 3063 (w) 2941 (w), 1677 (sh), 1577 (sh), 1470 (m), 1431 (m), 1297 (sh), 1242 (m), 1009 (m), 790 (sh), 756 (sh), 705 (m). Elemental Analysis **4Sr.½Et$_2$O**, Expected: C:59.07 H:5.12, Found: C59.37 H:4.84. CCDC: 1938261.

2.6.10. Tris-o-methoxyphenyl antimony S-mandelate, ***4Ss***

Tris-*o*-methoxyphenyl antimony (0.221 g, 0.5 mmol) was reacted with S-mandelic acid (0.071 g, 0.5 mmol) according to GP. White solid (0.231 g. 78%), m.p: 196–198 °C; δ = 7.56–7.48 (m, 8H, CH_{ar}), 7.37–7.28 (m, 2H, CH_{ar}), 7.28–7.24 (m, 1H, CH_{ar}), 7.17–7.08 (m, 6H, CH_{ar}), 5.23 (s, 1H, CH), 3.56 (s, 9H, OCH_3); ^{13}C NMR (151 MHz, DMSO-d_6) δ = 173.5 (COOH), 160.2 ($COCH_3$), 140.9 (SbC), 133.2 (C_{ar}), 132.5 (C_{ar}), 129.0 (C_{ar}), 127.8 (C_{ar}), 127.1 (C_{ar}), 126.5 (C_{ar}), 121.8 (C_{ar}), 111.9 (OCH_3), 72.9 (COH), 55.8 (CCH); FT-IR [cm $^{-1}$]: 3063 (w) 2941 (w), 1677 (sh), 1577 (sh), 1470 (m), 1431 (m), 1297 (sh), 1242 (m), 1009 (m), 790 (sh), 756 (sh), 705 (m). Elemental Analysis **4Ss.½Et$_2$O** , Expected: C:59.07 H:5.12, Found: C59.45 H:4.91. CCDC: 1938262.

2.6.11. Tris-mesityl antimony R-mandelate, ***5Sr***

Tris-mesityl antimony (0.238 g, 0.5 mmol) was reacted with R-mandelic acid (0.071 g, 0.5 mmol) according to GP6. White solid (0.297 g, 78%), m.p: 230–232 °C; ^{1}H NMR (600 MHz, DMSO-d_6) δ = 7.30–7.25 (m, 3H, CH_{ar}), 7.11 (m, 2H, CH_{ar}), 7.02 (m, 3H, CH_{ar}), 6.88–6.81 (m, 3H, CH_{ar}), 5.02 (s, 1H, CH), 2.38 (s, 9H, CH_3), 2.30–2.26 (m, 9H, CH_3), 2.21–2.12 (m, 9H, CH_3); ^{13}C NMR (151 MHz, DMSO-d_6) δ = 143.7 (SbC), 141.4 (C_{ar}), 140.8 (C_{ar}), 139.3 (C_{ar}), 139.2 (C_{ar}), 130.5 (C_{ar}), 129.9 (C_{ar}), 127.9 (C_{ar}), 127.5 (C_{ar}), 74.2 (COH), 23.5 (CH_3), 22.3 (CH_3), 20.5 (CH_3); FT-IR [cm $^{-1}$]: 3017 (w) 2921 (w), 1677 (sh), 1449 (m), 1311 (sh), 1291 (m), 1256 (sh), 1017 (sh), 945 (m), 785 (m), 765 (sh), 697 (m). Elemental Analysis, Expected: C:66.79H:6.25, Found: C66.87H:6.57. CCDC: 1938256.

2.6.12. Tris-mesityl antimony S-mandelate, ***5Ss***

Tris-mesityl antimony (0.238 g, 0.5 mmol) was reacted with S-mandelic acid (0.071 g, 0.5 mmol) according to GP. White solid (0.300 g, 82%), m.p: 230–232 °C; ^{1}H NMR (600 MHz, DMSO-d_6) δ = 7.30–7.25 (m, 3H, CH_{ar}), 7.11 (m, 2H, CH_{ar}), 7.02 (m, 3H, CH_{ar}), 6.88–6.81 (m, 3H, CH_{ar}), 5.02 (s, 1H, CH), 2.38 (s, 9H, CH_3), 2.30–2.26 (m, 9H, CH_3), 2.21–2.12 (m, 9H, CH_3); ^{13}C NMR (151 MHz, DMSO-d_6) δ = 143.7 (SbC), 141.4 (C_{ar}), 140.8 (C_{ar}), 139.3 (C_{ar}), 139.2 (C_{ar}), 130.5 (C_{ar}), 129.9 (C_{ar}), 127.9 (C_{ar}), 127.5 (C_{ar}), 74.2 (COH), 23.5 (CH_3), 22.3 (CH_3), 20.5 (CH_3); FT-IR [cm $^{-1}$]: 3021 (w) 2919 (w), 1677 (sh), 1448 (m), 1311 (sh), 1291 (m), 1255 (sh), 1017 (sh), 945 (m), 785 (m), 765 (sh), 697 (m). Elemental Analysis, Expected: C:66.79H:6.25, Found: C66.97H:6.52. CCDC: 1938258.

2.6.13. Tris-p-tert-butylphenyl antimony R-mandelate, ***6Sr***

Tris-*p*-tertbutylphenyl antimony (0.260 g, 0.5 mmol) was reacted with R-mandelic acid (0.071 g, 0.5 mmol) according to GP. White solid (0.252 g, 75%), m.p: 196–198 °C; ^{1}H NMR (600 MHz, DMSO-d_6) δ = 7.61–7.50 (m, 6H, CH_{ar}), 7.49–7.43 (m, 6H, CH_{ar}), 7.41–7.33 (m, 2H, CH_{ar}), 7.21–7.16 (m, 3H, CH_{ar}), 5.14 (s, 1H, CH), 1.28 (s, 27H, CH_3); ^{13}C NMR (151 MHz, DMSO-d_6) δ = 174.5 (COOH), 152.5 (SbC), 139.8 (C_{ar}), 134.2 (C_{ar}), 127.5 (C_{ar}), 127.4 (C_{ar}), 125.6 (C_{ar}), 74.1 (COH), 56.2 (CCH), 34.7 (CH_3), 31.1 (CH_3), 18.7 (CH_3); FT-IR [cm $^{-1}$]: 3059 (w) 2957 (sh), 2902 (m), 1665 (sh), 1491 (m), 1311 (sh), 1267 (m), 1200 (m), 1064 (sh), 947 (w), 818 (sh), 800 (w), 698 (m). Elemental Analysis (6R.1.5H_2O), Expected: C:65.34 H6.93, Found: C65.47H:7.10. CCDC: 1938257.

2.6.14. Tris-p-tert-butylphenyl antimony S-mandelate, ***6Ss***

Tris-*p*-tertbutylphenyl antimony (0.260 g, 0.5 mmol) was reacted with S-mandelic acid (0.071 g, 0.5 mmol) according to GP. White solid (0.241 g, 73%), m.p: 197–199 °C; ^{1}H NMR (600 MHz, DMSO-d_6) δ = 7.61–7.50 (m, 6H, CH_{ar}), 7.49–7.43 (m, 6H, CH_{ar}), 7.41–7.33 (m, 2H, CH_{ar}), 7.21–7.16 (m, 3H, CH_{ar}), 5.14 (s, 1H, CH), 1.28 (s, 27H, CH_3); ^{13}C NMR (151 MHz, DMSO-d_6) δ = 174.1 (COOH), 152.5 (SbC), 139.8 (C_{ar}), 134.2 (C_{ar}), 127.6 (C_{ar}), 127.6 (C_{ar}), 125.6 (C_{ar}), 74.1 (COH), 56.2 (CCH), 34.7 (CH_3), 31.1 (CH_3), 18.7 (CH_3); FT-IR [cm $^{-1}$]: 3058 (w) 2957 (sh), 2902 (m), 1665 (sh), 1491 (m), 1311 (sh), 1267 (m), 1200 (m), 1064 (sh), 949 (w), 818 (sh), 798 (w), 697 (m). Elemental Analysis (6S.1.5H_2O), Expected: C:65.34 H6.93, Found: C65.30H:7.12. CCDC: 1938253.

3. Results and discussion

3.1. Synthesis

All complexes were synthesised by a conventional oxidative addition reaction of hydrogen peroxide to the selected $SbAr_3$ before addition of one equivalent of either *R* or *S* mandelic acid (Fig. 4) [19,21,22,39].

Due to the close pK_a values of *tert*-BuOH and the α-hydroxyl proton of mandelic acid, H_2O_2 was used in place of the common alternative oxidant *tert*-BuOOH to encourage cyclometallation [40]. Thus, the only by-product from the reaction was H_2O, produced upon condensation of the $[SbAr_3(OH)_2]$ intermediate with the acid.

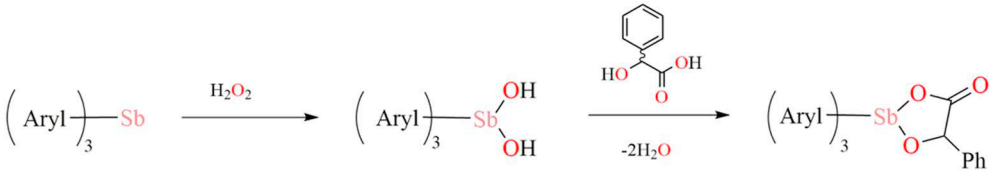

Fig. 4. Reaction scheme for the formation of complexes **1Sr/s,** [Sb(o-tol)$_3$(man)], **2Sr/s,** [Sb(*m*-tol)$_3$(man)], **3Sr/s,** [(Sb(*p*-tol)$_3$(manH)$_2$O$_2$], **4Sr/s,** [Sb(o-PhOMe)$_3$(man)], **5Sr/s,** [Sb(Mes)$_3$(man)] and **6Sr/s,** [Sb(*p*-tert-BuPh)$_3$(man)].

Despite the anticipated simplicity of the reaction procedure, the synthesis of complexes **1Sr/s,** [Sb(*o*-tol)$_3$(man)], **2Sr/s,** [Sb(*m*-tol)$_3$(man)], **3Sr/s,** [(Sb(*p*-tol)$_3$(manH)$_2$O$_2$], **4Sr/s,** [Sb(*o*-PhOMe)$_3$(man)], **5Sr/s,** [Sb(Mes)$_3$(man)] and **6Sr/s,** [Sb(*p*-*tert*-BuPh)$_3$(man)], gave rise to several issues. The reaction would often generate oily residues. ^{1}H NMR spectra of these residues indicated that the reactions had not gone to completion. On increasing the reaction time and heating to 60 °C in H_2O under sonication the target compounds were isolated as white solids in high purity and yield. Any remaining peroxide and mandelic acid was removed in the water. Complexes **1Sr/s**, **2Sr/s, 4Sr/s, 5Sr/s,** and **6Sr/s** all formed the desired cyclometallates of general formula [SbAr$_3$(man)].

Interestingly, and somewhat surprisingly, the reaction with Sb(*p*-tol)$_3$ generated the μ^2-peroxo complex [(SbAr$_3$(manH))$_2$O$_2$], illustrated in Fig. 5. This product was obtained on every occasion the reaction was conducted, as verified by elemental analysis and through X-ray diffraction data collected on four sets of crystals from four separate reactions. We saw no evidence for the formation of the cyclometallate from the solid-state data. However, solution ^{1}H NMR spectral analysis of the complex in d$_6$-DMSO over a period of 24 h showed the formation of the cyclometallate and liberation of H_2O_2 (Fig. 5). This result is consistent with the formation and identification of the only other complex of this type, [Sb(*p*-tol)$_3$(OC$_6$H$_4$Br-4)$_2$O$_2$)], which stems from the treatment of Sb(*p*-tol)$_3$ with 2-bromophenol mediated by H_2O_2 [41].

3.2. Characterisation

All complexes were characterised by ^{1}H and ^{13}C NMR spectroscopy, mp, FT-IR spectroscopy, and elemental analysis. Yields ranged from 72 to 86%. Complexes **1Sr/s**, **2Sr/s, 4Sr/s, 5Sr/s,** and **6Sr/s** were able to be structurally elucidated by single crystal X-ray crystallography. Repeated attempts to obtain the solid-state structures of the peroxo complexes **3Sr/s** resulted only in poor data, though connectivity of these complexes was able to be determined.

As expected for enantiomers, the *R* and *S* complexes are spectroscopically identical. Inclusion of the mandelate dianion as a cyclometallate was confirmed by the absence of the hydroxyl and carboxylic acid proton signals in the ^{1}H NMR spectra. The NMR spectra for all complexes can be found in the ESI along with an example in Fig. S1. The formation of the cyclometallate form of **3Sr/s,** [(SbAr$_3$(manH))$_2$O$_2$], was able to be determined through ^{1}H NMR, exhibiting clear differences in the solid-state *versus* solution state stability of the complex. When the μ^2-peroxo complex was dissolved into d$_6$-DMSO, a signal corresponding to H_2O_2 was observed along with the lack of the α-hydroxyl signal that would be expected for the μ^2-peroxo complex. After 24 h, the H_2O_2 signal disappears due to rapid degradation of H_2O_2, leaving only the signals that correspond to the formation of the cyclometallate (Fig. 6).

The FT-IR spectrum of each complex confirmed binding of the carboxylate by the shift in the wavenumber of the CO_2 stretching frequencies, detailed in the ESI (Table S1), along with the IR spectrum of each complex. The only technique able to successfully distinguish the two enantiomers was X-ray crystallography. The FT-IR was able to further confirm the presence of the peroxide bond in complexes **3Sr/s.** A sharp signals at 1187 cm^{-1} that is not found in any other complex correlates to the presence of a metal – peroxide bond [42,43]. A signal at ~3500 cm^{-1} representative of the α-hydroxyl can also be seen, and is absent in the remaining complexes. All IR spectral data can be found in the ESI.

3.3. X-ray crystallography

All complexes were structurally authenticated through single crystal X-ray diffraction. Complexes **1Ss** and **1Sr**, [Sb(*o*-tol)$_3$(man)]; **2Ss** and **2Sr,** [Sb(*m*-tol)$_3$(man)]; **4Sr** and **4Ss,** [Sb(*o*-PhOMe)$_3$(man)]; **5Ss** and **5Sr,** [Sb(Mes)$_3$(man)], all crystallised from either the toluene or ether reaction mixture, without solvent molecules present. Crystals of complexes **6Ss** and **6Sr**, [Sb(*p*-*tert*-BuPh)$_3$(man)], were crystallised through dissolution in hot DMSO and subsequent cooling, and shown to incorporate a datively bound DMSO molecule in the asymmetric unit, increasing the coordination number of Sb to six in a distorted octahedral environment.

Each complex solved in a non-centrosymmetric space group due to the pure enantiomeric form of the mandelate. A summary of the X-ray data for all complexes is provided in the ESI, Table S2. All complexes, with the exception of **2Ss/r** and **6Ss/r**, are five-coordinate adopting distorted trigonal bipyramidal geometry. Complexes **2Ss** and **2Sr**, [Sb(*m*-tol)$_3$(man)] are dimeric, with one Sb(*V*) datively interacting with the carboxyl of the other, forming a mixed five-coordinate, six-coordinate Sb complex. The structures are shown in the ESI with a detailed description of bond length and angles.

A description of the *o*-methoxyphenyl complex **4Sr** is given below (Fig. 7). The **4Ss** complex is analogous in structure, with the only

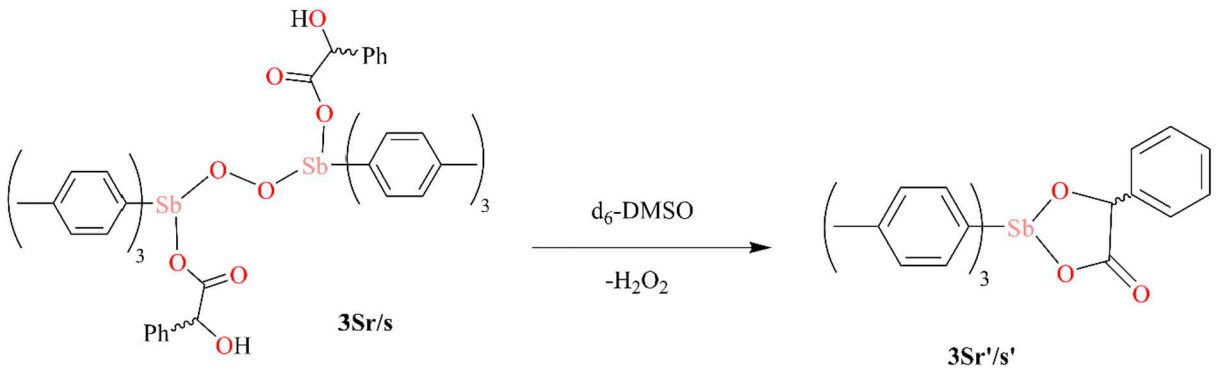

Fig. 5. General structures of complexes **3Sr/s,** [(Sb(*p*-tol)$_3$(manH)$_2$O$_2$] and the cyclometallate form **3Sr'/s'**, [Sb(*p*-tol)$_3$(man)].

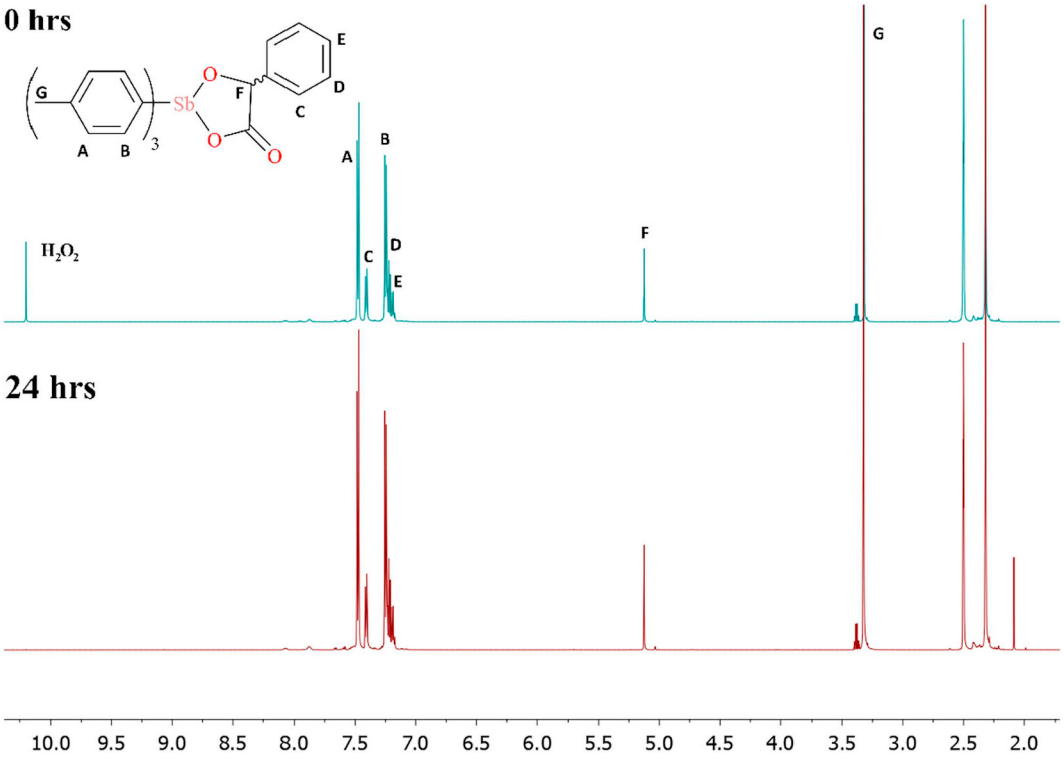

Fig. 6. ^{1}H NMR of complex **3Sr'**, [(Sb(*p*-tol)$_3$(man)], in d_6-DMSO at 0 and 24 h, highlighting the liberation of H_2O_2 and cyclometallate formation. The residual solvent signal and H_2O signal can be found at 2.50 and 3.33 ppm respectively.

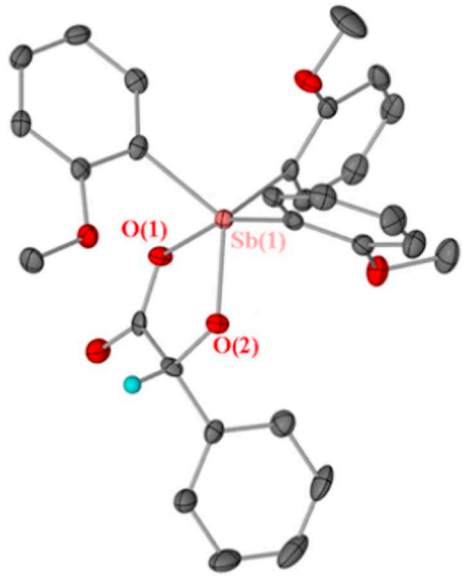

Fig. 7. Solid-state structure of [Sb($C_6H_4(OCH_3)$)$_3$(*R*-man)], **4Sr**. Thermal ellipsoids at 50% probability. Hydrogen atoms have been omitted for clarity. Selected bonds lengths (Å) and angles (o). Sb(1) – O(1), 1.956(3), Sb(1) – O(2), 2.162(3), Sb(1) – C(1), 2.118(5), Sb(1) – C(7), 2.103(4), Sb(1) – C(15), 2.100(5); C(1) – Sb(1) – C(15), 101.5(2), C(1) – Sb(1) – C(7), 108.1(2), C(7) – Sb(1) – O(1), 124.9(18), O(1) – Sb(1) – O(2), 77.00(14).

difference the position of the hydrogen of the α-carbon of the mandelate, bond lengths will still be discussed. The hydrogen of **4Sr** has been included in order to demonstrate the different enantiomers.

The trigonal bipyramidal geometry of the complexes is a common geometrical preference for *tris*-aryl antimony carboxylates [19,20,23,44–47]. In terms of cyclometallates, very little has been elucidated by X-ray crystallography, with most trigonal bipyramid complexes found to have the general formula [$SbPh_3L_2$]. Only two other instances of cyclometallate structures can be found in the literature, an α-hydroxy complex characterised by Barucki *et al*, [$SbPh_3(O_2CC(O)CH_3(CH_2CH_3O)$], and a pinanediol complex synthesised by Coles *et al,* [$SbPh_3(C_{10}H_{18}O_2)$] [24,25]. Complexes **4Sr** and **4Ss,** [Sb(*o*-PhOMe)$_3$(man)] were found to have similar bond lengths for the Sb – O interaction. These bond lengths were identified as covalent in nature (1.961(12); 2.165(13), **4Ss**, 1.956(3); 2.162(3), **4Sr**, for Sb(1) – O(1); Sb(1) – O(2)). Widening of the trigonal angle was also observed for the complexes from the ideal 120 °. For example: angles of 108.1(2) and 107.7(7) were observed for **4Sr** and **4Ss** for C(1) – Sb(1) – C(7). A similar degree of distortion was observed for the two cyclometallates synthesised by Barucki *et al* and Coles *et al*, with an average trigonal angle of 111.9 ° and 100.8 ° respectively [24,25].

3.4. Biological activity

3.4.1. Mammalian cytotoxicity assay

All complexes: **1Sr/s,** [Sb(*o*-tol)$_3$(man)], **2Sr/s,** [Sb(*m*-tol)$_3$(man)], **4Sr/s,** [Sb(*o*-PhOMe)$_3$(man)], **5Sr/s,** [Sb(Mes)$_3$(man)] and **6Sr/s,** [Sb(*p*-*tert*-BuPh)$_3$(man)], were dissolved in DMSO to a concentration of 10 mM. Complexes **6Sr/s** required heating to fully solubilise. All complexes were sufficiently soluble as DMSO solution in the biological media DMEM. As the solution state of complexes **3Sr/s,** [(Sb(*p*-tol)$_3$(manH)$_2$O$_2$] indicates cyclometallation in d_6-DMSO, it can be assumed that the biologically active complexes tested are **3Sr'/s'**, [Sb(*p*-tol)$_3$(man)].

Initial human fibroblast assays revealed a varying level of toxicity. An IC_{50} range of 2.07 - ≥ 100 μM was observed for the *R*-complexes and a range of 2.90–100 μM for the analogous *S*-enantiomers. Graphs showing the IC_{50} values can be found in the ESI, Figs. S2, S3, S4 and S5. The *p*-*tert*-butylphenyl complexes, **6Sr/s**, were found to be the most toxic, with the *o*-methoxyphenyl complexes **4Sr/s** exhibiting little or no toxicity at the highest concentration tested. Amphotericin B was used as a control, showing no toxicity towards the mammalian cells. IC_{50} values

Table 1
Selectivity indices of complexes **1Sr/s – 6Sr/s**. Indices calculated based on IC_{50}(mammalian)/IC_{50}(parasite).

Complex	Ar	IC_{50} (μM) fibroblasts	IC_{50} (μM) promastigotes	Selectivity index (SI)	CLogP[a]
1Ss	*o*-tolyl	19.3	14.6	1.32	8.516
1Sr		16.2	15.7	1.03	
2Ss	*m*-tolyl	21.8	4.56	4.78	8.516
2Sr		22.8	4.29	5.31	
3Ss'	*p*-tolyl	16.1	2.65	6.08	8.516
3Sr'		15.7	5.04	3.16	
4Ss	*o*-MeO	≥100	≥100	–	6.776
4Sr		≥100	≥100	–	
5Ss	mesityl	6.04	0.21	28.8	11.51
5Sr		5.01	0.33	15.2	
6Ss	*p-tert*-Bu	2.90	0.58	5.00	12.51
6Sr		2.07	0.60	3.45	

[a] Calculated using ChemDraw Professional 15.0, Perkin Elmer Informatics Inc.

for each complex and the selectivity indices (SI) are shown in Table 1.

3.4.2. Leishmania promastigote activity

A large variation was found in the anti-promastigote activity of the complexes with IC_{50} ranges from 0.21 to ≥100 μM, and also between the *R* and *S* enantiomers of each complex. Surprisingly, complexes **4Sr/s**, [Sb(*o*-PhOMe)$_3$(man)], showed little activity towards the promastigotes with only an approximate 75% reduction in parasite viability at 100 μM, the highest concentration used. The *o*-tolyl complexes **1Sr/s**, [Sb(*o*-tol)$_3$(man)], proved to be non-selective in their toxicity towards the promastigotes and fibroblasts, with SI values of 1.03 and 1.32 for the *R* and *S* enantiomers respectively. The more substituted mesityl and *p-tert*-butylphenyl complexes, **5Sr/s,** [Sb(Mes)$_3$(man)] and **6Sr/s,** [Sb(*p-tert*-BuPh)$_3$(man)], proved to have exceptional activity towards the promastigotes at the significantly low concentration range of 0.21–0.60 μM.

In contrast to our earlier observations on the effect of the aryl groups in *tris*-aryl Sb(V) benzoates on fibroblast toxicity, it is discernible from the data in Table 1 that there is very little difference in the *o-, m-* and *p*-tolyl complexes, though the *m-* and *p*-tolyl complexes give the best selectivity due to higher promastigote activity, matching in part some of our earlier data [23]. The clear standout complexes in terms of selectivity are those in which Ar = mesityl (SI = 15.2 *R* and 28.8 *S*), followed by the *p-tert*-butyl complexes (3.45 *R* and 5.00 *S*). The standout complexes in terms of showing little or no activity at 100 μM were the Ar = *o*-MeOPh complexes. This was repeated with an identical outcome. It is not clear at this time why this should be the case.

All complexes that exhibited a selectivity index of three or greater were assessed for their anti-amastigote activity.

3.4.3. Amastigote invasion assay

Due to a lack of selectivity, complexes **1Sr/s,** [Sb(*o*-tol)$_3$(man)] and **4Sr/s,** [Sb(*o*-PhOMe)$_3$(man)], were disqualified from the assay. Complexes **2Sr/s,** [Sb(*m*-tol)$_3$(man)], **3Sr'/s',** [Sb(*p*-tol)$_3$(man)] were sufficiently selective and were tested at a standard 10 μM concentration. Though complexes **5Sr/s** [Sb(Mes)$_3$(man)] and **6Sr/s** [Sb(*p*-tert-BuPh)$_3$(man)] were exceptionally selective, their mammalian toxicity was significant, and so were tested at half the standard concentration (5 μM). All complexes exhibited excellent anti-amastigote activity, with percentage infection values ranging from 0.75–3.00% for those tested at 10 μM and 0.25–2.50% for the remaining 5 μM complexes (Figs. 8 and 9). All individual values have been provided in Table 2.

These complexes were found to be more potent than previously analysed *tris*-phenyl antimony(V)

mandelates, confirming that a change in aryl group has a significant effect on the biological activity [19]. In terms of their anti-amastigote activity, the following trend was obtained: mes > *p*-tol > *p*-tert-BuPh = *m*-tol (based on the average between *R* and *S*). Chirality often plays an important role in biological activity, with the greatest examples of this are the morning sickness medication thalidomide and the over the counter NSAID ibuprofen. The *R*-enantiomer of thalidomide was found to be a potent sedative, whereas the *S*-enantiomer led to serious teratogenic effects [48]. Due to the interconversion of the drug, no fine chiral control was able to be obtained. Similarly, for ibuprofen, the *S*-enantiomer is the bio-active form and interconversion will occur for *R* to *S* but not *S* to *R* [49]. For the mandelate complexes no statistical difference was observed between both enantiomers, leading to the

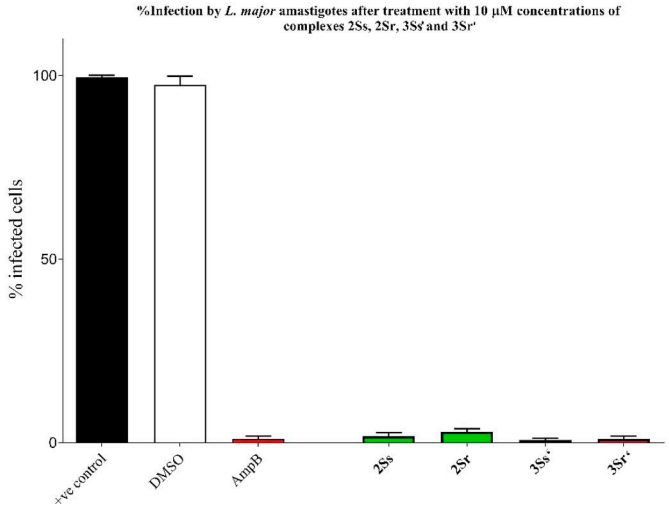

Fig. 8. Infected macrophages after treatment of complexes **2Ss, 2Sr, 3Ss'** and **3Sr',** after 48 h. Number of infected macrophages was determined microscopically, in duplicate of fixed specimens. Amphotericin B (AmpB) was used as a positive control at 10 μM concentration. A DMSO control was also employed at a 1% concentration. Error bars indicate SEM, one-way ANOVA. Dunnett's multiple comparison test was used to determine the statistical significance between all test compounds and a positive control lacking treatment (+ve control).

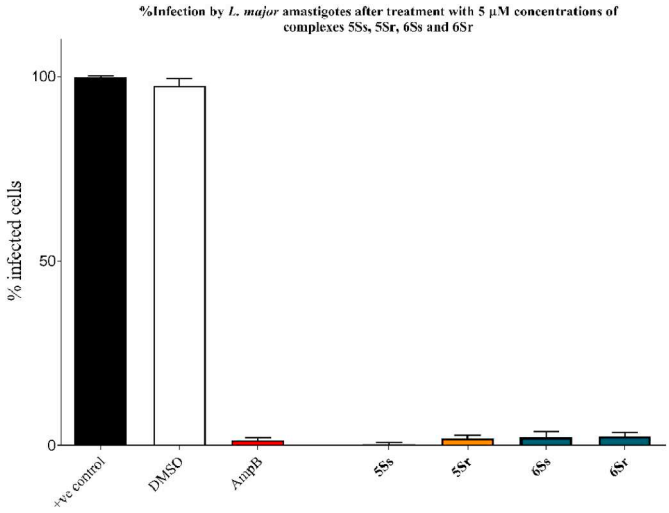

Fig. 9. Infected macrophages after treatment of complexes **5Ss, 5Sr**, **6Ss** and **6Sr**, after 48 h. Number of infected macrophages was determined microscopically, in duplicate of fixed specimens. Amphotericin B (AmpB) was used as a positive control at 5 μM concentration. A DMSO control was also employed at a 1% concentration. Error bars indicate SEM, one-way ANOVA. Dunnett's multiple comparison test was used to determine the statistical significance between all test compounds and a positive control lacking treatment (+ve control).

Table 2
Percentage infection values for the Sb(V) aryl mandelate complexes **2Sr/s, 3Sr'/s', 5Sr/s** and **6Sr/s.**

Complex	Conc^{n} (μM)	% Infection
2Ss	10	1.75 + 0.56
2Sr		3.00 + 0.50
3Ss'	10	0.75 + 0.83
3Sr'		1.00 + 0.50
5Ss	5.0	0.25 + 0.35
5Sr		2.00 + 0.48
6Ss	5.0	2.25 + 0.79
6Sr		2.50 + 0.56

conclusion that chirality of the mandelic acid plays little to no role in the biological activity.

4. Conclusion

A series of *tris*-aryl Sb(*V*) mandelato complexes: {**1Sr/s,** [Sb(*o*-tol)$_3$(man)], **2Sr/s,** [Sb(*m*-tol)$_3$(man)], **3Sr/s,** [(Sb(*p*-tol)$_3$(manH)$_2$O$_2$], **4Sr/s,** [Sb(*o*-PhOMe)$_3$(man)], **5Sr/s,** [Sb(Mes)$_3$(man)] and **6Sr/s,** [Sb(*p*-tert-BuPh)$_3$(man)]}, bearing different aryl groups with either *R* or *S* mandelate co-ligands, were synthesised, compositionally and structurally characterised, and their biological activity towards Leishmania promastigotes and amastigotes, and mammalian cells, assessed. Complexes **3Sr/s** were found to undergo cyclometallation in d$_6$-DMSO to the products **3Sr'/s',** [Sb(*p*-tol)$_3$(man)$_2$], therefore, the cyclometallates were the biological relevant complexes.

In the solid-state, complexes **1Sr/s, 4Sr/s,** and **5Sr/s** are all five-coordinate distorted trigonal bipyramids with the phenyl rings occupying the equatorial plane in the common propeller-like orientation. The oxygen atoms of the mandelate dianion occupy the two remaining axial positions. Complexes **6Sr/s** incorporate a datively bound DMSO molecule, raising the coordination number to six and having distorted octahedral geometry. The *m*-tolyl complexes **2Sr/s** have two moieties within the asymmetric unit, with one Sb(V) interacting with the carbonyl of the mandelate of the neighbouring Sb(V) centre forming a mixed five/six coordinate Sb(V) complex.

No clear trend was discernible from the initial toxicity assays on the fibroblast and promastigote for all the Sb(V) complexes. IC$_{50}$ values for the promastigotes ranged from 0.33 (**5Sr**) – ≥ 100 (**4Sr**) μM and 0.21 (**5Ss**) – ≥ 100 (**4Ss**) μM, and from 2.07 (**6Sr**) – ≥ 100 (**4Sr**) μM and 2.90 (**6Ss**) – ≥ 100 (**4Ss**) μM for fibroblast cells, for the *R* and *S* enantiomers respectively. Despite the high degree of mammalian cytotoxicity observed for complexes **5Ss**, **5Sr**, **6Ss** and **6Sr,** each were extremely potent anti-leishmanials, presenting with selectivity indices (SI) of 28.8, 15.2, 5.00 and 3.45 respectively. Those complexes with the highest SI values, **2Ss**, **2Sr**, **3Ss'** and **3Sr'**, were analysed in an amastigote invasion assay at the standard 10 μM, but due to the higher degree of toxicity of complexes, **5Ss**, **5Sr**, **6Ss** and **6Sr**, they were tested at only 5 μM. All complexes were found to exhibit excellent activity towards the amastigotes with ranges of 0.75–3.00% for **2Ss**, **2Sr**, **3Ss'** and **3Sr'** and 0.25–2.50% for **5Ss**, **5Sr**, **6Ss** and **6Sr**. Selectivity of the complexes was found to decrease in the following order: mes ≥ *p-tert*-BuPh ≥ *m*-tol ≥ *p*-tol ≥ *o*-tol ≥ *o*-MeOPh, which correlates with the CLogP values suggesting the lipophilicity of the complexes plays a role in their selectivity.

Though chirality can often lead to changes in biological activity this was not observed for the mandelate complexes with no statistical difference notable for either *R* or *S*. Nevertheless, the change in aryl group had a substantial effect on the overall activity of the complexes. Activity of these cyclometallate far out-classed our previously synthesised *bis*-substituted carboxylates [20], however an increased cytotoxicity is of concern. Despite this, the selectivity of these cyclometallates is still substantially high due to their potency towards the parasite. This study has highlighted the further need for further research into modification of the aryl substituents of both conventional *bis*-substituted and cyclometallate *tris*-aryl Sb(*V*) carboxylates.

List of abbreviations

GSH	Gluathione
TSH	Trypanthione
GSSG	oxidised glutathione
^{1}H NMR	Proton nuclear magnetic resonance.
FT-IR	Fourier transform infrared
m.p	Melting point
o,m,p-tol	ortho, meta, para-tolyl
tert-BuPh	tertiary butyl phenyl
MeOPh	methoxyphenyl
Mes	Mesityl
CLogP	Partition co-efficient
IC$_{50}$	Inhibitory concentration at 50%
d$_6$_DMSO	deuterated dimethyl sulfoxide

Declaration of competing interest

There are no conflicts to declare.

Acknowledgements

The authors would like to thank the Australian Research Council (DP170103624) and Monash University for financial support. We would also like to thank Dr. Craig Forsyth (Monash) for assistance with X-ray crystallography.

Appendix A. Supplementary data

Supplementary data to this article can be found online at https://doi.org/10.1016/j.jinorgbio.2019.110932.

References

[1] World Health Organization (WHO), Interregional Meeting on Leishmaniasis among Neighbouring Endemic Countries in the Eastern Mediterranean, African and European Regions, https://apps.who.int/iris/bitstream/handle/10665/311922/IC_Meet_Rep_2019_EN_20619.pdf, (2019).
[2] S.M. Gossage, M.E. Rogers, P.A. Bates, Int. J. Parasitol. 33 (2003) 1027–1034.
[3] H.A. Fletcher, M. Chatterjee, A. Cooper, T. Hussell, P.M. Kaye, J. Prior, R. Reljic, S. Vermaak, M. Vordermeier, A. Williams, F100Research, (2018), pp. 1–5.
[4] J. Alvar, I.D. Vélez, C. Bern, M. Herrero, P. Desjeux, J. Cano, J. Jannin, M. den Boer, W.L.C. Team, PLoS One 7 (2012) e35671.
[5] D. Légaré, M. Ouellette, Handbook of Antimicrobial Resistance, (2017), pp. 313–341.
[6] G. Mandal, V. Govindarajan, M. Sharma, H. Bhattacharjee, R. Mukhopadhyay, Antimicrob. Drug. Resist, Springer, 2017, pp. 649–665.
[7] A. Ponte-Sucre, F. Gamarro, J.-C. Dujardin, M.P. Barrett, R. López-Vélez, R. García-Hernández, A.W. Pountain, R. Mwenechanya, B. Papadopoulou, PLoS Negl. Trop. Dis. 11 (2017) e0006052.
[8] B.L. Herwaldt, J.D. Berman, Am. J. Trop. Med. Hyg. 46 (1992) 296–306.
[9] J. Chulay, L. Fleckenstein, D. Smith, Trans. R. Soc. Trop. Med. Hyg. 82 (1988) 69–72.
[10] P. Rees, P. Kager, M. Keating, W. Hockmeyer, Lancet 316 (1980) 226–229.
[11] B. Purkait, A. Kumar, N. Nandi, A.H. Sardar, S. Das, S. Kumar, K. Pandey, V. Ravidas, M. Kumar, T. De, Antimicrob. Agents Chemother. (2011) 1031–1041.
[12] S. Sundar, T.K. Jha, C.P. Thakur, S.K. Bhattacharya, M. Rai, Trans. R. Soc. Trop. Med. Hyg. 100 (2006) 26–S33.
[13] J. Veronica, S. Chandrasekaran, A. Dayakar, M. Devender, V.K. Prajapati, S. Sundar, R. Maurya, FEBS J. 286 (2019) 3488–3503 https://febs.onlinelibrary.wiley.com/doi/abs/10.1111/febs.14923 (accessed 26 September 2019).
[14] World Health Organization (WHO), Investing to Overcome the Global Impact of Neglected Tropical Diseases: Third WHO Report on Neglected Tropical Diseases, 3 (2015).
[15] A.K. Haldar, P. Sen, S. Roy, Mol. Biol. Int. 2011 (2011) 23 571242 https://www.hindawi.com/journals/mbi/2011/571242/abs/ , Accessed date: 26 September 2019.
[16] A.H. Fairlamb, A. Cerami, Annu. Rev. Microbiol. 46 (1992) 695–729.
[17] M.K. Pathak, T. Yi, J. Immunol. 167 (2001) 3391–3397.
[18] Y.C. Ong, S. Roy, P.C. Andrews, G. Gasser, Chem. Rev. 119 (2018) 730–796.
[19] R.N. Duffin, V.L. Blair, L. Kedzierski, P.C. Andrews, Dalton Trans. 47 (2018)

971–980.
[20] R.N. Duffin, V.L. Blair, L. Kedzierski, P.C. Andrews, J. Inorg. Biochem. 189 (2018) 151–162.
[21] Y.C. Ong, V.L. Blair, L. Kedzierski, K.L. Tuck, P.C. Andrews, Dalton Trans. 44 (2015) 18215–18226.
[22] Y.C. Ong, V.L. Blair, L. Kedzierski, P.C. Andrews, Dalton Trans. 43 (2014) 12904–12916.
[23] M.I. Ali, M.K. Rauf, A. Badshah, I. Kumar, C.M. Forsyth, P.C. Junk, L. Kedzierski, P.C. Andrews, Dalton Trans. 42 (2013) 16733–16741.
[24] H. Barucki, S.J. Coles, J.F. Costello, M.B. Hursthouse, J. Organomet. Chem. 622 (2001) 265–273.
[25] S.J. Coles, J.F. Costello, M.B. Hursthouse, S. Smith, J. Organomet. Chem. 662 (2002) 98–104.
[26] M. Mohamadyan, M. Moosazadeh, A. Borji, N. Khanjani, S.R. Moghadam, Environ. Monit. Assess. 191 (2019) 62.
[27] J. Gromiec, J. Piotrowski, Int. Arch. Occup. Environ. Health 55 (1984) 61–72.
[28] P. Putten, Antonie van Leeuwenhoek, 45, (1979), 622–623.
[29] M.L. Rosenheim, Lancet 225 (1935) 1032–1037.
[30] M. Ikeda, T. Imamura, M. Hayashi, T. Tabuchi, I. Hara, Int. Arch. Arbeitsmed. 32 (1974) 93–101.
[31] A. Slob, Occup. Environ. Med. 30 (1973) 390–393.
[32] C.D. Stan, A. Ştefanache, G. Tătărîngă, M. Drăgan, C. Tuchiluş, FARMACIA 63 (2015) 577–580.
[33] M. Motamedifar, A. Bazargani, M.R. Namazi, E. Sarai, H. Sedigh, World Appl. Sci. J. 31 (2014) 925–929.
[34] CrysAlisPro, version 1.171. 34.36, Oxford Diffraction Ltd.: Oxford, UK, 2010.
[35] G.M. Sheldrick, Acta Crystallogr. A 64 (2008) 112–122.
[36] O.V. Dolomanov, L.J. Bourhis, R.J. Gildea, J.A. Howard, H. Puschmann, J. Appl. Crystallogr. 42 (2009) 339–341.
[37] A. Pathak, V.L. Blair, R.L. Ferrero, L. Kedzierski, P.C. Andrews, J. Inorg. Biochem. 177 (2017) 266–275.
[38] K. Lackovic, J.P. Parisot, N. Sleebs, J.B. Baell, L. Debien, K.G. Watson, J.M. Curtis, E. Handman, I.P. Street, L. Kedzierski, Antimicrob. Agents Chemother. 54 (2010) 1712–1719.
[39] D.V. Moiseev, Y.B. Malysheva, A.S. Shavyrin, Y.A. Kurskii, A.V. Gushchin, J. Organomet. Chem. 690 (2005) 3652–3663.
[40] W. Reeve, C.M. Erikson, P.F. Aluotto, Can. J. Chem. 57 (1979) 2747–2754 NRC Research Press.
[41] V. Sharutin, A. Pakusina, O. Subacheva, O. Sharutina, A. Gerasimenko, Russ. J. Coord. Chem. 29 (2003) 395–399.
[42] J.C. Maxwell, J.A. Volpe, C.H. Barlow, W.S. Caughey, Biochem. Biophys. Res. Commun. 58 (1974) 166–171.
[43] K. Shikama, Prog. Biophys. Mol. Biol. 91 (2006) 83–162.
[44] T. Iftikhar, M.K. Rauf, S. Sarwar, A. Badshah, D. Waseem, M.N. Tahir, A. Khan, K.M. Khan, G.M. Khan, J. Organomet. Chem. 851 (2017) 89–96.
[45] R. Mushtaq, M.K. Rauf, M. Bolte, A. Nadhman, A. Badshah, M.N. Tahir, M. Yasinzai, K.M. Khan, Appl. Organomet. Chem. 31 (2017) e3606.
[46] L. Saleem, A.A. Altaf, A. Badshah, M.K. Rauf, A. Waseem, M. Danish, S.S. Azam, M.N. Arshad, A.M. Asiri, S. Ahmad, Inorg. Chim. Acta 474 (2018) 148–155.
[47] S. Sarwar, T. Iftikhar, M.K. Rauf, A. Badshah, D. Waseem, M.N. Tahir, K.M. Khan, G.M. Khan, Inorg. Chim. Acta 476 (2018) 12–19.
[48] M.E. Franks, G.R. Macpherson, W.D. Figg, Lancet 63 (2004) 1802–1811.
[49] A.M. Evans, Clin. Rheumatol. 20 (2001) 9–14.